

# Phosphorus and Arsenic Based Ligands in Supramolecular Chemistry



DISSERTATION

ZUR ERLANGUNG DES DOKTORGRADES DER NATURWISSENSCHAFTEN

(DR. RER. NAT.) DER FAKULTÄT FÜR CHEMIE UND PHARMAZIE

DER UNIVERSITÄT REGENSBURG

vorgelegt von

**Jana Schiller**

aus Laaber

im Jahr 2020

Diese Arbeit wurde angeleitet von Prof. Dr. Manfred Scheer.

Promotionsgesuch eingereicht am: 28. April 2020

Tag der mündlichen Prüfung am: 29. Mai 2020

Vorsitzender: Prof. Dr. Hubert Motschmann

Prüfungsausschuss: Prof. Dr. Manfred Scheer

Prof. Dr. Henri Brunner

PD Dr. David Díaz Díaz



Universität Regensburg



The experimental work presented in this thesis was performed from August 2016 until February 2020 in the Institute of Inorganic Chemistry at the University of Regensburg, under the supervision of Prof. Dr. Manfred Scheer. Parts of the results presented in chapter 7 were obtained from experiments performed at the INSA, Rennes in June 2018, May-July 2019 and February 2020 under the supervision of Dr. Christophe Lescop.

Parts of this work have already been published:

J. Schiller, E. V. Peresykina, A. V. Virovets, M. Scheer, *Angew. Chem. Int. Ed.* **2020**, online; <https://doi.org/10.1002/anie.202004988>.

M. Elsayed Moussa, J. Schiller, E. Peresykina, M. Seidl, G. Balázs, P. Shelyganov, M. Scheer, *Chem. Eur. J.* **2020**, accepted manuscript; <https://doi.org/10.1002/chem.202002513>.



*"Wer das Geheimnis seiner Herstellung kennt,  
der kann jedes Metall in den Kristall der Ewigkeit  
verwandeln."*

*aus „Jim Knopf und die wilde 13“*

**Michael Ende**



## Abstract and Preface

This thesis reports of various aspects of the coordination chemistry of phosphorus and arsenic based complexes towards coinage metal salts. The first part (chapters 3-5) deals with the reaction behavior of the tetrahedral complex  $[\text{Cp}_2\text{Mo}_2(\text{CO})_4(\mu, \eta^2\text{-As}_2)]$  (**1**) with Cu(I) and Ag(I) salts containing weakly coordinating anions (WCAs) and the three component reactions of **1** with Ag(I)WCA salts and organic pyridyl linkers. In chapter 3 the reactions of the organometallic diarsenic complex **1** with the weakly coordinating  $\text{Ag}[\text{FAI}\{\text{OC}(\text{C}_6\text{F}_5)(\text{C}_6\text{F}_{10})\}_3]$  (AgFAI) and  $\text{Ag}[\text{Al}\{\text{OC}(\text{CF}_3)_3\}_4]$  (AgTEF), respectively are presented. Chapter 4 focuses on the synthesis of  $[\text{Ag}\{\text{Cp}_2\text{Mo}_2(\text{CO})_4(\mu, \eta^2\text{-As}_2)\}_3][\text{PF}_6]$  and its coordination chemistry towards organic pyridyl linkers. The reaction of  $[\text{Cp}_2\text{Mo}_2(\text{CO})_4(\mu, \eta^2\text{-As}_2)]$  with Cu(I) WCA salt is reported in chapter 5. The second part (chapter 6) presents the formation of the superdeficient supramolecule  $[(\text{Cp}''\text{Fe}(\eta^5\text{-P}_5))_{12}\{\text{CuNCMe}\}_8]^{8+}$  under weakly coordinating conditions. The unique structure of the sphere is discussed in terms of its vacancies, the inner cavity and its potential for further supramolecular reactions. The last part (chapter 7) displays the syntheses of the metallacycles  $[\text{Cu}_4(\mu_2\text{-dppm})_4(\text{CN})_2][\text{X}]_2$  ( $\text{X} = \text{TEF}^-$  (**2**),  $\text{BAr}^{\text{Cl-}}$  (**3**)), their photophysical properties and the reactions of **2** and **3** with pyridyl linkers and the resulting luminescence properties. Finally, chapter 8 contains the thesis treasury and describes additional results which were obtained during the preparation of this work.

At the beginning of each chapter a list of authors, who contributed to the respective part, is given. If results from collaborations are in part also discussed in other theses, it is stated there.

To ensure a uniform design of this work, all chapters are subdivided into 'Introduction', 'Results and Discussion', 'Conclusion', 'Supporting Information' and 'References'. Furthermore, all chapters have the same text settings and the compound numeration begins anew. In addition, a general introduction is given at the beginning and a comprehensive conclusion of all chapters is presented at the end of the thesis.



## Table of Contents

1. Introduction	1
1.1 Supramolecular Chemistry	1
1.1.1 Coordination Chemistry of E <sub>n</sub> (E=P, As) Ligand Complexes	2
1.1.2 Discrete Nano-sized Aggregates	7
1.2 The Myth of the Non-Coordinating Anions	9
1.3 The Potential of Luminescent Cu(I) Complexes	12
1.4 References	16
2. Research Objectives	24
3. The Diarsenic Complex [(C <sub>5</sub> H <sub>5</sub> ) <sub>2</sub> Mo <sub>2</sub> (CO) <sub>4</sub> (μ,η <sup>2</sup> -As <sub>2</sub> )] as a Building Block in Supramolecular Chemistry	26
3.1 Introduction	27
3.2 Results and Discussion	29
3.3 Conclusion	34
3.4 Supporting Information	34
3.4.1 General	34
3.4.2 Synthesis of [{{CpMo(CO) <sub>2</sub> }} <sub>2</sub> {η <sup>2</sup> :η <sup>2</sup> -As <sub>2</sub> }} <sub>4</sub> Ag <sub>2</sub> ][FAI{OC(C <sub>6</sub> F <sub>5</sub> )(C <sub>6</sub> F <sub>10</sub> )}} <sub>3</sub> ] <sub>2</sub> ( <b>4</b> )	35
3.4.3 Synthesis of [{{CpMo(CO) <sub>2</sub> }} <sub>2</sub> {η <sup>2</sup> :η <sup>2</sup> -As <sub>2</sub> }} <sub>3</sub> Ag][Al{OC(CF <sub>3</sub> ) <sub>3</sub> }} <sub>4</sub> ] ( <b>5</b> )	35
3.4.4 Synthesis of [{{CpMo(CO) <sub>2</sub> }} <sub>2</sub> {η <sup>2</sup> :η <sup>2</sup> -As <sub>2</sub> }} <sub>2</sub> [[{{CpMo(CO) <sub>2</sub> }} <sub>2</sub> {η <sup>1</sup> :η <sup>2</sup> :η <sup>2</sup> -As <sub>2</sub> }} <sub>3</sub> Ag][Al{OC(CF <sub>3</sub> ) <sub>3</sub> }} <sub>4</sub> ] ( <b>6</b> )	36
3.4.5 Synthesis of [{{CpMo(CO) <sub>2</sub> }} <sub>2</sub> {η <sup>1</sup> :η <sup>2</sup> :η <sup>2</sup> -As <sub>2</sub> }} <sub>4</sub> Ag <sub>3</sub> ][Al{OC(CF <sub>3</sub> ) <sub>3</sub> }} <sub>4</sub> ] <sub>3</sub> ( <b>7</b> )	37
3.4.6 Crystallographic Data	37
3.4.7 DFT Calculations	53
3.5 References	58
4. Discrete and Polymeric Organometallic-Organic Assemblies Based on the Diarsene Complex [(C <sub>5</sub> H <sub>5</sub> ) <sub>2</sub> Mo <sub>2</sub> (CO) <sub>4</sub> (μ,η <sup>2</sup> -As <sub>2</sub> )], AgPF <sub>6</sub> and Organic N-donor Molecules	62
4.1 Introduction	63
4.2 Results and Discussion	66
4.3 Conclusion	69
4.4 Supporting Information	70
4.4.1 General	70

4.4.2	Synthesis of $[(\mu, \eta^2\text{-B})_3\text{Ag}][\text{PF}_6]_2$ ( <b>C</b> )	70
4.4.3	Synthesis of $[\{(\eta^2\text{-B})_2\text{Ag}\}_2(\mu\text{-L}_1)][\text{PF}_6]_2$ ( <b>1</b> )	71
4.4.4	Synthesis of $[\{(\eta^2\text{-B})_2\text{Ag}\}_2(\mu\text{-L}_2)][\text{PF}_6]_2$ ( <b>2</b> )	71
4.4.5	Synthesis of $[\{(\eta^2\text{-B})\text{Ag}\}(\mu\text{-L}_3)]_n[\text{PF}_6]_{2n}$ ( <b>3</b> )	72
4.4.6	Synthesis of $[\{(\eta^1:\eta^2\text{-B})_2(\text{CH}_3\text{CN})_2\text{Ag}_2\}(\mu\text{-L}_4)]_n[\text{PF}_6]_{2n}$ ( <b>4</b> )	73
4.4.7	Synthesis of $[\{(\eta^1:\eta^2\text{-B})_2(\eta^1:\eta^1\text{-B})\text{Ag}_2\}(\mu\text{-L}_5)]_n[\text{PF}_6]_{2n}$ ( <b>5</b> )	73
4.4.8	Synthesis of $[\{(\eta^1:\eta^2\text{-B})_2(\text{CH}_3\text{CN})_2\text{Ag}_2\}(\mu\text{-L}_5)]_n[\text{PF}_6]_{2n}$ ( <b>6</b> )	74
4.4.9	Crystallographic Data	74
4.5	References	85
5.	Unprecedented Linking Behavior of Tetrahedral $\text{Mo}_2\text{E}_2$ Complexes (E = P, As) towards Cu(I) Units	88
5.1	Introduction	89
5.2	Results and Discussion	91
5.3	Conclusion	96
5.4	Supporting Information	97
5.4.1	General	97
5.4.2	Synthetic Procedure	97
5.4.3	Crystallographic Data	102
5.4.4	DFT Calculations	108
5.4.5	Results and Discussion – Additional Compounds	121
5.5	References	132
6.	Metal-Deficient Supramolecule based on a Fivefold-Symmetric Building Block	136
6.1	Introduction	137
6.2	Results and Discussion	139
6.3	Conclusion	142
6.4	Supporting Information	143
6.4.1	General	143
6.4.2	Synthetic Procedure	143
6.4.3	Crystallographic Data	144
6.4.3.1	The Crystal Structure of the by-product $[\{\text{Cp}''\text{FeP}_5\}_2\text{Cu}_4(\text{CH}_3\text{CN})_{10}[\text{TEF}]_4$ ( <b>4</b> )	147
6.4.3.2	The Crystal Structure of the Super-vacant Supramolecule $(\text{CH}_2\text{Cl}_2)_{1.25}@\{[\text{Cp}''\text{FeP}_5]_{12}\}$ $\{\text{Cu}(\text{CH}_3\text{CN})\}_8[\text{TEF}]_8$ ( <b>3</b> )	150
6.4.4	Powder Diffraction	156



6.4.5	Additional Solid-State Structures Mentioned in the Introduction	159
6.5	References	160
7.	Tuning Emission Properties of Cu(I) Metallacycles by Introducing Bulky Weakly Coordinating Anions	162
7.1	Introduction	163
7.2	Results and Discussion	164
7.3	Conclusion	175
7.4	Supporting Information	176
7.4.1	Chemicals	176
7.4.2	Spectroscopic Methods	176
7.4.3	Synthetic Procedure	177
7.4.4	Crystallographic Data	180
7.4.5	Additional Variable Temperature UV-Vis Spectra	188
7.4.6	Variable Temperature Excited State Lifetime Measurements of $\mathbf{A}_2$	192
7.4.7	Thermogravimetric Analyses and Differential Scanning Calorimetry	194
7.4.8	Additional IR Spectra	196
7.5	References	204
8.	Thesis Treasury	208
8.1	Coordination Compounds Based on $[(\text{C}_5\text{H}_5)_2\text{Mo}_2(\text{CO})_4(\mu, \eta^2\text{-As}_2)]$	208
8.1.1	Reaction of $[(\text{C}_5\text{H}_5)_2\text{Mo}_2(\text{CO})_4(\mu, \eta^2\text{-As}_2)]$ with $\text{Au}(\text{tht})\text{Cl}$	208
8.1.2	Reaction of $[(\text{C}_5\text{H}_5)_2\text{Mo}_2(\text{CO})_4(\mu, \eta^2\text{-As}_2)]$ with $\text{CuCl}$	209
8.1.3	Reaction of $[(\text{C}_5\text{H}_5)_2\text{Mo}_2(\text{CO})_4(\mu, \eta^2\text{-As}_2)]$ with hydrolyzed $\text{AgPF}_6$ and 2,2'-bipyrimide	209
8.1.4	Reaction of $[(\text{C}_5\text{H}_5)_2\text{Mo}_2(\text{CO})_4(\mu, \eta^2\text{-As}_2)]$ with hydrolyzed $\text{AgPF}_6$ and 2,2'-bipyridine	210
8.1.5	Reaction of $[(\text{C}_5\text{H}_5)_2\text{Mo}_2(\text{CO})_4(\mu, \eta^2\text{-As}_2)]$ with $[\text{Cu}(\text{CH}_3\text{CN})_4][\text{Al}\{\text{OC}(\text{CF}_3)_3\}_4]$ and 1,2-di(4-pyridyl)ethylene	211
8.2	Coordination Compounds Based on $[(\text{C}_5\text{Me}_5)\text{Fe}(\eta^5\text{-P}_5)]$	212
8.2.1	Reaction of $[(\text{C}_5\text{Me}_5)\text{Fe}(\eta^5\text{-P}_5)]$ with $\text{Ag}[\text{B}(3,5\text{-C}_6\text{H}_3\text{Cl}_2)_4]$	212
8.2.2	Reaction of $[(\text{C}_5\text{Me}_5)\text{Fe}(\eta^5\text{-P}_5)]$ with $\text{Ag}[\text{B}(3,5\text{-C}_6\text{H}_3\text{Cl}_2)_4]$ and 4,4'-bipyridine	214
8.3	Supporting Information	218
8.3.1	General	218

8.3.2 Synthetic Procedure	218
8.3.3 Crystallographic Data	221
8.4 References	227
9. Conclusion	228
A. Appendices	242
List of Abbreviations	242
Danksagung	244
Lebenslauf	245
Eidstattliche Erklärung	248





# 1. Introduction

## 1.1 Supramolecular Chemistry

Jean-Marie Lehn defined supramolecular chemistry as the “chemistry beyond the molecule”.<sup>1</sup> Its principles do not only help to understand chemical mechanisms but also biological phenomena, such as the structure of DNA or protein-protein interactions based on the lock-and-key model. Its principles are found in many different areas.<sup>2,3</sup> For their pioneering “development and use of molecules with structure-specific interactions of high selectivity” Jean-Marie Lehn, Donald J. Cram and Charles Pedersen were jointly awarded with the Nobel Prize in chemistry in 1987.<sup>1,4,5</sup> As, for most of the 150 years between Wöhler’s urea synthesis<sup>6</sup> and the 1987 Nobel Prize, the main focus of chemists were molecules containing only covalently linked atoms, this was an important turning point in the history of chemistry. The coordinative bond turned out to be an exceptional tool, since it incorporates the advantages of both weak interactions (van-der Waals forces, hydrogen bonds,  $\pi,\pi$ -, electrostatic interactions) and covalent bonds. These bonds are comparatively strong, but also weak enough to allow dynamic behavior in solution.

The work in supramolecular chemistry started with the selective binding of alkali metal cations by natural<sup>7</sup> and synthetic<sup>5,8,9</sup> macro(poly)cyclic ligands, such as crown ethers and cryptands. This led to the appearance of molecular recognition as a new field of chemical research that expanded and became supramolecular chemistry.<sup>8,10</sup> Many different receptor types, such as crown ethers, cryptands and calixarenes have been explored with regard to molecular recognition based on supramolecular principles.<sup>5,11–13</sup> During the last decades supramolecular chemistry gained impact in modern chemistry, with regard to biological systems and beyond. The Lewis acid/base interaction between a metal center and a ligand is also included in the field and was named metallosupramolecular chemistry.<sup>14,15</sup>

It has become evident that the key concept of supramolecular chemistry is not size but information. In keeping with Richard Feynman’s motto ‘there’s plenty of room at the bottom’<sup>16</sup> the capability of supramolecular species to spontaneously build up networks and achieve complex roles on the basis of encoded instructions and information demonstrates that with supramolecular chemistry ‘there’s even more room at the top’.<sup>10</sup>

### 1.1.1 Coordination Chemistry of E<sub>n</sub> (E = P, As) Ligand Complexes

The term E<sub>n</sub> ligand complexes describes organometallic complexes with a limited number n (n = 2 - 6) of substituent-free pnictogen atoms E (E = P, As, Sb, Bi) only bound to other pnictogen atoms or transition metals.<sup>17-20</sup> Since the first examples of P<sub>n</sub> ligand complexes (1971: [RhCl(P<sub>4</sub>)L<sub>2</sub>], L = P(C<sub>6</sub>H<sub>5</sub>)<sub>3</sub>, P(*p*-CH<sub>3</sub>C<sub>6</sub>H<sub>4</sub>)<sub>3</sub>, P(*m*-CH<sub>3</sub>-C<sub>6</sub>H<sub>4</sub>)<sub>3</sub>, As(C<sub>6</sub>H<sub>5</sub>)<sub>3</sub>;<sup>21</sup> 1973: [Co<sub>4</sub>(η<sup>5</sup>-C<sub>5</sub>H<sub>5</sub>)<sub>4</sub>P<sub>4</sub>];<sup>22</sup> 1973: [(Co(CO)<sub>3</sub>)<sub>2</sub>(μ,η<sup>2,2</sup>-P<sub>2</sub>)];<sup>23</sup>) were published around 50 years ago a variety of other examples have been reported. E<sub>n</sub> ligand complexes can act as electron-donors towards Lewis acids due to their sterically accessible lone pairs, as well as their occupied σ-orbitals of E-E bonds. This enables a unique coordination chemistry. The tetrahedrane complexes [{Cp<sup>R</sup>Mo(CO)<sub>2</sub>]<sub>2</sub>(η<sup>2</sup>-E<sub>2</sub>)] (E = P (**1**), As (**2**); Cp = C<sub>5</sub>H<sub>5</sub>) and [Cp<sup>R</sup>Mo(CO)<sub>2</sub>(η<sup>3</sup>-P<sub>3</sub>)] (**3**), the P<sub>4</sub> complex [Cp<sup>R</sup>Ta(CO)<sub>2</sub>(η<sup>4</sup>-P<sub>4</sub>)] (**4**), the cyclo-E<sub>5</sub> complexes [Cp<sup>R</sup>Fe(η<sup>5</sup>-E<sub>5</sub>)] (E = P (**5**), As (**6**)) as well as the tripledecker complex [(Cp<sup>R</sup>Mo)<sub>2</sub>(μ,η<sup>6,6</sup>-P<sub>6</sub>)] (**7**) are versatile synthetic building blocks in supramolecular chemistry (Figure 1.1).

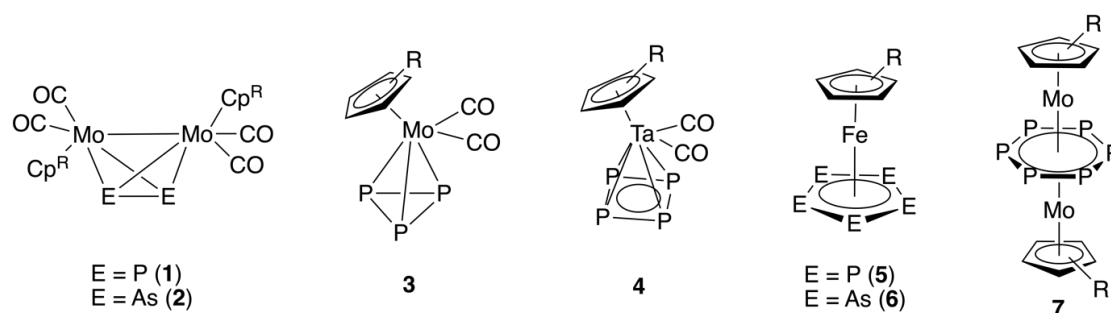


**Figure 1.1.** Selected E<sub>n</sub> (E = P, As; n = 2 – 6) complexes suitable as building blocks for supramolecular chemistry.

Compounds **1**, **3**, **5** and **7** can be easily obtained by the thermolysis of [Cp<sup>R</sup>Mo(CO)<sub>3</sub>]<sub>2</sub> (Cp<sup>R</sup> = C<sub>5</sub>H<sub>5</sub>, C<sub>5</sub>Me<sub>5</sub>) and [Cp<sup>R</sup>Fe(CO)<sub>2</sub>]<sub>2</sub> (Cp<sup>R</sup> = η<sup>5</sup>-C<sub>5</sub>Me<sub>5</sub>, η<sup>5</sup>-C<sub>5</sub>H<sub>3</sub><sup>t</sup>Bu<sub>2</sub>, η<sup>5</sup>-C<sub>5</sub>H<sub>2</sub><sup>t</sup>Bu<sub>3</sub>), respectively, with white phosphorus (P<sub>4</sub>).<sup>24-28</sup> Compound **4** containing a Cp<sup>R</sup> ligand (Cp<sup>R</sup> = η<sup>5</sup>-C<sub>5</sub>H<sub>3</sub><sup>t</sup>Bu<sub>2</sub>) can be synthesized by photolysis of [Cp<sup>R</sup>Ta(CO)<sub>4</sub>] with P<sub>4</sub>.<sup>29</sup> The polyarsenic complexes **2** and **6** are formed when reacting hexaphenylcyclohexaarsine with [CpMo(CO)<sub>3</sub>]<sub>2</sub> or by thermolysis of [Cp<sup>R</sup>Fe(CO)<sub>2</sub>]<sub>2</sub> with yellow arsenic (As<sub>4</sub>).<sup>30,31</sup> The first example of the coordination behavior of a P<sub>n</sub> ligand complex was reported by Scherer *et al.* in 1984 who observed the coordination of **1** with the 16 valence electron (VE) complexes [Re(CO)<sub>4</sub>Br] and [Cr(CO)<sub>5</sub>].<sup>32</sup>

The conversion of **1** with coinage metal salts results in 1D coordination polymers (CPs) or dimers depending on the counterion. The first reports on this reactivity included the formation of the neutral 1D polymer **8**<sup>33,34</sup> as well as the charged polymer **9**<sup>33</sup> and the

discrete complex **10**<sup>33</sup> (Figure 1.2) from the reaction of **1** with CuX (X = Cl, Br, I), AgNO<sub>3</sub> and Ag(OTf) (Otf = CF<sub>3</sub>SO<sub>3</sub>), respectively.

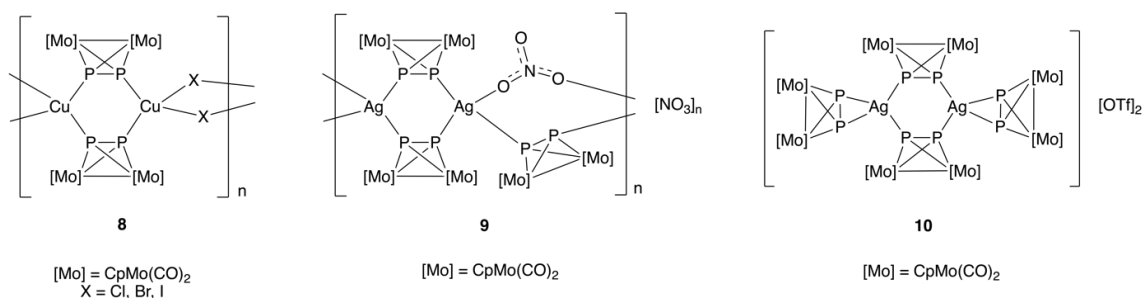
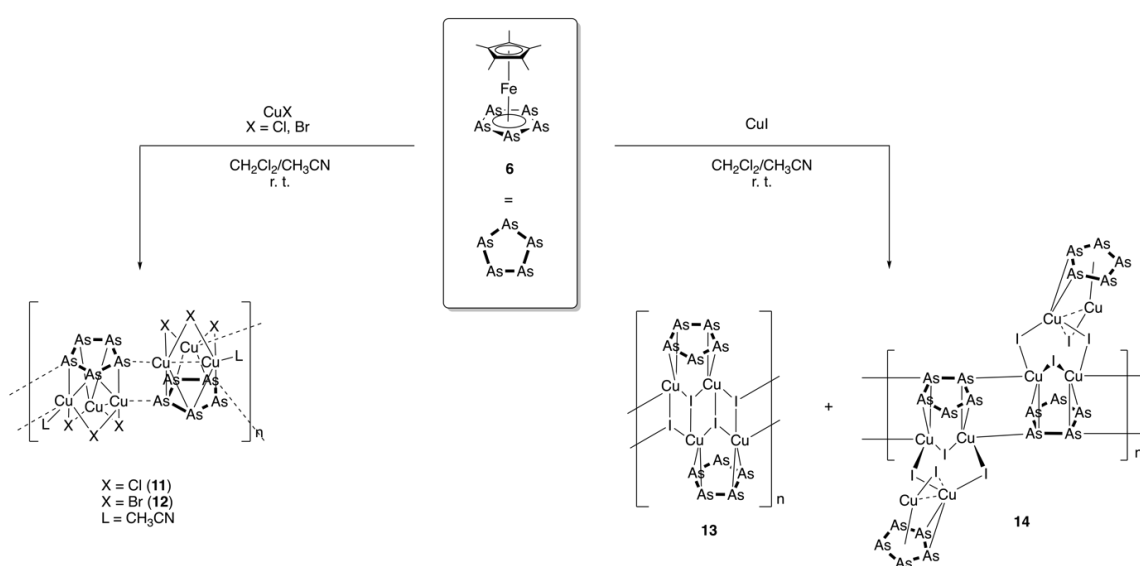


**Figure 1.2.** First polymeric and oligomeric coordination compounds based on **1**.

Compound **8** consists of six-membered Cu<sub>2</sub>P<sub>4</sub> rings in which two P<sub>2</sub> units coordinate side-on to the Cu atoms. Additionally, each copper atom coordinates to two halides forming a one-dimensional neutral polymer. Using the strongly coordinating anion [NO<sub>3</sub>]<sup>−</sup> instead of a halide the charged 1D polymer **9** is obtained, which features Ag<sub>2</sub>P<sub>4</sub> rings similar to the Cu<sub>2</sub>P<sub>4</sub> rings in **8**. The Ag<sub>2</sub>P<sub>4</sub> rings are linked by coordination of each Ag atom to a bridging NO<sub>3</sub><sup>−</sup> and an additional Mo<sub>2</sub>P<sub>2</sub> fragment. Interestingly, compound **10** is not a coordination polymer (CP) but a discrete compound containing an Ag<sub>2</sub>P<sub>4</sub> ring, similar to **9**. The Ag cations are additionally side-on coordinated by one molecule of **1** each. Due to the relatively weakly coordinating anion (WCA) [Otf]<sup>−</sup> compound **10** is slightly soluble, but dissociates in solution. Using other first generation WCA salts (AgBF<sub>4</sub>,<sup>35</sup> AgClO<sub>4</sub>,<sup>35</sup> AgPF<sub>6</sub>,<sup>35</sup> AgSbF<sub>6</sub>,<sup>35</sup> Ag[Al{OC(CF<sub>3</sub>)<sub>3</sub>]<sub>4</sub>],<sup>35</sup> [(Ph<sub>3</sub>P)Au(thf)][PF<sub>6</sub>],<sup>35</sup> [Cu(CH<sub>3</sub>CN)<sub>4</sub>][PF<sub>6</sub>],<sup>35</sup> [Cu(CH<sub>3</sub>CN)<sub>4</sub>][BF<sub>4</sub>],<sup>36</sup> [Cu(CH<sub>3</sub>CN)<sub>4</sub>][Al{OC(CF<sub>3</sub>)<sub>3</sub>]<sub>4</sub>],<sup>37</sup> [Cu(CH<sub>3</sub>CN)<sub>3.5</sub>][Fai{OC(C<sub>6</sub>F<sub>10</sub>)(C<sub>6</sub>F<sub>5</sub>)<sub>3</sub>}]<sup>38</sup>) leads to isostructural compounds comparable to **10**. The structural differences in **8-10** illustrate how small differences in the binding properties of the anions present in solution can dramatically change the structure of the product.

Interestingly, the reaction of the *cyclo*-P<sub>5</sub> compound **5** with CuCl leads to a structure similar to that of **8**, which consists of planar six-membered Cu<sub>2</sub>P<sub>4</sub> and four-membered Cu<sub>2</sub>Cl<sub>2</sub> rings, arranged alternately in an orthogonal fashion.<sup>39</sup> However, using CuBr or CuI rather than CuCl, the 2D coordination compounds [(Cp\*Fe(μ,η<sup>1,1,1,5</sup>-P<sub>5</sub>))CuX]<sub>n</sub> (X = Br, I; Cp\* = η<sup>5</sup>-C<sub>5</sub>Me<sub>5</sub>) are formed under otherwise identical reaction conditions. The polymers feature a 1,2,4-substitution pattern of the P<sub>5</sub> ring which causes the formation of two-dimensional layers in the solid-state structure.<sup>39</sup> Since organophosphorus and organoarsenic compounds generally show comparable behavior, one would assume a similar reactivity of As<sub>n</sub> and P<sub>n</sub> ligand complexes. Electronic structures of **5** and **6**

modelled by DFT calculations using the hybrid B3LYP functional show only minor differences, which seems to support this hypothesis.<sup>40</sup> The energies of the highest occupied molecular orbital (HOMO) and the HOMO-1 in **6** are higher than in **5**. Furthermore, the lowest unoccupied molecular orbital (LUMO) of **6** is doubly degenerate ( $e_2$  symmetry) involving mainly  $\pi$  orbital contribution from the  $As_5$  ligand, and the LUMO+1 ( $e_1$  symmetry) contains metal,  $Cp^*$  and  $As_5$  ligand contributions. In **5** the relative energies of the unoccupied  $e_1$  and  $e_2$  orbitals are reversed. This and the relative energy of the HOMO in **6** compared to **5** suggest a somewhat more electron releasing character of the  $As_5$  moiety in comparison to the  $P_5$  unit in **5**. Consequently, **6** should be a slightly weaker ligand than **5**. Nevertheless, the experimental results contradict this prediction.<sup>40</sup>



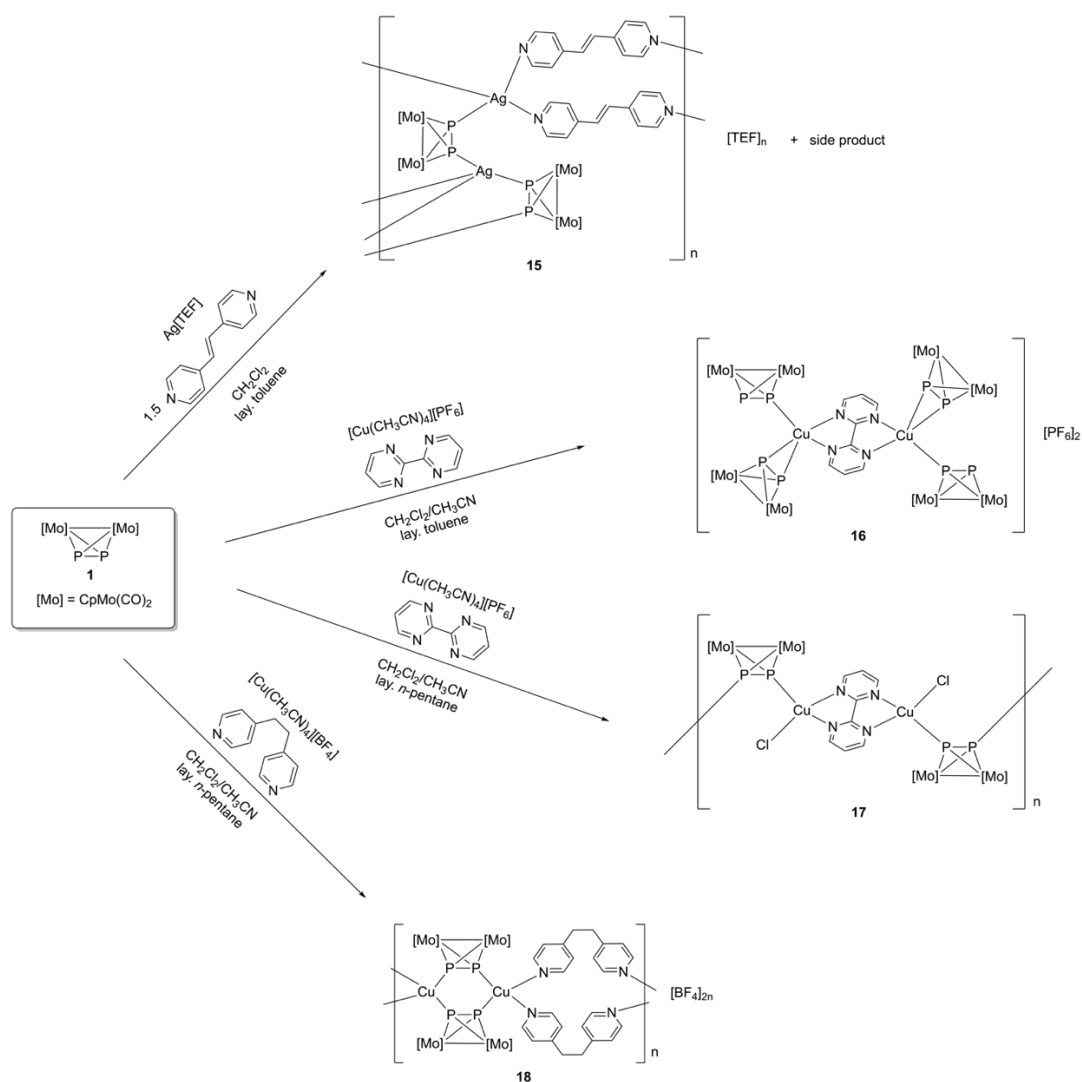
**Scheme 1.1.** Reaction behavior of  $[Cp^*Fe(\eta^5-As_5)]$  (**6**) with  $CuX$  ( $X = Cl, Br, I$ ) yielding the 1D polymers **11-14**.<sup>40</sup>

The reaction of the *cyclo-As<sub>5</sub>* compound **6** with  $CuX$  ( $X = Cl, Br$ ) leads to the isostructural 1D coordination polymers **11** and **12**, respectively (Scheme 1.1). **11** and **12** are chain-like polymers comprised of building blocks in which an  $As_5$  moiety coordinates to the copper atoms of a  $(CuX)_3$  six-membered ring in an  $\eta^2:\eta^2:\eta^2$  coordination mode. The  $(CuX)_3$  ring shows a distorted chair conformation with the  $Cu_3$  plane parallel to that of the  $As_5$  ring. The building blocks are linked *via* an end-on coordination of two copper atoms to arsenic atoms of the neighboring building units. The third copper atom of each building block is coordinated by a  $CH_3CN$  molecule. Surprisingly, two one-dimensional CPs (**13** and **14**) are obtained by reacting **6** with  $CuI$ . The polymeric structure of **13** reveals a  $(CuI)_n$  ladder structure coordinated by molecules of **6** (Scheme 1.1). Four arsenic atoms of the *cyclo-As<sub>5</sub>* unit coordinate side-on in an  $\eta^2:\eta^2$  fashion towards two copper atoms.



Compound **14** combines structural motifs of **11**, **12** and **13** with new ones. The linked building blocks of **14** consist of two **6** units in which one *cyclo*-As<sub>5</sub> adopts an  $\eta^2:\eta^2$  coordination mode towards two copper atoms. These two copper atoms form a six-membered (CuI)<sub>3</sub> ring with a third Cu atom that is  $\eta^2$  coordinated by two arsenic atoms of the second As<sub>5</sub> unit in the building unit. Furthermore, this second molecule **6** coordinates in a  $\eta^5$  fashion to another Cu atom of a dumbbell shaped CuI located nearly perpendicular above the As<sub>5</sub> plane. This structural motif is reminiscent of a triple-decker sandwich complex. These units are linked by end-on coordination of a copper atom towards an arsenic atom of a neighboring unit and *vice versa*. This structural variety demonstrates the extended  $\pi$  coordination behavior of **6** compared to a more  $\sigma$  donating character of **5**.<sup>40</sup>

Going beyond the domain of CPs comprised of organometallic building blocks and metal salts, organometallic-organic hybrid materials can be built up by reacting E<sub>n</sub> ligand complexes, metal salts and organic N-donor linkers. This field is increasingly attracting interest due to the great potential of hybrid materials, including metal-organic frameworks (MOF), e.g. in catalysis or for gas storage and separation. Reactions of **1**, different coinage metal salts and ditopic pyridyl-based linkers leading to the CPs **15-18** are depicted in Scheme 1.2. The 3D coordination polymer  $[\{\text{Cp}_2\text{Mo}_2(\text{CO})_4(\mu_4, \eta^{1,1,2,2}\text{-P}_2)\}(\mu, \eta^{1,1}\text{-C}_{12}\text{H}_{10}\text{N}_2)\text{Ag}]_n[\text{Al}\{\text{OC}(\text{CF}_3)_3\}_4]_n$  (**15**), comprised of distorted octahedral building blocks, crystallizes upon layering with toluene (Scheme 2).<sup>41</sup> Interestingly, layering the reaction mixture of **1**, [Cu(CH<sub>3</sub>CN)<sub>4</sub>][PF<sub>6</sub>] and 2,2'-bipyrimidine with toluene results in the formation of the discrete compound **16** in which the copper atoms are side-on coordinated by two nitrogen atoms of the linker and one P<sub>2</sub> unit, and end-on coordinated by a phosphorus atom of another **1** moiety (Scheme 1.2).<sup>42</sup>



**Scheme 1.2.** Coordination compounds **15-18** containing the tetrahedral  $P_2$  complex **1**, organic pyridyl based linkers and coinage metal salts.

Unexpectedly, when the reaction is conducted with the same reactants and reaction conditions except *n*-pentane is used as layering solvent instead of toluene, the neutral 1D CP **17** is obtained.<sup>42</sup>

The repeating unit of **17** consists of one 2,2'-bipyrimidine molecule, two  $P_2$  ligand complexes **1**, two chloride atoms bound to two copper atoms. A copper atom is side-on coordinated by two nitrogen atoms of the linker,  $\eta^1$  coordinated by one P atom and one chloride ion resulting in a tetrahedral coordination sphere. Switching to the flexible ditopic linker 1,2-bis(4-pyridyl)ethane leads to the expected coordination polymer **18**.<sup>36</sup> In **18** the  $Cu_2P_4$  six-membered ring is still intact and two linker molecules coordinate each copper atom to form a one-dimensional hybrid compound.

These examples only give a brief insight into the enormous variety of accessible hybrid materials and show that the structure of the organometallic-organic hybrid materials can

be easily tuned by changing either the metal center, the anion, the organic linker or the layering solvent.

### 1.1.2 Discrete Nano-sized Aggregates

Discrete nano-sized aggregates, particularly spheres with distinct inner cavities, display great potential for a broad range of applications, such as storage of small molecules, for molecular recognition, in catalysis or as molecular containers. Therefore, the field of large spherical molecules and clusters has attracted unprecedented attention within the last years. With regard to molecular recognition, smaller supramolecules such as crown ethers,<sup>9</sup> cryptands<sup>9</sup> and calixarenes gained popularity.<sup>12</sup> (Figure 1.3).

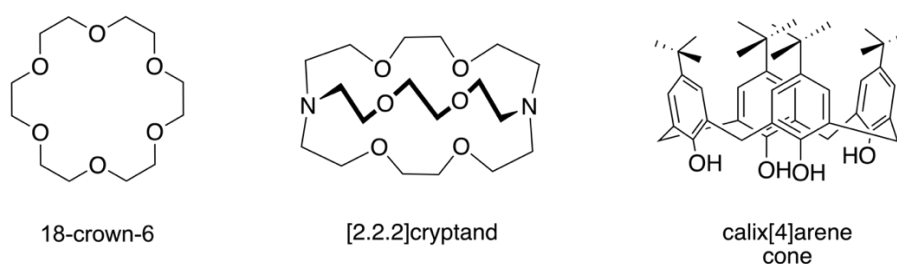


**Figure 1.3.** Representatives for crown ethers, cryptands and calixarenes, respectively.

These classes of supramolecules are able to bind selectively cations in their cavities or the interior of the ring.

Polyoxometallates (POMs) are another prominent example for nano-sized supramolecules.<sup>43</sup> POMs are defined by  $\text{MO}_6$  octahedra ( $\text{M} = \text{Mo}, \text{W}, \text{V}, \text{Mn}, \dots$ ) connected *via* their faces, edges or vertices to form *inter alia* larger polyanions with the basic structural motif of the Keggin ion  $[(\text{XO}_4)(\text{M}_{12}\text{O}_{36})]^{n-}$  ( $\text{X} = \text{P}^{5+}, \text{Si}^{4+}, \text{B}^{3+}, \dots$ ;  $\text{M} = \text{Mo}^{6+}, \text{W}^{6+}, \text{V}^{6+}, \dots$ ).<sup>44,45</sup>

Furthermore, *Schnöckel et al.* defined compounds which contain more metal-metal bonds than metal-ligand bonds as metalloids clusters.<sup>46–48</sup> They succeeded in the synthesis of the metalloid  $\text{Au}_{102}(\text{SR})_{44}$  ( $\text{SR} = p$ -mercaptobenzoic acid) which emphasizes ‘the outstanding position of metalloids clusters as intermediates between the bulk metal and the bulk salts on the one hand and of naked metal atom clusters and salt-like clusters on the other hand’.<sup>46</sup>

The discovery of the third allotropic modification of carbon, the fullerenes,<sup>49</sup> was awarded with the Nobel Prize to Robert F. Curl,<sup>50</sup> Harold W. Kroto<sup>51</sup> and Richard E. Smalley<sup>52</sup> in 1996. Fullerenes consist of twelve five- and any even number of six-

membered rings with the pentagons not bordering each other.<sup>53,54</sup> The smallest and most prominent fullerene is the highly symmetric Buckminster fullerene  $I_h$ -C<sub>60</sub><sup>49</sup> which is associated with the geodesic domes designed by the architect R. Buckminster Fuller.<sup>55–57</sup> It contains twelve five-membered and twenty six-membered carbon rings. Most of the reported fullerenes are restricted to the most stable derivatives such as C<sub>60</sub> and C<sub>70</sub>. Our group was able to show that [Cp\*Fe( $\eta^5$ -P<sub>5</sub>)] (**5a**) and [Cp<sup>R</sup>Ta(CO)<sub>2</sub>( $\eta^4$ -P<sub>4</sub>)] (**4**) (Cp<sup>R</sup> = Cp<sup>''</sup> (**4a**), Cp<sup>'''</sup> (**4b**)) self-assemble with Cu(I) halides to give a supramolecular aggregate with fullerene-like topology. The carbon-free fullerene analogues of the  $I_h$ -C<sub>80</sub> frameworks embody less stable representatives.<sup>58,59</sup> It became evident that larger spherical molecules of this fullerene type are only accessible by using large guest molecules such as **5a**,<sup>60</sup> *o*-carborane,<sup>58</sup> C<sub>60</sub>,<sup>61</sup> ferrocene,<sup>62</sup> cobaltocene<sup>63</sup> or [MCp<sub>2</sub>][PF<sub>6</sub>] (M = Fe, Co)<sup>63</sup> as a template (Figure 1.4a). Using **5** with the sterically more demanding Cp<sup>Bn</sup> substituent (**5b**, Cp<sup>Bn</sup> =  $\eta^5$ -C<sub>5</sub>(CH<sub>2</sub>Ph)<sub>5</sub>) leads to the formation of the nano-sized supramolecule (CH<sub>2</sub>Cl<sub>2</sub>)<sub>3.4</sub>@[(Cp<sup>Bn</sup>FeP<sub>5</sub>)<sub>12</sub>(CuI)<sub>54</sub>(CH<sub>3</sub>CN)<sub>1.46</sub>] (Figure 1.4b).<sup>64</sup> The size of the supramolecular aggregates can even be increased to a 140-vertex<sup>65</sup> core and a 168-vertex core<sup>66</sup> using Cp<sup>BIG</sup> and Cp<sup>Bn</sup> substituents (Cp<sup>BIG</sup> =  $\eta^5$ -C<sub>5</sub>(4-*n*BuC<sub>6</sub>H<sub>4</sub>)<sub>5</sub>), respectively. Furthermore, the *cyclo*-P<sub>4</sub> complexes **4a** and **4b** form highly symmetric non-classical fullerene-like 32-vertex cores of solely four- and six-membered rings upon reaction with CuX (X = Cl, Br) (Figure 1.4c-d).<sup>67</sup>

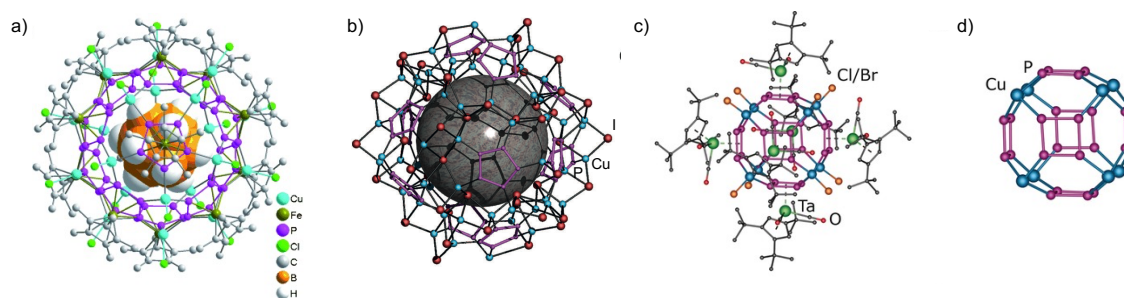


**Figure 1.4.** a) Molecular structure of C<sub>2</sub>B<sub>10</sub>H<sub>12</sub>@[(**5a**)<sub>12</sub>(CuCl)<sub>20</sub>],<sup>58</sup> b) idealized scaffold of [(**5b**)<sub>12</sub>(CuI)<sub>54</sub>],<sup>64</sup> c) molecular structure of [(**4a**)<sub>6</sub>(CuBr)<sub>8</sub>],<sup>67</sup> d) scaffold of 32-vertex core.<sup>67</sup>

## 1.2 The Myth of the Non-Coordinating Anion

Over 50 years ago the dogmatic term ‘non-coordinating anions’ was introduced for more complex anions such as  $[\text{BF}_4]^-$ ,  $[\text{CF}_3\text{SO}_3]^-$ ,  $[\text{ClO}_4]^-$  or  $[\text{MF}_6]^-$  ( $M = \text{P, As, Sb}$ ) compared to covalently binding halides. However, it has been shown that these anions can indeed easily be coordinated.<sup>68</sup> Also, ‘non-coordinating’ implies the lack of cation-anion interactions, which is physically impossible, since opposite charges attract each other, resulting in the Coulomb force  $F$  (equation 1.1).<sup>69</sup>

$$F = \frac{1}{4\pi\epsilon} \frac{q_1 q_2}{r^2} = \frac{1}{4\pi\epsilon} \frac{z_1 z_2 e^2}{r^2} \quad (\text{equation 1.1})$$

$q_1, q_2$  = point charges,  $z_1, z_2$  = ionic charges,  $e$  = elemental charge,  $r$  = distance between charges,  $\epsilon_0$  = dielectric constant.

The force decreases with an increasing distance between the charges ( $r$ ) and is dependent on the ionic charges ( $z_1$  and  $z_2$ ). In other words, to minimize the Coulomb force a small negative charge should be delocalized over a large surface area. Consequently, the more precise expression ‘Weakly Coordinating Anion’ (WCA) is commonly used in literature today. In order to achieve a nearly non-coordinating WCA many efforts in fundamental<sup>70,71</sup> as well as in applied<sup>72</sup> chemistry were undertaken. A large number of approaches to obtain the best approximation of non-coordinating anions have been tried, resulting in many ‘superweak anions’.<sup>73–76</sup> These groups of WCAs include carborane-based anions,<sup>70,77</sup> teflate-based anions,<sup>78–80</sup> anions formed by reaction with Lewis acids,<sup>81,82</sup> borate-based anions and aluminates. The last two examples will be described in more detail.

The first group of anions to be introduced are borates. The well-known  $[\text{BPh}_4]^-$  anion is obtained by the substitution the fluorine atoms in  $[\text{BF}_4]^-$  with phenyl groups. Since this anion is susceptible to hydrolysis, the phenyl groups can be fluorinated or exchanged with  $-\text{C}_6\text{F}_5$  or  $-\text{C}_6\text{H}_3-3,5-(\text{CF}_3)_2$  groups in order to avoid this drawback. Several salts of  $[\text{B}(\text{C}_6\text{F}_5)_4]^-$ <sup>83</sup> and  $[\text{B}(\text{Ar}^{\text{F}})_4]^-$  ( $\text{Ar}^{\text{F}} = -\text{C}_6\text{H}_3-3,5-(\text{CF}_3)_2$ ),<sup>84,85</sup> respectively, are commercially available and broadly used for example in homogenous catalysis.<sup>72</sup> The EMIM<sup>+</sup> (1-ethyl-3-methyl imidazolium) salt with the weakly coordinating anion  $[\text{B}\{(\text{C}_6\text{H}_3(\text{CF}_3)_2)_4\}]^-$ , used as an ionic liquid, can enhance the conversions in hydrovinylation reactions.<sup>86</sup> In order to further reduce the coordinating strength of the anion, the  $-\text{CF}_3$  substituent can be replaced by larger perfluoroalkyl groups leading to the modified  $[\text{B}(\text{Ar}^{\text{F}})_4]^-$  ( $\text{Ar}^{\text{F}} = -\text{C}_6\text{H}_3-3,5-(\text{R}^{\text{F}})_2$ ;  $\text{R}^{\text{F}} = n\text{-C}_6\text{F}_{13}$ ,<sup>87</sup>  $n\text{-C}_4\text{F}_9$ ,<sup>88</sup>  $2\text{-C}_3\text{F}_7$ <sup>88</sup>). It was shown that such  $[\text{B}(\text{Ar}^{\text{F}})_4]^-$  anions can

lead to very high conductivities when used in lithium-ion batteries.<sup>89</sup> Our group investigates the potential of the closely related chlorinated borate anion  $[\text{B}(3,5\text{-C}_6\text{H}_3\text{Cl}_2)_4]^-$  ( $= [\text{BAR}^{\text{Cl}}_4]^-$ , **19**, Figure 1.5). The corresponding Ag(I) salt  $\text{Ag}[\text{BAR}^{\text{Cl}}_4]$  was first reported by *Braunschweig et al.* in 2014,<sup>90</sup> followed by the synthesis of  $[\text{Cu}(\text{CH}_3\text{CN})_3][\text{BAR}^{\text{Cl}}_4]$  by *Scheer et al.*<sup>91</sup>

Another prominent type of WCAs are weakly coordinating aluminate anions, such as  $[\text{Al}\{\text{OC}(\text{CF}_3)_3\}_4]^-$  ( $= [\text{TEF}]^-$ , **20**, Figure 1.5) and  $[\text{FAI}\{\text{OC}_6\text{F}_{10}(\text{C}_6\text{F}_5)\}_3]^-$  ( $= [\text{FAI}]^-$ , **21**, Figure 1.5). This class of anions was introduced by *Strauss et al.* in 1996<sup>92–94</sup> and complemented by *Krossing et al.*<sup>95,96</sup> and our group.<sup>38</sup>

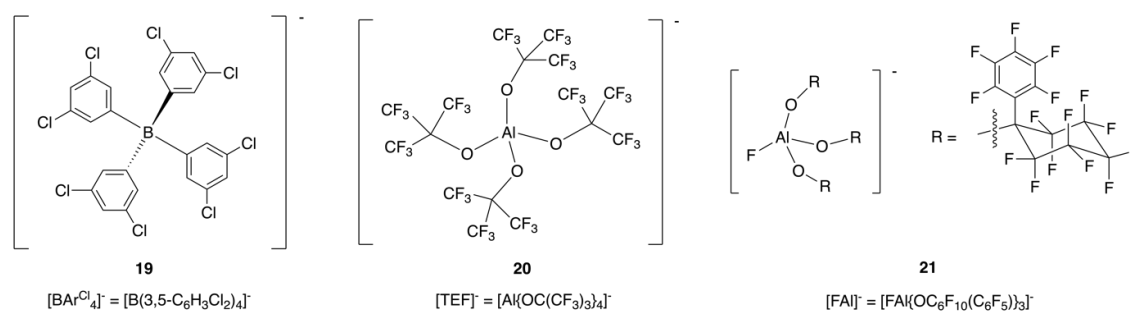
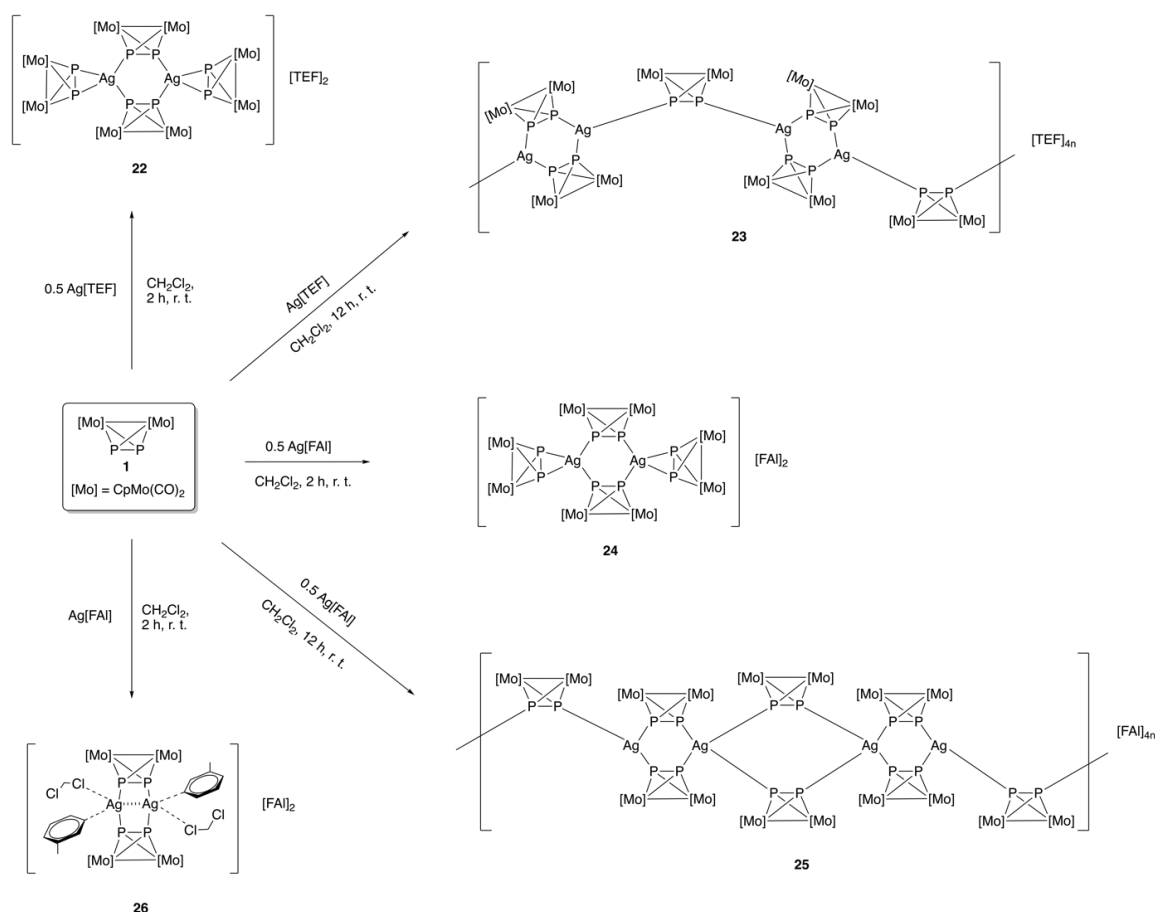


**Figure 1.5.** Representation of the WCAs  $[\text{BAR}^{\text{Cl}}_4]^-$  (**19**),  $[\text{TEF}]^-$  (**20**) and  $[\text{FAI}]^-$  (**21**).

These perfluorinated alkoxy metalates with the oxophilic and highly Lewis acidic Al(III) centers offer the advantage of being easily accessible on a large scale compared to some borates anions.<sup>76</sup> The reaction of  $\text{Li}[\text{AlH}_4]$  with four equivalents of the appropriate fluorinated alcohol  $\text{R}^{\text{F}}\text{OH}$  ( $\text{R}^{\text{F}} = \text{C}(\text{CF}_3)_3$ ,  $\text{C}_6\text{F}_{10}(\text{C}_6\text{F}_5)$ ) leads to the corresponding Li(I) salts.<sup>93,97,98</sup> The facile conversion of the lithium  $[\text{TEF}]$  salt yields the monovalent M(I)  $[\text{TEF}]$  ( $\text{M}(\text{I}) = \text{Ag}^+$ ,<sup>95</sup>  $\text{Cu}^+$ ,<sup>38,99–101</sup>  $\text{In}^+$ ,<sup>102</sup>  $\text{Tl}^+$ <sup>103</sup>) salts. The  $[\text{TEF}]^-$  anion shows a low coordinative strength,<sup>75</sup> a high stability in nitric acid<sup>95</sup> and its Brønsted acid  $[\text{H}(\text{OEt})_2]^+[\text{TEF}]^-$  can be produced in high yields.<sup>104</sup> This stability towards hydrolysis is a result of the steric shielding of the oxygen atoms and the electronic stabilization caused by the perfluorination. In addition, the chemical robustness of **20** is also shown in the synthesis of its salts with the highly electrophilic cations  $[\text{PX}_4]^+$ ,<sup>105</sup>  $[\text{P}_2\text{X}_5]^+$ ,<sup>105</sup>  $[\text{P}_5\text{X}_2]^+$  ( $\text{X} = \text{Br}, \text{I}$ )<sup>105,106</sup> and  $[\text{Cl}_3]^+$ .<sup>107</sup> This class of WCAs has also proven to act as very good counterions in ionic liquids for polymerization catalysis, as conducting salts for cyclic voltammetry or in electric cells and many more.<sup>108</sup> Furthermore, *Krossing et al.* reported the Ag(I) complexes  $[\text{Ag}(\eta^4\text{-S}_8)_2][\text{TEF}]$ , with two  $\text{S}_8$  crowns coordinating to the Ag(I) atoms,<sup>109</sup> and  $[\text{Ag}(\eta^2\text{-P}_4)_2][\text{TEF}]$ , with two  $\eta^2$ -coordinated  $\text{P}_4$  tetrahedra.<sup>110</sup> Remarkably, the  $\text{P}_4$  tetrahedra remain intact and are easily displaced from the silver center, which is why this compound is one of the first known  $\text{P}_4$  transfer reagents. In 2013, *Scheer et al.*

synthesized the isostructural arsenic analogue  $[\text{Ag}(\eta^2\text{-As}_4)]\text{[TEF]}^{111}$ . For the  $[\text{FAI}]^-$  anion, only  $\text{Li(I)}$ ,<sup>98</sup> the  $\text{Ag(I)}$ <sup>98</sup> and  $\text{Cu(I)}$ <sup>38</sup> salts have been reported so far. The  $[\text{FAI}]^-$  anion facilitates the isolation of unstable cations in condensed phase. **21** can stabilize the dication  $[\text{Ag}_2\text{Se}_{14}]^{2+}$  by the coordination of the fluorine atom of the WCA to the silver atoms ( $d(\text{Ag}\cdots\text{F}) = 2.4198(2)$ ).<sup>98</sup>

The weakly coordinating aluminate anions are also used in supramolecular chemistry. The reaction of the polypnictogen complexes  $[\text{Cp}^*\text{Fe}(\eta^5\text{-E}_5)]$  ( $\text{Cp}^* = \eta^5\text{-C}_5\text{Me}_5$ ;  $\text{E} = \text{P}$  (**5a**),  $\text{As}$  (**6a**)) with the monovalent  $\text{M[TEF]}$  salts ( $\text{M} = \text{Tl(I)}$ ,  $\text{In(I)}$  and  $\text{Ga(I)}$ ) yields one-dimensional coordination polymers  $[\text{M}(\mu, \eta^5:\eta^1\text{-E}_5\text{FeCp}^*)_3]\text{[TEF]}_n$ .<sup>112</sup> The dimers **22**, **24** and **26** and the 1D polymers **23** and **25** were obtained by reacting the tetrahedral diphosphorus complex  $[\text{Cp}_2\text{Mo}_2(\text{CO})_4(\eta^2\text{-P}_2)]$  (**1a**;  $\text{Cp} = \text{C}_5\text{H}_5$ ) with  $\text{Ag[TEF]}$  and  $\text{Ag[FAI]}$ , respectively (Scheme 1.3).<sup>113</sup>



**Scheme 1.3.** Reaction of  $[\text{Cp}_2\text{Mo}_2(\text{CO})_4(\eta^2\text{-P}_2)]$  with  $\text{Ag[TEF]}$  and  $\text{Ag[FAI]}$ , respectively, yielding dimers **22**, **24**, **26** and the 1D coordination polymers **23** and **25**.

The special properties of WCAs enable a broad range of applications, for example in the area of ionic liquids,<sup>86</sup> lithium batteries<sup>114,115</sup> and photoacid generators (PAGs).<sup>116–118</sup>

Hygroscopic diaryl iodonium salts containing  $[\text{SbF}_6]^-$  are used as photoacid generators for cationic polymerization of many different substrates. The counterions of these toxic salts can be exchanged for a series of WCAs, including  $[(\text{F}_5\text{C}_6)_3\text{B}(\mu\text{-X})\text{B}(\text{C}_6\text{F}_5)_3]^{n-}$  ( $\text{X} = \text{C}_3\text{N}_2\text{H}_3$ ,  $n = 1$ ;  $\text{X} = \text{C}_6\text{F}_4$ ,  $n = 2$ ) making them more stable and less toxic.<sup>118</sup> PAGs are used in many applications, such as printing inks, optical fibers, holography, and photolithography.<sup>76</sup>

These examples demonstrate how the unique properties of WCAs allow the synthesis and isolation of unprecedented compounds and lead to improvements in a number of technical applications. Therefore, WCA salts of coinage metals hold great promise for the generation of new coordination polymers and hybrid materials.

### 1.3 The Potential of Luminescent Cu(I) Complexes

Intense research efforts are currently focused on the development of novel phosphorescent transition metal complexes as building blocks for a number of applications, such as components in organic light emitting diodes (OLEDs).<sup>119–122</sup> The recognition of the potential of third row transition metal complexes for this type of application was a breakthrough. The advantage of these metal complexes is that they can display strong spin-orbit coupling (SOC) which can result in high phosphorescence emission quantum yields and fast emission decays from the lowest triplet state ( $T_1$ ) and thus, efficient harvesting of electrically generated excitons.<sup>123–127</sup> This was successfully applied in the conception of red and green OLEDs, but the development of blue and white light emitting phosphorescent materials is still challenging. Furthermore, unclear toxicity, and high costs of third row transition metal complexes may be disadvantageous. Therefore, other abundant emitter materials are highly sought after, such as first row transition metals. Unfortunately, the triplet emission (phosphorescence) decay times of these compounds are usually too long due to relatively ineffective SOC. As a consequence, transitions between the excited triplet states ( $T_x$ ) and the singlet ground state ( $S_0$ ) are highly forbidden. The application of these metal compounds in OLEDs could therefore result in undesired saturation effects. However, selected Cu(I) complexes with reducible ligands, *i.e.* with energetically low-lying  $\pi^*$  orbitals, can overcome these severe restraints and thus have gained rising attractiveness, due to the extensive metal-to-ligand charge transfer (MLCT) character of their lowest excited states.<sup>123,128–132</sup> The associated transitions induce distinct spatial separations of the involved orbitals, especially of the HOMO and the LUMO, leading to comparatively small exchange integrals and, consequently, to a small energy gap  $\Delta E$  ( $S_1 - T_1$ ) between the



lowest triplet state  $T_1$  and the lowest excited singlet state  $S_1$  (e.g.  $<1000\text{ cm}^{-1}$  or  $0.12\text{ eV}$ ).<sup>133</sup> Following thermal induction, the excitons can undergo a reversed intersystem crossing (RISC) from  $T_1$  to  $S_1$ . Consequently, these materials can show a very efficient Thermally Activated Delayed Fluorescence (TADF, Figure 1.6).<sup>133–142</sup>

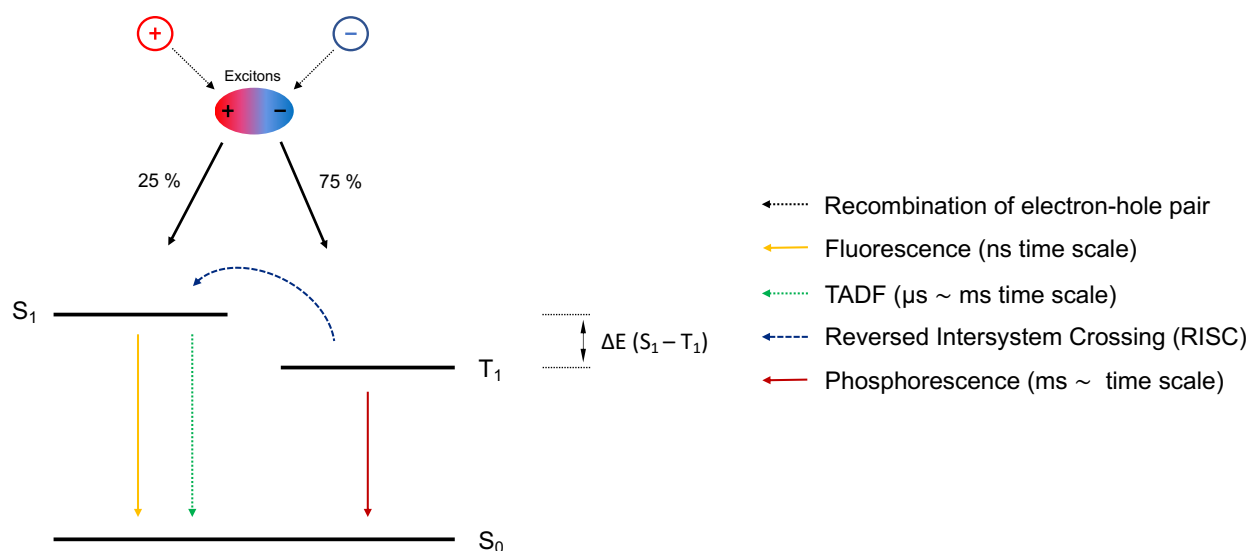


**Figure 1.6.** Thermally Activated Delayed Fluorescence (TADF), reversed intersystem crossing, fluorescence and phosphorescence processes in Cu(I) complexes.

This mechanism allows consuming all introduced excitons for light generation by making use of the singlet harvest effect.<sup>129,131,143,144</sup> Different structural motifs in Cu(I) complexes have been in the focus of research. In particular, wide-ranging photophysical studies were performed for copper(I) complexes that exhibit a pseudo-tetrahedral coordination of the Cu center by two bidentate chelating ligands, such as  $[\text{Cu}(\text{N}^{\wedge}\text{N})_2]^+$  ( $\text{N}^{\wedge}\text{N}$  indicates a bisimine ligand),<sup>131,145–148</sup> heteroleptic  $[\text{Cu}(\text{N}^{\wedge}\text{N})(\text{P}^{\wedge}\text{P})]^+$  complexes,<sup>149–151</sup> amidophosphane derivatives ( $[\text{Cu}(\text{P}^{\wedge}\text{N})(\text{P}^{\wedge}\text{P})]^+$ )<sup>152,153</sup> as well as  $[\text{Cu}(\text{P}^{\wedge}\text{P})_2]^+$  (bisphosphane derivatives) complexes<sup>129,138,154–158</sup> (Figure 1.7).

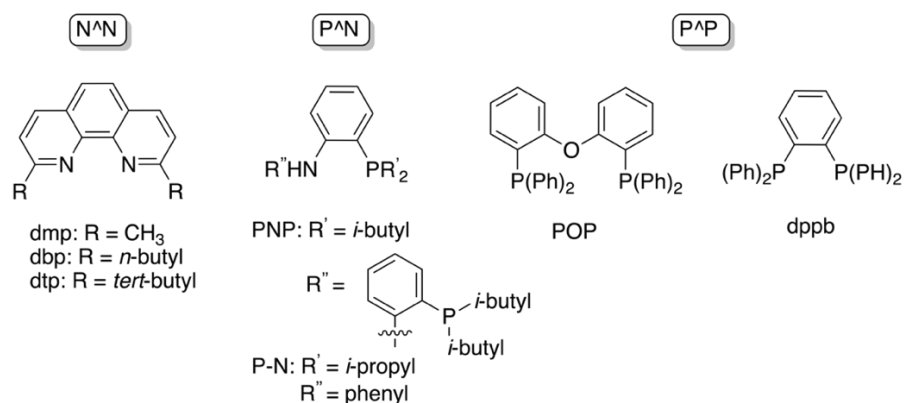
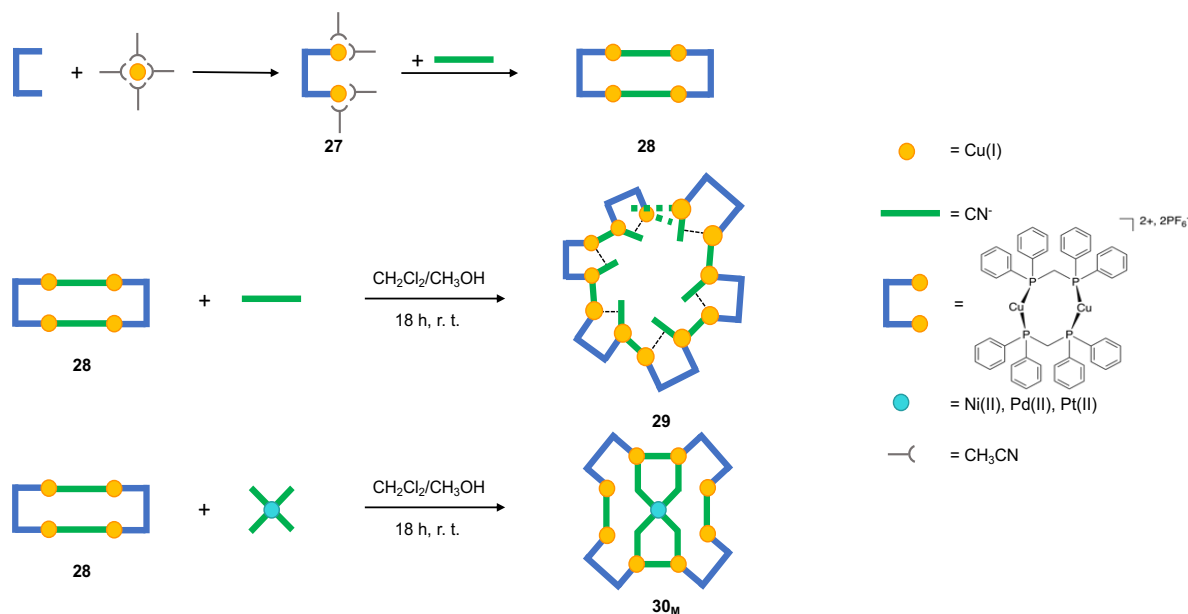


**Figure 1.7.** Examples of ligands used to form luminescent Cu(I) complexes with the general formulas [Cu(N<sup>N</sup>)<sub>2</sub>]<sup>+</sup>, [Cu(N<sup>N</sup>)(P<sup>P</sup>)]<sup>+</sup>, [Cu(P<sup>N</sup>)(P<sup>P</sup>)]<sup>+</sup> or [Cu(P<sup>P</sup>)<sub>2</sub>]<sup>+</sup>. dmp = 2,9-dimethyl-1,10-phenanthroline; dbp = 2,9-di-*n*-butyl-1,10-phenanthroline; dtp = 2,9-di-*tert*-butyl-1,10-phenanthroline; PNP = bis[2-(diisobutylphosphino)phenyl]amide); P-N = [2-(diisopropylphosphino)diphenyl]amide; POP = bis[2-(diphenylphosphino)phenyl]ether; dppb = 1,2-bis-(diphenylphosphino)benzene. For P<sup>N</sup> ligands, “N” refers to an amide, not to an imine ligand, as for N<sup>N</sup>.

[Cu(N<sup>N</sup>)(P<sup>P</sup>)]<sup>+</sup> complexes, where P<sup>P</sup> denotes a bisphosphane ligand, exhibit highly enhanced emission properties compared to complexes containing N<sup>N</sup> ligands.<sup>159</sup> Only a few examples of light emitting coordination-driven supramolecular assemblies are reported as yet. For example, the reaction of the P<sup>P</sup> ligand dppm (dppm = 1,1-bis(diphenylphosphino)methane) with Cu(I) salts yields luminescent dinuclear Cu(I) complexes such as **27** with a clip-like structure (Scheme 1.4).<sup>160,161</sup> Reacting this clip with different substrates leads to a variety of room temperature solid-state luminescent polymetallic assemblies **28-30<sub>M</sub>** (Scheme 1.4).<sup>93,97</sup> Compound **28** ([Cu<sub>4</sub>(μ<sub>2</sub>-dppm)<sub>4</sub>(CN)<sub>2</sub>][PF<sub>6</sub>]<sub>2</sub>) exhibits blue luminescence in the solid state at room temperature (λ<sub>em</sub> = 457 nm; excitation at 320 nm) with an emission quantum yield of 72% and interestingly, displays a reversible red-shift of its emission maximum upon cooling.<sup>158</sup> The neutral 1D helicoidal coordination polymer **29** is based on repeating units of [Cu<sub>2</sub>(μ<sub>2</sub>-dppm)<sub>2</sub>]<sup>2+</sup> fragments and two sorts of cyano ligands coordinated to the Cu(I) center. One CN<sup>-</sup> ligand acts as a μ<sub>2</sub>-ditopic linker between two metal centers of neighboring Cu<sub>2</sub>(μ<sub>2</sub>-dppm)<sub>2</sub> moieties while the second cyano ligand bridges the two metal centers within each Cu<sub>2</sub>(μ<sub>2</sub>-dppm)<sub>2</sub> moiety in a rare end-on/side-on coordination mode. Compound **29** demonstrates a broad emission maximum at 538 nm upon excitation at 320 nm with an emission quantum yield (EQY) of 20% at room temperature. However, cooling to 77 K results in a blue-shift to an emission maximum at 468 nm.<sup>162</sup> The isostructural derivatives **30<sub>M</sub>** (M = Ni(II), Pd(II), Pt(II)) are discrete polymetallic compounds. The asymmetric unit contains one dicationic [Cu<sub>8</sub>M(CN)<sub>8</sub>(dppm)<sub>8</sub>]<sup>2+</sup> entity and two hexafluorophosphate anions. The central M cation is square planar coordinated by four cyano ligands, which

connect the center atom with four  $[\text{Cu}_2\text{dppm}(\text{CN})]$  units. The luminescence properties in the solid state at room temperature are dependent on the metal atom **M**. Compounds **30<sub>Ni</sub>** shows a very weak turquoise luminescence, **30<sub>Pd</sub>** displays a moderate luminescence ( $\lambda_{\text{em}} = 500 \text{ nm}$ ; EQY = 2%) upon excitation at 350 nm and **30<sub>Pt</sub>** exhibits an intense luminescence with an emission maximum at 510 nm (EQY = 18%).<sup>162</sup> These data reveal a crucial impact of the spin-orbit coupling offered by the central metal center **M** on the emission properties of the heterobimetallic compounds **30<sub>M</sub>**.



**Scheme 1.4.** Synthesis of the tetrametallic dicationic assembly **28**. Synthesis of the derivatives **29** and **30<sub>M</sub>**. Simplified top view along the *c* axis of **29** showing six repetition units  $[\text{Cu}_2(\mu_2\text{-dppm})_2(\text{CN})_2]$ . Simplified top view of **30<sub>M</sub>**.

The previous section shows that only minor changes of the ligand can have an essential influence on the photophysical properties of Cu(I) complexes. This versatility and the need for new luminescent materials for OLEDs drive many scientists to develop more innovative compounds.

## 1.4 References

- [1] J. M. Lehn, *Angew. Chem.* **1988**, *100*, 91-116.
- [2] E. Fischer, *Berichte d. Dt. Chem. Gesellschaft zu Berlin* **1894**, *27*, 2985-2993.
- [3] X. Zhou, P. Pathak, J. Jayawickramarajah, *Chem. Commun.* **2018**, *54*, 11668-11680.
- [4] D. J. Cram, *Angew. Chem.* **1988**, *100*, 1041-1052.
- [5] C. J. Pedersen, *Angew. Chem.* **1988**, *100*, 1053-1059.
- [6] F. Wöhler, *Annalen der Physik und Chemie* **1828**, *88*, 253-256.
- [7] Y. A. Ovchinnikov, V. T. Ivanov, A. M. Scrob, *Membrane Active Complexones*, Elsevier, New York, **1974**.
- [8] J. M. Lehn, *Pure Appl. Chem.* **1978**, *50*, 871-892.
- [9] G. W. Gokel, *Crown Ethers and Cryptands*, **1991**.
- [10] J. M. Lehn, *Science* **1993**, *260*, 1762-1763.
- [11] F. Diederich, *Cyclophanes*, Royal Society of Chemistry, **1991**.
- [12] D. C. Gutsche, *Calixarenes*, Royal Society of Chemistry, **1989**.
- [13] A. Collet, *Tetrahedron* **1987**, *43*, 5725-5759.
- [14] E. C. Constable, A. M. W. C. Thompson, *Supramol. Chem.* **1994**, *4*, 95-99.
- [15] E. C. Constable, *Pure Appl. Chem.* **1996**, *68*, 253-260.
- [16] R. Feynman, *Eng. Sci.* **1960**, *23*, 22-36.
- [17] O. J. Scherer, *Chem. Unserer Zeit* **2000**, *34*, 374-381.
- [18] O. J. Scherer, *Acc. Chem. Res.* **1999**, *32*, 751-762.
- [19] O. J. Scherer, *Angew. Chem.* **1990**, *102*, 1137-1155.
- [20] B. M. Cossairt, N. A. Piro, C. C. Cummins, *Chem. Rev.* **2010**, *110*, 4164-4177.
- [21] A. P. Ginsberg, W. E. Lindsell, *J. Am. Chem. Soc.* **1971**, *93*, 2082-2084.
- [22] G. L. Simon, L. F. Dahl, *J. Am. Chem. Soc.* **1973**, *95*, 2175-2183.
- [23] A. Vizi-Orosz, G. Pályi, L. Markó, *J. Organomet. Chem.* **1973**, *60*, C25-C26.
- [24] M. Fleischmann, C. Heindl, M. Seidl, G. Balázs, A.V. Virovets, E. V. Peresytkina, M. Tsunoda, F. P. Gabbai, M. Scheer, *Angew. Chemie - Int. Ed.* **2012**, *51*, 9918-9921.
- [25] O. J. Scherer, J. Schwalb, H. Sitzmann, *Inorg. Synth.* **1990**, *27*, 224-227.
- [26] O. J. Scherer, H. Sitzmann, *Angew. Chem.* **1985**, *47*, 5-6.
- [27] O. J. Scherer, H. Sitzmann, G. Wolmershäuser, *J. Organomet. Chem.* **1984**, *268*, C9-C12.
- [28] O. J. Scherer, T. Brück, *Angew. Chem.* **1987**, *99*, 59.
- [29] O. J. Scherer, R. Winter, G. Wolmershäuser, *Z. anorg. allg. Chem.* **1993**, *619*, 827-835.

- [30] P. J. Sullivan, A. L. Rheingold, *Organometallics* **1982**, *1*, 1547-1549.
- [31] O. J. Scherer, C. Blath, G. Wolmershäuser, *J. Organomet. Chem.* **1990**, *387*, 21-24.
- [32] O. J. Scherer, H. Sitzmann, G. Wolmershäuser, *Angew. Chem.* **1984**, *96*, 979-980.
- [33] J. Bai, E. Leiner, M. Scheer, *Angew. Chem. Int. Ed.* **2002**, *41*, 783-786.
- [34] M. Scheer, L. Gregoriades, J. Bai, M. Sierka, G. Brunklaus, H. Eckert, *Chem. Eur. J.* **2005**, *11*, 2163-2169.
- [35] M. Scheer, L. Gregoriades, M. Zabel, J. Bai, I. Krossing, G. Brunklaus, H. Eckert, *Chem. Eur. J.* **2008**, *14*, 282-295.
- [36] M. Elsayed Moussa, B. Attenberger, E. V. Peresykina, M. Fleischmann, G. Balázs, M. Scheer, *Chem. Commun.* **2016**, *52*, 10004–10007.
- [37] M. Fleischmann, S. Welsch, E. V. Peresykina, A. V. Virovets, M. Scheer, *Chem. Eur. J.* **2015**, *21*, 14332–14336.
- [38] M. Elsayed Moussa, M. Piesch, M. Fleischmann, A. Schreiner, M. Seidl, M. Scheer, *Dalton Trans.* **2018**, *47*, 16031–16035.
- [39] J. Bai, A. V. Virovets, M. Scheer, *Angew. Chem. Int. Ed.* **2002**, *41*, 1737–1740.
- [40] H. Krauss, G. Balázs, M. Bodensteiner, M. Scheer, *Chem. Sci.* **2010**, *1*, 337–342.
- [41] B. Attenberger, E. V. Peresykina, M. Scheer, *Inorg. Chem.* **2015**, *54*, 7021–7029.
- [42] M. Elsayed Moussa, B. Attenberger, M. Seidl, A. Schreiner, M. Scheer, *Eur. J. Inorg. Chem.* **2017**, *47*, 5616–5620.
- [43] J. J. Berzelius, *Poggendorffs Ann. Phys. Chem.* **1826**, *6*, 380.
- [44] J. F. Keggin, *Proc. R. Soc. London Ser. A* **1934**, *144*, 75–100.
- [45] M. T. Pope, A. Müller, *Angew. Chemie* **1991**, *103*, 56–70.
- [46] H. Schnöckel, A. Schnepf, R. L. Whetten, C. Schenk, P. Henke, *Z. Anorg. Allg. Chem.* **2011**, *637*, 15–23.
- [47] J. Vollet, J. R. Hartig, H. Schnöckel, *Angew. Chem. Int. Ed.* **2004**, *43*, 3186–3189.
- [48] H. Schnöckel, A. Schnepf, *Aluminium and Gallium Clusters*; John Wiley & Sons Ltd., **2011**.
- [49] H. W. Kroto, J.R. Heath, S. C. O'Brien, R. F. Curl, R. E. Smalley, *Nature* **1985**, *318*, 162–163.
- [50] R. F. Curl, *Angew. Chem. Int. Ed.* **1997**, *36*, 1567–1576.
- [51] H. W. Kroto, J. R. Heath, *Angew. Chem. Int. Ed.* **1997**, *36*, 1578–1593.
- [52] R. E. Smalley, *Angew. Chem. Int. Ed.* **1997**, *36*, 1594–1601.

- [53] M. S. Dresselhaus, G. Dresselhaus, P. C. Eklund, *Science of Fullerenes and Carbon Nanotubes*; Academic Press, **1996**.
- [54] P. W. Fowler, D. E. Manopoulos, *An Atlas of Fullerenes*; Claredon Press, **1995**.
- [55] R. B. Fuller, *Inventions-The patented works of Buckminster Fuller*; St. Martin's Press: New York, **1983**.
- [56] J. Baldwin, *Bucky Works- Buckminster Fuller's Idea for Today*; Wiley, New York, **1996**.
- [57] R. W. Marx, *The Dymaxion World of Buckminster Fuller*; Reinhold, New York, **1960**.
- [58] M. Scheer, A. Schindler, C. Gröger, A. V. Virovets, E. V. Peresyphkina, *Angew. Chem. Int. Ed.* **2009**, *48*, 5046–5049.
- [59] F. Dielmann, M. Fleischmann, C. Heindl, E. V. Peresyphkina, A. V. Virovets, R. M. Gschwind, M. Scheer, *Chem. Eur. J.* **2015**, *21*, 6208–6214.
- [60] M. Scheer, J. Bai, B. P. Johnson, R. Merkle, A. V. Virovets, C. E. Anson, *Eur. J. Inorg. Chem.* **2005**, *20*, 4023–4026.
- [61] M. Scheer, A. Schindler, R. Merkle, B. P. Johnson, M. Linseis, R. Winter, C. E. Anson, A. V. Virovets, *J. Am. Chem. Soc.* **2007**, *129*, 13386–13387.
- [62] A. Schindler, C. Heindl, G. Balázs, C. Gröger, A. V. Virovets, E. V. Peresyphkina, M. Scheer, *Chem. Eur. J.* **2012**, *18*, 829–835.
- [63] E. Peresyphkina, C. Heindl, A. V. Virovets, H. Brake, E. Mädl, M. Scheer, *Chem. Eur. J.* **2018**, *24*, 2503–2508.
- [64] F. Dielmann, C. Heindl, F. Hastreiter, E.V. Peresyphkina, A. V. Virovets, R. M. Gschwind, M. Scheer, *Angew. Chem. Int. Ed.* **2014**, *53*, 13605–13608.
- [65] S. Heini, E. V. Peresyphkina, J. Sutter, M. Scheer, *Angew. Chem. Int. Ed.* **2015**, *54*, 13431–13435.
- [66] C. Heindl, E. V. Peresyphkina, A. V. Virovets, W. Kremer, M. Scheer, *J. Am. Chem. Soc.* **2015**, *137*, 10938–10941.
- [67] F. Dielmann, E. V. Peresyphkina, B. Krämer, F. Hastreiter, B. P. Johnson, M. Zabel, C. Heindl, M. Scheer, *Angew. Chem. Int. Ed.* **2016**, *55*, 14833–14837.
- [68] W. Beck, K. Sünkel, *Chem. Rev.* **1988**, *88*, 1405–1421.
- [69] N. Trapp, I. Krossing, *Nachrichten aus der Chemie* **2009**, *57*, 632–637.
- [70] C. A. Reed, *Acc. Chem. Res.* **1998**, *31*, 133–139.
- [71] S. H. Strauss, *Chem. Rev.* **1993**, *93*, 927–942.
- [72] E. Y. X. Chen, T. J. Marks, *Chem. Rev.* **2000**, *100*, 1391–1434.
- [73] A. J. Lupinetti, S. H. Strauss, *Chemtracts: Inorg. Chem.* **1998**, *11*, 565–595.
- [74] J. A. Johnson, B. M. Petersen, A. Kormos, E. Echeverría, Y. S. Chen, J. Zhang, *J. Am. Chem. Soc.* **2016**, *138*, 10293–10298.

- [75] I. M. Riddlestone, A. Kraft, J. Schaefer, I. Krossing, *Angew. Chem. Int. Ed.* **2018**, *57*, 13982–14024.
- [76] I. Krossing, I. Raabe, *Angew. Chem. Int. Ed.* **2004**, *43*, 2066–2090.
- [77] T. Jelinek, J. Plešek, S. Hermanek, B. Stibr, *Collect. Czech. Chem. Commun.* **1986**, *51*, 819–829.
- [78] D. M. Van Seggen, P. K. Hurlburt, M. D. Noirot, O. P. Anderson, S. H. Strauss, *Inorg. Chem.* **1992**, *31*, 1423–1430.
- [79] H. P. A. Mercier, J. C. P. Sanders, G. J. Schrobilgen, *J. Am. Chem. Soc.* **1994**, *116*, 2921–2937.
- [80] T. S. Cameron, I. Krossing, J. Passmore, *Inorg. Chem.* **2001**, *40*, 4488–4490.
- [81] W. E. Piers, T. Chivers, *Chem. Soc. Rev.* **1997**, *26*, 345–354.
- [82] R. Minkwitz, F. Neikes, *Inorg. Chem.* **1999**, *38*, 5960–5963.
- [83] A. G. Massey, A. J. Park, *J. Organomet. Chem.* **1964**, *2*, 245–250.
- [84] J. H. Golden, P. F. Mutolo, E. B. Lobkovsky, F. DiSalvo, *Inorg. Chem.* **1994**, *33*, 5374–5375.
- [85] K. Fujiki, S.-Y. Ikeda, H. Kobayashi, A. Mori, A. Nahira, J. Nie, T. Sonoda, Y. Yagupolskii, *Chem. Lett.* **2000**, *1*, 62–63.
- [86] A. Bösmann, G. Francio, E. Janssen, M. Solinas, W. Leitner, P. Wasserscheid, *Angew. Chem. Int. Ed.* **2001**, *113*, 2769–2771.
- [87] J. Van Den Broeke, B. J. Deelman, G. Van Koten, *Tetrahedron Lett.* **2001**, *42*, 8085–8087.
- [88] K. Fujiki, J. Ichikawa, H. Kobayashi, A. Sonoda, T. Sonoda, *J. Fluor. Chem.* **2000**, *102*, 293–300.
- [89] F. Kita, H. Sakata, S. Sinomoto, A. Kawakami, H. Kamizori, T. Sonoda, H. Nagashima, J. Nie, N. V. Pavlenko, Y. L. Yagupolskii, *J. Power Sources* **2000**, *90*, 27–32.
- [90] H. Braunschweig, R. D. Dewhurst, F. Hupp, C. Schneider, *Chem. Commun.* **2014**, *50*, 15685–15688.
- [91] L. Dütsch, Master thesis, University Regensburg, 2015.
- [92] T. J. Barbarich, S. T. Handy, S. M. Miller, O. P. Anderson, P. A. Grieco, S. H. Strauss, *Organometallics* **1996**, *15*, 3776–3778.
- [93] S. M. Ivanova, B. G. Nolan, Y. Kobayashi, S. M. Miller, O. P. Anderson, S. H. Strauss, *Chem. Eur. J.* **2001**, *7*, 503–510.
- [94] T. J. Barbarich, S. M. Miller, O. P. Anderson, S. H. Strauss, *J. Mol. Catal. A Chem.* **1998**, *128*, 289–331.
- [95] I. Krossing, *Chem. Eur. J.* **2001**, *7*, 490–502.

- [96] I. Krossing, H. Brands, R. Feuerhake, S. Koenig, *J. Fluor. Chem.* **2001**, *112*, 83–90.
- [97] I. Krossing *Chem. Eur. J.* **2001**, *7*, 490–502.
- [98] T. Köchner, N. Trapp, T. A. Engesser, A. J. Lehner, C. Röhr, S. Riedel, C. Knapp, H. Scherer, I. Krossing, *Angew. Chem. Int. Ed.* **2011**, *50*, 11253–11256.
- [99] G. Santiso-Quiñones, R. Brückner, C. Knapp, I. Dionne, J. Passmore, I. Krossing, *Angew. Chem. Int. Ed.* **2009**, *48*, 1133–1137.
- [100] G. Santiso-Quiñones, A. Reisinger, J. M. Slattery, I. Krossing, *Chem. Commun.* **2007**, *47*, 5046–5048.
- [101] G. Santiso-Quiñones, A. Higelin, J. Schaefer, R. Brückner, C. Knapp, I. Krossing, *Chem. Eur. J.* **2009**, *15*, 6663–6677.
- [102] S. Welsch, M. Bodensteiner, M. Dušek, M. Sierka, M. Scheer, *Chem. Eur. J.* **2010**, *16*, 13041–13045.
- [103] M. Gonsior, I. Krossing, N. Mitzel, *Z. anorg. allg. Chem.* **2002**, *628*, 1821–1830.
- [104] A. Reisinger, I. Krossing Diplomarbeit, University Karlsruhe, 2003.
- [105] M. Gonsior, I. Krossing, L. Müller, I. Raabe, M. Jansen, L. Van Wullen, *Chem. Eur. J.* **2002**, *8*, 4475–4492.
- [106] I. Krossing, I. Raabe, *Angew. Chem. Int. Ed.* **2001**, *40*, 4406–4409.
- [107] I. Krossing, A. Bihlmeier, I. Raabe, N. Trapp, *Angew. Chem. Int. Ed.* **2003**, *42*, 1531–1534.
- [108] A. B. Rupp, I. Krossing, *Acc. Chem. Res.* **2015**, *48*, 2537–2546.
- [109] T. S. Cameron, A. Decken, I. Dionne, M. Fang, I. Krossing, J. Passmore, *Chem. Eur. J.* **2002**, *8*, 3386–3401.
- [110] I. Krossing, *J. Am. Chem. Soc.* **2001**, *123*, 4603–4604.
- [111] C. Schwarzmaier, M. Sierka, M. Scheer, *Angew. Chem. Int. Ed.* **2013**, *52*, 858–861.
- [112] M. Fleischmann, S. Welsch, H. Krauss, M. Schmidt, M. Bodensteiner, E. V. Peresykina, M. Sierka, C. Gröger, M. Scheer, *Chem. Eur. J.* **2014**, *20*, 3759–3768.
- [113] M. Elsayed Moussa, M. Fleischmann, E. V. Peresykina, L. Dütsch, M. Seidl, G. Balázs, M. Scheer, *Eur. J. Inorg. Chem.* **2017**, *25*, 3222–3226.
- [114] H. J. Frohn, V. V. Bardin, *Z. anorg. allg. Chem.* **2001**, *627*, 15–16.
- [115] L. M. Yagupolskii, Y. L. Yagupolskii, *J. Fluor. Chem.* **1995**, *72*, 225–229.
- [116] K. Ren, A. Mejiritski, J. H. Malpert, O. Grinevich, H. Gu, D. C. Neckers, *Tetrahedron Lett.* **2000**, *41*, 8669–8672.
- [117] H. Li, K. Ren, W. Zhang, J. H. Malpert, D. C. Neckers, *Macromolecules* **2001**, *34*, 2019–2021.



- [118] K. Ren, J. H. Malpert, H. Li, H. Gu, D. C. Neckers, *Macromolecules* **2002**, *35*, 1632–1637.
- [119] V. W. W. Yam, V. K. M. Au, S. Y. L. Leung, *Chem. Rev.* **2015**, *115*, 7589–7728.
- [120] H. Yersin, *Highly Efficient OLEDs with Phosphorescent Materials*; Wiley-VCH Verlag, **2008**.
- [121] P. Ai, M. Mauro, L. De Cola, A. A. Danopoulos, P. Braunstein, *Angew. Chem. Int. Ed.* **2016**, *55*, 3338–3341.
- [122] R. Czerwieniec, M. Leidl, H. H. Homeier, H. Yersin, *Coord. Chem. Rev.* **2016**, *325*, 2–28.
- [123] H. Yersin, A. F. Rausch, R. Czerwieniec, T. Hofbeck, T. Fischer, *Coord. Chem. Rev.* **2011**, *255*, 2622–2652.
- [124] T. A. Niehaus, T. Hofbeck, H. Yersin, *RSC Adv.* **2015**, *5*, 63318–63329.
- [125] A. Bossi, A. F. Rausch, M. J. Leidl, R. Czerwieniec, M. T. Whited, P. Djurovich, H. Yersin, M. E. Thompson, *Inorg. Chem.* **2013**, *52*, 12403–12415.
- [126] W. Brütting, C. Adachi, *Physics of Organic Semiconductors*; Wiley-VCH Verlag, **2012**.
- [127] K. Udagawa, H. Sasabe, C. Cai, J. Kido, *Adv. Mater.* **2014**, *26*, 5062–5066.
- [128] A. Tsuboyama, K. Kuge, M. Furugori, S. Okada, M. Hoshino, K. Ueno, *Inorg. Chem.* **2007**, *46*, 1992–2001.
- [129] R. Czerwieniec, J. Yu, H. Yersin, *Inorg. Chem.* **2011**, *50*, 8293–8301.
- [130] J. C. Deaton, S. C. Switalski, D. Y. Kondakov, R. H. Young, T. D. Pawlik, D. J. Giesen, S. B. Harkins, A. J. M. Miller, S. F. Mickenberg, J. C. Peters, *J. Am. Chem. Soc.* **2010**, *132*, 9499–9508.
- [131] R. Czerwieniec, K. Kowalski, H. Yersin, *Dalton Trans.* **2013**, *42*, 9826–9830.
- [132] D. M. Zink, T. Grab, T. Baumann, M. Nieger, E. C. Barnes, W. Klopffer, S. Bräse, *Organometallics* **2011**, *30*, 3275–3283.
- [133] T. Hofbeck, U. Monkowius, H. Yersin, *J. Am. Chem. Soc.* **2015**, *137*, 399–404.
- [134] M. J. Leidl, V. A. Krylova, P. I. Djurovich, M. E. Thompson, H. Yersin, *J. Am. Chem. Soc.* **2014**, *136*, 16032–16038.
- [135] Q. Zhang, J. Li, K. Shizu, S. Huang, S. Hirata, H. Miyazaki, C. Adachi, *J. Am. Chem. Soc.* **2012**, *134*, 14706–14709.
- [136] H. Yersin, L. Mataranga-Popa, R. Czerwieniec, Y. Dovbii, *Chem. Mater.* **2019**, *31*, 6110–6116.
- [137] L. Bergmann, G. J. Hedley, T. Baumann, S. Bräse, I. D. W. Samuel, *Sci. Adv.* **2016**, *2*, 1–7.
- [138] M. Osawa, M. Hoshino, M. Hashimoto, I. Kawata, S. Igawa, M. Yashima, *Dalton Trans.* **2015**, *44*, 8369–8378.

- [139] S. Evariste, M. Elsayed Moussa, H. L. Wong, G. Calvez, V. W. W. Yam, C. Lescop, *Z. anorg. allg. Chem.* **2020**, 1–8.
- [140] M. Elsayed Moussa, A. M. Khalil, S. Evariste, H.-L. Wong, V. Delmas, B. Le Guennic, G. Calvez, K. Costuas, V. W. W. Yam, C. Lescop, *Inorg. Chem. Front.* **2020**, 7, 1334–1344.
- [141] F. B. Dias, K. N. Bourdakos, V. Jankus, K. C. Moss, K. T. Kamtekar, V. Bhalla, J. Santos, M. R. Bryce, A. P. Monkman, *Adv. Mater.* **2013**, 25, 3707–3714.
- [142] T. Gneuß, M. J. Leitzl, L. H. Finger, N. Rau, H. Yersin, J. Sundermeyer, *Dalton Trans.* **2015**, 44, 8506–8520.
- [143] M. J. Leitzl, F. R. Küchle, H. A. Mayer, L. Wesemann, H. Yersin, *J. Phys. Chem. A* **2013**, 117, 11823–11836.
- [144] D. M. Zink, M. Bächle, T. Baumann, M. Nieger, M. Kühn, C. Wang, W. Klopfer, U. Monkowius, T. Hofbeck, H. Yersin, S. Bräse, *Inorg. Chem.* **2013**, 52, 2292–2305.
- [145] N. Armaroli, G. Accorsi, F. Cardinali, A. Listorti, *Photochemistry and Photophysics of Coordination Compounds I*; Springer Verlag, **2007**.
- [146] N. Armaroli, *Chem. Soc. Rev.* **2001**, 30, 113–124.
- [147] D. W. Thompson, D. V. Scaltrito, D. W. Thompson, J. A. O. Callaghan, G. J. Meyer, *Coord. Chem. Rev.* **2015**, 208, 243–266.
- [148] D. R. McMillin, K. M. McNett *Chem. Rev.* **1998**, 98, 1201–1219.
- [149] D. G. Cuttell, S. M. Kuang, P. E. Fanwick, D. R. McMillin, R. A. Walton, *J. Am. Chem. Soc.* **2002**, 124, 6–7.
- [150] N. Armaroli, G. Accorsi, M. Holler, O. Moudam, J. F. Nierengarten, Z. Zhou, R. T. Wegh, R. Welter, *Adv. Mater.* **2006**, 18, 1313–1316.
- [151] K. Saito, T. Arai, N. Takahashi, T. Tsukuda, T. Tsubomura, *Dalton Trans.* **2006**, 37, 4444–4448.
- [152] A. J. M. Miller, J. L. Dempsey, J. C. Peters, *Inorg. Chem.* **2007**, 46, 7244–7246.
- [153] S. B. Harkins, J. C. Peters, *J. Am. Chem. Soc.* **2005**, 127, 2030–2031.
- [154] M. Hashimoto, S. Igawa, M. Yashima, I. Kawata, M. Hoshino, M. Osawa, *J. Am. Chem. Soc.* **2011**, 133, 10348–10351.
- [155] S. Igawa, M. Hashimoto, I. Kawata, M. Yashima, M. Hoshino, M. Osawa, *J. Mater. Chem. C* **2013**, 1, 542–551.
- [156] A. Schinabeck, N. Rau, M. Klein, J. Sundermeyer, H. Yersin, *Dalton Trans.* **2018**, 47, 17067–17076.
- [157] O. Moudam, A. Kaeser, B. Delavaux-Nicot, C. Duhayon, M. Holler, G. Accorsi, N. Armaroli, I. Seguy, J. Navarro, P. Destruel, J. F. Nierengarten, *Chem. Commun.* **2007**, 29, 3077–3079.

- 
- [158] M. Elsayed Moussa, S. Evariste, H. L. Wong, L. Le Bras, C. Roiland, L. Le Polles, B. Le Guennic, K. Costuas, V. W. W. Yam, C. Lescop, *Chem. Commun.* **2016**, 52, 11370–11373.
- [159] A. Barbieri, G. Accorsi, N. Armaroli, *Chem. Commun.* **2008**, 19, 2185–2193.
- [160] B. Nohra, S. Graule, C. Lescop, R. Réau, *J. Am. Chem. Soc.* **2006**, 128, 3520–3521.
- [161] M. Elsayed Moussa, K. Guillois, W. Shen, R. Réau, J. Crassous, C. Lescop, *Chem. Eur. J.* **2014**, 20, 14853–14867.
- [162] S. Evariste, A. M. Khalil, M. E. Moussa, A. K. W. Chan, E. Y. H. Hong, H. L. Wong, B. Le Guennic, G. Calvez, K. Costuas, V. W. W. Yam, C. Lescop, *J. Am. Chem. Soc.* **2018**, 140, 12521–12526.

## 2. Research Objectives

This thesis is divided into three main parts dealing with various aspects of the coordination chemistry of coinage metals and their use in the self-assembly of oligonuclear aggregates as well as two- and three-dimensional coordination polymers.

### Reactions of an $As_2$ ligand complex with coinage metal salts and organic linkers

This chapter is concerned with the reactivity of the  $As_2$  ligand complex  $[(C_5H_5)_2Mo_2(CO)_4(\mu, \eta^2-As_2)]$  towards coinage metal (I) salts of weakly coordinating anions (WCAs). The reaction behavior of the resulting coordination complexes towards organic pyridyl-based linkers are of interest. The investigated topics include:

- coordination chemistry of  $[(CpMo(CO)_2)_2(\mu, \eta^2: \eta^2-As_2)]$  with CuWCAs and AgWCAs
- reaction of  $[(CpMo(CO)_2)_2(\mu, \eta^2: \eta^2-As_2)]$  with  $Ag[PF_6]$  and organic linkers

### Spherical Aggregates based on the self-assembly of $[Cp''Fe(\eta^5-P_5)]$ and $Cu[TEF]$

This chapter deals with the reaction of  $Cp''Fe(\eta^5-P_5)$  ( $Cp'' = 1,3-C_5H_3tBu_2$ ) with  $[Cu(CH_3CN)_4][TEF]$  ( $TEF^- = [Al\{OC(CF_3)_3\}_4]^-$ ) yielding the unprecedented cationic supramolecule  $[(Cp''Fe(\eta^5-P_5))_{12}\{CuNCMe\}_8]^{8+}$  as a salt of the WCA  $TEF^-$ . The investigated topics include:

- synthesis and characterization in solution of the supramolecule
- structural characterization of  $[(Cp''Fe(\eta^5-P_5))_{12}\{CuNCMe\}_8][TEF]_8$  in the solid state and comparison to other supramolecular spheres

## Reactivity of tetranuclear Cu(I) metallacycle towards organic pyridyl linkers

In collaboration with Dr. Christophe Lescop (Institut des Sciences Chimiques de Rennes, UMR 6226 at the Institut National des Sciences Appliquées de Rennes) the influence on the coordination chemistry and the photophysical properties of a blue emissive tetranuclear Cu(I) metallacycle is investigated. The work on this topic focuses on the complexes  $[\text{Cu}_4(\mu_2\text{-dppm})_4(\text{CN})_2](\text{X})_2$  ( $\text{X} = \text{PF}_6^-$ ,  $[\text{Al}\{\text{OC}(\text{CF}_3)_3\}_4]^-$  (TEF<sup>-</sup>),  $[\text{B}(\text{C}_6\text{H}_3\text{Cl}_2)_4]^-$  (BAR<sup>Cl-</sup>), dppm = 1,1-bis(diphenylphosphino)methane). For the systematic investigation of this chemistry the following challenges arise:

- synthesis of Cu (I) metallacycles containing the WCAs [TEF] and [BAR<sup>Cl</sup>]
- reaction of  $[\text{Cu}_4(\mu_2\text{-dppm})_4(\text{CN})_2](\text{X})_2$  ( $\text{X} = \text{PF}_6^-$ , TEF<sup>-</sup>, BAR<sup>Cl-</sup>) with pyridyl linkers
- structural characterization of  $[\text{Cu}_4(\mu_2\text{-dppm})_4(\text{CN})_2][\text{TEF}]_2$ ,  $[\text{Cu}_4(\mu_2\text{-dppm})_4(\text{CN})_2][\text{BAR}^{\text{Cl}}]_2$  and the coordination polymers resulting from reactions of the metallacycles with pyridyl spacers in the solid state
- characterization of the photophysical properties of selected 1D polymers

## Preface

## Authors

Mehdi Elsayed Moussa,<sup>†</sup> Jana Schiller,<sup>†</sup> Eugenia Peresykina, Michael Seidl, Gábor Balázs, and Manfred Scheer\*

## Author contributions

Jana Schiller and Mehdi Elsayed Moussa contributed equally to this work. The first preparation of compounds **4-7** was done by Mehdi Elsayed Moussa. The reproduction and characterization of compounds **4-7** was done by Jana Schiller. The preparation of the manuscript was done by Mehdi Elsayed Moussa and Jana Schiller. Eugenia V. Peresykina and Michael Seidl have done the X-ray structural characterization of all compounds and revised the experimental part for the X-ray structural analyses. Gábor Balázs performed supporting DFT calculations. Manfred Scheer supervised the research and revised the manuscript prior to publication.

## Acknowledgements

This work was supported by the European Research Council (Grant ERC-2013-AdG 339072).

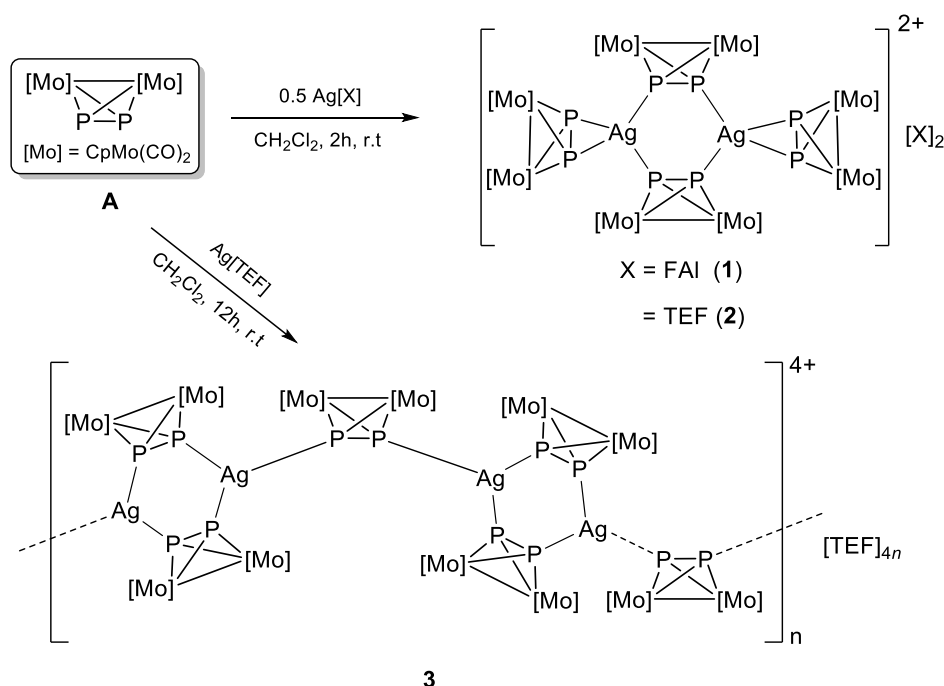
A revised version of this chapter was accepted for publication in Chemistry – A European Journal. <https://doi.org/10.1002/chem.202002513>.

# 1. The Diarsene Complex $[(C_5H_5)_2Mo_2(CO)_4(\mu,\eta^2-As_2)]$ as a Building Block in Supramolecular Chemistry

**Abstract:** The reaction of the organometallic diarsenic complex  $[Cp_2Mo_2(CO)_4(\mu,\eta^2-As_2)]$  (**B**) ( $Cp = C_5H_5$ ) with  $Ag[FAI\{OC(C_6F_5)(C_6F_{10})\}_3]$  ( $Ag[FAI]$ ) and  $Ag[Al\{OC(CF_3)_3\}_4]$  ( $Ag[TEF]$ ), respectively, yields four unprecedented supramolecular assemblies  $[(\eta^2-B)_4Ag_2][FAI]_2$  (**4**),  $[(\eta^2-B)_3Ag][TEF]$  (**5**),  $[(\mu,\eta^1:\eta^2-B)_3(\eta^2-B)_2Ag_3][TEF]_3$  (**6**) and  $[(\mu,\eta^1:\eta^2-B)_4Ag_3][TEF]_3$  (**7**). These compounds characterized with X-Ray crystallography represent the first homoleptic complexes of **B** and  $Ag(I)$ . Additionally, **6** and **7** are unique supramolecular assemblies bearing **B** as a linking unit and the first examples of  $[Ag(I)]_3$  units stabilized by organometallic bichelating ligands.

## 3.1 Introduction

The interest in using metal-directed self-assembly for the design of well-defined solid state structures have remarkably increased in the past decades.<sup>1</sup> The majority of these assemblies are obtained from the association of multitopic organic linkers featuring N-, O- or S- donor atoms with Lewis acidic metal cations.<sup>2</sup> In addition, only few examples of organometallic building blocks have been also used as linking moieties to metal centers.<sup>3</sup> To fill this gap, our group developed the concept of using organometallic polyphosphorus ( $P_n$ ) ligand complexes with flexible coordination modes as connectors between metal ions.<sup>4</sup> This new approach allowed for the synthesis of a large variety of unprecedented supramolecular aggregates including 1D, 2D and 3D coordination polymers (CPs),<sup>5</sup> inorganic nanospheres,<sup>6</sup> nanosized bowls<sup>7</sup> and capsules.<sup>8</sup> One of the simplest of these  $P_n$  compounds is the diphosphorus complex  $[Cp_2Mo_2(CO)_4(\mu,\eta^2-P_2)]$  (**A**) ( $Cp = \eta^5-C_5H_5$ ).<sup>9</sup> Its reaction with a large number of  $Ag(I)$  salts including those of the weakly coordinating anions  $[Al\{OC(CF_3)_3\}_4]^-$  ( $[TEF]^-$ ) and  $[FAI\{OC(C_6F_5)(C_6F_{10})\}_3]^-$  ( $[FAI]^-$ ) allowed for the isolation of  $Ag(I)$  dimers of the general formula  $[Ag_2(\eta^2-A)_2(\mu,\eta^1:\eta^1-A)_2][X]_2$  ( $X = [FAI]^-$  (**1**),  $[TEF]^-$  (**2**); Scheme 3.1).<sup>5a</sup> It is only possible to isolate selectively these products if **A** is used in excess compared to the  $Ag(I)$  salts. However, for example, when a stoichiometric reaction of **A** and  $Ag[TEF]$  is conducted, the 1D polymer  $[Ag_2(\mu,\eta^1:\eta^1-A)_3]_n[TEF]_{2n}$  is formed instead (Scheme 3.1). Interestingly, within the dimers **1** and **2**, due to the weaker coordination of the terminal  $\eta^2$ -coordinated ligands **A** compared to the  $\eta^1:\eta^1$ -coordinated ones, these can be easily substituted by pyridyl functions upon the reaction of the  $Ag(I)$  dimers with ditopic pyridine-based organic molecules to form a new class of hybrid CPs, in which both organometallic and organic units link  $Ag(I)$  ions.<sup>10</sup>



**Scheme 3.1.** Reaction of **A** with  $Ag[FAI\{OC(C_6F_5)(C_6F_{10})\}_3]$  ( $Ag[FAI]$ ) and  $Ag[Al\{OC(CF_3)_3\}_4]$  ( $Ag[TEF]$ ). Synthesis of the dimers **1** and **2** and the 1D CP **3**.

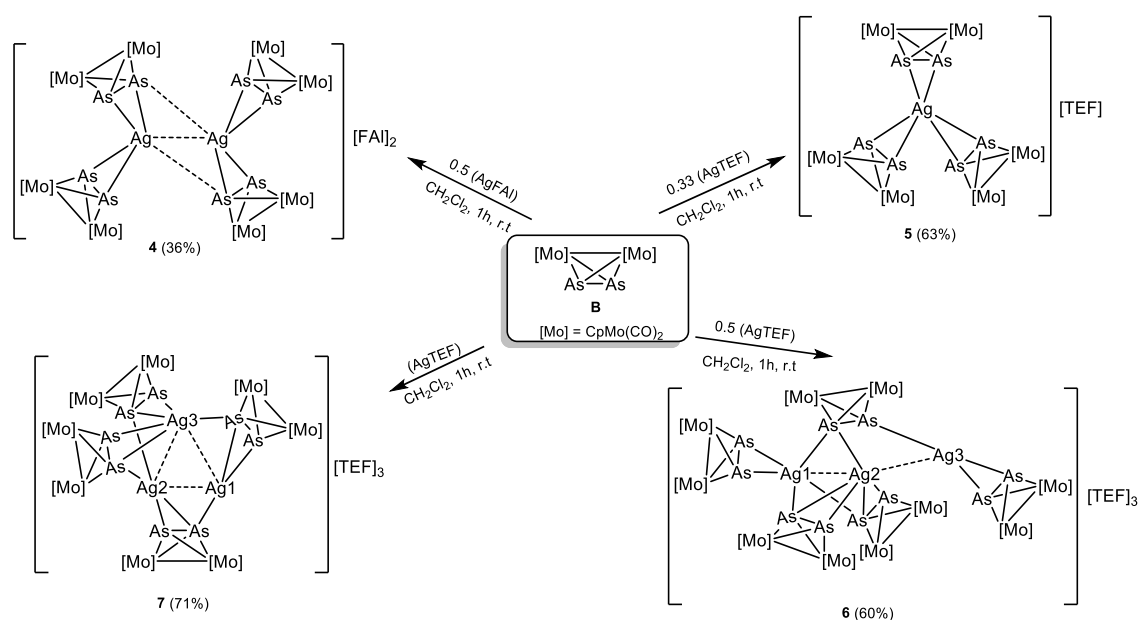
In addition to  $P_n$  complexes, arsenic-based organometallic complexes have been known also for decades.<sup>11</sup> However, their coordination chemistry is only very little investigated,<sup>12a-d</sup> and their use as linkers in supramolecular chemistry is rare. In fact, coordination compounds of any polyarsenic linker and silver ions are extremely rare.<sup>12a,c-e</sup> Thus, expanding this field can be of great interest for organometallic and supramolecular chemists, since the coordination behavior of the much weaker As in comparison to P may significantly differ. Moreover, due to the flexible coordination sphere of the Ag(I) ion and its tendency to form  $Ag \cdots Ag$  interactions,<sup>13,14</sup> the question arise whether it is possible to stabilize short Ag-Ag distances using a certain combination of the diarsene complex  $[Cp_2Mo_2(CO)_4(\mu, \eta^2-As_2)]$  (**B**)<sup>11a</sup> and Ag(I) ions. Accordingly, we became captivated in expanding our research by studying the supramolecular chemistry of polyarsenic  $As_n$  complexes and its comparison to their phosphorus analogues. Herein, we show that the reaction of the diarsenic complex  $[Cp_2Mo_2(CO)_4(\mu, \eta^2-As_2)]$  (**B**) with  $Ag[FAI]$  and  $Ag[TEF]$  using various reactants ratios allowed for the isolation of the first homoleptic coordination compounds of **B** and silver;  $[(\eta^2-B)_4Ag_2][FAI]_2$  (**4**),  $[(\eta^2-B)_3Ag][TEF]$  (**5**),  $[(\mu, \eta^1: \eta^2-B)_3](\eta^2-B)_2Ag_3[TEF]_3$  (**6**) and  $[(\mu, \eta^1: \eta^2-B)_4Ag_3][TEF]_3$  (**7**). Moreover, compounds **6** and **7** show that **B** has the potential as a connector between the Ag(I) centers, stabilizing short  $Ag \cdots Ag$  distances. Compounds **6** and **7** are the only known supramolecular compounds featuring **B** as a linking moiety and to the best of our



knowledge, are the first examples of trinuclear  $[Ag(I)]_3$  units stabilized by organometallic bichelating ligands.

### 3.2 Results and Discussion

In the first step, **B** was reacted with the Ag(I) salt ( $Ag[FAI]$ ). This reaction was conducted using a 2:1 ratio of **B**: $Ag[FAI]$  in  $CH_2Cl_2$  at room temperature (Scheme 3.2). This specific ratio of reactants was studied in order to compare the formed product to that obtained from a similar reaction of the P-containing analogue **A** affording the Ag(I) dimer **1** (Scheme 3.1).



**Scheme 3.2.** Reaction of **B** with  $Ag[FAI\{OC(C_6F_5)(C_6F_{10})\}_3]$  ( $Ag[FAI]$ ) and  $Ag[Al\{OC(CF_3)_3\}_4]$  ( $Ag[TEF]$ ). Synthesis of the supramolecular compounds **4-7**. Yields are shown in parentheses.

From this reaction however compound **4** was isolated as red prisms in 36% yield suitable for X-ray structure analysis. Compound **4** is well soluble in common organic solvents like  $CH_2Cl_2$  and  $CH_3CN$  and insoluble in *n*-pentane. In the solid state, it is air- and light-stable for several hours while it decomposes gradually after one hour in  $CH_3CN$  under air. Compound **4** crystallizes in the orthorhombic space group *Pccn*. Its solid-state structure (Figure 3.1) reveals an Ag(I) dimer stabilized by four  $As_2$  ligands **B**. The whole molecular complex lies on the 2-fold axis along the *z* direction and is additionally disordered over 2 close laying positions with occupancies 0.75 and 0.25, respectively. This type of disorder is ambiguous for the interpretation of the structure and allows for three possible individual cores for **4**, two of them, core **4a** and core **4b**, possess 2-fold rotational symmetry, and

core **4c** is asymmetric (Figure 3.1; for further details see SI). The disorder implies that the crystal structure **4** is always a mixture of complexes with different cores. If cores **4a** and **4b** co-crystallize, they should form the mixture of 75% of **4a** and 25% of **4b**. The core **4c** can co-exist with the core **4a** in a 1:1 ratio. In principle, any mixture of all three complexes **4a-4c** is possible with a ratio that does not contradict the crystallographic occupancies of the atoms. As one of such examples, the mixture of the **4a**, **4b** and **4c** in a ratio of 0.25:0.25:0.5 also does not contradict to the experimental data. Thus, the question as to which of these alternatives would really exist cannot be answered by using X-ray structural data alone.

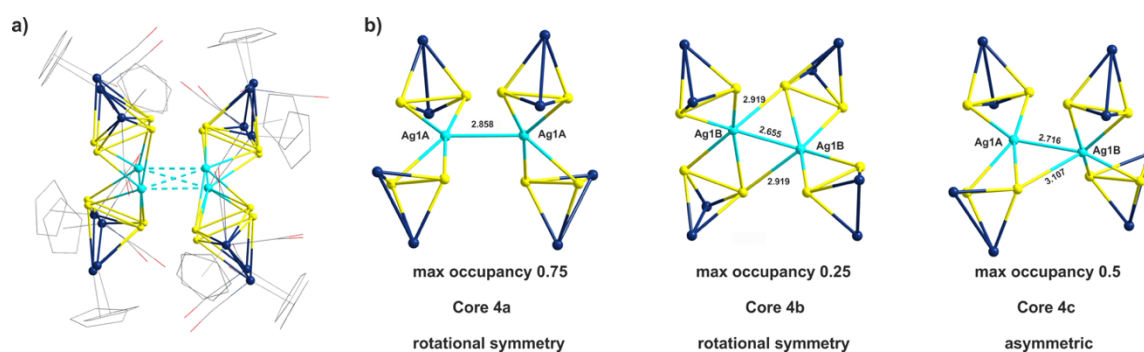


**Figure 3.1.** a) The disordered complex **4** ( $2_z$  axis is directed vertically to the plane of the picture). b) Possible individual cores of **4** in the disordered structure.

In order to elucidate which of the above-mentioned cores represents an energy minimum in the gas phase, we performed DFT calculations using the range separated hybrid functional  $\omega$ B97XD,<sup>15</sup> which also incorporates dispersion corrections together with the def2SVP basis set. Starting from the experimental geometry of core **4b**, the geometry optimization in the gas phase leads to an optimized geometry, which is very similar to that of the core **4a**, solely, the Ag $\cdots$ Ag distance in the optimized geometry is with 3.188 Å longer than that found experimentally for core **4a** (Figure 3.2, left). Interestingly, the geometry optimization of a  $[\{CpMo(CO)_2\}_2As_2]_2Ag^+$  unit, starting from the experimental coordinates of a half of core **4a**, leads to a more symmetric geometry containing a distorted tetrahedrally coordinated Ag center (Figure 3.2, right). This indicates that between the two  $[\{CpMo(CO)_2\}_2As_2]_2Ag^+$  units attraction forces should be present in the solid state. This is also reflected by the gas phase “dimerization” energy of two  $[\{CpMo(CO)_2\}_2As_2]_2Ag^+$  units to the gas phase optimized geometry of **4** of  $-9.90$  kJ $\cdot$ mol $^{-1}$  (for further details see SI).

Whichever structures **4** adopts in the solid state, its composition (an Ag(I) dimer stabilized by four  $As_2$  ligands **B**) is related to the Ag(I) dimer **2**, obtained from a similar reaction with the phosphorus analogue **A** (Scheme 3.1). Still however, two main

differences are realized between both dimers **2** and **4**. Firstly, although two of the E<sub>2</sub> units (E = P, As) in both dimers possess each a η<sup>2</sup>-coordination mode, the other ones possess each a bridging μ,η<sup>1</sup>:η<sup>1</sup>-coordination in **2** and a bridging μ,η<sup>1</sup>:η<sup>2</sup>-coordination or a η<sup>2</sup>-coordination in **4**.

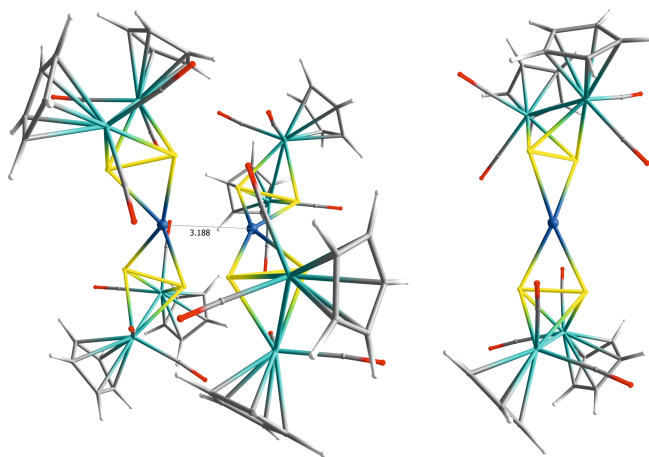


**Figure 3.2.** Gas-phase optimized geometry of **4** at the ωB97XD/def2SVP level of theory.

Additionally, the distance between the metal centers in **2** [ $d(\text{Ag}\cdots\text{Ag}) > 4.85 \text{ \AA}$ ]<sup>5a</sup> are much larger than those in **4** [ $2.65 \text{ \AA} > d(\text{Ag}\cdots\text{Ag}) > 2.86 \text{ \AA}$ ]. So, no argentophilic interaction is present in **2**, while a possible metal-metal interaction is present in **4** (the sum of the van der Waals radii for silver (3.44 Å)).<sup>16</sup> The As-As (2.331(1)-2.414(2) Å) bond lengths in **4** are slightly elongated compared to those in the non-coordinated ligand complexes **1** (As-As = 2.312(3) Å).<sup>11c</sup> The As-Ag bond lengths are in the range of 2.613(1)-2.919(6) Å. These lengths are expectedly longer than the P-Ag bond lengths (2.442(5)-2.688(5) Å) found in the Ag(I) dimer based on the lighter analog  $[\text{Cp}_2\text{Mo}_2(\text{CO})_4(\mu, \eta^2\text{-P}_2)]$ .<sup>5a</sup>

The crystallographic features of **4**, including the flexible coordination mode of the As<sub>2</sub> ligand complex **B** and the short Ag⋯Ag contacts, raised the question as to whether a change in the stoichiometry of the reactants would lead to products with different compositions. Obviously if, a higher amount of Ag(I) salts is used as reactants would lead to a higher number of Ag(I) ions with possible metal-metal interaction in the formed solid-state products. Thus, **B** was treated with the Ag(I) salt Ag[Al{OC(CF<sub>3</sub>)<sub>3</sub>]<sub>4</sub>] (Ag[TEF]), due to the very high solubility of the [TEF]<sup>-</sup> salts, for which the dependence of the composition of the product on the stoichiometry of the reactants was studied by varying the **B**:Ag[TEF] ratio. Interestingly, very different solid-state products were obtained in these reactions directed by the ratio of the used starting materials. All these reactions were performed in CH<sub>2</sub>Cl<sub>2</sub> and subsequently layered with *n*-pentane. The 3:1 reaction

gave compound **5**, the 2:1 reaction compound **6** and the 1:1 reaction compound **7** in yields of 63%, 60% and 71%, respectively. Compounds **5-7** are selectively isolated from their corresponding crude reaction mixtures as red crystals and show air- and light stability in the solid state. Single-crystal X-ray structure analysis of **5-7** reveal composition ratios of 3:1 (for **5**), 5:3 (for **6**) and 4:3 (for **7**) of **B**:Ag(I) (Figure 3.3). Compound **5** represents a Ag(I) monomer with the general formula [Ag(μ,η<sup>2</sup>-**B**)<sub>3</sub>][TEF] while compounds **6** and **7** are unprecedented Ag(I) trimers with the formulas [Ag<sub>3</sub>(μ,η<sup>2</sup>-**B**)<sub>2</sub>(μ,η<sup>1</sup>:η<sup>2</sup>-**B**)<sub>3</sub>][TEF]<sub>3</sub> and [Ag<sub>3</sub>(μ,η<sup>1</sup>:η<sup>2</sup>-**B**)<sub>4</sub>][TEF]<sub>3</sub> respectively. The silver monomer **5** crystallizes in the monoclinic space group *P2<sub>1</sub>/c*.

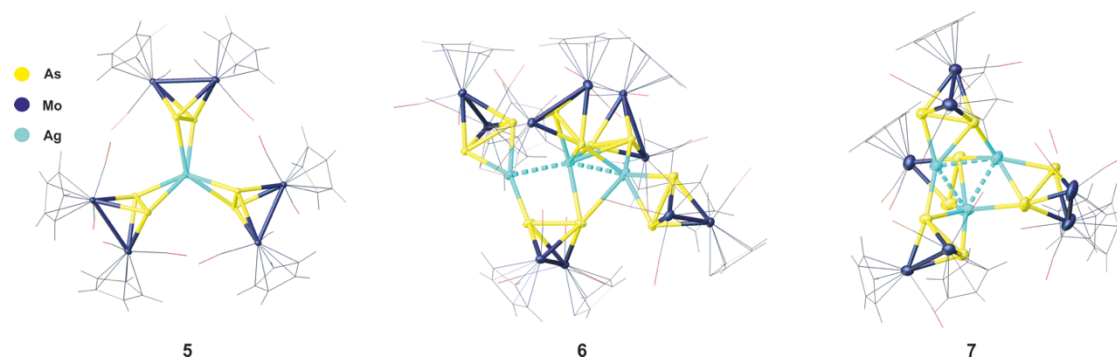


**Figure 3.3.** Molecular structures of the supramolecular assemblies **5-7** in the solid state.

The Ag(I) core in **5** is stabilized by three Mo<sub>2</sub>As<sub>2</sub> ligand complexes **B** each possessing a η<sup>2</sup>-coordination mode, thus the Ag(I) center is hexacoordinated to six As atoms. According to the CSD database,<sup>16</sup> only one other coordination compound in which a silver center has been stabilized by six arsenic atoms has been previously reported.<sup>12d</sup> The As<sub>2</sub>AgAs<sub>2</sub> plane to plane normal angles range from 71.77(3) to 108.77(3)°. As a consequence, the Ag(I) center adopts a distorted trigonal prismatic coordination sphere. The As-As bond lengths in **5** (2.3572(4)-2.3734(3) Å) are slightly elongated compared to those in the non-coordinated ligand complex **B** (2.312(3) Å).<sup>11c</sup> The Ag-As bond lengths in **5** range between 2.7337(3) and 2.9186(3) Å.

Compounds **6** and **7** crystallize in the monoclinic space groups *P2<sub>1</sub>/n* and *P2<sub>1</sub>/c* with three crystallographically unique Ag(I) atoms, five (in **6**) and four (in **7**) Mo<sub>2</sub>As<sub>2</sub> ligands **B**, four (in **6**) and one (in **7**) CH<sub>2</sub>Cl<sub>2</sub> solvent molecules and three [TEF]<sup>-</sup> anions in the asymmetric units. The central structural motif of **6** consists of a bent trinuclear Ag<sub>3</sub> chain while it shows an almost perfect equilateral Ag<sub>3</sub> triangle in **7**. In **6**, these Ag(I) ions are stabilized by five Mo<sub>2</sub>As<sub>2</sub> ligands **B** with two of them showing an η<sup>2</sup>-coordination mode and three others a μ,η<sup>2</sup>:η<sup>1</sup>-coordination. Interestingly, one of these bridging ligands **B** connects all the three Ag(I) ions, Ag1, Ag2 and Ag3, while the other two ligands **B**

connect each only the Ag1 and Ag2 ions. Additionally, the intermetallic Ag...Ag distances in **6** (2.8376(3)-2.9053(3) Å) are significantly shorter than the sum of the van der Waals radii for two silver atoms (3.44 Å) indicating a possible existence of argentophilic interactions.<sup>17</sup> As a consequence, all the Ag(I) ions in **6** show different coordination environments: Ag1 is hexacoordinated to five As atoms and one Ag(I) ion, Ag2 is heptacoordinated to five As atoms and two Ag(I) ions and Ag3 is tetracoordinated to three As atoms and one Ag(I) ion. The Ag<sub>3</sub> core in **7** is stabilized by four bridging Mo<sub>2</sub>As<sub>2</sub> ligands **B** each showing a η<sup>2</sup>:η<sup>1</sup>-coordination. All Ag(I) ions in **7** show different coordination spheres; Ag3 is heptacoordinated to five As atoms and two Ag(I) ions, Ag2 is hexacoordinated to four As atoms and two Ag(I) ions and Ag1 is pentacoordinated to three As atoms and two Ag(I) ions. The intermetallic Ag...Ag distances in **7** range between 2.858(2) and 2.980(1) Å, are also within the range of possible metal-metal interactions.<sup>[17]</sup> The As-As bond lengths in **6** (2.321(1)-2.458(3) Å) and **7** (2.378(5)-2.409(5) Å) are elongated compared to those in the non-coordinated complex **B** (2.312(3) Å).<sup>11c</sup> The Ag-As bond lengths are in the range of 2.438(1)-3.123(1) Å for **6** and 2.573(8)-2.989(8) Å for **7**, respectively. The 3:1 and the 2:1 stoichiometric ratio reactions of the Mo<sub>2</sub>P<sub>2</sub> ligand complex (**A**) and Ag[TEF] afforded the Ag(I) dimer **2**, whereas a 1:1 reaction gave the 1D polymer **3**. Similar reactions of the Mo<sub>2</sub>As<sub>2</sub> ligand complex (**B**) using similar ratios afforded totally different products (**5-7**). This is caused by the very flexible coordination behavior of the As<sub>2</sub> moiety in **B** which can adopt easily both η<sup>2</sup>:η<sup>1</sup>- and η<sup>2</sup>-coordination modes.

Compounds **4-7** are well soluble in common organic solvents like CH<sub>2</sub>Cl<sub>2</sub> and CH<sub>3</sub>CN, little soluble in THF and insoluble in *n*-pentane. Their <sup>1</sup>H and <sup>13</sup>C{<sup>1</sup>H} NMR spectra in CD<sub>3</sub>CN at room temperature show typical signals for Cp and CO ligands. In the ESI mass spectra in CH<sub>3</sub>CN peaks for the cations [Ag(**B**)<sub>2</sub>]<sup>+</sup> and [Ag(**B**)(CH<sub>3</sub>CN)]<sup>+</sup> are mainly detected in the positive ion mode and a peak for the [TEF]<sup>-</sup> or the [FAI]<sup>-</sup> anions in the negative ion mode. These data indicate that only a partial dissociation of the assemblies **4-7** occurs in solutions of CH<sub>3</sub>CN. The solid-state IR spectra of **4** and **5** show each three strong broad absorptions between 1921 and 2048 cm<sup>-1</sup> while those of **6** and **7** show each two absorptions between 1942 and 1980 cm<sup>-1</sup>. These are attributed to the stretching vibrations of the CO ligands in the coordinated ligand units **B**. These vibrations appear at lower energies from those reported for the free complex **B** (1900 and 1949 cm<sup>-1</sup>).<sup>11c</sup>

### 3.3 Conclusion

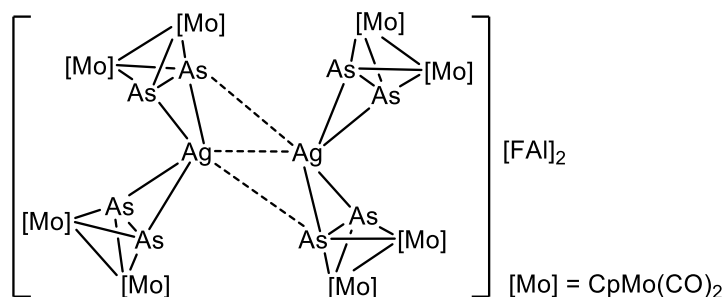
In summary we have synthesized the first homoleptic complexes (**4-7**) of the tetrahedral diarsenic complex  $\text{Mo}_2\text{As}_2$  (**B**) and Ag(I) ions. Thereby, the potential of **B** as a connector in supramolecular chemistry stabilizing short  $\text{Ag}\cdots\text{Ag}$  distances was demonstrated. By using the right stoichiometric ratios of the starting materials and careful experimental conditions, a large variety of solid-state Ag(I) coordination compounds stabilized by three, four or five of these ligand complexes is accessible. The solid-state structures of these products allow a comparison to corresponding P-containing derivatives obtained from similar reactions using the lighter analogue  $\text{P}_2$  complex **A** as a building block. The higher potential of the  $\text{As}_2$  units to form  $\eta^2:\eta^1$ -coordination towards Ag(I) promotes the formation of trimers as cycle (**7**) or catena (**6**) compounds showing  $\text{Ag}\cdots\text{Ag}$  interactions in the solid state. DFT calculations show that core **4a** represents the ground state of complex **4**, and indicates attractive interactions between the two units. Current investigations in this field focus on the reaction of the Ag(I) monomer (**5**) with N-donor organic molecules to build more complex supramolecular architectures with (As,N) mixed donor ligands.

### 3.4 Supporting Information

#### 3.4.1 General

All manipulations were carried out under an inert atmosphere of dry nitrogen using standard glovebox and Schlenk techniques. The nitrogen/argon was dried and purified from traces of oxygen with a Cu/MgSO<sub>4</sub> catalyst, concentrated H<sub>2</sub>SO<sub>4</sub> and orange gel. The ligand complex  $[\text{Cp}_2\text{Mo}_2(\text{CO})_4(\mu,\eta^2\text{-As}_2)]$  (**B**)<sup>18</sup> and the Ag(I) salts  $\text{Ag}[\text{FAl}\{\text{OC}(\text{C}_6\text{F}_5)(\text{C}_6\text{F}_{10})\}_3]$ <sup>19</sup> and  $\text{Ag}[\text{Al}\{\text{OC}(\text{CF}_3)_3\}_4]$ <sup>20</sup> were prepared according to literature procedures. All used solvents were taken from the solvent drying machine MB SPS-800 of the company MBRAUN. IR spectra were recorded as solids using a ThermoFisher Nicolet iS5 FT-IR spectrometer with an ATR-Ge disc. <sup>1</sup>H and <sup>13</sup>C {<sup>1</sup>H} spectra were recorded on a Bruker Avance 400 spectrometer at room temperature. <sup>1</sup>H and <sup>13</sup>C {<sup>1</sup>H} chemical shifts were reported in parts per million (ppm) relative to Me<sub>4</sub>Si as external standard. Mass spectra were recorded on an Agilent Q-TOF 6540 UHD mass spectrometer with acetonitrile as solvent. Elemental analyses were performed on an Elementar Vario MICRO cube apparatus by the microanalytical laboratory of the University of Regensburg.

### 3.4.2 Synthesis of $[\{\{\text{CpMo}(\text{CO})_2\}_2\{\eta^2\text{-As}_2\}\}_4\text{Ag}_2][\text{FAI}\{\text{OC}(\text{C}_6\text{F}_5)(\text{C}_6\text{F}_{10})\}_3]_2$ (**4**)



A solution of  $\text{Ag}[\text{FAI}]$  (76 mg, 0.05 mmol, 1 eq.) in 5 mL of  $\text{CH}_2\text{Cl}_2$  and slowly added to a stirred solution of  $[\text{CpMo}_2(\text{CO})_4(\eta^2\text{-As}_2)]$  (**B**) (58 mg, 0.1 mmol, 2 eq.) in 10 ml of  $\text{CH}_2\text{Cl}_2$ . The red solution was stirred for 1 h at room temperature, after which, it was carefully layered with 30 ml of n-pentane. In two days, red crystals of **4** were obtained, washed with n-pentane and dried *in vacuo*. Yield (48 mg, 36% referred to **B**).

$^1\text{H}$  NMR (400 MHz,  $\text{CD}_3\text{CN}$ ):  $\delta = 5.34$  ppm (s,  $\text{H}_{\text{Cp}}$ ).

$^{13}\text{C}\{^1\text{H}\}$  NMR (100 MHz,  $\text{CD}_3\text{CN}$ ):  $\delta = 86.7$  (s,  $\text{C}_{\text{Cp}}$ ), 224.5 ppm (s,  $\text{C}_{\text{CO}}$ ).

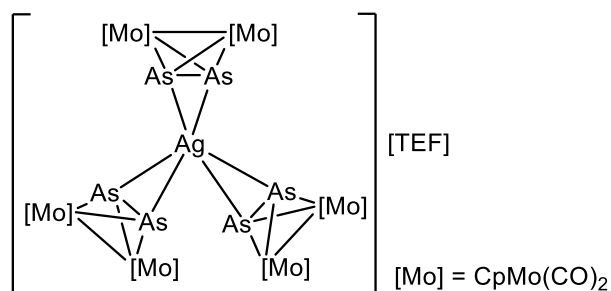
Positive ion ESI-MS ( $\text{CH}_3\text{CN}$ , RT):  $m/z$  (%) = 1276.3 (100)  $[\{\text{Cp}_2(\text{CO})_4\text{Mo}_2\text{As}_2\}_2\text{Ag}]^+$ , 731.6 (80)  $[\{\text{Cp}_2(\text{CO})_4\text{Mo}_2\text{As}_2\}\text{Ag}(\text{CH}_3\text{CN})]^+$ , 690.6 (30)  $[\{\text{Cp}_2(\text{CO})_4\text{Mo}_2\text{As}_2\}\text{Ag}]^+$ , 583.7 (7)  $[\text{Cp}_2(\text{CO})_4\text{Mo}_2\text{As}_2]^+$ .

Negative ion ESI-MS ( $\text{CH}_3\text{CN}$ , RT):  $m/z$  (%) = 1380.9  $[\text{FAI}\{\text{OC}_6\text{F}_{10}(\text{C}_6\text{F}_5)\}_3]^-$ .

Elemental analysis, calcd (%) for  $\text{C}_{128}\text{H}_{40}\text{Ag}_2\text{Al}_2\text{As}_8\text{F}_{92}\text{Mo}_8\text{O}_{22}$  (5314.16 g/mol): C, 28.93; H, 0.76; found: C, 28.69; H, 0.79;

IR (solid, CO bands):  $\tilde{\nu}/\text{cm}^{-1}$ : 1971 (vs), 1933 (vs), 1921 (vs).

### 3.4.3 Synthesis of $[\{\{\text{CpMo}(\text{CO})_2\}_2\{\eta^2\text{-As}_2\}\}_3\text{Ag}][\text{Al}\{\text{OC}(\text{CF}_3)_3\}_4]$ (**5**)



A solution of  $\text{Ag}[\text{TEF}]$  (54 mg, 0.05 mmol, 1 eq.) in 5 mL of  $\text{CH}_2\text{Cl}_2$  and slowly added to a stirred solution of  $[\text{CpMo}_2(\text{CO})_4(\eta^2\text{-As}_2)]$  (**B**) (87 mg, 0.15 mmol, 3 eq.) in 10 ml of  $\text{CH}_2\text{Cl}_2$ . The red solution was stirred for 1 h at room temperature, after which, it was carefully layered with 30 ml of n-pentane. In four days, orange crystals of **5** were obtained, washed with n-pentane and dried *in vacuo*. Yield (88 mg, 63% referred to **B**).

$^1\text{H}$  NMR (400 MHz,  $\text{CD}_3\text{CN}$ ):  $\delta = 5.31$  ppm (s,  $\text{H}_{\text{Cp}}$ ).

$^{13}\text{C}\{^1\text{H}\}$  NMR (100 MHz,  $\text{CD}_3\text{CN}$ ):  $\delta = 86.3$  (s,  $\text{C}_{\text{Cp}}$ ), 225.4 ppm (s,  $\text{C}_{\text{CO}}$ ).

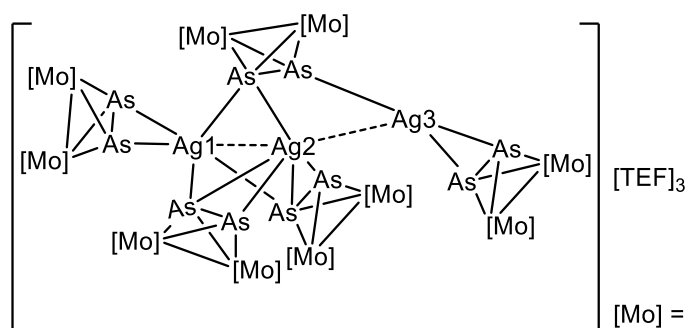
Positive ion ESI-MS ( $\text{CH}_3\text{CN}$ , RT):  $m/z$  (%) = 1276.3 (55) [ $\{\text{Cp}_2(\text{CO})_4\text{Mo}_2\text{As}_2\}_2\text{Ag}\}^+$ , 731.6 (100) [ $\{\text{Cp}_2(\text{CO})_4\text{Mo}_2\text{As}_2\}\text{Ag}(\text{CH}_3\text{CN})\}^+$ , 583.7 (16) [ $\text{Cp}_2(\text{CO})_4\text{Mo}_2\text{As}_2\}^+$ .

Negative ion ESI-MS ( $\text{CH}_3\text{CN}$ , RT):  $m/z$  (%) = 966.9 (100) [ $\text{Al}\{\text{OC}(\text{CF}_3)_3\}_4\}^-$ .

Elemental analysis, calcd (%) for  $\text{C}_{58}\text{H}_{30}\text{AgAlAs}_6\text{F}_{36}\text{Mo}_6\text{O}_{16}$  (2826.83): C, 24.64; H, 1.07; found: C, 24.70; H, 1.01;

IR (solid, CO bands):  $\tilde{\nu}/\text{cm}^{-1}$ : 2048 (s), 1985 (s), 1946 (s).

### 3.4.4 Synthesis of [ $\{\{\text{CpMo}(\text{CO})_2\}_2\{\eta^2:\eta^2\text{-As}_2\}\}_2\{\{\text{CpMo}(\text{CO})_2\}_2\{\eta^1:\eta^2:\eta^2\text{-As}_2\}\}_3\text{Ag}_3\}[\text{Al}\{\text{OC}(\text{CF}_3)_3\}_4\}_3$ ] (**6**)



A solution of  $\text{Ag}[\text{TEF}]$  (54 mg, 0.05 mmol, 1 eq.) in 5 mL of  $\text{CH}_2\text{Cl}_2$  and slowly added to a stirred solution of [ $\text{CpMo}_2(\text{CO})_4(\eta^2\text{-As}_2)$ ] (**B**) (58 mg, 0.1 mmol, 2 eq.) in 10 ml of  $\text{CH}_2\text{Cl}_2$ . The red solution was stirred for 1 h at room temperature, after which, it was carefully layered with 30 ml of n-pentane. After one week, red crystals of **6** were obtained, washed with n-pentane and dried *in vacuo*. Yield (61 mg, 60% referred to **B**).

$^1\text{H}$  NMR (400 MHz,  $\text{CD}_3\text{CN}$ ):  $\delta = 5.34$  ppm (s,  $\text{H}_{\text{Cp}}$ ).

$^{13}\text{C}\{^1\text{H}\}$  NMR (100 MHz,  $\text{CD}_3\text{CN}$ ):  $\delta = 86.7$  (s,  $\text{C}_{\text{Cp}}$ ), 224.5 ppm (s,  $\text{C}_{\text{CO}}$ ).

Positive ion ESI-MS ( $\text{CH}_3\text{CN}$ , RT):  $m/z$  (%) = 1276.3 (42) [ $\{\text{Cp}_2(\text{CO})_4\text{Mo}_2\text{As}_2\}_2\text{Ag}\}^+$ , 731.7 (100) [ $\{\text{Cp}_2(\text{CO})_4\text{Mo}_2\text{As}_2\}\text{Ag}(\text{CH}_3\text{CN})\}^+$ , 690.6 (16) [ $\{\text{Cp}_2(\text{CO})_4\text{Mo}_2\text{As}_2\}\text{Ag}\}^+$ .

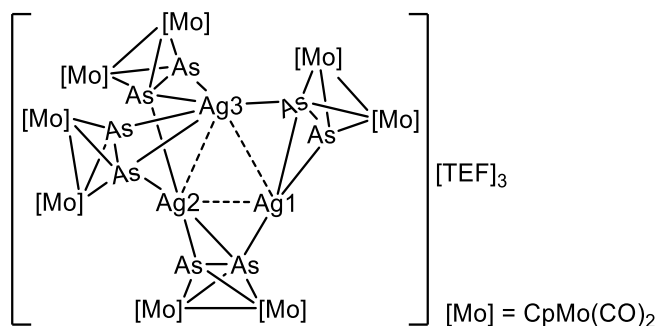
Negative ion ESI-MS ( $\text{CH}_3\text{CN}$ , RT):  $m/z$  (%) = 966.9 (100) [ $\text{Al}\{\text{OC}(\text{CF}_3)_3\}_4\}^-$ .

Elemental analysis, calcd (%) for  $\text{C}_{118}\text{H}_{50}\text{Ag}_3\text{Al}_3\text{As}_{10}\text{F}_{108}\text{Mo}_{10}\text{O}_{32}$  (6144.67): C, 23.07; H, 0.82; found: C, 23.11; H, 0.93;

IR (solid, CO bands):  $\tilde{\nu}/\text{cm}^{-1}$ : 1980 (vs), 1949 (vs).



### 3.4.5 Synthesis of $[\{\{\text{CpMo}(\text{CO})_2\}_2\{\eta^1:\eta^2\text{-As}_2\}\}_4\text{Ag}_3][\text{Al}\{\text{OC}(\text{CF}_3)_3\}_4]_3$ (**7**)



A solution of Ag[TEF] (54 mg, 0.05 mmol, 1 eq.) in 5 mL of CH<sub>2</sub>Cl<sub>2</sub> and slowly added to a stirred solution of [CpMo<sub>2</sub>(CO)<sub>4</sub>(η<sup>2</sup>-As<sub>2</sub>)] (**B**) (29 mg, 0.05 mmol, 1 eq.) in 5 ml of CH<sub>2</sub>Cl<sub>2</sub>. The red solution was stirred for 1 h at room temperature, after which, it was carefully layered with 30 ml of n-pentane. In four days, red crystals of **7** were obtained, washed with n-pentane and dried *in vacuo*. Yield (65 mg, 71% referred to **B**).

<sup>1</sup>H NMR (400 MHz, CD<sub>3</sub>CN): δ = 5.34 ppm (s, H<sub>Cp</sub>).

<sup>13</sup>C{<sup>1</sup>H} NMR (100 MHz, CD<sub>3</sub>CN): δ = 86.7 (s, C<sub>Cp</sub>), 224.5 ppm (s, C<sub>CO</sub>).

Positive ion ESI-MS (CH<sub>3</sub>CN, RT): *m/z* (%) = 1276.3 (100) [Cp<sub>2</sub>(CO)<sub>4</sub>Mo<sub>2</sub>As<sub>2</sub>]<sub>2</sub>Ag]<sup>+</sup>, 731.7 (79) [Cp<sub>2</sub>(CO)<sub>4</sub>Mo<sub>2</sub>As<sub>2</sub>Ag(CH<sub>3</sub>CN)]<sup>+</sup>, 690.6 (37) [Cp<sub>2</sub>(CO)<sub>4</sub>Mo<sub>2</sub>As<sub>2</sub>Ag]<sup>+</sup>, 583.7 (14) [Cp<sub>2</sub>(CO)<sub>4</sub>Mo<sub>2</sub>As<sub>2</sub>]<sup>+</sup>.

Negative ion ESI-MS (CH<sub>3</sub>CN, RT): *m/z* (%) = 966.9 (100) [Al{OC(CF<sub>3</sub>)<sub>3</sub>}]<sub>4</sub><sup>-</sup>.

Elemental analysis, calcd (%) for C<sub>104</sub>H<sub>40</sub>Ag<sub>3</sub>Al<sub>3</sub>As<sub>8</sub>F<sub>108</sub>Mo<sub>8</sub>O<sub>28</sub> (5560.72): C, 23.06; H, 0.82; found: C, 22.82; H, 0.68;

IR (solid, CO bands):  $\tilde{\nu}/\text{cm}^{-1}$ : 1977 (vs), 1942 (vs).

### 3.4.6 Crystallographic Data

Crystals of **4** – **7** were taken from a Schlenk flask under a stream of argon and immediately covered with mineral oil to prevent a loss of solvent. The quickly chosen single crystals covered by a thin oil layer were taken to the pre-centered goniometer head with CryoMount® and directly attached to the diffractometer into a stream of cold nitrogen.

The diffraction experiments for **4** – **7** were collected on a Rigaku Oxford Diffraction diffractometers, Gemini R-ultra equipped with a sealed tube (MoK $\alpha$  radiation,  $\lambda$  = 0.71073 Å) and Atlas CCD detector (**4**, **6**, **7**) or on a SuperNova micro-focus source (CuK $\alpha$  radiation,  $\lambda$  = 1.54178 Å) or Titan CCD detector (**5**), respectively, using  $\omega$  scans of 0.5° frames. The measurements for **4**, **6**, **7** were performed at 123 K, whereas **5** at 90 K. Absorption corrections were applied analytically using *CrysAlis PRO* Software.<sup>21</sup> The

crystal structures were solved by direct methods with *SHELXT*<sup>21</sup> or *Olex*<sup>22</sup> programs and refined by full-matrix least-squares method against  $|F|^2$  in anisotropic approximation using multiprocessor versions of SHELXTL.<sup>23</sup> Hydrogen atoms were refined in calculated positions using riding on pivot atom model. In case of the disorder, the site occupancies of the disordered components were refined with their  $U_{\text{iso}}$  fixed at average  $U_{\text{eq}}$  for fully occupied atoms in given structure in order to avoid correlations. After refinement, occupancies were fixed at the resulting values and the refinement of the atomic displacement parameters was performed. The light atoms with site occupation factors less than 0.5 were refined isotropically.

The Cp<sub>2</sub>Mo<sub>2</sub>P<sub>2</sub>(CO)<sub>4</sub> dimers in **4**, **6** and **7** demonstrate different type of disorder. It can be rotational caused by re-orientations of Cp groups about the direction of  $\pi$ -bond (the tendency can be seen in **6**), or positional, related to different mutual orientation of the CO, Cp ligands coordinated to Mo atoms (**4**, **6**, **7**). In the case of **6** the introduction of the minor (refined to 0.03) disorder of the three of 5 {Mo<sub>2</sub>P<sub>2</sub>} dimers allowed to describe otherwise meaningless electron density (2.40–3.23 e·Å<sup>-2</sup>) and improve quality factors from  $R_1 = 0.0384$ ,  $wR_2 = 0.0905$  to  $R_1 = 0.0271$ ,  $wR_2 = 0.0522$  and maximal ED peak of 0.82 e·Å<sup>-2</sup>

In all structures with the weakly coordinating anion [TEF], it is disordered. The disorder patterns varied according to different orientations or conformations of the [TEF] anion caused by rotation around O-*tert*C (**5**, **6**, **7**) or C-C(F<sub>3</sub>) bonds of OC<sub>4</sub>F<sub>9</sub> groups (**6**, **7**). In all structures the solvent CH<sub>2</sub>Cl<sub>2</sub> molecules are also either disordered or partly occupied. The disorder patterns are illustrated in the Figures S6, S8 and S10.

The supplementary crystallographic data for this publication (Tables S1-S2: CCDC-1985242 (**4**), CCDC-1985243 (**5**), CCDC-1985244 (**6**), CCDC-1985245 (**7**)) can be obtained free of charge at [www.ccdc.cam.ac.uk/conts/retrieving.html](http://www.ccdc.cam.ac.uk/conts/retrieving.html) (or from the Cambridge Crystallographic Data Centre, 12 Union Road, Cambridge CB2 1EZ, UK; Fax: +44-1223-336-033; e-mail: [deposit@ccdc.cam.ac.uk](mailto:deposit@ccdc.cam.ac.uk)).

All ORTEP drawings for **4** – **7** were made in Olex2 software.<sup>22</sup>

**Table S3.1.** Crystallographic details for **4** and **5**.

Compound	4	5
CCDC Code	CCDC-1985242	CCDC-1985243
Structural formula	[Ag <sub>2</sub> (Cp <sub>2</sub> Mo <sub>2</sub> As <sub>2</sub> (CO) <sub>4</sub> ) <sub>4</sub> ] (FAIO <sub>3</sub> C <sub>36</sub> H <sub>45</sub> )·1.675(CH <sub>2</sub> Cl <sub>2</sub> )	[Ag(Cp <sub>2</sub> Mo <sub>2</sub> As <sub>2</sub> (CO) <sub>4</sub> ) <sub>3</sub> ] (Al(OC <sub>4</sub> F <sub>9</sub> ) <sub>4</sub> )
Chemical formula	C <sub>129.68</sub> H <sub>43.35</sub> Ag <sub>2</sub> Al <sub>2</sub> As <sub>8</sub> Cl <sub>3.35</sub> F <sub>92</sub> Mo <sub>8</sub> O <sub>22</sub>	C <sub>42</sub> H <sub>30</sub> AgAs <sub>6</sub> Mo <sub>6</sub> O <sub>12</sub> ·C <sub>16</sub> AlF <sub>36</sub> O <sub>4</sub>
<i>M<sub>r</sub></i>	5456.43	2826.83
Crystal system, space group	Orthorhombic, <i>Pccn</i>	Monoclinic, <i>P2<sub>1</sub>/c</i>
Temperature (K)	123	90
<i>a</i> , <i>b</i> , <i>c</i> (Å)	18.5126 (3), 33.8843 (8), 25.6612 (6)	14.08967 (13), 13.71359 (11), 39.9112 (3)
β (°)	90, 90, 90	90.3681 (8)
<i>V</i> (Å <sup>3</sup> )	16096.9 (6)	7711.49 (11)
<i>Z</i>	4	4
<i>F</i> (000)	10409	5360
<i>D<sub>x</sub></i> (Mg m <sup>-3</sup> )	2.252	2.435
Radiation type	Mo <i>K</i> α	Cu <i>K</i> α
μ (mm <sup>-1</sup> )	2.71	14.10
Crystal shape	Prism	Plate
Colour	Red	Orange
Crystal size (mm)	0.73 × 0.68 × 0.51	0.07 × 0.06 × 0.04
Diffractometer	Xcalibur, Atlas <sup>S2</sup> , Gemini ultra	SuperNova, Titan <sup>S2</sup>
Absorption correction	Analytical	Gaussian
<i>T<sub>min</sub></i> , <i>T<sub>max</sub></i>	0.273, 0.398	0.513, 0.681
No. of measured, independent and observed [ <i>I</i> > 2σ( <i>I</i> )] reflections	82022, 26113, 12482	93514, 15595, 13932
<i>R<sub>int</sub></i>	0.042	0.038
(sin θ/λ) <sub>max</sub> (Å <sup>-1</sup> )	0.756	0.623
Range of <i>h</i> , <i>k</i> , <i>l</i>	<i>h</i> = -27→16, <i>k</i> = -50→32, <i>l</i> = -21→38	<i>h</i> = -17→16, <i>k</i> = -17→17, <i>l</i> = -48→49
<i>R</i> [ <i>F</i> <sup>2</sup> > 2σ( <i>F</i> <sup>2</sup> )], <i>wR</i> ( <i>F</i> <sup>2</sup> ), <i>S</i>	0.044, 0.101, 0.90	0.022, 0.055, 0.96
No. of reflections	26110	15595
No. of parameters	1359	1153
No. of restraints	0	0
H-atom treatment	H-atom parameters constrained	H-atom parameters constrained
Δρ <sub>max</sub> , Δρ <sub>min</sub> (e Å <sup>-3</sup> )	1.78, -1.47	0.64, -1.18

Computer programs: *CrysAlis PRO* 1.171.38.41, 1.171.38.46 (Rigaku OD, 2015), *SHELXT2015/7* (Sheldrick, 2015), *SHELXL2014/7* (Sheldrick, 2014).

**Table S3.2.** Crystallographic details for **6** and **7**.

Compound	6	7
CCDC Code	CCDC-1985244	CCDC-1985245
Structural formula	[Ag <sub>3</sub> (Cp <sub>2</sub> Mo <sub>2</sub> As <sub>2</sub> (CO) <sub>4</sub> ) <sub>5</sub> ] (AlO <sub>4</sub> C <sub>16</sub> F <sub>36</sub> ) <sub>3</sub> ·4CH <sub>2</sub> Cl <sub>2</sub>	[Ag <sub>3</sub> (Cp <sub>2</sub> Mo <sub>2</sub> As <sub>2</sub> (CO) <sub>4</sub> ) <sub>4</sub> ] (AlO <sub>4</sub> C <sub>16</sub> F <sub>36</sub> ) <sub>3</sub> ·CH <sub>2</sub> Cl <sub>2</sub>
Chemical formula	C <sub>122</sub> H <sub>58</sub> Ag <sub>3</sub> Al <sub>3</sub> As <sub>10</sub> Cl <sub>8</sub> F <sub>108</sub> Mo <sub>10</sub> O <sub>32</sub>	C <sub>105</sub> H <sub>42</sub> Ag <sub>3</sub> Al <sub>3</sub> As <sub>8</sub> Cl <sub>2</sub> F <sub>108</sub> Mo <sub>8</sub> O <sub>28</sub>
<i>M<sub>r</sub></i>	6484.43	5645.71
Crystal system, space group	Monoclinic, <i>P</i> 2 <sub>1</sub> / <i>n</i>	Monoclinic, <i>P</i> 2 <sub>1</sub> / <i>c</i>
Temperature (K)	123	123
<i>a</i> , <i>b</i> , <i>c</i> (Å)	20.20026(19), 30.0466(3), 31.0089(3)	22.6469(5), 23.0028(4), 30.4515(4)
β (°)	103.4982 (10)	91.9714(16)
<i>V</i> (Å <sup>3</sup> )	18301.0 (3)	15854.1(5)
<i>Z</i>	4	4
<i>F</i> (000)	12336	10728
<i>D<sub>x</sub></i> (Mg m <sup>-3</sup> )	2.353	2.365
Radiation type	Mo <i>K</i> α	Cu <i>K</i> α
μ (mm <sup>-1</sup> )	3.07	12.025
Crystal shape	prism	plate
Colour	red	red
Crystal size (mm)	0.71 × 0.62 × 0.38	0.32 × 0.17 × 0.05
Diffractometer	Xcalibur, Atlas <sup>S2</sup> , Gemini ultra	Atlas <sup>S2</sup> , SuperNova
Absorption correction	Analytical	Analytical
<i>T<sub>min</sub></i> , <i>T<sub>max</sub></i>	0.221, 0.431	0.143, 0.650
No. of measured, independent and observed [ <i>I</i> > 2σ( <i>I</i> )] reflections	169943, 58279, 38192	69104, 32402, 26756
<i>R<sub>int</sub></i>	0.029	0.0353
(sin θ/λ) <sub>max</sub> (Å <sup>-1</sup> )	0.744	0.746
Range of <i>h</i> , <i>k</i> , <i>l</i>	<i>h</i> = -29→28, <i>k</i> = -40→44, <i>l</i> = -46→43	<i>h</i> = -28→27, <i>k</i> = -25→29, <i>l</i> = -38→29
<i>R</i> [ <i>F</i> <sup>2</sup> > 2σ( <i>F</i> <sup>2</sup> )], <i>wR</i> ( <i>F</i> <sup>2</sup> ), <i>S</i>	0.027, 0.054, 0.90	0.0634, 0.1804, 1.02
No. of reflections	58279	32402
No. of parameters	2975	4201
No. of restraints	0	7150
H-atom treatment	H-atom parameters constrained	H-atom parameters constrained
Δρ <sub>max</sub> , Δρ <sub>min</sub> (e Å <sup>-3</sup> )	1.26, -1.19	1.67, -1.18

Computer programs: *CrysAlis PRO* 1.171.38.41 and 1.171.39.45g (Rigaku OD, 2018), *SHELXL2014/7* (Sheldrick, 2014), *Olex2* (Dolomanov *et al.*, 2009).

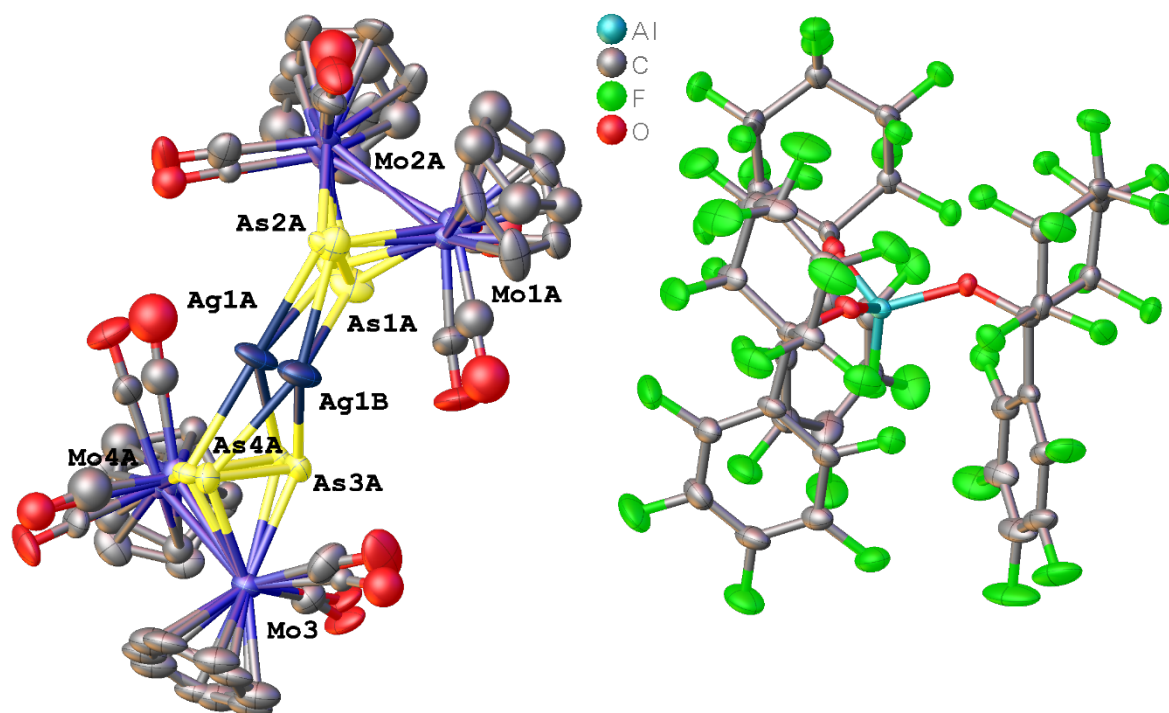


**Figure S3.1.** Molecular structure of the compound **4** (a.d.p. ellipsoids at 50% probability).

**Table S3.3.** Selected geometric parameters (Å, °) for **4**.

Ag1A—As4A	2.6188 (15)	Ag1B—Ag1B <sup>i</sup>	2.655 (4)
Ag1A—As2A	2.678 (3)	Ag1B—As1B	2.656 (8)
Ag1A—As1A	2.705 (2)	Ag1B—As4B	2.718 (5)
Ag1A—As3A	2.706 (2)	Ag1B—As3B	2.726 (7)
Ag1A—Ag1A <sup>i</sup>	2.8583 (12)	Ag1B—As4B <sup>i</sup>	2.919 (6)
Mo1A—As2A	2.553 (5)	Mo1B—As2B	2.549 (15)
Mo1A—As1A	2.629 (4)	Mo1B—As1B	2.607 (12)
Mo2A—As1A	2.545 (2)	Mo2B—As1B	2.559 (7)
Mo2A—As2A	2.623 (3)	Mo2B—As2B	2.664 (12)
Mo4A—As3A	2.5510 (18)	Mo4B—As3B	2.550 (6)
Mo4A—As4A	2.6546 (17)	Mo4B—As4B	2.603 (6)
As1A—As2A	2.413 (4)	As1B—As2B	2.331 (14)
As3A—As4A	2.414 (2)	As3B—As4B	2.346 (9)
Ag1B—As2B	2.613 (10)	As4B—Ag1B <sup>i</sup>	2.919 (6)
As4A—Ag1A—As2A	164.27 (8)	As1B—Ag1B—As4B	127.2 (2)
As4A—Ag1A—As1A	142.24 (6)	As2B—Ag1B—As3B	138.7 (3)
As2A—Ag1A—As1A	53.27 (9)	Ag1B <sup>i</sup> —Ag1B—As3B	116.47 (16)
As4A—Ag1A—As3A	53.88 (5)	As1B—Ag1B—As3B	86.2 (2)

As2A—Ag1A—As3A	138.18 (10)	As4B—Ag1B—As3B	51.05 (18)
As1A—Ag1A—As3A	90.92 (6)	As2B—Ag1B—As4B <sup>i</sup>	91.0 (3)
As4A—Ag1A—Ag1A <sup>i</sup>	92.18 (4)	Ag1B <sup>i</sup> —Ag1B—As4B <sup>i</sup>	58.15 (12)
As2A—Ag1A—Ag1A <sup>i</sup>	72.23 (7)	As1B—Ag1B—As4B <sup>i</sup>	131.75 (18)
As1A—Ag1A—Ag1A <sup>i</sup>	125.49 (5)	As4B—Ag1B—As4B <sup>i</sup>	99.69 (12)
As3A—Ag1A—Ag1A <sup>i</sup>	137.24 (4)	As3B—Ag1B—As4B <sup>i</sup>	122.51 (13)
As2A—As1A—Ag1A	62.79 (9)	As2B—As1B—Ag1B	62.8 (3)
Mo2A—As1A—Ag1A	116.34 (10)	Mo2B—As1B—Ag1B	120.6 (3)
Mo1A—As1A—Ag1A	107.36 (9)	Mo1B—As1B—Ag1B	105.1 (3)
As1A—As2A—Ag1A	63.94 (8)	As1B—As2B—Ag1B	64.7 (3)
Mo1A—As2A—Ag1A	110.47 (14)	Mo1B—As2B—Ag1B	108.0 (5)
Mo2A—As2A—Ag1A	114.61 (11)	Ag1B—As2B—Mo2B	118.3 (4)
As4A—As3A—Ag1A	61.21 (6)	As4B—As3B—Ag1B	64.3 (2)
Mo4A—As3A—Ag1A	105.44 (7)	Mo3—As3B—Ag1B	117.1 (2)
Mo3—As3A—Ag1A	115.24 (7)	Mo4B—As3B—Ag1B	109.8 (2)
As3A—As4A—Ag1A	64.90 (6)	As3B—As4B—Ag1B	64.6 (2)
Mo3—As4A—Ag1A	120.91 (6)	Mo3—As4B—Ag1B	120.05 (18)
Ag1A—As4A—Mo4A	105.00 (6)	Mo4B—As4B—Ag1B	108.5 (2)
As2B—Ag1B—Ag1B <sup>i</sup>	101.2 (3)	As3B—As4B—Ag1B <sup>i</sup>	120.3 (2)
As2B—Ag1B—As1B	52.5 (3)	Mo3—As4B—Ag1B <sup>i</sup>	146.48 (15)
Ag1B <sup>i</sup> —Ag1B—As1B	146.34 (14)	Mo4B—As4B—Ag1B <sup>i</sup>	143.3 (2)
As2B—Ag1B—As4B	153.8 (3)	Ag1B—As4B—Ag1B <sup>i</sup>	56.06 (12)
Ag1B <sup>i</sup> —Ag1B—As4B	65.79 (14)		

Symmetry code(s): (i)  $-x+1/2, -y+3/2, z$ .

### Interpretation of the disorder of the core in the cationic complex **4**

The cationic complex  $[\text{Ag}_3(\text{Cp}_2\text{Mo}_2\text{As}_2(\text{CO})_4)_5]^{3+}$  (**4**) is disordered over two close positions with occupancies 0.75 and 0.25. It occupies special position on the 2-fold axis along z direction. The half of each two disordered components is located in the asymmetric unit (Figure S3.2). The symmetrically generated disordered complex is depicted in Figure S3.3.

If symmetry operation of  $2_z$  axis is applied only to the major (0.75) part of the complex **4**, the resulting core will include only 'green-bonded' atoms in the Figure S3.3b, if the same procedure is repeated for the minor part (0.25) – the 'red-bonded' atoms. This would be the easiest and straightforward interpretation of the disorder. However, it is also possible, that the red part in the asymmetric part combines with the green part of the symmetrically generated part of the disorder. Then two more combinations 'green-red' and 'red-green' are allowed, which correspond to potentially different cores of the complex **4** (Figure S3.4).

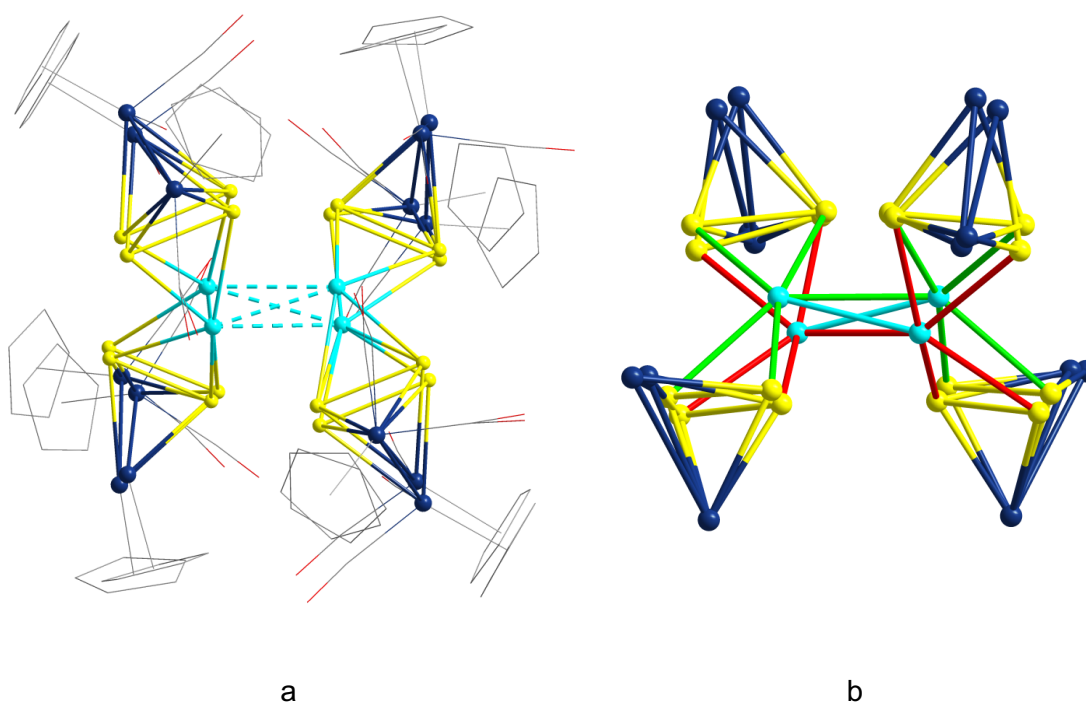


**Figure S3.3.** (a) Disordered cationic part in **4** and (b) the view of the disordered core with highlighted major (0.75, green bonds) and minor (0.25, red bonds).

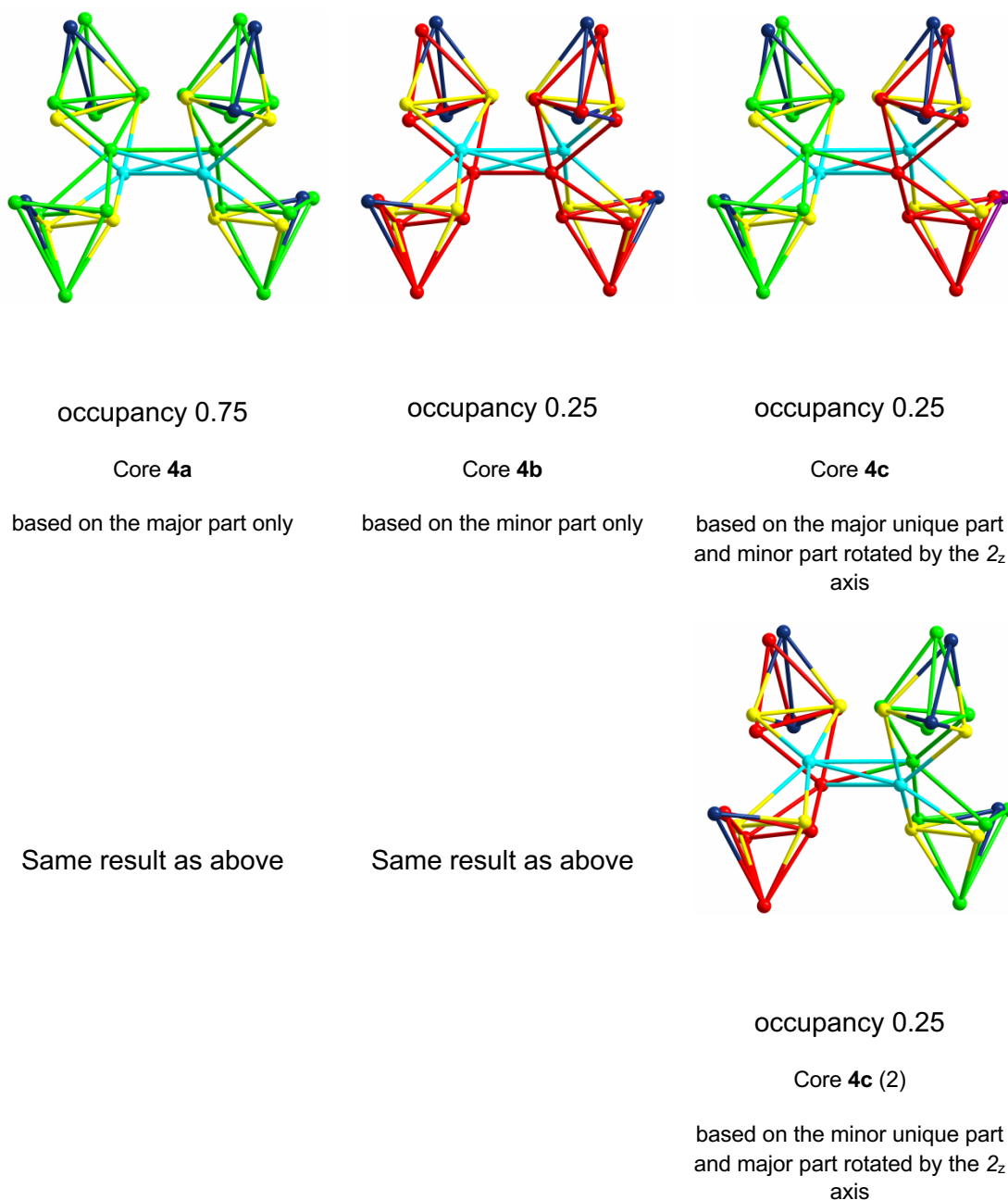


**Figure S3.4.** Possible individual cores of **4** in the disordered structure.

There is no unambiguous interpretation of the structure model, as it is impossible to distinguish if it is either cores **4a** and **4b** co-exist (and have local rotational symmetry as they can be generated by 2-fold axis) or the core **4c** (which has no rotational symmetry) is disordered by the 2-folds axis and co-exists with the core **4a** (Figure S3.5). Obviously, co-existence of **4b** and **4c** is less probable if the occupancies are taken into account.



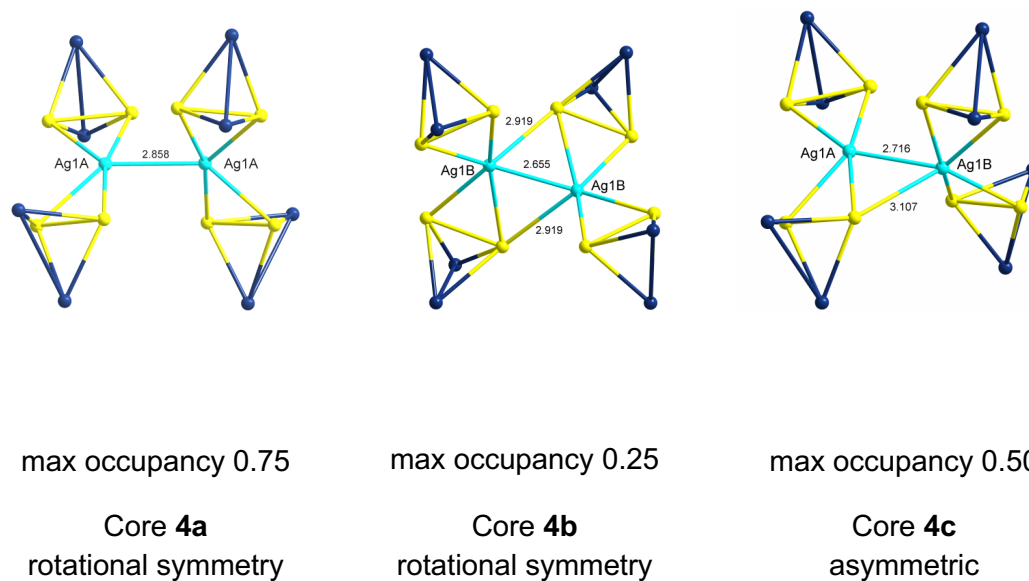


**Figure S3.5.** Possible inorganic cores of the complex **4**.

**Two (simplest) possible situations:** in the crystal structure co-exist different complexes:

Situation 1:  $0.75 \times (\text{Core I}) + 0.25 \times (\text{Core II})$

Situation 2:  $0.5 \times (\text{Core III}) + 0.5 \times (\text{Core I})$

or **any mixture** of all three complexes with a ratio that does not contradict crystallographic occupancies of the atoms. As one of possible examples, the solid solution of  $0.25 \times (\text{core 4a}) + 0.25 \times (\text{core 4b}) + 0.5 \times (\text{core 4c})$  is non-contradicting to the experimental data. More possible compositions can also be devised. Therefore, the answer to the question as to which of these alternatives do really exist, cannot be obtained from the X-ray structural data as the symmetry of the special position hides the initial forms.

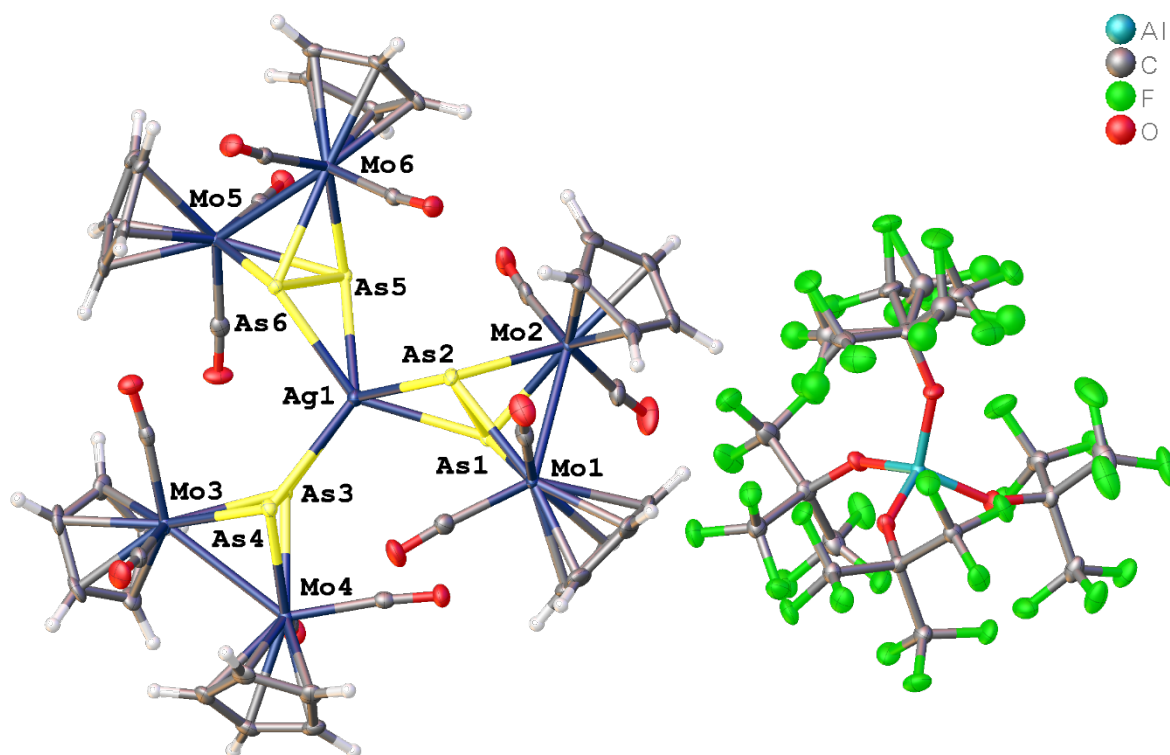


**Figure S3.6.** Molecular structure of the compound **5** (a.d.p. ellipsoids at 50% probability).

**Table S3.4.** Selected geometric parameters ( $\text{\AA}$ ,  $^\circ$ ) for **5**.

Ag1—As6	2.7337 (3)	Mo4—C42	2.332 (3)
Ag1—As1	2.7507 (3)	Mo4—C44	2.342 (3)
Ag1—As3	2.7760 (3)	Mo4—C43	2.371 (3)
Ag1—As2	2.7843 (3)	Mo4—As4	2.5751 (3)
Ag1—As4	2.9053 (3)	Mo4—As3	2.6637 (3)
Ag1—As5	2.9186 (3)	Mo5—C52C	1.973 (3)
Mo1—C12C	1.992 (3)	Mo5—C51C	2.005 (3)
Mo1—C11C	1.993 (3)	Mo5—C51	2.299 (2)
Mo1—C13	2.300 (3)	Mo5—C52	2.318 (2)
Mo1—C12	2.304 (3)	Mo5—C55	2.321 (2)
Mo1—C14	2.328 (3)	Mo5—C53	2.363 (3)
Mo1—C11	2.343 (3)	Mo5—C54	2.372 (2)
Mo1—C15	2.359 (3)	Mo5—As6	2.5621 (3)
Mo1—As1	2.5690 (4)	Mo5—As5	2.6615 (3)
Mo1—As2	2.6496 (3)	Mo5—Mo6	3.0511 (3)
Mo1—Mo2	3.0431 (3)	Mo6—C61C	1.983 (3)
Mo2—C22C	1.987 (3)	Mo6—C62C	1.997 (3)
Mo2—C21C	1.987 (3)	Mo6—C64	2.304 (2)

Mo2—C21	2.291 (3)	Mo6—C63	2.316 (3)
Mo2—C25	2.311 (3)	Mo6—C65	2.346 (3)
Mo2—C22	2.325 (3)	Mo6—C62	2.353 (3)
Mo2—C24	2.355 (3)	Mo6—C61	2.381 (3)
Mo2—C23	2.376 (3)	Mo6—As5	2.5828 (3)
Mo2—As2	2.5750 (3)	Mo6—As6	2.6656 (3)
Mo2—As1	2.6540 (3)	As1—As2	2.3734 (4)
Mo3—C31C	1.982 (3)	As3—As4	2.3572 (4)
Mo3—C32C	1.992 (3)	As5—As6	2.3583 (4)
Mo3—C32	2.298 (3)	O11C—C11C	1.142 (4)
Mo3—C31	2.316 (3)	O12C—C12C	1.148 (4)
Mo3—C33	2.328 (3)	O21C—C21C	1.145 (4)
Mo3—C35	2.357 (3)	O22C—C22C	1.144 (4)
Mo3—C34	2.374 (3)	O31C—C31C	1.150 (3)
Mo3—As3	2.5665 (3)	O32C—C32C	1.148 (4)
Mo3—As4	2.6664 (3)	O41C—C41C	1.138 (3)
Mo3—Mo4	3.0354 (3)	O42C—C42C	1.149 (3)
Mo4—C42C	1.987 (3)	O51C—C51C	1.141 (3)
Mo4—C41C	1.999 (3)	O52C—C52C	1.154 (3)
Mo4—C41	2.303 (3)	O61C—C61C	1.148 (3)
Mo4—C45	2.305 (3)	O62C—C62C	1.143 (3)
As6—Ag1—As1	141.568 (10)	As3—Mo4—Mo3	53.045 (8)
As6—Ag1—As3	108.360 (10)	As6—Mo5—As5	53.635 (9)
As1—Ag1—As3	107.412 (10)	As6—Mo5—Mo6	55.886 (8)
As6—Ag1—As2	101.731 (10)	As5—Mo5—Mo6	53.229 (7)
As1—Ag1—As2	50.778 (8)	As5—Mo6—As6	53.375 (9)
As3—Ag1—As2	145.678 (11)	As5—Mo6—Mo5	55.635 (8)
As6—Ag1—As4	103.923 (10)	As6—Mo6—Mo5	52.730 (7)
As1—Ag1—As4	109.932 (10)	As2—As1—Mo1	64.696 (11)
As3—Ag1—As4	48.961 (8)	As2—As1—Mo2	61.320 (10)
As2—Ag1—As4	108.209 (10)	As2—As1—Ag1	65.344 (10)
As6—Ag1—As5	49.186 (8)	As1—As2—Mo2	64.720 (10)
As1—Ag1—As5	108.649 (10)	As1—As2—Mo1	61.229 (10)
As3—Ag1—As5	103.252 (10)	As1—As2—Ag1	63.878 (10)
As2—Ag1—As5	108.847 (10)	As4—As3—Mo3	65.417 (10)
As4—Ag1—As5	137.923 (10)	As4—As3—Mo4	61.352 (10)
As1—Mo1—As2	54.075 (9)	As4—As3—Ag1	68.380 (10)
As1—Mo1—Mo2	55.675 (8)	As3—As4—Mo4	65.200 (10)
As2—Mo1—Mo2	53.242 (8)	As3—As4—Mo3	61.080 (10)

As2—Mo2—As1	53.960 (9)	As3—As4—Ag1	62.659 (10)
As2—Mo2—Mo1	55.527 (8)	As6—As5—Mo6	65.110 (10)
As1—Mo2—Mo1	53.074 (8)	As6—As5—Mo5	61.026 (10)
As3—Mo3—As4	53.503 (9)	As6—As5—Ag1	61.320 (10)
As3—Mo3—Mo4	56.032 (8)	As5—As6—Mo5	65.339 (10)
As4—Mo3—Mo4	53.219 (8)	As5—As6—Mo6	61.515 (10)
As4—Mo4—As3	53.448 (9)	As5—As6—Ag1	69.494 (10)
As4—Mo4—Mo3	56.031 (8)		

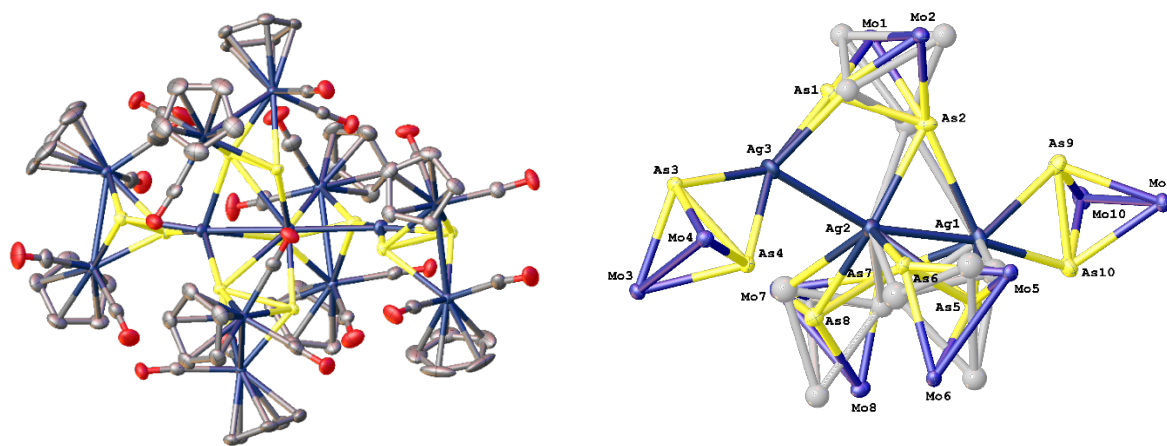


**Figure S3.7.** (left) Molecular structure of the cation of the compound **6** (H atoms are omitted); (right) the disorder of the  $\{Mo_2As_2\}$  units with a ratio of 0.97:0.03 a.d.p. ellipsoids at 50% probability).

**Table S3.5.** Selected geometric parameters (Å) for **6**.

Ag1—As10	2.6709 (3)	Mo1A—As2A	2.537 (15)
Ag1—As5A	2.694 (11)	Mo1A—Mo2A	3.036 (13)
Ag1—As9	2.7340 (3)	Mo2A—As1A	2.542 (15)
Ag1—As5	2.7382 (3)	Mo2A—As2A	2.664 (14)
Ag1—As7	2.7541 (3)	As1A—As2A	2.400 (17)
Ag1—As7A	2.826 (10)	Mo5A—As5A	2.560 (15)
Ag1—Ag2	2.8376 (3)	Mo5A—As6A	2.615 (15)
Ag1—As2	3.0218 (4)	Mo5A—Mo6A	3.057 (13)
Ag1—As2A	3.123 (11)	Mo6A—As5A	2.600 (14)
Ag2—As6A	2.438 (12)	Mo6A—As6A	2.609 (15)
Ag2—As8	2.7204 (3)	As5A—As6A	2.387 (16)
Ag2—As6	2.7513 (3)	Mo7A—As8A	2.553 (14)
Ag2—As2	2.7566 (3)	Mo7A—As7A	2.565 (13)
Ag2—As2A	2.858 (11)	Mo7A—Mo8A	2.989 (12)
Ag2—Ag3	2.9053 (3)	Mo8A—As7A	2.524 (13)
Ag2—As7A	2.942 (10)	Mo8A—As8A	2.594 (14)
Ag2—As8A	2.995 (11)	As7A—As8A	2.321 (15)
Ag2—As7	3.0159 (3)	Mo1—As1	2.5144 (4)
Ag2—As5	3.0225 (3)	Mo1—As2	2.6539 (4)
Ag3—As1	2.4642 (3)	Mo1—Mo2	3.0689 (3)
Ag3—As4	2.5699 (3)	Mo2—As2	2.5635 (3)
Ag3—As1A	2.604 (12)	Mo2—As1	2.6140 (4)
Ag3—As3	2.6519 (3)	Mo5—As6	2.5716 (3)
Mo3—As4	2.5824 (3)	Mo5—As5	2.6271 (3)
Mo3—As3	2.6023 (3)	Mo5—Mo6	3.0641 (3)
Mo3—Mo4	3.1375 (3)	Mo6—As5	2.5636 (3)
Mo4—As3	2.5511 (3)	Mo6—As6	2.6665 (3)
Mo4—As4	2.5940 (3)	Mo7—As7	2.5587 (3)
Mo9—As9	2.5514 (3)	Mo7—As8	2.6519 (3)
Mo9—As10	2.6323 (3)	Mo7—Mo8	3.0465 (3)
Mo9—Mo10	3.0480 (3)	Mo8—As8	2.5792 (3)
Mo10—As10	2.5589 (3)	Mo8—As7	2.6359 (3)
Mo10—As9	2.6304 (3)	As1—As2	2.3748 (4)
As3—As4	2.4585 (3)	As5—As6	2.3693 (4)
As9—As10	2.3968 (4)	As7—As8	2.3738 (4)
Mo1A—As1A	2.536 (16)		

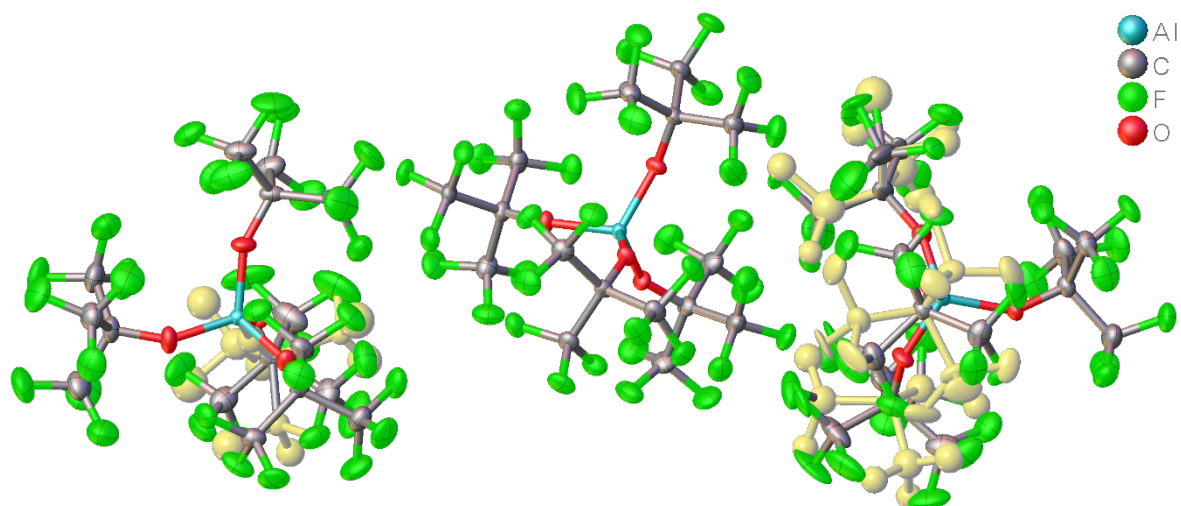


**Figure S3.8.** The TEF anions (disordered groups are shown in pale yellow) in the structure of the compound **6** (a.d.p. ellipsoids at 50% probability).

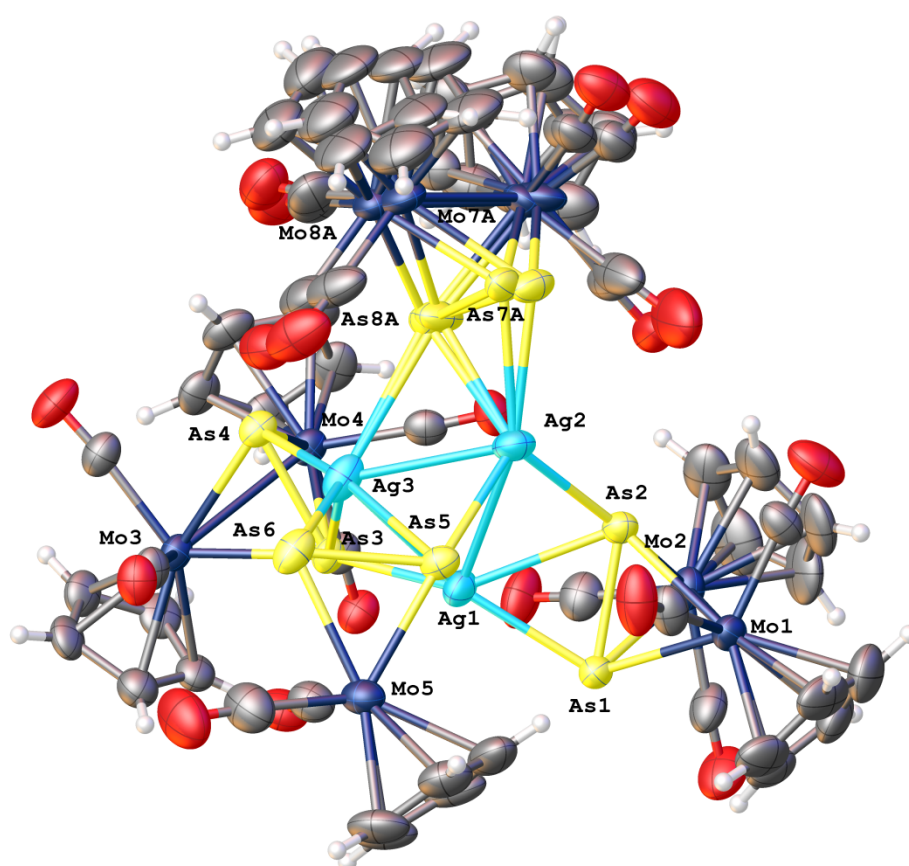


**Figure S3.9.** The structure of the cationic complex in the compound **7** (a.d.p. ellipsoids at 50% probability).

**Table S3.6.** Selected geometric parameters (Å) for **7**.

Ag1—Ag3	2.8904 (8)	Mo1—Mo2	3.0627 (9)
Ag1—Ag2	2.9800 (8)	Mo1—As2	2.6069 (9)
Ag1—As3	2.5738 (8)	Mo1—As1	2.5643 (10)
Ag1—As2	2.7923 (9)	Mo2—As2	2.5357 (10)
Ag1—As1	2.6133 (9)	Mo2—As1	2.6413 (10)
Mo3—Mo4	3.0759 (8)	Mo5—As5	2.5566 (10)
Mo3—As3	2.5424 (9)	Mo5—As6	2.6267 (11)
Mo3—As4	2.6345 (10)	As3—As4	2.4066 (10)
Ag3—Ag2	2.8625 (9)	Mo7A—As8A	2.540 (9)
Ag3—As3	2.8582 (9)	Mo7A—Mo8A	3.064 (7)
Ag3—As4	2.6054 (9)	Mo7A—As7A	2.649 (5)
Ag3—As5	2.8190 (9)	As2—As1	2.4095 (11)
Ag3—As8A	2.989 (8)	As5—As6	2.4066 (12)
Ag3—As6	2.6312 (11)	As8A—Mo8A	2.596 (7)
Ag2—As2	2.6718 (10)	As8A—As7A	2.378 (5)
Ag2—As5	2.7041 (10)	Mo8A—As7A	2.529 (4)
Ag2—As8A	2.737 (7)	Mo8B—As7B	2.579 (5)
Ag2—As7A	2.730 (5)	Mo8B—Mo7B	3.029 (8)
Ag2—As7B	2.680 (4)	Mo8B—As8B	2.627 (9)
Ag2—As8B	2.683 (9)	As7B—Mo7B	2.585 (5)
Mo4—As3	2.6042 (9)	As7B—As8B	2.365 (6)
Mo4—As4	2.5564 (9)	Mo7B—As8B	2.550 (11)

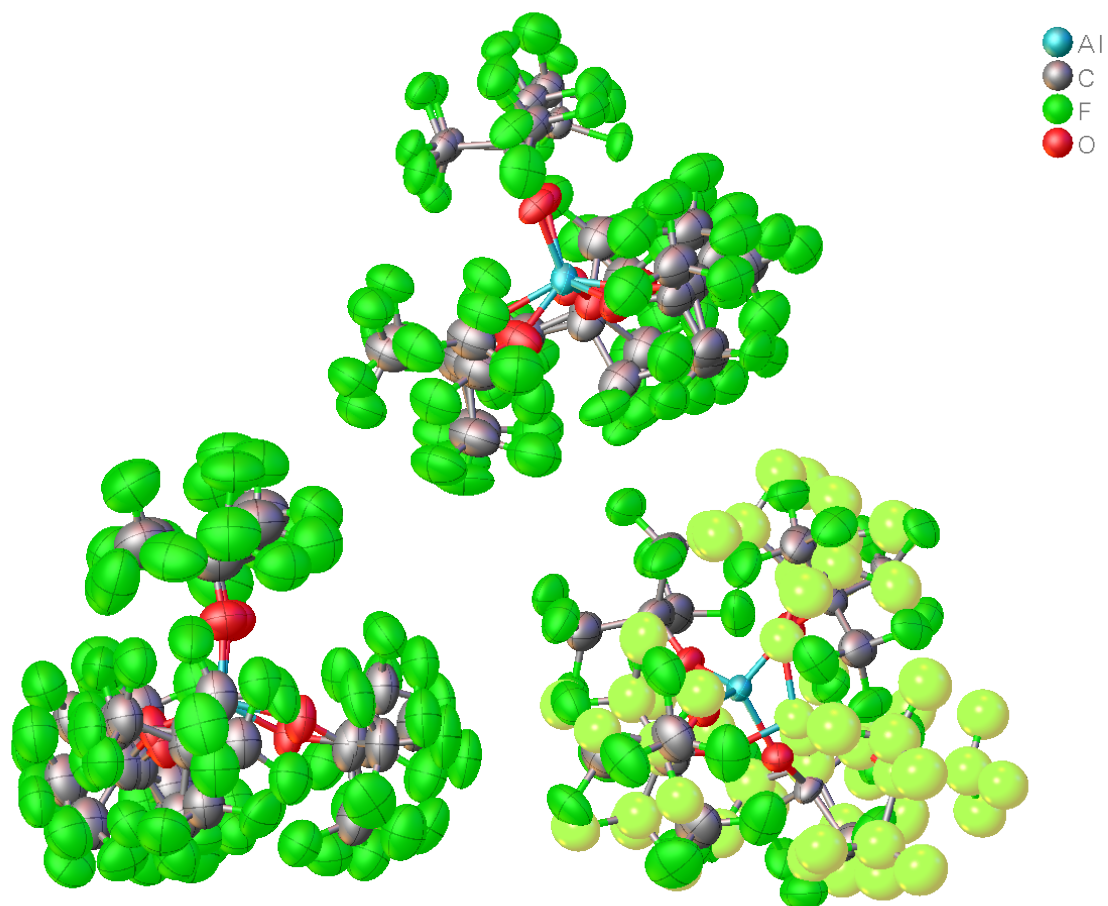


**Figure S3.10.** The TEF anions (disordered groups are shown in pale yellow) in the structure of the compound 7 (a.d.p. ellipsoids at 50% probability).

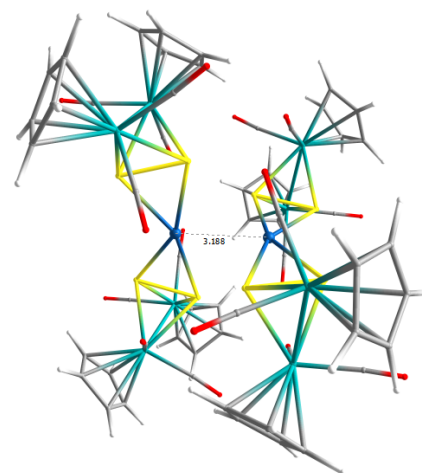


### 3.4.7 DFT Calculations

The DFT calculations have been performed with Gaussian 09<sup>24</sup> at the  $\omega$ B97XD<sup>25</sup> functional together with the def2-SVP<sup>26</sup> basis set. For the calculation of reaction energies, the SCF energies were used without corrections for zero point vibrations.

**Table S3.7.** Cartesian coordinates of the gas-phase optimized geometry of  $[\{(\text{Cp}(\text{CO})_2\text{Mo})_2(\text{As}_2)\}_4\text{Ag}_2]^{2+}$  at the  $\omega$ B97XD/def2-SVP level of theory.  $E = -22083.8841414$  Hartree.

Atom	x	y	z
Ag	-0.000866000	-1.594029000	-0.026443000
Ag	0.000866000	1.594029000	-0.026443000
As	1.515199000	-3.335603000	-1.450448000
As	1.940414000	-1.007319000	-1.853091000
As	-1.485453000	-3.253201000	1.573342000
As	-1.989238000	-0.908669000	1.693120000
Mo	4.011374000	-2.496227000	-1.554668000
Mo	2.028208000	-2.703223000	-3.871395000
Mo	-3.977864000	-2.658945000	1.536702000
Mo	-2.108387000	-2.198671000	3.906483000
As	-1.515199000	3.335603000	-1.450448000
As	-1.940414000	1.007319000	-1.853091000
As	1.485453000	3.253201000	1.573342000
As	1.989238000	0.908669000	1.693120000
Mo	-4.011374000	2.496227000	-1.554668000
Mo	-2.028208000	2.703223000	-3.871395000
Mo	3.977864000	2.658945000	1.536702000
Mo	2.108387000	2.198671000	3.906483000
C	2.137965000	1.836553000	6.160565000
H	1.446672000	2.321408000	6.846963000
C	3.436039000	2.309748000	5.803808000
H	3.895788000	3.228895000	6.163348000
C	4.049441000	1.343001000	4.964910000
H	5.061819000	1.392809000	4.574991000
C	3.133166000	0.269675000	4.782761000
H	3.312079000	-0.644116000	4.219765000
C	1.958637000	0.570148000	5.523407000
H	1.102040000	-0.089282000	5.628433000



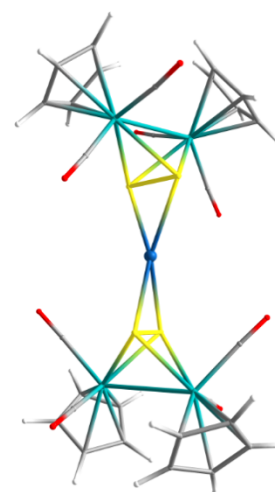
C	-4.035706000	4.483947000	-1.476566000
	-4.140102000	5.625976000	-1.439355000
C	2.039701000	4.173861000	4.147826000
O	2.020450000	5.298045000	4.371097000
O	-3.506698000	2.412349000	1.534924000
O	0.835362000	1.492291000	-4.203163000
O	-3.329851000	0.104952000	-5.050037000
O	-1.014673000	2.140633000	4.055659000
O	3.671416000	1.982062000	-1.499321000
C	4.791278000	0.897744000	1.940526000
O	5.365354000	-0.068671000	2.183406000
C	-3.663634000	2.454078000	0.399227000
C	-5.672044000	0.961928000	-1.128553000
H	-5.614794000	0.251313000	-0.309565000
C	-6.233031000	2.276416000	-1.062093000
H	-6.690288000	2.740207000	-0.190582000
C	-6.161403000	2.836110000	-2.371345000
H	-6.541719000	3.813383000	-2.664713000
C	-5.564384000	1.882530000	-3.235458000
H	-5.417659000	1.997185000	-4.305624000
C	-5.254702000	0.725909000	-2.464895000
H	-4.816164000	-0.194462000	-2.842525000
C	-0.223648000	1.906145000	-4.050847000
C	-2.834605000	1.016441000	-4.563595000
C	-3.368750000	4.510205000	-4.607539000
H	-4.335878000	4.788716000	-4.198830000
C	-3.146476000	3.614524000	-5.685412000
H	-3.915933000	3.085321000	-6.245211000
C	-1.746838000	3.580772000	-5.960551000
H	-1.266107000	3.038048000	-6.771746000
C	-1.106409000	4.462432000	-5.033525000
H	-0.044126000	4.697235000	-5.003289000
C	-2.108387000	5.029717000	-4.199787000
H	-1.950632000	5.777757000	-3.425804000
C	0.128432000	2.179253000	3.960998000
C	3.753381000	2.181520000	-0.371441000
C	4.335219000	4.963335000	1.855081000

H	3.550494000	5.711708000	1.942721000
C	4.968597000	4.289587000	2.937328000
H	4.759019000	4.437565000	3.992551000
C	5.977552000	3.447856000	2.400934000
H	6.667555000	2.832619000	2.975993000
C	5.983246000	3.601909000	0.982584000
H	6.685846000	3.143380000	0.289874000
C	4.961357000	4.545535000	0.650231000
H	4.735621000	4.919792000	-0.346645000
C	-2.137965000	-1.836553000	6.160565000
H	-1.446672000	-2.321408000	6.846963000
C	-3.436039000	-2.309748000	5.803808000
H	-3.895788000	-3.228895000	6.163348000
C	-4.049441000	-1.343001000	4.964910000
H	-5.061819000	-1.392809000	4.574991000
C	-3.133166000	-0.269675000	4.782761000
H	-3.312079000	0.644116000	4.219765000
C	-1.958637000	-0.570148000	5.523407000
H	-1.102040000	0.089282000	5.628433000
C	4.035706000	-4.483947000	-1.476566000
O	4.140102000	-5.625976000	-1.439355000
C	-2.039701000	-4.173861000	4.147826000
O	-2.020450000	-5.298045000	4.371097000
O	3.506698000	-2.412349000	1.534924000
O	-0.835362000	-1.492291000	-4.203163000
O	3.329851000	-0.104952000	-5.050037000
O	1.014673000	-2.140633000	4.055659000
O	-3.671416000	-1.982062000	-1.499321000
C	-4.791278000	-0.897744000	1.940526000
O	-5.365354000	0.068671000	2.183406000
C	3.663634000	-2.454078000	0.399227000
C	5.672044000	-0.961928000	-1.128553000
H	5.614794000	-0.251313000	-0.309565000
C	6.233031000	-2.276416000	-1.062093000
H	6.690288000	-2.740207000	-0.190582000
C	6.161403000	-2.836110000	-2.371345000
H	6.541719000	-3.813383000	-2.664713000

C	5.564384000	-1.882530000	-3.235458000
H	5.417659000	-1.997185000	-4.305624000
C	5.254702000	-0.725909000	-2.464895000
H	4.816164000	0.194462000	-2.842525000
C	0.223648000	-1.906145000	-4.050847000
C	2.834605000	-1.016441000	-4.563595000
C	3.368750000	-4.510205000	-4.607539000
H	4.335878000	-4.788716000	-4.198830000
C	3.146476000	-3.614524000	-5.685412000
H	3.915933000	-3.085321000	-6.245211000
C	1.746838000	-3.580772000	-5.960551000
H	1.266107000	-3.038048000	-6.771746000
C	1.106409000	-4.462432000	-5.033525000
H	0.044126000	-4.697235000	-5.003289000
C	2.108387000	-5.029717000	-4.199787000
H	1.950632000	-5.777757000	-3.425804000
C	-0.128432000	-2.179253000	3.960998000
C	-3.753381000	-2.181520000	-0.371441000
C	-4.335219000	-4.963335000	1.855081000
H	-3.550494000	-5.711708000	1.942721000
C	-4.968597000	-4.289587000	2.937328000
H	-4.759019000	-4.437565000	3.992551000
C	-5.977552000	-3.447856000	2.400934000
H	-6.667555000	-2.832619000	2.975993000
C	-5.983246000	-3.601909000	0.982584000
H	-6.685846000	-3.143380000	0.289874000
C	-4.961357000	-4.545535000	0.650231000
H	-4.735621000	-4.919792000	-0.346645000

**Table S3.8.** Cartesian coordinates of the gas-phase optimized geometry of  $\{[(\text{Cp}(\text{CO})_2\text{Mo})_2(\text{As}_2)]_2\text{Ag}\}^{1+}$  at the  $\omega\text{B97XD/def2-SVP}$  level of theory.  $E = -11041.940186$  Hartree.

Atom	x	y	z
Ag	-0.001021000	-0.000373000	-0.000068000
As	-2.389062000	0.689827000	0.979702000
As	-2.389157000	-0.690014000	-0.979720000
As	2.388013000	-0.507348000	1.085472000
As	2.388002000	0.507102000	-1.085535000
Mo	-4.110070000	-1.297193000	0.812890000
Mo	-4.109837000	1.297286000	-0.812948000
Mo	4.110057000	1.352855000	0.722413000
Mo	4.110387000	-1.352761000	-0.722338000
C	5.439321000	-2.757969000	-1.939482000
H	5.424200000	-3.826150000	-1.800533000
C	6.303621000	-1.838899000	-1.283998000
H	7.049807000	-2.093328000	-0.548626000
C	6.056987000	-0.547839000	-1.803828000
H	6.582604000	0.352158000	-1.537103000
C	5.030178000	-0.655264000	-2.775011000
H	4.637282000	0.152315000	-3.369879000
C	4.648856000	-2.014941000	-2.862652000
H	3.915319000	-2.420661000	-3.540100000
C	-4.597070000	-0.220722000	2.413801000
O	-4.948873000	0.339837000	3.344968000
C	4.602556000	-2.200638000	1.009759000
O	4.957763000	-2.726334000	1.959653000
O	-1.825962000	-2.664274000	2.455528000
O	-1.825444000	2.664102000	-2.455410000
O	-4.949052000	-0.339771000	-3.344871000
O	1.829594000	-3.463927000	-1.071768000
O	1.828835000	3.463587000	1.071682000
C	4.602211000	2.200817000	-1.009642000
O	4.957454000	2.726608000	-1.959471000
C	-2.636072000	-2.127611000	1.861583000
C	-4.647424000	-3.479372000	0.304268000
H	-3.909407000	-4.264748000	0.305450000
C	-5.429545000	-3.062832000	1.419839000
H	-5.404108000	-3.486511000	2.409983000
C	-6.303793000	-2.037931000	0.967480000
H	-7.045893000	-1.535027000	1.566606000
C	-6.069732000	-1.829034000	-0.410380000
H	-6.605868000	-1.146293000	-1.045986000
C	-5.042368000	-2.715990000	-0.819696000
H	-4.657119000	-2.817376000	-1.820632000
C	-2.635695000	2.127467000	-1.861632000
C	-4.596974000	0.220906000	-2.413879000
C	-6.069430000	1.829426000	0.410297000
H	-6.605688000	1.146764000	1.045887000
C	-6.303438000	2.038376000	-0.967564000
H	-7.045611000	1.535597000	-1.566705000
C	-5.429025000	3.063146000	-1.419899000
H	-5.403507000	3.486834000	-2.410038000
C	-4.646852000	3.479548000	-0.304312000
H	-3.908715000	4.264810000	-0.305475000
C	-5.041935000	2.716218000	0.819638000
H	-4.656689000	2.817537000	1.820582000
C	2.638969000	-2.678678000	-0.909237000
C	2.638360000	2.678489000	0.909169000
C	5.029821000	0.655638000	2.775198000
H	4.637012000	-0.151966000	3.370089000
C	6.056711000	0.548311000	1.804090000
H	6.582485000	-0.351622000	1.537453000
C	6.303174000	1.839375000	1.284189000
H	7.049373000	2.093874000	0.548853000
C	5.438679000	2.758352000	1.939550000
H	5.423392000	3.826521000	1.800530000
C	4.648271000	2.015260000	2.862716000
H	3.914628000	2.420909000	3.540092000



### 3.5 References

- [1] a) T. L. Mako, J. M. Racicot, M. Levine, *Chem. Rev.* **2019**, *119*, 322-477; b) M.-M. Gan, J.-Q. Liu, L. Zhang, Y.-Y. Wang, F. E. Hahn, Y.-F. Han, *Chem. Rev.* **2018**, *118*, 9587-9641; c) Y. Lu, H.-N. Zhang, G.-X. Jin, *Acc. Chem. Res.* **2018**, *51*, 2148-2158; d) C. Lescop, *Acc. Chem. Res.* **2017**, *50*, 885-894; e) T. R. Cook, P. Stang, *Chem. Rev.* **2015**, *115*, 7001-7045; f) M. Han, D. M. Engelhard, G. H. Clever, *Chem. Soc. Rev.* **2014**, *43*, 1848-1860; g) K. Harris, D. Fujita, M. Fujita, *Chem. Commun.* **2013**, *49*, 6703-6712; h) M. M. J. Smulders, I. A. Riddell, C. Browne, J. R. Nitschke, *Chem. Soc. Rev.* **2013**, *42*, 1728-1754.
- [2] a) T. R. Cook, Y. -R. Zheng, P. J. Stang, *Chem. Rev.* **2013**, *113*, 734-777; b) S. Park, S. Y. Lee, K.-M. Park, S. S. Lee, *Acc. Chem. Res.* **2012**, *3*, 391-403; c) R. Chakrabarty, P. S. Mukherjee, P. J. Stang, *Chem. Rev.* **2011**, *111*, 6810-6918; d) K.-M. Park, I. Yoon, J. Seo, J.-E. Lee, J. Kim, K. S. Choi, O.-S. Jung, S. S. Lee, *Cryst. Growth Des.* **2005**, *5*, 1707-1709.
- [3] a) K. Škoch, I. Císařová, J. Schulz, U. Siemeling, P. Štěpnička, *Dalton Trans.* **2017**, *46*, 10339-10354. b) J. Moussa, K. M.-C. Wong, X. F. Le Goff, M. N. Rager, C. K.-M. Chan, V. W.-W. Yam, H. Amouri, *Organometallics* **2013**, *32*, 4985-4992; c) K.-J. Wei, J. Ni, Y. Liu, *Inorg. Chem.* **2010**, *49*, 1834-1848; d) J. Moussa, H. Amouri, *Angew. Chem. Int. Ed.* **2008**, *47*, 1372-1380.
- [4] a) K. H. Whitmire, *Coord. Chem. Rev.* **2018**, *376*, 114-195; b) M. Scheer, *Dalton Trans.* **2008**, 4372-4386.
- [5] a) M. E. Moussa, M. Fleischmann, E. V. Peresykina, L. Dütsch, M. Seidl, G. Balázs, M. Scheer, *Eur. J. Inorg. Chem.* **2017**, *25*, 3222-3226; b) C. Heindl, E. Peresykina, D. Lüdeker, G. Bruncklaus, A. V. Virovets, M. Scheer, *Chem. Eur. J.* **2016**, *22*, 2599-2604; c) M. Fleischmann, S. Welsch, E. V. Peresykina, A. V. Virovets, M. Scheer, *Chem. Eur. J.* **2015**, *21*, 14332-14336; d) F. Dielmann, C. Heindl, F. Hastreiter, E. V. Peresykina, A. V. Virovets, R. M. Gschwind, M. Scheer, *Angew. Chem. Int. Ed.* **2014**, *53*, 13605-13608; e) M. Scheer, L. J. Gregoriades, A. V. Virovets, W. Kunz, R. Neueder, I. Krossing, *Angew. Chem. Int. Ed.* **2006**, *45*, 5689-5693; f) J. Bai, A. V. Virovets, M. Scheer, *Angew. Chem. Int. Ed.* **2002**, *41*, 1737-1740.
- [6] a) E. Peresykina, C. Heindl, A. Virovets, H. Brake, E. Mädl, M. Scheer, *Chem. Eur. J.* **2018**, *24*, 2503-2508; b) C. Heindl, E. Peresykina, A. V. Virovets, I. S. Bushmarinov, M. G. Medvedev, B. Krämer, B. Dittrich, M. Scheer, *Angew. Chem. Int. Ed.* **2017**, *43*, 13237-13243; c) E. Peresykina, C. Heindl, A. Virovets, M. Scheer, *Inorganic Superspheres*. In: Dehnen S. (eds) *Clusters – Contemporary*

- Insight in Structure and Bonding. *Structure and Bonding* **2016**, 174, 321-373; d) C. Heindl, E. V. Peresyphkina, A. V. Virovets, W. Kremer, M. Scheer, *J. Am. Chem. Soc.* **2015**, 137, 10938-10941; e) F. Dielmann, C. Heindl, F. Hastreiter, E. V. Peresyphkina, A. V. Virovets, R. M. Gschwind, M. Scheer, *Angew. Chem. Int. Ed.* **2014**, 53, 13605-13608; f) M. Scheer, A. Schindler, R. Merkle, B. P. Johnson, M. Linseis, R. Winter, C. E. Anson, A. V. Virovets, *J. Am. Chem. Soc.* **2007**, 129, 13386-13387; g) J. Bai, A. V. Virovets, M. Scheer, *Science* **2003**, 300, 781-783.
- [7] H. Brake, E. Peresyphkina, C. Heindl, A. V. Virovets, W. Kremer, M. Scheer, *Chem. Sci.* **2019**, 10, 2940-2944.
- [8] S. Welsch, C. Gröger, M. Sierka, M. Scheer, *Angew. Chem. Int. Ed.* **2011**, 50, 1435-1438.
- [9] a) O. J. Scherer, J. Schwalb, H. Sitzmann, *Inorg. Synth.* **1990**, 27, 224-227; b) O. J. Scherer, H. Sitzmann, G. Wolmershäuser, *J. Organomet. Chem.* **1984**, 268, C9-C12.
- [10] a) M. E. Moussa, E. Peresyphkina, A. V. Virovets, D. Venus, G. Balázs, M. Scheer, *CrystEngComm.* **2018**, 20, 7417-7422; b) B. Attenberger, S. Welsch, M. Zabel, E. Peresyphkina, M. Scheer, *Angew. Chem. Int. Ed.* **2011**, 50, 11516-11519.
- [11] a) O. J. Scherer, C. Blath, G. Wolmershäuser, *J. Organomet. Chem.* **1990**, 387, C21-C24; b) K. Blechschmitt, H. Pfisterer, T. Zahn, M. Ziegler, *Angew. Chem. Int. Ed.* **1985**, 24, 66-67; c) P. J. Sullivan and A. L. Rheingold, *Organometallics* **1982**, 1, 1547-1549.
- [12] a) C. Schwarzmaier, M. Sierka, M. Scheer, *Angew. Chem. Int. Ed.* **2013**, 52, 858-861; b) H. Krauss, G. Balázs, M. Bodensteiner, M. Scheer, *Chem. Sci.* **2010**, 1, 337-342; c) M. Scheer, L. J. Gregoriades, A. V. Virovets, W. Kunz, R. Neueder, I. Krossing, *Angew. Chem. Int. Ed.* **2006**, 45, 5689-5693; d) L. J. Gregoriades, H. Krauss, J. Wachter, A. V. Virovets, M. Sierka, M. Scheer, *Angew. Chem. Int. Ed.* **2006**, 45, 4189-4192; e) D. Fenske, F. Simon, *Z. Anorg. Allg. Chem.* **1996**, 622, 45-52.
- [13] R. Meijboom, R. J. Bowen, S. J. Berners-Price, *Coord. Chem. Rev.* **2009**, 253, 325-342.
- [14] A. N. Khlobystov, A. J. Blake, N. R. Champness, D. A. Lemenovskii, A. G. Majouga, N. V. Zyk, M. Schröder, *Coord. Chem. Rev.* **2001**, 222, 155-192;
- [15] J.-D. Chai, M. Head-Gordon, *Phys. Chem. Chem. Phys.* **2008**, 10, 6615-6620. H. Schmidbaur, A. Schier, *Angew. Chem. Int. Ed.* **2015**, 54, 746-784.
- [16] C. R. Groom, I. J. Bruno, M. P. Lightfoot, S. C. Ward, *Acta Cryst.* **2016**, B72, 171-179.
- [17] H. Schmidbaur, A. Schier, *Angew. Chem. Int. Ed.* **2015**, 54, 746-784.

- [18] O. J. Scherer, C. Blath, G. Wolmershäuser, *J. Organomet. Chem.* **1990**, *387*, C21-C24.
- [19] T. Köchner, N. Trapp, T. A. Engesser, A. J. Lehner, C. Röhr, S. Riedel, C. Knapp, H. Scherer, I. Krossing, *Angew. Chem. Int. Ed.* **2011**, *50*, 11253-11256; *Angew. Chem.* **2011**, *123*, 11449-11452.
- [20] I. Krossing, *Chem. Eur. J.* **2001**, *7*, 490-502.
- [21] *CrysAlisPRO*, different versions 2006-2020, Rigaku Oxford Diffraction.
- [22] O.V. Dolomanov, L.J. Bourhis, R.J. Gildea, J.A.K. Howard, H. Puschmann, *J. Appl. Cryst.* **2009**, *42*, 339-341.
- [23] G. M. Sheldrick. *Acta Cryst.* (**2015**). C71, 3-8.
- [24] Gaussian 09, Revision E.01, M. J. Frisch, G. W. Trucks, H. B. Schlegel, G. E. Scuseria, M. A. Robb, J. R. Cheeseman, G. Scalmani, V. Barone, B. Mennucci, G. A. Petersson, H. Nakatsuji, M. Caricato, X. Li, H. P. Hratchian, A. F. Izmaylov, J. Bloino, G. Zheng, J. L. Sonnenberg, M. Hada, M. Ehara, K. Toyota, R. Fukuda, J. Hasegawa, M. Ishida, T. Nakajima, Y. Honda, O. Kitao, H. Nakai, T. Vreven, J. A. Montgomery, Jr., J. E. Peralta, F. Ogliaro, M. Bearpark, J. J. Heyd, E. Brothers, K. N. Kudin, V. N. Staroverov, T. Keith, R. Kobayashi, J. Normand, K. Raghavachari, A. Rendell, J. C. Burant, S. S. Iyengar, J. Tomasi, M. Cossi, N. Rega, J. M. Millam, M. Klene, J. E. Knox, J. B. Cross, V. Bakken, C. Adamo, J. Jaramillo, R. Gomperts, R. E. Stratmann, O. Yazyev, A. J. Austin, R. Cammi, C. Pomelli, J. W. Ochterski, R. L. Martin, K. Morokuma, V. G. Zakrzewski, G. A. Voth, P. Salvador, J. J. Dannenberg, S. Dapprich, A. D. Daniels, O. Farkas, J. B. Foresman, J. V. Ortiz, J. Cioslowski, and D. J. Fox, Gaussian, Inc., Wallingford CT, **2013**.
- [25] J.-D. Chai, M. Head-Gordon, *Phys. Chem. Chem. Phys.* **2008**, *10*, 6615-6620.
- [26] a) F. Weigend, M. Häser, H. Patzelt, R. Ahlrichs, *Chem. Phys. Letters* **1998**, *294*, 143-152; b) F. Weigend, R. Ahlrichs, *Phys. Chem. Chem. Phys.* **2005**, *7*, 3297-3305; c) F. Weigend, *Phys. Chem. Chem. Phys.* **2006**, *8*, 1057-1065.





## **Preface**

## **Authors**

Jana Schiller,<sup>†</sup> Mehdi Elsayed Moussa,<sup>†</sup> Michael Seidl and Manfred Scheer\*

## **Author contributions**

Jana Schiller and Mehdi Elsayed Moussa contributed equally to this work. The first preparation of compounds **1-3** and **5** was done by Mehdi Elsayed Moussa. The syntheses of compounds **4** and **6**, as well as the reproduction and characterization of compounds **1-3** and **5** was done by Jana Schiller. The preparation of the manuscript was mainly done by Jana Schiller. Michael Seidl has done the X-ray structural characterization of all compounds. Manfred Scheer supervised the research and revised the manuscript prior to publication.

## **Acknowledgements**

This work was supported by the European Research Council (Grant ERC-2013-AdG 339072)

## 4. Discrete and Polymeric Organometallic-Organic Assemblies Based on the Diarsene Complex $[(C_5H_5)_2Mo_2(CO)_4(\mu,\eta^2-As_2)]$ , $AgPF_6$ and Organic N-donor Molecules

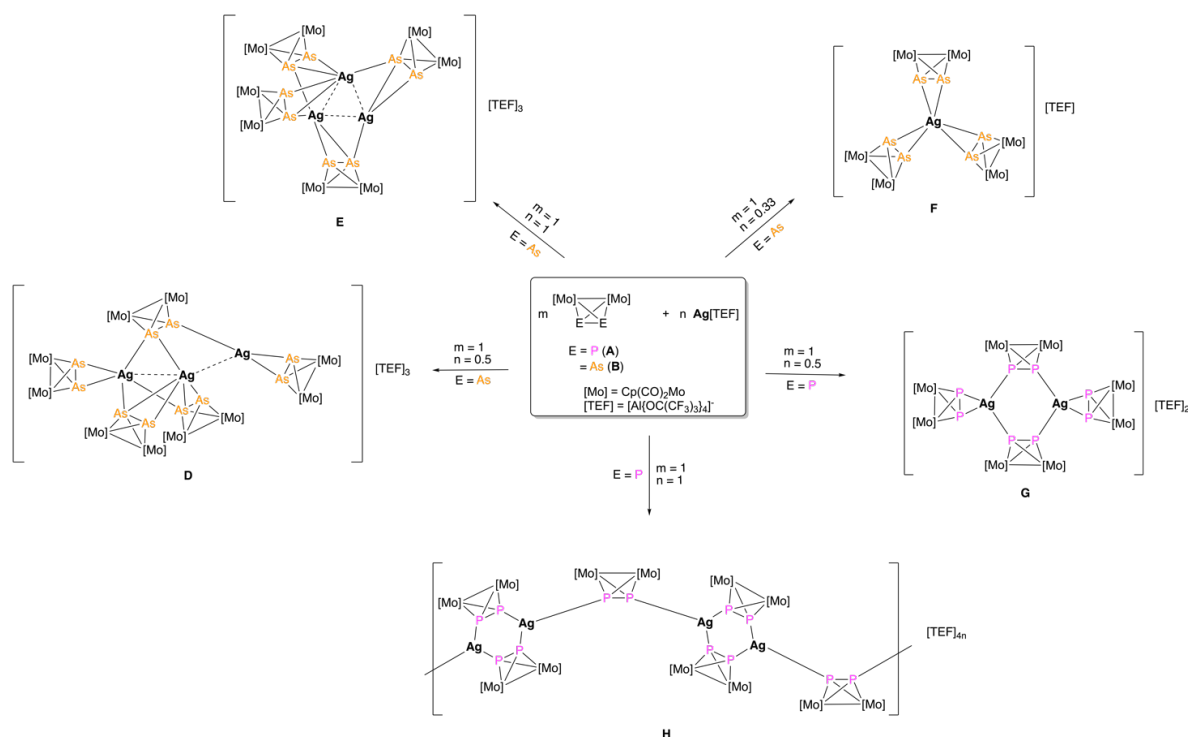
**Abstract:** The three component reactions of the organometallic diarsene complex  $[Cp_2Mo_2(CO)_4(\mu,\eta^2-As_2)]$  (**B**) ( $Cp = C_5H_5$ ) with  $AgPF_6$  in the presence of N-donor linkers 1,2-di(4-pyridyl)ethylene (**L**<sub>1</sub>), 1,2-di(4-pyridyl)ethyne (**L**<sub>2</sub>), 2,2'-bipyrimidine (**L**<sub>3</sub>), 1,3-di(4-pyridyl)propane (**L**<sub>4</sub>) and 4,4'-bipyridine (**L**<sub>5</sub>) are studied. Depending on the organic linker used, a variety of new coordination compounds are accessible: the novel dicationic molecular organometallic-organic hybrid complexes  $\{[(\eta^2-B)_2Ag]_2(\mu-L_1)\}[PF_6]_2$  (**1**) and  $\{[(\eta^2-B)_2Ag]_2(\mu-L_2)\}[PF_6]_2$  (**2**), as well as the one-dimensional organometallic-organic hybrid polymers  $\{[(\eta^2-B)Ag](\mu-L_3)\}_n[PF_6]_{2n}$  (**3**),  $\{[(\eta^1:\eta^2-B)_2(CH_3CN)_2Ag_2](\mu-L_4)\}_n[PF_6]_{2n}$  (**4**),  $\{[(\eta^1:\eta^2-B)_2(\eta^1:\eta^1-B)Ag_2](\mu-L_5)\}_n[PF_6]_{2n}$  (**5**) and  $\{[(\eta^1:\eta^2-B)_2(CH_3CN)_2Ag_2](\mu-L_5)\}_n[PF_6]_{2n}$  (**6**). All compounds **1-6** were characterized by X-ray crystallography. Compounds **4-6** have unique solid-state structures in which the organometallic diarsene complex **B** and organic dipyridine units cooperate together as linkers between Ag(I) ions.

### 4.1 Introduction

The design of Ag(I) complexes represent an interesting research area because of their rich structural diversity and wide range of applications.<sup>1</sup> This diversity is due to the flexible coordination sphere of the Ag(I) ion on one hand which can adopt various coordination geometries (linear, trigonal planar, tetrahedral, square-planar, trigonal bipyramidal, etc...)<sup>2</sup> And on the other hand due to its ability to coordinate a variety of multitopic organic ligands bearing mainly N-, O-, S- or P- and minorly Se-, C-, As- or mixed-donor atoms.<sup>3</sup> However, only few examples of organometallic building blocks have been used as ligands to stabilize Ag(I) centers.<sup>4</sup> Due to the lack of such investigations, our group focuses on studying the potential of organometallic polyphosphorus ( $P_n$ ) and polyarsenic ( $As_n$ ) complexes with flexible coordination modes as connectors between metal ions.<sup>5</sup> This novel approach allowed for the synthesis of a large variety of discrete and extended supramolecular aggregates including 1D, 2D and 3D coordination polymers (CPs),<sup>5a,b,d-g</sup> inorganic nanospheres,<sup>6</sup> and nanosized capsules.<sup>7</sup> Furthermore, we investigated the possibility of conducting reactions in which both organic molecules and organometallic complexes are used together to link metal

centers.<sup>8</sup> Within this field, the most studied compound is the diphosphorus complex [Cp<sub>2</sub>Mo<sub>2</sub>(CO)<sub>4</sub>(μ,η<sup>2</sup>-P<sub>2</sub>)] (Cp = C<sub>5</sub>H<sub>5</sub>, **A**). Its reaction with Ag(I) or Cu(I) salts in the presence of a variety of ditopic pyridine-based linkers allowed for the formation of unprecedented solid state organometallic-organic hybrid polymers.<sup>8a-9</sup> Interestingly, such reactions with Ag(I) ions can be performed in two ways: *i*) either in one step three component reactions by mixing all starting materials together under certain experimental conditions<sup>8e,9</sup> or *ii*) in two step reactions in which the first step involves the preparation of a preorganized precursor composed of the Ag(I) ions and the P<sub>2</sub> ligand complex and the second step involves the reaction of this precursor with the N-donor organic molecules.<sup>8c,d</sup>

More recently, we became interested in studying the supramolecular chemistry of similar molybdenum complexes bearing unsubstituted heavier homo- and heterodiatom group 15 elements as connectors between metal ions. For example the diarsene complex [Cp<sub>2</sub>Mo<sub>2</sub>(CO)<sub>4</sub>(μ,η<sup>2</sup>-As<sub>2</sub>)] (**B**) was reacted with the Ag(I) salt of the weakly coordinating anion [Al{OC(CF<sub>3</sub>)<sub>3</sub>}<sub>4</sub>]<sup>-</sup> ([TEF]<sup>-</sup>) allowing the synthesis of first compounds [(μ,η<sup>1</sup>:η<sup>2</sup>-**B**)<sub>3</sub>(η<sup>2</sup>-**B**)<sub>2</sub>Ag<sub>3</sub>][TEF]<sub>3</sub> (**D**) and [(μ,η<sup>1</sup>:η<sup>2</sup>-**B**)<sub>4</sub>Ag<sub>3</sub>][TEF]<sub>3</sub> (**E**) containing [Ag(I)]<sub>3</sub> units stabilized by organometallic bichelating ligands and [(μ,η<sup>1</sup>-**B**)<sub>3</sub>Ag][TEF] (**F**) (Scheme 4.1).<sup>9</sup> Within the compounds **D** and **E**, the complex **B** was found to possess either an η<sup>2</sup>- or an η<sup>1</sup>:η<sup>2</sup>-coordination mode. These results were particularly interesting considering the fact that similar reactions from the P<sub>2</sub> analogue complex **A** and Ag[TEF] yield totally different products: the Ag(I) dimers of the general formula [Ag<sub>2</sub>(η<sup>2</sup>-**A**)<sub>2</sub>(μ,η<sup>1</sup>:η<sup>1</sup>-**A**)<sub>2</sub>][TEF]<sub>2</sub> (**G**) or the 1D polymer [Ag<sub>2</sub>(μ,η<sup>1</sup>:η<sup>1</sup>-**A**)<sub>3</sub>]<sub>n</sub>[TEF]<sub>2n</sub> (**H**) (Scheme 4.1).<sup>8e,f</sup> Compound **F** contains one Ag(I) ion coordinated by three complexes **B** only in an η<sup>2</sup>-coordination mode. The accessibility of these products of two-component reactions rises the question whether it would be possible to conduct three component reactions of complex **B** with metal ions in the presence of N-donor organic molecules. Accordingly, Ag(I) is an attractive ion due to its adaptive coordination sphere which would result in a greater variety of the formed products compared to other coinage metal salts. Herein, we show that the reaction of **B** with AgPF<sub>6</sub> yields a cationic moiety similar to **F**, [(μ,η<sup>2</sup>-**B**)<sub>3</sub>Ag][TEF] (**C**) (Scheme 4.2).



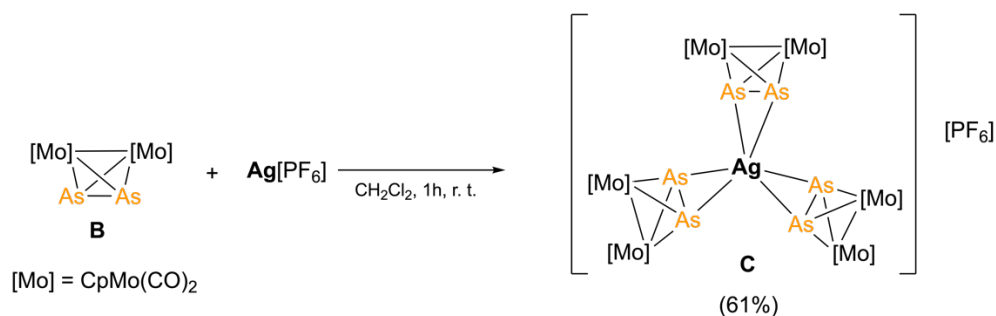
**Scheme 4.1.** Reactions of **A** and **B**, respectively, with Ag[TEF] in different ratios.<sup>8e,f,9</sup>

Furthermore, the three component reactions of **B** with AgPF<sub>6</sub> and the N-donor organic molecules 2-di(4-pyridyl)ethylene (**L**<sub>1</sub>), 1,2-di(4-pyridyl)ethyne (**L**<sub>2</sub>), 2,2'-bipyrimidine (**L**<sub>3</sub>), 1,3-di(4-pyridyl)propane (**L**<sub>4</sub>) and 4,4'-bipyridine (**L**<sub>5</sub>) allowed for the synthesis of the novel dicationic molecular organometallic-organic hybrid complexes  $\{[\text{Cp}_2\text{Mo}_2(\text{CO})_4(\mu_3, \eta^{2:2:2}\text{-As}_2)]_4(\mu_2, \eta^{1:1}\text{-C}_{12}\text{H}_8\text{N}_2)\text{Ag}_2\}[\text{PF}_6]_2$  (**1**) and  $\{[\text{Cp}_2\text{Mo}_2(\text{CO})_4(\mu_3, \eta^{2:2:2}\text{-As}_2)]_4(\mu_2, \eta^{1:1}\text{-C}_{12}\text{H}_{10}\text{N}_2)\text{Ag}_2\}[\text{PF}_6]_2$  (**2**), the new one-dimensional (1D) organometallic-organic hybrid polymer  $\{[\text{Cp}_2\text{Mo}_2(\text{CO})_4(\mu_3, \eta^{2:2:2}\text{-As}_2)](\mu_2, \eta^{1:1:1:1}\text{-C}_6\text{H}_8\text{N}_4)\text{Ag}\}[\text{PF}_6]_{2n}$  (**3**) as well as the unique 1D organometallic-organic hybrid polymers  $\{[\text{Cp}_2\text{Mo}_2(\text{CO})_4(\mu_4, \eta^{2:2:1:2}\text{-As}_2)]_2(\mu_2, \eta^{1:1}\text{-C}_{13}\text{H}_{14}\text{N}_2)(\text{CH}_3\text{CN})_2\text{Ag}_2\}[\text{PF}_6]_{2n}$  (**4**),  $\{[\text{Cp}_2\text{Mo}_2(\text{CO})_4(\mu_4, \eta^{2:2:1:2}\text{-As}_2)]_2(\mu_2, \eta^{1:1}\text{-C}_{10}\text{H}_8\text{N}_2)(\text{CH}_3\text{CN})_2\text{Ag}_2\}[\text{PF}_6]_{2n}$  (**5**) and  $\{[\text{Cp}_2\text{Mo}_2(\text{CO})_4(\mu_4, \eta^{2:2:1:2}\text{-As}_2)]_2\{[\text{Cp}_2\text{Mo}_2(\text{CO})_4(\mu_4, \eta^{2:2:1:1}\text{-As}_2)](\mu_2, \eta^{1:1}\text{-C}_{13}\text{H}_{14}\text{N}_2)\text{Ag}_2\}[\text{PF}_6]_{2n}$  (**6**) (Scheme 4.3).

## 4.2 Results and Discussion

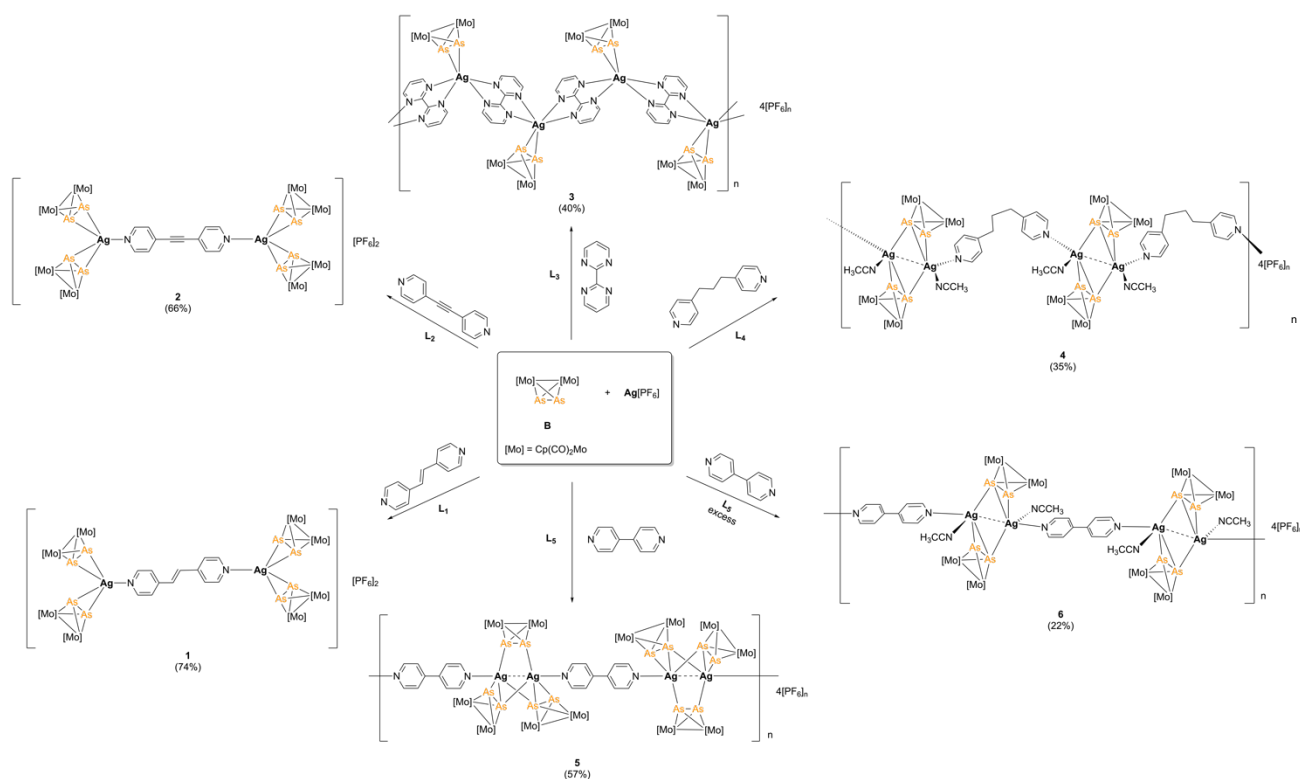
The reaction of **B** and AgPF<sub>6</sub> was conducted using a 3:1 ratio of **B**:AgPF<sub>6</sub> in CH<sub>2</sub>Cl<sub>2</sub>:CH<sub>3</sub>CN 1:1 at room temperature (Scheme 4.2). Layering with *n*-pentane affords red blocks of **C** suitable for X-ray structure analysis in a good yield within several day. Compound **C** crystallizes in the trigonal space group  $P\bar{3}1c$ . The Ag(I) center is  $\eta^2$ -coordinated by three complexes **B**. The As-As bonds (2.3676(17) Å) are slightly elongated compared to the uncoordinated complex **A** (2.311(3) Å).<sup>10</sup> Additionally, the distances of the coordinating As atoms to Ag are rather long (2.752(4) Å). The As<sub>2</sub>AgAs<sub>2</sub> plane to plane angle is 76°, resulting in a distorted trigonal prismatic coordination sphere of the Ag(I) center.

Compound **C** is well soluble in donor solvents such as CH<sub>3</sub>CN and slightly soluble in CH<sub>2</sub>Cl<sub>2</sub> but insoluble in *n*-pentane. The ESI mass spectra of **C** show the expected peaks for the cationic fragments [AgB<sub>2</sub>]<sup>+</sup> and [AgB(CH<sub>3</sub>CN)]<sup>+</sup> and one peak for the PF<sub>6</sub><sup>-</sup> anion in the negative ion mode. The solid-state IR spectrum of **C** reveals four strong broad absorptions between 1889 and 1985 cm<sup>-1</sup>. These vibration bands are attributed to the stretching of the CO ligands of the coordinated **B** and are shifted to lower energies compared to the free complex **B** (1900 and 1949 cm<sup>-1</sup>).<sup>10</sup>



**Scheme 4.2.** Reaction of **B** with Ag[PF<sub>6</sub>] yielding compound **C**. Yield is given in parenthesis.

Reacting **B** and AgPF<sub>6</sub> with the linkers 1,2-di(4-pyridyl)ethylene (**L**<sub>1</sub>) and 1,2-di(4-pyridyl)ethyne (**L**<sub>2</sub>) lead to two discrete coordination complexes **1** and **2**, respectively (Scheme 4.3). The straightforward synthetic approach, mixing **B** and AgPF<sub>6</sub> in CH<sub>2</sub>Cl<sub>2</sub>:CH<sub>3</sub>CN 1:1 and add **L**<sub>1</sub> or **L**<sub>2</sub>, respectively, after 1 h of stirring at room temperature, yields in red blocks suitable for X-ray structure analysis. Compounds **1** and **2** crystallize in the triclinic space group  $P\bar{1}$  in very good yields. Both solid-state structures reveal two [AgB<sub>2</sub>]<sup>+</sup> units connected with linker **L**<sub>1</sub> or **L**<sub>2</sub>, respectively, *via* the free coordination site at the Ag(I) (Figure 4.1). Surprisingly, also an excess of the linkers **L**<sub>1</sub> and **L**<sub>2</sub> did not lead to the formation of a higher dimensional coordination compound.



**Scheme 4.3.** Reaction of **B** and  $\text{AgPF}_6$  with the linkers  $\text{L}_1$ - $\text{L}_5$  conducted at r. t. in  $\text{CH}_2\text{Cl}_2:\text{CH}_3\text{CN}$  1:1 yielding compounds **1-6**. Yields are given in parentheses.

Though, the reaction of **B** and  $\text{AgPF}_6$  with  $\text{L}_3$  under the same reaction conditions resulted in the 1D zig-zag polymer **3** (Scheme 4.3). Compound **3** crystallizes in the monoclinic space group  $P2_1/c$  as red blocks in a good yield. The solid-state structure reveals  $[\text{AgB}]^+$  moieties, which are linked with  $\text{L}_3$ . The Ag(I) centers are trigonal prismatic coordinated with  $\text{As}_2$ ,  $\text{N}_2$  of one linker molecule and  $\text{N}_2$  of another linker molecule forming the edges of the prism (Figure 4.4). The  $\text{NAgN}$  plane to plane angle is  $83^\circ$ , leading to a distorted coordination sphere on the Ag(I) center.

Moreover, compound **4** was obtained by reacting **B** and  $\text{AgPF}_6$  with  $\text{L}_4$  (Scheme 4.3). Interestingly, the  $[\text{Ag}_2\text{B}_2(\text{CH}_3\text{CN})_2]^+$  units were linked with  $\text{L}_4$  to yield a 1D coordination polymer (Figure 4.1). The Ag(I) centers are  $\eta^2$ -coordinated by one molecule **B**,  $\eta^1$ -coordinated by a second **B** unit. The nitrogen atoms of  $\text{L}_4$  coordinate in an end-on coordination mode towards the Ag(I) centers. Additionally, every Ag(I) ion is coordinated by one  $\text{CH}_3\text{CN}$  molecule. The  $\text{Ag1AsAg2}/\text{Ag1'AsAg2'}$  planes deviate from planarity ( $21^\circ$ ). The intermetallic  $\text{Ag}\cdots\text{Ag}$  distance in **4** is significantly short ( $2.9690(4)$  Å) compared to the sum of the van der Waals radii for  $\text{Ag}\cdots\text{Ag}$  ( $3.44$  Å)<sup>11</sup> demonstrating the possible existence of argentophilic interactions. The  $[\text{Ag}_2\text{B}_2(\text{CH}_3\text{CN})_2]^+$  moieties show a cis-like coordination sphere concerning the linker  $\text{L}_4$  and the solvent molecules, resulting in the same coordination environments of all Ag(I) centers. Attempts to substitute the solvent molecule by adding an excess of linker  $\text{L}_4$  to build up 2D coordination polymers failed.

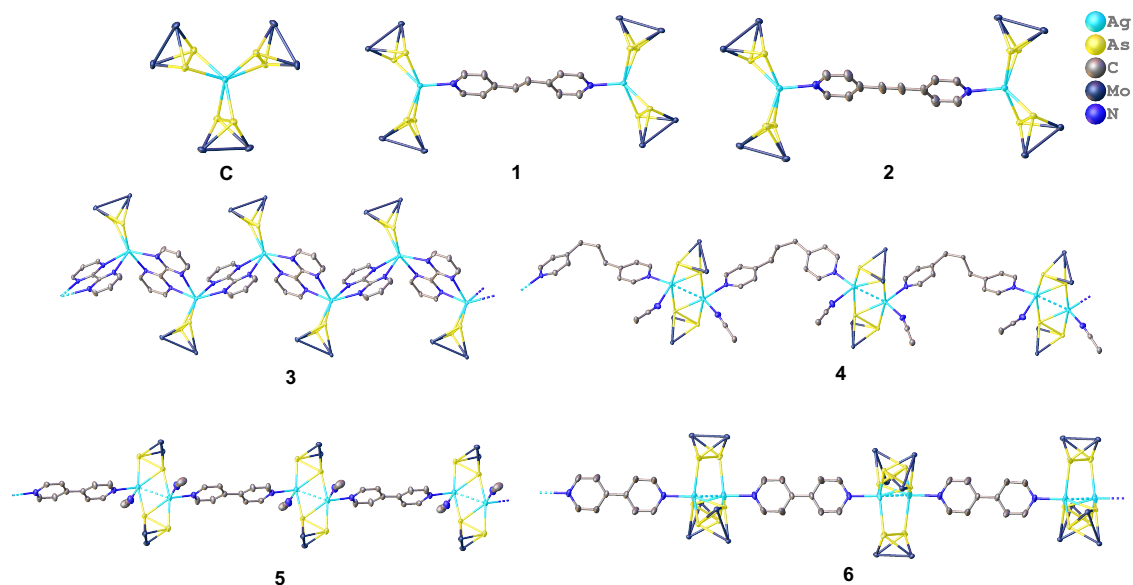


**Figure 4.1.** Solid-state structures of the compounds **C** and **1-6**. Cp-, CO-fragments, hydrogen atoms and anions are not depicted for clarity. Ellipsoids are shown at 50% probability level.

Compounds **1-4** are formed regardless of the ratio of  $\text{B}:\text{AgPF}_6$ :linker. In contrast, linker  $\text{L}_5$  forms two structurally distinct compounds **5** and **6**, depending on the stoichiometry. Reacting **B**,  $\text{AgPF}_6$  and  $\text{L}_5$  in a 3:1:2 ratio results in the formation of **5**, while using a threefold excess of  $\text{L}_5$  yields compound **6** (Scheme 4.3).

The central structural motif of **5** consists of  $[\text{Ag}_2\text{B}_3]^+$  units linked with  $\text{L}_5$ . Each Ag(I) center is  $\eta^2$ -coordinated by one **B** moiety and  $\eta^1$ -coordinated by the other two **B** molecules, whereby, one of the three **B** only coordinate towards the silver ions in an  $\eta^1$  fashion (Figure 4.1 and 4.2). Such structural motif is unique and has not been observed so far. Furthermore, the  $\text{Ag}\cdots\text{Ag}$  distance is found to be even shorter than in **4** (2.7867(6) Å), also proposing argentophilic interactions.

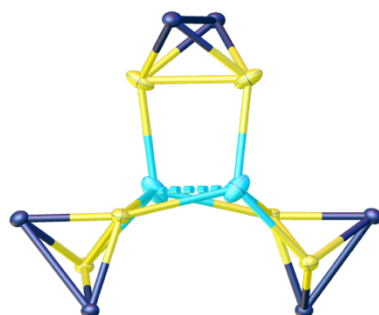


**Figure 4.2.** Section of the solid-state structure of **5** showing a rare  $\eta^1$ -coordination mode of the  $\text{As}_2$  complex **B** towards the Ag(I) centers. Cp-, CO- and anions were omitted for clarity. Ellipsoids shown at 50% probability level.



The coordination polymer **6** consists of linked  $[\text{Ag}_2\text{B}_2(\text{CH}_3\text{CN})_2]^+$  entities. Surprisingly, the third molecule **B** of compound **6** was not substituted by a linker molecule as expected, but the free coordination site of the silver ion is occupied by an acetonitrile molecule. The difference between the  $[\text{Ag}_2\text{B}_2(\text{CH}_3\text{CN})_2]^+$  unit of **4** and **6** is the direction of the solvent molecules. Compound **6** shows a trans arrangement of the  $\text{CH}_3\text{CN}$  molecules coordinated to the  $\text{Ag}(\text{I})$  centers. The  $\text{Ag}\cdots\text{Ag}$  distance in **6** is similar to the distance in **4** (2.9798(4) Å).

As already discussed in chapter 3 of this work, compounds **4-6** demonstrate that the tetrahedral complex **B** has a high potential to form a  $\eta^2:\eta^1$ -coordination towards  $\text{Ag}(\text{I})$  and to stabilize short  $\text{Ag}\cdots\text{Ag}$  distances. Compounds **1-6** are all well soluble in  $\text{CH}_3\text{CN}$ , slightly soluble in  $\text{CH}_2\text{Cl}_2$  and insoluble in *n*-pentane. The  $^1\text{H}$  and  $^{13}\text{C}\{^1\text{H}\}$  NMR spectra, recorded in acetonitrile- $d_3$  at room temperature, of compounds of **3** and **4** show signals corresponding to the proton and carbon nuclei of the Cp and CO ligands of the coordinated **B**, respectively, and the corresponding linkers. Since the products can only be dissolved in the donor solvent  $\text{CH}_3\text{CN}$ , the NMR data of compounds **1**, **2** and **5** reveal depolymerization in solution as only signals for uncoordinated **B** (5.45 ppm) and the linkers are detectable.<sup>i</sup> The ESI mass spectra in  $\text{CH}_3\text{CN}$  show mainly peaks for the cationic fragments  $[\text{AgB}_2]^+$ ,  $[\text{AgB}(\text{CH}_3\text{CN})]^+$  and  $[\text{AgB}]^+$ . Some peaks lower in intensities are detected for  $[\text{L}_x]^+$  and  $[\text{Ag}(\text{CH}_3\text{CN})]^+$  in the positive ion mode. The assignment of some higher aggregated cationic fragments in very low intensities was not possible. In the negative ion mode, the peak for  $\text{PF}_6^-$  is detected. These data indicate a partial dissociation of all compounds in solutions of  $\text{CH}_3\text{CN}$ . In the solid-state IR spectra of compounds **1-5**<sup>ii</sup> the CO bands are shifted to higher wavenumbers (between 1905 and 1983  $\text{cm}^{-1}$ ) compared to the uncoordinated complex **B** (1900, 1949  $\text{cm}^{-1}$ ).<sup>12</sup>

### 4.3 Conclusion

To conclude, we were able to obtain compound **C** by reacting the tetrahedral diarsenic complex  $[\text{Cp}_2\text{Mo}_2(\text{CO})_4(\mu, \eta^2\text{-As}_2)]$  (**B**) with  $\text{AgPF}_6$ . Furthermore, we synthesized two discrete (**1**, **2**) and four polymeric (**3-6**) coordination compounds by using  $\text{Ag}(\text{I})$ , **B** and the organic pyridyl linker **L**<sub>1</sub>-**L**<sub>5</sub>, respectively. The one-dimensional polymers show a variety of  $\text{Ag}(\text{I})$  coordination modes. The supramolecular polymers **4**, **5** and **6** contain  $[\text{Ag}_2]^{2+}$  units with very short  $\text{Ag}\cdots\text{Ag}$  distances stabilized by the tetrahedral complex **B**. Additionally, compound **5** shows an unprecedented mix of coordination modes of **B**

<sup>i</sup> NMR measurements for compound **6** could not be performed within this work.

<sup>ii</sup> IR measurements for compound **6** and **4** could not be performed within this work.

towards the silver atoms ( $[(\eta^1:\eta^2\text{-B})_2(\eta^1:\eta^1\text{-B})\text{Ag}_2]^{2+}$ ), leading to very short Ag...Ag distance (2.7866(6) Å), indicating even stronger argentophilic interactions. Linker **L<sub>5</sub>** (4,4'-bipyridine) was the only one to form different coordination compounds (**5** and **6**) depending on the linker stoichiometry used.

## 4.4 Supporting Information

### 4.4.1 General

All experiments were performed under an atmosphere of dry argon or nitrogen using standard Schlenk and glovebox techniques. The nitrogen/argon was dried and purified from traces of oxygen with a Cu/MgSO<sub>4</sub> catalyst, concentrated H<sub>2</sub>SO<sub>4</sub> and orange gel. All used solvents were taken from the solvent drying machine MB SPS-800 of the company MBRAUN. The precursor [Cp<sub>2</sub>Mo<sub>2</sub>(CO)<sub>4</sub>(μ,η<sup>2:2</sup>-As<sub>2</sub>)] (**B**) was prepared according to literature procedures.<sup>12</sup> AgPF<sub>6</sub> (abcr), 1,2-di(4-pyridyl)ethylene (**L<sub>1</sub>**) (TCI), 1,2-di(4-pyridyl)ethyne (**L<sub>2</sub>**) (TCI), 2,2'-bipyrimidine (**L<sub>3</sub>**) (TCI), 1,3-di(4-pyridyl)propane (**L<sub>4</sub>**) (TCI) and 4,4'-bipyridine (**L<sub>5</sub>**) (TCI) were used as received without further purification. Solution NMR spectra were recorded on a Bruker Avance III HD 400 spectrometer (<sup>1</sup>H: 400 MHz, <sup>31</sup>P: 161 MHz, <sup>13</sup>C: 100 MHz, <sup>19</sup>F: 376 MHz) with acetonitrile -d<sub>3</sub> as solvent at room temperature. The chemical shifts δ are presented in parts per million ppm and coupling constants *J* in Hz. The following samples were used as external reference: TMS (<sup>1</sup>H, <sup>13</sup>C), CFCI<sub>3</sub> (<sup>19</sup>F), H<sub>3</sub>PO<sub>4</sub> 85 % (<sup>31</sup>P). The spectra were processed and analyzed using the software Bruker TopSpin 3.0. IR spectra were recorded as solids with an ATR-Ge disc on a Thermo Fisher Nicolet iS5 spectrometer. Elemental analyses were performed on an Elementar Vario MICRO cube apparatus. Mass spectra were recorded on an Agilent Q-TOF 6540 UHD mass spectrometer with acetonitrile as solvent.

### 4.4.2 Synthesis of [(μ,η<sup>2</sup>-B)<sub>3</sub>Ag][PF<sub>6</sub>]<sub>2</sub> (**C**)

0.15 mmol AgPF<sub>6</sub> (39 mg) in 5 mL CH<sub>2</sub>Cl<sub>2</sub>:CH<sub>3</sub>CN 1:1 was added to a stirred solution of [Cp<sub>2</sub>Mo<sub>2</sub>(CO)<sub>4</sub>(η<sup>2</sup>-As<sub>2</sub>)] (30 mg, 0.05 mmol) in 5 mL CH<sub>2</sub>Cl<sub>2</sub>, respectively, and stirred for 1 h at room temperature. The red solution was filtered and carefully layered with threefold amount of *n*-pentane and stored at room temperature in the dark. After several days red blocks were formed. The crystals were washed with *n*-pentane and dried *in vacuo*. Yield 20 mg (61% referred to [Cp<sub>2</sub>Mo<sub>2</sub>(CO)<sub>4</sub>(η<sup>2</sup>-As<sub>2</sub>)]).

<sup>1</sup>H NMR (CD<sub>3</sub>CN): δ/ppm = 5.29 (s).

<sup>13</sup>C {<sup>1</sup>H} NMR (CD<sub>3</sub>CN): δ/ppm = 226.32 (CO), 86.21 (C<sub>5</sub>H<sub>5</sub>).

Positive ion ESI-MS (CH<sub>3</sub>CN, RT):  $m/z$  (%) = 1276.3 (100) [ $\{\text{Cp}_2(\text{CO})_4\text{Mo}_2\text{As}_2\}_2\text{Ag}\}^+$ , 731.6 (12) [ $\{\text{Cp}_2(\text{CO})_4\text{Mo}_2\text{As}_2\}\text{Ag}(\text{CH}_3\text{CN})\}^+$ , 690.6 (5) [ $\{\text{Cp}_2(\text{CO})_4\text{Mo}_2\text{As}_2\}\text{Ag}\}^+$ .

Negative ion ESI-MS (CH<sub>3</sub>CN, RT):  $m/z$  (%) = 145.0 (100) PF<sub>6</sub><sup>-</sup>.

Elemental analysis, calcd (%) for C<sub>42</sub>H<sub>30</sub>AgAs<sub>6</sub>F<sub>6</sub>Mo<sub>6</sub>O<sub>12</sub>P (2004.70 g/mol): C, 25.16; H, 1.51; found: C, 25.37; H, 1.52;

IR (solid, CO bands):  $\tilde{\nu}/\text{cm}^{-1}$ : 1985 (vs), 1951 (vs), 1919 (vs), 1889 (vs);

#### 4.4.3 Synthesis of [ $\{(\eta^2\text{-B})_2\text{Ag}\}_2(\mu\text{-L}_1)\text{][PF}_6\text{]}_2$ (**1**)

AgPF<sub>6</sub> (1 eq., 4 mg, 0.016 mmol) in 5 mL CH<sub>2</sub>Cl<sub>2</sub>:CH<sub>3</sub>CN 1:1 was added to a stirred solution of compounds **B** (3 eq., 29 mg, 0.05 mmol) in 5 mL CH<sub>2</sub>Cl<sub>2</sub>:CH<sub>3</sub>CN 1:1 and stirred for 1 h at room temperature. Then 0.1 mmol (6 eq., 18 mg) of the linker 1,2-di(4-pyridyl)ethylene (**L**<sub>1</sub>) was added and stirred for another 2 h. The red solution was filtered and carefully layered with the threefold amount of *n*-pentane and stored at room temperature in the dark. After several days, compound **1** was obtained as clear red blocks. The supernatant was decanted off, the remaining crystals washed with *n*-pentane and dried *in vacuo*. Yield = 28 mg (74% referred to [Cp<sub>2</sub>Mo<sub>2</sub>(CO)<sub>4</sub>(η<sup>2</sup>-As<sub>2</sub>)]).

<sup>1</sup>H NMR (CD<sub>3</sub>CN):  $\delta/\text{ppm}$  = 8.57 (m, 4H), 7.54 (m, 4H), 7.42 (s, 2H), 5.33 (s, 40H).

<sup>13</sup>C {<sup>1</sup>H} NMR (CD<sub>3</sub>CN):  $\delta/\text{ppm}$  = 225.11 (CO), 151.41 (*o*-C<sub>Ar</sub>), 131.64 (*m*-C<sub>Ar</sub>), 122.38 (C<sub>Et</sub>), 86.53 (C<sub>5</sub>H<sub>5</sub>).

<sup>31</sup>P {<sup>1</sup>H} NMR (CD<sub>3</sub>CN):  $\delta/\text{ppm}$  = -143.13 (sept, <sup>1</sup>J<sub>P,F</sub> = 705.3 Hz).

<sup>19</sup>F {<sup>1</sup>H} NMR (CD<sub>3</sub>CN):  $\delta/\text{ppm}$  = -71.76 (d, <sup>1</sup>J<sub>F,P</sub> = 705.3 Hz).

Positive ion ESI-MS (CH<sub>3</sub>CN, r. t.):  $m/z$  (%) = 1276.33 (100) [ $\{\text{Cp}_2(\text{CO})_4\text{Mo}_2\text{As}_2\}_2\text{Ag}\}^+$ , 731.65 (19) [ $\{\text{Cp}_2(\text{CO})_4\text{Mo}_2\text{As}_2\}\text{Ag}(\text{CH}_3\text{CN})\}^+$ , 690.62 (5) [ $\{\text{Cp}_2(\text{CO})_4\text{Mo}_2\text{As}_2\}\text{Ag}\}^+$ , 183.09 (6) [N<sub>2</sub>C<sub>12</sub>H<sub>10</sub>]<sup>+</sup>.

Negative ion ESI-MS (CH<sub>3</sub>CN, r. t.):  $m/z$  (%) = 144.97 (100) PF<sub>6</sub><sup>-</sup>.

Elemental analysis, calcd (%) for C<sub>68</sub>H<sub>50</sub>Ag<sub>2</sub>As<sub>8</sub>F<sub>12</sub>Mo<sub>8</sub>N<sub>2</sub>O<sub>16</sub>P<sub>2</sub> (3023.71 g/mol): C, 27.01; H, 1.67; N, 0.93; found: C, 26.93; H, 1.78; N, 1.03;

IR (solid, CO bands):  $\tilde{\nu}/\text{cm}^{-1}$ : 1953.42 (w), 1912.22 (w).

#### 4.4.4 Synthesis of [ $\{(\eta^2\text{-B})_2\text{Ag}\}_2(\mu\text{-L}_2)\text{][PF}_6\text{]}_2$ (**2**)

AgPF<sub>6</sub> (1 eq., 4 mg, 0.016 mmol) in 5 mL CH<sub>2</sub>Cl<sub>2</sub>:CH<sub>3</sub>CN 1:1 was added to a stirred solution of compounds **B** (3 eq., 29 mg, 0.05 mmol) in 5 mL CH<sub>2</sub>Cl<sub>2</sub>:CH<sub>3</sub>CN 1:1 and stirred for 1 h at room temperature. Then 0.1 mmol (6 eq., 18 mg) of the linker 1,2-di(4-pyridyl)ethyne (**L**<sub>2</sub>) was added and stirred for another 2 h. The red solution was filtered and carefully layered with the threefold amount of *n*-pentane and stored at room

temperature in the dark. After several days, compound **2** was obtained as clear red blocks. The supernatant was decanted off, the remaining crystals washed with *n*-pentane and dried *in vacuo*. Yield = 25 mg (66% referred to [Cp<sub>2</sub>Mo<sub>2</sub>(CO)<sub>4</sub>(η<sup>2</sup>-As<sub>2</sub>)]).

<sup>1</sup>H NMR (CD<sub>3</sub>CN): δ/ppm = 8.64 (m, 4H), 7.49 (m, 4H), 5.32 (s, 40H).

<sup>13</sup>C {<sup>1</sup>H} NMR (CD<sub>3</sub>CN): δ/ppm = 225.39 (CO), 151.12 (*o*-C<sub>Ar</sub>), 126.57 (*m*-C<sub>Ar</sub>), 86.47 (C<sub>5</sub>H<sub>5</sub>).

<sup>31</sup>P {<sup>1</sup>H} NMR (CD<sub>3</sub>CN): δ/ppm = -143.08 (sept, 1P, <sup>1</sup>J<sub>P,F</sub> = 706.3 Hz).

<sup>19</sup>F {<sup>1</sup>H} NMR (CD<sub>3</sub>CN): δ/ppm = -71.76 (d, <sup>1</sup>J<sub>F,P</sub> = 706.7 Hz).

Positive ion ESI-MS (CH<sub>3</sub>CN, r. t.): *m/z* (%) = 1276.33 (100) [(Cp<sub>2</sub>(CO)<sub>4</sub>Mo<sub>2</sub>As<sub>2</sub>)<sub>2</sub>Ag]<sup>+</sup>, 731.65 (28) [(Cp<sub>2</sub>(CO)<sub>4</sub>Mo<sub>2</sub>As<sub>2</sub>)Ag(CH<sub>3</sub>CN)]<sup>+</sup>, 690.62 (7) [(Cp<sub>2</sub>(CO)<sub>4</sub>Mo<sub>2</sub>As<sub>2</sub>)Ag]<sup>+</sup>, 181.08 (19) [N<sub>2</sub>C<sub>12</sub>H<sub>8</sub>]<sup>+</sup>.

Negative ion ESI-MS (CH<sub>3</sub>CN, r. t.): *m/z* (%) = 144.97 (100) PF<sub>6</sub><sup>-</sup>.

Elemental analysis, calcd (%) for C<sub>68</sub>H<sub>48</sub>Ag<sub>2</sub>As<sub>8</sub>F<sub>12</sub>Mo<sub>8</sub>N<sub>2</sub>O<sub>16</sub>P<sub>2</sub> (3021.69 g/mol): C, 27.03; H, 1.60; N, 0.93; found: C, 27.27; H, 1.84; N, 1.22;

IR (solid, CO bands):  $\tilde{\nu}/\text{cm}^{-1}$ : 1951.88 (s), 1917.12 (s).

#### 4.4.5 Synthesis of [(η<sup>2</sup>-B)Ag](μ-L<sub>3</sub>)<sub>n</sub>[PF<sub>6</sub>]<sub>2n</sub> (**3**)

AgPF<sub>6</sub> (1 eq., 4 mg, 0.016 mmol) in 5 mL CH<sub>2</sub>Cl<sub>2</sub>:CH<sub>3</sub>CN 1:1 was added to a stirred solution of compounds **B** (3 eq., 29 mg, 0.05 mmol) in 5 mL CH<sub>2</sub>Cl<sub>2</sub>:CH<sub>3</sub>CN 1:1 and stirred for 1 h at room temperature. Then 0.1 mmol (6 eq., 16 mg) of the linker 2,2'-bipyrimidine (L<sub>3</sub>) was added and stirred for another 2 h. The red solution was filtered and carefully layered with the threefold amount of *n*-pentane and stored at room temperature in the dark. After several days, compound **3** was obtained as dark red blocks. The supernatant was decanted off, the remaining crystals washed with *n*-pentane and dried *in vacuo*. Yield = 20 mg (40% referred to [Cp<sub>2</sub>Mo<sub>2</sub>(CO)<sub>4</sub>(η<sup>2</sup>-As<sub>2</sub>)]).

<sup>1</sup>H NMR (CD<sub>3</sub>CN): δ/ppm = 9.03 (d, J<sub>HH</sub> = 4.91 Hz, 6H), 7.64 (t, J<sub>HH</sub> = 4.92 Hz, 3H), 5.31 (s, 10H).

<sup>13</sup>C {<sup>1</sup>H} NMR (CD<sub>3</sub>CN): δ/ppm = 225.03 (CO), 161.56 (NC<sub>q</sub>N), 159.49 (NCC), 123.65 (CCC), 86.51 (C<sub>5</sub>H<sub>5</sub>).

<sup>31</sup>P {<sup>1</sup>H} NMR (CD<sub>3</sub>CN): δ/ppm = -143.14 (sept, 1P, <sup>1</sup>J<sub>P,F</sub> = 706.9 Hz).

<sup>19</sup>F {<sup>1</sup>H} NMR (CD<sub>3</sub>CN): δ/ppm = -71.76 (d, <sup>1</sup>J<sub>F,P</sub> = 705.5 Hz).

Positive ion ESI-MS (CH<sub>3</sub>CN, r. t.): *m/z* (%) = 1276.33 (12) [(Cp<sub>2</sub>(CO)<sub>4</sub>Mo<sub>2</sub>As<sub>2</sub>)<sub>2</sub>Ag]<sup>+</sup>, 848.68 (100) [Ag(Cp<sub>2</sub>(CO)<sub>4</sub>Mo<sub>2</sub>As<sub>2</sub>)(N<sub>2</sub>C<sub>10</sub>H<sub>8</sub>)]<sup>+</sup>, 423.02 (18) [Ag(N<sub>4</sub>C<sub>8</sub>H<sub>6</sub>)<sub>2</sub>]<sup>+</sup>, 181.05 (17), 147.93 (8) [Ag(CH<sub>3</sub>CN)]<sup>+</sup>.

Negative ion ESI-MS (CH<sub>3</sub>CN, r. t.): *m/z* (%) = 144.97 (100) PF<sub>6</sub><sup>-</sup>.

Elemental analysis, calcd (%) for  $C_{22}H_{16}AgAs_2F_6Mo_2N_4O_4P$  (994.95 g/mol): C, 26.56; H, 1.62; N, 5.63; found: C, 26.50; H, 1.44; N, 5.53;

IR (solid, CO bands):  $\tilde{\nu}/\text{cm}^{-1}$ : 1942.85 (s), 1915.93 (vs), 1900.98 (vs).

#### 4.4.6 Synthesis of $[(\eta^1:\eta^2\text{-B})_2(\text{CH}_3\text{CN})_2\text{Ag}_2](\mu\text{-L}_4)_n[\text{PF}_6]_{2n}$ (**4**)

$\text{AgPF}_6$  (1 eq., 4 mg, 0.016 mmol) in 5 mL  $\text{CH}_2\text{Cl}_2:\text{CH}_3\text{CN}$  1:1 was added to a stirred solution of compounds **B** (3 eq., 29 mg, 0.05 mmol) in 5 mL  $\text{CH}_2\text{Cl}_2:\text{CH}_3\text{CN}$  1:1 and stirred for 1 h at room temperature. Then 0.1 mmol (6 eq., 20 mg) of the linker 1,3-di(4-pyridyl)propane (**L**<sub>4</sub>) was added and stirred for another 2 h. The red solution was filtered and carefully layered with the threefold amount of *n*-pentane and stored at room temperature in the dark. After 3-5 weeks, compound **4** was obtained as clear orange blocks. The supernatant was decanted off, the remaining crystals washed with *n*-pentane and dried *in vacuo*. Yield = 17 mg (35% referred to  $[\text{Cp}_2\text{Mo}_2(\text{CO})_4(\eta^2\text{-As}_2)]$ ).

$^1\text{H}$  NMR ( $\text{CD}_3\text{CN}$ ):  $\delta/\text{ppm}$  = 8.44 (d,  $J_{\text{HH}}$  = 4.85 Hz, 4H), 7.22 (d,  $J_{\text{HH}}$  = 4.85 Hz, 4H), 5.34 (s, 20H), 2.67 (t,  $J_{\text{HH}}$  = 7.7 Hz, 4H), second linker signal is overlaid by solvent signal.

$^{13}\text{C}$   $\{^1\text{H}\}$  NMR ( $\text{CD}_3\text{CN}$ ):  $\delta/\text{ppm}$  = 224.60 (CO), 153.85 ( $\text{C}_{\text{Ar,q}}$ ), 150.27 ( $o\text{-C}_{\text{Ar}}$ ), 125.54 ( $m\text{-C}_{\text{Ar}}$ ), 86.64 ( $\text{C}_5\text{H}_5$ ), 35.13 ( $\text{C}_{\text{Ar,q}}\text{-CH}_2\text{-CH}_2$ ), 31.33 ( $\text{CH}_2\text{-CH}_2\text{-CH}_2$ ).

$^{31}\text{P}$   $\{^1\text{H}\}$  NMR ( $\text{CD}_3\text{CN}$ ):  $\delta/\text{ppm}$  = -143.08 (sept, 1P,  $^1J_{\text{P,F}}$  = 705.8 Hz).

$^{19}\text{F}$   $\{^1\text{H}\}$  NMR ( $\text{CD}_3\text{CN}$ ):  $\delta/\text{ppm}$  = -71.74 (d,  $^1J_{\text{F,P}}$  = 707.2 Hz).

Positive ion ESI-MS ( $\text{CH}_3\text{CN}$ , r. t.):  $m/z$  (%) = 1276.3 (15)  $[(\text{Cp}_2(\text{CO})_4\text{Mo}_2\text{As}_2)_2\text{Ag}]^+$ , 731.6 (33)  $[(\text{Cp}_2(\text{CO})_4\text{Mo}_2\text{As}_2)\text{Ag}(\text{CH}_3\text{CN})]^+$ , 147.9 (100)  $[\text{Ag}(\text{CH}_3\text{CN})]^+$ , 189.0 (24)  $[\text{N}_2\text{C}_{13}\text{H}_{14}]^+$ .

Negative ion ESI-MS ( $\text{CH}_3\text{CN}$ , r. t.):  $m/z$  (%) = 144.97 (100)  $\text{PF}_6^-$ .

#### 4.4.7 Synthesis of $[(\eta^1:\eta^2\text{-B})_2(\eta^1:\eta^1\text{-B})\text{Ag}_2](\mu\text{-L}_5)_n[\text{PF}_6]_{2n}$ (**5**)

$\text{AgPF}_6$  (1 eq., 4 mg, 0.016 mmol) in 5 mL  $\text{CH}_2\text{Cl}_2:\text{CH}_3\text{CN}$  1:1 was added to a stirred solution of compounds **B** (3 eq., 29 mg, 0.05 mmol) in 5 mL  $\text{CH}_2\text{Cl}_2:\text{CH}_3\text{CN}$  1:1 and stirred for 1 h at room temperature. Then 0.032 mmol (2 eq., 5 mg) of the linker 4,4'-bipyridine (**L**<sub>5</sub>) was added and stirred for another 2 h. The red solution was filtered and carefully layered with the threefold amount of *n*-pentane and stored at room temperature in the dark. After several days, compound **5** was obtained as red blocks. The supernatant was decanted off, the remaining crystals washed with *n*-pentane and dried *in vacuo*. Yield = 23 mg (57% referred to  $[\text{Cp}_2\text{Mo}_2(\text{CO})_4(\eta^2\text{-As}_2)]$ ).

$^1\text{H}$  NMR ( $\text{CD}_3\text{CN}$ ):  $\delta/\text{ppm}$  = 8.71 (dd, 4H,  $^4J_{\text{H,H}}$  = 1.7,  $^3J_{\text{H,H}}$  = 4.6 Hz), 7.71 (m, 4H), 5.34 (s, 30H).

<sup>13</sup>C {<sup>1</sup>H} NMR (CD<sub>3</sub>CN): δ/ppm = 224.44 (CO), 151.74 (*o*-C<sub>Ar</sub>), 122.69 (*m*-C<sub>Ar</sub>), 86.62 (C<sub>5</sub>H<sub>5</sub>), 55.26 (*p*-C<sub>Ar</sub>).

<sup>31</sup>P {<sup>1</sup>H} NMR (CD<sub>3</sub>CN): δ/ppm = -143.13 (sept, <sup>1</sup>J<sub>P,F</sub> = 705.2 Hz).

<sup>19</sup>F NMR (CD<sub>3</sub>CN): δδ/ppm = -71.75 (d, <sup>1</sup>J<sub>F,P</sub> = 705.3 Hz).

Positive ion ESI-MS (CH<sub>3</sub>CN, r. t.): *m/z* (%) = 1276.3 (100) [{Cp<sub>2</sub>(CO)<sub>4</sub>Mo<sub>2</sub>As<sub>2</sub>}<sub>2</sub>Ag]<sup>+</sup>, 731.7 (82) [{Cp<sub>2</sub>(CO)<sub>4</sub>Mo<sub>2</sub>As<sub>2</sub>}Ag(CH<sub>3</sub>CN)]<sup>+</sup>, 690.6 (22) [{Cp<sub>2</sub>(CO)<sub>4</sub>Mo<sub>2</sub>As<sub>2</sub>}Ag]<sup>+</sup>, 147.9 (22) [Ag(CH<sub>3</sub>CN)]<sup>+</sup>.

Negative ion ESI-MS (CH<sub>3</sub>CN, r. t.): *m/z* (%) = 144.97 (100) PF<sub>6</sub><sup>-</sup>.

Elemental analysis, calcd (%) for C<sub>52</sub>H<sub>38</sub>Ag<sub>2</sub>As<sub>6</sub>F<sub>12</sub>Mo<sub>6</sub>N<sub>2</sub>O<sub>12</sub>P<sub>2</sub> (2413.72 g/mol): C, 25.88; H, 1.59; N, 1.16; found: C, 25.49; H, 1.61; N, 1.16;

IR (solid, CO bands):  $\tilde{\nu}/\text{cm}^{-1}$ : 1983.19 (s), 1956.80 (s), 1905.60 (vs).

#### 4.4.8 Synthesis of [{(η<sup>1</sup>:η<sup>2</sup>-B)<sub>2</sub>(CH<sub>3</sub>CN)<sub>2</sub>Ag<sub>2</sub>}(μ-L<sub>5</sub>)]<sub>n</sub>[PF<sub>6</sub>]<sub>2n</sub> (**6**)

AgPF<sub>6</sub> (1 eq., 4 mg, 0.016 mmol) in 5 mL CH<sub>2</sub>Cl<sub>2</sub>:CH<sub>3</sub>CN 1:1 was added to a stirred solution of compounds **B** (3 eq., 29 mg, 0.05 mmol) in 5 mL CH<sub>2</sub>Cl<sub>2</sub>:CH<sub>3</sub>CN 1:1 and stirred for 1 h at room temperature. Then 0.1 mmol (6 eq., 16 mg) of the linker 4,4'-bipyridine (L<sub>5</sub>) was added and stirred for another 2 h. The red solution was filtered and carefully layered with the threefold amount of *n*-pentane and stored at room temperature in the dark. After several days, compound **5** was obtained as clear orange blocks. The supernatant was decanted off, the remaining crystals washed with *n*-pentane and dried *in vacuo*. Yield = 10 mg (22% referred to [Cp<sub>2</sub>Mo<sub>2</sub>(CO)<sub>4</sub>(η<sup>2</sup>-As<sub>2</sub>)]).

Positive ion ESI-MS (CH<sub>3</sub>CN, RT): *m/z* (%) = 1276.33 (43) [{Cp<sub>2</sub>(CO)<sub>4</sub>Mo<sub>2</sub>As<sub>2</sub>}<sub>2</sub>Ag]<sup>+</sup>, 731.65 (100) [{Cp<sub>2</sub>(CO)<sub>4</sub>Mo<sub>2</sub>As<sub>2</sub>}Ag(CH<sub>3</sub>CN)]<sup>+</sup>, 690.62 (25) [{Cp<sub>2</sub>(CO)<sub>4</sub>Mo<sub>2</sub>As<sub>2</sub>}Ag]<sup>+</sup>, 147.93 (69) Ag(CH<sub>3</sub>CN)<sup>+</sup>.

Negative ion ESI-MS (CH<sub>3</sub>CN, RT): *m/z* (%) = 144.97 (100) PF<sub>6</sub><sup>-</sup>.

#### 4.4.9 Crystallographic Data

Crystals of **1-6** were taken from a Schlenk flask under a stream of argon and immediately covered with mineral oil to prevent a loss of solvent. The quickly chosen single crystals covered by a thin oil/Fomblin layer were taken to the pre-centered goniometer head with CryoMount® and directly attached to the diffractometer into a stream of cold nitrogen.

The diffraction experiments for **1-6** were collected on Rigaku Oxford Diffraction diffractometers; on a GV50 diffractometer equipped with a TitanS2 detector (CuKα radiation, λ = 1.54178 Å) (**C, 1, 3, 4, 5, 6**) or on a GV1000 diffractometer equipped with a TitanS2 detector (CuKα radiation, λ = 1.54178 Å) (**2**), respectively. The crystals were

kept at  $T = 123(1)$  K during data collection. Data collection and reduction were performed with *CrysAlis PRO* [Version V1.171.40.14a, 2018 (**1**), V1.171.38.41h, 2015 (**C**, **2**, **3**, **5**), V1.171.41.54a, 2020 (**4**, **6**)].<sup>13</sup> For all compounds a numerical absorption correction based on gaussian integration over a multifaceted crystal model and an empirical absorption correction using spherical harmonics as implemented in SCALE3 ABSPACK scaling algorithm was applied. The crystal structures were solved by dual methods or intrinsic phasing solution method with *SHELXT*<sup>14</sup> or *Olex2*<sup>15</sup> programs and refined by full-matrix least-squares method against  $|F|^2$  in anisotropic approximation using multiprocessor versions of SHELXL.<sup>16</sup> Hydrogen atoms were refined in calculated positions using riding on pivot atom model. In case of the disorder, the site occupancies of the disordered components were refined with their  $U_{\text{iso}}$  fixed at average  $U_{\text{eq}}$  for fully occupied atoms in given structure in order to avoid correlations. After refinement, occupancies were fixed at the resulting values and the refinement of the atomic displacement parameters was performed.

The  $\text{PF}_6^-$  molecule and one  $\text{CH}_2\text{Cl}_2$  molecule in **1** demonstrate disorder. Compound **2** shows an anion disordered over two positions. In compound **5** one As atom and the CO, Cp ligands coordinated to Mo atoms of half a  $\text{Cp}_2\text{Mo}_2\text{P}_2(\text{CO})_4$  dimer, as well as one  $\text{CH}_2\text{Cl}_2$  molecule show positional disorder, related to different mutual orientation. All CO and Cp ligands, as well as the  $\text{PF}_6^-$  molecule and one the linker molecule in compound **6** demonstrate positional disorder, related to different mutual orientation.

All ORTEP drawings for **C**, **1-6** were made with the Olex2 software.<sup>15</sup>

Table S4.1. Crystallographic details for C, 1, 2 and 3.

Compound	C · CH <sub>2</sub> Cl <sub>2</sub>	1 · 2 CH <sub>2</sub> Cl <sub>2</sub> / 1 CH <sub>3</sub> CN	2 · CH <sub>3</sub> CN	3
Data set (internal naming)	ems_282f_ hp_abs	ems_405_aP_ abs_gaus	ems_407_aP_ abs	ems_542f_mP_ abs
Formula	C <sub>44</sub> H <sub>34</sub> AgAs <sub>6</sub> Cl <sub>4</sub> F <sub>6</sub> Mo <sub>6</sub> O <sub>12</sub>	C <sub>74.7</sub> H <sub>61.4</sub> Ag <sub>2</sub> As <sub>8</sub> Cl <sub>5.4</sub> F <sub>12</sub> Mo <sub>8</sub> N <sub>4</sub> O <sub>16</sub> P <sub>2</sub>	Ag <sub>2</sub> As <sub>8</sub> C <sub>75</sub> Cl <sub>6</sub> F <sub>12</sub> H <sub>60</sub> Mo <sub>8</sub> N <sub>4</sub> O <sub>16</sub> P <sub>2</sub>	C <sub>22</sub> H <sub>16</sub> AgAs <sub>2</sub> F <sub>6</sub> Mo <sub>2</sub> N <sub>4</sub> O <sub>4</sub> P
<i>D</i> <sub>calc.</sub> / g · cm <sup>-3</sup>	2.352	2.142	2.162	2.348
μ/mm <sup>-1</sup>	18.306	15.754	15.937	16.591
Formula Weight	2174.51	3335.06	3358.53	994.95
Colour	red	red	red	red
Shape	block	block	block	block
Size/mm <sup>3</sup>	0.22×0.17×0.12	0.33×0.25×0.21	0.35×0.23×0.15	0.20×0.14×0.10
<i>T</i> /K	293.82(10)	122.97(13)	123.0(2)	123.01(10)
Crystal System	trigonal	triclinic	triclinic	monoclinic
Space Group	<i>P</i> 3̄1 <i>c</i>	<i>P</i> 1̄	<i>P</i> 1̄	<i>P</i> 2 <sub>1</sub> / <i>c</i>
<i>a</i> /Å	16.35(3)	12.9052(4)	12.8682(7)	12.5558(3)
<i>b</i> /Å	16.35(3)	12.9624(3)	13.0664(6)	21.4306(5)
<i>c</i> /Å	13.264(7)	16.0579(5)	15.9420(8)	10.6865(2)
α/°	90	97.822(2)	98.621(4)	90
β/°	90	103.366(3)	103.144(4)	101.817(2)
γ/°	120	91.281(2)	90.062(4)	90
<i>V</i> /Å <sup>3</sup>	3070(11)	2585.09(13)	2579.1(2)	2814.56(11)
<i>Z</i>	2	1	1	4
<i>Z</i> '	0.16667	0.5	0.5	1
Wavelength/Å	1.54184	1.54184	1.54184	1.54184
Radiation type	Cu K <sub>α</sub>	Cu K <sub>α</sub>	Cu K <sub>α</sub>	CuK <sub>α</sub>
θ <sub>min</sub> /°	3.121	2.859	2.881	3.596
θ <sub>max</sub> /°	74.442	74.232	74.868	74.231
Measured Refl.	33019	24671	16268	15640
Independent Refl.	2101	10080	9907	5559
Reflections with <i>I</i> > 2( <i>I</i> )	2093	9574	9310	5096
<i>R</i> <sub>int</sub>	0.0513	0.0347	0.0359	0.0547
Parameters	192	696	615	379
Restraints	219	130	150	18
Largest Peak	1.002	1.132	0.917	2.640
Deepest Hole	-0.790	-1.386	-1.075	-1.871
GooF	1.161	1.050	1.031	1.056
<i>wR</i> <sub>2</sub> (all data)	0.0906	0.0971	0.1015	0.1588
<i>wR</i> <sub>2</sub>	0.0905	0.0955	0.0996	0.1532
<i>R</i> <sub>1</sub> (all data)	0.0361	0.0372	0.0375	0.0628
<i>R</i> <sub>1</sub>	0.0361	0.0355	0.0359	0.0590



Table S4.2. Crystallographic details for 4, 5 and 6.

Compound	4	5 · CH <sub>2</sub> Cl <sub>2</sub>	6 · CH <sub>3</sub> CN
Data set (internal naming)	js2016_aP_abs_gaus	ems_404_mC_abs	js233_aP_abs_gaus
Formula	C <sub>90</sub> H <sub>80</sub> Ag <sub>4</sub> As <sub>8</sub> F <sub>24</sub> Mo <sub>8</sub> N <sub>8</sub> O <sub>16</sub> P <sub>4</sub>	C <sub>27</sub> H <sub>21</sub> AgAs <sub>3</sub> Cl <sub>2</sub> F <sub>6</sub> Mo <sub>3</sub> NO <sub>6</sub> P	C <sub>26</sub> AgAs <sub>2</sub> F <sub>6</sub> H <sub>24.5</sub> Mo <sub>2</sub> N <sub>4.5</sub> O <sub>4</sub> P
<i>D</i> <sub>calc.</sub> / g · cm <sup>-3</sup>	2.273	2.371	1.891
μ/mm <sup>-1</sup>	16.312	18.091	9.962
Formula Weight	3907.86	1291.77	996.98
Colour	clear orange	red	clear orange
Shape	block	block	block
Size/mm <sup>3</sup>	0.15×0.12×0.11	0.18×0.09×0.07	0.15×0.07×0.06
<i>T</i> /K	122.97(12)	123.11(10)	123.00(10)
Crystal System	triclinic	monoclinic	triclinic
Space Group	<i>P</i> $\bar{1}$	<i>C</i> 2/ <i>c</i>	<i>P</i> $\bar{1}$
<i>a</i> /Å	10.7861(2)	24.8486(4)	10.8770(2)
<i>b</i> /Å	20.7482(4)	18.8751(3)	13.3926(2)
<i>c</i> /Å	26.5944(5)	15.5925(3)	13.6762(2)
α/°	79.429(2)	90	100.5570(10)
β/°	87.128(2)	98.2656(17)	111.5570(10)
γ/°	77.470(2)	90	100.6310(10)
<i>V</i> /Å <sup>3</sup>	5710.9(2)	7237.2(2)	1751.07(5)
<i>Z</i>	2	8	2
<i>Z</i> '	1	1	1
Wavelength/Å	1.54184	1.54184 Cu K <sub>α</sub>	1.39222 Cu K <sub>β</sub>
Radiation type	Cu K <sub>α</sub>	Cu K <sub>α</sub>	Cu K <sub>β</sub>
<i>θ</i> <sub>min</sub> /°	3.381	2.951	3.153
<i>θ</i> <sub>max</sub> /°	74.148	74.254	69.506
Measured Refl.	63285	21960	21688
Independent Refl.	22500	7156	8567
Reflections with <i>I</i> > 2( <i>I</i> )	20378	6547	7586
<i>R</i> <sub>int</sub>	0.0468	0.0305	0.0324
Parameters	1463	559	705
Restraints	0	234	342
Largest Peak	1.064	0.868	1.020
Deepest Hole	-0.742	-0.760	-1.200
Goof	1.047	1.038	1.034
<i>wR</i> <sub>2</sub> (all data)	0.0754	0.0650	0.0746
<i>wR</i> <sub>2</sub>	0.0730	0.0627	0.0718
<i>R</i> <sub>1</sub> (all data)	0.0348	0.0286	0.0350
<i>R</i> <sub>1</sub>	0.0306	0.0254	0.0301

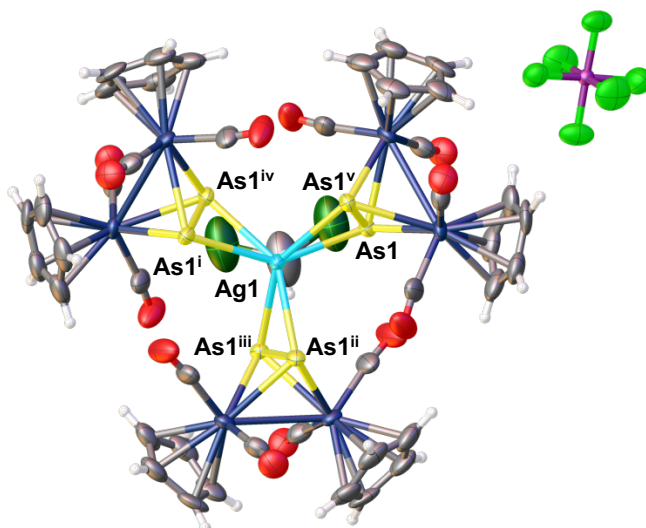


**Figure S4.1.** Molecular structure in the solid state of compound **C**. Thermal ellipsoids are depicted at 50% probability level.

**Table S4.3.** Selected geometric parameters (Å, °) for **C**.

Ag1—As1 <sup>i</sup>	2.752(4)	Ag1—As1 <sup>v</sup>	2.752(4)
Ag1—As1 <sup>ii</sup>	2.752(4)	Ag1—As1	2.752(4)
Ag1—As1 <sup>iii</sup>	2.752(4)	As1—As1 <sup>v</sup>	2.3676(17)
Ag1—As1 <sup>iv</sup>	2.752(4)		
As1 <sup>i</sup> —Ag1—As1 <sup>ii</sup>	50.95(7)	As1 <sup>i</sup> —Ag1—As1 <sup>v</sup>	105.06(3)
As1 <sup>iii</sup> —Ag1—As1	50.95(7)	As1 <sup>ii/iii</sup> —Ag1—As1 <sup>iv/v</sup>	145.76(2)
As1 <sup>iii</sup> —Ag1—As1 <sup>iv</sup>	105.77(4)	As1 <sup>v</sup> —Ag1—As1 <sup>iv</sup>	50.95(7)
As1 <sup>i</sup> —Ag1—As1 <sup>iii-iv</sup>	105.77(4)	As1—Ag1—As1 <sup>iv</sup>	105.06(3)

<sup>i</sup> Symmetry code:  $y-x, y, 3/2-z$ ; <sup>ii</sup> Symmetry code:  $1-y, 1-x, 3/2-z$ ; <sup>iii</sup> Symmetry code:  $y-x, 1-x, z$ ;

<sup>iv</sup> Symmetry code:  $1-y, 1+x-y, z$ ; <sup>v</sup> Symmetry code:  $x, 1+x-y, 3/2-z$ .

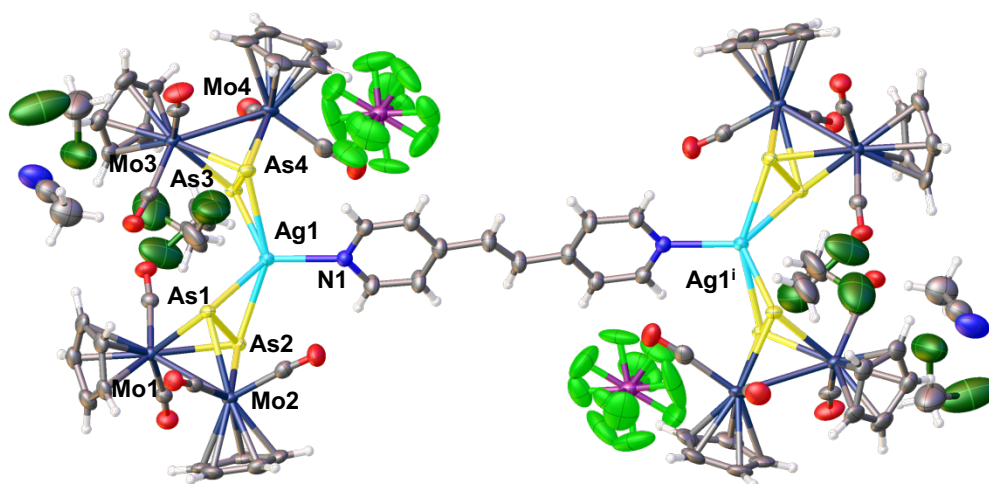


**Figure S4.2.** Molecular structure in the solid state of compound **1**. Thermal ellipsoids are depicted at 50% probability level. <sup>†</sup> symmetry codes: -x, -y, 1-z.

**Table S4.4.** Selected geometric parameters (Å, °) for **1**.

Ag1—As1	2.6823(5)	Ag1—N1	2.302(3)
Ag1—As2	2.7393(5)	As1—As2	2.3858(6)
Ag1—As3	2.7164(5)	As3—As4	2.3726(6)
Ag1—As4	2.7637(6)		
As1—Ag1—As2	52.201(13)	As3—Ag1—As4	51.302(14)
As1—Ag1—As3	118.165(16)	N1—Ag1—As1	127.19(9)
As1—Ag1—As4	105.770(16)	N1—Ag1—As2	109.78(9)
As2—Ag1—As4	149.395(16)	N1—Ag1—As3	114.12(9)
As3—Ag1—As2	115.542(17)	N1—Ag1—As4	100.60(9)

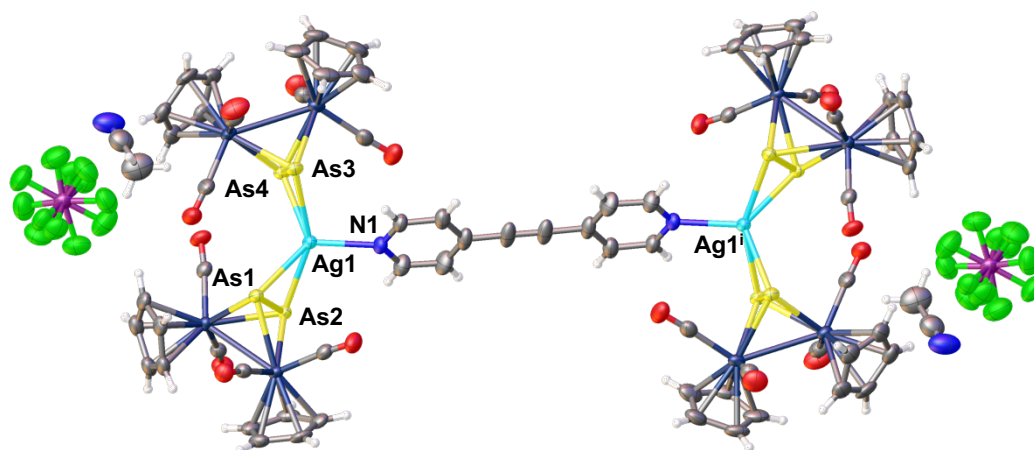


**Figure S4.3.** Molecular structure in the solid state of compound **2**. Thermal ellipsoids are depicted at 50% probability level. <sup>†</sup> symmetry codes: 2-x, 2-y, 1-z.

**Table S4.5.** Selected geometric parameters (Å, °) for **2**.

Ag1—As1	2.6764(5)	Ag1—N1	2.324(4)
Ag1—As2	2.7230(6)	As1—As2	2.3842(7)
Ag1—As3	2.7246(6)	As3—As4	2.3749(7)
Ag1—As4	2.7230(6)		
As1—Ag1—As2	52.398(15)	As4—Ag1—As3	51.693(15)
As1—Ag1—As3	108.037(19)	N1—Ag1—As1	127.01(10)
As1—Ag1—As4	119.285(18)	N1—Ag1—As2	107.58(10)
As2—Ag1—As3	151.525(19)	N1—Ag1—As3	100.85(10)
As4—Ag1—As2	115.296(19)	N1—Ag1—As4	113.55(10)

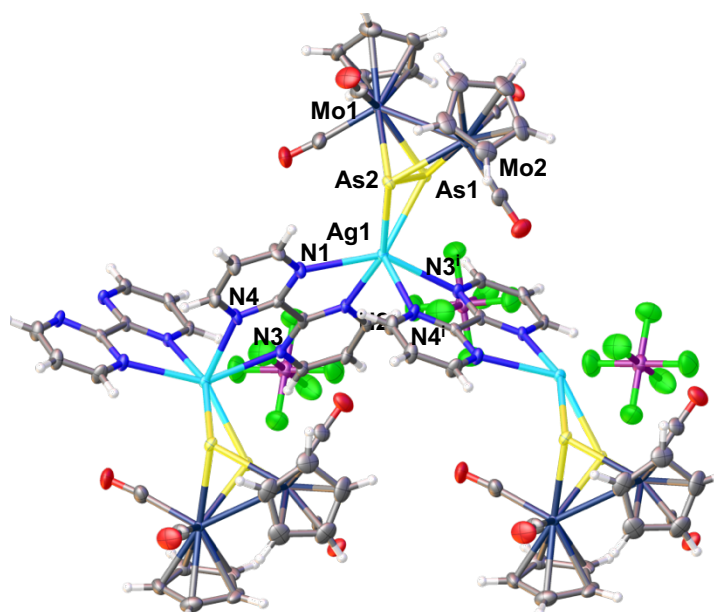


**Figure S4.4.** Part of the polymeric structure in the solid state of compound **3**. Thermal ellipsoids are depicted at 50% probability level. <sup>i</sup> symmetry codes:  $x, 1/2-y, 1/2+z$ .

**Table S4.6.** Selected geometric parameters (Å, °) for **3**.

Ag1—As1	2.7298(8)	Ag1—N3 <sup>i</sup>	2.596(5)
Ag1—As2	2.6314(8)	Ag1—N4 <sup>i</sup>	2.423(5)
Ag1—N1	2.553(5)	As1—As2	2.3777(8)
Ag1—N2	2.387(5)		
As2—Ag1—As1	52.61(2)	N4 <sup>i</sup> —Ag1—As1	124.83(13)
N3 <sup>i</sup> —Ag1—As1	84.29(12)	N4 <sup>i</sup> —Ag1—As2	101.77(14)
N3 <sup>i</sup> —Ag1—As2	118.01(12)	N4 <sup>i</sup> —Ag1—N3 <sup>i</sup>	65.51(17)
N2—Ag1—As1	128.78(12)	N4 <sup>i</sup> —Ag1—N1	94.12(18)
N2—Ag1—As2	154.87(12)	N1—Ag1—As1	130.07(14)
N2—Ag1—N3 <sup>i</sup>	85.81(16)	N1—Ag1—As2	93.45(13)
N2—Ag1—N4 <sup>i</sup>	95.30(18)	N1—Ag1—N3 <sup>i</sup>	144.67(18)
N2—Ag1—N1	66.81(17)		

<sup>i</sup> Symmetry code:  $x, 1/2-y, 1/2+z$ .

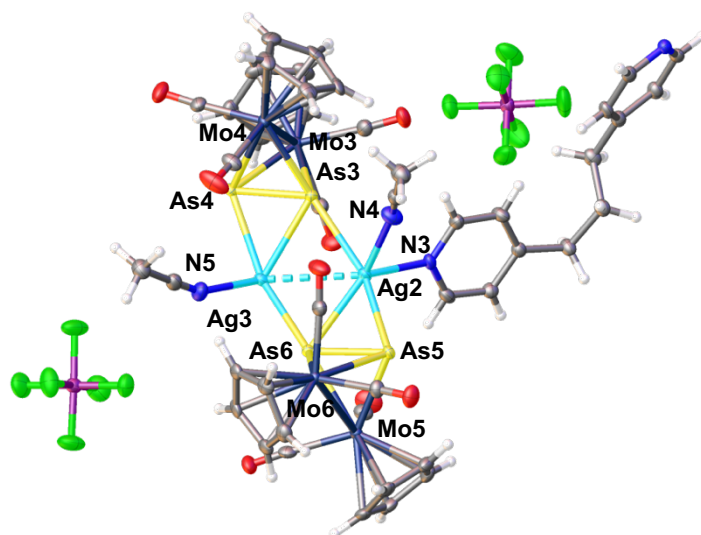


**Figure S4.5.** Part of the polymeric structure in the solid state of compound **4**. Thermal ellipsoids are depicted at 50% probability level.

**Table S4.7.** Selected geometric parameters (Å, °) for **4**.

Ag2—Ag3	2.9690(4)	Ag3—N5	2.463(4)
Ag2—As5	2.7177(4)	Mo4—Mo3	3.0704(4)
Ag2—As6	2.6953(4)	Mo4—As3	2.5518(5)
Ag2—As3	2.7257(5)	Mo4—As4	2.6589(5)
Ag2—N3	2.274(3)	Mo5—As5	2.5498(5)
Ag2—N4	2.482(4)	Mo5—As6	2.6216(5)
Ag3—As6	2.8073(4)	Mo6—Mo5	3.0644(4)
Ag3—As3	2.6912(5)	Mo6—As5	2.6632(4)
Ag3—As4	2.7096(5)	Mo6—As6	2.5569(4)
Ag3—N6	2.267(3)		
As5—Ag2—Ag3	111.542(12)	N4—Ag2—Ag3	121.41(10)
As5—Ag2—As3	155.758(15)	N4—Ag2—As5	93.18(9)
As6—Ag2—Ag3	59.186(11)	N4—Ag2—As6	121.59(9)
As6—Ag2—As3	52.407(11)	N4—Ag2—As3	79.43(10)
As3—Ag2—Ag3	56.207(11)	As6—Ag3—Ag2	55.544(10)
N3—Ag2—Ag3	126.56(8)	As3—Ag3—Ag2	57.323(11)
N3—Ag2—As5	105.17(8)	As3—Ag3—As6	109.941(14)
N3—Ag2—As6	136.56(8)	As3—Ag3—As4	52.595(12)
N3—Ag2—As3	98.30(8)	As4—Ag3—Ag2	109.798(12)
N3—Ag2—N4	92.96(13)	As4—Ag3—As6	158.611(16)

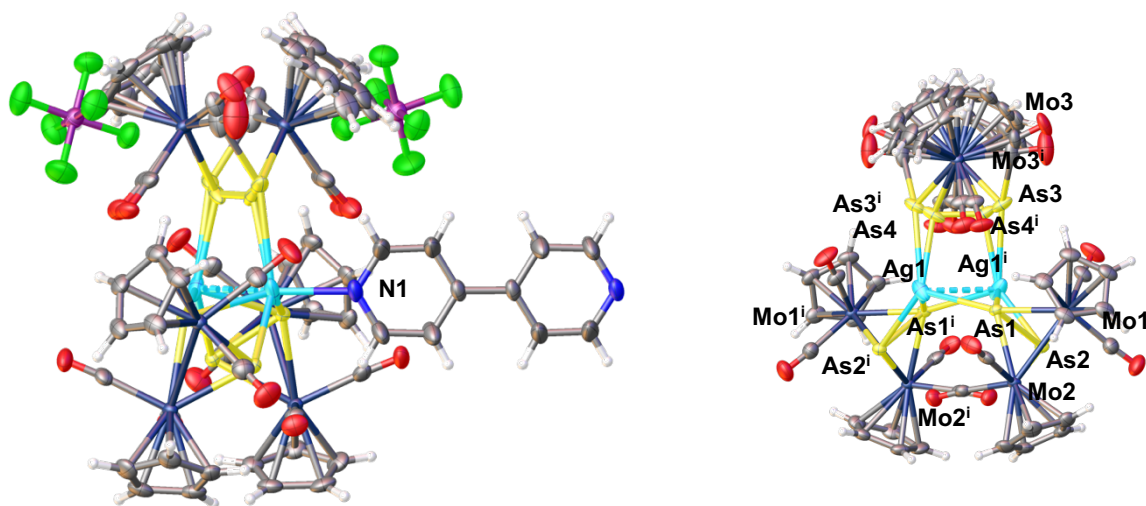


**Figure S4.6.** Part of the polymeric structure in the solid state of compound **5** (left). Disordered [Ag<sub>2</sub>B<sub>3</sub>]<sup>2+</sup> unit (right). Thermal ellipsoids are depicted at 50% probability level. <sup>i</sup> symmetry codes: 1-x, y, 3/2-z.

**Table S4.8.** Selected geometric parameters (Å, °) for **5**.

Mo1—Mo2	3.0653(3)	Ag1—Ag1 <sup>i</sup>	2.7866(6)
Mo1—As1	2.5787(4)	Ag1—As1	2.6997(4)
Mo1—As2	2.6464(4)	Ag1—As1 <sup>i</sup>	3.0965(5)
Mo2—As1	2.6364(4)	Ag1—As2	2.7515(4)
Mo2—As2	2.5599(4)	Ag1—As3	2.9209(14)
Mo3—Mo3 <sup>i</sup>	3.0745(5)	Ag1—N1	2.254(3)
Mo3—As3	2.6399(13)	As1—As2	2.3908(5)
Mo3—As4	2.6361(13)	As3—As4	2.350(3)
As1—Mo1—Mo2	54.878(10)	As2—Ag1—As1 <sup>i</sup>	121.065(16)
As1—Mo1—As2	54.440(12)	As2—Ag1—As3	126.36(3)
As2—Mo1—Mo2	52.633(10)	As3—Ag1—As1 <sup>i</sup>	110.95(3)
As1—Mo2—Mo1	53.133(10)	N1—Ag1—Ag1 <sup>i</sup>	138.87(9)
As2—Mo2—Mo1	55.249(10)	N1—Ag1—As1	150.00(9)
As2—Mo2—As1	54.763(12)	N1—Ag1—As1 <sup>i</sup>	85.95(10)
Ag1 <sup>i</sup> —Ag1—As1 <sup>i</sup>	54.324(13)	N1—Ag1—As2	99.50(8)
Ag1 <sup>i</sup> —Ag1—As3	89.73(3)	N1—Ag1—As3	96.09(9)
As1—Ag1—Ag1 <sup>i</sup>	68.697(13)	Ag1—As1—Ag1 <sup>i</sup>	56.979(12)
As1—Ag1—As2	52.016(11)	As2—As1—Ag1 <sup>i</sup>	110.353(16)
As1—Ag1—As3	95.36(3)	As2—As1—Ag1	65.107(13)
As2—Ag1—Ag1 <sup>i</sup>	109.492(13)	As4—As3—Ag1	79.70(5)

<sup>i</sup> Symmetry code: 1-x, y, 3/2-z.

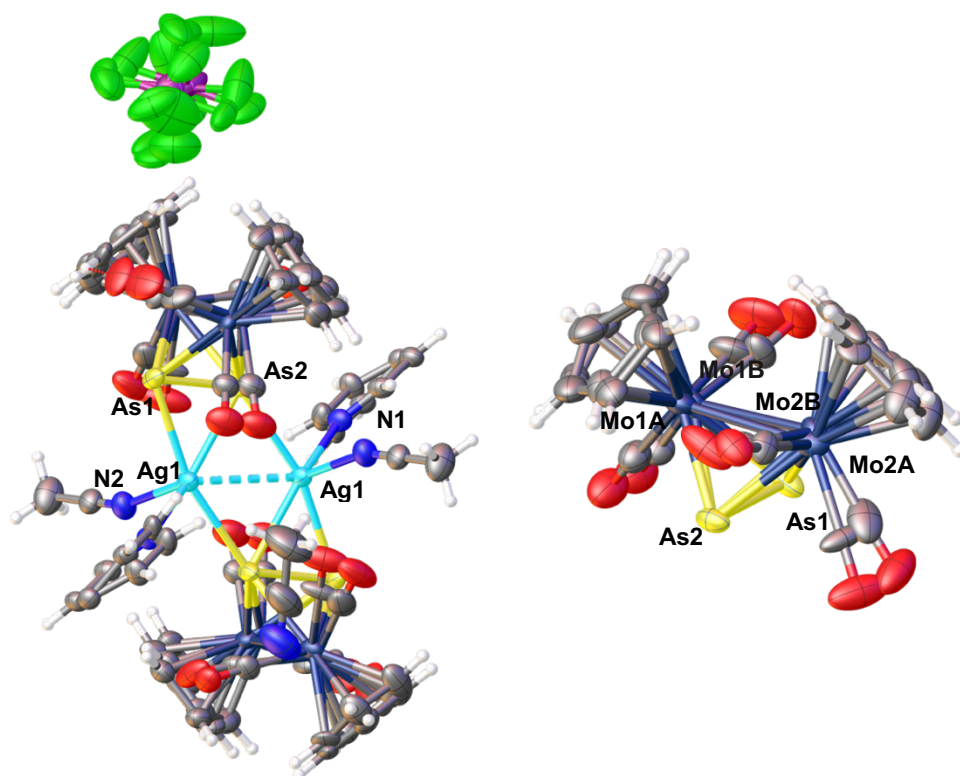


**Figure S4.7.** Part of polymeric structure in the solid state of compound **6** (left). Disordered molecular structure of the  $[\text{Cp}_2(\text{CO})_4\text{Mo}_2\text{As}_2]$  moiety (right). Thermal ellipsoids are depicted at 50% probability level.

**Table S4.9.** Selected geometric parameters (Å, °) for **6**.

Ag1—Ag1 <sup>i</sup>	2.9798(4)	Mo2A—As1	2.583(3)
Ag1—As2	2.6599(4)	Mo1A—As2	2.5180(13)
Ag1—As2 <sup>i</sup>	2.7437(4)	Mo1A—As1	2.7055(11)
Ag1—As1	2.7235(4)	As2—As1	2.3734(4)
Ag1—N1	2.309(2)	As2—Mo1B	2.615(4)
Ag1—N2	2.393(3)	As2—Mo2B	2.685(3)
Mo2A—Mo1A	3.108(3)	As1—Mo1B	2.450(3)
Mo2A—As2	2.543(3)	As1—Mo2B	2.511(3)
As2 <sup>i</sup> —Ag1—Ag1 <sup>i</sup>	55.199(9)	As1—Ag1—Ag2 <sup>i</sup>	164.634(13)
As2—Ag1—Ag1 <sup>i</sup>	57.888(9)	N1—Ag1—Ag1 <sup>i</sup>	131.56(7)
As2—Ag1—As2 <sup>i</sup>	113.087(10)	N1—Ag1—As2	145.00(7)
As2—Ag1—Ag1	52.302(10)	N1—Ag1—As2 <sup>i</sup>	85.77(7)
As1—Ag1—Ag1 <sup>i</sup>	109.998(12)	N1—Ag1—As1	104.49(7)
N1—Ag1—N2	94.78(10)	N2—Ag1—As2	114.17(7)
N2—Ag1—Ag1 <sup>i</sup>	109.69(8)	N2—Ag1—As1	102.03(8)
N2—Ag1—As2 <sup>i</sup>	88.23(8)		

<sup>i</sup> Symmetry code: 2-x, 1-y, 1-z.



## 4.5 References

- [1] a) L. Bai, Y. Li, X. Chen, L. Ji, X. Zhang, F. Yang, *ACS Appl. Nano Mater.* **2019**, *2*, 7728-7736; b) Y.-A. Sun, L.-T. Chen, S.-Y. Hsu, C.-C. Hu, D.-H. Tsai, *Langmuir* **2019**, *35*, 14203-14212; c) H.-M. Song, J. I. Zink, *RSC Adv.* **2019**, *9*, 4380-4389; d) Y. Luo, R. Li, J. Wnag, M. Zhang, L. Zou, L. Ling, *Science China: Chemistry* **2017**, *60*, 1575-1580; e) X. He, W. Wang, S. Li, Q. Wang, W. Zheng, Q. Shi, Y. Liu, *Nanoscale Research Lett.* **2015**, *10*, 1-6; f) J. Mucelini, I. Oestroem, A. O. Ortolan, K. F. Andriani, G. F. Caramori, R. L. T. Parreira, K. K. Laali, *Dalton Trans.* **2019**, *48*, 13281-13292.
- [2] a) I. Krossing, *J. Am. Chem. Soc.* **2001**, *123*, 4603-4604; b) N. Sinha, F. E. Hahn, *Acc. Chem. Res.* **2017**, *50*, 2167-2184; c) Y. Zhu, X. Li, Y. Li, Q. Wang, X. Lu, *Inorg. Chim. Acta* **2019**, *484*, 42-46; d) R. Donamaría, V. Lippolis, J. M. López-de-Luzuriaga, M. Monge, M. Nieddu, M. E. Olmos, *Inorg. Chem.* **2018**, *57*, 11099-11112; e) I. Krossing, *Chem. Eur. J.* **2001**, *7*, 490-502; f) B. Alvarez, M. A. Alvarez, I. Amor, M. E. García, M. A. Ruiz, *Inorg. Chem.* **2014**, *53*, 10325-10339.
- [3] a) A. A. Shmakova, A. S. Berezin, P. A. Abramov, M. N. Sokolov, *Inorg. Chem.* **2020**, *59*, 1853-1862; b) X.-N. Kuang, Y. Wang, N. Zhu, M. Liu, Y.-P. Yang, Z.-F. Li, H.-L. Han, Q.-H. Jin, *Wuji Huaxue Xuebao* **2018**, *34*, 1733-1738; c) S. Lin, Y.-Z. Cui, Q.-M. Qiu, H.-L. Han, Z.-F. Li, X. Liu, X.-L. Xin, Q.-H. Jin, *Polyhedron* **2017**, *134*, 319-329; d) W.-T. Chang, P.-Y. Lee, J.-H. Liao, K. K. Chakrahari, S. Kahlal, Y.-C. Liu, M.-H. Chiang, J.-Y. Saillard, C. W. Liu, *Angew. Chem. Int. Ed.* **2017**, *56*, 10178-10182; e) C. Schwarzmeier, A. Schindler, C. Heindl, S. Scheuermayer, E. V. Peresyphkina, A. V. Virovets, M. Neumeier, R. M. Gschwind, M. Scheer, *Angew. Chem. Int. Ed.* **2013**, *52*, 10896-10899; f) D. F. Gonzalez-Ramirez, P. Avila-Perez, L. G. Torres-Bustillos, R. Aguilar-Lopez, F. J. Esparza-Garcia, R. Rodriguez-Vazquez, *Int. J. Environ. Sci. Dev.* **2017**, *8*, 635-641.
- [4] a) K. Škoch, I. Císarová, J. Schulz, U. Siemeling, P. Štepička, *Dalton Trans.* **2017**, *46*, 10339-10354; b)
- [5] Selected publications: a) J. Bai, E. Leiner, M. Scheer, *Angew. Chem. Int. Ed.* **2002**, *41*, 783-786; b) M. Elsayed Moussa, P. A. Shelyganov, B. Wegley, M. Seidl, M. Scheer, *Eur. J. Inorg. Chem.* **2019**, 4241-4248; c) M. Fleischmann, F. Dielmann, L. J. Gregoriades, E. V. Peresyphkina, A. V. Virovets, S. Huber, A. T. Timoshkin, G. Balázs, M. Scheer, *Angew. Chem. Int. Ed.* **2015**, *54*, 13110-13115; d) M. Fleischmann, S. Welsch, H. Krauss, M. Schmidt, M. Bodensteiner,

- E. V. Peresyphkina, M. Sierka, C. Gröger, M. Scheer, *Chem. Eur. J.* **2014**, *20*, 3759-3768; e) C. Heindl, E. V. Peresyphkina, A. V. Virovets, V. Y. Komarov, M. Scheer, *Dalton Trans.* **2015**, *44*, 10245-10252; f) M. Elsayed Moussa, S. Welsch, L. J. Gregoriades, G. Balázs, M. Seidl, M. Scheer, *Eur. J. Inorg. Chem.* **2018**, 1683-1687.
- [6] a) M. Scheer, A. Schindler, R. Merkle, B. P. Johnson, M. Linseis, R. Winter, C. E. Anson, A. V. Virovets, *J. Am. Chem. Soc.* **2007**, *129*, 13386-13387; b) M. Scheer, J. Bai, B. P. Johnson, R. Merkle, A. V. Virovets, C. E. Anson, *Eur. J. Inorg. Chem.* **2005**, 4023-4026; c) C. Heindl, E. V. Peresyphkina, A. V. Virovets, W. Kremer, M. Scheer, *J. Am. Chem. Soc.* **2015**, *137*, 10938-10941; d) F. Dielmann, E. V. Peresyphkina, B. Krämer, F. Hastreiter, B. P. Johnson, M. Zabel, C. Heindl, M. Scheer, *Angew. Chem. Int. Ed.* **2016**, *55*, 14833-14837; e) F. Dielmann, M. Fleischmann, C. Heindl, E. V. Peresyphkina, A. V. Virovets, R. M. Gschwind, M. Scheer, *Chem. Eur. J.* **2015**, *21*, 6208-6214.
- [7] S. Welsch, C. Gröger, M. Sierka, M. Scheer, *Angew. Chem. Int. Ed.* **2011**, *50*, 1435-1438.
- [8] a) M. Elsayed Moussa, B. Attenberger, E. V. Peresyphkina, M. Fleischmann, G. Balázs, M. Scheer, *Chem. Commun.* **2016**, *52*, 10004-10007; b) M. Elsayed Moussa, B. Attenberger, M. Seidl, A. Schreiner, M. Scheer, *Eur. J. Inorg. Chem.* **2017**, 5616-5620; c) B. Attenberger, S. Welsch, M. Zabel, E. V. Peresyphkina, M. Scheer, *Angew. Chem. Int. Ed.* **2011**, *50*, 11516-11519; d) M. Elsayed Moussa, M. Seidl, G. Balázs, M. Zabel, A. V. Virovets, B. Attenberger, A. Schreiner, M. Scheer, *Chem. Eur. J.* **2017**, *23*, 16199-16203; e) B. Attenberger, E. V. Peresyphkina, M. Scheer, *Inorg. Chem.* **2015**, *54*, 7021-7029; f) M. Elsayed Moussa, M. Fleischmann, E. V. Peresyphkina, L. Dütsch, M. Seidl, G. Balázs, M. Scheer, *Eur. J. Inorg. Chem.* **2017**, 3222-3226; g) M. Elsayed Moussa, B. Attenberger, M. Fleischmann, A. Schreiner, M. Scheer, *Eur. J. Inorg. Chem.* **2016**, 4538-4541; h) M. Fleischmann, L. Dütsch, M. Elsayed Moussa, G. Balázs, W. Kremer, C. Lescop, M. Scheer, *Inorg. Chem.* **2016**, *55*, 2840-2854; i) M. Elsayed Moussa, B. Attenberger, E. V. Peresyphkina, M. Scheer, *Dalton Trans.* **2018**, *47*, 1014-1017.
- [9] M. Elsayed Moussa, J. Schiller, E. V. Peresyphkina, M. Seidl, G. Balázs, M. Scheer *manuscript in preparation*.
- [10] M. L. Ziegler, K. Blechschmitt, B. Nuber, T. Zahn, *Chem. Ber.* **1988**, *121*, 159-171.
- [11] H. Schmidbauer, A. Schier, *Angew. Chem. Int. Ed.* **2015**, *54*, 746-784.
- [12] P. J. Sullivan, A. L. Rheingold, *Organometallics* **1982**, *1*, 1547-1549.

- 
- [13] CrysAlisPro Software System, Rigaku Oxford Diffraction, (**2018**).
- [14] Sheldrick, G.M., ShelXT-Integrated space-group and crystal-structure determination, *Acta Cryst.* **2015**, *A71*, 3-8.5.G.
- [15] O.V. Dolomanov and L.J. Bourhis and R.J. Gildea and J.A.K. Howard and H. Puschmann, Olex2: A complete structure solution, refinement and analysis program, *J. Appl. Cryst.* **2009**, *42*, 339-341.
- [16] M. Sheldrick, Crystal structure refinement with ShelXL, *Acta Cryst.* **2015**, *C27*, 3-8.

## **Preface**

### **Authors**

Jana Schiller,<sup>†</sup> Andrea Schreiner,<sup>†</sup> Michael Seidl, Gábor Balázs and Manfred Scheer\*

### **Author contributions**

Jana Schiller and Andrea Schreiner contributed equally to this work. The manuscript was written by Jana Schiller and Andrea Schreiner. The synthesis, characterization and X-ray measurement of all phosphorus containing compounds (compounds **1-3**, **8,9**) and the X-ray measurement of compound **7** were performed by Andrea Schreiner. The synthesis, characterization and X-ray measurement of all arsenic containing compounds (compounds **4-7** and **10**) were performed by Jana Schiller, apart from the X-ray measurement of compound **7**. Michael Seidl performed the refinement of the solid-state structures and also wrote the experimental part of the X-ray measurement. Michael Seidl also contributed by supporting the X-ray measurements and revision of the manuscript. Gábor Balázs performed the DFT calculations, including the manuscript regarding the DFT calculations. Manfred Scheer contributed by supervising the research and revision of the manuscript.

### **Acknowledgements**

This work was supported by the Deutsche Forschungsgemeinschaft.

## 5. Unprecedented linking behavior of tetrahedral Mo<sub>2</sub>E<sub>2</sub> complexes (E = P, As) towards Cu(I) units

**Abstract:** The reaction of [Cp<sub>2</sub>Mo<sub>2</sub>(CO)<sub>4</sub>(μ,η<sup>2:2</sup>-E<sub>2</sub>)] (E = P (**A**), E = As (**B**), Cp = C<sub>5</sub>H<sub>5</sub>) with the WCA containing Cu(I) salts ([Cu(CH<sub>3</sub>CN)<sub>4</sub>][Al{OC(CF<sub>3</sub>)<sub>3</sub>}<sub>4</sub>] (Cu[TEF], **C**), [Cu(CH<sub>3</sub>CN)<sub>4</sub>][BF<sub>4</sub>] (**D**) and [Cu(CH<sub>3</sub>CN)<sub>3.5</sub>][FAI{OC<sub>6</sub>F<sub>12</sub>(C<sub>6</sub>F<sub>5</sub>)<sub>3</sub>] (Cu[FAI], **E**)) affords seven unprecedented coordination compounds (Scheme 5.1). Depending on the E<sub>2</sub> ligand complex, the anion of the copper salt and the stoichiometry, four novel dinuclear copper dimers and three trinuclear copper compounds are accessible. The latter complexes reveal first linear Cu<sub>3</sub> arrays linked by E<sub>2</sub> units (E = P, As) coordinated in a η<sup>2.1.1</sup> coordination mode. All compounds were characterized by X-ray crystallography, NMR and IR spectroscopy, mass spectrometry and elemental analysis. To define the nature of the Cu⋯Cu⋯Cu interactions DFT calculations were performed.

### 5.1 Introduction

In the last two decades the number of organometallic aggregates bearing Cu(I) units increased rapidly, owing to their wide range of applications and their versatile coordination chemistry.<sup>1</sup> Cu(I) compounds have proven to be useful in mimicking enzyme interactions,<sup>1a</sup> as anticancer drugs,<sup>1b</sup> and in other materials.<sup>1c</sup> Furthermore, Cu(I) derivatives turned out to be smart and novel solid-state emitters because of their accessibility and low costs.<sup>2</sup> Therefore, the development of *inter alia* extended linear Cu(I) arrays for potential applications in molecular electronics and luminescent materials gets more and more important. Some linear trinuclear cationic Cu(I) complexes bridged by P/N hybrid ligands, such as 7-diphenylphosphino-2,4-dimethyl-1,8-naphthyridine,<sup>3</sup> *N,N,N',N'',N'''*-pentamethyl-diethylen-triamine,<sup>4</sup> diphosphine/*N*-heterocyclic-carbene hybrid ligands<sup>5</sup> or the synthesis of halide-bridged trinuclear Cu(I) complexes connected by (diphenylphosphinomethyl)phenyl-phosphine<sup>6</sup> with Cu⋯Cu distances below the sum of the van der Waals radii were reported. However, Cu⋯Cu interactions were not confirmed by calculations. A variety of compounds containing different Cu(I) and organometallic polyphosphorus ligand complexes were previously reported by us.<sup>7</sup> We were able to show the formation of 1D, 2D and even 3D coordination polymers,<sup>8</sup> metal-organic nanosized capsules<sup>9</sup> and inorganic spherical supramolecules.<sup>10</sup> Additional to polyphosphorus complexes, organometallic polyarsenic ligand complexes have been known for many years.<sup>11</sup> However, their coordination chemistry is a rather uncharted area so far.<sup>12</sup> To bring metals in a close proximity for metallophilic interactions special building blocks are needed. One of such potential materials is the tetrahedral Mo<sub>2</sub>E<sub>2</sub>

moiety in the compounds  $[\text{Cp}_2\text{Mo}_2(\text{CO})_4(\mu, \eta^{2:2}\text{-E}_2)]$ , ( $\text{E} = \text{P}$  (**A**),  $\text{As}$  (**B**)).<sup>13</sup> Until now, basically three coordination modes have been observed for these  $\text{E}_2$  ligand complexes (Figure 5.1).<sup>7c,e</sup>

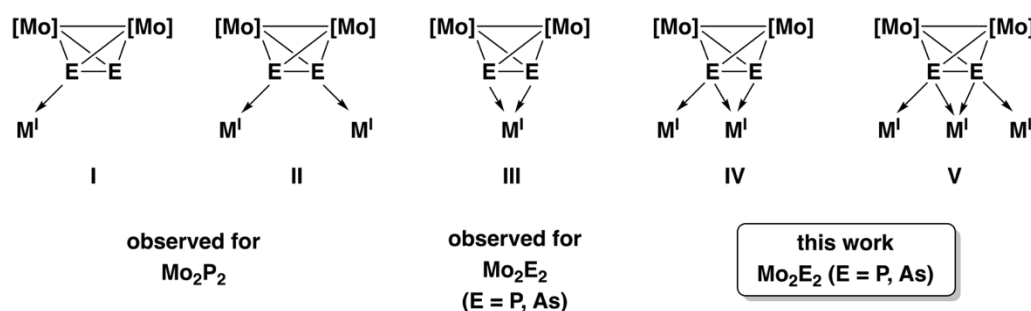


**Figure 5.1.** Reported and new coordination modes of  $\text{Mo}_2\text{E}_2$  complexes.  $\text{M}' = \text{Ag}(\text{I}), \text{Cu}(\text{I}), \text{Au}(\text{I})$ .  $[\text{Mo}] = [\text{CpMo}_2(\text{CO})_2]$ .<sup>7c,e</sup>

The lone pairs of one or two E atoms can either coordinate towards one or two metal centers *via*  $\sigma$ -coordination of the lone pairs (type **I** and **II**),<sup>7c,e</sup> or the E-E  $\sigma$ -orbital binds in a  $\pi$ -coordination to the metal center (type **III**).<sup>7e</sup> However, to bring metal cations in a close proximity, the coordination modes **IV** and **V** are needed, which are unknown for heteroelement  $\text{Mo}_2\text{E}_2$  compounds. Note, that the coordination mode **IV** have so far only be observed for mixed  $\text{EE}'$  derivatives ( $\text{E} = \text{P}, \text{E}' = \text{As}, \text{Sb}$ ).<sup>7b</sup> Herein we report the reactions of the polypnictogen ligand complexes  $[\text{Cp}_2\text{Mo}_2(\text{CO})_4(\mu, \eta^{2:2}\text{-E}_2)]$  (**A**:  $\text{E} = \text{P}$ , **B**:  $\text{E} = \text{As}$ ,  $\text{Cp} = \text{C}_5\text{H}_5$ ) with the  $\text{Cu}(\text{I})$  salts  $[\text{Cu}(\text{CH}_3\text{CN})_4][\text{BF}_4]$ ,  $[\text{Cu}(\text{CH}_3\text{CN})_3.5][\text{FAl}\{\text{OC}_6\text{F}_{12}(\text{C}_6\text{F}_5)\}_3]$  ( $\text{Cu}[\text{FAl}]$ ) and  $([\text{Cu}(\text{CH}_3\text{CN})_4][\text{Al}\{\text{OC}(\text{CF}_3)_3\}_4])$  ( $\text{Cu}[\text{TEF}]$ ) which lead, by variation of the stoichiometry of the used reactants, to seven unprecedented coordination compounds (**1-7**, Scheme 5.1) showing a novel  $\eta^{2:1:1}$  and  $\eta^{2:1}$  coordination behavior, respectively, of the  $\text{E}_2$  ligand complexes ( $\text{E} = \text{P}$ ). Moreover, compounds **1**, **2** and **6** show  $\text{Cu}\cdots\text{Cu}\cdots\text{Cu}$  interactions, which were analyzed by DFT calculations. For the first time a  $\eta^{2:1,1}$  coordination mode of both  $\text{E}_n$  ligand complexes **A** and **B** have been detected, in which both P/As atoms contribute *via*  $\sigma$ -bonding and  $\pi$ -coordination. To the best of our knowledge, these unprecedented linear  $\text{Cu}_3$  chains stabilized by  $\eta^{2:1,1}$ -coordination of only polypnictogen ligand complexes are the first ones to be observed.

## 5.2 Results and Discussion

The reaction of  $[\text{Cu}(o\text{-DFB})][\text{TEF}]$  ( $o\text{-DFB}$  = *ortho*-difluorobenzene) with **A** to give the dimeric compound  $[\text{Cu}_2(\text{Cp}_2\text{Mo}_2(\text{CO})_4(\mu_4, \eta^{2:2:1:1}\text{-P}_2)_2(\text{Cp}_2\text{Mo}_2(\text{CO})_4(\mu_3, \eta^{2:2:1}\text{-P}_2)_2)][\text{TEF}]$  (**F**), containing a  $\text{P}_4\text{Cu}_2$  6-membered ring, was reported a time ago (Figure 5.2).<sup>8c</sup>

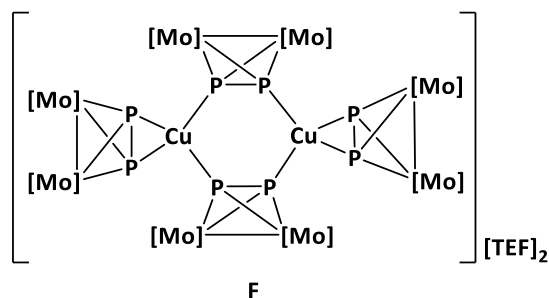
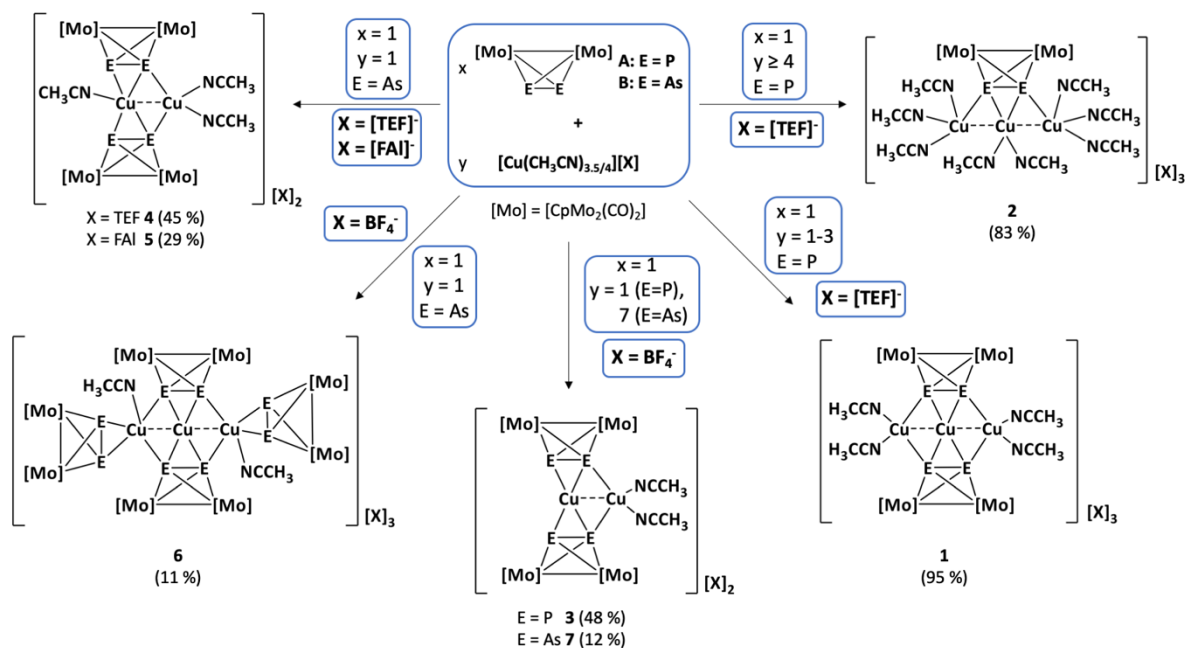


**Figure 5.2.** Structure of the dimeric compound **F**.<sup>8c</sup>

By using the different Cu(I) source  $[\text{Cu}(\text{CH}_3\text{CN})_4][\text{TEF}]$  (**C**)<sup>7a</sup> in the reaction with **A** we have been surprised to receive the new coordination compound  $[\text{Cu}\{\text{Cu}(\text{CH}_3\text{CN})_2\}_2\{\text{Cp}_2\text{Mo}_2(\text{CO})_4(\mu_5, \eta^{2:2:2:1:1}\text{-P}_2)_2\}][\text{TEF}]_3$  (**1**, Figure 5.3). Crystals of **1** as orange blocks in the trigonal space group  $P3_2$  were obtained by diffusion of *n*-pentane or toluene into the crude reaction mixture. When *n*-pentane was used, **1** crystallizes as red plates in the monoclinic space group  $P2_1/c$ . In compound **1**, two  $\text{P}_2$  ligand complexes **A** are coordinated to a molecular chain of three copper atoms ( $\text{Cu}\cdots\text{Cu}$  2.4344(10)-2.4537(19) Å) in a  $\eta^{2:2:2:1:1}$ -coordination mode. The peripheral copper atoms  $\text{Cu}_{\text{per}}$  are coordinated by two acetonitrile ligands each. Unlike other known structures, which feature a characteristic six-membered  $\text{Cu}_2\text{P}_4$  ring with **A** being coordinated in a  $\eta^{2:2:1:1}$ -coordination mode,<sup>8c,7c</sup> in **1**, a third additional copper atom is located in the center of this six-membered ring with an unprecedented type **V** like coordination (Scheme 5.1). Therefore, the P-P bonds in **1** (2.4344(10)-2.4537(19) Å) are elongated compared to the free **A** (2.0798(3) Å).<sup>13a</sup> The bonds between the peripheral copper atoms and the respective phosphorus atoms have values from 2.3830(19) to 2.460(3) Å, which are significantly longer than in the dimer **F** (2.240(3)-2.277(2) Å). The Cu-Cu-Cu angles in **1** are between 177.95(9)° and 180°, depending on the space group of the product, and the angles around the central copper atom are between 57.70(6)-62.39(9)°. Compound **1** presents the first trinuclear Cu(I) complex with such short  $\text{Cu}\cdots\text{Cu}$  distances, stabilized by the  $\eta^{2:1:1}$  coordination of a polypnictogen unit.



**Scheme 5.1.** Products of the reaction of **A** with  $[\text{Cu}(\text{CH}_3\text{CN})_4][\text{Al}\{\text{OC}(\text{CF}_3)_3\}_4]$  (**1/2**, depending on the stoichiometry), and with  $[\text{Cu}(\text{CH}_3\text{CN})_4][\text{BF}_4]$  (**3**) and reaction of **B** with the Cu(I) salts  $[\text{Cu}(\text{CH}_3\text{CN})_4][\text{Al}\{\text{OC}(\text{CF}_3)_3\}_4]$  (**4**),  $[\text{Cu}(\text{CH}_3\text{CN})_{3.5}][\text{FAI}\{\text{OC}_6\text{F}_{12}(\text{C}_6\text{F}_5)_3\}_3]$  (**5**) and  $[\text{Cu}(\text{CH}_3\text{CN})_4][\text{BF}_4]$  (**6/7**, depending on the stoichiometry). Yields are given in parentheses.

By using an excess of the Cu(I) salt **C** in the reaction with **A** ( $\text{CH}_2\text{Cl}_2$ , room temperature), the novel compound  $[\{\text{Cu}(\text{CH}_3\text{CN})_2\}\{\text{Cu}(\text{CH}_3\text{CN})_3\}_2\{\text{Cp}_2\text{Mo}_2(\text{CO})_4(\mu_5, \eta^{2:2:2:1:1}\text{-P}_2)\}][\text{TEF}]_3$  (**2**, Figure 5.3) was obtained. Compound **2** crystallizes as yellow blocks in the monoclinic space group  $P2_1/c$  and consists of only one ligand complex **A** coordinated to three copper atoms in a  $\eta^{2:2:2:1:1}$ -coordination mode type **V**. The peripheral copper atoms are saturated with three acetonitrile ligands each; the central copper atom has two acetonitrile ligands attached. The  $\text{Cu}\cdots\text{Cu}$  distances in **2** (3.0013(6) Å and 3.0593(6) Å) are significantly elongated compared to **1**. The distance between the two peripheral copper atoms are also significantly larger in **2** (5.8238(8) Å; **1**: 4.869(2)-4.904(2) Å). The Cu-P bonds are slightly longer for  $\text{Cu}_{\text{cen}}\text{-P}$  (2.3706(8) and 2.3909(8) Å), but shorter for  $\text{Cu}_{\text{per}}\text{-P}$  (2.2446(8) and 2.2520(8) Å), compared to **1**. Also, the Cu-Cu-Cu angle is with  $147.861(19)^\circ$  significantly more bent. The angles around the central copper atom possess values between  $47.55(2)$  and  $53.56(3)^\circ$ .

Furthermore, we were interested in the reactivity of the  $\text{As}_2$  ligand complex  $[\text{Cp}_2\text{Mo}_2(\text{CO})_4(\mu, \eta^2\text{-As}_2)]$  (**B**) towards  $[\text{Cu}(\text{CH}_3\text{CN})_4][\text{TEF}]$  (**C**). In a straightforward synthetic approach, mixing **B** with an equimolar amount of **C** in  $\text{CH}_2\text{Cl}_2$  at room



temperature, the new compound  $[\{\{\text{CpMo}(\text{CO})_2\}_2(\mu_5, \eta^{2:2:2:1}\text{-As}_2)\}\{\text{Cu}(\text{CH}_3\text{CN})_2\}]_2\text{Cu}(\text{CH}_3\text{CN})[\text{TEF}]_2$  (**4**) was obtained.

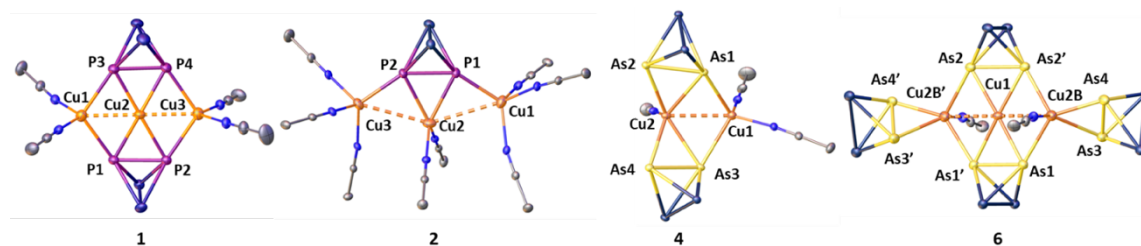


**Figure 5.3.** Molecular structures of the cationic parts of compounds **1**, **2**, **4** and **6** in the solid state. Cp- and CO-ligands and hydrogen atoms are omitted for clarity. Thermal ellipsoids are shown at 50% probability level. Only the major part of compound **6** is depicted (for further information see SI).

Layering with *n*-pentane afforded **4** in a moderate yield as red needles suitable for X-ray structure analysis (Figure 5.3).<sup>14</sup> **4** crystallizes in the triclinic space group  $P\bar{1}$  and reveals a Cu dimer stabilized by two  $\text{As}_2$  ligands **B**. Additionally, the copper atom Cu1 is coordinated by two and the copper atom Cu2 is coordinated by one acetonitrile ligand. Cu1 is  $\eta^1$ -coordinated by one As atom from both  $\text{As}_2$  ligand complexes **B**, Cu2 is  $\eta^2$ -coordinated by two complexes **B** in a new  $\eta^{2:1}$  coordination mode **IV**. The Cu $\cdots$ Cu distance (2.6925(7) Å) is elongated compared to **1**. The As-As bonds (2.3905(5)-2.3901(5) Å) are slightly elongated compared to the uncoordinated complex **B** (2.311(3) Å).<sup>15</sup> Additionally, the distances of the coordinating As atoms to Cu2 ( $\eta^2$ -coordination) are slightly longer (2.4849(6)-2.5312(6) Å) than the As-Cu1 distances ( $\eta^1$ -coordination, 2.4582(6)-2.4850(6) Å). A to **4** isostructural compound **5** containing a different counterion was formed by the reaction of **B** with the Cu(I) salt  $[\text{Cu}(\text{CH}_3\text{CN})_{3.5}][\text{FAI}]$  (**E**) (cf. Supporting Information).

Moreover, the unprecedented trinuclear complex **6** was obtained by reacting **B** with  $[\text{Cu}(\text{CH}_3\text{CN})_4][\text{BF}_4]$  in  $\text{CH}_2\text{Cl}_2$  at room temperature using equimolar amounts. By diffusion of *n*-pentane into the crude reaction mixture **6** crystallizes as dark red blocks in the monoclinic space groups  $C2/c$ . X-ray crystallography of **6** revealed that the central Cu atom has an occupancy of 0.8. Therefore, a complex with only the peripheral copper atoms is present with an occupancy of only 0.2. Furthermore, the acetonitrile molecules coordinated to the outer Cu atoms have an occupancy of 0.59 (for further details see SI). The major part (Figure 5.3) consists of a Cu<sub>3</sub> ( $d(\text{Cu}-\text{Cu}) = 2.587(4)$  Å) chain coordinated by four  $\text{As}_2$  ligand complexes **B**, with the peripheral copper atoms (Cu2B and Cu2B') coordinated additionally by one acetonitrile ligand each. While Cu2B and Cu2B' are  $\eta^2$ -side-on-coordinated by one molecule of **B** and  $\eta^1$ -end-on coordinated by two other  $[\text{Cp}_2\text{Mo}_2(\text{CO})_4(\mu, \eta^{2:2}\text{-As}_2)]$  moieties, Cu1 shows only  $\eta^2$ -side-on-coordination of two

molecules of **B**. The As-As bonds of the side-on-coordinated molecules **B** are tilted by an angle of 133° with regard to the plane As1-Cu1-As2'-Cu2B and accordingly tilted to an angle of 47° to the symmetry generated plane.

By using a 1:1 stoichiometry of **B** and **D** the product **6** was obtained with a composition of 2:1. It was expected that a higher ratio of **D** would lead to a product, which is similar to complex **1**. In contrast, using an excess of **D** compound **7** was formed. The structure of **7** is comparable to those of compounds **4** and **5** with the difference that Cu2 atom is not coordinated by a CH<sub>3</sub>CN molecule. However, the synthesis of a Mo<sub>2</sub>P<sub>2</sub> containing compound [Cu(CH<sub>3</sub>CN)<sub>2</sub>{Cu{Cp<sub>2</sub>Mo<sub>2</sub>(CO)<sub>4</sub>(μ<sub>4</sub>,η<sup>2:2:2:1</sup>-P<sub>2</sub>)<sub>2</sub>}[BF<sub>4</sub>]<sub>2</sub> (**3**) (Figure 5.3), which is isostructural with **7** was achieved by reacting equimolar amounts of **A** with **D**. The use of two equivalents of **A** lead to a compound containing a P<sub>4</sub>Cu<sub>2</sub> 6-membered ring similar to compound **F** (Figure 5.2).<sup>8c</sup> Compounds **3** (orange plates) and **7** (red plates) crystallize both in the monoclinic space group *I2/m*. For detailed information on their structures, see the Supporting Information.

The products **1-7** are well soluble in donor solvents such as CH<sub>3</sub>CN and slightly soluble in CH<sub>2</sub>Cl<sub>2</sub>, but insoluble in other common organic solvents such as THF, toluene and *n*-pentane. The NMR spectra of all compounds have been recorded in acetonitrile-*d*<sub>3</sub> at room temperature. The <sup>1</sup>H and <sup>13</sup>C{<sup>1</sup>H} NMR spectra of compounds **1-7** indicate decomplexation by showing signals corresponding to the proton and carbon nuclei of the Cp and CO ligands of **A** or **B**, respectively. The <sup>31</sup>P NMR spectra of compounds **1-3** show broad signals upfield shifted compared to the free P<sub>2</sub> ligand complex **A** (δ = -43.2 ppm).<sup>13a</sup> The broad signals in combination with already reported *variable-temperature* NMR studies on the Ag-dimer [Ag<sub>2</sub>(Cp<sub>2</sub>Mo<sub>2</sub>(CO)<sub>4</sub>(μ,η<sup>2:2:1:1</sup>-P<sub>2</sub>)<sub>2</sub>(Cp<sub>2</sub>Mo<sub>2</sub>(CO)<sub>4</sub>(μ,η<sup>2:2:1</sup>-P<sub>2</sub>)<sub>2</sub>)[TEF]<sub>7</sub><sup>c</sup> indicate a dynamic behavior in solution between **1-3** and monomeric fragments of them. Therefore, with acetonitrile being a coordinating solvent, decomplexation is most likely observed in solution. In the ESI mass spectra of **1-3**, peaks for the cationic fragments ([Cu{Cp<sub>2</sub>Mo<sub>2</sub>(CO)<sub>2</sub>P<sub>2</sub>}]<sup>+</sup>, [Cu(CH<sub>3</sub>CN){Cp<sub>2</sub>Mo<sub>2</sub>(CO)<sub>2</sub>P<sub>2</sub>}]<sup>+</sup> and [Cu(CH<sub>3</sub>CN)<sub>2</sub>]<sup>+</sup>) were detected. While the ESI mass spectra of **4-5** show peaks for the cationic fragments [{Cp<sub>2</sub>(CO)<sub>4</sub>Mo<sub>2</sub>As<sub>2</sub>}<sub>2</sub>Cu]<sup>+</sup> and [{Cp<sub>2</sub>(CO)<sub>4</sub>Mo<sub>2</sub>As<sub>2</sub>}Cu(CH<sub>3</sub>CN)]<sup>+</sup>, compounds **6-7** reveal an additional peak for [Cp<sub>2</sub>(CO)<sub>4</sub>Mo<sub>2</sub>As<sub>2</sub>]<sup>+</sup>. All compounds are air- and light-stable in the solid state for several days, but decompose within hours in solution when exposed to air.

The Cu...Cu distances in **1**, **2** and **6** are below the sum of the van-der-Waals radii<sup>16</sup> and are in the range of Cu(I)-Cu(I) single bonds (2.24 Å)<sup>17</sup> suggesting intramolecular metallophilic interactions. In order to elucidate the bonding situation in [{{CpMo(CO)<sub>2</sub>}}<sub>2</sub>(μ<sub>5</sub>,η<sup>2:2:2:1:1</sup>-P<sub>2</sub>)<sub>2</sub>]{Cu(CH<sub>3</sub>CN)<sub>2</sub>Cu]<sup>3+</sup> (**1**) and [{{CpMo(CO)<sub>2</sub>}}<sub>2</sub>(μ<sub>5</sub>,η<sup>2:2:2:1:1</sup>-

$P_2\})\{Cu(CH_3CN)_3\}_2Cu(CH_3CN)_2\}^{3+}$  (**2**), DFT calculations at the B3LYP/def2-TZVP level of theory have been performed. The Cu $\cdots$ Cu distances in **1** in the gas phase (2.559 Å) are similar to the distances in the solid state (2.4344(10) - 2.4537(19) Å). For **2**, the Cu $\cdots$ Cu distances are even longer in the gas phase (3.380 and 3.384 Å) compared to the solid state (3.0013(6) and 3.0593(6) Å). This indicates that the chelating effect of a second  $[[CpMo(CO)_2]_2(\mu, \eta^{2-2}-P_2)]$  is responsible for the relatively short Cu $\cdots$ Cu distances in **1**. The calculations also show that the bonding of the peripheral Cu ions to the  $P_2$  ligands in **1** takes place via the coordination of the phosphorus lone pairs, while the central Cu ion binds to the P-P  $\sigma$ -orbital of the  $P_2$  unit. This is clearly revealed by the Localized Molecular Orbitals (LMOs) (Figure 5.4).

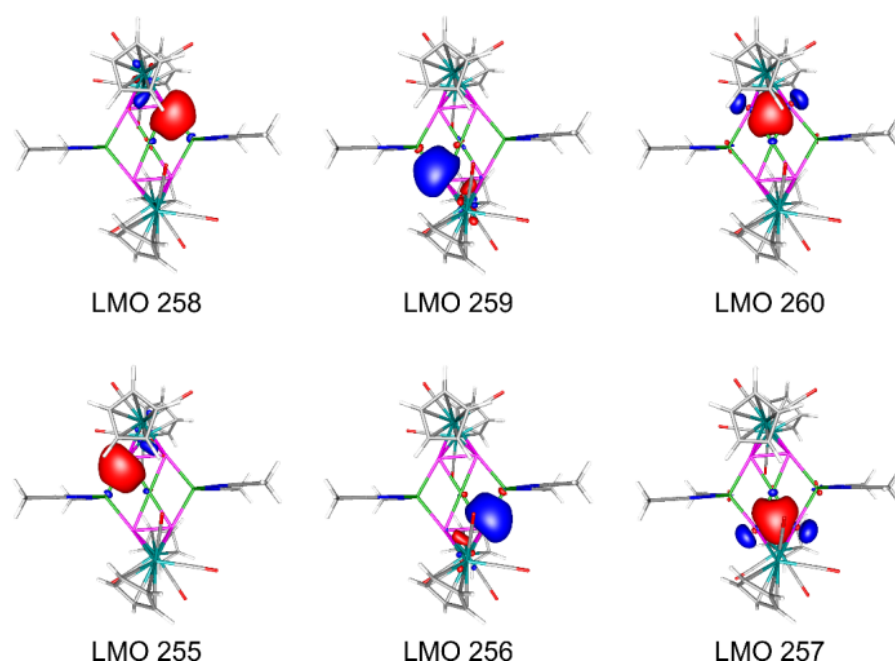


**Figure 5.4.** Selected Localized Molecular Orbitals (LMOs) representing the Cu-P bonding in  $[[[CpMo(CO)_2]_2(\mu_5, \eta^{2:2:2:1:1}-P_2)]_2\{Cu(CH_3CN)_2\}_2Cu]^{3+}$ , calculated at the B3LYP/def2-TZVP level of theory.

A small orbital contribution of the central Cu ion to the LMOs of the P-Cu<sub>per</sub> bond of roughly 7% has been detected for **1**. A comparison of the LMOs of **1** with that of  $[[[CpMo(CO)_2]_2(\mu_4, \eta^{2:2:1:1}-P_2)]_2\{Cu(CH_3CN)_2\}_2]^{2+}$  (**G**)<sup>7a</sup> shows that the bonding of the  $P_2$  ligand **A** to the peripheral Cu ions is very similar (Figure S5.3). The Wiberg Bond Indexes (WBIs) of the P-P bond in **G** is close to unity (1.06), while in **1** and **2** the WBIs of the P-P bonds are lower (0.78 in **1**; 0.72 in **2**), indicating a weaker P-P bond. This is not unexpected if considering the coordination of the P-P  $\sigma$ -bond additionally to the central Cu ion, which leads to depletion of the electron density in this bonding orbital. The WBIs of the peripheral Cu-P bonds in **1**, *i.e.* 0.40-0.44, are slightly lower than in **G** (0.53-0.55) and **2** (0.55), respectively. The WBIs of the Cu<sub>cen</sub>-P bonds in **1** are 0.29 (Cu9-P6, Cu9-

P8) and 0.40 (Cu9-P5, Cu9-P7) indicating a slightly asymmetric bonding and a preference for a linear coordination geometry of the central Cu ion. This is an explanation for the elongation of the P-P bond in **1** (WBI (Wiberg Bond Index) 0.78) compared to **G** (1.06). The calculations indicate that between the three Cu ions an interaction is present since a WBI of 0.11 has been found.

### 5.3 Conclusion

In conclusion, we synthesized seven unprecedented coordination compounds (**1-7**), obtained by reacting the  $\text{P}_2$  (**A**) and  $\text{As}_2$  (**B**) ligand complexes with three different Cu(I) salts (**C**, **D** and **E**) containing a WCA as counterion. Thus, four novel dinuclear copper dimers (**3**, **4**, **5** and **7**) and three trinuclear copper complexes (**1**, **2** and **6**) have been obtained. For the first time, a tetrahedral  $\text{Mo}_2\text{E}_2$  ligand complex is able to connect different metal atoms forming a chain of three Cu atoms. These complexes reveal the decisive influence of WCAs as a counterion in addition to the use Cu(I) salts with different coordinating solvent, as  $[\text{Cu}(\text{CH}_3\text{CN})_4][\text{TEF}]$  forms a novel trinuclear Cu(I) chain coordinated by two **A** units and  $[\text{Cu}(o\text{-DFB})][\text{TEF}]$  forms a  $\text{Cu}_2\text{P}_4$  ring.<sup>8c</sup> The  $\text{Cu}\cdots\text{Cu}$  distances in the trinuclear copper complexes **1**, **2** and **6** (2.4344(10)-2.4537(19) Å; 3.0013(6)/3.0593(6) Å; 2.587(4) Å) are below the sum of the van-der-Waals radii and in the range of Cu(I)-Cu(I) single bonds, suggesting intramolecular metallophilic interactions. DFT calculations for **1** at the B3LYP/def2-TZVP level of theory revealed that the bonding of the peripheral Cu ions to the  $\text{Mo}_2\text{P}_2$  ligands in **1** takes place via the coordination of the phosphorus lone pairs, while the central Cu ion binds to the P-P  $\sigma$ -orbital of the  $\text{Mo}_2\text{P}_2$  unit. Therefore, it can be concluded that there is an interaction present between the central and peripheral Cu ions, as a WBI of 0.11 has been found. Moreover, under the same reaction conditions, the  $\text{As}_2$  ligand complex **B** has a higher tendency to coordinate in an  $\eta^2$ -fashion and additionally, in a  $\eta^1:\eta^1$ -mode in comparison to the  $\text{P}_2$  complex **A**.

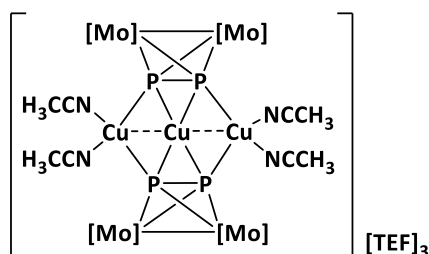
## 5.4 Supporting Information

### 5.4.1 General

All experiments were carried out in an inert atmosphere of nitrogen or argon using standard Schlenk techniques. The nitrogen/argon was dried and purified from traces of oxygen with a Cu/MgSO<sub>4</sub> catalyst, concentrated H<sub>2</sub>SO<sub>4</sub> and orange gel. Reactants were stored in a glovebox under argon atmosphere. All used solvents were taken from the solvent drying machine MB SPS-800 of the company MBRAUN. The precursors [Cp<sub>2</sub>Mo<sub>2</sub>(CO)<sub>4</sub>(μ,η<sup>2:2</sup>-P<sub>2</sub>)]<sup>13a</sup> (**A**), [Cp<sub>2</sub>Mo<sub>2</sub>(CO)<sub>4</sub>(μ,η<sup>2:2</sup>-As<sub>2</sub>)]<sup>13b</sup> (**B**), [Cu(CH<sub>3</sub>CN)<sub>4</sub>][Al{OC(CF<sub>3</sub>)<sub>3</sub>}<sub>4</sub>] (Cu[TEF], **C**)<sup>7a</sup> and [Cu(CH<sub>3</sub>CN)<sub>3.5</sub>][FAI{OC<sub>6</sub>F<sub>10</sub>(C<sub>6</sub>F<sub>6</sub>)<sub>3</sub>}] (Cu[FAI], **E**)<sup>7a</sup> were prepared according to literature procedures. [Cu(CH<sub>3</sub>CN)<sub>4</sub>][BF<sub>4</sub>] (**D**) was purchased from the company TCI and used without further purification. IR spectra were recorded as solids with an ATR-Ge disc on a Thermo Fisher Nicolet iS5 spectrometer. Solution NMR spectra were recorded on a Bruker Avance III HD 400 spectrometer (<sup>1</sup>H: 400 MHz, <sup>31</sup>P: 161 MHz, <sup>13</sup>C: 100 MHz, <sup>19</sup>F: 376 MHz, <sup>11</sup>B: 128 MHz) with acetonitrile-d<sub>3</sub> as solvent at room temperature. The signals of tetramethylsilane (<sup>1</sup>H, <sup>13</sup>C), CFC<sub>3</sub> (<sup>19</sup>F), Et<sub>2</sub>O x BF<sub>3</sub> (<sup>11</sup>B) and 85% H<sub>3</sub>PO<sub>4</sub> (<sup>31</sup>P) were used as reference for determining chemical shifts. The chemical shifts δ are presented in parts per million ppm and coupling constants *J* in Hz. The spectra were processed and analyzed using the software Bruker TopSpin 3.0. Elemental analyses were performed on an Elementar vario MICRO cube apparatus. Mass spectra were recorded on an Agilent Q-TOF 6540 UHD mass spectrometer with acetonitrile as solvent.

### 5.4.2 Synthetic procedure

Synthesis of [{{CpMo(CO)<sub>2</sub>}}<sub>2</sub>(μ<sub>5</sub>,η<sup>2:2:2:1:1</sup>-P<sub>2</sub>)}<sub>2</sub>{Cu(CH<sub>3</sub>CN)<sub>2</sub>}}<sub>2</sub>Cu[TEF]<sub>3</sub> (**1**):



Compounds **A** (1 eq., 5 mg, 0.01 mmol) and Cu[TEF] (3 eq., 79.4 mg, 0.05 mmol) were dissolved in CH<sub>2</sub>Cl<sub>2</sub> (5 mL each). Subsequently, the solution of **C** was added dropwise to the solution of **A**. The clear reaction mixture was stirred for 3h, filtered and stored at -30 °C. After one day, compound **1** was obtained as clear orange blocks (**1a**) or red plates

(1b). The supernatant was decanted off, the remaining crystals washed with *n*-pentane and dried *in vacuo*. Crystalline Yield: 39 mg (95 %, related to **A**).

<sup>1</sup>H NMR (CD<sub>3</sub>CN): δ = 5.32 (s, 10H, C<sub>5</sub>H<sub>5</sub>).

<sup>13</sup>C {<sup>1</sup>H} NMR (CD<sub>3</sub>CN): δ = 226.1 (CO), 87.6 (C<sub>5</sub>H<sub>5</sub>).

<sup>31</sup>P {<sup>1</sup>H} NMR (CD<sub>3</sub>CN): δ = -54.0 - -59.5 (bs).<sup>18</sup>

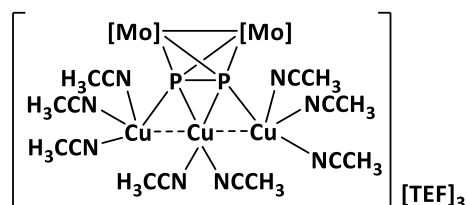
<sup>19</sup>F {<sup>1</sup>H} NMR (CD<sub>3</sub>CN): δ = -74.8 (s).

Positive ion ESI-MS (CH<sub>3</sub>CN, RT): *m/z* (%) = 1056.56 (60) [Cu{Cp<sub>2</sub>Mo<sub>2</sub>(CO)<sub>2</sub>P<sub>2</sub>}]<sup>+</sup>, 599.77 (100) [Cu(CH<sub>3</sub>CN){Cp<sub>2</sub>Mo<sub>2</sub>(CO)<sub>2</sub>P<sub>2</sub>}]<sup>+</sup>.

Elemental analysis, calc. for C<sub>84</sub>H<sub>32</sub>Al<sub>3</sub>Cu<sub>3</sub>F<sub>108</sub>Mo<sub>4</sub>N<sub>4</sub>O<sub>20</sub>P<sub>4</sub> (4253.24 g/mol) (%): C, 23.75; H, 0.76; N 1.31; found: C, 23.89; H, 0.83; N, 1.29.

IR (solid, CO bands):  $\tilde{\nu}/\text{cm}^{-1}$ : 2037 (w), 2013 (w), 1983 (w).

Synthesis of [{{CpMo(CO)<sub>2</sub>}}<sub>2</sub>(μ<sub>5,η</sub><sup>2:2:2:1:1</sup>-P<sub>2</sub>)]{Cu(CH<sub>3</sub>CN)<sub>3</sub>}}<sub>2</sub>Cu(CH<sub>3</sub>CN)<sub>2</sub>][TEF]<sub>3</sub> (**2**):



Compounds **A** (1 eq., 5 mg, 0.01 mmol) and Cu[TEF] (4 eq., 64 mg, 0.04 mmol) were dissolved in CH<sub>2</sub>Cl<sub>2</sub> (5 mL each). Subsequently, the solution of **C** was added dropwise to the solution of **A**. The clear reaction mixture was stirred for 3h, filtered and stored at -30 °C. After one day, compound **2** was obtained as yellow blocks. The supernatant was decanted off, the remaining crystals washed with *n*-pentane and dried *in vacuo*. Crystalline Yield: 38.7 mg (99 %, reverved to **A**).

<sup>1</sup>H NMR (CD<sub>3</sub>CN): δ = 5.32 (s, 10H, C<sub>5</sub>H<sub>5</sub>).

<sup>13</sup>C {<sup>1</sup>H} NMR (CD<sub>3</sub>CN): δ = 226.2 (s, CO), 87.5 (C<sub>5</sub>H<sub>5</sub>).

<sup>31</sup>P {<sup>1</sup>H} NMR (CD<sub>3</sub>CN): δ = -57.8 - -64.3 (bs).<sup>18</sup>

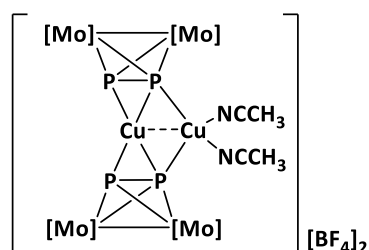
<sup>19</sup>F {<sup>1</sup>H} NMR (CD<sub>3</sub>CN): δ = -74.8 (s).

Positive ion ESI-MS (CH<sub>3</sub>CN, RT): *m/z* (%) = 1056.56 (60) [Cu{Cp<sub>2</sub>Mo<sub>2</sub>(CO)<sub>2</sub>P<sub>2</sub>}]<sup>+</sup>, 599.77 (100) [Cu(CH<sub>3</sub>CN){Cp<sub>2</sub>Mo<sub>2</sub>(CO)<sub>2</sub>P<sub>2</sub>}]<sup>+</sup>.

Elemental analysis, calc. for C<sub>78</sub>H<sub>34</sub>Al<sub>3</sub>Cu<sub>3</sub>F<sub>108</sub>Mo<sub>2</sub>N<sub>8</sub>O<sub>16</sub>P<sub>2</sub> (3917,53 g/mol) (%): C, 23.89; H, 0.87; N 2.86; found: C, 24.22; H, 0.70; N, 2.82.

IR (solid, CO bands):  $\tilde{\nu}/\text{cm}^{-1}$ : 2009 (w), 1972 (w).

Synthesis of  $[\{\{\text{CpMo}(\text{CO})_2\}_2(\mu_5, \eta^{2:2:2:1}\text{-P}_2)\}\{\text{Cu}(\text{CH}_3\text{CN})_2\}\text{Cu}][\text{BF}_4]_2$  (**3**):



Compounds **A** (1.9 eq., 88 mg, 0.28 mmol) and  $[\text{Cu}(\text{CH}_3\text{CN})_4][\text{BF}_4]$  (1 eq., 351.7 mg, 0.15 mmol) were dissolved in  $\text{CH}_2\text{Cl}_2$  (5 mL each) and the solution of **D** was added dropwise to the solution of **A**. The clear reaction mixture was stirred for 3h, filtered and stored at  $-30\text{ }^\circ\text{C}$ . After one day, compound **3** was obtained as clear intense red blocks. The supernatant was decanted, the remaining crystals were washed with *n*-pentane and dried *in vacuo*. Crystalline yield: 46 mg (48 %, related to **A**).

$^1\text{H}$  NMR ( $\text{CD}_3\text{CN}$ ):  $\delta = 5.33$  (s, 10H,  $\text{C}_5\text{H}_5$ ).

$^{13}\text{C}$   $\{^1\text{H}\}$  NMR ( $\text{CD}_3\text{CN}$ ):  $\delta = 225.4$  (**CO**), 87.7 ( $\text{C}_5\text{H}_5$ ).

$^{31}\text{P}$   $\{^1\text{H}\}$  NMR ( $\text{CD}_3\text{CN}$ ):  $\delta = -69.5$ - $59.8$  (bs).<sup>18</sup>

$^{19}\text{F}$   $\{^1\text{H}\}$  NMR ( $\text{CD}_3\text{CN}$ ):  $\delta = -150.6$  (bs).

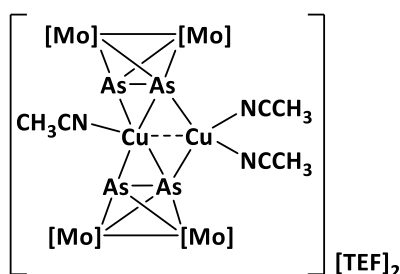
$^{11}\text{B}$   $\{^1\text{H}\}$  NMR ( $\text{CD}_3\text{CN}$ ):  $\delta = -0.56$  (s).

Positive ion ESI-MS ( $\text{CH}_3\text{CN}$ , RT):  $m/z$  (%) = 1056.56 (60)  $[\text{Cu}\{\text{Cp}_2\text{Mo}_2(\text{CO})_2\text{P}_2\}_2]^+$ , 599.77 (100)  $[\text{Cu}(\text{CH}_3\text{CN})\{\text{Cp}_2\text{Mo}_2(\text{CO})_2\text{P}_2\}]^+$ , 144.98 (100)  $[\text{Cu}(\text{CH}_3\text{CN})_2]^+$ .

Elemental analysis, calc. for  $\text{C}_{32}\text{H}_{26}\text{B}_2\text{Cu}_2\text{F}_8\text{Mo}_4\text{N}_2\text{O}_8\text{P}_4$  (1381,55 g/mol) (%): C, 27.79; H, 1.90; N 2.03; found: C, 27.97; H, 1.89; N, 2.03.

IR (solid, CO bands):  $\tilde{\nu}/\text{cm}^{-1}$ : 1971 (s), 1932 (w), 1911(s).

Synthesis of  $[\{\{\text{CpMo}(\text{CO})_2\}_2(\mu_5, \eta^{2:2:2:1}\text{-As}_2)\}\{\text{Cu}(\text{CH}_3\text{CN})_2\}\text{Cu}(\text{CH}_3\text{CN})][\text{TEF}]_2$  (**4**):



$[\text{Cu}(\text{CH}_3\text{CN})_4][\text{Al}\{\text{OC}(\text{CF}_3)_3\}_4]$  (1 eq., 60 mg, 0.05 mmol) was dissolved in  $\text{CH}_2\text{Cl}_2$  (5 mL) and was added to a solution of  $\text{Cp}_2\text{Mo}_2(\text{CO})_4(\eta^2\text{-As}_2)$  (**B**) (1 eq., 29 mg, 0.05 mmol) in  $\text{CH}_2\text{Cl}_2$  (5 mL) and stirred for 2h at room temperature. The red solution was carefully layered with threefold amount of *n*-pentane and stored at room temperature. After one

day, red needles were formed. The crystals were washed with *n*-pentane and dried *in vacuo*. Crystalline Yield: 75 mg (89 %, referred to **B**).

<sup>1</sup>H NMR (CD<sub>3</sub>CN): δ = 5.45 (s, 10H, C<sub>5</sub>H<sub>5</sub>) + 5.26 Mo<sub>2</sub>As<sub>2</sub>.

<sup>13</sup>C {<sup>1</sup>H} NMR (CD<sub>3</sub>CN): δ = 227.59 (CO), 85.80 (C<sub>5</sub>H<sub>5</sub>).

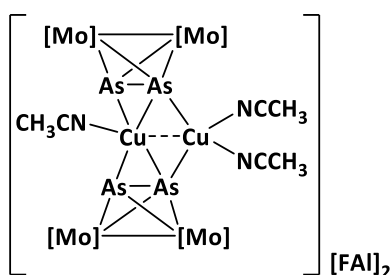
<sup>19</sup>F {<sup>1</sup>H} NMR (CD<sub>3</sub>CN): δ = -74.78.

Positive ion ESI-MS (CH<sub>3</sub>CN, RT): *m/z* (%) = 1232.3 (60) [Cp<sub>2</sub>(CO)<sub>4</sub>Mo<sub>2</sub>As<sub>2</sub>]<sub>2</sub>Cu]<sup>+</sup>, 687.7 (100) [Cp<sub>2</sub>(CO)<sub>4</sub>Mo<sub>2</sub>As<sub>2</sub>]<sub>2</sub>Cu(CH<sub>3</sub>CN)]<sup>+</sup>, 583.7 (12) [Cp<sub>2</sub>(CO)<sub>4</sub>Mo<sub>2</sub>As<sub>2</sub>]<sup>+</sup>.

Elemental analysis, calc. for C<sub>66</sub>H<sub>29</sub>Al<sub>2</sub>As<sub>4</sub>Cu<sub>2</sub>F<sub>72</sub>Mo<sub>4</sub>N<sub>3</sub>O<sub>16</sub> (3352.35 g/mol) (%): C, 23.92; H, 0.88; N 2.86; found: C, 24.22; H, 0.70; N, 2.82.

IR (solid, CO bands):  $\tilde{\nu}/\text{cm}^{-1}$ : 1275 (s), 1298 (s), 1240 (vs), 1215 (vs).

Synthesis of [CpMo(CO)<sub>2</sub>]<sub>2</sub>(μ<sub>5</sub>,η<sup>2:2:2:1</sup>-As<sub>2</sub>){Cu(CH<sub>3</sub>CN)<sub>2</sub>}[Cu(CH<sub>3</sub>CN)] [FAI]<sub>2</sub> (**5**):



[Cu(CH<sub>3</sub>CN)<sub>3.5</sub>][FAI{OC(C<sub>6</sub>F<sub>10</sub>)(C<sub>6</sub>F<sub>5</sub>)<sub>3</sub>}] (1 eq., 79 mg, 0.05 mmol) dissolved in CH<sub>2</sub>Cl<sub>2</sub> (5 mL), was added to a solution of Cp<sub>2</sub>Mo<sub>2</sub>(CO)<sub>4</sub>(η<sup>2</sup>-As<sub>2</sub>) (**B**) (1 eq., 29 mg, 0.05 mmol) in CH<sub>2</sub>Cl<sub>2</sub> (5 mL) and stirred for 2h at room temperature. The red solution was carefully layered with threefold amount of *n*-pentane and stored at room temperature. After one day, orange plates crystallized. The crystals were washed with *n*-pentane and dried *in vacuo*. Crystalline Yield: 60 mg (57 %, referred to **B**).

<sup>1</sup>H NMR (CD<sub>3</sub>CN): δ = 5.45 (s, 10H, C<sub>5</sub>H<sub>5</sub>) + 5.26 Mo<sub>2</sub>As<sub>2</sub>.

<sup>13</sup>C {<sup>1</sup>H} NMR (CD<sub>3</sub>CN): δ = 227.75 (CO), 85.85 (C<sub>5</sub>H<sub>5</sub>).

<sup>19</sup>F {<sup>1</sup>H} NMR (CD<sub>3</sub>CN): δ = -111.64 (d, *J*<sub>F,F</sub> = 283 Hz, 2F), -116.14 (d, *J*<sub>F,F</sub> = 280Hz, 2F), -121.13 (d, *J*<sub>F,F</sub> = 280Hz, 2F), -127.84 (s, 2F), -129.77 (d, *J*<sub>F,F</sub> = 280Hz, 2F), -136.46 (d, *J*<sub>F,F</sub> = 280Hz, 2F), -140.79 (d, *J*<sub>F,F</sub> = 280Hz 1F), -154.00 (tt, <sup>2</sup>*J*<sub>F,F</sub> = 21Hz, <sup>3</sup>*J*<sub>F,F</sub> = 6Hz, 1F), 164.70 (td, <sup>2</sup>*J*<sub>F,F</sub> = 21Hz, <sup>3</sup>*J*<sub>F,F</sub> = 6Hz, 1F), -170.63 (s, 1F).

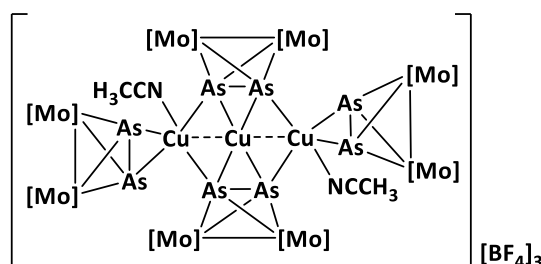
Positive ion ESI-MS (CH<sub>3</sub>CN, RT): *m/z* (%) = 1232.3 (51) [Cp<sub>2</sub>(CO)<sub>4</sub>Mo<sub>2</sub>As<sub>2</sub>]<sub>2</sub>Cu]<sup>+</sup>, 687.7 (100) [Cp<sub>2</sub>(CO)<sub>4</sub>Mo<sub>2</sub>As<sub>2</sub>]<sub>2</sub>Cu(CH<sub>3</sub>CN)]<sup>+</sup>, 583.7 (37) [Cp<sub>2</sub>(CO)<sub>4</sub>Mo<sub>2</sub>As<sub>2</sub>]<sup>+</sup>.

Elemental analysis, calc. for C<sub>106</sub>H<sub>29</sub>Al<sub>2</sub>As<sub>4</sub>Cu<sub>2</sub>F<sub>92</sub>Mo<sub>4</sub>N<sub>3</sub>O<sub>14</sub> (4180.73 g/mol) (%): C, 30.45; H, 0.70; N, 1.01; found: C, 30.38; H, 0.61; N, 0.61.

IR (solid, CO bands):  $\tilde{\nu}/\text{cm}^{-1}$ : 2005 (s), 1979 (s), 1950 (s), 1934 (s).



Synthesis of  $[\{\{\text{CpMo}(\text{CO})_2\}_2(\mu_5, \eta^{2:2:2:1:1}\text{-As}_2)\}_2\{\{\text{CpMo}(\text{CO})_2\}_2(\mu_5, \eta^{2:2:2}\text{-As}_2)\}_2\{\text{Cu}(\text{CH}_3\text{CN})\}_2\text{Cu}][\text{BF}_4]_3$  (**6**):



$[\text{Cu}(\text{CH}_3\text{CN})_4][\text{BF}_4]$  (1 eq., 16 mg, 0.05 mmol), dissolved in  $\text{CH}_2\text{Cl}_2$  (5 mL), was added to a solution of  $\text{Cp}_2\text{Mo}_2(\text{CO})_4(\eta^2\text{-As}_2)$  (**B**) (1 eq., 29 mg, 0.05 mmol) in  $\text{CH}_2\text{Cl}_2$  (5 mL) and stirred for 2h at room temperature. The red solution was filtered and carefully layered with threefold amount of *n*-pentane and stored at room temperature. After one day dark red block-shaped crystals were formed. The crystals were washed with *n*-pentane and dried *in vacuo*. Crystalline Yield: 15 mg (43%, referred to **B**).

$^1\text{H}$  NMR ( $\text{CD}_3\text{CN}$ ):  $\delta = 5.45$  (s, 10H, Cp) + 5.26  $\text{Mo}_2\text{As}_2$ .

$^{13}\text{C}$   $\{^1\text{H}\}$  NMR ( $\text{CD}_3\text{CN}$ ):  $\delta = 227.22$  (CO), 85.82 ( $\text{C}_5\text{H}_5$ ).

$^{19}\text{F}$   $\{^1\text{H}\}$  NMR ( $\text{CD}_3\text{CN}$ ):  $\delta = -150.66$  (d,  $^1J_{\text{B,F}} = 19.8$  Hz).

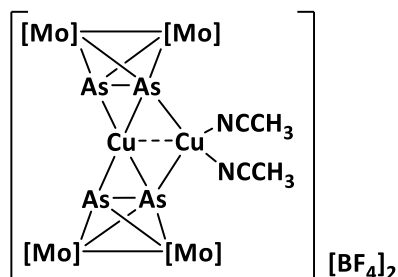
$^{11}\text{B}$   $\{^1\text{H}\}$  NMR ( $\text{CD}_3\text{CN}$ ):  $\delta = -0.57$  (s).

Positive ion ESI-MS ( $\text{CH}_3\text{CN}$ , RT):  $m/z$  (%) = 1232.4 (100)  $[\{\{\text{Cp}_2(\text{CO})_4\text{Mo}_2\text{As}_2\}_2\text{Cu}\}]^+$ , 687.7 (99)  $[\{\{\text{Cp}_2(\text{CO})_4\text{Mo}_2\text{As}_2\}_2\text{Cu}(\text{CH}_3\text{CN})\}]^+$ .

IR (solid, CO bands):  $\tilde{\nu}/\text{cm}^{-1}$ : 1953 (vs), 1917 (vs).

Elemental analysis, calc. (%) for  $\text{C}_{56}\text{H}_{40}\text{As}_8\text{B}_3\text{Cu}_3\text{F}_{12}\text{Mo}_8\text{O}_{16}$  (2786.85 g/mol): C, 24.13; H, 1.45; found: C, 24.11; H, 1.57.

Synthesis of  $[\{\{\text{CpMo}(\text{CO})_2\}_2(\mu_5, \eta^{2:2:2:1}\text{-As}_2)\}_2\{\text{Cu}(\text{CH}_3\text{CN})_2\text{Cu}\}][\text{BF}_4]_2$  (**7**):



$[\text{Cu}(\text{CH}_3\text{CN})_4][\text{BF}_4]$  (7 eq., 110 mg, 0.35 mmol), dissolved in  $\text{CH}_2\text{Cl}_2$  (5 mL), was added to a solution of **B** (1 eq., 29 mg, 0.05 mmol) in  $\text{CH}_2\text{Cl}_2$  (8 mL) and stirred for 2h at room temperature. The light red solution was carefully layered with threefold amount of *n*-pentane and stored at room temperature. After one day dark red block-shaped crystals

were formed. The crystals were washed with *n*-pentane and dried *in vacuo*. Crystalline yield: 21 mg (47%, referred to **B**).

<sup>1</sup>H NMR (CD<sub>3</sub>CN): δ = 5.45 (s, C<sub>5</sub>H<sub>5</sub>), 5.26 Mo<sub>2</sub>As<sub>2</sub>.

<sup>13</sup>C {<sup>1</sup>H} NMR (CD<sub>3</sub>CN): δ = 226.8 (CO), 85.45 (C<sub>5</sub>H<sub>5</sub>).

<sup>19</sup>F {<sup>1</sup>H} NMR (CD<sub>3</sub>CN): δ = -150.65 (d, <sup>1</sup>J<sub>B,F</sub> = 19.7 Hz). <sup>11</sup>B NMR (CD<sub>3</sub>CN): δ = -0.56 (s).

Positive ion ESI-MS (CH<sub>3</sub>CN, RT): *m/z* (%) = 1232.4 (100) [{Cp<sub>2</sub>(CO)<sub>4</sub>Mo<sub>2</sub>As<sub>2</sub>}<sub>2</sub>Cu]<sup>+</sup>, 687.7 (48) [{Cp<sub>2</sub>(CO)<sub>4</sub>Mo<sub>2</sub>As<sub>2</sub>}Cu(CH<sub>3</sub>CN)]<sup>+</sup>.

Elemental analysis did not deliver matching values, because an excess of starting material is used which crystallizes simultaneously with the product. [Cu(CH<sub>3</sub>CN)<sub>4</sub>][BF<sub>4</sub>] cannot be separated from the product, due to similar solubilities.

IR (solid, CO bands):  $\tilde{\nu}/\text{cm}^{-1}$ : 1992 (s), 1939 (s).

### 5.4.3 Crystallographic Data

**Crystal Structure Analysis:** The crystals were selected and measured on a Gemini Ultra diffractometer equipped with an AtlasS2 CCD detector (**1** (2 CH<sub>2</sub>Cl<sub>2</sub>), **1** (toluene), **2**, **3**) and a GV50 diffractometer equipped with a TitanS2 detector (**4-7**), respectively. The crystals were kept at *T* = 123(1) K during data collection. Data collection and reduction were performed with **CrysAlisPro** [Version V1.171.38.46, 2015 (**1** (2 CH<sub>2</sub>Cl<sub>2</sub>)), V1.171.40.14a, 2018 (**1** (toluene), **2**, **3**, **4**, **5**, **6**, **7**)].<sup>19</sup> For the compounds **1** (toluene), **2**, **3** and **6** an analytical numeric absorption correction using a multifaceted crystal model based on expressions derived by R.C. Clark & J.S. Reid<sup>20</sup> and an empirical absorption correction using spherical harmonics as implemented in SCALE3 ABSPACK was applied. For the compounds **1** (2 CH<sub>2</sub>Cl<sub>2</sub>), **4**, **5** and **7** a numerical absorption correction based on gaussian integration over a multifaceted crystal model and an empirical absorption correction using spherical harmonics as implemented in SCALE3 ABSPACK was applied. Using **Olex2**,<sup>21</sup> the structures were solved with **ShelXT**<sup>22</sup> and a least-square refinement on *F*<sup>2</sup> was carried out with **ShelXL**<sup>23</sup> for all structures. All non-hydrogen atoms were refined anisotropically. Hydrogen atoms at the carbon atoms were located in idealized positions and refined isotropically according to the riding model.

Compound **1** (2 CH<sub>2</sub>Cl<sub>2</sub>): The asymmetric unit contains two CH<sub>2</sub>Cl<sub>2</sub> solvent molecules, which are respectively disordered over two positions (79:21; 74:26). Further, the asymmetric unit contains two halves of the complex [{{CpMo(CO)<sub>2</sub>}<sub>2</sub>(μ<sub>5,η</sub><sup>2:2:2:1:1</sup>-P<sub>2</sub>)<sub>2</sub>]{Cu(CH<sub>3</sub>CN)<sub>2</sub>}<sub>2</sub>Cu] and additionally three [Al{OC(CF<sub>3</sub>)<sub>3</sub>}<sub>4</sub>]<sup>-</sup> anions. Almost all the {OC(CF<sub>3</sub>)<sub>3</sub>} units at the three [Al{OC(CF<sub>3</sub>)<sub>3</sub>}<sub>4</sub>]<sup>-</sup> anions are disordered over at least two positions. Further, one Cp ligand at one half of a [{{CpMo(CO)<sub>2</sub>}<sub>2</sub>(μ<sub>5,η</sub><sup>2:2:2:1:1</sup>-

$P_2\}_2\{Cu(CH_3CN)_2\}_2Cu$  complex is disordered over two positions (53:47). To describe these disorders the FLAT, DFIX, SADI, SIMU, RIGU and ISOR restraints were applied.

**Compound 1 (toluene):** The asymmetric unit contains one toluene solvent molecule, the cationic complex  $[\{CpMo(CO)_2\}_2(\mu_5, \eta^{2:2:2:1:1}-P_2)]_2\{Cu(CH_3CN)_2\}_2Cu$  and three  $[Al\{OC(CF_3)_3\}_4]^-$  anions. One Cp and one CO ligand of the complex  $[\{CpMo(CO)_2\}_2(\mu_5, \eta^{2:2:2:1:1}-P_2)]_2\{Cu(CH_3CN)_2\}_2Cu$  are disordered over two positions (73:27). Further, almost all the  $\{OC(CF_3)_3\}$  units at the three  $[Al\{OC(CF_3)_3\}_4]^-$  anions are disordered over at least two positions. To describe these disorders the SADI, SIMU and RIGU restraints were applied.

**Compound 2:** The asymmetric unit contains one  $CH_2Cl_2$  solvent molecule, the cationic complex  $[\{CpMo(CO)_2\}_2(\mu_5, \eta^{2:2:2:1:1}-P_2)]\{Cu(CH_3CN)_3\}_2Cu(CH_3CN)_2$  and three  $[Al\{OC(CF_3)_3\}_4]^-$  anions. The Cl atoms of  $CH_2Cl_2$  solvent molecule are disordered over two positions (69:31). Further, almost all the  $\{OC(CF_3)_3\}$  units at the three  $[Al\{OC(CF_3)_3\}_4]^-$  anions are disordered over at least two positions. To describe these disorders the SADI, SIMU, RIGU and ISOR restraints were applied.

**Compound 3:** The asymmetric unit contains half a  $BF_4^-$  anion and one quarter of the complex  $[\{CpMo(CO)_2\}_2(\mu_4, \eta^{2:2:2:1}-P_2)]\{Cu(CH_3CN)_2\}Cu$  at which one CO group is disordered over two positions (50:50). To describe this disorder, the SIMU restraint was applied.

**Compound 4:** The asymmetric unit contains one  $CH_2Cl_2$  solvent molecule, the cationic complex  $[\{CpMo(CO)_2\}_2(\mu_4, \eta^{2:2:2:1}-As_2)]_2\{Cu(CH_3CN)_2\}Cu(CH_3CN)_1$  and three  $[Al\{OC(CF_3)_3\}_4]^-$  anions. At one  $[Al\{OC(CF_3)_3\}_4]^-$  anion two  $\{OC(CF_3)_3\}$  units are disordered over two (60:40) and one  $\{OC(CF_3)_3\}$  unit is disordered over three positions (37:37:26). To describe these disorders the SADI, SIMU and RIGU restraints were applied.

**Compound 5:** The asymmetric unit contains 1.75  $CH_2Cl_2$  solvent molecules, two  $[FAl\{OC_6F_{10}(C_6F_6)\}_3]^-$  anions and the cationic complex  $[\{Cp_2Mo_2(CO)_4(\mu_4, \eta^{2:2:2:1}-As_2)]\{Cu(CH_3CN)_2\}\{Cu(CH_3CN)\}]$ . One and a half of the  $CH_2Cl_2$  solvent molecules were heavily disordered. Therefore, a solvent mask was calculated and 252 electrons were found in a volume of 1252 Å<sup>3</sup> in two voids per unit cell. This is consistent with the presence of 1.5  $CH_2Cl_2$  molecules per asymmetric unit, which account for 252 electrons per unit cell. Additionally 0.25  $CH_2Cl_2$  molecules were disordered over two positions (15:10). Further, one Cp ligand (70:30) and a  $CH_3CN$  molecule (53:47) of the complex  $[\{Cp_2Mo_2(CO)_4(\mu_4, \eta^{2:2:2:1}-As_2)]\{Cu(CH_3CN)_2\}\{Cu(CH_3CN)\}]$  are disordered over two positions. Furthermore, two of the three  $\{OC_6F_{10}(C_6F_6)\}$  substituents of one

[FAl{OC<sub>6</sub>F<sub>10</sub>(C<sub>6</sub>F<sub>6</sub>)<sub>3</sub>}<sub>3</sub>]<sup>-</sup> anion are disordered over two positions (72:28; 61:39). To describe these disorders the SADI, SIMU and ISOR restraints were applied.

Compound **6**: The asymmetric unit contains 2.19 CH<sub>2</sub>Cl<sub>2</sub> solvent molecules and 1.4 BF<sub>4</sub><sup>-</sup> anions. It further contains four overlaying complexes [{Cp<sub>2</sub>Mo<sub>2</sub>(CO)<sub>4</sub>(μ<sub>5</sub>,η<sup>2:2:2:1:1</sup>-As<sub>2</sub>)<sub>2</sub>{Cp<sub>2</sub>Mo<sub>2</sub>(CO)<sub>4</sub>(μ<sub>3</sub>,η<sup>2:2:2</sup>-As<sub>2</sub>)<sub>2</sub>{Cu(NCMe)}<sub>2</sub>Cu}] (**6a**, 39 - 59% occupancy), [{Cp<sub>2</sub>Mo<sub>2</sub>(CO)<sub>4</sub>(μ<sub>5</sub>,η<sup>2:2:2:1:1</sup>-As<sub>2</sub>)<sub>2</sub>{Cp<sub>2</sub>Mo<sub>2</sub>(CO)<sub>4</sub>(μ<sub>3</sub>,η<sup>2:2:2</sup>-As<sub>2</sub>)<sub>2</sub>Cu<sub>3</sub>}] (**6b**, 21 - 41% occupancy), [{Cp<sub>2</sub>Mo<sub>2</sub>(CO)<sub>4</sub>(μ<sub>4</sub>,η<sup>2:2:1:1</sup>-As<sub>2</sub>)<sub>2</sub>{Cp<sub>2</sub>Mo<sub>2</sub>(CO)<sub>4</sub>(μ<sub>3</sub>,η<sup>2:2:2</sup>-As<sub>2</sub>)<sub>2</sub>Cu<sub>2</sub>}] (**6c**; 0 - 20% occupancy) and [{Cp<sub>2</sub>Mo<sub>2</sub>(CO)<sub>4</sub>(μ<sub>5</sub>,η<sup>2:2:2:1:1</sup>-As<sub>2</sub>)<sub>2</sub>{Cp<sub>2</sub>Mo<sub>2</sub>(CO)<sub>4</sub>(μ<sub>3</sub>,η<sup>2:2:2</sup>-As<sub>2</sub>)<sub>2</sub>{Cu(NCMe)}<sub>2</sub>}] (**6d**; 0 - 20% occupancy), which are located on a 2-fold rotation axis and therefore only half present in the asymmetric unit. The vague allocation of these complexes is a result of the unequal occupation of the central Cu atom (0.8% occupancy) and the NCMe ligands (0.59% occupancy). The SADI and SIMU restraints were applied to describe one BF<sub>4</sub><sup>-</sup> anion, which is located on a 2-fold rotation axis. Further, these restraints were also used to describe a CH<sub>2</sub>Cl<sub>2</sub> molecule, which shares the same position with an NCMe molecule coordinated to a Cu atom.

Compound **7**: The asymmetric unit contains one quarter of a BF<sub>4</sub><sup>-</sup> anion and one quarter of the complex [{Cp<sub>2</sub>Mo<sub>2</sub>(CO)<sub>4</sub>(μ<sub>4</sub>,η<sup>2:2:2:1</sup>-As<sub>2</sub>)<sub>2</sub>{Cu(NCCH<sub>3</sub>)<sub>2</sub>Cu}]. Due to the special position of the [Cu(NCCH<sub>3</sub>)<sub>2</sub>]<sup>+</sup> fragment on a mirror plane near an inversion center the SIMU restraint was applied to this fragment.

**Table S5.1.** Crystallographic data and details of diffraction experiments for compounds **1a - 3**.

<b>Compound</b>	<b>1a · 2 CH<sub>2</sub>Cl<sub>2</sub></b>	<b>1b</b>	<b>2 · CH<sub>2</sub>Cl<sub>2</sub></b>	<b>3 · 4 CH<sub>3</sub>CN · 4 CH<sub>2</sub>Cl<sub>2</sub></b>
Data set (internal naming)	abs268	abs461a	abs437a	abs444b_2
Formula	C <sub>86</sub> H <sub>36</sub> Al <sub>3</sub> Cl <sub>4</sub> Cu <sub>3</sub> F <sub>108</sub> Mo <sub>4</sub> N <sub>4</sub> O <sub>20</sub> P <sub>4</sub>	C <sub>91</sub> H <sub>40</sub> Al <sub>3</sub> Cu <sub>3</sub> F <sub>108</sub> Mo <sub>4</sub> N <sub>4</sub> O <sub>20</sub> P <sub>4</sub>	C <sub>79</sub> H <sub>36</sub> Al <sub>3</sub> Cl <sub>2</sub> Cu <sub>3</sub> F <sub>108</sub> Mo <sub>2</sub> N <sub>8</sub> O <sub>16</sub> P <sub>2</sub>	C <sub>32</sub> H <sub>26</sub> B <sub>2</sub> Cu <sub>2</sub> F <sub>8</sub> Mo <sub>4</sub> N <sub>2</sub> O <sub>8</sub> P <sub>4</sub>
<i>D</i> <sub>calc.</sub> / g · cm <sup>-3</sup>	2.117	2.059	2.008	2.077
<i>m</i> /mm <sup>-1</sup>	6.645	5.879	0.954	2.284
Formula Weight	4418.19	4340.47	4001.44	1374.89
Colour	red	clear orange	yellow	clear orange
Shape	plate	block	block	plate
Size/mm <sup>3</sup>	0.46×0.28×0.06	0.25×0.16×0.08	0.41×0.31×0.28	0.44×0.22×0.07
<i>T</i> /K	123(1)	123(1)	123.15	123(1)
Crystal System	monoclinic	trigonal	monoclinic	monoclinic
Flack Parameter	-	-0.010(8)	-	-
Hooft Parameter	-	-0.007(4)	-	-
Space Group	<i>P</i> 2 <sub>1</sub> / <i>c</i>	<i>P</i> 3 <sub>2</sub>	<i>P</i> 2 <sub>1</sub> / <i>c</i>	<i>I</i> 2/ <i>m</i>
<i>a</i> /Å	28.5401(2)	17.35370(10)	27.3674(7)	8.3221(3)
<i>b</i> /Å	18.57590(14)	17.35370(10)	23.2498(6)	25.8028(9)
<i>c</i> /Å	26.6845(2)	40.2585(2)	20.7996(5)	10.2632(4)
<i>α</i> <sup>o</sup>	90	90	90	90
<i>β</i> <sup>o</sup>	101.5352(8)	90	90.654(2)	94.027(3)
<i>γ</i> <sup>o</sup>	90	120	90	90
<i>V</i> /Å <sup>3</sup>	13861.24(19)	10499.58(13)	13233.6(6)	2198.41(14)
<i>Z</i>	4	3	4	2
<i>Z</i> '	1	1	1	0.25
Wavelength/Å	1.54184	1.54184	0.71073	0.71073
Radiation type	Cu K <sub>α</sub>	Cu K <sub>α</sub>	Mo K <sub>α</sub>	Mo K <sub>α</sub>
<i>θ</i> <sub>min</sub> <sup>o</sup>	3.434	3.293	3.278	3.411
<i>θ</i> <sub>max</sub> <sup>o</sup>	72.915	73.056	32.310	32.327
Measured Refl.	57598	39410	119824	16969
Independent Refl.	26486	23136	41829	3773
Reflections with <i>I</i> > 2( <i>I</i> )	20576	22123	31376	3435
<i>R</i> <sub>int</sub>	0.0551	0.0304	0.0296	0.0255
Parameters	3249	3327	3116	229
Restraints	4244	2605	3335	24
Largest Peak	3.618	0.958	1.232	0.454
Deepest Hole	-1.195	-0.541	-0.788	-0.651
GooF	1.049	1.016	1.073	1.179
<i>wR</i> <sub>2</sub> (all data)	0.2255	0.1421	0.1453	0.0535
<i>wR</i> <sub>2</sub>	0.2104	0.1395	0.1332	0.0520
<i>R</i> <sub>1</sub> (all data)	0.0971	0.0551	0.0802	0.0319
<i>R</i> <sub>1</sub>	0.0783	0.0530	0.0559	0.0267

**Table S5.2.** Crystallographic data and details of diffraction experiments for compounds **4** - **7**.

Compound	<b>4</b>	<b>5</b> · 1.75 CH <sub>2</sub> Cl <sub>2</sub>	<b>6</b> · 4.38 CH <sub>2</sub> Cl <sub>2</sub>	<b>7</b>
Data set (internal naming)	JS200	JS151	JS120_2	JS164_2
Formula	C <sub>67</sub> H <sub>31</sub> Al <sub>2</sub> As <sub>4</sub> Cl <sub>2</sub> Cu <sub>2</sub>	Al <sub>2</sub> As <sub>4</sub> C <sub>107.75</sub> Cl <sub>3.5</sub> Cu <sub>2</sub>	C <sub>62.74</sub> H <sub>52.3</sub> As <sub>8</sub> B <sub>2.58</sub> Cl <sub>8.76</sub>	C <sub>16</sub> H <sub>13</sub> As <sub>2</sub> BCuF <sub>4</sub>
<i>D</i> <sub>calc.</sub> / g · cm <sup>-3</sup>	2.213	2.080	2.309	2.316
<i>m</i> /mm <sup>-1</sup>	8.170	4.958	11.674	10.433
Formula Weight	3437.33	4329.42	3157.42	775.34
Colour	orange	clear orange	orange	orange
Shape	block	plate	plate	plate
Size/mm <sup>3</sup>	0.20×0.15×0.12	0.22×0.12×0.04	0.26×0.15×0.05	0.12×0.06×0.05
<i>T</i> /K	122.97(11)	122.98(14)	123.00(12)	123.00(11)
Crystal System	triclinic	monoclinic	monoclinic	monoclinic
Space Group	<i>P</i> -1	<i>P</i> 21/ <i>n</i>	<i>C</i> 2/ <i>c</i>	<i>I</i> 2/ <i>m</i>
<i>a</i> /Å	15.2567(3)	23.5326(6)	14.6204(4)	8.2869(2)
<i>b</i> /Å	15.8605(3)	18.9404(4)	26.8116(5)	26.2286(6)
<i>c</i> /Å	23.6139(5)	31.4016(8)	23.3084(5)	10.2500(2)
$\alpha^\circ$	72.159(2)	90	90	90
$\beta^\circ$	75.865(2)	98.942(2)	96.168(2)	93.660(2)
$\gamma^\circ$	74.451(2)	90	90	90
<i>V</i> /Å <sup>3</sup>	5157.7(2)	13826.1(6)	9083.9(3)	2223.33(9)
<i>Z</i>	2	4	4	4
<i>Z</i> '	1	1	0.5	0.5
Wavelength/Å	1.54184	1.39222	1.39222	1.39222
Radiation type	Cu K $\alpha$	Cu K $\alpha$	Cu K $\alpha$	Cu K $\alpha$
$\theta_{min}^\circ$	3.342	1.978	3.123	3.043
$\theta_{max}^\circ$	74.188	61.639	57.000	60.027
Measured Refl.	58028	129209	29745	9499
Independent Refl.	20296	28445	8329	2274
Reflections with <i>I</i> > 2( <i>I</i> )	18284	22099	8089	2230
<i>R</i> <sub>int</sub>	0.0361	0.0505	0.0384	0.0498
Parameters	1939	2601	618	181
Restraints	471	1303	49	36
Largest Peak	1.444	0.706	2.503	1.389
Deepest Hole	-0.908	-0.711	-1.120	-1.052
Goof	1.011	1.029	1.185	1.243
<i>wR</i> <sub>2</sub> (all data)	0.0827	0.0996	0.1868	0.1280
<i>wR</i> <sub>2</sub>	0.0796	0.0899	0.1860	0.1275
<i>R</i> <sub>1</sub> (all data)	0.0384	0.0605	0.0697	0.0487
<i>R</i> <sub>1</sub>	0.0336	0.0420	0.0685	0.0481

**Table S5.3.** Selected bond lengths and atom-atom distances of **1-7** in Å. Only the major part of compound **6** is described.

	<b>1</b> abs268 / abs461a E = P	<b>2</b> abs437a E = P	<b>3</b> abs444b E = P	<b>4</b> JS200 E = As	<b>5</b> JS151 E = As	<b>6</b> JS120 E = As	<b>7</b> JS164 E = As
Cu <sub>peripheral</sub> -	2.4344(10)/ 2.4537(19)	3.0013(6) /	2.5645(9)	2.6925(7)	2.6668(10)	2.587(4)	2.470(3)
Cu <sub>peripheral</sub> -	4.869(2) -	5.8238(8)	-	-	-	5.175(9)	-
Cu <sub>peripheral</sub> -	4.904(2)						
<b>Cu-E</b>	2.2830(19)- 2.437(2)	2.2446(8) -	2.3545(6)/ 2.491(7)	2.4582(6) -	2.4465(8) -	2.382(4) -	2.4197(7) / 2.4488(18)
Cu <sub>central</sub> -E	2.2838(17)- 2.3132(16)	2.3706(8) /	2.491(7)	2.4849(6) -	2.4647(8) -	2.410(3) /	2.4197(7)
Cu <sub>peripheral</sub> -E	2.3830(19)- 2.460(3)	2.2446(8) /	2.3545(6)	2.4582(6) /	2.4465(8) /	2.382(4) -	2.4488(18)
<b>E-E</b>	2.213(3) -	2.1455(10)	2.1796(11)	2.3901(5)- 2.3905(5)	2.3816(6) /	2.3860(16) -	2.4282(14) /
	2.238(2)				2.3849(6)	2.4372(2)	

### Disorder of compound **6**

The solid-state molecular structure of **6** shows a superposition of four possible species (**6a- 6d**) with different occupancies (Figure S5.1). For the central copper atom Cu1, an occupancy of 0.8 was determined, while the acetonitrile molecules have an occupancy of 0.59. Hence, the resulting occupancies are 0.39-0.59 for **6a**, 0.21-0.41 for **6b**, 0-0.20 for **6c** and **6d**, respectively. As **6a** appears to be the species with the highest occupancy, it is considered as the major product in this work.

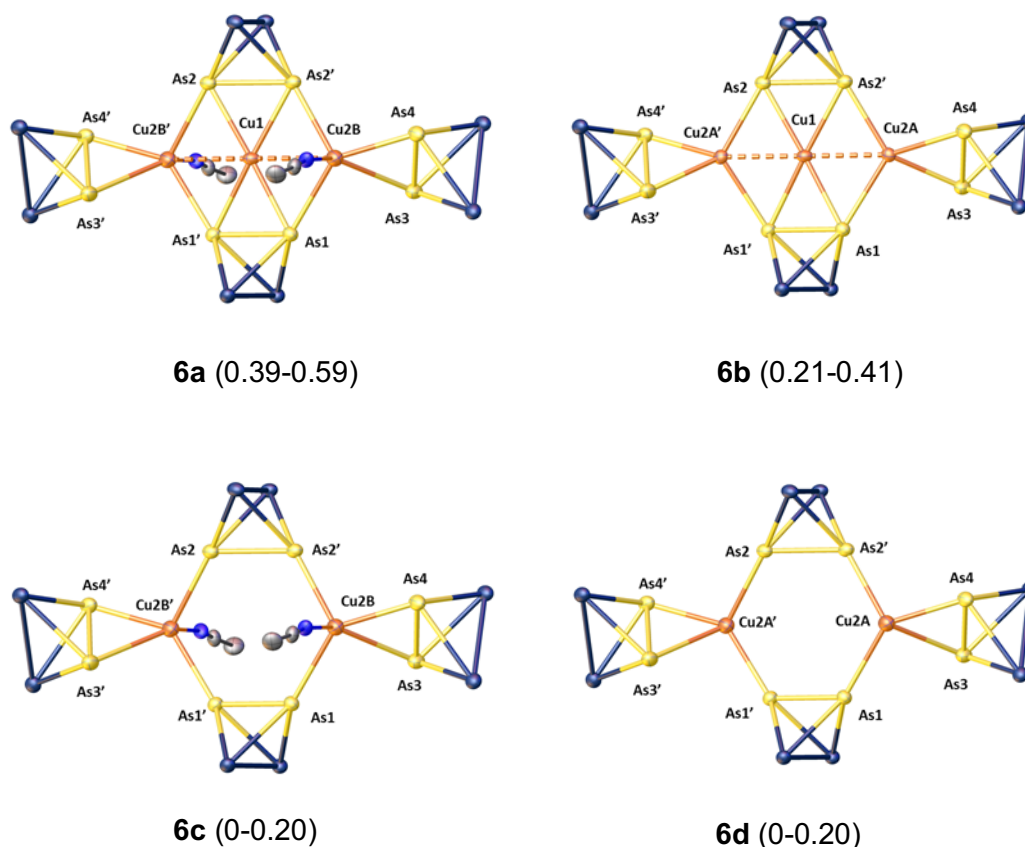


**Figure S5.1.** Possible occupancies of the compounds **6a-6d** in brackets. Only the cationic fragments are depicted. Cp-, CO-ligands and hydrogen atoms were omitted for clarity. Thermal ellipsoids are shown at 50% probability level.

#### 5.4.4 DFT Calculations

All calculations have been performed with the TURBOMOLE program package<sup>24</sup> at the RI<sup>25</sup>-B3LYP<sup>26</sup>/def2-TZVP<sup>27</sup> level of theory. The geometries were optimized in the gas phase using the Multipole Accelerated Resolution of Identity (MARI-J)<sup>28</sup> approximation during the geometry optimization steps. The solvent effects were incorporated as single point calculations (without the RI approximation) on the gas phase optimized geometries via the Conductor-like Screening Model (COSMO)<sup>29</sup> using the dielectric constant of  $\text{CH}_2\text{Cl}_2$  ( $\epsilon = 8.930$ ). For the reaction energies the SCF energies, corrected for the “outlying charge” were used. The energy minimum structure of  $[\{\{\text{CpMo}(\text{CO})_2\}_2(\mu_5, \eta^{2:2:2:1:1}\text{-P}_2)\}_2\{\text{Cu}(\text{CH}_3\text{CN})_2\}_2\text{Cu}]^{3+}$  (**1**) have been proven by frequency calculations which shows no imaginary frequencies. The population analysis has been performed on the gas phase optimized geometries.

In order to elucidate the bonding situation in  $[\{\{\text{CpMo}(\text{CO})_2\}_2(\mu_5, \eta^{2:2:2:1:1}\text{-P}_2)\}_2\{\text{Cu}(\text{CH}_3\text{CN})_2\}_2\text{Cu}]^{3+}$  (**1**) and  $[\{\{\text{CpMo}(\text{CO})_2\}_2(\mu_5, \eta^{2:2:2:1:1}\text{-P}_2)\}_2\{\text{Cu}(\text{CH}_3\text{CN})_3\}_2$



$\text{Cu}(\text{CH}_3\text{CN})_2]^{3+}$  (**2**) DFT calculations at the B3LYP/def2-TZVP level of theory have been performed. The optimized geometry of **1** in the gas phase is very similar to the experimental structure determined by single crystal X-ray diffraction, i.e. the Cu-Cu distances in the gas phase optimized geometry of 2.559 Å are similar to the experimental values of 2.4344(10) - 2.4537(19) Å. In the case of **3** the Cu-Cu distances are longer in the gas phase optimized geometry (Cu...Cu 3.380 and 3.384 Å) compared to that in the solid state (Cu...Cu 3.0013(6) and 3.0593(6) Å). This indicates that the chelating effect of a second  $[\{\text{CpMo}(\text{CO})_2\}_2(\mu, \eta^{2:2}\text{-P}_2)]$  is responsible for the relatively short Cu-Cu distances in **1**. The energy minimum structure of **1** have been proven by frequency calculations which shows no imaginary frequencies.

The calculations also show that the bonding of the peripheral Cu ions to the  $\text{Mo}_2\text{P}_2$  ligand in **1** takes place via the coordination of the phosphorus lone pairs, while the central Cu ion binds to the P-P sigma orbital of the  $\text{Mo}_2\text{P}_2$  unit. This is nicely shown by the Localized Molecular Orbitals (LMOs) (Figure S5.2). A small orbital contribution of the central Cu ion to the LMOs of the P-Cu<sub>peripheral</sub> bonding of roughly 7% has been observed. This is not the case for **2**. A comparison of the LMOs of **1** with that of  $[\{\{\text{CpMo}(\text{CO})_2\}_2(\mu_4, \eta^{2:2:1:1}\text{-P}_2)\}_2\{\text{Cu}(\text{CH}_3\text{CN})_2\}_2]^{2+}$  (**G**) shows that the bonding of the  $\text{Mo}_2\text{P}_2$  Ligand to the peripheral Cu ions is very similar (Figure S5.3). The Wiberg Bond Indexes (WBIs) of the P-P bond in **G** is close to unity (1.06), while in **1** and **2** the WBIs of the P-P bonds are lower (0.78 in **1** and 0.72 in **2**) indicating a weaker P-P bond. This is not unexpected if consider that the coordination of the P-P sigma bond to the central Cu ion, which leads to depletion of the electron density in this bonding orbital. The WBIs of the peripheral Cu-P bonds in **1** are slightly lower than in **G** and **2**, i.e. 0.40 – 0.44 in **1** and 0.53 – 0.55 and 0.55 in **G** and **2**, respectively. The WBIs of the Cu<sub>central</sub>-P bonds are 0.29 (Cu9-P6, Cu9-P8) and 0.40 (Cu9-P5, Cu9-P7) indicating a slightly asymmetric bonding and a preference for a linear coordination geometry of the central Cu ion (for labeling see Figure S5.4). The calculations indicate that between the three Cu ions an interaction is presence since a WBI of 0.11 has been found.

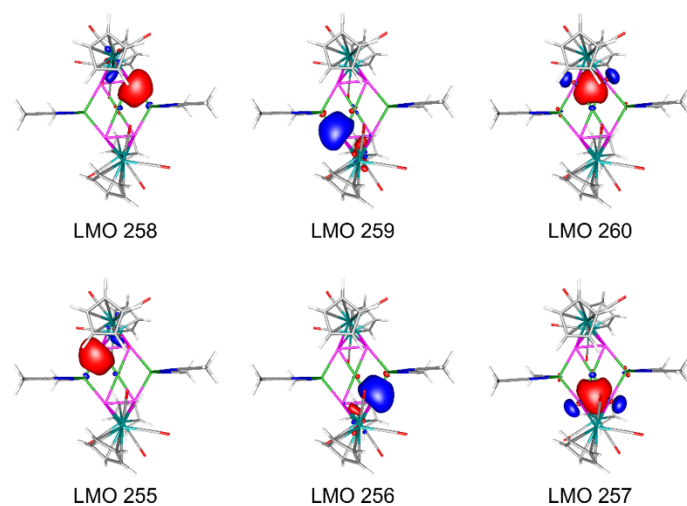


**Figure S5.2.** Selected Localized Molecular Orbitals (LMOs) representing the Cu-P bonding in  $[\{\{\text{CpMo}(\text{CO})_2\}_2(\mu_5, \eta^{2:2:2:1:1}\text{-P}_2)\}_2\{\text{Cu}(\text{CH}_3\text{CN})_2\}_2\text{Cu}]^{3+}$  (**1**). Calculated at the B3LYP/def2-TZVP level of theory.

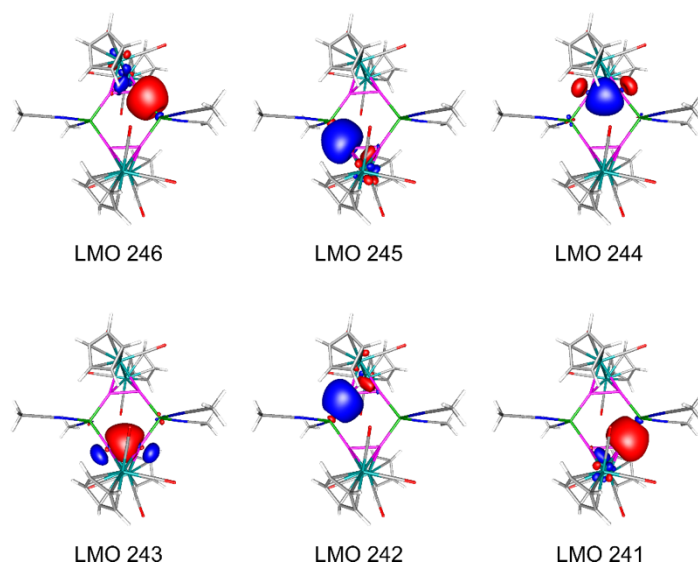


**Figure S5.3.** Selected Localized Molecular Orbitals (LMOs) representing the Cu-P bonding in  $[\{\{\text{CpMo}(\text{CO})_2\}_2(\mu_4, \eta^{2:2:1:1}\text{-P}_2)\}_2\{\text{Cu}(\text{CH}_3\text{CN})_2\}_2]^{2+}$  (**G**). Calculated at the B3LYP/def2-TZVP level of theory.

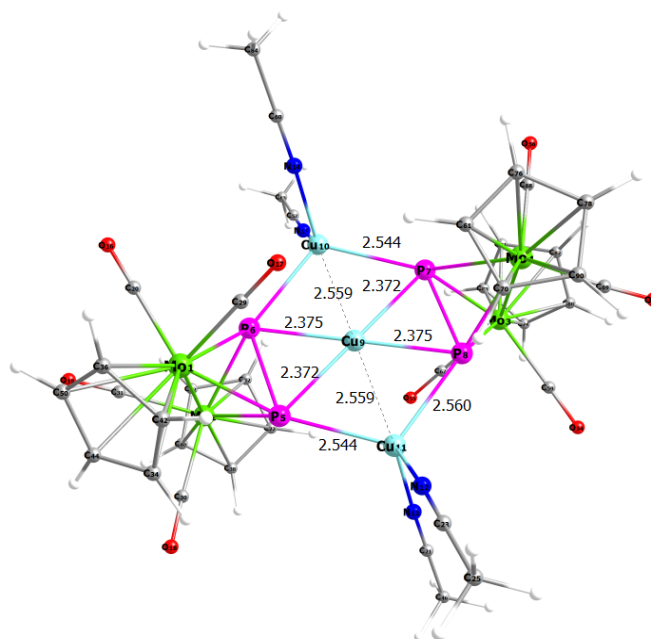


**Figure S5.4.** Optimized geometry and selected geometric parameters of  $[[\{\text{CpMo}(\text{CO})_2\}_2(\mu_5, \eta^{2:2:2:1:1}\text{-P}_2)]_2\{\text{Cu}(\text{CH}_3\text{CN})_2\}_2\text{Cu}]^{3+}$  (**1**) at the B3LYP/def2-TZVP level of theory.

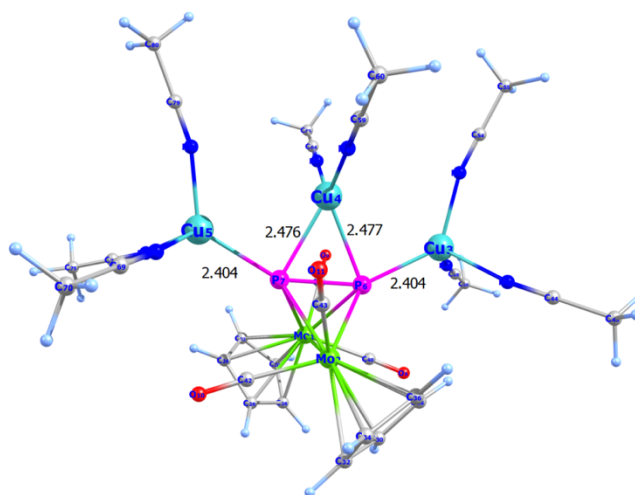
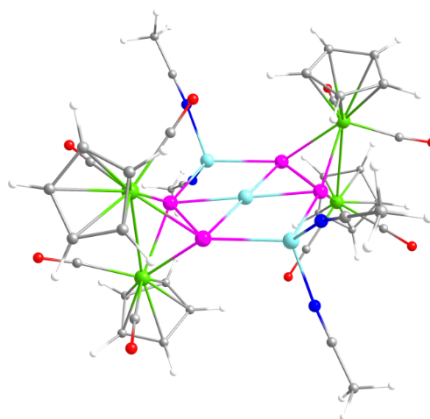


**Figure S5.5.** Optimized geometry and selected geometric parameters of  $[[\{\text{CpMo}(\text{CO})_2\}_2(\mu_5, \eta^{2:2:2:1:1}\text{-P}_2)]\{\text{Cu}(\text{CH}_3\text{CN})_3\}_2\text{Cu}(\text{CH}_3\text{CN})_2]^{3+}$  (**2**) at the B3LYP/def2-TZVP level of theory.

**Table S5.4.** Cartesian coordinates of the optimized geometry of  $[\{\{\text{CpMo}(\text{CO})_2\}_2(\mu_5, \eta^{2:2:2:1:1}\text{-P}_2)\}_2\{\text{Cu}(\text{CH}_3\text{CN})_2\}_2\text{Cu}]^{3+}$  (**1**).

Atom	x	y	z
Mo	1.6912025	3.2304868	-1.6450839
Mo	1.9990712	3.1753909	1.5251320
Mo	-1.6911198	-3.2304863	1.6449352
Mo	-1.9989085	-3.1753706	-1.5252966
P	2.0140406	1.2468919	-0.1183611
P	0.1175368	2.3689693	0.1213012
P	-2.0139739	-1.2468899	0.1182200
P	-0.1174381	-2.3689319	-0.1214054
Cu	0.0000291	0.0000106	0.0000022
Cu	-2.2025092	1.2893836	0.1929427
Cu	2.2024820	-1.2894585	-0.1929527
N	3.2031299	-1.9347044	-1.8448166
N	3.2971686	-1.9774515	1.3692341
N	-3.2974532	1.9775323	-1.3689751
N	-3.2030104	1.9346190	1.8449216
O	-0.6164617	5.3932285	-1.5928664
O	-0.1678400	1.4871114	-3.4694739
O	5.0917287	3.0572322	0.9267115
O	1.9237373	6.2091307	0.7100018
C	0.2100544	4.6114691	-1.5714240
C	4.0062542	-2.4590205	2.1333324
C	1.6129283	1.8423368	3.4760805
C	3.9208651	-2.3934233	-2.6156718
H	1.5649104	0.7659719	3.4545258
C	4.8322419	-2.9779966	-3.5815378
H	4.4869410	-2.7744672	-4.5961615
H	5.8295464	-2.5541238	-3.4535909
H	4.8854830	-4.0578123	-3.4336736
C	0.4890097	2.1223548	-2.7809440
C	3.9639736	3.1241706	1.0904378
C	1.9371295	5.0840674	0.9198213
C	0.5098626	2.7294313	3.3502430
H	-0.5205034	2.4413040	3.2235791
C	3.9870577	3.0506915	-2.3027542



---

H	4.6723524	2.3281781	-1.8916364
C	2.4509201	4.0846951	-3.6751102
H	1.7913214	4.2881416	-4.5031985
C	2.7804130	2.6217382	3.6721140
H	3.7740749	2.2419248	3.8485094
C	2.4038854	3.9968184	3.6635119
H	3.0560648	4.8354060	3.8477096
C	3.1550972	2.8625524	-3.4350418
H	3.1077270	1.9770220	-4.0476985
C	3.8116550	4.3845799	-1.8463924
H	4.3403307	4.8536518	-1.0339160
C	4.9057555	-3.0723545	3.0919656
H	4.5602870	-2.8772018	4.1081012
H	4.9400590	-4.1507364	2.9290735
H	5.9102525	-2.6634553	2.9723663
C	2.8620519	5.0184295	-2.6832318
H	2.5442250	6.0467130	-2.6084615
C	0.9922637	4.0572015	3.4624085
H	0.3943782	4.9543015	3.4506854
O	0.6166455	-5.3931238	1.5928270
O	0.1677627	-1.4869608	3.4693555
O	-5.0915979	-3.0573459	-0.9269733
C	-3.9207591	2.3933049	2.6157848
O	-1.9235447	-6.2091181	-0.7101974
C	-0.2099051	-4.6114004	1.5713445
C	-4.0068335	2.4591301	-2.1327821
C	-1.6128378	-1.8422793	-3.4762501
H	-1.5649676	-0.7659077	-3.4547167
C	-4.8321580	2.9778300	3.5816593
H	-4.4868439	2.7743092	4.5962801
H	-5.8294426	2.5539099	3.4537140
H	-4.8854516	4.0576445	3.4338051
C	-0.4890258	-2.1222695	2.7808258
C	-3.9638361	-3.1242285	-1.0906761
C	-1.9369473	-5.0840523	-0.9200035
C	-0.5096620	-2.7292219	-3.3503163

H	0.5206563	-2.4409565	-3.2235826
C	-3.9870032	-3.0507762	2.3025008
H	-4.6722945	-2.3282831	1.8913453
C	-2.4508998	-4.0847309	3.6749248
H	-1.7913327	-4.2881566	4.5030426
C	-2.7802040	-2.6218406	-3.6723419
H	-3.7739065	-2.2421652	-3.8488061
C	-2.4034951	-3.9968679	-3.6636908
H	-3.0555511	-4.8355437	-3.8479202
C	-3.1551107	-2.8626147	3.4348323
H	-3.1077981	-1.9770841	4.0474935
C	-3.8115290	-4.3846542	1.8461390
H	-4.3401422	-4.8537396	1.0336311
C	-4.9067171	3.0724886	-3.0910390
H	-4.5615856	2.8774753	-4.1073158
H	-4.9410618	4.1508503	-2.9280209
H	-5.9111347	2.6634838	-2.9711350
C	-2.8619446	-5.0184740	2.6830194
H	-2.5440685	-6.0467416	2.6082499
C	-0.9918782	-4.0570616	-3.4624872
H	-0.3938750	-4.9540815	-3.4507110

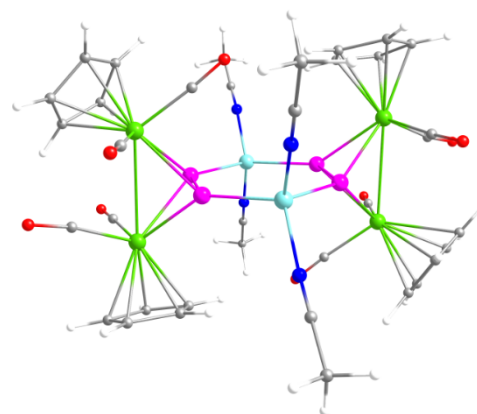
ENERGIES [a.u.]:

Total energy = -8771.0678177315

Total energy + OC corr. = -8771.0608050097

**Table S5.5.** Cartesian coordinates of the optimized geometry of  $[\{\{\text{CpMo}(\text{CO})_2\}_2(\mu_4, \eta^{2:2:1:1}\text{-P}_2)\}_2\{\text{Cu}(\text{CH}_3\text{CN})_2\}_2]^{2+}$  (**G**).

Atom	x	y	z
Mo	1.5636762	3.1668807	-1.6165327
Mo	1.9579801	3.1052378	1.5232183
Mo	-1.5636666	-3.1668293	1.6164772
Mo	-1.9579561	-3.1052715	-1.5232450
P	1.9073930	1.1535960	-0.1299055
P	0.0958917	2.1401870	0.1823365
P	-1.9073760	-1.1535798	0.1298150
P	-0.0958676	-2.1401677	-0.1824039
Cu	-2.1083992	1.2226720	0.2534735
Cu	2.1084037	-1.2226449	-0.2535302
N	3.2021402	-1.8576163	-1.8971982
N	3.2498971	-1.9830596	1.2718297
N	-3.2499522	1.9831285	-1.2718143
N	-3.2020532	1.8575402	1.8972017
O	-0.7461471	5.2966273	-1.3229077
O	-0.4426161	1.5363698	-3.3821857
O	4.9841502	2.4773146	0.9716905
O	2.3288308	6.0567915	0.5634651
C	0.0855754	4.5165659	-1.3875733
C	3.9103554	-2.4517902	2.0846672
C	1.3130961	1.9587824	3.5293399
C	3.9380449	-2.2724902	-2.6750032
H	1.1485648	0.8938865	3.5562723
C	4.8717681	-2.8016244	-3.6526463
H	4.5358610	-2.5596224	-4.6617154
H	5.8603816	-2.3686699	-3.4940698
H	4.9399049	-3.8856517	-3.5517270
C	0.2689951	2.1169995	-2.6937695
C	3.8725375	2.7206188	1.1183011
C	2.1775047	4.9399401	0.8010644
C	0.3222224	2.9533387	3.2924922
H	-0.7243868	2.7687222	3.1181166
C	3.8174540	2.8551443	-2.4057941
H	4.4638392	2.0629474	-2.0672763



C	2.2879367	4.0685026	-3.6333689
H	1.5984820	4.3598306	-4.4086184
C	2.5475306	2.6181898	3.7475446
H	3.4841872	2.1452593	3.9948310
C	2.3270913	4.0211236	3.6346224
H	3.0605351	4.7943078	3.7960514
C	2.9144748	2.7909712	-3.4969968
H	2.7642132	1.9431218	-4.1452510
C	3.7550345	4.1647316	-1.8655296
H	4.3462599	4.5404761	-1.0479848
C	4.7450875	-3.0479269	3.1111154
H	4.3361281	-2.8269346	4.0977569
H	4.7824820	-4.1297320	2.9764332
H	5.7572488	-2.6464141	3.0473373
C	2.8062885	4.9103487	-2.6099315
H	2.5578143	5.9475570	-2.4519301
C	0.9411198	4.2222759	3.3565873
H	0.4502401	5.1760798	3.2506291
O	0.7461838	-5.2965665	1.3229681
O	0.4425859	-1.5362251	3.3820831
O	-4.9841062	-2.4773192	-0.9716678
C	-3.9379298	2.2723811	2.6750495
O	-2.3287831	-6.0568063	-0.5634162
C	-0.0855497	-4.5165111	1.3875810
C	-3.9104806	2.4518472	-2.0846020
C	-1.3131265	-1.9588469	-3.5294004
H	-1.1486218	-0.8939479	-3.5563648
C	-4.8716200	2.8014665	3.6527426
H	-4.5356620	2.5594394	4.6617874
H	-5.8602303	2.3684954	3.4941962
H	-4.9397811	3.8854954	3.5518592
C	-0.2690166	-2.1168923	2.6936901
C	-3.8724986	-2.7206360	-1.1183021
C	-2.1774591	-4.9399596	-0.8010407
C	-0.3222230	-2.9533705	-3.2925424
H	0.7243845	-2.7687227	-3.1181901



---

C	-3.8174433	-2.8550475	2.4057290
H	-4.4638171	-2.0628486	2.0671970
C	-2.2879497	-4.0684019	3.6333269
H	-1.5984997	-4.3597230	4.4085830
C	-2.5475426	-2.6182970	-3.7475766
H	-3.4842154	-2.1454029	-3.9948717
C	-2.3270669	-4.0212218	-3.6346163
H	-3.0604936	-4.7944305	-3.7960086
C	-2.9144676	-2.7908665	3.4969337
H	-2.7641982	-1.9430113	4.1451758
C	-3.7550429	-4.1646454	1.8654843
H	-4.3462762	-4.5403997	1.0479536
C	-4.7452972	3.0479573	-3.1109918
H	-4.3363972	2.8269731	-4.0976596
H	-4.7827109	4.1297620	-2.9763075
H	-5.7574413	2.6464135	-3.0471427
C	-2.8063057	-4.9102603	2.6099036
H	-2.5578362	-5.9474710	2.4519163
C	-0.9410868	-4.2223269	-3.3565996
H	-0.4501788	-5.1761140	-3.2506200

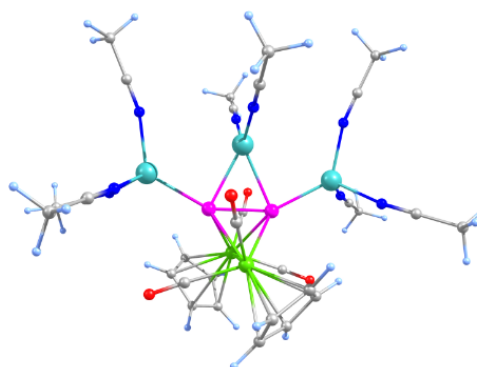
## ENERGIES [a.u.]:

Total energy = -7130.7434091722

Total energy + OC corr. = -7130.7381750726

**Table S5.6.** Cartesian coordinates of the optimized geometry of  $[\{\{\text{CpMo}(\text{CO})_2\}_2(\mu_5, \eta^{2:2:2:1:1}-\text{P}_2)\}\{\text{Cu}(\text{CH}_3\text{CN})_3\}_2\text{Cu}(\text{CH}_3\text{CN})_2\}]^{3+}$  (**2**).

Atom	x	y	z
Mo	-1.4764508	-0.2411396	2.2242238
Mo	1.5859373	0.3398631	2.1283441
Cu	0.5357696	-3.1609302	-0.5573098
Cu	-0.0546305	-0.0354771	-1.7126697
Cu	-0.5675516	3.1373673	-0.6679758
P	0.2859753	-1.0313115	0.5297532
P	-0.2664491	1.0573640	0.4990335
O	-0.7712909	-3.1364112	3.2472733
O	-3.3745933	-1.5215576	0.0825565
O	0.9361374	3.2804819	3.0552226
O	3.3625655	1.5183828	-0.1703459
N	2.2573691	-4.1077019	0.1313365
N	-0.9673046	-4.4177119	0.0603291
N	0.6634930	-3.4792297	-2.5766409
N	1.5849703	0.2477298	-2.8167359
N	-1.7610229	-0.3698998	-2.6959545
N	0.9932545	4.3946439	-0.2190323
N	-2.2218444	4.1425348	0.0995445
N	-0.8424115	3.3628348	-2.6844520
C	-3.4003863	-0.1147126	3.5390969
H	-4.1517834	-0.8874330	3.5406526
C	-3.3798451	1.0416245	2.7013857
H	-4.1062132	1.2847179	1.9431153
C	-2.2755629	1.8423754	3.0871317
H	-2.0066602	2.7946501	2.6620126
C	-1.6167154	1.1963373	4.1682370
H	-0.7758360	1.5812099	4.7191988
C	-2.3047089	-0.0108630	4.4406324
H	-2.0725511	-0.7072175	5.2308782
C	1.8323513	-1.0097031	4.1240694
H	1.0232325	-1.3677336	4.7371305
C	2.5339941	0.2068563	4.3042501
H	2.3453035	0.9384394	5.0740274
C	3.5787146	0.2681147	3.3405343



---

H	4.3284669	1.0388822	3.2662879
C	3.5126854	-0.9244323	2.5577320
H	4.1962190	-1.2026163	1.7722751
C	2.4312727	-1.7047699	3.0384909
H	2.1403162	-2.6746529	2.6719053
C	-0.9929313	-2.0876538	2.8479119
C	-2.6431024	-1.0668105	0.8369939
C	1.1364659	2.2140814	2.6931802
C	2.6742313	1.0998295	0.6434183
C	3.1014519	-4.8430872	0.3891135
C	4.1630605	-5.7786260	0.7132724
H	4.0230217	-6.7048364	0.1538839
H	4.1482603	-6.0056496	1.7802235
H	5.1323703	-5.3512476	0.4531951
C	-1.6936642	-5.2433166	0.3897430
C	-2.6061500	-6.2910282	0.8082460
H	-3.3082971	-6.5179664	0.0049503
H	-3.1635979	-5.9702062	1.6891246
H	-2.0453483	-7.1938620	1.0544221
C	0.7555711	-3.9374140	-3.6253772
C	0.8730164	-4.5310175	-4.9448730
H	1.8699007	-4.9547490	-5.0747125
H	0.7051886	-3.7766828	-5.7144927
H	0.1352107	-5.3263219	-5.0608094
C	2.5636797	0.4551461	-3.3788906
C	3.8058004	0.7223676	-4.0782235
H	3.6040292	1.2363183	-5.0189633
H	4.3228553	-0.2142475	-4.2912159
H	4.4485672	1.3491813	-3.4584009
C	-2.7747529	-0.6045561	-3.1799138
C	-4.0607101	-0.9060665	-3.7787612
H	-3.9223923	-1.4761909	-4.6983574
H	-4.5893892	0.0189624	-4.0127896
H	-4.6617571	-1.4913578	-3.0813077
C	1.7565063	5.2179778	0.0202725
C	2.7162374	6.2624289	0.3259698

H	2.5455974	7.1246369	-0.3202861
H	3.7311783	5.8958400	0.1671210
H	2.6076961	6.5724308	1.3662829
C	-3.0343808	4.9040300	0.3817460
C	-4.0559785	5.8727694	0.7354490
H	-4.8241274	5.9039099	-0.0384878
H	-3.6089631	6.8633526	0.8317015
H	-4.5194586	5.6009521	1.6847895
C	-1.0086860	3.7706895	-3.7447588
C	-1.2193756	4.3008090	-5.0796070
H	-2.2174615	4.7349241	-5.1541237
H	-1.1215932	3.5068204	-5.8208900
H	<u>-0.4819956</u>	<u>5.0765312</u>	<u>-5.2913130</u>

## ENERGIES [a.u.]:

Total energy = -7130.7434091722

Total energy + OC corr. = -7130.7381750726

### 5.4.5 Results and Discussion – Additional Compounds

During the studies on this work, additional experiments were performed. The additional compounds obtained during these studies will be discussed in the following.

#### $[\{\{\text{CpMo}(\text{CO})_2\}_2(\mu_4, \eta^{2:2:2:1}\text{-E}_2)\}_2\{\text{Cu}(\text{CH}_3\text{CN})_2\}\text{Cu}(\text{CH}_3\text{CN})][\text{TEF}]_2$ (E = 56% P, 44% As) (**8**)

The  $\text{P}_2$  ligand complex **A** was reacted with  $[\text{Cu}(\text{CH}_3\text{CN})_4][\text{TEF}]$  (**C**,  $[\text{TEF}]^- = [\text{Al}\{\text{OC}(\text{CF}_3)_3\}_4]^-$ ) and the  $\text{As}_2$  ligand complex **B** in one reaction in order to synthesize a mixed coordination compound. Single crystal X-ray analysis revealed the formation of a  $\text{Cu}_2\text{E}_4^{2+}$  unit (Figure S5.6) with the formula  $[\{\{\text{CpMo}(\text{CO})_2\}_2(\mu_4, \eta^{2:2:2:1}\text{-E}^1_2)\}\{\{\text{CpMo}(\text{CO})_2\}_2(\mu_4, \eta^{2:2:2:1}\text{-E}^2_2)\}\{\text{Cu}(\text{CH}_3\text{CN})_2\}\text{Cu}(\text{CH}_3\text{CN})][\text{TEF}]_2$  ( $\text{E}^1 = 50\% \text{ P}, 50\% \text{ As}; \text{E}^2 = 62\% \text{ As}, 38\% \text{ P}$ ) (**8**).

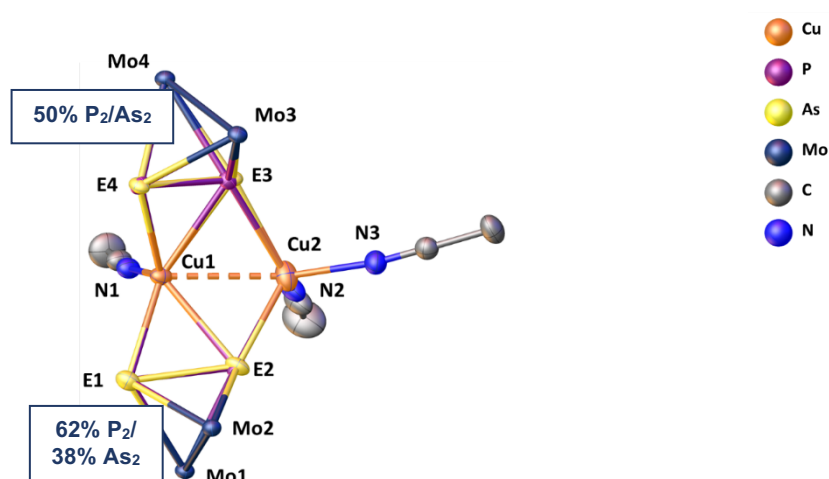


**Figure S5.6:** Molecular structure of the cationic fragment of **8** in the solid state. Cp- and CO- ligands and hydrogen atoms are omitted for clarity. Thermal ellipsoids are shown at 50% probability level. Average of selected bond lengths [Å] and angles [°]: Cu1-Cu2 2.6494(7), Cu1-N1 1.994(3), Cu2-N3 1.982(3), Cu2-N2 1.988(3), N1-Cu1-Cu2 97.79(9), N3-Cu2-Cu1 146.96(9), N2-Cu2-Cu1 105.77(9), N3-Cu2-N2 107.0(1).

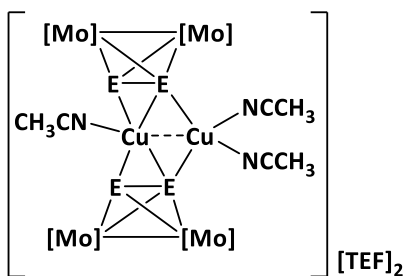
Crystals of compound **8** were obtained as clear orange blocks in 97% yield (referred to **A**) by diffusion of *n*-pentane into the crude reaction mixture. **8** crystallized in the triclinic space group  $\text{P}\bar{1}$ . Single crystal X-ray analysis (Figure S5.6) showed that **8** is isostructural to compounds **4** and **5**. The  $\text{E}_2$  position have an  $\text{As}_2:\text{P}_2$  ratio of 50:50 and 62:38, respectively. The stoichiometry of  $\text{P}_2:\text{As}_2$  in the compound therefore is approximately 1.12:0.88. Compound **8** could be also be characterized by NMR and mass spectrometry, IR spectroscopy and elemental analysis. In the  $^1\text{H}$  NMR (400 MHz,  $\text{CD}_3\text{CN}$ , r.t.) of **8**, the signals for the  $\text{P}_2$  and  $\text{As}_2$  ligand complexes can be observed. The signal in the  $^{31}\text{P}$  NMR

is observed at -47.5 ppm. In the <sup>13</sup>C{<sup>1</sup>H} NMR, signals for the CO and Cp ligand of **P**<sub>2</sub> and **As**<sub>2</sub> are observed. In the positive ESI mass spectrum, the signals for [Cu(CH<sub>3</sub>CN){Cp<sub>2</sub>Mo<sub>2</sub>(CO)<sub>4</sub>P<sub>2</sub>}]<sup>+</sup>, [Cu{Cp<sub>2</sub>Mo<sub>2</sub>(CO)<sub>4</sub>P<sub>2</sub>}]<sub>2</sub><sup>+</sup>, [Cu(CH<sub>3</sub>CN){Cp<sub>2</sub>Mo<sub>2</sub>(CO)<sub>4</sub>As<sub>2</sub>}]<sup>+</sup>, [Cu{Cp<sub>2</sub>Mo<sub>2</sub>(CO)<sub>4</sub>P<sub>2</sub>}{Cp<sub>2</sub>Mo<sub>2</sub>(CO)<sub>4</sub>As<sub>2</sub>}]<sup>+</sup> and [Cu{Cp<sub>2</sub>Mo<sub>2</sub>(CO)<sub>4</sub>As<sub>2</sub>}]<sub>2</sub><sup>+</sup> are detected. Compound **8** is well soluble in acetonitrile, moderately soluble in dichloromethane and insoluble in other common solvents.

**Table S5.7.** Comparison of selected bond length [Å] and angles [°] of compound **8**.

	E = P	E = As
E1-E2	2.17(2), 2.258(8)	2.314(7), 2.38(1)
Cu1-E	2.402(6) - 2.489(5)	2.422(5) - 2.531(8)
Cu2-E2	2.373(7)	2.344(5)
Cu2-E3	2.469(19)	2.409(8)
E-Mo	2.474(6) - 2.608(10)	2.491(5) - 2.633(5)
E1-Cu1-Cu2, E4-Cu1-Cu2	109.7(1), 107.1(3)	110.2(1), 107.8(1)
E2-Cu1-Cu2, E3-Cu1-Cu2	54.9(2), 57.8(4)	54.2(1), 55.4(2)
E1-Cu1-E2, E3-Cu1-E4	55.0(2), 53.2(5)	56.2(2), 57.1(2)
E1-Cu1-E3	150.6(4)	152.0(2)
E1-Cu1-E4	118.4(3)	117.1(2)
E2-Cu1-E3	105.2(4)	103.3(2)
E2-Cu1-E4	128.0(2)	127.4(2)
N1-Cu1-E	101.9(4) - 115.5(2)	99.89(2) - 115.9(1)
Cu1-Cu2-E2, Cu1-Cu2-E3	59.1(1), 57.0(5)	59.4(1), 59.8(2)
E2-Cu2-E3	108.2(5)	111.9(2)
N-Cu2-E	103.5(4) - 117.0(4)	102.1(2) - 114.6(2)

Synthesis of  $[\{\{\text{CpMo}(\text{CO})_2\}_2(\mu_4, \eta^{2:2:2:1}\text{-E}^1_2)\}\{\{\text{CpMo}(\text{CO})_2\}_2(\mu_4, \eta^{2:2:2:1}\text{-E}^2_2)\}\{\text{Cu}(\text{CH}_3\text{CN})_2\} \text{Cu}(\text{CH}_3\text{CN})][\text{TEF}]_2$  ( $\text{E}^1 = 50\% \text{P}, 50\% \text{As}$ ;  $\text{E}^2 = 62\% \text{As}, 38\% \text{P}$ ) (**8**):



The **P**<sub>2</sub> ligand complex **A** (1 eq., 25 mg, 0.05 mmol), the **As**<sub>2</sub> ligand complex **B** (1.5 eq., 148.8 mg, 0.1 mmol) and the Cu<sup>I</sup> salt **C** (1 eq., 29.4 mg, 0.05 mmol) were each dissolved in dichloromethane (4 mL). The solution of **B** was slowly added to the solution of **A** and the mixture stirred for half an hour. The solution of **C** was slowly added and the reaction stirred for 3 h. The crude reaction mixture was filtered and layered with *n*-pentane. After one day, crystals of compound **8** were obtained as clear orange blocks. The supernatant was decanted off, the remaining crystals washed with *n*-pentane and dried in vacuo. Crystalline Yield: 72 mg (97%, related to **A**).

<sup>1</sup>H NMR δ[ppm] = 5.32 (s, C<sub>5</sub>H<sub>5</sub>, **P**<sub>2</sub>), 5.26 (s, C<sub>5</sub>H<sub>5</sub>, **As**<sub>2</sub>).

<sup>13</sup>C {<sup>1</sup>H} NMR δ[ppm] = 226.6 (s, **CO**), 87.5 (s, C<sub>5</sub>H<sub>5</sub>, **P**<sub>2</sub>), 85.9 (s, C<sub>5</sub>H<sub>5</sub>, **As**<sub>2</sub>).

<sup>31</sup>P {<sup>1</sup>H} NMR δ[ppm] = -47.5 (s).

<sup>19</sup>F {<sup>1</sup>H} NMR δ[ppm] = -74.8 (s).

Positive ion ESI-MS (CH<sub>3</sub>CN, RT): *m/z* (%) = 599.77 (100) [Cu(CH<sub>3</sub>CN){Cp<sub>2</sub>Mo<sub>2</sub>(CO)<sub>4</sub>P<sub>2</sub>}<sup>+</sup>, 1056.56 (60) [Cu{Cp<sub>2</sub>Mo<sub>2</sub>(CO)<sub>4</sub>P<sub>2</sub>}<sub>2</sub>]<sup>+</sup>, 689.67 (100) [Cu(CH<sub>3</sub>CN){Cp<sub>2</sub>Mo<sub>2</sub>(CO)<sub>4</sub>As<sub>2</sub>}<sup>+</sup>, 1144.46 (64) [Cu{Cp<sub>2</sub>Mo<sub>2</sub>(CO)<sub>4</sub>P<sub>2</sub>}{Cp<sub>2</sub>Mo<sub>2</sub>(CO)<sub>4</sub>As<sub>2</sub>}]<sup>+</sup>, 1231.35 (58) [Cu{Cp<sub>2</sub>Mo<sub>2</sub>(CO)<sub>4</sub>As<sub>2</sub>}<sub>2</sub>]<sup>+</sup>.

Negative ion ESI-MS (CH<sub>3</sub>CN, RT): *m/z* (%) = 966.9 (100) [Al(OC(CF<sub>3</sub>)<sub>3</sub>)<sub>4</sub>]<sup>-</sup>.

Elemental analysis calculated for C<sub>66</sub>H<sub>29</sub>Al<sub>2</sub>As<sub>1.8</sub>Cu<sub>2</sub>F<sub>72</sub>Mo<sub>4</sub>N<sub>3</sub>O<sub>16</sub>P<sub>2.2</sub> (3255,6 g·mol<sup>-1</sup>): 24.3 %C, 0.90 %H, 1.29 %N; Found: 24.53 %C, 0.79 %H, 1.26 %N.

IR (solid, CO bands):  $\tilde{\nu}/\text{cm}^{-1}$ : 2015 (vs), 1991 (s), 1980 (s), 1967 (vs), 1954 (vs), 1941 (s), 1933 (s), 1918 (vs).

**Crystal Structure Analysis:** The crystal was selected and measured on a Gemini Ultra diffractometer equipped with an AtlasS2 CCD detector. The crystal was kept at  $T = 123(1)$  K during data collection. Data collection and reduction was performed with **CrysAlisPro** [Version 171.40.14a, 2018].<sup>19</sup> An analytical numeric absorption correction using a multifaceted crystal model based on expressions derived by R.C. Clark & J.S. Reid<sup>20</sup> and an empirical absorption correction using spherical harmonics as implemented

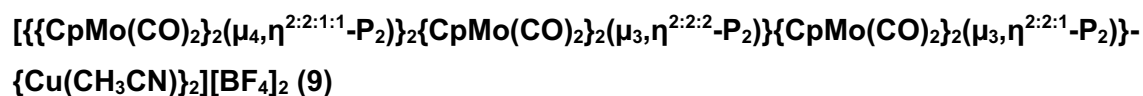
in SCALE3 ABSPACK was applied. Using **Olex2**,<sup>21</sup> the structure was solved with **ShelXT**<sup>22</sup> and a least-square refinement on  $F^2$  was carried out with ShelXL.<sup>23</sup> All non-hydrogen atoms were refined anisotropically. Hydrogen atoms at the carbon atoms were located in idealized positions and refined isotropically according to the riding model.

Compound **8**: The asymmetric unit contains a CH<sub>2</sub>Cl<sub>2</sub> solvent molecule, two [Al{OC(CF<sub>3</sub>)<sub>3</sub>}<sub>4</sub>]<sup>-</sup> anions and the cationic complex [{CpMo(CO)<sub>2</sub>}<sub>2</sub>(μ<sub>4</sub>,η<sup>2:2:2:1</sup>-E<sub>2</sub>)}<sub>2</sub>{Cu(CH<sub>3</sub>CN)<sub>2</sub>}<sub>2</sub>Cu(CH<sub>3</sub>CN)] (E = P, As). In this cationic complex, the complex fragments **A** and **B** superpose each other in a ratio of 50:50 and 62:38, respectively. Further, one of the two [Al{OC(CF<sub>3</sub>)<sub>3</sub>}<sub>4</sub>]<sup>-</sup> anions shows a disorder of two OC(CF<sub>3</sub>)<sub>3</sub> groups in the ratio 86:14. The second [Al{OC(CF<sub>3</sub>)<sub>3</sub>}<sub>4</sub>]<sup>-</sup> anion shows a disorder of three of the four OC(CF<sub>3</sub>)<sub>3</sub> groups over two (56:44; 64:36) and three (40:30:30) positions respectively. To describe these disorders the restrains SADI, ISOR, SIMU and RIGU were applied.



**Table S5.8.** Crystallographic data and details of diffraction experiments for compound **8**.

Compound	<b>8</b> · CH <sub>2</sub> Cl <sub>2</sub>
Data set (internal naming)	abs445
Formula	C <sub>67</sub> H <sub>31</sub> Al <sub>2</sub> As <sub>1.76</sub> Cl <sub>2</sub> Cu <sub>2</sub> F <sub>72</sub> Mo <sub>4</sub> N <sub>3</sub> O <sub>16</sub> P <sub>2.24</sub>
<i>D</i> <sub>calc.</sub> / g · cm <sup>-3</sup>	2.152
<i>m</i> /mm <sup>-1</sup>	7.707
Formula Weight	3338.88
Colour	clear orange
Shape	block
Size/mm <sup>3</sup>	0.39×0.31×0.22
<i>T</i> /K	123(1)
Crystal System	triclinic
Space Group	<i>P</i> -1
<i>a</i> /Å	15.1935(3)
<i>b</i> /Å	15.8577(3)
<i>c</i> /Å	23.6045(5)
<i>α</i> °	72.586(2)
<i>β</i> °	76.091(2)
<i>γ</i> °	74.721(2)
<i>V</i> /Å <sup>3</sup>	5153.4(2)
<i>Z</i>	2
<i>Z</i> '	1
Wavelength/Å	1.54184
Radiation type	Cu K <sub>α</sub>
<i>θ</i> <sub>min</sub> °	3.653
<i>θ</i> <sub>max</sub> °	73.264
Measured Refl.	57168
Independent Refl.	20098
Reflections with <i>I</i> > 2( <i>I</i> )	19381
<i>R</i> <sub>int</sub>	0.0293
Parameters	2299
Restraints	1599
Largest Peak	0.923
Deepest Hole	-0.753
GooF	1.056
<i>wR</i> <sub>2</sub> (all data)	0.0854
<i>wR</i> <sub>2</sub>	0.0844
<i>R</i> <sub>1</sub> (all data)	0.0354
<i>R</i> <sub>1</sub>	0.0341



Compound **9** was obtained by the reaction of **A** with the Cu<sup>I</sup> salt [Cu(CH<sub>3</sub>CN)<sub>4</sub>][BF<sub>4</sub>] (**D**) and characterized by single crystal X-ray crystallography (Figure S5.7). The reaction was performed in CH<sub>2</sub>Cl<sub>2</sub> using a 1:1 stoichiometry. The storage of the reaction mixture at -30°C resulted in crystals of **9**, which crystallize as clear intense red blocks in the triclinic space group P-1. Single crystal X-ray analysis revealed the presence of two units of **A**, which are coordinated in a  $\eta^{2:2:1:1}$ -coordination mode to two Cu atoms, resulting in a Cu<sub>2</sub>P<sub>4</sub> dimer. Two additional complexes **A** coordinated to the Cu<sup>I</sup> centers in a  $\eta^{2:2:1}$  and  $\eta^{2:2:1}$  coordination mode, respectively. Additionally, each Cu<sup>I</sup> center is coordinated by one acetonitrile ligand.

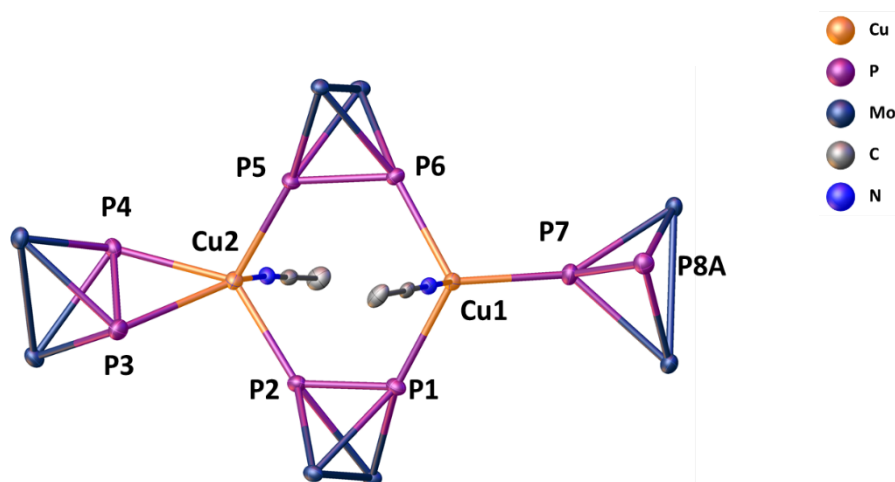
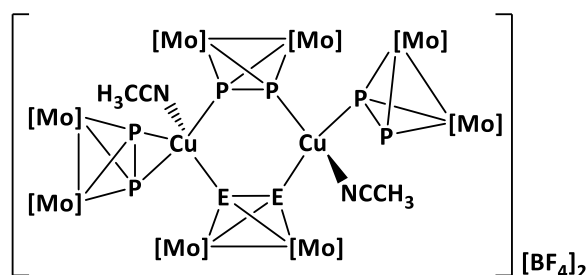


**Figure S5.7:** Molecular structure of the cation of compound **9** in the solid state. Cp- and CO-ligands, the hydrogen atoms and the minor parts of the disorder are omitted for clarity. Thermal ellipsoids are shown at 50% probability level. Average of selected bond lengths [Å] and angles [°]: Cu1-P1 2.3339(5), Cu1-P6 2.3267(5), Cu1-P7 2.2844(5), Cu1-N2 2.017(2), Cu2-P2 2.3357(6), Cu2-P3 2.6306(7), Cu2-P4 2.4184(8), Cu2-P5 2.3214(6), Cu2-N1 2.080(2), P6-Cu1-P1 114.76(2), P7-Cu1-P1 116.61(2), P7-Cu1-P6 110.99(2), N2-Cu1-P1 98.33(5), N2-Cu1-P6 100.97(5), N2-Cu1-P7 113.44(5), P2-Cu2-P3 92.49(2), P2-Cu2-P4 137.19(2), P4-Cu2-P3 49.55(2), P5-Cu2-P2 109.32(2), P5-Cu2-P3 121.59(3), P5-Cu2-P4 108.06(2), N1-Cu2-P2 96.32(5), N1-Cu2-P3 131.54(5), N1-Cu2-P4 97.07(5), N1-Cu2-P5 99.97(5).

The <sup>1</sup>H NMR spectra (400 MHz, CD<sub>3</sub>CN, r.t.) of **9** reveals signals for the Cp ligand and free acetonitrile. In the <sup>31</sup>P NMR spectra, a chemical shift of -49.1 ppm (s) was observed. In the <sup>13</sup>C {<sup>1</sup>H} NMR, the signals referring to the CO- and Cp-ligands are observed. In the positive ion ESI mass spectrum, signals for [Cu(CH<sub>3</sub>CN)<sub>2</sub>]<sup>+</sup>, [Cu(CH<sub>3</sub>CN){Cp<sub>2</sub>Mo<sub>2</sub>(CO)<sub>4</sub>P<sub>2</sub>}]<sup>+</sup> and [Cu{Cp<sub>2</sub>Mo<sub>2</sub>(CO)<sub>4</sub>P<sub>2</sub>}]<sup>+</sup> were detected.

Synthesis of  $[\{\{\text{CpMo}(\text{CO})_2\}_2(\mu_4, \eta^{2:2:1:1}\text{-P}_2)\}_2\{\text{CpMo}(\text{CO})_2\}_2(\mu_3, \eta^{2:2:2}\text{-P}_2)\}\{\text{CpMo}(\text{CO})_2\}_2(\mu_3, \eta^{2:2:1}\text{-P}_2)\}\{\text{Cu}(\text{CH}_3\text{CN})\}_2][\text{BF}_4]_2$  (**9**):



A solution of **A** (35 mg, 0.07 mmol) in  $\text{CH}_2\text{Cl}_2$  (5 mL) was added dropwise to a solution of **D** (22 mg, 0.07 mmol) in  $\text{CH}_2\text{Cl}_2$  (5 mL). The clear reaction mixture was stirred for 3h, filtered and stored at  $-30\text{ }^\circ\text{C}$ . After one day, compound **9** was obtained as clear orange plates. The supernatant was decanted off, the remaining crystals washed with *n*-pentane and dried in vacuo. Crystalline Yield: 23 mg (28 %, related to **A**).

$^1\text{H}$  NMR (400 MHz,  $\text{CD}_3\text{CN}$ ):  $\delta = 5.30$  (s, 10H,  $\text{C}_5\text{H}_5$ ), 2.11 (s,  $\text{CH}_3\text{CN}$ ).

$^{31}\text{P}$   $\{^1\text{H}\}$  NMR (400 MHz,  $\text{CD}_3\text{CN}$ ):  $\delta = -49.10$  (s).

$^{13}\text{C}$   $\{^1\text{H}\}$  NMR (400 MHz,  $\text{CD}_3\text{CN}$ ):  $\delta = 226.5$  (s, **CO**), 87.5 (s,  $\text{C}_5\text{H}_5$ ).

$^{19}\text{F}$   $\{^1\text{H}\}$  NMR (400 MHz,  $\text{CD}_3\text{CN}$ ):  $\delta = -150.7$  (s).

$^{11}\text{B}$   $\{^1\text{H}\}$  NMR (400 MHz,  $\text{CD}_3\text{CN}$ ):  $\delta = 0.57$  (s).

Positive ion ESI-MS ( $\text{CH}_3\text{CN}$ , RT):  $m/z$  (%) = 144.98 (100)  $[\text{Cu}(\text{CH}_3\text{CN})_2]^+$ , 599.77 (100)  $[\text{Cu}(\text{CH}_3\text{CN})\{\text{Cp}_2\text{Mo}_2(\text{CO})_4\text{P}_2\}]^+$ , 1056.56 (60)  $[\text{Cu}\{\text{Cp}_2\text{Mo}_2(\text{CO})_4\text{P}_2\}_2]^+$ .

Negative ion ESI-MS ( $\text{CH}_3\text{CN}$ , RT):  $m/z$  (%) = 87.00 (100)  $[\text{BF}_4]^-$ .

Elemental analysis, calc. for  $\text{B}_2\text{C}_{62}\text{Cl}_4\text{Cu}_2\text{F}_8\text{H}_{50}\text{Mo}_8\text{N}_2\text{O}_{16}\text{P}_8$  ( $= \mathbf{9} \cdot 2 \text{CH}_2\text{Cl}_2$ ) (2549 g/mol) (%): C, 29.35; H, 1.99; N 1.10; found: C, 29.13; H, 1.98; N, 1.04.

IR (solid, CO bands):  $\tilde{\nu}/\text{cm}^{-1}$ : 1972 (s), 1932 (s), 1912 (s).

**Crystal Structure Analysis:** The crystal was selected and measured on a Gemini Ultra diffractometer equipped with an AtlasS2 CCD detector. The crystal was kept at  $T = 123(1)$  K during data collection. Data collection and reduction were performed with **CrysAlisPro** [Version 171.39.37b, 2017].<sup>19</sup> An analytical numeric absorption correction using a multifaceted crystal model based on expressions derived by R.C. Clark & J.S. Reid<sup>20</sup> and an empirical absorption correction using spherical harmonics as implemented in SCALE3 ABSPACK was applied. Using **Olex2**,<sup>21</sup> the structure was solved with **SheIXT**<sup>22</sup> and a least-square refinement on  $F^2$  was carried out with **SheIXL**.<sup>21</sup> All non-hydrogen atoms were refined anisotropically. Hydrogen atoms at the carbon atoms were located in idealized positions and refined isotropically according to the riding model.

Compound **9**: The asymmetric unit contains two  $\text{CH}_2\text{Cl}_2$  and two  $\text{CH}_3\text{CN}$  solvent molecules, which are heavily disordered. Therefore, a solvent mask was calculated and 268 electrons were found in a volume of  $774 \text{ \AA}^3$  in two voids per unit cell. This is consistent with the presence of two  $\text{CH}_2\text{Cl}_2$  and two  $\text{CH}_3\text{CN}$  solvent molecules per asymmetric unit, which account for 256 electrons per unit cell. The asymmetric unit further contains the cationic complex  $[\{\{\text{CpMo}(\text{CO})_2\}_2(\mu_4, \eta^{2:2:1:1}\text{-P}_2)\}_2\{\text{CpMo}(\text{CO})_2\}_2(\mu_3, \eta^{2:2:2}\text{-P}_2)\}\{\text{CpMo}(\text{CO})_2\}_2(\mu_3, \eta^{2:2:1}\text{-P}_2)\}\text{-}\{\text{Cu}(\text{CH}_3\text{CN})\}_2]^{2+}$  and two  $\text{BF}_4$  anions. One of the two  $\text{BF}_4$  anions is disordered over three positions (39:36:25), a Cu atom is disordered over two positions (96:4) and further both of the terminal complexes **A** are disordered over two positions (96:4; 93:7). To model this disorders the restraints DFIX, SADI, FLAT, ISOR, SIMU and RIGU were applied.

**Table S9.** Crystallographic data and details of diffraction experiments for compound **9**.

Compound	Compound <b>9</b> · 2 CH <sub>2</sub> Cl <sub>2</sub> · 2 CH <sub>3</sub> CN
Data set (internal naming)	abs444b_2
Formula	B <sub>2</sub> C <sub>66</sub> Cl <sub>4</sub> Cu <sub>2</sub> F <sub>8</sub> H <sub>56</sub> Mo <sub>8</sub> N <sub>4</sub> O <sub>16</sub> P <sub>8</sub>
<i>D</i> <sub>calc.</sub> / g · cm <sup>-3</sup>	2.247
<i>m</i> /mm <sup>-1</sup>	2.066
Formula Weight	2952.99
Colour	clear intense red
Shape	block
Size/mm <sup>3</sup>	0.38×0.31×0.28
<i>T</i> /K	123.15
Crystal System	triclinic
Space Group	P-1
<i>a</i> /Å	14.5777(3)
<i>b</i> /Å	14.8078(3)
<i>c</i> /Å	23.6001(4)
<i>α</i> /°	100.584(2)
<i>β</i> /°	93.8500(10)
<i>γ</i> /°	117.715(2)
<i>V</i> /Å <sup>3</sup>	4364.53(16)
<i>Z</i>	2
<i>Z</i> '	1
Wavelength/Å	0.71073
Radiation type	Mo K <sub>α</sub>
<i>θ</i> <sub>min</sub> /°	3.348
<i>θ</i> <sub>max</sub> /°	32.546
Measured Refl.	78860
Independent Refl.	28165
Reflections with <i>I</i> > 2( <i>I</i> )	23497
<i>R</i> <sub>int</sub>	0.0267
Parameters	1265
Restraints	497
Largest Peak	1.222
Deepest Hole	-0.975
GooF	1.030
<i>wR</i> <sub>2</sub> (all data)	0.0587
<i>wR</i> <sub>2</sub>	0.0557
<i>R</i> <sub>1</sub> (all data)	0.0378
<i>R</i> <sub>1</sub>	0.0281

**$[\{\text{Cp}_2(\text{CO})_4\text{Mo}_2(\mu_3, \eta^{2:2:2}\text{-As}_2)\}_2(\eta^1\text{-CH}_3\text{CN})\text{Cu}][\text{TEF}]$  (10)**

As mentioned before, the  $\text{E}_2/\text{Cu}^{\text{I}}$  systems are highly dynamic in solution. Due to this, the compound  $[\{\text{Cp}_2(\text{CO})_4\text{Mo}_2(\mu, \eta^{2:2:2}\text{-As}_2)\}_2(\text{CH}_3\text{CN})\text{Cu}][\text{TEF}]$  (10), once co-crystallized with compound 4. Except of preliminary X-ray measurements (Figure S5.8), no further characterization was performed for 10. The measurement revealed a Cu(I) monomer with the Cu(I) center  $\eta^{2:2:1}$ -coordinated by two molecules of  $\text{As}_2$  and saturated with one acetonitrile ligand.

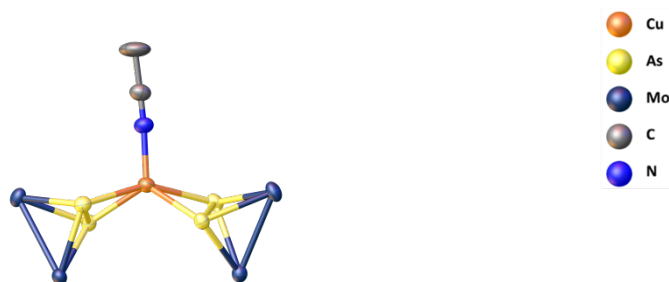


**Figure S5.8.** Molecular structure of the cationic fragment of compound 10. Cp-, Co-ligands and hydrogen atoms are omitted for clarity. Thermal ellipsoids are shown at 50% probability level.

**Crystal Structure Analysis:** The crystal was selected and measured on a GV50 diffractometer equipped with a TitanS2 CCD detector. The crystal was kept at  $T = 153(1)$  K during data collection. Data collection and reduction were performed with **CrysAlisPro** [Version V1.171.41.21a, 2019].<sup>19</sup> A numerical absorption correction based on gaussian integration over a multifaceted crystal model and an empirical absorption correction using spherical harmonics as implemented in SCALE3 ABSPACK was applied. Using **Olex2**,<sup>21</sup> the structure was solved with **ShelXT**<sup>22</sup> and a least-square refinement on  $F^2$  was carried out with **ShelXL**.<sup>23</sup> All non-hydrogen atoms were refined anisotropically. Hydrogen atoms at the carbon atoms were located in idealized positions and refined isotropically according to the riding model.

**Compound 10:** The asymmetric unit contains two  $\text{CH}_2\text{Cl}_2$  solvent molecule, two independent units of the cationic complex  $[\{\text{Cp}_2(\text{CO})_4\text{Mo}_2(\mu_3, \eta^{2:2:2}\text{-As}_2)\}_2(\eta^1\text{-CH}_3\text{CN})\text{Cu}]^+$  and two  $[\text{Al}\{\text{OC}(\text{CF}_3)_3\}_4]^-$  anions. For one of the complexes  $[\{\text{Cp}_2\text{Mo}_2(\text{CO})_4(\mu_3, \eta^{2:2:2}\text{-As}_2)\}_2(\eta^1\text{-CH}_3\text{CN})\text{Cu}]^+$  a  $[\text{Cp}_2\text{Mo}_2(\text{CO})_4(\text{As}_2)]$  unit and a  $\text{CH}_3\text{CN}$  molecule are disordered over two positions (78:22; 68:32). Further, one of the  $\text{CH}_2\text{Cl}_2$  molecules is disordered (72:28). One of the two  $[\text{Al}\{\text{OC}(\text{CF}_3)_3\}_4]^-$  anions shows a disorder of one  $\text{OC}(\text{CF}_3)_3$  group over two positions (73:27). For the second  $[\text{Al}\{\text{OC}(\text{CF}_3)_3\}_4]^-$  anion all four  $\text{OC}(\text{CF}_3)_3$  groups are disordered over two positions (60:40; 54:46; 55:45; 54:46). To describe this disorder the restraints DFIX, SADI and SIMU were applied.

**Table S5.10.** Crystallographic data and details of diffraction experiments for compound **10**.

<b>Compound</b>	<b>10 · 2 CH<sub>2</sub>Cl<sub>2</sub></b>
Data set (internal naming)	JS200_3
Formula	C <sub>47</sub> H <sub>25</sub> AlAs <sub>4</sub> Cl <sub>2</sub> Cu F <sub>36</sub> Mo <sub>4</sub> NO <sub>12</sub>
$D_{calc.} / \text{g} \cdot \text{cm}^{-3}$	2.223
$m/\text{mm}^{-1}$	10.465
Formula Weight	2324.54
Colour	clear orange
Shape	needle
Size/mm <sup>3</sup>	0.50×0.09×0.06
$T/\text{K}$	152.96(13)
Crystal System	triclinic
Space Group	P-1
$a/\text{Å}$	11.9908(2)
$b/\text{Å}$	19.2373(3)
$c/\text{Å}$	31.4734(3)
$\alpha^\circ$	87.8510(10)
$\beta^\circ$	88.7130(10)
$\gamma^\circ$	73.2230(10)
$V/\text{Å}^3$	6945.57(18)
$Z$	4
$Z'$	2
Wavelength/Å	1.54184
Radiation type	Cu K $\alpha$
$\theta_{min}^\circ$	3.637
$\theta_{max}^\circ$	74.218
Measured Refl.	79129
Independent Refl.	27517
Reflections with $I > 2(I)$	25208
$R_{int}$	0.0738
Parameters	2614
Restraints	1833
Largest Peak	1.468
Deepest Hole	-1.351
GooF	1.101
$wR_2$ (all data)	0.1825
$wR_2$	0.1803
$R_1$ (all data)	0.0784
$R_1$	0.746

## 5.5 References

- [1] a) S. T. Li, B. B. Cula, S. Hoof and C. Limberg, *Dalton Trans.* **2018**, 47, 544-560; b) C. Marzano, V. Gandin, M. Pellei, D. Colavito, G. Papini, G. G. Lobbia, E. D. Giudice, M. Porchia, F. Tisato, C. Santini, *J. Med. Chem.* **2008**, 51, 798; c) O. A. Filippov, A. A. Titov, E. A. Guseva, D. A. Loginov, A. F. Smol'yakov, F. M. Dolgushin, N. V. Belkova, L. M. Epstein, E. S. Shubina, *Chem. Eur. J.* **2015**, 21, 13176-13180.
- [2] a) B. Hupp, C. Schiller, C. Lenczyk, M. Stanoppi, K. Edkins, A. Lorbach A. Steffen, *Inorg. Chem.* **2017**, 56, 8996-9008; b) M. E. Moussa, S. Evariste, H.-L. Wong, L. Le Bras, C. Roiland, L. Le Polles, B. Le Guennic, K. Costuas, V. W.-W. Yam, C. Lescop, *Chem. Commun.* **2016**, 52, 11370-11373; c) F. Bappler, M. Zimmer, F. Dietrich, M. Gruppe, M. Wallesch, D. Volz, S. Brase, M. Gerhards, R. Diller, *Phys. Chem. Chem. Phys.* **2017**, 19, 29438-29448; d) T. Hofbeck, U. Monkowius, H. Yersin, *J. Am. Chem. Soc.* **2015**, 137, 399-404.
- [3] W.-H. Chan, S.-M. Peng, C.-M. Che, *J. Chem. Soc. Dalton Trans.* **1998**, 2867-2871.
- [4] X. He, K. Ruhlandt-Senge, P. P. Power, S. H. Bertz, *J. Am. Chem. Soc.* **1994**, 116, 6963-6964.
- [5] P. Ai, A. A. Danopoulos, P. Braunstein. K. Y. Monakhov, *Chem. Commun.* **2014**, 50, 103-105.
- [6] M. Fleischmann, L. Dutsch, M. E. Moussa, G. Balazs, W. Kremer, C. Lescop, M. Scheer, *Inorg. Chem.* **2016**, 55, 2840-2854.
- [7] a) M. E. Moussa, M. Piesch, M. Fleischmann, A. Schreiner, M. Seidl, M. Scheer, *Dalton Trans.* **2018**, 47, 16031-16035; b) M. E. Moussa, M. Seidl, G. Balazs, M. Hautmann, M. Scheer, *Angew. Chem.* **2019**, 131, 13035-13039; *Angew. Chem. Int. Ed.* **2019**, 58, 12903-12907; c) M. Scheer, L. J. Gregoriades, M. Zabel, J. Bai, I. Krossing, G. Brunklaus, H. Eckert, *Chem. Eur. J.* **2008**, 14, 282-295; d) M. E. Moussa, B. Attenberger, E. V. Peresyphkina, M. Fleischmann, G. Balazs, M. Scheer, *Chem. Commun.* **2016**, 52, 10004-10007; e) J. Bai, E. Leiner, M. Scheer, *Angew. Chem.* **2002**, 114, 820-823; *Angew. Chem. Int. Ed.* **2002**, 41, 783-786; f) M. Scheer, L. Gregoriades, J. Bai, M. Sierka, G. Brunklaus, H. Eckert, *Chem. Eur. J.* **2005**, 11, 2163-2169; g) M. E. Moussa, P. A. Shelyganov, B. Wegley, M. Seidl, M. Scheer, *Eur. J. Inorg. Chem.* **2019**, 4241-4248.
- [8] a) C. Heindl, A. Kuntz, E. V. Peresyphkina, A. V. Virovets, M. Zabel, D. Ludeker, G. Brunklaus, M. Scheer, *Dalton Trans.* **2015**, 44, 6502-6509; b) C. Heindl, E. V. Peresyphkina, A. V. Virovets, V. Y. Komarov, M. Scheer, *Dalton Trans.* **2015**, 44,



- 10245-10252; c) M. Fleischmann, S. Welsch, E. V. Peresyphkina, A. V. Virovets, M. Scheer, *Chem. Eur. J.* **2015**, *21*, 14332-14336; d) E.-M. Rummel, M. Eckhardt, M. Bodensteiner, E. V. Peresyphkina, W. Kremer, C. Groger, M. Scheer, *Eur. J. Inorg. Chem.* **2014**, 1625-1637; e) M. E. Moussa, E. Peresyphkina, A. V. Virovets, D. Venus, G. Balázs, M. Scheer, *CrystEngComm* **2018**, *20*, 7417-7422; f) M. E. Moussa, S. Welsch, M. Lochner, E. Peresyphkina, A. V. Virovets, M. Scheer, *Eur. J. Inorg. Chem.* **2018**, 2689-2694; g) M. E. Moussa, B. Attenberger, E. V. Peresyphkina, M. Scheer, *Dalton Trans.* **2018**, *47*, 1014; h) M. E. Moussa, B. Attenberger, M. Seidl, A. Schreiner, M. Scheer, *Eur. J. Inorg. Chem.* **2017**, 5616-5620; i) C. Heindl, E. V. Peresyphkina, D. Ludeker, G. Brunklaus, A. V. Virovets, M. Scheer, *Chem. Eur. J.* **2016**, *22*, 2599-2604.
- [9] S. Welsch, C. Groger, M. Sierka, M. Scheer, *Angew. Chem.* **2011**, *123*, 1471; *Angew. Chem. Int. Ed.* **2011**, *50*, 1435; *Angew. Chem.* **2011**, *123*, 1471.
- [10] a) C. Heindl, E. Peresyphkina, A. V. Virovets, I. S. Bushmarinov, M. G. Medvedev, B. Krämer, B. Dittrich, M. Scheer, *Angew. Chem.* **2017**, *129*, 13420; *Angew. Chem. Int. Ed.* **2017**, *56*, 13237-13243; *Angew. Chem.* **2017**, *129*, 13420; b) F. Dielmann, E. V. Peresyphkina, B. Krämer, F. Hastreiter, B. P. Johnson, M. Zabel, C. Heindl, M. Scheer, *Angew. Chem. Int. Ed.* **2016**, *55*, 14833-14837; c) C. Heindl, E. V. Peresyphkina, A. V. Virovets, W. Kremer, M. Scheer, *J. Am. Chem. Soc.* **2015**, *137*, 10938-10941; d) M. Scheer, A. Schindler, R. Merkle, B. P. Johnson, M. Linseis, R. Winter, C. E. Anson, A. V. Virovets, *J. Am. Chem. Soc.* **2007**, *129*, 13386-13387; e) J. Bai, A. V. Virovets, M. Scheer, *Science* **2003**, *300*, 781-783; f) F. Dielmann, C. Heindl, F. Hastreiter, E. V. Peresyphkina, A. V. Virovets, R. M. Gschwind, M. Scheer, *Angew. Chem.* **2014**, *53*, 13605-13608; *Angew. Chem. Int. Ed.* **2014**, *53*, 13605-13608; *Angew. Chem.* **2014**, *126*, 13823-13826.
- [11] a) P. J. Sullivan, A. L. Rheingold, *Organometallics* **1982**, *1*, 1547-1549; b) O. J. Scherer, C. Blath, G. Wolmershäuser, *J. Organomet. Chem.* **1990**, *387*, C21-C24.
- [12] a) H. Krauss, G. Balázs, M. Bodensteiner, M. Scheer, *Chem. Sci.* **2010**, *1*, 337-342; C. Schwarzmaier, M. Sierka, M. Scheer, *Angew. Chem. Int. Ed.* **2013**, *52*, 858-861; c) L. J. Gregoriades, H. Krauss, J. Wachter, A. V. Virovets, M. Sierka, M. Scheer, *Angew. Chem.* **2006**, *118*, 4295-4298; *Angew. Chem. Int. Ed.* **2006**, *45*, 4189-4192; d) M. Scheer, L. J. Gregoriades, A. V. Virovets, W. Kunz, R. Neueder, I. Krossing, *Angew. Chem.* **2006**, *118*, 5818-5822; *Angew. Chem. Int. Ed.* **2006**, *45*, 5689-5693.
- [13] a) O. J. Scherer, H. Sitzmann, G. Wolmershäuser, *J. Organomet. Chem.* **1984**, *268*, C9-C12; b) O. J. Scherer, H. Sitzmann, G. Wolmershäuser, *J. Organomet. Chem.*, **1986**, *309*, 77-86.

- [14] Once another compound could be isolated (cf. Supporting information).
- [15] M. L. Ziegler, K. Blechschmitt, B. Nuber, T. Zahn, *Chem. Ber.* **1988**, *121*, 159-171.
- [16] A. Bondi, *J. Phys. Chem.* **1964**, *68*, 441-451.
- [17] P. Pykkö, M. Atsumi, *Chem. Eur. J.* **2009**, *15*, 186-197.
- [18] In the <sup>31</sup>P{<sup>1</sup>H} spectra of compounds **1-3**, broad signals are detected. This is most likely due to an equilibrium in a highly dynamic solution. This has already been discussed in the main part of this paper.
- [19] CrysAlisPro Software System, Rigaku Oxford Diffraction, (2018).
- [20] Clark, R. C. & Reid, J. S. *Acta Cryst.* **1995**, *A51*, 887-897.
- [21] O.V. Dolomanov and L.J. Bourhis and R.J. Gildea and J.A.K. Howard and H. Puschmann, Olex2: A complete structure solution, refinement and analysis program, *J. Appl. Cryst.* **2009**, *42*, 339-341.
- [22] Sheldrick, G.M., ShelXT-Integrated space-group and crystal-structure determination, *Acta Cryst.* **2015**, *A71*, 3-8.5.G.
- [23] M. Sheldrick, Crystal structure refinement with ShelXL, *Acta Cryst.* **2015**, *C27*, 3-8.
- [24] a) F. Furche, R. Ahlrichs, C. Hättig, W. Klopper, M. Sierka, F. Weigend, *WIREs Comput. Mol. Sci.* **2014**, *4*, 91-100. b) R. Ahlrichs, M. Bär, M. Häser, H. Horn, C. Kölmel, *Chem. Phys. Lett.* **1989**, *162*, 165-169; c) O. Treutler, R. Ahlrichs, *J. Chem. Phys.* **1995**, *102*, 346-354. d) TURBOMOLE V6.4, <http://www.turbomole.com>.
- [25] a) K. Eichkorn, O. Treutler, H. Oehm, M. Häser, R. Ahlrichs, *Chem. Phys. Lett.* **1995**, *242*, 652-660; b) K. Eichkorn, F. Weigend, O. Treutler, R. Ahlrichs, *Theor. Chem. Acc.* **1997**, *97*, 119.
- [26] a) P. A. M. Dirac, *Proc. Royal Soc.A.* **1929**, *123*, 714. b) J. C. Slater, *Phys. Rev.* **1951**, *81*, 385. c) S. H. Vosko, L. Wilk, M. Nusair, *Can. J. Phys.* **1980**, *58*, 1200. d) A. D. Becke, *Phys. Rev. A*, **1988**, *38*, 3098. e) C. Lee, W. Yang, R. G. Parr, *Phys. Rev. B.* **1988**, *37*, 785. f) A. D. Becke, *J. Chem. Phys.* **1993**, *98*, 5648.
- [27] a) A. Schäfer, C. Huber, R. Ahlrichs, *J. Chem. Phys.* **1994**, *100*, 5829; b) K. Eichkorn, F. Weigend, O. Treutler, R. Ahlrichs, *Theor. Chem. Acc.* **1997**, *97*, 119.
- [28] M. Sierka, A. Hogekamp, R. Ahlrichs, *J. Chem. Phys.* **2003**, *118*, 9136.
- [29] A. Klamt, G. Schüürmann *J. Chem. Soc. Perkin Trans.* **1993**, *2*, 799-805; A. Schäfer, A. Klamt, D. Sattel, J. C. W. Lohrenz, F. Eckert *Phys. Chem. Chem. Phys.*, **2000**, *2*, 2187-2193.



## **Preface**

## **Authors**

Jana Schiller, Eugenia Peresykina, Alexander V. Virovets and Manfred Scheer\*

## **Author contributions**

The manuscript was written by Jana Schiller, Eugenia Peresykina and Alexander V. Virovets. The synthesis and characterization of compound **3** and **4** were performed by Jana Schiller. The X-ray measurements of compounds **3** and **4** were performed by Eugenia V. Peresykina and Alexander V. Virovets. Manfred Scheer contributed by supervising the research and revision of the manuscript.

## **Acknowledgements**

This work was supported by the Deutsche Forschungsgemeinschaft. Parts of this research (projects II-20180597 and I-20190225) were carried out at PETRA III at DESY, a member of the Helmholtz Association (HGF). We thank Dr. Martin Tolkiehn and Dr. Sofiane Saouane for the assistance regarding the use of the beamlines P24 and P11, respectively. The authors thank Christian Klimas for performing PXRD measurements.

This chapter is published as an open access article by *Angewandte Chemie* and is reprinted with permission. <https://doi.org/10.1002/anie.202004988>.

## 6. Metal-Deficient Supramolecule Based on a Fivefold-Symmetric Building Block

**Abstract:** An unprecedented cationic supramolecule  $[(\text{Cp}^{\text{R}}\text{Fe}(\eta^5\text{-P}_5))_{12}\{\text{CuNCMe}\}_8]^{8+}$  2.66 nm in diameter was selectively isolated as a salt of the weakly coordinating anion  $[\text{Al}\{\text{OC}(\text{CF}_3)_3\}_4]^-$  for the first time and characterized by X-ray structure analysis, PXRD, NMR spectroscopy and mass spectrometry. Its metal-deficient core contains the lowest possible number of Cu atoms to connect 12 pentaphosphaferrocene units providing a supramolecule with fullerene topology which, topologically, also represents the simplest homologue in the family of metal-deficient pentaphosphaferrocene-based supramolecules  $[(\text{Cp}^{\text{R}}\text{Fe}(\eta^5\text{-P}_5))_{12}(\text{CuX})_{20-n}]$ . The 12 vacant metal sites between *cyclo*-P<sub>5</sub> rings, the largest number attained to date, make this compound a facile precursor for potential inner and outer modification of the core as well as for functionalization *via* the substitution of labile acetonitrile ligands.

### 6.1 Introduction

Giant self-assembled supramolecules based on metal cations and rigid bi- or multidentate organic ligands have been met with growing interest over the last decade.<sup>1</sup> They represent an attractive combination of solubility and functionality such as selective encapsulation of enantiomers and catalytic as well as photochemical activity.<sup>2</sup> Generally, these supramolecules contain dozens of metal atoms in their hollow cores as, for example, spherical  $[\text{Pd}_{30}(\text{L1})_{60}](\text{BF}_4)_{60}$ ,  $[\text{Pd}_{48}(\text{L1})_{96}](\text{BF}_4)_{60}$  (L1 = selenophene-based spacer), octahedral  $[\text{M}_{24}\{\text{pyrogallol}[4]\text{arene}\}_6]$  (M = Cu, Fe, Mg, V), or icosahedral  $[\text{M}_{48}\{\mu_3\text{-L2}\}_{18}\{\text{TC4A}\}_{12}]$  (M = Co, Ni; H<sub>4</sub>TC4A = *p-tert*-butylthiacalix[4]arene; L2 = 1H-tetrazol-1-yl)isophthalate) (Figure S6.14 in the Supporting Information).<sup>3</sup> Although usually all positions of metal cations in the supramolecule are fully occupied, it is nonetheless entirely conceivable that some of these metal cations are absent without harming the integrity of the core of the supramolecule in any way. Such '*metal-deficient*' supramolecules might be interesting as a precursor for the design of mixed-metal supramolecules *via* subsequent saturation of vacant coordination sites with heterometals, opening a way to tailor the total charge/spin state of the supramolecule or electronic structure of the spacers. Moreover, modification by additional ligands coordinated to heterometallic sites becomes possible. Nevertheless, the general principles of achieving such metal-deficient supramolecules have not been developed.

During our studies of coordination chemistry of polyphosphorus ligand complexes as for instance pentaphosphaferrocene,  $[\text{Cp}^{\text{R}}\text{Fe}(\eta^5\text{-P}_5)]$  ( $\text{Cp}^{\text{R}} = \text{C}_5(\text{CH}_2\text{Ph})_5$  ( $\text{Cp}^{\text{Bn}}$ , **1a**),  $\text{C}_5(\text{CH}_3)_5$  ( $\text{Cp}^*$ , **1b**), 1,3- $\text{C}_5\text{H}_3\text{tBu}_2$  ( $\text{Cp}^{\text{H}}$ , **1c**)) we found a way to construct various giant supramolecules reaching 4.6 nm in size *via* coordination of Cu cations to P atoms of *cyclo-P*<sub>5</sub> rings.<sup>4</sup> In a homologous family of supramolecules with the formula  $[\{\text{Cp}^{\text{R}}\text{Fe}(\eta^5\text{-P}_5)\}_{12}(\text{CuX})_{20}]$  (**2**:  $\text{Cp}^{\text{R}} = \text{Cp}^*$ ,  $\text{Cp}^{\text{Bn}}$ ; X = Cl, Br, Figure 6.1a), all phosphorus atoms of all *cyclo-P*<sub>5</sub> rings coordinate towards Cu cations, ideally forming an 80-vertex  $\{\text{Cu}_{20}\text{P}_{60}\}$  core with the fullerene  $I_h\text{-C}_{80}$  topology and a pentagonal dodecahedral arrangement of Cu (Figure 6.1b). However, the comprehensive study of **1a**- and **1b**-based supramolecules in solid state and solution revealed the fact that some of the  $\{\text{CuX}\}$  sites are statistically vacant. Therefore, instead of an individual compound, a solid solution of various  $[\{\text{1a}\}_{12}(\text{CuX})_{20-n}]$  *n*-vacant supramolecules with  $0 < n < 4.8$  crystallizes in the solid state.<sup>4f</sup> The question arises as to how an individual compound containing a supramolecule with given *n* can be selectively obtained? Moreover, what is the maximal achievable value of metal-deficiency *n*?

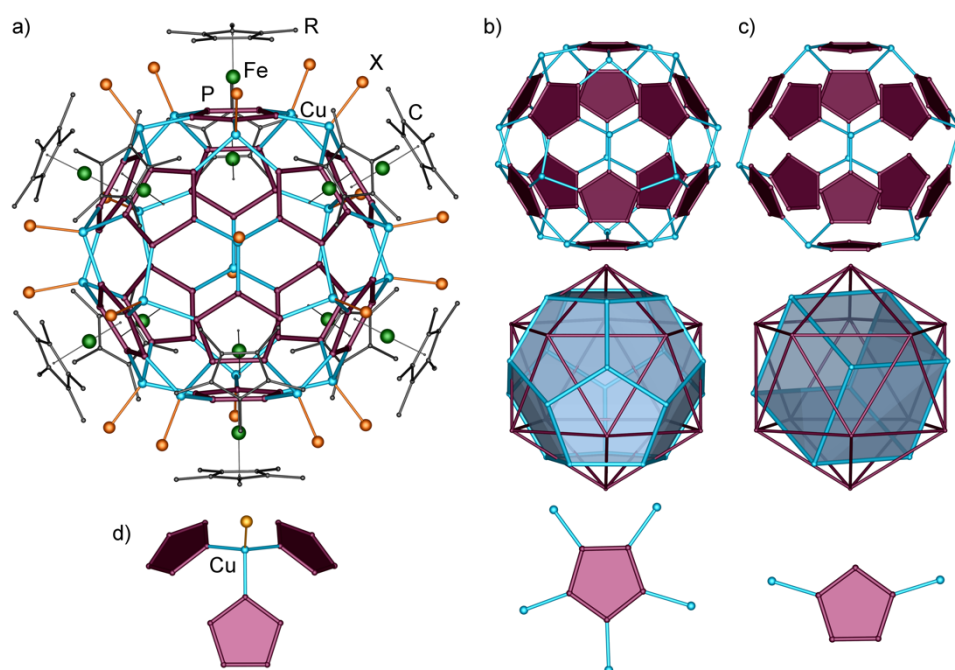


**Figure 6.1.** a) Spherical supramolecule  $[\{\text{Cp}^{\text{R}}\text{Fe}(\eta^5\text{-P}_5)\}_{12}(\text{CuX})_{20}]$  (**2**), b) its inorganic core  $\{\text{Cu}_{20}\text{P}_{60}\}$ , corresponding icosahedral representation for centres of *cyclo-P*<sub>5</sub> units and dodecahedral for copper. c) Hypothetic 12-fold deficient  $\{\text{Cu}_8\text{P}_{60}\}$  core and its respective polyhedral representation. D) Coordination environment of Cu.

All  $[\{\text{1}\}_{12}(\text{CuX})_{20-n}]$  80-vertex supramolecules known so far are neutral due to the presence of copper-bonded halide anions X and are similar in size and shape as predefined by substituted cyclopentadienyl ligands of 12 units of **1**. Obviously, this is the

reason why they readily co-crystallize. At the same time, molecular modeling of these spherical systems revealed that eight copper(I) cations is the minimal number to keep a sphere of this overall size together, if they are distributed in a cube-like arrangement (Figure 6.1c), leaving  $20 - 8 = 12$  vacant metal sites. After numerous attempts, such a super-vacant sphere was considered as unattainable in both **1a**/CuX and **1b**/CuX systems.<sup>4b,f</sup>

## 6.2 Results and Discussion

One of the possible approaches to control the formation of a Cu-deficient sphere with a given  $n$  is to obtain positively charged analogues of the supramolecule **2** using weakly coordinating anions (WCAs). As the stability of the ionic structure strongly depends on the mutual size and charge of ions (function of  $n$  in the present case), the size of the WCA should play an important role. Firstly, every additional metal position will require an additional counter anion, and with a large WCA, different  $[\{\mathbf{1}\}_{12}\text{Cu}_{20-n}]^{(20-n)+}(\text{WCA}^-)_{20-n}$  salts are not able to crystallize in the same structure type. In this way, an undesirable co-crystallization of salts with different  $n$  can be prevented. In addition, different salts are also expected to have different solubilities, which allows fractional crystallization. Secondly, the degree of metal deficiency can be controlled to a certain extent by the size of the WCA, because only a restricted number of large anions can surround multi-charged cations, avoiding anion-anion repulsive interactions. Therefore, a larger WCA can afford a higher degree of metal-deficiency. Following these considerations, herein we report on the synthesis of a Cu salt of a bulky WCA  $[\text{Al}(\text{OC}_4\text{F}_9)_4]^-$  (teflonate,  $[\text{TEF}]^-$ ) with  $[\text{Cp}^*\text{Fe}(\eta^5\text{-P}_5)]$  (**1c**) allowing an isolation of the 8+ charged supramolecule

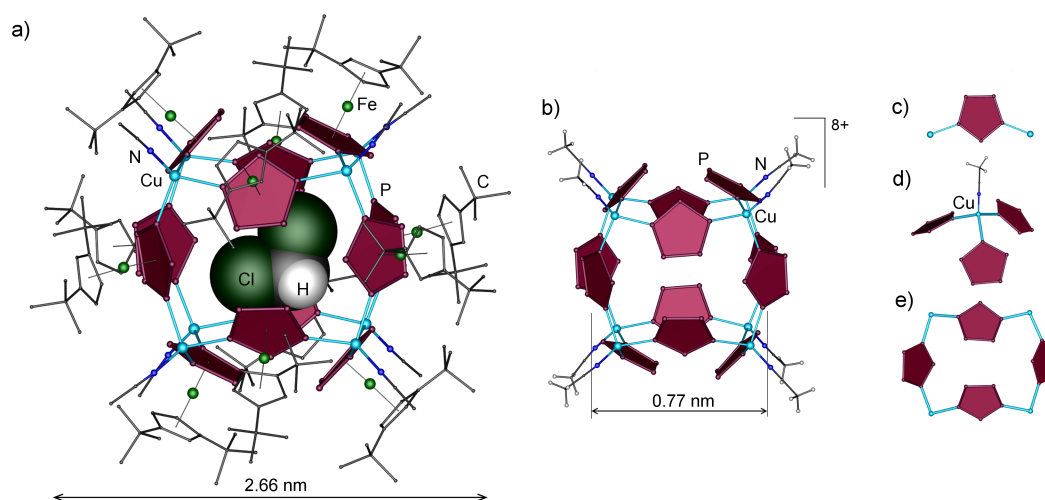
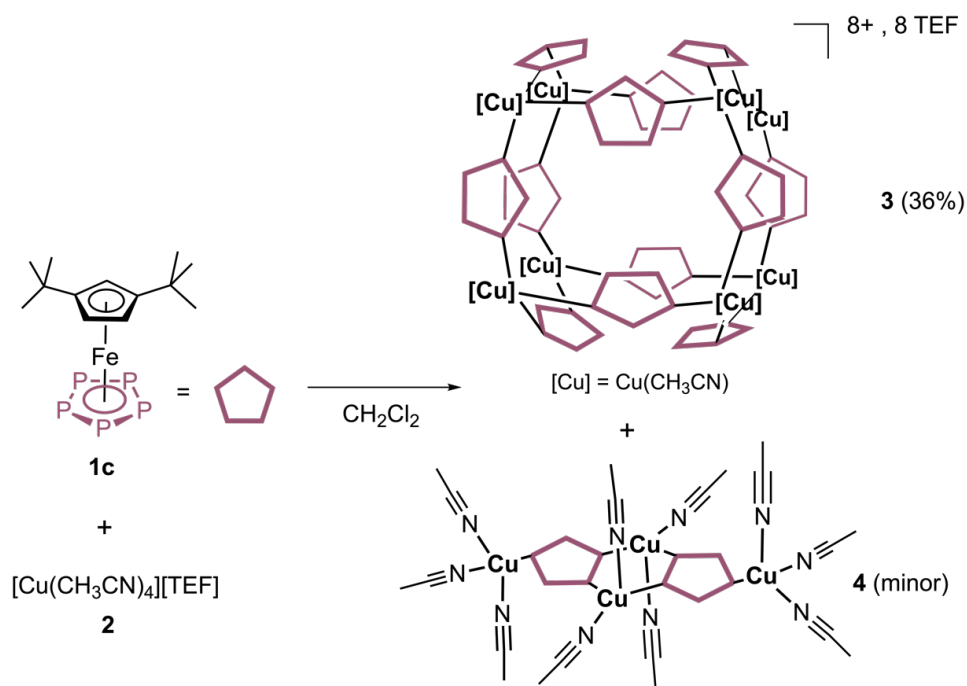


**Figure 6.2.** a) The cationic supramolecular assembly of **3**: b) the 68-vertex cube-like inorganic core, c) 1,3-coordination mode of the **1c** unit, d) coordination environment of Cu, and e) 18-membered  $\{\text{Cu}_4\text{P}_{14}\}$  cycles.

$[(\mathbf{1c})_{12}\{\text{CuNCMe}\}_8](\text{TEF})_8$  (**3**, Figure 6.2b) possessing the first metal-deficient 68-vertex  $\{\text{Cu}_8\text{P}_{60}\}$  core with the lowest possible number of copper atoms sufficing to bind 12 *cyclo*- $\text{P}_5$  ligands as required by the fullerene topology.<sup>4b,f</sup>

The reaction of two equivalents of **1c** with three equivalents of  $[\text{Cu}(\text{CH}_3\text{CN})_4][\text{Al}\{\text{OC}(\text{CF}_3)_3\}_4]$  (**2**) in  $\text{CH}_2\text{Cl}_2$  at room temperature led to the formation of an olive green solution. Layering the solution with *n*-pentane afforded green octahedra of  $(\text{CH}_2\text{Cl}_2)_{1.25}@[(\text{Cp}''\text{FeP}_5)_{12}\{\text{Cu}(\text{CH}_3\text{CN})\}_8](\text{TEF})_8$  (**3**, Scheme 6.1) and green plates of  $[(\text{Cp}''\text{FeP}_5)_2\text{Cu}_4(\text{CH}_3\text{CN})_{10}](\text{TEF})_4$  (**4**). By changing the stoichiometry of the reaction, only the ratio of **3** to **4** could be varied, with **3** always being the major product. Surprisingly, compound **3** was formed during a first unsuccessful attempt to fill the free coordination sites at the *cyclo*- $\text{P}_5$  units with Ni(0) by adding  $\text{Ni}(\text{cod})_2$  (cod = 1,5-cyclooctadiene) to the reaction mixture. Within a few minutes, black metallic Ni precipitated. After filtration and layering the olive-green solution with *n*-pentane, **3** could be isolated in a moderate yield with its phase purity confirmed by PXRD (Figure S6.12 in the Supporting Information).



**Scheme 6.1.** Reaction of **1c** with  $[\text{Cu}(\text{CH}_3\text{CN})_4][\text{TEF}]$  (**2**) leading to **3**.

Compound **3** crystallizes as green octahedra in the trigonal space group  $R\bar{3}$ . Single crystal X-ray structure analysis of **3** revealed a 68-vertex sphere  $[(\text{CH}_2\text{Cl}_2)@[(\text{Cp}''\text{Fe}(\eta^5:\eta^1:\eta^1\text{-P}_5))_{12}\text{Cu}_8]^{8+}]$  (Figure 6.2), consisting of 12 units of **1c** arranged in an icosahedron in which Cu(I) ions systematically cap eight of the 20 available trigonal faces (Figure 6.1c). The remaining 12 trigonal faces furnish six 18-membered rings  $\{\text{Cu}_4\text{P}_{14}\}$  corresponding to a face of an underlying cube of the inorganic



core (Figure 6.2e). Each ring edge-shares four analogous rings and carries two positions potentially available to metal coordination. Every *cyclo*-P<sub>5</sub> ligand coordinates to Cu in a 1,3-mode with the Cu-P distances of 2.287(2)-2.314(2) Å and bond angles P-Cu-P 99.53(8)-103.80(8)°. A spherical assembly solely composed of two-coordinated units of **1** was predicted, but never observed before.<sup>4b,f</sup> The Cu atoms are tetrahedrally coordinated by three units of **1c** and one acetonitrile molecule (Cu-N: 1.98(1) - 1.974(7) Å, Figure 6.2d). The two-fold coordinated pentaphosphaferrocene unit allows a restricted rotation around all Cu-P coordinative bonds and thus provides some adaptability to the inorganic core. The Cu...Cu separation in this cube-like arrangement amounts to 7.53-7.59 Å, which points to a certain deformation of the core along one of the body diagonals.

Another feature of the inorganic core is a guest-accessible inner cavity of 0.77 nm (Figure 6.2). In **3**, the cavity is statistically occupied by one or two CH<sub>2</sub>Cl<sub>2</sub> molecules. Therefore, guest encapsulation of small molecules appears feasible.<sup>4f,5</sup>

The metal-deficient supramolecule possesses an outer diameter of 2.66 nm, which is twice that of a TEF anion (1.32 nm).<sup>6</sup> Charge balance requirements in **3** dictate a 1:8 ratio of supramolecule to the outer sphere TEF anions. Therefore, each supramolecule is completely isolated from any contacts with neighboring supramolecules by TEF anions as well as solvent CH<sub>2</sub>Cl<sub>2</sub> molecules (Figure S6.11 in the Supporting Information).

Notably, the formation of **3** is not accompanied by more metal-rich [(**1b**)<sub>12</sub>{CuN(CMe)<sub>8+m</sub>}]<sup>8+m</sup> salts. It is possible that these phases with  $m > 0$  are less favorable because of electrostatic repulsion of 8+m large anions per supramolecule in the crystal.

The minor product **4** crystallizes as green plates in the triclinic space group  $P\bar{1}$ . In the crystal structure of [(Cp''Fe(η<sup>5</sup>:η<sup>1</sup>,η<sup>1</sup>,η<sup>1</sup>-P<sub>5</sub>))<sub>2</sub>Cu<sub>4</sub>(CH<sub>3</sub>CN)<sub>10</sub>](TEF)<sub>4</sub> (**4**, Figure 6.3), tetracationic dimers are surrounded by bulky TEF anions and solvent molecules. The complexes [(**1c**)<sub>2</sub>Cu<sub>4</sub>(CH<sub>3</sub>CN)<sub>10</sub>]<sup>4+</sup> consist of two units of **1c** which coordinate three copper cations in a 1,2,4-mode. Two Cu(I) ions are coordinated by two units of **1c** each to give a 4-membered {Cu<sub>2</sub>P<sub>4</sub>} cycle with Cu-P bond lengths of 2.2592(9) - 2.278(1) Å and P-Cu-P angles of 107.11(4) - 108.13(4)° falling into the usual range.<sup>7</sup> Two acetonitrile ligands coordinate the copper ions to complete their tetrahedral environment with Cu-N bond lengths of 1.997(3) - 2.019(3) Å. Two more Cu cations are coordinated to the *cyclo*-P<sub>5</sub> in the position 4 (Cu-P: 2.216(1) - 2.224(1) Å); their coordination sphere is saturated by three acetonitrile ligands with Cu-N bond distances of 1.974(3) - 2.008(3) Å (Figure 6.3).

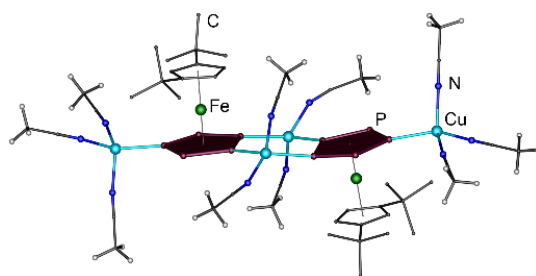


**Figure 6.3.** Molecular structure of the tetracationic dimer **4**.

The supramolecular aggregate **3** and the by-product **4** are slightly soluble in  $\text{CH}_2\text{Cl}_2$ , and completely insoluble in other common organic solvents such as THF, toluene and *n*-pentane. In donor solvents such as  $\text{CH}_3\text{CN}$ , **3** and **4** are well soluble at the cost of partial fragmentation. Therefore, all characterizations in solution were performed in a mixture of  $\text{CH}_2\text{Cl}_2(\text{CD}_2\text{Cl}_2)/\text{CH}_3\text{CN}(\text{CD}_3\text{CN})$ . The  $^1\text{H}$  NMR spectrum of **3** shows three singlets for the hydrogen atoms of  $\text{Cp}''$  at 4.12 ppm (2H), 3.98 ppm (1H) and 1.18 ppm (18H). In the room-temperature  $^{13}\text{C}\{^1\text{H}\}$  NMR spectra of **3**, five signals for the  $\text{Cp}''$  ligands can be detected (31.35 ppm, 32.90 ppm, 72.37 ppm, 73.94 ppm, 111.84 ppm). The signals in the  $^1\text{H}$  and  $^{13}\text{C}\{^1\text{H}\}$  NMR spectra are all slightly low-field shifted compared to the uncoordinated **1c**, which prefigures a dynamic behavior of **3** in solution. The  $^{31}\text{P}$  NMR of **3** exhibits one high-field shifted singlet at 163.2 ppm for the coordinated *cyclo*- $\text{P}_5$  ligand complex **1c** compared to free **1c** (168.9 ppm). The ESI mass spectra show peaks for the cationic fragments  $[\{\mathbf{1c}\}_2\text{Cu}]^+$ ,  $[\{\mathbf{1c}\}\text{Cu}(\text{CH}_3\text{CN})]^+$ ,  $[\text{Cu}(\text{CH}_3\text{CN})_2]^+$  and  $[\text{Cu}(\text{CH}_3\text{CN})]^+$ . Both compounds are air- and light-stable in the solid state for several days, but decompose within hours in solution when exposed to air.

### 6.3 Conclusion

In conclusion, a novel approach to metal-deficient pentaphosphaferrocene-based supramolecules was demonstrated relying on the usage of WCAs as counter anions, making it possible to control metal-deficiency of the inorganic core. In this way, the hollow supramolecule **3** was obtained based on 12 *cyclo*- $\text{P}_5$  rings and so far the smallest possible number (eight) of coinage metal atoms bearing labile acetonitrile ligands. These features open a way to using this promising multitasking precursor in supramolecular chemistry, which was beyond the scope of this first report about the fundamental accessibility of such metal-deficient spheres. The future perspectives are: (i) the presence of unprecedented 12 free metal site makes it an interesting starting material for further substitution of the supramolecule with heterometals or with metal complexes;

(ii) the central cavity of 0.77 nm, which is accessible for small molecules, allows inner functionalization; (iii) the terminal acetonitrile ligands could be substituted by various bridging N-donor ligands, opening the way to expanded networks of the supramolecules. This approach will be fine-tuned in the future with respect to the nature of the corresponding Cp ligands or the coinage metals and further extended to any supramolecules having cores that are constructed from metal cations and neutral polydentate ligands.

## 6.4 Supporting Information

### 6.4.1 General

All experiments were carried out in an inert atmosphere of nitrogen or argon using standard Schlenk techniques. The nitrogen/argon was dried and purified from traces of oxygen with a Cu/MgSO<sub>4</sub> catalyst, concentrated H<sub>2</sub>SO<sub>4</sub> and orange gel. Reactants were stored in a glovebox under argon atmosphere. All used solvents were taken from the solvent drying machine MB SPS-800 of the company MBRAUN.

The precursors [Cp''Fe(η<sup>5</sup>-P<sub>5</sub>)]<sup>8</sup> (**1c**), [Cu(CH<sub>3</sub>CN)<sub>4</sub>][Al{OC(CF<sub>3</sub>)<sub>3</sub>}]<sup>9</sup> (**2**) were prepared according to literature procedures.

Solution NMR spectra were recorded on a Bruker Avance 400 spectrometer (<sup>1</sup>H: 400 MHz, <sup>31</sup>P: 161 MHz, <sup>13</sup>C: 100 MHz, <sup>19</sup>F: 376 MHz,) with a mixture of CD<sub>3</sub>CN and CD<sub>2</sub>Cl<sub>2</sub> as solvent at room temperature. The signals of tetramethylsilane (<sup>1</sup>H, <sup>13</sup>C), CFC<sub>3</sub> (<sup>19</sup>F) and 85% H<sub>3</sub>PO<sub>4</sub> (<sup>31</sup>P) were used as reference for determining chemical shifts. The chemical shifts δ are presented in parts per million ppm. The spectra were processed and analyzed using the software Bruker TopSpin 3.0. Elemental analyses were performed on an Elementar vario MICRO cube apparatus. Mass spectra were recorded on an Agilent Q-TOF 6540 UHD mass spectrometer with a mixture of CH<sub>2</sub>Cl<sub>2</sub> and CH<sub>3</sub>CN as solvents.

### 6.4.2 Synthetic Procedure

Synthesis of **3** and **4**: [Cu(CH<sub>3</sub>CN)<sub>4</sub>][Al{OC(CF<sub>3</sub>)<sub>3</sub>}] (2 eq., 60 mg, 0.05 mmol), dissolved in CH<sub>2</sub>Cl<sub>2</sub> (5 mL), was added to a solution of Cp''FeP<sub>5</sub> (3 eq., 29 mg, 0.075 mmol) in CH<sub>2</sub>Cl<sub>2</sub> (5 mL) and stirred for 1.5h at room temperature under inert gas atmosphere. The greenish brown solution was carefully layered with threefold amount of *n*-pentane and stored at room temperature. After 3h green octahedra (compound **3**) and green plates

(compound **4**) were formed. The crystals were washed with *n*-pentane and dried *in vacuo*.

Synthesis of **3**: [Cu(CH<sub>3</sub>CN)<sub>4</sub>][Al{OC(CF<sub>3</sub>)<sub>3</sub>}<sub>4</sub>] (2 eq., 60 mg, 0.05 mmol), dissolved in CH<sub>2</sub>Cl<sub>2</sub> (5 mL), was added to a solution of Cp''FeP<sub>5</sub> (3 eq., 29 mg, 0.075 mmol) in CH<sub>2</sub>Cl<sub>2</sub> (5 mL) and stirred for 1.5h at room temperature. A suspension of Ni(cod)<sub>2</sub> (3 eq., 21 mg, 0.075 mmol) in 5 mL CH<sub>2</sub>Cl<sub>2</sub> was added to the reaction mixture. The directly afterwards formed black precipitate (Ni(0)) was removed by filtration and the greenish brown solution was carefully layered with threefold amount of *n*-pentane and stored at room temperature. After 2d only green hexagonal plates **3** were formed. The crystals were washed with *n*-pentane and dried *in vacuo*. Crystalline yield: 30 mg (36 %, referred to **2**).  
<sup>1</sup>H NMR (CH<sub>2</sub>Cl<sub>2</sub>/CD<sub>3</sub>CN):  $\delta$  = 4.12 (s, 2H), 3.98 (s, 1H), 1.18 (s, 18H).

<sup>13</sup>C {<sup>1</sup>H} NMR (CH<sub>2</sub>Cl<sub>2</sub>/CD<sub>3</sub>CN):  $\delta$  = 111.84 (s, C<sub>Cp,q</sub>), 73.94 (s, C<sub>Cp,2</sub>), 72.37 (s, C<sub>Cp,1</sub>), 32.90 (s, C(CH<sub>3</sub>)), 31.35 (s, C(CH<sub>3</sub>)).

<sup>31</sup>P {<sup>1</sup>H} NMR (CH<sub>2</sub>Cl<sub>2</sub>/CD<sub>3</sub>CN):  $\delta$  = 163.2 (s).

<sup>19</sup>F {<sup>1</sup>H} NMR (CH<sub>2</sub>Cl<sub>2</sub>/CD<sub>3</sub>CN):  $\delta$  = -75.76 (s).

Positive ion ESI-MS (CH<sub>2</sub>Cl<sub>2</sub>/CD<sub>3</sub>CN, RT): *m/z* (%) = 838.9 (25) [C<sub>5</sub>H<sub>3</sub>(C(CH<sub>3</sub>)<sub>3</sub>)<sub>2</sub>FeP<sub>5</sub>]<sub>2</sub>Cu<sup>+</sup>, 491.9 (42) [C<sub>5</sub>H<sub>3</sub>(C(CH<sub>3</sub>)<sub>3</sub>)<sub>2</sub>FeP<sub>5</sub>]<sub>2</sub>Cu(CH<sub>3</sub>CN)<sup>+</sup>, 145.0 (100) [Cu(CH<sub>3</sub>CN)<sub>2</sub>]<sup>+</sup>, 104.0 (38) [Cu(CH<sub>3</sub>CN)]<sup>+</sup>.

Negative ion ESI-MS (CH<sub>2</sub>Cl<sub>2</sub>/CD<sub>3</sub>CN, RT): *m/z* (%) = 966.9 (100) [TEF]<sup>-</sup>.

Elemental analysis, calc. for C<sub>300</sub>H<sub>276</sub>Al<sub>8</sub>Cu<sub>8</sub>F<sub>288</sub>Fe<sub>12</sub>N<sub>8</sub>O<sub>32</sub>P<sub>60</sub> (13229.88 g/mol) (%): C, 27.24; H, 2.10; N, 0.85; found: C, 27.93; H, 2.25; N, 0.82.

As mentioned before, compound **3** shows a partial fragmentation in pure CH<sub>3</sub>CN. Due to this, the analytics in solution have been performed in a mixture of CH<sub>2</sub>Cl<sub>2</sub> and CH<sub>3</sub>CN. However, the signals of **3** in the <sup>1</sup>H and <sup>13</sup>C {<sup>1</sup>H} NMR spectra are all slightly low-field shifted compared to the uncoordinated **1c**, which prefigures a dynamic behavior of **3** in solution.

### 6.4.3 Crystallographic Data

Crystals of **3** and **4** were taken from a Schlenk flask under a stream of argon and immediately covered with perfluorinated Fomblin® mineral oil to prevent a loss of solvent. The quickly chosen single crystals covered by a thin layer of the oil were taken to the pre-centered goniometer head with suitable CryoMount® and directly attached to the goniometer into a stream of cold gas. The X-ray diffraction study of **3** faced many challenges, since the crystals were systematically twinned and quickly decomposed due to the loss of solvent.

The data for **3** were collected using  $0.5^\circ$   $\omega$  scans on a Rigaku Oxford Diffraction diffractometer equipped with a Titan<sup>S2</sup> CCD detector and a SuperNova CuK $\alpha$  microfocus source at 90 K. The data for **4** were collected at P24 beamline of PETRA III (DESY, Hamburg) using 22.11 keV synchrotron radiation ( $\lambda = 0.56076$  Å) and scan width 0.5 deg. The experiment for **4** was performed at 14 K to suppress thermal contribution to the disorder for usually severely disordered teflonate anions. The partial ordering in fact took place in the case of **4**. Numerous attempts were also performed to measure the structure of **3** at helium temperatures at DESY PETRA synchrotron for the same purpose. Unfortunately, pre-selected crystals kept in liquid nitrogen either lost their quality upon storing or immediately cracked when tried at P24 beamline with manual sample mounting. At P11 beamline we used robotic mounting, but considerable radiolysis took place and the resulting data proved worse than those obtained with in-house diffractometer at 90 K.

The data processing and reduction for all experiments was performed with CrysAlisPRO Software.<sup>10</sup> The structures were solved by direct methods with *SHELXT* and refined by full-matrix least-squares method on  $|F^2|$  using multiprocessor and variable memory version *SHELXL2015-2018*.<sup>11</sup> All positionally ordered non-hydrogen atoms were refined in an anisotropic approximation, while the disordered light atoms with occupation factors less than 0.5 were refined isotropically. The hydrogen atoms were refined as riding on pivot atoms. The disordered anions were treated in the following procedure. The occupancy factors of the atoms of the disordered fragments were refined with fixed isotropic a.d.p. parameters. When all positions of the disordered atoms were localized, the relative contribution of a disordered group was refined with *FVAR* instructions in *SHELX*. Then the occupancies were fixed at refined-to values and isotropic followed by anisotropic (for major component) refinement of the a.d.p. parameters was performed. In this way the positional disorder of the TEF<sup>-</sup> anion over  $\bar{3}$  position was refined in **3** (Fig. S6.9). The extra low temperatures during the X-ray experiment made the refinement of the structure of the **4** with four unique TEF anions considerably easier. A few <sup>t</sup>Bu-groups become ordered at 14 K compared to the in-house preliminary measurement at 90 K.

Crystallographic data and details of the diffraction experiments are given in Table S1, bond lengths and angles are listed in Tables S6.2 and S6.3, and molecular structures **3** and **4** are depicted in Figs. S6.1-S6.11.

CIF files with comprehensive information on the details of the diffraction experiments and full tables of bond lengths and angles for **3** and **4** are deposited in Cambridge

Crystallographic Data Centre under the deposition codes CCDC-1988183 and CCDC-1988184, respectively.

**Table S6.1.** Crystallographic details for **3** and **4**.

Crystal data	<b>3</b>	<b>4</b>
CCDC Deposition Code	CCDC-1988183	CCDC-1988184
Structural formula	(CH <sub>2</sub> Cl <sub>2</sub> ) <sub>1.25</sub> [(Cp''FeP <sub>5</sub> ) <sub>12</sub> {Cu(CH <sub>3</sub> CN)} <sub>8</sub> ](AlO <sub>4</sub> C <sub>16</sub> F <sub>36</sub> ) <sub>8</sub> ·4.33CH <sub>2</sub> Cl <sub>2</sub>	[(Cp''FeP <sub>5</sub> ) <sub>2</sub> Cu <sub>4</sub> (CH <sub>3</sub> CN) <sub>10</sub> ](AlO <sub>4</sub> C <sub>16</sub> F <sub>36</sub> ) <sub>4</sub> ·0.8CH <sub>2</sub> Cl <sub>2</sub> ·0.45CH <sub>3</sub> CN
Chemical formula	C <sub>300</sub> H <sub>276</sub> Cu <sub>8</sub> Fe <sub>12</sub> N <sub>8</sub> P <sub>60</sub> ·8(AlO <sub>4</sub> C <sub>16</sub> F <sub>36</sub> )·5.89(CH <sub>2</sub> Cl <sub>2</sub> )	C <sub>110</sub> H <sub>72</sub> Cu <sub>4</sub> Fe <sub>2</sub> N <sub>10</sub> P <sub>10</sub> ·4(AlO <sub>4</sub> C <sub>16</sub> F <sub>36</sub> )·0.8(CH <sub>2</sub> Cl <sub>2</sub> )·0.45(CH <sub>3</sub> CN)
<i>M<sub>r</sub></i>	13704.00	5395.67
Crystal system, space group	Trigonal, <i>R</i> $\bar{3}$ : <i>H</i>	Triclinic, <i>P</i> $\bar{1}$
Temperature (K)	90	14
<i>a</i> , <i>b</i> , <i>c</i> (Å)	26.5534 (4), 64.0248 (18)	19.2003 (4), 22.1827 (5), 25.7710 (7)
$\alpha$ , $\beta$ , $\gamma$ (°)	90, 90, 120	67.188 (2), 68.385 (2), 85.8176 (16)
<i>V</i> (Å <sup>3</sup> )	39094.7 (16)	9374.9 (4)
<i>Z</i>	3	2
<i>F</i> (000)	20288	5279
<i>D<sub>x</sub></i> (Mg m <sup>-3</sup> )	1.746	1.911
Radiation type	Cu <i>K</i> $\alpha$	Synchrotron, $\lambda$ = 0.56076 Å
$\mu$ (mm <sup>-1</sup> )	6.77	0.49
Crystal shape and colour	Green hexagonal prism	Green plate
Crystal size (mm)	0.17 × 0.14 × 0.06	0.3 × 0.2 × 0.1
Data collection		
Diffractometer	SuperNova, Titan <sup>S2</sup>	P24 beamline, PETRA III synchrotron
Absorption correction	Gaussian	Multi-scan
<i>T<sub>min</sub></i> , <i>T<sub>max</sub></i>	0.313, 1.000	0.832, 1.000
No. of measured, independent and observed [ <i>I</i> > 2 $\sigma$ ( <i>I</i> )] reflections	25899, 15426, 10647	102710, 36450, 31708
<i>R<sub>int</sub></i>	0.054	0.031
( <i>sin</i> $\theta$ / $\lambda$ ) <sub>max</sub> (Å <sup>-1</sup> )	0.600	0.625
Range of <i>h</i> , <i>k</i> , <i>l</i>	<i>h</i> = -31→31, <i>k</i> = -22→25, <i>l</i> = -55→75	<i>h</i> = -24→24, <i>k</i> = -27→27, <i>l</i> = -29→30
Refinement		
<i>R</i> [ <i>F</i> <sup>2</sup> > 2 <i>s</i> ( <i>F</i> <sup>2</sup> )], <i>wR</i> ( <i>F</i> <sup>2</sup> ), <i>S</i>	0.107, 0.305, 1.16	0.057, 0.158, 1.02
No. of reflections	15426	36450
No. of parameters	1197	3665
No. of restraints	24	4
H-atom treatment	H-atom parameters constrained	H-atom parameters constrained
$\Delta\rho_{max}$ , $\Delta\rho_{min}$ (e Å <sup>-3</sup> )	1.72, -1.15	1.55, -0.72

Computer programs: *CrysAlis PRO 1.171.40.18c* and *1.171.41.21a* (Rigaku OD, 2018), *SHELXL2015/3* (Sheldrick, 2015), *SHELXL2018/3* (Sheldrick, 2018).

### 6.4.3.1 The Crystal Structure of the By-Product $[(\text{Cp}''\text{FeP}_5)_2\text{Cu}_4(\text{CH}_3\text{CN})_{10}][\text{TEF}]_4$ (4)

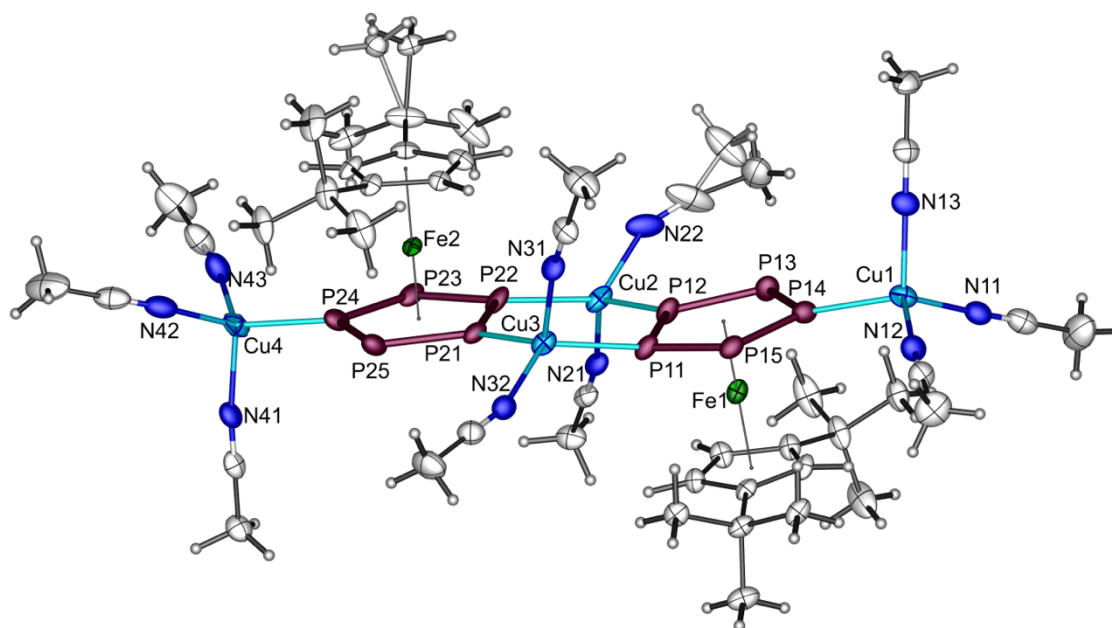


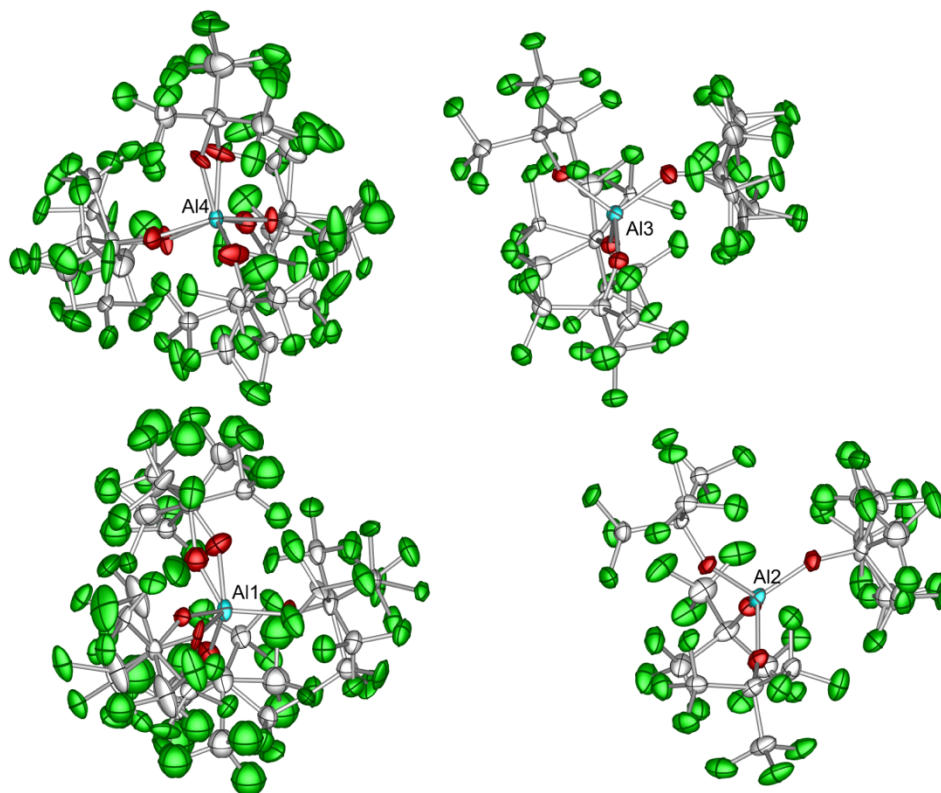
**Figure S6.3.** Asymmetric unit and enumeration scheme in **4** (a.d.p. ellipsoids at 50% probability).

**Table S6.2.** Selected geometric parameters (Å, °) for **4**.

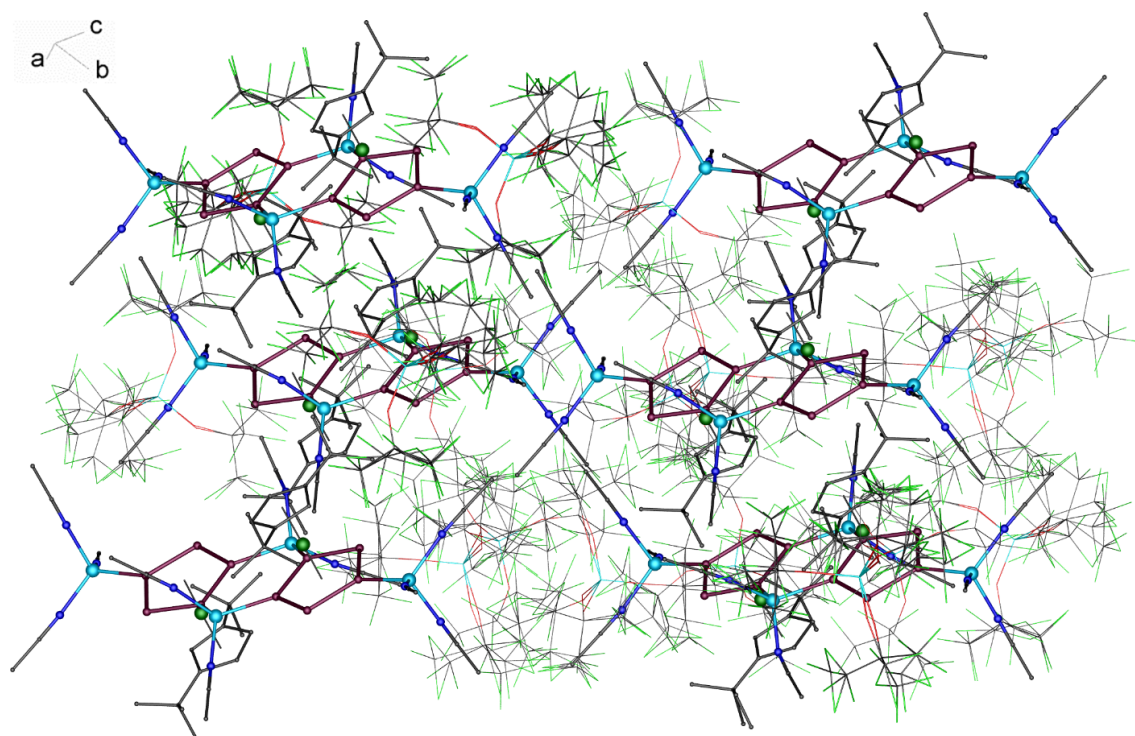
Cu1—N11	1.974 (3)	Fe1—P14	2.3572 (10)
Cu1—N12	1.993 (3)	Fe1—P13	2.4102 (11)
Cu1—N13	2.002 (3)	Fe1—P15	2.4266 (9)
Cu1—P14	2.2235 (10)	Fe2—P24	2.3445 (10)
Cu2—N21	2.006 (3)	Fe2—P22	2.3451 (9)
Cu2—N22	2.011 (4)	Fe2—P21	2.3567 (10)
Cu2—P22	2.2679 (10)	Fe2—P25	2.4091 (10)
Cu2—P12	2.2757 (10)	Fe2—P23	2.4279 (9)
Cu3—N32	1.997 (3)	P11—P12	2.1014 (12)
Cu3—N31	2.019 (3)	P11—P15	2.1077 (13)
Cu3—P21	2.2592 (9)	P12—P13	2.1062 (14)
Cu3—P11	2.2756 (10)	P13—P14	2.1065 (13)
Cu4—N42	1.989 (4)	P14—P15	2.1045 (13)
Cu4—N43	2.003 (4)	P21—P22	2.1018 (13)
Cu4—N41	2.008 (3)	P21—P25	2.1043 (14)
Cu4—P24	2.2158 (10)	P22—P23	2.1009 (13)
Fe1—P12	2.3503 (10)	P23—P24	2.1089 (14)

Fe1—P11	2.3547 (10)	P24—P25	2.1106 (13)
N11—Cu1—N12	108.73(14)	P22—Cu2—P12	107.11(4)
N11—Cu1—N13	108.36(13)	N32—Cu3—N31	99.42(12)
N12—Cu1—N13	106.69(13)	N32—Cu3—P21	106.17(9)
N11—Cu1—P14	118.46(9)	N31—Cu3—P11	99.86(9)
N12—Cu1—P14	108.79(10)	P21—Cu3—P11	108.13(4)
N13—Cu1—P14	105.20(10)	N42—Cu4—N43	102.51(15)
N21—Cu2—N22	100.34(13)	N42—Cu4—N41	110.73(13)
N21—Cu2—P22	103.99(9)	N43—Cu4—N41	104.11(14)
N22—Cu2—P22	127.83(12)	N42—Cu4—P24	121.29(10)
N21—Cu2—P12	121.16(9)	N43—Cu4—P24	114.35(10)
N22—Cu2—P12	98.17(10)	N41—Cu4—P24	102.79(9)





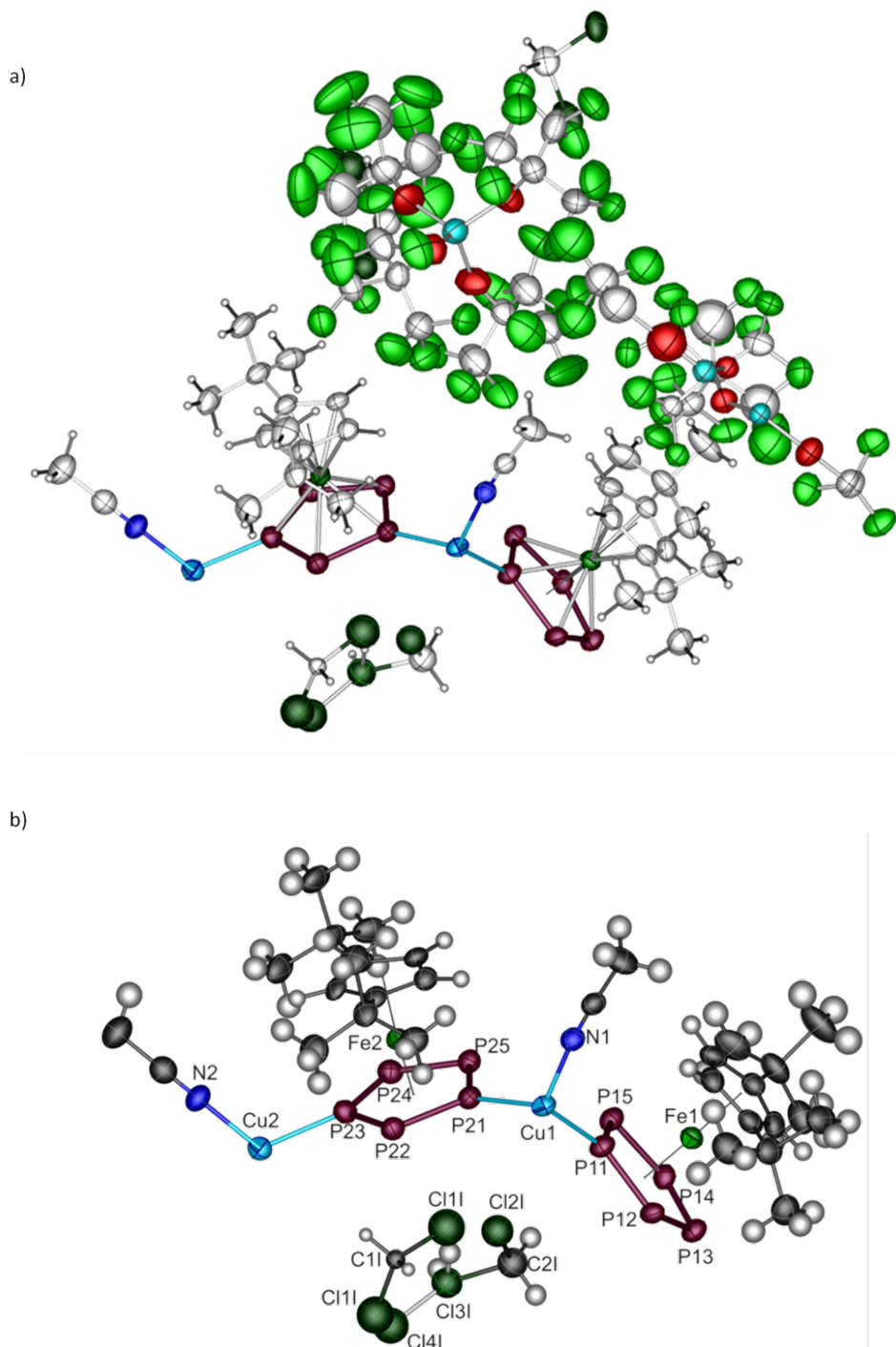
**Figure S6.4.** Anionic part in **4** (a.d.p. ellipsoids at 50% probability).



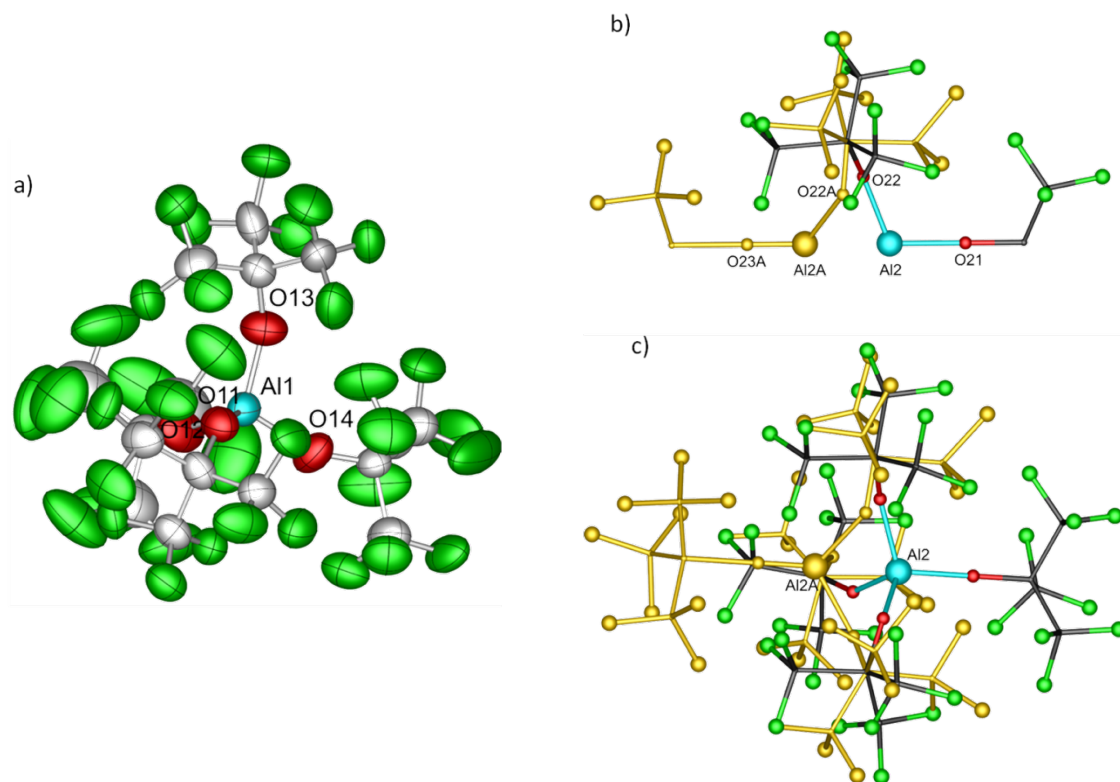
**Figure S6.5.** Crystal packing in **4**. The TEF anions are shown in thin lines, solvent molecules are not shown.

### 6.4.3.2 The Crystal Structure of the Super-vacant Supramolecule $(\text{CH}_2\text{Cl}_2)_{1.25}@[ (\text{Cp}''\text{FeP}_5)_{12}\{\text{Cu}(\text{CH}_3\text{CN})\}_8][\text{TEF}]_8$ (**3**)

Compound **3** crystallizes in a trigonal  $R\bar{3}$  space group. The supramolecular cation and one of the TEF cations lie on the three-fold rotoinversion axis. The other TEF anion occupies general position.



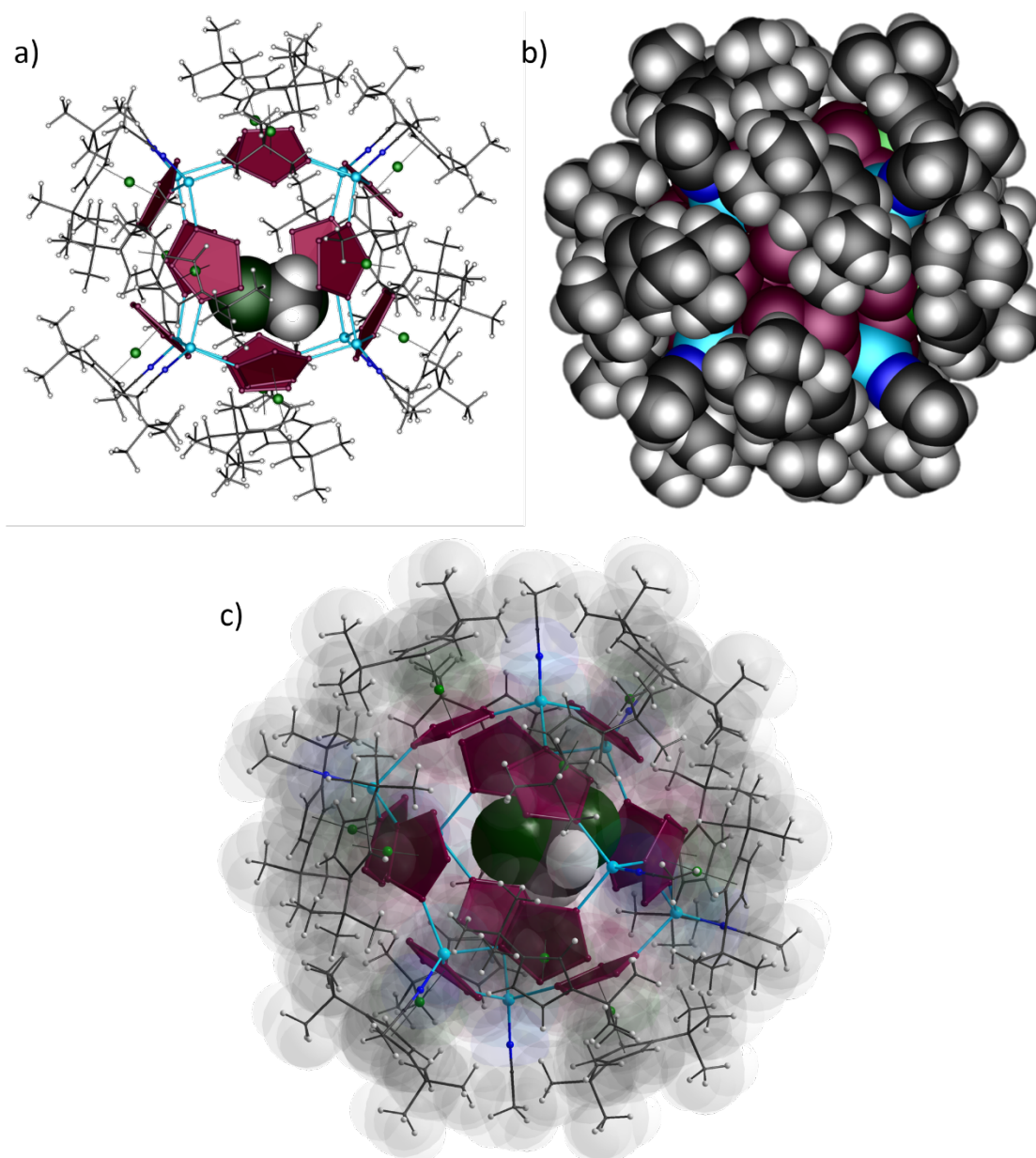
**Figure S6.6.** a) Asymmetric unit in **3** and b) enumeration scheme of the cationic part (a.d.p. ellipsoids at 50% probability). Cl3i position is shared between C and Cl.



**Figure S6.7.** The anionic part of the structure **3**. TEF<sup>-</sup> anions a) in general position (a.d.p. ellipsoids at 50% probability) and b) two positions of TEF<sup>-</sup> anions in  $\bar{3}$  position (balls-and-sticks model). c) Disordered TEF<sup>-</sup> anions over  $\bar{3}$  axis with relative ratio 5/6 and 1/6.

**Table S6.3.** Selected geometric parameters (Å, °) for **3**.

C4I—C14I <sup>i</sup>	2.01 (5)	Fe1—P12	2.398 (2)
Cu1—N1	1.974 (7)	Fe2—P23	2.337 (2)
Cu1—P11	2.287 (2)	Fe2—P21	2.340 (2)
Cu1—P21	2.296 (2)	Fe2—P25	2.390 (2)
Cu1—P14 <sup>i</sup>	2.314 (2)	Fe2—P24	2.402 (2)
Cu2—N2	1.984 (12)	Fe2—P22	2.407 (2)
Cu2—P23	2.303 (2)	P11—P12	2.104 (3)
Cu2—P23 <sup>ii</sup>	2.303 (2)	P11—P15	2.107 (3)
Cu2—P23 <sup>iii</sup>	2.303 (2)	P12—P13	2.107 (3)
N1—C11N	1.132 (10)	P13—P14	2.107 (3)
C11N—C12N	1.444 (12)	P14—P15	2.104 (3)
N2—C21N	1.114 (19)	P21—P22	2.108 (3)
C21N—C22N	1.48 (2)	P21—P25	2.111 (3)
Fe1—P11	2.344 (2)	P22—P23	2.102 (3)
Fe1—P13	2.373 (2)	P23—P24	2.114 (3)
Fe1—P15	2.378 (2)	P24—P25	2.112 (3)
Fe1—P14	2.385 (2)		
N1—Cu1—P11	113.8 (2)	P11—P12—P13	106.48 (11)
N1—Cu1—P21	117.7 (2)	P14—P13—P12	106.50 (11)
P11—Cu1—P21	99.53 (8)	P15—P14—P13	111.49 (11)
N1—Cu1—P14 <sup>i</sup>	117.8 (2)	P15—P14—Cu1 <sup>iv</sup>	122.50 (11)
P11—Cu1—P14 <sup>i</sup>	101.57 (8)	P13—P14—Cu1 <sup>iv</sup>	122.36 (10)
P21—Cu1—P14 <sup>i</sup>	103.80 (8)	P14—P15—P11	103.36 (11)
N2—Cu2—P23	116.92 (6)	P22—P21—P25	111.76 (11)
N2—Cu2—P23 <sup>ii</sup>	116.92 (6)	P22—P21—Cu1	123.02 (10)
P23—Cu2—P23 <sup>ii</sup>	101.10 (8)	P25—P21—Cu1	125.18 (10)
N2—Cu2—P23 <sup>iii</sup>	116.92 (6)	P23—P22—P21	103.77 (11)
P23—Cu2—P23 <sup>iii</sup>	101.11 (8)	P22—P23—P24	111.43 (11)
P23 <sup>ii</sup> —Cu2—P23 <sup>iii</sup>	101.10 (8)	P22—P23—Cu2	119.02 (10)
P12—P11—P15	111.68 (11)	P24—P23—Cu2	128.73 (10)
P12—P11—Cu1	125.98 (11)	P25—P24—P23	106.80 (11)
P15—P11—Cu1	122.34 (11)	P21—P25—P24	106.20 (11)

**The host supramolecule**

**Figure S6.8.** Cationic supramolecule in **3** (a) in ball-and-stick representation with one orientation of positionally disordered  $\text{CH}_2\text{Cl}_2$  guest molecule is shown in van der Waals spheres; (b, c) in van der Waals spheres.

### Disorder of the guest molecule

The guest molecule is disordered over 12 equatorial positions (2 unique positions are shown in green) and 6 apical positions (yellow). Two atom positions are shared between C and Cl atoms in the apical part; they lie on the 3-fold rotainversion axis (Figure S6.9)

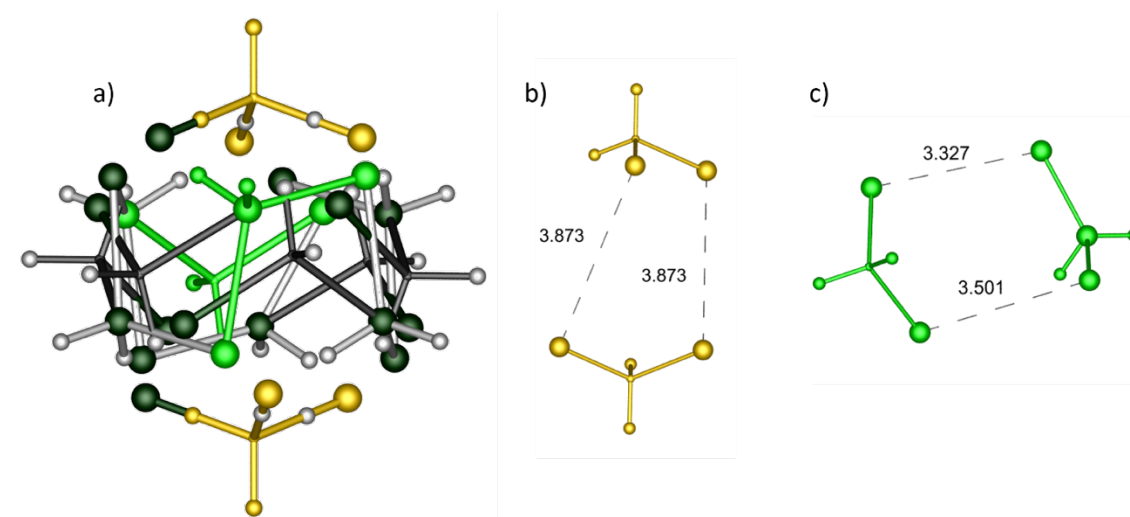


**Figure S6.9.** a) The disorder pattern of the CH<sub>2</sub>Cl<sub>2</sub> guest molecule in the cavity of the cationic **3**. Two pairwise non-contradictory positions of the CH<sub>2</sub>Cl<sub>2</sub> b) in the apical positions (the molecule on the  $\bar{3}$  axis) and c) in the equator (the molecules in general position).

### Crystal packing

In crystal the supramolecules form abundant arrangement topologically identical to face-centered cubic packing of equal spheres (Figure S6.10). However, here the supramolecules are not in direct contact with each other, but well-isolated by bulky TEF anions. Each 8-fold positively charged cation forms van der Waals contact with 24 TEF anions (Figure S6.11).



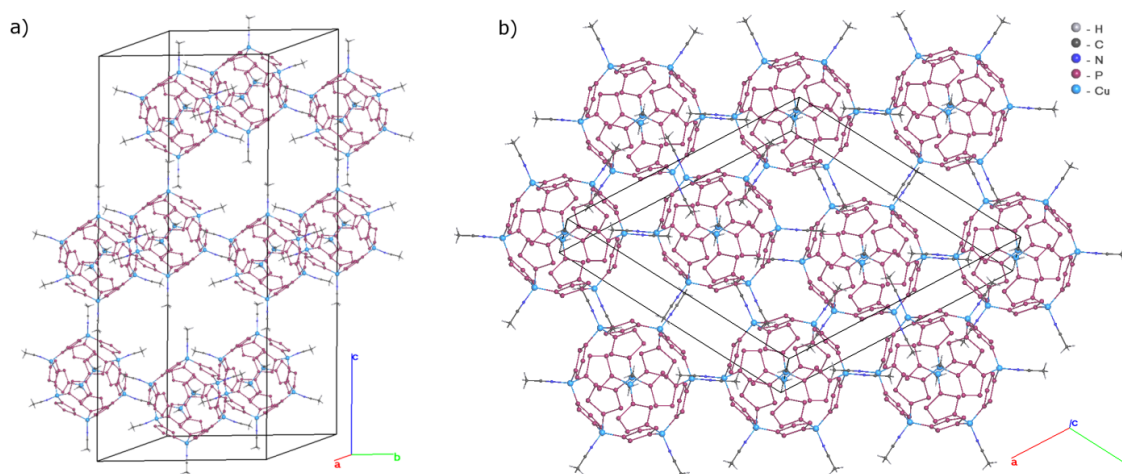


**Figure S6.10.** The face-centered cubic (fcc)<sup>12</sup> arrangement of spherical cations in crystal packing of **3**. TEF anions, solvent molecules and {Cp<sup>III</sup>Fe} fragments are omitted.

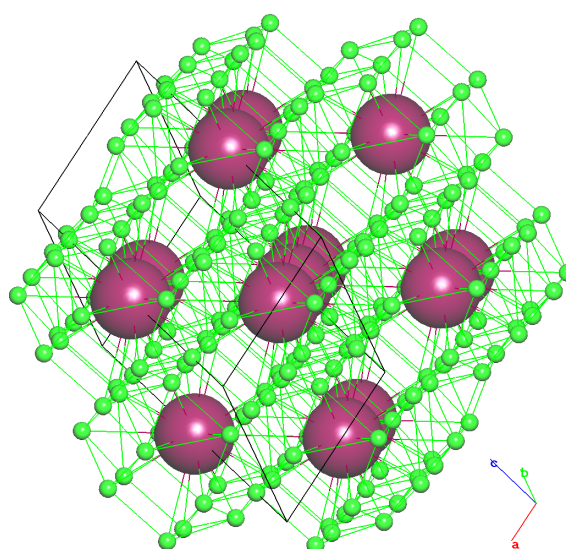


**Figure S6.11.** The schematic arrangement of spherical cations (purple) with TEF anions (green) in crystal packing of **3**.

### **Minimal and complete inorganic cores: a comparison**

The inorganic core of the minimal possible core derived from a well-known 80-vertex core  $[(\text{Cp}^{\text{R}}\text{FeP}_5)_{12}(\text{CuX})_{20}]$  ( $\text{X} = \text{Cl}, \text{Br}$ ) for the neutral supramolecules based on pentaphosphaferrocenes ( $\text{Cp}^{\text{R}} = \text{Cp}^{\text{Bn}}, \text{Cp}^*$ ). The interrelation is schematically shown in Figure S6.11. Two inserted polyhedra describe the mutual orientation of the pentaphosphaferrocene molecules (Fe atoms are chosen as vertices of a resultant icosahedron) and Cu cations (blue polyhedra). In the complete core the copper

arrangement corresponds to pentagonal dodecahedron (Figure S6.11a), whereas in the minimal core this arrangement is a cube (Figure S6.11b).

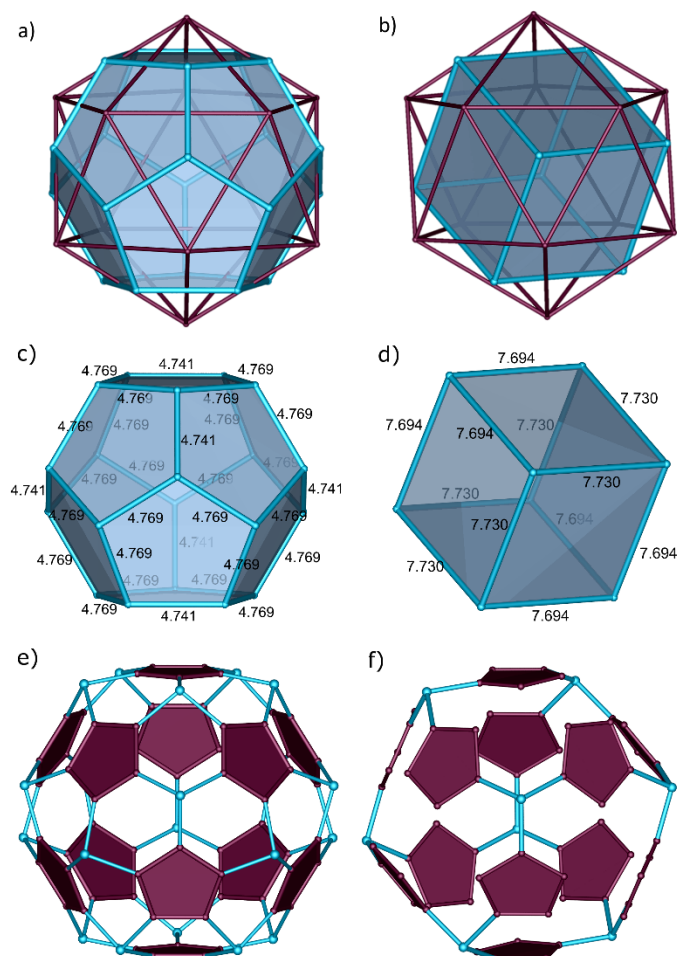


**Figure S6.11.** Comparison of the complete 80-vertex and 68-vertex minimal possible cores.

#### 6.4.4 Powder Diffraction

Phase purity for the compound **3** was confirmed by X-ray powder diffraction. The PXRD measurements were performed with a STADI-P powder diffractometer from STOE with  $\text{CuK}\alpha_1$  radiation at room temperature. The shift of peak positions to higher  $2\theta$  angles for the theoretical diffraction pattern compared to the experimental one occurs due to thermal constriction of the unit cell constants, as the single crystal data used for simulation were obtained at 90 K for **3** and at 14 K for **4**.



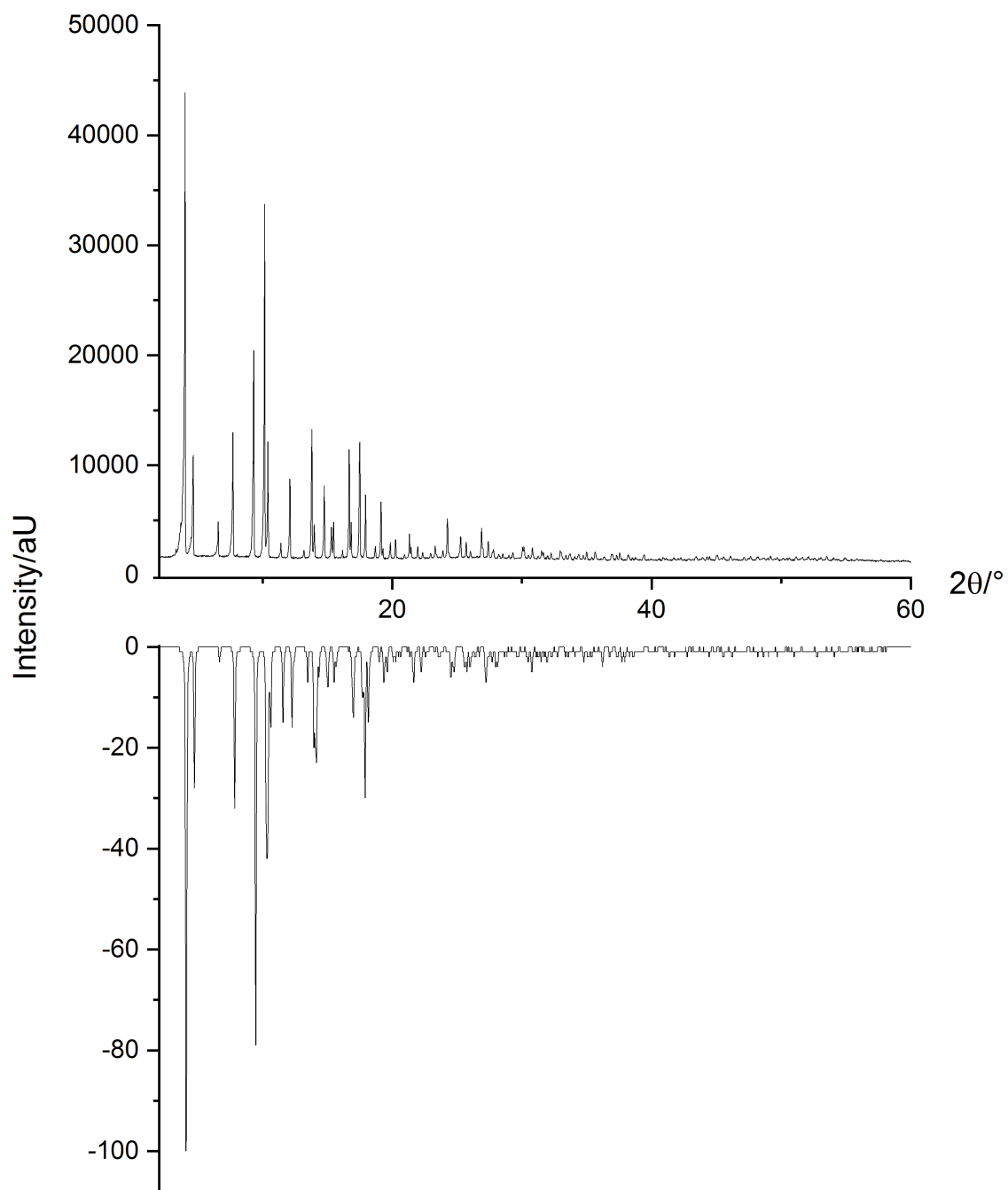


**Figure S6.12.** Comparison of measured (top) at room temperature and theoretical (bottom) PXRD pattern of **3** calculated from the single crystal data at 90K ( $2\theta$  range 2-60°).

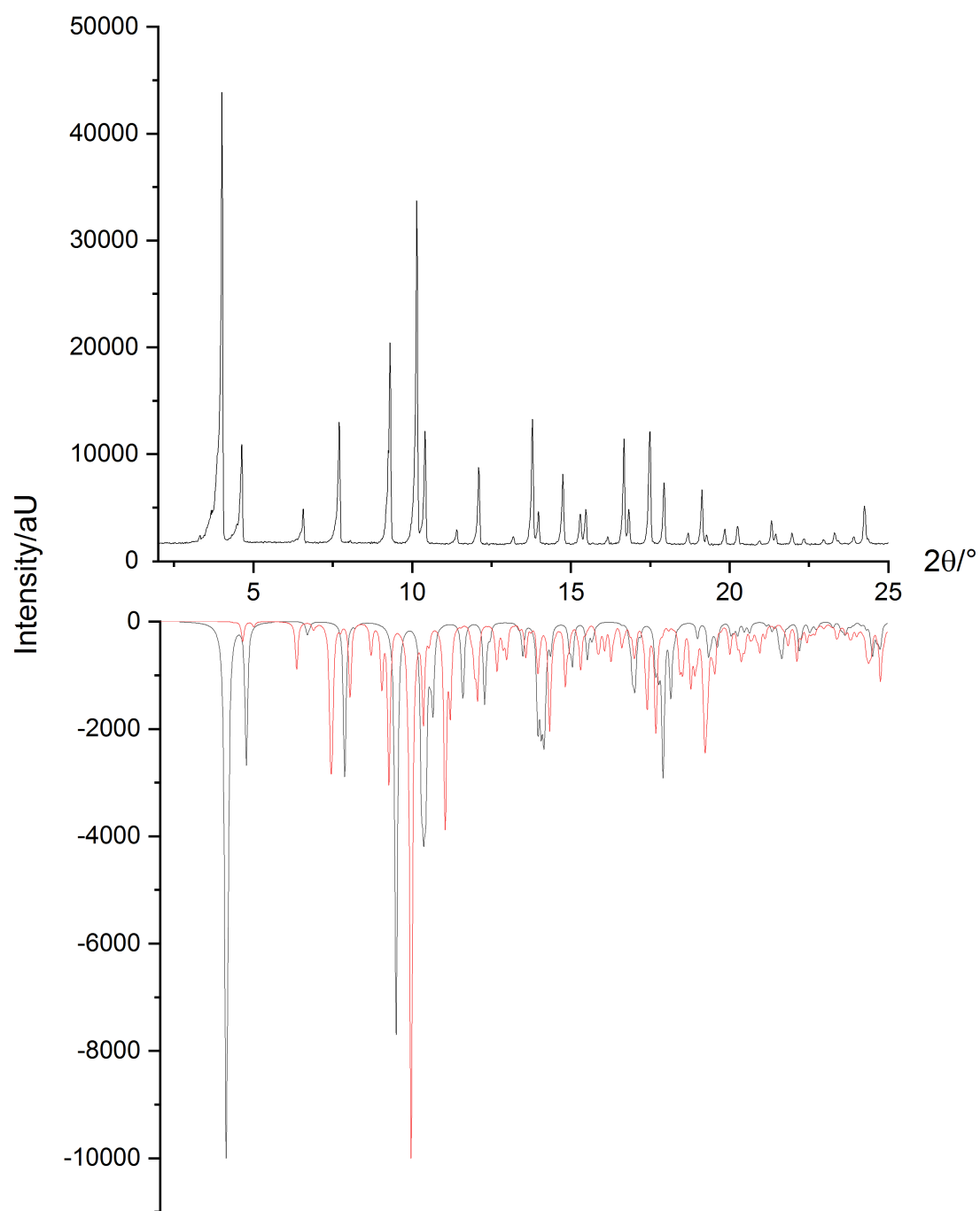


**Figure S6.13.** Comparison of measured (top) at room temperature and theoretical (bottom) PXRD patterns of **3** (black) and **4** (red) calculated from the single crystal data at 90K and 14K, respectively ( $2\theta$  range 2-25°).

### 6.4.5 Additional Solid-State Structures Mentioned in the Introduction

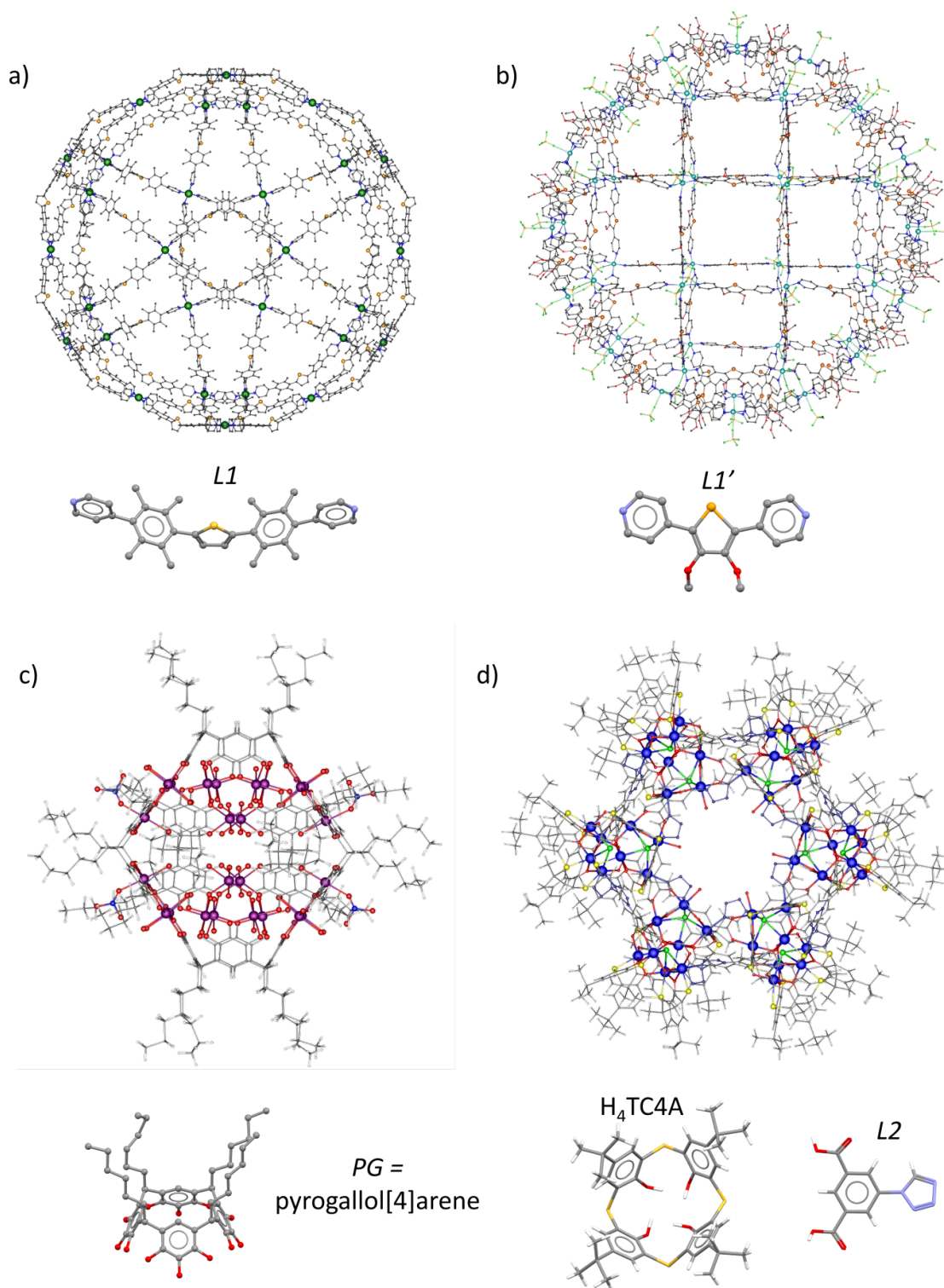


**Figure S14.** a) Ligand  $L1$  and  $[Pd_{30}(L1)_{60}]^{60+}$  cationic supramolecule; b) ligand  $L1'$  and  $[Pd_{48}(L1')_{96}](BF_4)_{96}$  cationic supramolecule; c)  $[Mg_{24}(PG)_6(H_2O)_{44}(NO_3)_4]^{4-}$  anion and pyrogallol[4]arene ( $PG$ ) ligand; d)  $[Co_{48}\{\mu_3-L2\}_{18}\{TC4A\}_{12}]$  supramolecule,  $H_4TC4A$  (p-tert-butylthiacalix[4]arene) and  $L2$  (1H-tetrazol-1-yl) ligands.

## 6.5 References

- [1] a) F. J. Rizzuto, L. K. S. von Krbek, J. R. Nitschke, *Nat. Rev. Chem.* **2019**, *3*, 204–222; b) M. Han, D. M. Engelhard, G. Clever, *Chem. Soc. Rev.* **2014**, *43*, 1848–1860; c) P. S. Bols, H. L. Anderson, *Acc. Chem. Res.* **2018**, *51*, 2083–2092; d) M. D. Ward, C. A. Hunter, N. H. Williams, *Acc. Chem. Res.* **2018**, *51*, 2073–2082; e) C. M. Hong, R. G. Bergman, K. N. Raymond, F. D. Toste, *Acc. Chem. Res.* **2018**, *51*, 2447–2455.
- [2] a) T. R. Schulte, J. J. Holstein, G. H. Clever, *Angew. Chem. Int. Ed.* **2019**, *58*, 5562–5566; b) Y. Lin, W. Massa, S. Dehnen, *J. Am. Chem. Soc.* **2012**, *134*, 4497–4500; c) R.-J. Li, J. J. Holstein, W. G. Hiller, J. Andréasson, G. H. Clever, *J. Am. Chem. Soc.* **2019**, *141*, 2097–2103; d) M. D. Pluth, R. G. Bergman, K. N. Raymond, *Science* **2007**, *316*, 85–88; e) Y. Ueda, H. Ito, D. Fujita, M. Fujita, *J. Am. Chem. Soc.*, **2017**, *139*, 6090–6093; f) R.-J. Li, M. Han, J. Tessarolo, J. J. Holstein, J. Lübben, B. Dittrich, C. Volkmann, M. Finze, C. Jenne, G. H. Clever, *ChemPhotoChem* **2019**, *3*, 378–383.
- [3] a) D. Fujita, Y. Ueda, S. Sato, N. Mizuno, T. Kumasaka, M. Fujita, *Nature* **2016**, *540*, 563–567; b) C. Zhang, R. S. Patil, C. Liu, C. L. Barnes, J. L. Atwood, *J. Am. Chem. Soc.* **2017**, *139*, 2920–2923; c) K. Su, M. Wu, D. Yuan, M. Hong, *Nat. Commun.* **2018**, *9*, 4941–4946; d) D. Geng, X. Han, Y. Bi, Y. Qin, Q. Li, L. Huang, K. Zhou, L. Song, Z. Zheng, *Chem. Sci.* **2018**, *9*, 8535–8541.
- [4] a) J. Bai, A. V. Virovets, M. Scheer, *Science* **2003**, *300*, 781–783; b) E. Peresytkina, C. Heindl, A. Virovets, M. Scheer in *Structure and Bonding*, Vol. 174 (Eds.: S. Dehnen), Springer International Publishing, Switzerland, **2016**, pp. 321–373; c) C. Schwarzmaier, A. Schindler, C. Heindl, S. Scheuermayer, E. Peresytkina, A. Virovets, M. Neumeier, R. Gschwind, M. Scheer. *Angew. Chem. Int. Ed.* **2013**, *52*, 10896–10899; d) C. Heindl, E. Peresytkina, A. V. Virovets, I. S. Bushmarinov, M. G. Medvedev, B. Krämer, B. Dittrich M. Scheer, *Angew. Chem. Int. Ed.*, **2017**, *56*, 13237–13243; e) H. Brake, E. Peresytkina, C. Heindl, A. V. Virovets, W. Kremer, M. Scheer, *Chem. Sci.* **2019**, *10*, 2940–2944; f) F. Dielmann, M. Fleischmann, C. Heindl, E.V. Peresytkina, A.V. Virovets, R. Gschwind, M. Scheer, *Chem. Eur. J.* **2015**, *21*, 6208–6214.
- [5] a) E. Peresytkina, C. Heindl, A. Virovets, E. Mädl, H. Brake, M. Scheer, *Chem. Eur. J.* **2018**, *24*, 2503–2508; b) E. Peresytkina, C. Heindl, A. Schindler, M. Bodensteiner, A. V. Virovets, M. Scheer, *Z. Kristallogr.* **2014**, *229*, 735–741; c) M. Scheer, A. Schindler, C. Gröger, A. V. Virovets, E. V. Peresytkina, *Angew. Chem.*

- Int. Ed.* **2009**, *48*, 5046-5049; d) A. Schindler, C. Heindl, G. Balazs, C. Groeger, A. V. Virovets, E. V. Peresyphkina, M. Scheer, *Chem. Eur. J.* **2012**, *18*, 829-835.
- [6] The outer diameter in supramolecule **3** is calculated as the distance between H atoms of two the most opposing Cp'' ligands plus twice the van der Waals radii of H (1.2 Å). The outer diameter for the TEF anion was calculated as the distance between H atoms of two the most opposing F atoms (1.47 Å). The size of the void in **3** is calculated as the distance between the centroids of every individual *cyclo*-P<sub>5</sub> unit and the centroid of the node minus twice the van der Waals radius of P (1.8 Å) according to M. Mantina, A. C. Chamberlin, R. Valero, C. J. Cramer and D. G. Truhlar, *Chemistry J. Phys. Chem. A* **2009**, *113*, 5806-5812.
- [7] a) F. Dielmann, A. Schindler, S. Scheuermayer, J. Bai, R. Merkle, M. Zabel, A. V. Virovets, E. V. Peresyphkina, G. Brunklaus, H. Eckert and M. Scheer, *Chem. Eur. J.* **2012**, *18*, 1168-1179; b) M. Elsayed Moussa, M. Piesch, M. Fleischmann, A. Schreiner, M. Seidl, M. Scheer, *Dalton Trans.* **2018**, *47*, 16031; c) A. Cavaille, N. Saffon-Merceron, N. Nebra, M. Fustier-Boutignon, N. Mezailles, *Angew. Chem. Int. Ed.* **2018**, *57*, 1874.
- [8] O. J. Scherer, H. Sitzmann, G. Wolmershäuser, *J. Organomet. Chem.* **1984**, *268*, C9-C12.
- [9] M. E. Moussa, M. Piesch, M. Fleischmann, A. Schreiner, M. Seidl, M. Scheer, *Dalton Trans.* **2018**, *47*, 16031-16035.
- [10] *CrysAlis PRO*, different versions (Rigaku OD, **2018**)
- [11] G. M. Sheldrick, *Acta Cryst. sect. C.*, **2015**, *C71*, 3.
- [12] a) V. A. Blatov, A. P. Shevchenko, D. M. Proserpio, *Cryst. Growth Des.*, 2014, **14**, 3576; b) V. A. Blatov, M. O'Keeffe, D. M. Proserpio, *CrystEngComm* 2010, **12**, 44; c) M. O'Keeffe, M. A. Peskov, S. J. Ramsden, O. M. Yaghi, *Accts. Chem. Res.*, 2008, **41**, 1782; <http://rcsr.net>

## Preface

### Authors

Jana Schiller, Florent Moutier, Ali Khalil, Guillaume Calvez, Michael Seidl, Christophe Lescop and Manfred Scheer

### Author contributions

This work was prepared in close cooperation with the group of Dr. Christophe Lescop in Rennes (Institut des Sciences Chimiques de Rennes, UMR 6226 at the Institut National des Sciences Appliquées de Rennes). The preparation and a part of the characterization of all compounds, except of **A<sub>1</sub>B<sub>1</sub>**, **A<sub>1</sub>B<sub>4</sub>**, **A<sub>1</sub>B<sub>5</sub>**, **A<sub>2</sub>B<sub>2</sub>** and **A<sub>2</sub>B<sub>3</sub>** was done by Jana Schiller. The preparation of compounds **A<sub>1</sub>B<sub>4</sub>**, **A<sub>1</sub>B<sub>5</sub>**, **A<sub>2</sub>B<sub>2</sub>** and **A<sub>2</sub>B<sub>3</sub>** was done together with Florent Moutier. The photophysical measurements of all compounds were done by Florent Moutier, Ali Khalil and Guillaume Calvez. The preparation of the manuscript was done by Jana Schiller. Jana Schiller and Christophe Lescop have measured the solid state structures of all compounds. Christophe Lescop finalized the calculations of compounds **A<sub>2</sub>**, **A<sub>3</sub>**, **A<sub>1</sub>B<sub>4</sub>**, **A<sub>1</sub>B<sub>6</sub>**, **A<sub>1</sub>B<sub>7</sub>**, **A<sub>2</sub>B<sub>2</sub>**, **A<sub>2</sub>B<sub>4</sub>**, **A<sub>2</sub>B<sub>6</sub>** and **A<sub>3</sub>B<sub>4</sub>**. Michael Seidl finalized the calculations for compounds **A<sub>1</sub>B<sub>5</sub>**, **A<sub>2</sub>B<sub>1a</sub>**, **A<sub>2</sub>B<sub>1b</sub>**, **A<sub>2</sub>B<sub>3</sub>** and **A<sub>2</sub>B<sub>7</sub>**. Christophe Lescop revised the experimental part for the X-ray structural analyses. Christophe Lescop and Manfred Scheer supervised the research and revised the manuscript prior to publication.

Parts of this work have already been reported in the Master thesis of Florent Moutier and the PhD thesis of Ali Khalil.

### Acknowledgements

This work was supported by the CNRS (including the PICS program SupraRe2), the French Research Ministry and Campus France (PHC Procope founding) and the German Academic Exchange Service (SUPRAFLEX). C.L. thanks the Alexander von Humboldt Foundation for a fellowship for experienced researcher.

## 7. Tuning Emission Properties of Cu(I) Metallacycles by Introducing Bulky Weakly Coordination Anions

**Abstract:** Herein is presented the impact of changing the nature of the counterion of **A** ( $[\text{Cu}_4(\mu_2\text{-dppm})_4(\text{CN})_2]^{2+}$ , Figure 7.1), from the ‘small’  $\text{PF}_6^-$  (**A**<sub>1</sub>) ion to the bulky weakly coordinating  $[\text{Al}\{\text{OC}(\text{CF}_3)_3\}_4]^-$  and  $[\text{B}(\text{C}_6\text{H}_3\text{Cl}_2)_4]^-$  ions, respectively, on the architecture of a self-assembled metallacycle and its photophysical properties. By doing so, we synthesized  $[\text{Cu}_4(\mu_2\text{-dppm})_4(\text{CN})_2][\text{Al}\{\text{OC}(\text{CF}_3)_3\}_4]_2$  (**A**<sub>2</sub>) and  $[\text{Cu}_4(\mu_2\text{-dppm})_4(\text{CN})_2][\text{B}(\text{C}_6\text{H}_3\text{Cl}_2)_4]_2$  (**A**<sub>3</sub>) (dppm= 1,1-bis(diphenyl-phosphino)methane) and extended our investigations by reacting **A**<sub>1</sub>, **A**<sub>2</sub> and **A**<sub>3</sub> with organic pyridyl linkers.

### 7.1 Introduction

The development of phosphorescent transition metal complexes as building blocks for a number of applications, particularly for organic light emitting diodes (OLEDs), drew a lot of attention in recent years.<sup>1</sup> Especially, complexes based on third row transition metals, such as Ir(III) and Pt(II) are suitable, as the metal center can induce spin-orbit coupling (SOC).<sup>2</sup> This results in short emission decay times for normally spin-forbidden transitions from the first excited triplet state to the ground state ( $T_1 \rightarrow S_0$ )<sup>1d,3</sup> and fast intersystem crossing.<sup>3a,4</sup> The consequential emission properties (fluorescence and phosphorescence) of metal complexes can be modulated using different combinations of Lewis acidic metals and organic ligands.<sup>5</sup> Cu(I) derivatives turned out to be smart novel solid-state emitters because of their low costs and accessibility.<sup>6</sup>

Recently, Thermally Activated Delayed Fluorescence (TADF) Cu(I) coordination complexes have experienced significant research attention<sup>1c,6b,7</sup> as they show exalted photophysical performances which are in no way inferior to “classical” expensive heavy metal complexes.<sup>8</sup> Up to now, luminescent Cu(I) precursors acting as pre-organized building blocks to form coordination-driven supramolecular assemblies have almost never been reported.<sup>9</sup> This is mostly assigned to the labile and non-directional coordination spheres that Cu(I) ions usually exhibit. Based on this knowledge, we were interested, how the photophysical properties of Cu(I) complexes can be tuned by introducing different anions and subsequently building up one-dimensional coordination polymers with organic linkers.

## 7.2 Results and Discussion

The blue emissive tetranuclear metallacycle  $[\text{Cu}_4(\mu_2\text{-dppm})_4(\text{CN})_2](\text{PF}_6)_2$  (**A**<sub>1</sub>) (dppm= 1,1-bis(diphenylphosphino) methane) was recently described as the first Cu(I) coordination-driven supramolecular assembly bearing solid-state Thermally Activated Delayed Fluorescence (TADF) properties.<sup>10</sup> Compound **A**<sub>1</sub> exhibits an absolute luminescence quantum yield of 72% at room temperature and displays a reversible red-shift of its emission spectra upon cooling. These results have triggered us to extend our investigation. We were interested how anions can influence the photophysical properties of precursor **A**. For this the bulky weakly coordinating  $[\text{Al}\{\text{OC}(\text{CF}_3)_3\}_4]^-$  and  $[\text{B}(\text{C}_6\text{H}_3\text{Cl}_2)_4]^-$  ions were introduced.

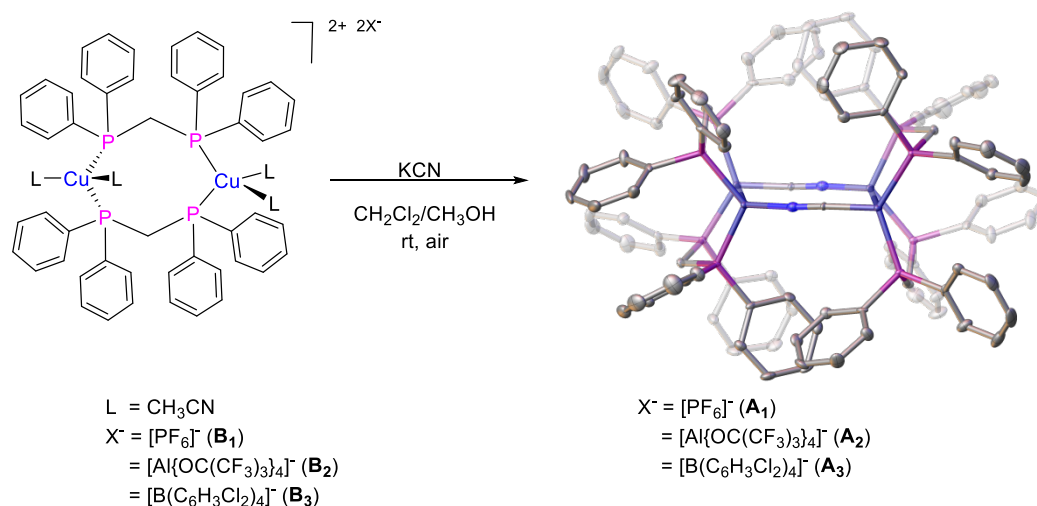


**Figure 7.1.** Synthesis of compounds **A**<sub>1</sub>-**A**<sub>3</sub>. Hydrogen atoms, counteranions and included solvent molecules were omitted for clarity. Thermal ellipsoids are shown at 50% probability level.

The reaction of the previously reported pre-assembled molecular clip **B**<sub>1</sub><sup>11</sup> with an equimolar amount of KCN at room temperature in air in a 2:1  $\text{CH}_2\text{Cl}_2/\text{CH}_3\text{OH}$  mixture leads to the formation of **A**<sub>1</sub> in a very good yield (Figure 7.1).<sup>10</sup> The analogous reaction with *in situ* prepared **B**<sub>2</sub> and **B**<sub>3</sub> yields the Cu(I) metallacycles **A**<sub>2</sub> and **A**<sub>3</sub>, respectively. Upon layering the crude solutions with *n*-pentane, homogenous batches of air stable colorless blocks suitable for X-ray crystallography were obtained in moderate to good yields. Compound **A**<sub>2</sub> crystallizes in the triclinic space group  $P\bar{1}$  and **A**<sub>3</sub> in the monoclinic space group  $P2_1/n$ . **A** is bearing two  $[\text{Cu}_2(\mu_2\text{-dppm}_2)]$  fragments, which are connected by two cyano ligands. The location of the C and N atom is arbitrary. The solid-state structures of the cationic fragments of **A**<sub>2</sub> and **A**<sub>3</sub>, respectively, are isomorphous to **A**<sub>1</sub>. The IR spectra of **A**<sub>2</sub> and **A**<sub>3</sub> show characteristic signals for the presence of the cyanide



groups coordinated to the metal centers ( $2135\text{ cm}^{-1}$  for **A<sub>2</sub>**<sup>12</sup> and  $2120\text{ cm}^{-1}$  for **A<sub>3</sub>**, Figure 7.2), while it is  $2117\text{ cm}^{-1}$  for **A<sub>1</sub>**.<sup>10</sup>

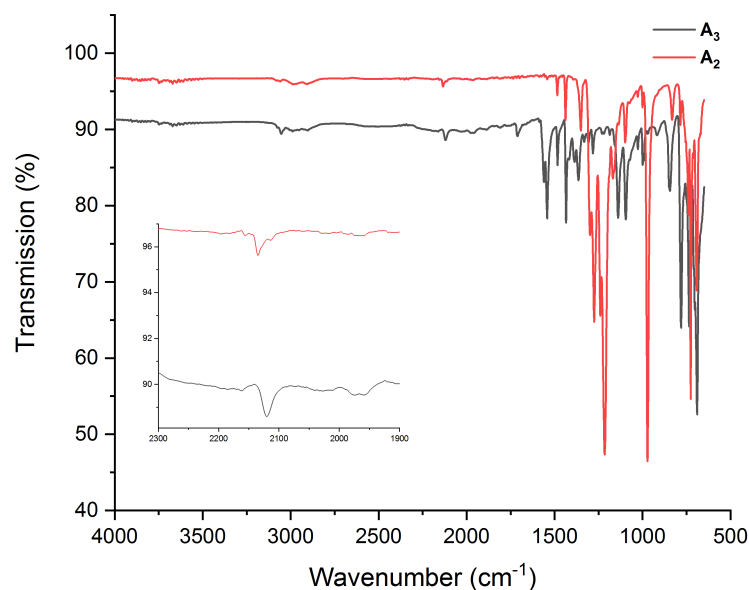


**Figure 7.2.** IR spectra of the metallacycle precursors **A<sub>2</sub>** and **A<sub>3</sub>**. Characteristic C≡N vibration band (inset).

In the solid state at room temperature, compounds **A<sub>2</sub>** and **A<sub>3</sub>** demonstrate blue luminescence (excitation at 325 nm) with an emission maximum of 456 nm and 473 nm, respectively. Interestingly, the emission quantum yield at room temperature of **A<sub>2</sub>** ( $\Phi_{298\text{K}} = 86\%$ ) and **A<sub>3</sub>** ( $\Phi_{298\text{K}} = 91\%$ ) was improved compared to compound **A<sub>1</sub>** ( $\Phi_{298\text{K}} = 72\%$ ).<sup>10</sup> Upon cooling both new derivatives show a similar behavior as **A<sub>1</sub>** ( $\lambda_{\text{max}} = 457\text{ nm}$  at r. t.,  $\lambda_{\text{max}} = 486\text{ nm}$  at 80 K<sup>10</sup>). Cooling from room temperature to 80 K the emission (excitation 325 nm) of compound **A<sub>2</sub>** shows a bathochromic shift to 472 nm (Figure 7.3 left, S7.3), associated with an intense visually perceived greenish luminescence. Cooling compound **A<sub>3</sub>** to 80 K affords an emission maximum (excitation 325 nm) at 489 nm (Figure 7.3 right, S7.6). The shift of the emission maxima is lower for **A<sub>2</sub>** and **A<sub>3</sub>**, respectively, compared to **A<sub>1</sub>**. Exciting compounds **A<sub>2</sub>** and **A<sub>3</sub>** at 360 nm does not significantly change the obtained emission spectra (Figures S7.4, S7.5 and S7.7, S7.8).

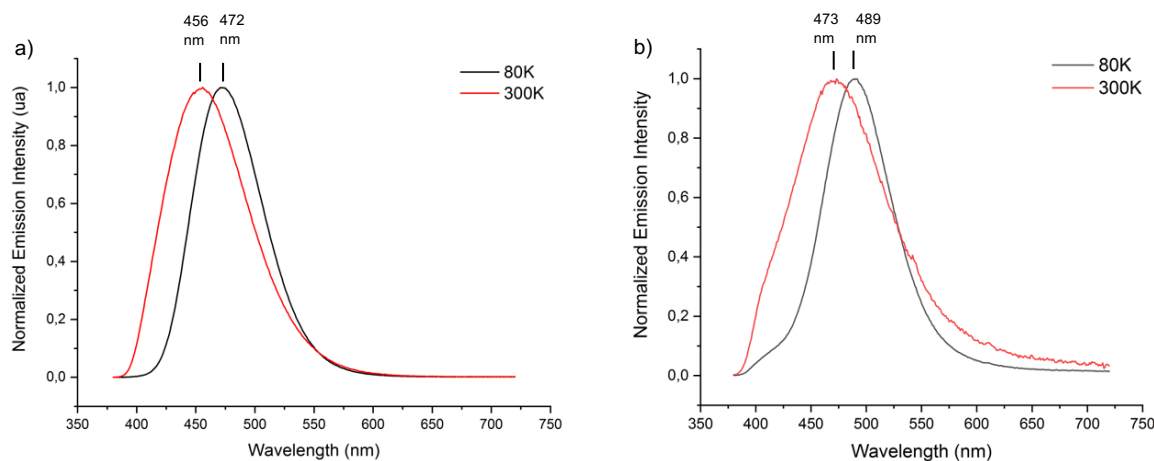


**Figure 7.3.** Solid-state emission spectra of **A**<sub>2</sub> (a) and **A**<sub>3</sub> (b) at 300 K and 80 K upon excitation at 325 nm.

Variable-temperature excited state lifetime measurements of **A**<sub>2</sub> could not make a statement to evidence the electronic processes responsible for the luminescence behavior (Figure S7.11, S7.12). Indeed, as for **A**<sub>2</sub> higher temperatures should be investigated and further measurements have to be performed. Nevertheless, the temperature dependence for both, the emission spectra and the lifetime of the excited states support a TADF mechanism.

Upon heating, compound **A**<sub>2</sub> undergoes a weight loss of less than 2% up to 270°C and an endothermic transition at 206°C followed by decomposition of the compound (Figure S7.13 left). The IR spectra recorded after this transition of **A**<sub>2</sub> shows a shift of the CN band to 2128 cm<sup>-1</sup> (Figure S7.19). The visually perceived emission changes from blue to more greenish after the transition. This fact could imply a change in the geometry of the metallacycle assigned to the phase transition in the solid state at high temperatures. Similar behavior was also observed for **A**<sub>1</sub> recently and is still under study. **A**<sub>3</sub> also loses 2% of its weight upon heating, but the thermal degradation starts at 180°C and no transition is observable (Figure S7.13 right). The weight loss could be attributable to solvent removal in both cases.

As Cu(I) complexes are popular building blocks in supramolecular chemistry,<sup>13</sup> compounds **A**<sub>1</sub>-**A**<sub>3</sub> were reacted with different organic pyridyl-based linkers (**B**<sub>1</sub>-**B**<sub>11</sub>, Figure 7.4). The coordination behavior of the precursor **A**<sub>1</sub> towards **B**<sub>1</sub>-**B**<sub>3</sub>, **B**<sub>9</sub>-**B**<sub>11</sub> and other 4-pyridyl linkers was mainly investigated by the cooperation partners in Rennes and already reported.<sup>14</sup> In this work only the compounds obtained within the cooperation will be discussed (**A**<sub>1</sub>**B**<sub>4</sub>, **A**<sub>1</sub>**B**<sub>5</sub>, **A**<sub>1</sub>**B**<sub>6</sub> and **A**<sub>1</sub>**B**<sub>7</sub>), further polymers will only serve as comparative samples (**A**<sub>1</sub>**B**<sub>1</sub>).

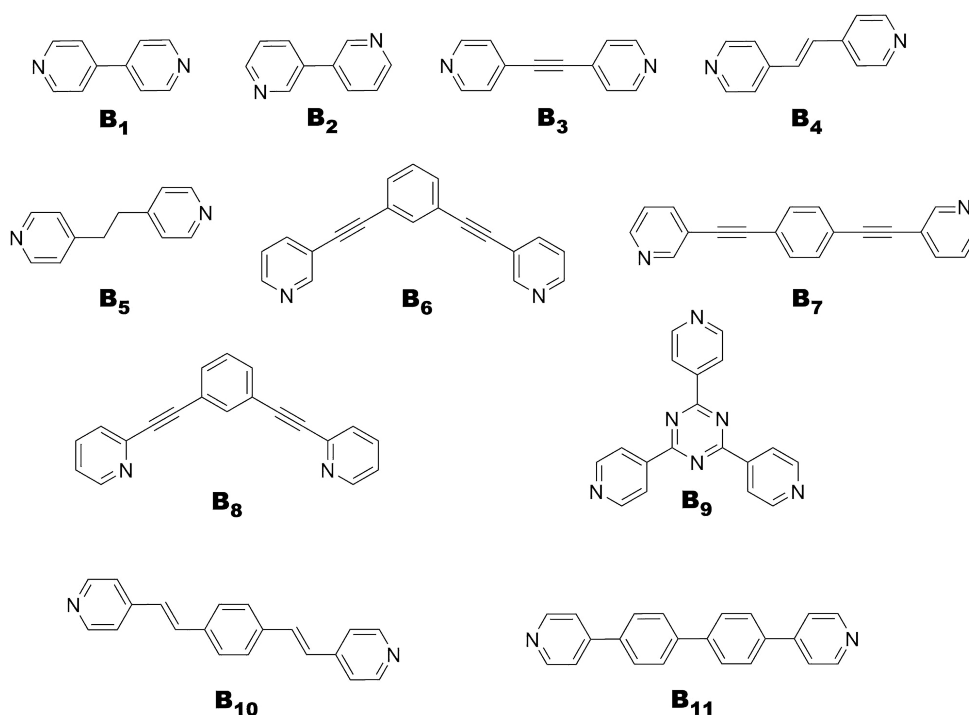


**Figure 7.4.** Organic pyridyl-based linkers **B**<sub>1</sub>-**B**<sub>11</sub> used in this work.

For the reactions with the metallacycle **A**<sub>1</sub> the precursor had to be isolated before adding the organic linkers **B**<sub>4</sub>, **B**<sub>5</sub>, **B**<sub>6</sub>, **B**<sub>7</sub> and **B**<sub>8</sub> in a 1:1 ratio. Whereas, the polymers **A**<sub>2</sub>**B**<sub>x</sub> and **A**<sub>3</sub>**B**<sub>x</sub> were obtained by *in situ* formation of the precursors **A**<sub>2</sub> and **A**<sub>3</sub>, respectively, followed by the addition of the linkers. X-ray diffraction studies of the isolated products performed at low temperatures on single crystals revealed the formation of the one-dimensional coordination polymers **A**<sub>1</sub>**B**<sub>4</sub>, **A**<sub>1</sub>**B**<sub>5</sub>, **A**<sub>1</sub>**B**<sub>6</sub> and **A**<sub>1</sub>**B**<sub>7</sub> (Figure 7.5).

The reaction of any precursor with the 2-pyridyl linker **B**<sub>8</sub> did only lead to the crystallization of the starting material **A**<sub>x</sub> most-likely due to sterical hindrance. The compounds **A**<sub>1</sub>**B**<sub>5</sub> and **A**<sub>1</sub>**B**<sub>6</sub>, obtained by the reaction of the preformed precursor **A**<sub>1</sub> and the linker **B**<sub>6</sub>, crystallizes in the monoclinic space group *P*2<sub>1</sub>/*n* in moderate yields. Compounds **A**<sub>1</sub>**B**<sub>4</sub> and **A**<sub>1</sub>**B**<sub>7</sub> crystallize in the triclinic space group *P* $\bar{1}$  in moderate to poor yields. In the solid-state structure, the metallacycles **A** are connected by linker units, resulting in four one-dimensional coordination polymers. The pyridyl rings in compound **A**<sub>1</sub>**B**<sub>6</sub> are tilted by an angle of 55° what causes also torsion of the metallacycle units to each other (Figure S7.5). Also, cumulated  $\pi \cdots \pi$  and  $\pi \cdots \text{CH}$  interactions are observed between the dppm ligands of the neighboring metallacycles. This stabilizes the structures and could be the reason for such torsion.

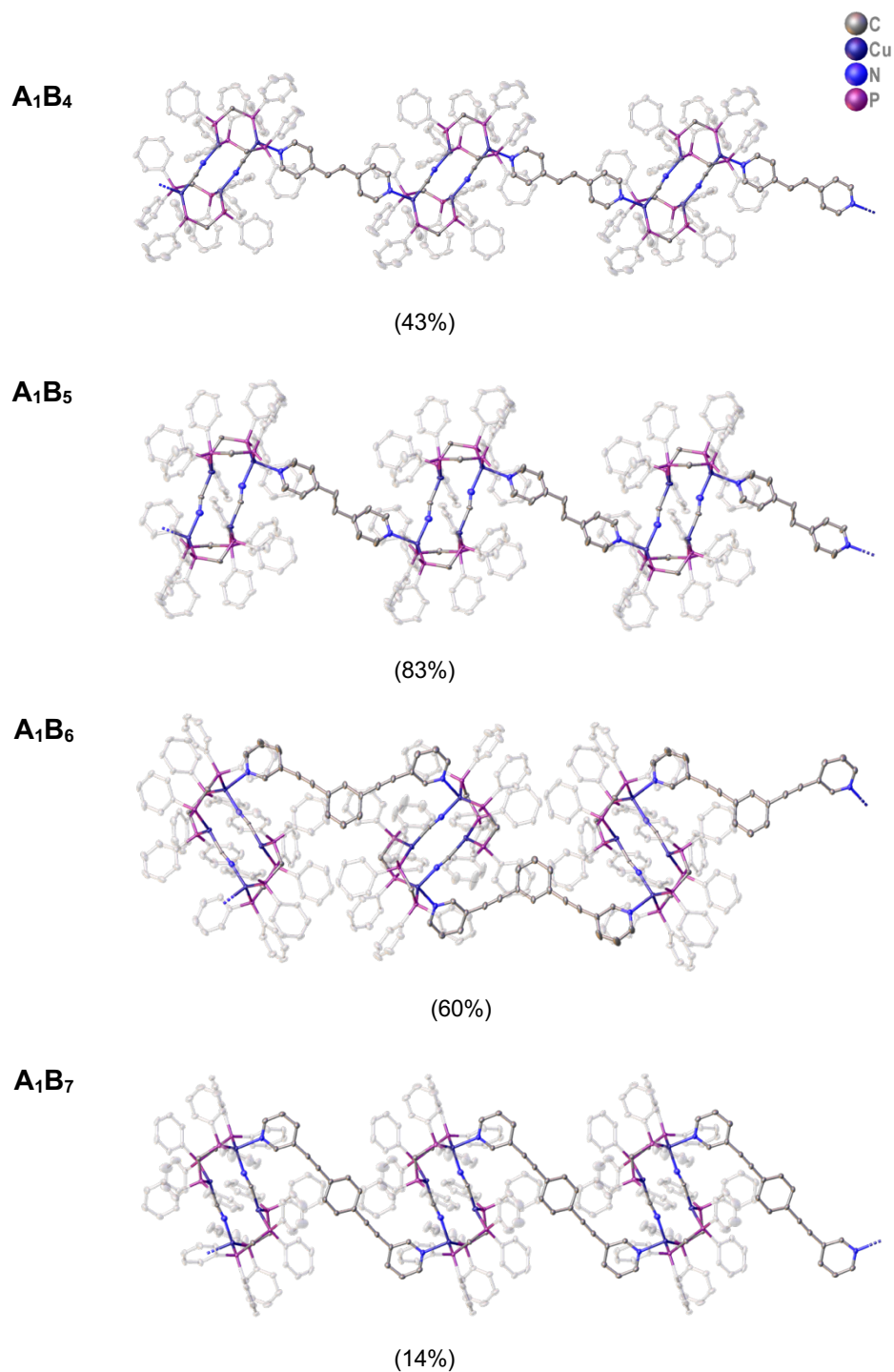


**Figure 7.5.** Solid-state structures of the 1D polymers **A<sub>1</sub>B<sub>4</sub>**, **A<sub>1</sub>B<sub>5</sub>**, **A<sub>1</sub>B<sub>6</sub>** and **A<sub>1</sub>B<sub>7</sub>**. Anions and hydrogen atoms are omitted for clarity. Phenyl rings are depicted transparent. Thermal ellipsoids are shown at 50% probability level. Yields are given in parenthesis.

The characteristic IR vibration bands of the CN groups of the obtained 1D polymers are shifted to lower wavenumbers compared to **A<sub>1</sub>** (Table 7.1).<sup>10</sup> Compound **A<sub>1</sub>B<sub>4</sub>** shows a red luminescence under UV irradiation. TGA-DSC measurements show that compound

**A<sub>1</sub>B<sub>4</sub>** undergoes no transition and shows a weight loss of only 1% upon heating to 250 °C, most-likely as a loss of solvent molecules, which co-crystallized in the crystal lattice, followed by a decomposition upon heating to 270 °C (Figure S7.14 left). The visually perceived emission at r. t. changed to blue after the thermal degradation. The IR spectra of **A<sub>1</sub>B<sub>4</sub>** recorded after the TGA-DSC measurement displays a shift of the CN vibration band to higher wavenumbers (2126 cm<sup>-1</sup>, Figure S7.22), that, however, differs from the infrared spectrum of **A<sub>1</sub>** (ν(C≡N) 2117 cm<sup>-1</sup>)<sup>10</sup> and shows that there is still a CN unit present.

**Table 7.1.** Values for IR vibration bands of C≡N groups in compounds **A<sub>1</sub>B<sub>4</sub>**-**A<sub>1</sub>B<sub>7</sub>** compared to **A<sub>1</sub>**.

compound	<b>A<sub>1</sub></b> <sup>10</sup>	<b>A<sub>1</sub>B<sub>4</sub></b>	<b>A<sub>1</sub>B<sub>5</sub></b>	<b>A<sub>1</sub>B<sub>6</sub></b>	<b>A<sub>1</sub>B<sub>7</sub></b>
ν <sub>CN</sub> (cm <sup>-1</sup> )	2117	2100	2102	2103	2106

The temperature dependent UV-Vis spectra of **A<sub>1</sub>B<sub>4</sub>** (excitation 325 nm) reveals three emission bands at 300 K at 581 nm, 635 nm and 698 nm, which do not significantly shift upon cooling to 80 K (578 nm, 637 nm and 706 nm). However, a new emission band arises at higher energies during cooling to 80 K centered at 445 nm (Figure S7.9). Investigations of the nature of this new emission band was not possible within this work. Compound **A<sub>1</sub>B<sub>7</sub>** indicates a visually perceived change in its weakly observable blue emission at room temperature upon cooling to 77 K (yellow emission). Upon heating to 50 °C compound **A<sub>1</sub>B<sub>7</sub>** loses 2% of its weight, up to 230 °C a weight loss of another 2% is evident followed by a thermal degradation at 270 °C. This loss of weight could indicate the evaporation of solvent incorporated in the crystal lattice. The DSC measurement revealed an exothermic transition at 199 °C (Figure S7.14 right). After the decomposition, the visibly black compound shows a stronger blue luminescence than before.

The reaction of equimolar amounts of **A<sub>2</sub>** and **B<sub>1</sub>**-**B<sub>4</sub>**, **B<sub>6</sub>** and **B<sub>7</sub>**, respectively, conducted at room temperature in air in CH<sub>2</sub>Cl<sub>2</sub> led to the formation of six novel one dimensional polymers (Figure 7.6). So far, an X-ray structural analysis of compound **A<sub>2</sub>B<sub>6</sub>** was not possible, though, the characterization, including elemental analysis and IR spectroscopy point to a 1D polymer with a 1:1 **A<sub>2</sub>** to **B<sub>6</sub>** composition, similar to the other obtained coordination polymers. The linking units of **A<sub>2</sub>B<sub>1</sub>** and **A<sub>2</sub>B<sub>2</sub>** deviate from planarity with a dihedral angle of 55° and 45°, respectively. This will be further examined later in this chapter for compound **A<sub>2</sub>B<sub>1</sub>** in comparison to **A<sub>1</sub>B<sub>1</sub>**.<sup>14</sup> Similar to the coordination polymers **A<sub>1</sub>B<sub>x</sub>** also the polymers shown in table 7.2 possess C≡N vibrations band shifted to lower wavenumbers compared to **A<sub>2</sub>**.

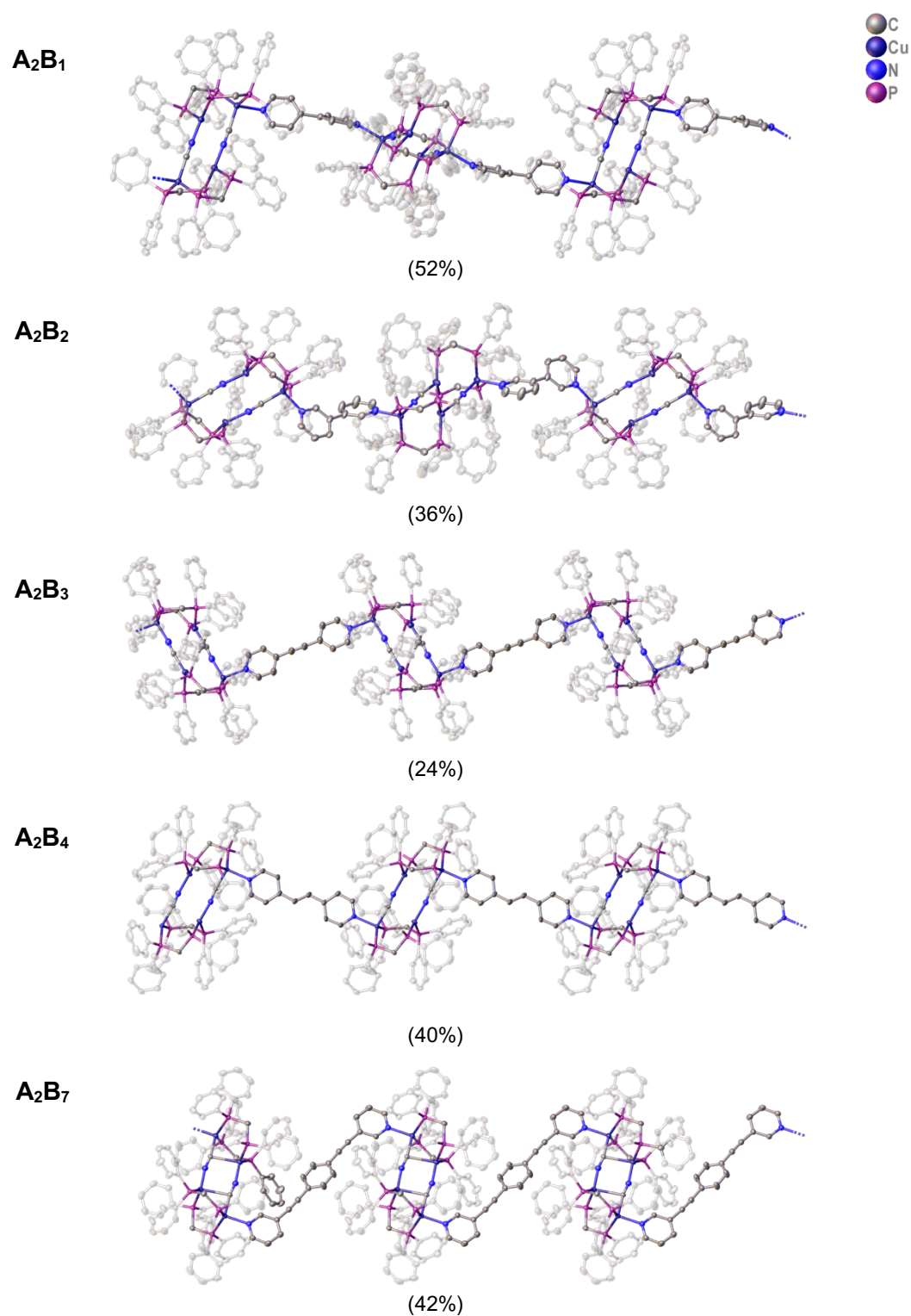


**Figure 7.6.** Solid-state structures of the 1D polymers **A<sub>2</sub>B<sub>1</sub>**, **A<sub>2</sub>B<sub>2</sub>**, **A<sub>2</sub>B<sub>3</sub>**, **A<sub>2</sub>B<sub>4</sub>**, **A<sub>2</sub>B<sub>6</sub>** and **A<sub>2</sub>B<sub>7</sub>**. Anions and hydrogen atoms are omitted for clarity. Phenyl rings are depicted transparent. Thermal ellipsoids are shown at 50% probability level. Yields are given in parenthesis.

**Table 7.2.** Values for IR vibration bands of C≡N groups in compounds **A<sub>2</sub>B<sub>1a</sub>**-**A<sub>2</sub>B<sub>4</sub>** and **A<sub>2</sub>B<sub>6</sub>**-**A<sub>2</sub>B<sub>7</sub>** compared to **A<sub>2</sub>**.

compound	<b>A<sub>2</sub></b>	<b>A<sub>2</sub>B<sub>1a</sub></b>	<b>A<sub>2</sub>B<sub>1b</sub></b> <sup>i</sup>	<b>A<sub>2</sub>B<sub>2</sub></b>	<b>A<sub>2</sub>B<sub>3</sub></b>	<b>A<sub>2</sub>B<sub>4</sub></b>	<b>A<sub>2</sub>B<sub>6</sub></b>	<b>A<sub>2</sub>B<sub>7</sub></b>
$\nu_{\text{CN}} \text{ (cm}^{-1}\text{)}$	2135	2096	2110	2096	2107	2106	2097 <sup>15</sup>	2100 <sup>16</sup>

<sup>i</sup> complexes **A<sub>2</sub>B<sub>1a</sub>** and **A<sub>2</sub>B<sub>1b</sub>** are indicated for completeness. This will be discussed in more detail later in this work.

The TGA-DSC measurement of compound **A<sub>2</sub>B<sub>3</sub>** shows a weight loss of 2% upon heating to 175°C and an endothermic transition at 186°C with another weight loss of 3.5% at 230°C and the thermal degradation of the polymer (Figure S7.16 left). The weight loss indicates that the linker sublimates during heating. After the transition an additional IR spectrum was recorded and the resulting C≡N vibration band of 2133 cm<sup>-1</sup> also designates, that the starting material **A<sub>2</sub>** is being formed (Figure S7.28). Furthermore, the TGA-DSC measurement of compound **A<sub>2</sub>B<sub>4</sub>** shows a similar behavior with a transition at 208 °C and a total weight loss of 5.5% pointing to the cleavage of linker **B<sub>4</sub>**. In this case it is an exothermic process. The IR spectrum after the conversion reveals a vibration band of 2135 cm<sup>-1</sup> matching the precursor **A<sub>2</sub>** (Figure S7.29). Also, the visible perceived emission corresponding to the fact that polymer **A<sub>2</sub>B<sub>4</sub>** is not luminescent under UV light but, the resulting compound after heating is blue emissive. The emission spectrum of **A<sub>2</sub>B<sub>4</sub>** at room temperature shows a maximum at 415 nm and two maxima lower in energy at 568 nm and 625 nm upon excitation at 325 nm. Cooling to 80 K reveals four additional emission maxima at 480 nm, 570 nm, 627 nm and a broad peak at 685 nm (Figure S7.10). All peaks do not shift significantly in energy upon cooling. The intense peak at 415 nm might be corresponding to an emission centered on the linker. The two coordination polymers containing the 3-pyridyl based linkers **A<sub>2</sub>B<sub>6</sub>** and **A<sub>2</sub>B<sub>7</sub>** do not show any evidence of linker cleavage upon heating to 200 °C and 220 °C, respectively (Figure S7.17). However, polymer **A<sub>2</sub>B<sub>6</sub>** shows an exothermic transition at 198 °C resulting in a change of visible perceived emission from not emissive to slightly green after the transition. The IR spectrum recorded after the transition shows a band in the range of those for the starting material (2134 cm<sup>-1</sup>, Figure S7.30). For the coordination polymers **A<sub>1</sub>B<sub>x</sub>** which also show this transition but no weight loss, the collaboration partners proposed a de-coordination of **A<sub>1</sub>** upon heating.<sup>14</sup>

In 2019 Kitamura *et al.* published the luminescent silver(I) halogenido coordination polymers [Ag<sub>2</sub>X<sub>2</sub>(PPh<sub>3</sub>)<sub>2</sub>(bpy)]<sub>n</sub> (X = I, Br, Cl; bpy = 4,4'-bipyridine), where the organic linker in the chlorido complex deviates from planarity which influences the emission properties compared to the planar iodide and bromide complexes.<sup>17</sup> Since compound **A<sub>1</sub>B<sub>1</sub>**<sup>14</sup> does not show any torsion of the linker (Figure S7.2), compounds **A<sub>2</sub>B<sub>1</sub>** and **A<sub>1</sub>B<sub>1</sub>**

will be compared in the following regarding their emission properties as well as the differences in their solid-state structures. As seen in figure 7.7 the emission maximum of compound **A<sub>2</sub>B<sub>1</sub>** (507 nm) is blue shifted compared to the emission maximum of **A<sub>1</sub>B<sub>1</sub>** (611 nm) upon excitation at 320 nm at 300 K. Furthermore, **A<sub>2</sub>B<sub>1</sub>** shows a drop in the emission intensity, as well as a slight bathochromic shift upon cooling to 130 K followed by an increase of the emission and a blue shift upon cooling to 80 K. Compound **A<sub>1</sub>B<sub>1</sub>**, instead, reveals an increase in emission upon cooling to 80 K with an additional emission maximum arising at 503 nm. Interestingly, **A<sub>2</sub>B<sub>1</sub>** is green emissive in the solid state when dried and blue emissive as crystals in the supernatant, suggesting a solvatochromic effect. The C≡N IR vibration band of **A<sub>2</sub>B<sub>1</sub>** is shifted to lower wavenumbers (2096 cm<sup>-1</sup>) compared to compound **A<sub>1</sub>B<sub>1</sub>** (2105 cm<sup>-1</sup>) (Figure S7.21, S7.26). The Cu•••Cu distances in the twisted polymer **A<sub>2</sub>B<sub>1</sub>** of 3.36 Å are slightly longer than in **A<sub>1</sub>B<sub>1</sub>** (3.21 Å). Since the metallacycle units and the linkers are the same in **A<sub>1</sub>B<sub>1</sub>** and **A<sub>2</sub>B<sub>1</sub>** the differences observed in the conformations have to be related to the packing in the solid state influenced by the anions.

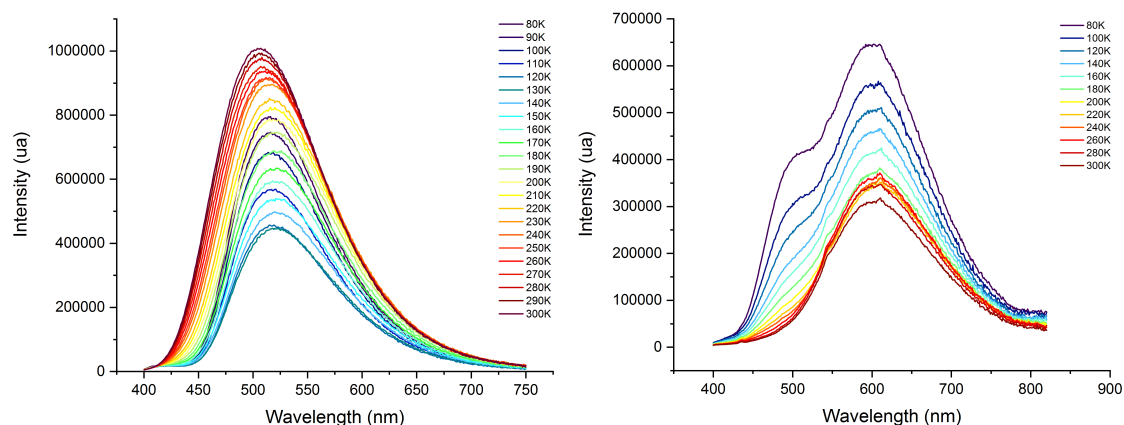


**Figure 7.7.** Temperature dependent emission spectra of **A<sub>2</sub>B<sub>1</sub>** (left) and **A<sub>1</sub>B<sub>1</sub>** (right) between 80 K and 300 K upon excitation at 320 nm.

Surprisingly, the crystals of **A<sub>2</sub>B<sub>1</sub>** transform quantitatively into yellow emissive crystals in the supernatant within 7 days. X-ray diffraction studies revealed the formation of the oligomer **A<sub>2</sub>B<sub>1</sub><sup>b</sup>** containing one metallacycle unit coordinated by two 4,4'-bipyridine linkers (Figure 7.8 top). The torsion angle between the two pyridyl rings in the linker decreases from 55° to 41° in the newly formed thermodynamic product **A<sub>2</sub>B<sub>1</sub><sup>b</sup>**. The transformation of **A<sub>2</sub>B<sub>1</sub><sup>a</sup>** to **A<sub>2</sub>B<sub>1</sub><sup>b</sup>** leads to a contraction of the Cu•••Cu distances (3.23 Å). The vibration bands of the CN groups shift to higher wavenumbers (2110 cm<sup>-1</sup>, Figure

<sup>i</sup> In the following the polymer will be named **A<sub>2</sub>B<sub>1</sub><sup>a</sup>** and the oligomer **A<sub>2</sub>B<sub>1</sub><sup>b</sup>**.



S7.27). The TGA-DSC measurements of both compounds show a cleavage of the pyridyl linker at around 175°C, directly followed by a thermal decomposition in the case of compound **A<sub>2</sub>B<sub>1</sub>b** (Figure S7.15 right).

The transformation could be driven by the higher stability of the  $\pi$ -stacked units (Figure 7.8 bottom). Within this work no photophysical measurements for compound **A<sub>2</sub>B<sub>1</sub>b** could be performed, but the transformation from the polymer **A<sub>2</sub>B<sub>1</sub>a** to the oligomer **A<sub>2</sub>B<sub>1</sub>b** and also the comparison to **A<sub>1</sub>B<sub>1</sub>** bear many interesting approaches worth to investigate in the future.

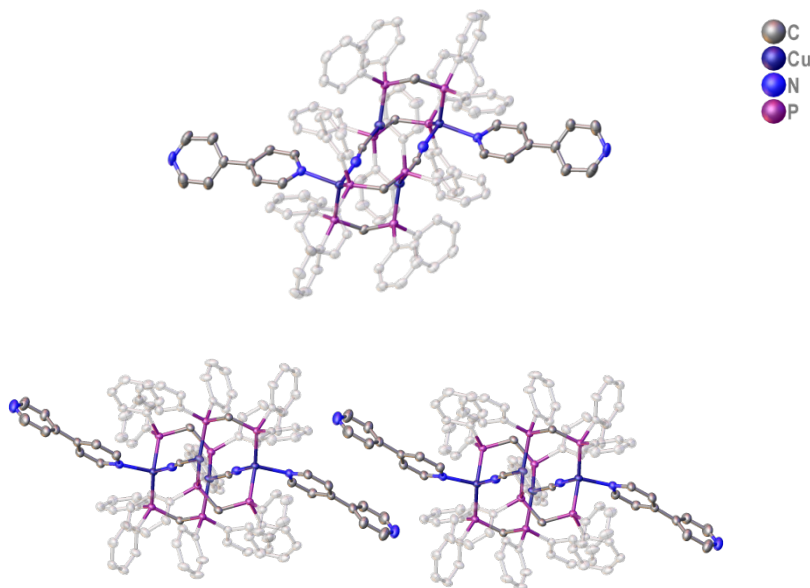


**Figure 7.8.** Solid-state structure of compound **A<sub>2</sub>B<sub>1</sub>b** (top).  $\pi$ -stacking via pyridyl rings (bottom). Anions and hydrogen atoms are omitted for clarity. Phenyl rings are depicted transparent. Thermal ellipsoids are shown at 50% probability level.

Precursor **A<sub>3</sub>** was used in a reaction with the 4-pyridyl linker **B<sub>4</sub>** yielding the 1D coordination polymer **A<sub>3</sub>B<sub>4</sub>** (Figure 7.9). Compared to **A<sub>2</sub>B<sub>4</sub>** the linker in this compound deviates from planarity with a dihedral angle of 34° between the two pyridine rings. The polymer shows no visually perceivable emission, though, after an exothermic transition at 147 °C the compound emits orange light under UV light. At 200 °C **A<sub>3</sub>B<sub>4</sub>** starts to decompose in combination with a high mass loss (Figure S7.18). The transition leads to a shift of the CN vibration band (2160 cm<sup>-1</sup>, Figure S7.32) to a significantly higher wavenumber relative to the precursor **A<sub>3</sub>** (2120 cm<sup>-1</sup>).

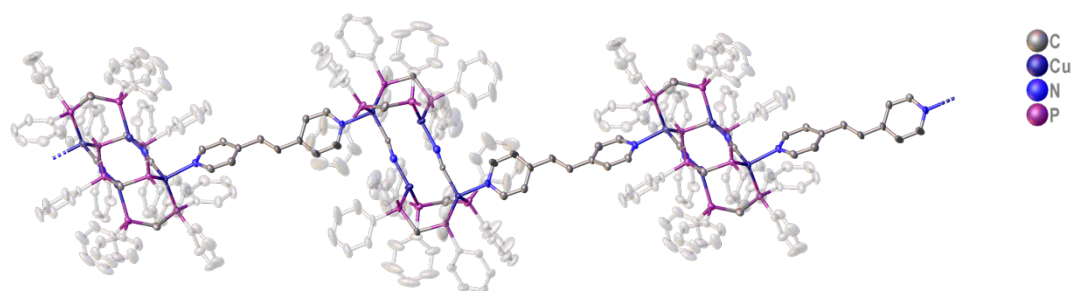


**Figure 7.9.** Solid-state structure of compound **A<sub>3</sub>B<sub>4</sub>**. Anions and hydrogen atoms are omitted for clarity. Phenyl rings are depicted transparent. Thermal ellipsoids are shown at 50% probability level.

The reactions of **A<sub>2</sub>** with **B<sub>9</sub>-B<sub>11</sub>** and **A<sub>3</sub>** with **B<sub>1</sub>-B<sub>3</sub>** and **B<sub>5</sub>-B<sub>11</sub>** did not lead to any results so far or still have to be performed.

### 7.3 Conclusion

In summary, we have presented the facile synthesis of 12 novel coordination compounds  $\mathbf{A}_1\mathbf{B}_4$ - $\mathbf{A}_1\mathbf{B}_7$ ,  $\mathbf{A}_2\mathbf{B}_1$ - $\mathbf{A}_2\mathbf{B}_4$ ,  $\mathbf{A}_2\mathbf{B}_6$ - $\mathbf{A}_2\mathbf{B}_7$  and  $\mathbf{A}_3\mathbf{B}_4$  containing the metallacycle unit  $\mathbf{A}$ , low and high sterically demanding anions and different pyridyl based organic linkers  $\mathbf{B}_1$ - $\mathbf{B}_7$ . We have demonstrated that the anions have a significant influence on the structure in the solid state and the luminescence of the coordination polymers, as well as on the luminescence of the precursors  $\mathbf{A}_2$  and  $\mathbf{A}_3$ . The comparison of  $\mathbf{A}_2\mathbf{B}_1\mathbf{a}$  with the coordination polymer  $\mathbf{A}_1\mathbf{B}_1$  shows a major difference in the solid-state structure due to the twisted linker in  $\mathbf{A}_2\mathbf{B}_1\mathbf{a}$ , resulting in distinctive photophysical properties. Furthermore, we detected a transformation of the green emissive  $\mathbf{A}_2\mathbf{B}_1\mathbf{a}$  after one week into the yellow luminescent oligomer  $\mathbf{A}_2\mathbf{B}_1\mathbf{b}$  (Figure 7.10). For the polymer with the smaller anion  $\text{PF}_6^-$  ( $\mathbf{A}_1\mathbf{B}_1$ ) this kind of transition was never observed.

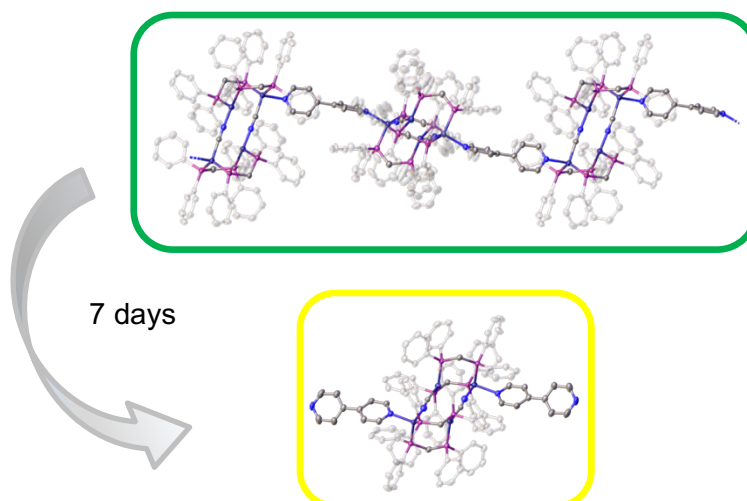


**Figure 7.10.** Transformation of  $\mathbf{A}_2\mathbf{B}_1\mathbf{a}$  into  $\mathbf{A}_2\mathbf{B}_1\mathbf{b}$  within 7 days in the supernatant. Anions and hydrogen atoms are omitted for clarity. Phenyl rings are depicted transparent. Thermal ellipsoids are shown at 50% probability level.

These different reactivities lead to a wide variety of photophysical properties of coordination polymers obtained by coordination of polytopic ligands with pyridyl terminations towards the precursors  $\mathbf{A}_1$ - $\mathbf{A}_3$ . Future efforts will focus on more detailed studies (*inter alia* variation of the lifetime of the excited state, quantum yield measurements, theoretical calculations, additional VT UV-Vis measurements) in order to rationalize the reported observations. The different thermal transitions are a subject of ongoing studies, as the  $\mathbf{A}_1\mathbf{B}_x$  compounds show various reactivities upon heating associated with irreversible change in the luminescence properties in the solid state.

## 7.4 Experimental Procedures

### 7.4.1 Chemicals

All solvents were used as received. The precursors,  $[\text{Cu}(\text{CH}_3\text{CN})_4][\text{Al}\{\text{OC}(\text{CF}_3)_3\}_4]^{18}$ ,  $[\text{Cu}(\text{CH}_3\text{CN})_3][\text{B}(\text{C}_6\text{H}_3\text{Cl}_2)_4]^{19}$  were prepared according to literature procedures. The organic linkers **B**<sub>6</sub>-**B**<sub>8</sub> were prepared in a modified synthesis according to literature.<sup>20</sup> The organic linker **B**<sub>10</sub> was prepared in a modified synthesis according to literature procedures from the collaboration partners.<sup>21</sup> The starting materials dpmm (1,1-bis(diphenyl-phosphino) methane) (Sigma Aldrich), KCN (Merck),  $\text{Cu}(\text{CH}_3\text{CN})_4\text{PF}_6$  (Sigma Aldrich), **B**<sub>1</sub> (Sigma Aldrich), **B**<sub>2</sub> (TCI), **B**<sub>3</sub> (TCI), **B**<sub>4</sub> (TCI), **B**<sub>5</sub> (TCI), **B**<sub>9</sub> (TCI) and **B**<sub>11</sub> (TCI) were purchased and used without further purification.

### 7.4.2 Spectroscopic Methods

Steady-state emission spectra and luminescence quantum yield measurements at room temperature were recorded on a Horiba Universal Attenuated Total Reflectance accessory. UV-Vis solid state measurements were performed with a Jobin Yvon (HJY) Fluorolog 3 (FL3-2iHR550) fluorescence spectrofluorometer equipped with an IR R928P PMT / HJY FL-1073 detector and with an integrating sphere. Low temperature measurements were allowed by using an Optistat CF (Oxford Inst.) in the range of 80 K to 300 K. Excited-state lifetimes at 77 K were measured with a delta hub (TCSPC: Time Correlated-Single-Photon-Counting) + delta diode system allowing to measure excited-state lifetimes between 500 ps et 10  $\mu\text{s}$  and with a pulsed xenon source (FL-1035) allowing to measure excited-state lifetimes longer than 10  $\mu\text{s}$ . Solid sample was placed in a quartz sample holders inside the integrating sphere and the cryostat and maintained at the desired temperature until equilibrium was reached before recording the spectrum. The experimental data of the variable-temperature excited state lifetime measurements were then fitted according to the following equation<sup>22</sup>

$$\tau(\text{obs}) = \frac{1 + \frac{1}{3} \exp\left(-\frac{\Delta E_{ST}}{k_B T}\right)}{\frac{1}{\tau(T_1)} + \frac{1}{3\tau(S_1)} \exp\left(-\frac{\Delta E_{ST}}{k_B T}\right)} \quad \text{equation (7.1)}$$

where  $\tau(\text{obs})$ ,  $\tau(S_1)$ ,  $\tau(T_1)$ ,  $k_B$ ,  $T$  and  $\Delta E_{ST}$  represent the observed lifetime, singlet state decay lifetime, triplet state decay lifetime, Boltzmann constant, temperature and singlet-

triplet energy difference, respectively. FT-IR measurements have been performed on a Perkin Elmer Frontier spectrometer using UATR (Universal Attenuated Total Reflectance) accessory. Spectra have been recorded between  $500\text{ cm}^{-1}$  and  $4000\text{ cm}^{-1}$  on pure samples. Elemental analyses were performed on an Elementar vario MICRO cube apparatus.

### 7.4.3 Synthetic procedure

The characterization of some compounds could not be finished within this work. Further measurements have to be performed.

#### Synthesis of compounds **A<sub>2</sub>** and **A<sub>3</sub>**

0.126 mmol 1,1-bis(diphenyl-phosphino) methane (48 mg) in 5 mL  $\text{CH}_2\text{Cl}_2$  was added to a solution of  $[\text{Cu}(\text{CH}_3\text{CN})_4][\text{Al}\{\text{OC}(\text{CF}_3)_3\}_4]$  (150 mg, 0.126 mmol) or  $[\text{Cu}(\text{CH}_3\text{CN})_3][\text{B}(\text{C}_6\text{H}_3\text{Cl}_2)_4]$  (99 mg, 0.126 mmol) in 5 mL  $\text{CH}_2\text{Cl}_2$ , respectively, and left without stirring for 0.5 h at room temperature. Then 0.063 mmol KCN (4 mg) in 2 mL  $\text{CH}_3\text{OH}$  was added and stirred for 18 h. The colorless solution was filtered. The diffusion of *n*-pentane and into the crude solution afforded colorless block-shaped crystals after 3-5 days.

#### Compound **A<sub>2</sub>**

Yield: 35 mg (34% referred to CuTEF)

Elemental analysis, calcd (%) for  $\text{C}_{354}\text{H}_{88}\text{Al}_2\text{Cu}_4\text{F}_{72}\text{N}_2\text{O}_8\text{P}_8$  (3778.00 g/mol): C, 45.58; H, 2.48; N, 1.38; found: C, 45.53; H, 2.36; N, 1.28;

IR (solid, CN bands):  $\tilde{\nu}/\text{cm}^{-1}$ : 2135 (w), 2114 (w);

IR after transition (solid, CN bands)  $\tilde{\nu}/\text{cm}^{-1}$ : 2128 (w), 2099 (w);

$\Phi_{298\text{K}} = 86\%$

#### Compound **A<sub>3</sub>**

Yield: 77 mg (79% referred to CuBArCl)

IR (solid, CN bands):  $\tilde{\nu}/\text{cm}^{-1}$ : 2115 (w)

$\Phi_{298\text{K}} = 91\%$

**Synthesis of compounds A<sub>1</sub>B<sub>4</sub>, A<sub>1</sub>B<sub>5</sub>, A<sub>1</sub>B<sub>6</sub> and A<sub>1</sub>B<sub>7</sub>**

0.0187 mmol of the preformed precursor **A<sub>1</sub>** (40 mg) in 10 mL CH<sub>2</sub>Cl<sub>2</sub> was added to a solution of linker (0.0187 mmol, **B<sub>4</sub>** 4.1 mg, **B<sub>5</sub>** 3.4 mg, **B<sub>6</sub>** or **B<sub>7</sub>**, respectively, 5.3 mg) in 10 mL CH<sub>2</sub>Cl<sub>2</sub>, and left without stirring for 18 h at room temperature. The colorless solution was filtered. The diffusion of vapors of *n*-pentane into the crude solution afforded colorless block-shaped crystals after 3-5 days.

**Compound A<sub>1</sub>B<sub>4</sub>**

Yield: 19 mg (43% referred to CuPF<sub>6</sub>)

IR (solid, CN bands):  $\tilde{\nu}/\text{cm}^{-1}$ : 2100 (w);

IR after transition (solid, CN bands)  $\tilde{\nu}/\text{cm}^{-1}$ : 2126 (w);

**Compound A<sub>1</sub>B<sub>5</sub>**

Yield: 36 mg (83% referred to CuPF<sub>6</sub>)

IR (solid, CN bands):  $\tilde{\nu}/\text{cm}^{-1}$ : 2102 (w);

**Compound A<sub>1</sub>B<sub>6</sub>**

Yield: 27 mg (60% referred to Cu PF<sub>6</sub>)

IR (solid, CN bands):  $\tilde{\nu}/\text{cm}^{-1}$ : 2103 (w);

**Compound A<sub>1</sub>B<sub>7</sub>**

Yield: 7 mg (14% referred to Cu PF<sub>6</sub>)

IR (solid, CN bands):  $\tilde{\nu}/\text{cm}^{-1}$ : 2106 (w);

**Synthesis of compounds A<sub>2</sub>B<sub>1a</sub>, A<sub>2</sub>B<sub>1b</sub>, A<sub>2</sub>B<sub>2</sub>-A<sub>2</sub>B<sub>4</sub>, and A<sub>2</sub>B<sub>6</sub>-A<sub>2</sub>B<sub>7</sub> and A<sub>3</sub>B<sub>4</sub>**

0.084 mmol 1,1-bis(diphenyl-phosphino) methane (32 mg) in 5 mL CH<sub>2</sub>Cl<sub>2</sub> was added to a solution of [Cu(CH<sub>3</sub>CN)<sub>4</sub>][Al{OC(CF<sub>3</sub>)<sub>3</sub>}<sub>4</sub>] (100 mg, 0.084 mmol) or [Cu(CH<sub>3</sub>CN)<sub>3</sub>][B(C<sub>6</sub>H<sub>3</sub>Cl<sub>2</sub>)<sub>4</sub>] (66 mg, 0.084 mmol) in 5 mL CH<sub>2</sub>Cl<sub>2</sub>, respectively, and left without stirred for 0.5 h at room temperature. Then 0.042 mmol KCN (3 mg) in 2 mL CH<sub>3</sub>OH was added and stirred for 2 h. 0.021 mmol of the linkers were dissolved in 2 mL CH<sub>2</sub>Cl<sub>2</sub>. The colorless solution was filtered. The diffusion of vapors of *n*-pentane into the crude solution afforded colorless block-shaped crystals after 3-5 days.

**Compound A<sub>2</sub>B<sub>1a</sub>**

Yield: 45 mg (52% referred to [Cu(CH<sub>3</sub>CN)<sub>4</sub>][Al{OC(CF<sub>3</sub>)<sub>3</sub>]<sub>4</sub>])

IR (solid, CN bands):  $\tilde{\nu}/\text{cm}^{-1}$ : 2096 (w);

IR after transition (solid, CN bands)  $\tilde{\nu}/\text{cm}^{-1}$ : 2130 (w);

**Compound A<sub>2</sub>B<sub>1b</sub>**

Yield: 45 mg (52% referred to [Cu(CH<sub>3</sub>CN)<sub>4</sub>][Al{OC(CF<sub>3</sub>)<sub>3</sub>]<sub>4</sub>])

IR (solid, CN bands):  $\tilde{\nu}/\text{cm}^{-1}$ : 2096 (w);

IR after transition (solid, CN bands)  $\tilde{\nu}/\text{cm}^{-1}$ : 2129 (w);

**Compound A<sub>2</sub>B<sub>2</sub>**

Yield: 30 mg (36% referred to [Cu(CH<sub>3</sub>CN)<sub>4</sub>][Al{OC(CF<sub>3</sub>)<sub>3</sub>]<sub>4</sub>])

IR (solid, CN bands):  $\tilde{\nu}/\text{cm}^{-1}$ : 2096 (w);

**Compound A<sub>2</sub>B<sub>3</sub>**

Yield: 20 mg (24% referred to [Cu(CH<sub>3</sub>CN)<sub>4</sub>][Al{OC(CF<sub>3</sub>)<sub>3</sub>]<sub>4</sub>])

Elemental analysis, calcd (%) for C<sub>146</sub>H<sub>96</sub>Al<sub>2</sub>Cu<sub>4</sub>F<sub>72</sub>N<sub>4</sub>O<sub>8</sub>P<sub>8</sub> (3958.21 g/mol): C, 44.30; H, 2.44; N, 1.42; found: C, 44.29; H, 2.50; N, 1.46;

IR (solid, CN bands):  $\tilde{\nu}/\text{cm}^{-1}$ : 2107 (w), 2233 (w);

IR after transition (solid, CN bands)  $\tilde{\nu}/\text{cm}^{-1}$ : 2133 (w);

**Compound A<sub>2</sub>B<sub>4</sub>**

Yield: 33 mg (40% referred to [Cu(CH<sub>3</sub>CN)<sub>4</sub>][Al{OC(CF<sub>3</sub>)<sub>3</sub>]<sub>4</sub>])

Elemental analysis, calcd (%) for C<sub>146</sub>H<sub>98</sub>Al<sub>2</sub>Cu<sub>4</sub>F<sub>72</sub>N<sub>4</sub>O<sub>8</sub>P<sub>8</sub> (3960.23 g/mol): C, 44.28; H, 2.49; N, 1.41; found: C, 44.31; H, 2.51; N, 1.26;

IR (solid, CN bands):  $\tilde{\nu}/\text{cm}^{-1}$ : 2106 (w);

IR after transition (solid, CN bands)  $\tilde{\nu}/\text{cm}^{-1}$ : 2135 (w);

**Compound A<sub>2</sub>B<sub>6</sub>**

Yield: 52 mg (61% referred to [Cu(CH<sub>3</sub>CN)<sub>4</sub>][Al{OC(CF<sub>3</sub>)<sub>3</sub>]<sub>4</sub>])

Elemental analysis, calcd (%) for C<sub>154</sub>H<sub>100</sub>Al<sub>2</sub>Cu<sub>4</sub>F<sub>72</sub>N<sub>4</sub>O<sub>8</sub>P<sub>8</sub> (4058.33 g/mol): C, 45.58; H, 2.48; N, 1.38; found: C, 45.20; H, 2.32; N, 1.26;

IR (solid, CN bands):  $\tilde{\nu}/\text{cm}^{-1}$ : 2097 (w), 2220 (w);

IR after transition (solid, CN bands)  $\tilde{\nu}/\text{cm}^{-1}$ : 2132 (w);

**Compound A<sub>2</sub>B<sub>7</sub>**

Yield: 36 mg (42% referred to  $[\text{Cu}(\text{CH}_3\text{CN})_4][\text{Al}\{\text{OC}(\text{CF}_3)_3\}_4]$ )

Elemental analysis, calcd (%) for  $\text{C}_{154}\text{H}_{100}\text{Al}_2\text{Cu}_4\text{F}_{72}\text{N}_4\text{O}_8\text{P}_8$  (4058.33 g/mol): C, 45.58; H, 2.48; N, 1.38; found: C, 45.53; H, 2.36; N, 1.28;

IR (solid, CN bands):  $\tilde{\nu}/\text{cm}^{-1}$ : 2100 (w), 2223 (w);

**Compound A<sub>3</sub>B<sub>4</sub>**

Yield: 21 mg (31% referred to  $[\text{Cu}(\text{CH}_3\text{CN})_3][\text{B}(\text{C}_6\text{H}_3\text{Cl}_2)_4]$ )

Elemental analysis, calcd (%) for  $\text{C}_{162}\text{H}_{122}\text{B}_2\text{Cl}_{16}\text{Cu}_4\text{N}_4\text{P}_8$  (3215.62 g/mol): C, 60.51; H, 3.82; N, 1.74; found: C, 60.41; H, 4.01; N, 1.50;

IR (solid, CN bands):  $\tilde{\nu}/\text{cm}^{-1}$ : 2101 (w);

IR after transition (solid, CN bands)  $\tilde{\nu}/\text{cm}^{-1}$ : 2160 (w);

**7.4.4 Crystallographic Data**

Single crystals of all compounds suitable for X-ray crystal analyses were obtained by slow diffusion of vapors of n-pentane into crude mother solutions. In the crystal lattices of the coordination complexes studied, dichloromethane solvent molecules were found in addition to the cationic coordination complexes and their counter-anions. These solvent molecules in most cases have a strong tendency to leave the bulk crystal via evaporation once the crystals are removed from their mother solution, a process that induce a rapid degradation of the single-crystal integrity of the crystals investigated. In order to slow down this process, single crystals of all these derivatives were always coated in paratone oil/Fomblin oil once removed from the mother solution, mounted at low temperature as quickly as possible on the diffractometer goniometer and X-ray data collection was performed at low temperature. Some solid state structures are only preliminary and could not be finalized during this work.

Single crystal data collection for **A<sub>2</sub>**, **A<sub>3</sub>**, **A<sub>1</sub>B<sub>4</sub>**, **A<sub>1</sub>B<sub>6</sub>**, **A<sub>1</sub>B<sub>7</sub>**, **A<sub>2</sub>B<sub>2</sub>**, **A<sub>2</sub>B<sub>4</sub>**, **A<sub>3</sub>B<sub>4</sub>** were performed at 150 K with a D8 Venture Bruker AXS (Centre de Diffractométrie, Université de Rennes 1, France) with Mo-K $\alpha$  radiation ( $\lambda = 0.71073 \text{ \AA}$ ), at 123 K with a GV50 diffractometer equipped with a TitanS2 detector (**A<sub>2</sub>B<sub>1a</sub>**, **A<sub>2</sub>B<sub>1b</sub>**, **A<sub>2</sub>B<sub>3</sub>**, **A<sub>2</sub>B<sub>7</sub>**) or at 123 K with a Xcalibur, AtlasS2, Gemini ultra diffractometer (**A<sub>1</sub>B<sub>5</sub>**), respectively.

For compounds **A<sub>2</sub>**, **A<sub>3</sub>**, **A<sub>1</sub>B<sub>4</sub>**, **A<sub>1</sub>B<sub>6</sub>**, **A<sub>1</sub>B<sub>7</sub>**, **A<sub>2</sub>B<sub>4</sub>**, **A<sub>2</sub>B<sub>2</sub>**, **A<sub>3</sub>B<sub>4</sub>** reflections were indexed, Lorentz-polarization corrected and integrated by the *DENZO* program of the KappaCCD software package. The data merging process was performed using the SCALEPACK



program.<sup>23</sup> Structure determinations were performed by direct methods with the solving program SIR97,<sup>24</sup> that revealed all the non-hydrogen atoms. SHELXL program<sup>25</sup> was used to refine the structures by full-matrix least-squares based on  $F^2$ .

The data collection and reduction were performed with **CrysAlisPro** [Version V1.171.40.14a, 2018 (**A<sub>1</sub>B<sub>5</sub>**, **A<sub>2</sub>B<sub>1b</sub>**, **A<sub>2</sub>B<sub>3</sub>**, **A<sub>2</sub>B<sub>7</sub>**), V1.171.41.54a, 2020 (**A<sub>2</sub>B<sub>1a</sub>**)].<sup>26</sup> For the compounds **A<sub>1</sub>B<sub>5</sub>** an analytical numeric absorption correction using a multifaceted crystal model based on expressions derived by R.C. Clark & J.S. Reid<sup>27</sup> and an empirical absorption correction using spherical harmonics as implemented in SCALE3 ABSPACK was applied. For the **A<sub>2</sub>B<sub>1a</sub>**, **A<sub>2</sub>B<sub>1b</sub>**, **A<sub>2</sub>B<sub>3</sub>**, **A<sub>2</sub>B<sub>7</sub>** a numerical absorption correction based on gaussian integration over a multifaceted crystal model and an empirical absorption correction using spherical harmonics as implemented in SCALE3 ABSPACK was applied. Using **Olex2**,<sup>28</sup> the structures were solved with **ShelXT**<sup>29</sup> and a least-square refinement on  $F^2$  was carried out with **ShelXL**<sup>30</sup> for all structures. All non-hydrogen atoms were refined with anisotropic displacement parameters. Hydrogen atoms were included in idealized positions and refined with isotropic displacement parameters.

The included dichloromethane solvent molecules (for derivatives **A<sub>1</sub>B<sub>4</sub>**, **A<sub>2</sub>B<sub>2</sub>**, **A<sub>2</sub>B<sub>4</sub>**, **A<sub>3</sub>B<sub>4</sub>**) were found to be highly disordered and a correct modelling of the disorder of these solvent molecules was not always possible leading to rather high anisotropic displacement parameters for some of their atoms. We have therefore proceeded to a 'squeeze' treatment<sup>31</sup> in order to remove the scattering contribution of these molecules which cannot be satisfactorily modelled (2 molecules of CH<sub>2</sub>Cl<sub>2</sub> for derivative **A<sub>1</sub>B<sub>4</sub>**, 4 CH<sub>2</sub>Cl<sub>2</sub> molecules and one pentane molecule for derivative **A<sub>2</sub>B<sub>2</sub>**, 2 CH<sub>2</sub>Cl<sub>2</sub> molecules for derivative **A<sub>2</sub>B<sub>4</sub>** and 7 CH<sub>2</sub>Cl<sub>2</sub> molecules for derivative **A<sub>3</sub>B<sub>4</sub>**). As a result, since these disordered molecules occupy a significant volume of the unit cell, several ALERTs A appear in the checkcif reports since "VERY LARGE Solvent Accessible VOIDS" are present in the structure resolution.

The data set of derivative **A<sub>3</sub>** has a low completeness what causes an ALERT B. This is only a preliminary structure and has to be measured again.

Compound **A<sub>2</sub>**: The asymmetric unit contains one half of the complex [Cu<sub>4</sub>(μ<sub>2</sub>-dppm)<sub>4</sub>(CN)<sub>2</sub>]<sup>2+</sup> and additionally one [Al{OC(CF<sub>3</sub>)<sub>3</sub>}]<sup>-</sup> anion. One of the {OC(CF<sub>3</sub>)<sub>3</sub>} units is disordered over at least two positions. The anion is not fully modeled yet.

Compound **A<sub>3</sub>**: The preliminary refinement shows an asymmetric unit containing three CH<sub>2</sub>Cl<sub>2</sub> molecules and half of the complex [Cu<sub>4</sub>(μ<sub>2</sub>-dppm)<sub>4</sub>(CN)<sub>2</sub>]<sup>2+</sup> and additionally one

[B(C<sub>6</sub>H<sub>3</sub>Cl<sub>2</sub>)<sub>4</sub>] anion. The measurement only has a completeness of 96% and has to be repeated.

Compound **A<sub>1</sub>B<sub>4</sub>**: The asymmetric unit contains two CH<sub>2</sub>Cl<sub>2</sub> molecules which were squeezed causing an ALERT A in the checkcif report. The squeeze does not change the R<sub>1</sub> factor. Furthermore, the asymmetric unit contains half of [Cu<sub>4</sub>(μ<sub>2</sub>-dppm)<sub>4</sub>(CN)<sub>2</sub>]<sup>2+</sup> and additionally one PF<sub>6</sub><sup>-</sup> anion.

Compound **A<sub>1</sub>B<sub>5</sub>**: The asymmetric unit contains two CH<sub>2</sub>Cl<sub>2</sub> solvent molecules, which are respectively disordered over two positions (70:30; 80:20). Further, the asymmetric unit contains one half of the complex [Cu<sub>4</sub>(μ<sub>2</sub>-dppm)<sub>4</sub>(CN)<sub>2</sub>]<sup>2+</sup> and additionally one PF<sub>6</sub><sup>-</sup> anion. The anion is also disordered over two positions (75:25). To describe these disorders the FLAT, DFIX, SADI, SIMU, RIGU and ISOR restraints were applied.

Compound **A<sub>1</sub>B<sub>6</sub>**: The asymmetric unit contains two PF<sub>6</sub><sup>-</sup> anions, two halves of the complex [Cu<sub>4</sub>(μ<sub>2</sub>-dppm)<sub>4</sub>(CN)<sub>2</sub>]<sup>2+</sup> and one linker molecule.

Compound **A<sub>1</sub>B<sub>7</sub>**: The asymmetric unit contains two CH<sub>2</sub>Cl<sub>2</sub> solvent molecules, one PF<sub>6</sub><sup>-</sup> anion, one half of the complex [Cu<sub>4</sub>(μ<sub>2</sub>-dppm)<sub>4</sub>(CN)<sub>2</sub>]<sup>2+</sup> and one half of the linker molecule.

Compound **A<sub>2</sub>B<sub>1a</sub>**: The asymmetric unit contains two halves of the complex [Cu<sub>4</sub>(μ<sub>2</sub>-dppm)<sub>4</sub>(CN)<sub>2</sub>]<sup>2+</sup>, one linker molecule and two [Al{OC(CF<sub>3</sub>)<sub>3</sub>}<sub>4</sub>]<sup>-</sup> anions. Both of the anions are disordered over more positions. To describe these disorders the FLAT, DFIX, SADI, SIMU, RIGU and ISOR restraints were applied.

Compound **A<sub>2</sub>B<sub>1b</sub>**: The asymmetric unit contains one half of the complex [Cu<sub>4</sub>(μ<sub>2</sub>-dppm)<sub>4</sub>(CN)<sub>2</sub>]<sup>2+</sup>, one linker molecule and one [Al{OC(CF<sub>3</sub>)<sub>3</sub>}<sub>4</sub>]<sup>-</sup> anion. One of the {OC(CF<sub>3</sub>)<sub>3</sub>} units is disordered over two positions (79:21). To describe these disorders the FLAT, DFIX, SADI, SIMU, RIGU and ISOR restraints were applied.

Compound **A<sub>2</sub>B<sub>2</sub>**: The preliminary asymmetric unit contains four CH<sub>2</sub>Cl<sub>2</sub> molecules and one *n*-pentane molecule which were squeezed causing an ALERT A. In addition, the asymmetric unit contains two [Al{OC(CF<sub>3</sub>)<sub>3</sub>}<sub>4</sub>]<sup>-</sup> anions, two halves of the complex [Cu<sub>4</sub>(μ<sub>2</sub>-dppm)<sub>4</sub>(CN)<sub>2</sub>]<sup>2+</sup> and one linker molecule. One of the {OC(CF<sub>3</sub>)<sub>3</sub>} units is disordered over two positions. It was necessary to apply isotropic displacement parameters to some of the atoms in these ponderations, implying several ALERTs in the checkcif report.

Compound **A<sub>2</sub>B<sub>3</sub>**: The asymmetric unit contains one half of the complex [Cu<sub>4</sub>(μ<sub>2</sub>-dppm)<sub>4</sub>(CN)<sub>2</sub>]<sup>2+</sup> and one linker molecule and additionally one [Al{OC(CF<sub>3</sub>)<sub>3</sub>}<sub>4</sub>]<sup>-</sup> anion. Two of the {OC(CF<sub>3</sub>)<sub>3</sub>} units are disordered over two positions (68:32; 66:34). To describe these disorders the FLAT, DFIX, SADI, SIMU, RIGU and ISOR restraints were applied.

Compound **A<sub>2</sub>B<sub>4</sub>**: The asymmetric unit contains one half of the complex  $[\text{Cu}_4(\mu_2\text{-dppm})_4(\text{CN})_2]^{2+}$ , one half of the linker molecule, one  $[\text{Al}\{\text{OC}(\text{CF}_3)_3\}_4]$  anion and additionally two  $\text{CH}_2\text{Cl}_2$  molecules, which were squeezed causing an ALERT A in the checkcif report.

Compound **A<sub>2</sub>B<sub>7</sub>**: The asymmetric unit contains one half of the complex  $[\text{Cu}_4(\mu_2\text{-dppm})_4(\text{CN})_2]^{2+}$ , one half of the linker molecule, one  $[\text{Al}\{\text{OC}(\text{CF}_3)_3\}_4]$  anion and additionally three  $\text{CH}_2\text{Cl}_2$  molecules. Two of the solvent molecules are disordered over two positions (70:30; 50:50). To describe these disorders the FLAT, DFIX, SADI, SIMU, RIGU and ISOR restraints were applied.

Compound **A<sub>3</sub>B<sub>4</sub>**: The preliminary asymmetric unit contains seven  $\text{CH}_2\text{Cl}_2$  molecules which were squeezed causing an ALERT A in the checkcif report. In addition, one  $\text{BArCl}$  anion was found highly disordered over two positions. This leaves a high residual density causing several ALERTs in the checkcif report.

Tables S7.1-S7.3 give the crystallographic data for all derivatives, the values for compounds **A<sub>1</sub>B<sub>4</sub>**, **A<sub>2</sub>B<sub>2</sub>**, **A<sub>2</sub>B<sub>4</sub>**, **A<sub>3</sub>B<sub>4</sub>** are depicted after the 'squeeze' treatment.

**Table S7.1.** Crystallographic data and details of diffraction experiments for compounds **A<sub>2</sub>**, **A<sub>3</sub>**, **A<sub>1</sub>B<sub>4</sub>**, **A<sub>1</sub>B<sub>5</sub>**.

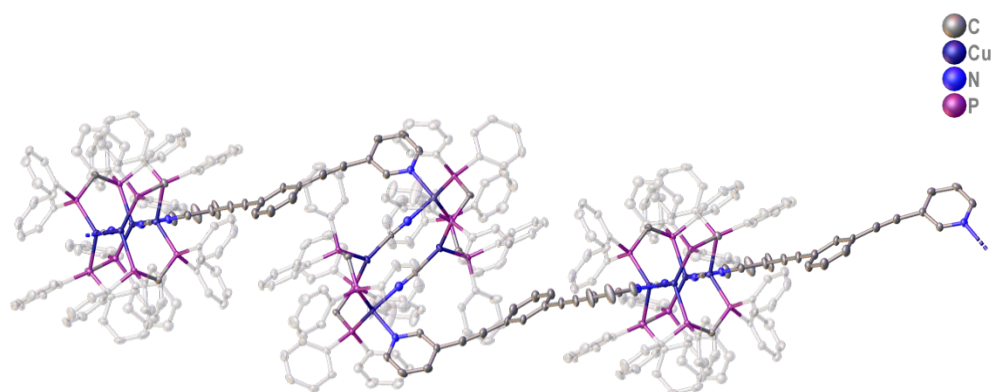
Compound	<b>A<sub>2</sub></b>	<b>A<sub>3</sub></b>	<b>A<sub>1</sub>B<sub>4</sub></b>	<b>A<sub>1</sub>B<sub>5</sub></b>
Data set (internal naming)	jsr41	jsr6	fm6	js153
Formula	C <sub>134</sub> H <sub>88</sub> F <sub>72</sub> Al <sub>2</sub> P <sub>8</sub> Cl Cu <sub>4</sub> N <sub>2</sub> O <sub>8</sub>	C <sub>156</sub> H <sub>124</sub> B <sub>2</sub> Cl <sub>28</sub> Cu <sub>4</sub> N <sub>2</sub> P <sub>8</sub>	C <sub>57</sub> H <sub>49</sub> ClCu <sub>2</sub> F <sub>6</sub> N <sub>2</sub> P <sub>5</sub>	C <sub>120</sub> Cl <sub>12</sub> Cu <sub>4</sub> F <sub>12</sub> H <sub>112</sub> N <sub>4</sub> P <sub>10</sub>
<i>D</i> <sub>calc.</sub> / g cm <sup>-3</sup>	1.659	1.495	1.291	1.485
<i>m</i> /mm <sup>-1</sup>	0.795	1.141	0.903	1.110
Formula Weight	3777.94	3542.71	1157.91	2827.39
Colour	white	white	yellow	colourless
Shape	block	block	block	block
Size/mm <sup>3</sup>	0.24×0.14×0.10	0.18×0.14×0.11	0.20×0.16×0.11	0.30×0.20×0.15
<i>T</i> /K	150(2)	150(2)	150(2)	123.0
Crystal System	triclinic	monoclinic	triclinic	monoclinic
Space Group	<i>P</i> $\bar{1}$	<i>P</i> <sub>2</sub> <sub>1</sub> / <i>n</i>	<i>P</i> $\bar{1}$	<i>P</i> <sub>2</sub> <sub>1</sub> / <i>n</i>
<i>a</i> /Å	15.266(2)	20.792(3)	13.003(2)	15.9335(7)
<i>b</i> /Å	16.105(2)	15.104(2)	14.326(2)	23.7619(9)
<i>c</i> /Å	16.751(2)	26.935(4)	18.407(2)	16.7993(6)
<i>a</i> <sup>o</sup>	103.655(4)	90	67.527(4)	90
<i>b</i> <sup>o</sup>	101.600(4)	111.526(5)	71.071(4)	96.028(4)
<i>γ</i> <sup>o</sup>	101.694(4)	90	77.265(4)	90
<i>V</i> /Å <sup>3</sup>	3782.4(8)	7869(2)	2978.8(7)	6325.2(4)
<i>Z</i>	1	2	2	2
<i>Z</i> '	0.5	0.5	1	0.5
Wavelength/Å	0.71069	0.71069	0.71069	0.71073
Radiation type	MoK <sub>α</sub>	MoK <sub>α</sub>	MoK <sub>α</sub>	MoK <sub>α</sub>
<i>θ</i> <sub>min</sub> <sup>o</sup>	2.55	2.11	2.15	3.420
<i>θ</i> <sub>max</sub> <sup>o</sup>	27.27	27.31	27.56	27.102
Measured Refl.	83843	72473	51085	37825
Independent Refl.	16913	16956	13714	13903
Reflections with >2σ (I)	12789	11966	12123	10483
<i>R</i> <sub>int</sub>	0.0951	0.1036	0.0223	0.0400
Parameters	997	901	651	820
Restraints	0	0	0	375
Largest Peak	1.531	0.858	0.622	0.986
Deepest Hole	-1.376	-0.567	-0.554	-0.429
GooF	1.027	1.042	1.101	1.017
<i>wR</i> <sub>2</sub> (all data)	0.2092	0.1255	0.1017	0.1204
<i>wR</i> <sub>2</sub>	0.1850	0.1116	0.0993	0.1102
<i>R</i> <sub>1</sub> (all data)	0.0962	0.0968	0.0392	0.0723
<i>R</i> <sub>1</sub>	0.0713	0.0589	0.0352	0.0494
Solution	ShelXS-97 (Sheldrick, 1990)	ShelXS-97 (Sheldrick, 1990)	ShelXS-97 (Sheldrick, 1990)	ShelXT (Sheldrick, 2015)
Refinement	ShelXL-97 (Sheldrick, 1997)	ShelXL-97 (Sheldrick, 1997)	ShelXL-97 (Sheldrick, 1997)	ShelXL 2018/3 (Sheldrick, 2015)

**Table S7.2.** Crystallographic data and details of diffraction experiments for compounds **A<sub>1</sub>B<sub>6</sub>**, **A<sub>1</sub>B<sub>7</sub>**, **A<sub>2</sub>B<sub>1a</sub>**, **A<sub>2</sub>B<sub>1b</sub>**.

Compound	A <sub>1</sub> B <sub>6</sub>	A <sub>1</sub> B <sub>7</sub>	A <sub>2</sub> B <sub>1a</sub>	A <sub>2</sub> B <sub>1b</sub>
Data set (internal naming)	jsr1	jsr3	js111_2	js111_cu_dw
Formula	C <sub>122</sub> H <sub>100</sub> ClCu <sub>4</sub> F <sub>12</sub> N <sub>4</sub> P <sub>10</sub>	C <sub>63</sub> H <sub>54</sub> Cl <sub>4</sub> Cu <sub>2</sub> F <sub>6</sub> N <sub>2</sub> P <sub>5</sub>	Al <sub>2</sub> C <sub>146.3</sub> Cl <sub>4.6</sub> Cu <sub>4</sub> F <sub>72</sub> H <sub>100.6</sub> N <sub>4</sub> O <sub>8.04</sub> P <sub>8</sub>	C <sub>77</sub> H <sub>52</sub> AlCu <sub>2</sub> F <sub>36</sub> N <sub>3</sub> O <sub>4</sub> P <sub>4</sub>
<i>D</i> <sub>calc.</sub> / g cm <sup>-3</sup>	1.130	1.476	1.602	1.602
<i>m</i> /mm <sup>-1</sup>	0.761	1.048	3.229	2.609
Formula Weight	2413.92	1376.81	4130.09	2045.15
Colour	white	white	dark orange	colorless
Shape	block	plate	block	block
Size/mm <sup>3</sup>	0.24×0.19×0.13	0.15×0.10×0.07	0.20×0.11×0.09	0.19×0.12×0.12
<i>T</i> /K	150(2)	150(2)	123.01(10)	100.00(10)
Crystal System	monoclinic	triclinic	triclinic	triclinic
Space Group	<i>P</i> 2 <sub>1</sub> / <i>n</i>	<i>P</i> $\bar{1}$	<i>P</i> $\bar{1}$	<i>P</i> $\bar{1}$
<i>a</i> /Å	22.618(2)	14.955(2)	16.1962(3)	15.3998(2)
<i>b</i> /Å	20.254(2)	15.537(2)	17.5331(3)	17.1112(3)
<i>c</i> /Å	32.549(4)	16.121(2)	30.7150(4)	18.5856(3)
<i>a</i> <sup>o</sup>	90.00	84.351(4)	90.6020(10)	64.762(2)
<i>b</i> <sup>o</sup>	107.878(4)	66.773(3)	99.6830(10)	73.7470(10)
<i>γ</i> <sup>o</sup>	90.00	64.601(3)	94.9150(10)	79.1130(10)
<i>V</i> /Å <sup>3</sup>	14191(3)	3098.2(2)	8563.5(2)	4239.28(13)
<i>Z</i>	4	2	2	2
<i>Z</i> '	1	1	1	1
Wavelength/Å	0.71073	0.71069	1.54184	1.54184
Radiation type	MoK <sub>α</sub>	MoK <sub>α</sub>	Cu K <sub>α</sub>	Cu K <sub>α</sub>
$\Theta_{min}$ <sup>o</sup>	2.06	2.09	3.352	2.697
$\Theta_{max}$ <sup>o</sup>	27.35	27.53	73.851	74.508
Measured Refl.	430858	69928	96008	79804
Independent Refl.	31915	14165	33616	16521
Reflections with >2 $\sigma$ ( <i>I</i> )	25890	12485	27068	15621
<i>R</i> <sub>int</sub>	0.0979	0.0289	0.0578	0.0184
Parameters	1364	740	3503	1271
Restraints	0	0	2115	73
Largest Peak	0.746	1.695	1.225	0.492
Deepest Hole	-0.858	-1.200	-0.673	-0.470
Goof	1.050	1.039	1.011	1.040
<i>wR</i> <sub>2</sub> (all data)	0.1251	0.1192	0.1508	0.0882
<i>wR</i> <sub>2</sub>	0.1168	0.1127	0.1404	0.0870
<i>R</i> <sub>1</sub> (all data)	0.0745	0.0502	0.0673	0.0351
<i>R</i> <sub>1</sub>	0.0537	0.0432	0.0549	0.0334
Solution	ShelXS-97 (Sheldrick, 1990)	ShelXS-97 (Sheldrick, 1990)	ShelXT (Sheldrick, 2015)	ShelXT (Sheldrick, 2015)
Refinement	ShelXL-97 (Sheldrick, 1997)	ShelXL-97 (Sheldrick, 1997)	ShelXL 2018/3 (Sheldrick, 2015)	ShelXL 2018/3 (Sheldrick, 2015)

**Table S7.3.** Crystallographic data and details of diffraction experiments for compounds **A<sub>2</sub>B<sub>2</sub>**, **A<sub>2</sub>B<sub>3</sub>**, **A<sub>2</sub>B<sub>6</sub>**, **A<sub>2</sub>B<sub>7</sub>**.

Compound	A <sub>2</sub> B <sub>2</sub>	A <sub>2</sub> B <sub>3</sub>	A <sub>2</sub> B <sub>4</sub>	A <sub>2</sub> B <sub>7</sub>
Data set (internal naming)	fm33	fm38	jsr21	js105
Formula	C <sub>145</sub> H <sub>96</sub> Al <sub>2</sub> ClCu <sub>4</sub> F <sub>72</sub> N <sub>3</sub> O <sub>8</sub> P <sub>8</sub>	AlC <sub>74.5</sub> Cl <sub>3</sub> Cu <sub>2</sub> F <sub>36</sub> H <sub>50</sub> N <sub>2</sub> O <sub>4</sub> P <sub>4</sub>	C <sub>73</sub> H <sub>49</sub> AlClCu <sub>2</sub> F <sub>36</sub> N <sub>2</sub> O <sub>4</sub> P <sub>4</sub>	C <sub>160</sub> H <sub>116.72</sub> Al <sub>2</sub> Cl <sub>12</sub> Cu <sub>4</sub> F <sub>72</sub> N <sub>4</sub> O <sub>8</sub> P <sub>8</sub>
<i>D</i> <sub>calc.</sub> / g cm <sup>-3</sup>	1.408	1.636	1.531	1.552
<i>m</i> /mm <sup>-1</sup>	0.651	3.445	0.704	3.796
Formula Weight	3932.13	2105.45	1980.08	4572.57
Colour	white	clear light yellow	white	colorless
Shape	rod	hexagonal	block	block
Size/mm <sup>3</sup>	0.25×0.10×0.08	0.54×0.30×0.25	0.29×0.22×0.19	0.65×0.27×0.16
<i>T</i> /K	150(2)	123.00(10)	150(2)	123.01(10)
Crystal System	triclinic	triclinic	triclinic	triclinic
Space Group	<i>P</i> $\bar{1}$	<i>P</i> $\bar{1}$	<i>P</i> $\bar{1}$	<i>P</i> $\bar{1}$
<i>a</i> /Å	19.062(4)	15.6580(5)	15.745(2)	16.5068(3)
<i>b</i> /Å	21.324(4)	17.1731(8)	17.263(2)	16.6060(4)
<i>c</i> /Å	24.783(4)	18.6088(6)	18.504(2)	18.2602(4)
<i>a</i> <sup>o</sup>	86.130(6)	63.166(4)	63.103(4)	91.918(2)
<i>b</i> <sup>o</sup>	78.772(6)	73.559(3)	73.704(4)	101.159(2)
<i>γ</i> <sup>o</sup>	69.840(6)	79.585(3)	79.280(4)	94.197(2)
<i>V</i> /Å <sup>3</sup>	9276(3)	4274.2(3)	4295.0(9)	4891.73(19)
<i>Z</i>	2	2	2	1
<i>Z</i> '	1	1	1	0.5
Wavelength/Å	0.71073	1.54184	0.71069	1.54184
Radiation type	MoK <sub>α</sub>	CuK <sub>α</sub>	MoK <sub>α</sub>	CuK <sub>α</sub>
<i>θ</i> <sub>min</sub> <sup>o</sup>	2.20	3.532	2.19	3.549
<i>θ</i> <sub>max</sub> <sup>o</sup>	27.82	74.164	27.54	75.936
Measured Refl.	197654	32834	96007	33241
Independent Refl.	42689	16786	19613	19469
Reflections with >2σ (I)	28086	14599	13901	17318
<i>R</i> <sub>int</sub>	0.0924	0.0597	0.0697	0.0311
Parameters	2024	1327	1101	1270
Restraints	0	347	0	130
Largest Peak	2.321	0.962	1.421	0.0917
Deepest Hole	-1.647	-0.573	-1.059	-1.008
Goof	1.111	1.018	1.108	1.044
<i>wR</i> <sub>2</sub> (all data)	0.3195	0.1461	0.2211	0.1744
<i>wR</i> <sub>2</sub>	0.2952	0.1393	0.2016	0.1671
<i>R</i> <sub>1</sub> (all data)	0.1378	0.0569	0.1038	0.0702
<i>R</i> <sub>1</sub>	0.1053	0.0514	0.0774	0.0636
Solution	ShelXS-97 (Sheldrick, 1990)	ShelXT (Sheldrick, 2015)	ShelXS-97 (Sheldrick, 1990)	ShelXT (Sheldrick, 2015)
Refinement	ShelXL-97 (Sheldrick, 1997)	ShelXL 2018/3 (Sheldrick, 2015)	ShelXL-97 (Sheldrick, 1997)	ShelXL 2018/3 (Sheldrick, 2015)

**Additional view of solid-state structure of compounds  $A_1B_6$  and  $A_1B_1$** 

**Figure S7.1.** Side view of the solid-state structure of compound  $A_1B_6$ . Anions and hydrogen atoms are omitted and phenyl rings are depicted transparent for clarity. Thermal ellipsoids are shown at 50% probability level.

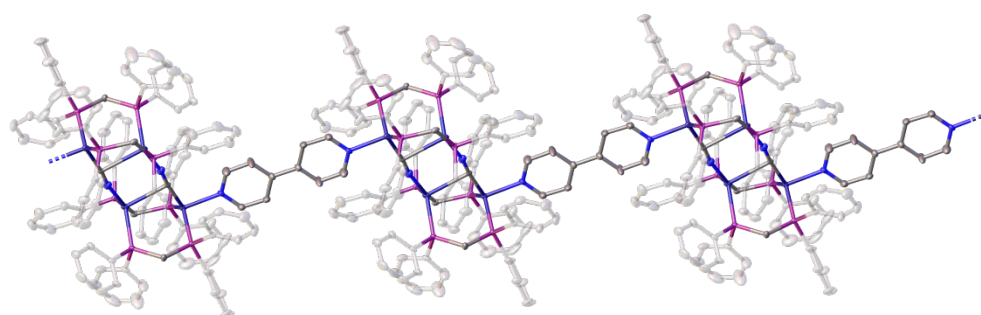


**Figure S7.2.** Solid-state structure of compound  $A_1B_1$ . Anions and hydrogen atoms are omitted and phenyl rings are depicted transparent for clarity. Thermal ellipsoids are shown at 50% probability level.

### 7.4.5 Additional Variable Temperature UV-Vis Spectra of Compounds $A_2$ , $A_3$ and $A_1B_4$

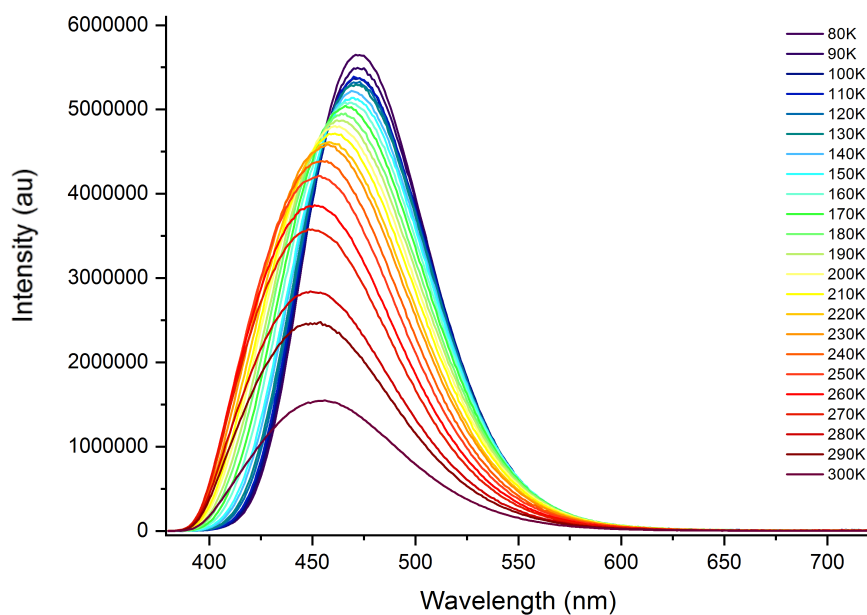


**Figure S7.3.** Solid-state emission spectra of  $A_2$  at different temperatures between 300 K and 80 K upon excitation at 325 nm.

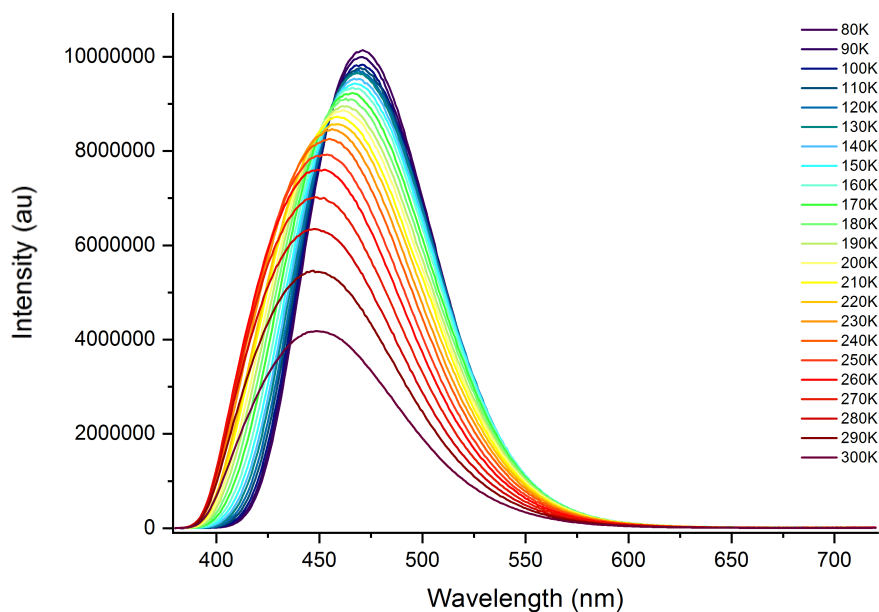


**Figure S7.4.** Solid-state emission spectra of  $A_2$  at different temperatures between 300 K and 80 K upon excitation at 360 nm.



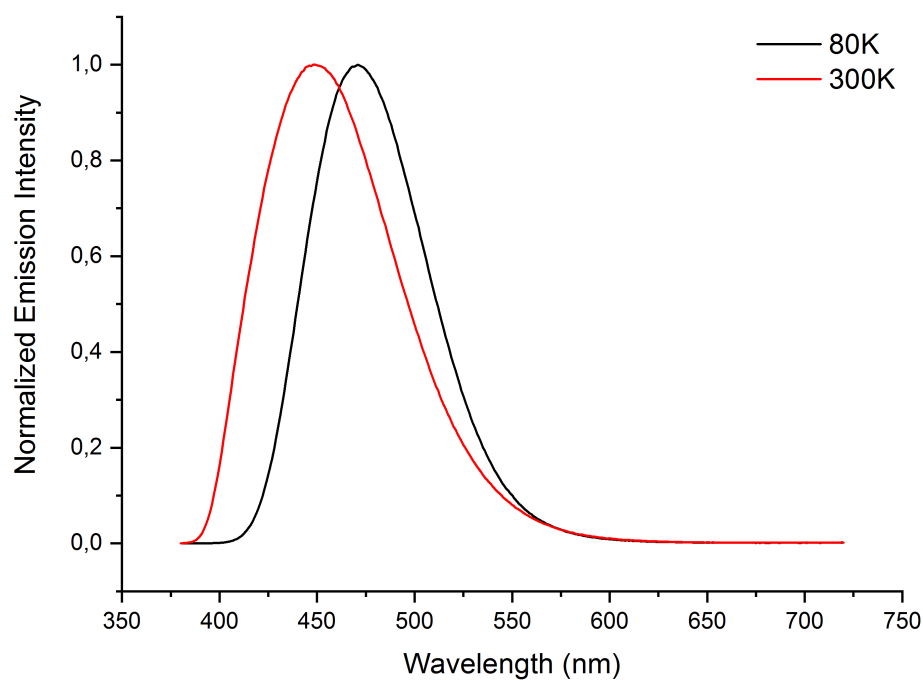


**Figure S7.5.** Solid-state emission spectra of  $A_2$  at 300 K and at 80 K upon excitation at 360 nm.

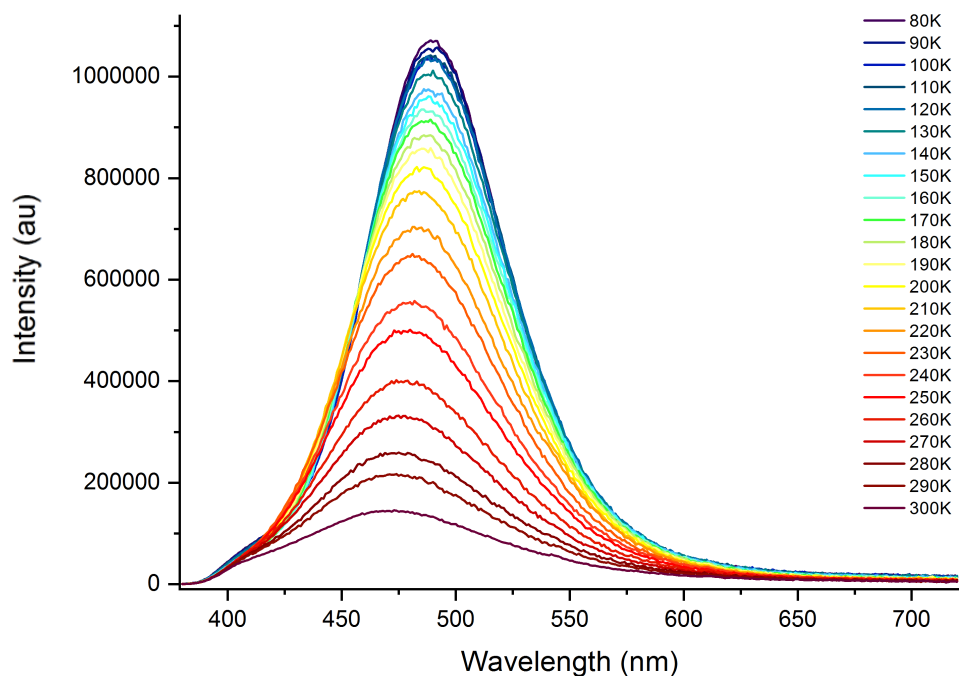


**Figure S7.6.** Solid-state emission spectra of  $A_3$  at different temperatures between 300 K and 80 K upon excitation at 325 nm.

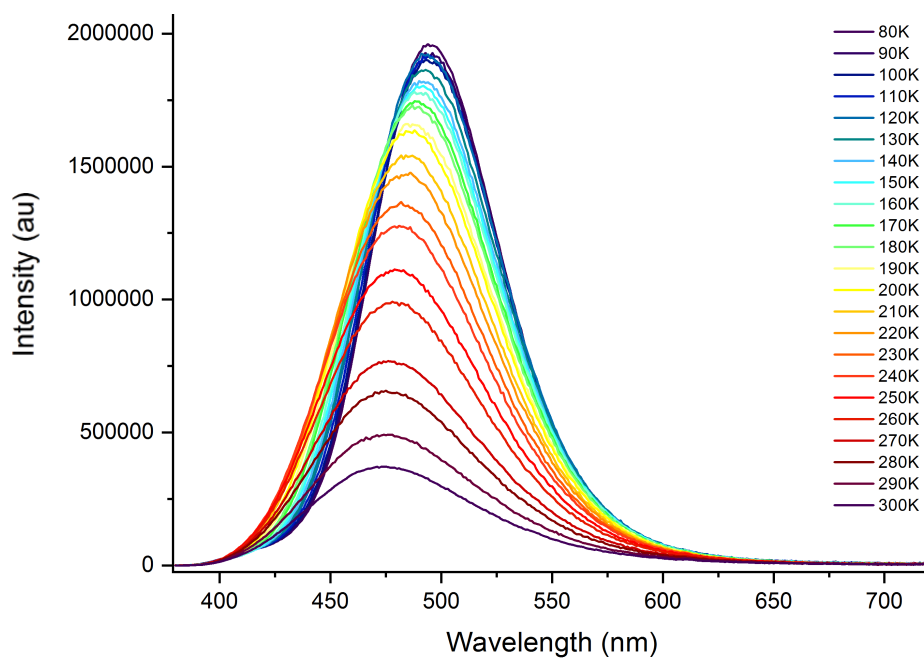


**Figure S7.7.** Solid-state emission spectra of  $A_3$  at different temperatures between 300 K and 80 K upon excitation at 360 nm.

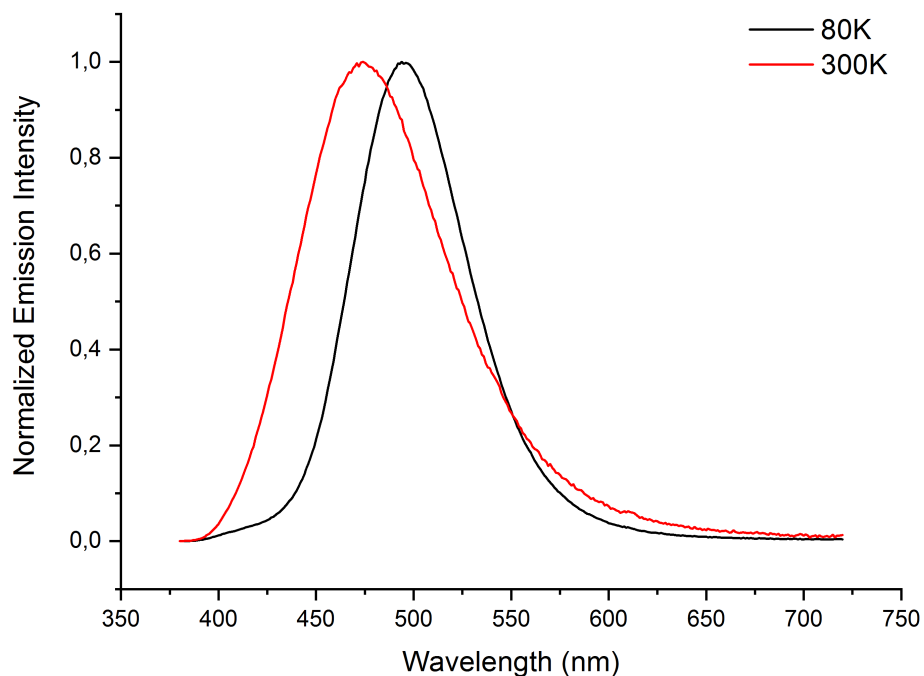


**Figure S7.8.** Solid-state emission spectra of  $A_3$  at 300 K and at 80 K upon excitation at 360 nm.

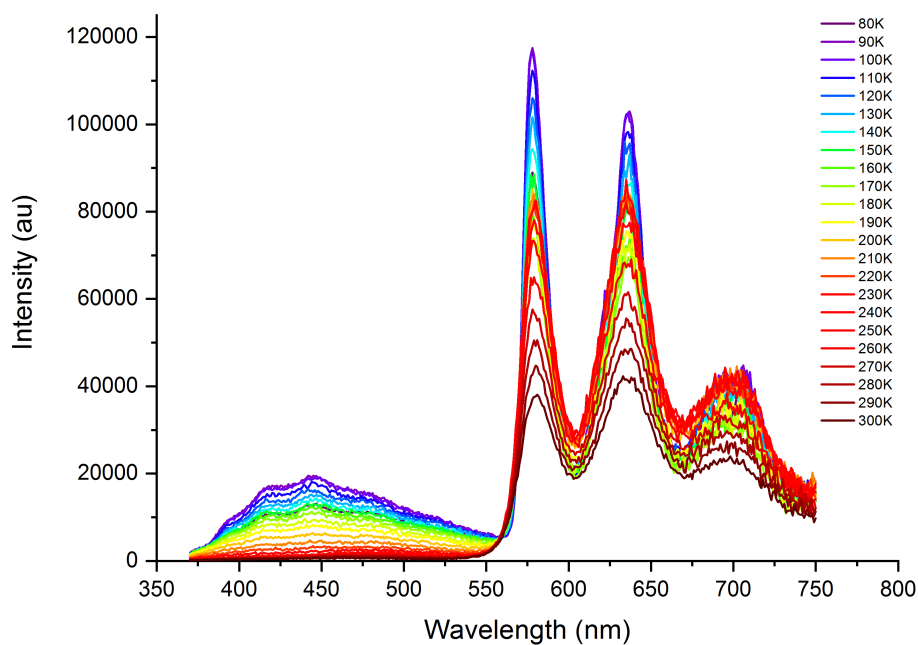


**Figure S7.9.** Solid-state emission spectra of  $A_1B_4$  at different temperatures between 300 K and 80 K upon excitation at 325 nm.

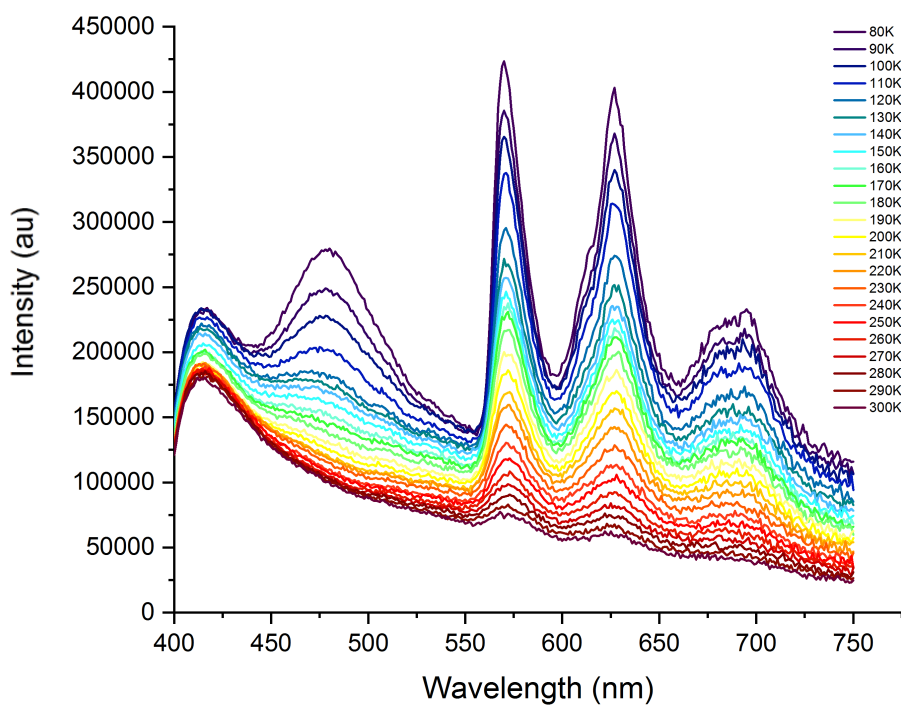


**Figure S7.10.** Solid-state emission spectra of  $A_2B_4$  at different temperatures between 300 K and 80 K upon excitation at 320 nm.

### 7.4.6 Variable Temperature Excited State Lifetimes of A<sub>2</sub>

Further measurements at higher temperatures have to be done to determine if a Thermally Activated Delayed Fluorescence is present, due to the absence of a plateau region at the range of the highest temperature measured so far.

**Table S7.4.** Calculated values for the excited state lifetimes of A<sub>2</sub> from 80K to 300K.

TEMPERATURE/K	BI-EXP. LIFETIME/ $\mu$ S	BI-EXP. LIFETIME/ $\mu$ S	MONO-EXP. LIFETIME/ $\mu$ S
80	298	158	234
90	281	130	233
100	306	168	230
110	300	166	22
120	315	175	217
130	316	176	210
140	316	175	205
150	298	172	200
160	288	168	192
170	266	162	186
180	263	158	178
190	238	150	171
200	237	145	162
210	232	129	156
220	206	128	145
230	198	121	135
240	185	114	126
250	169	102	113
260	152	92	103
270	158	82	91
280	142	70	78
290	104	55	68
300	84	42	58

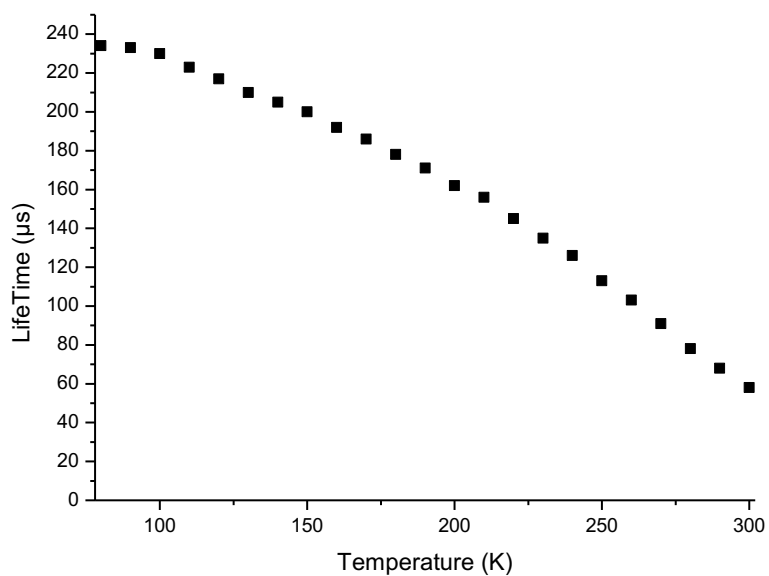


**Figure S7.11.** Plot of the mono-exponential excited state lifetimes of  $A_2$  from 80 K to 300 K.

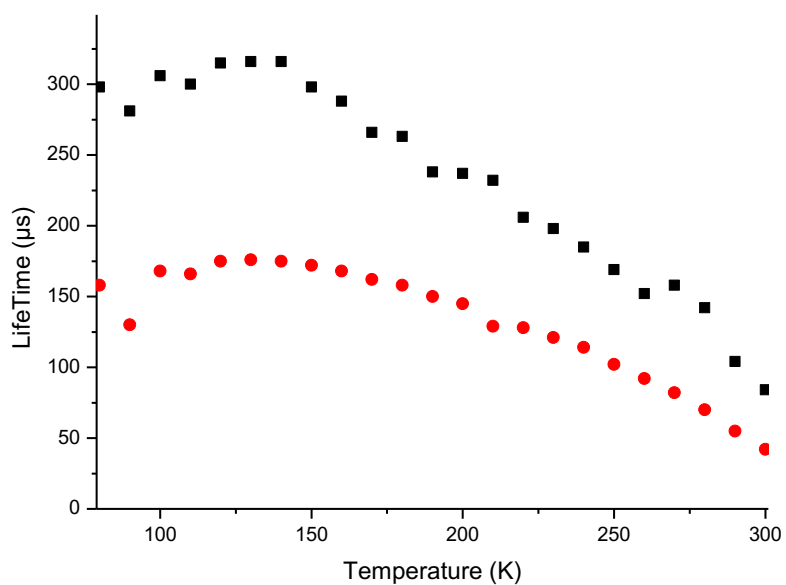


**Figure S7.12.** Plot of the bi-exponential excited state lifetimes of  $A_2$  from 80 K to 300 K.

### 7.4.7 Thermogravimetric Analyses and Differential Scanning Calorimetry

The samples were heated from room temperature up to 270.00 °C with a rate of 5.00 °C/min and a nitrogen gas flow of 100.0 mL/min. The temperature was held at 270.00 °C for five minutes before cooling again.

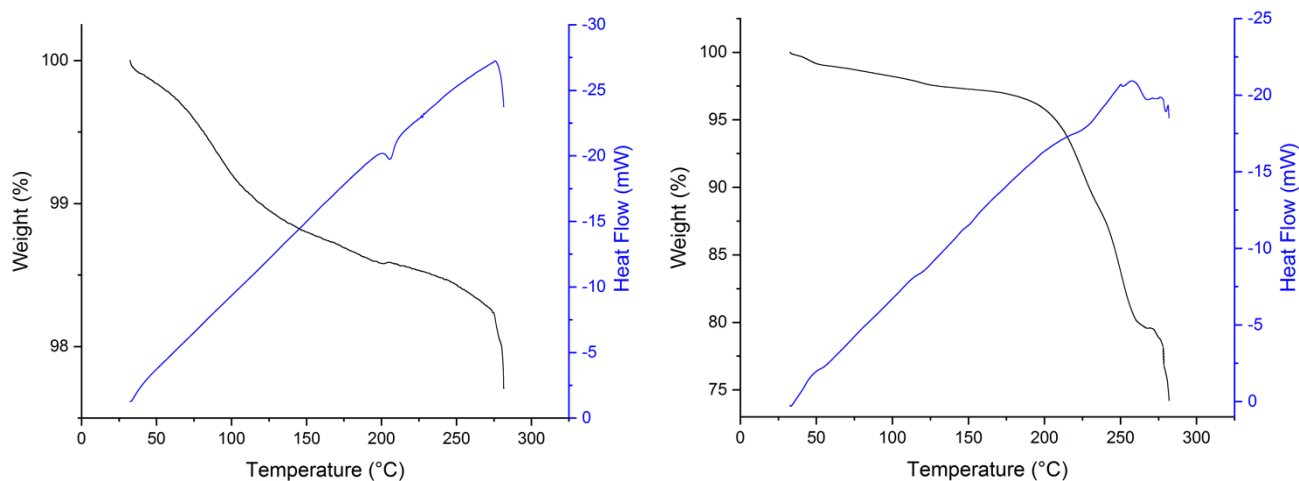


Figure S7.13. TGA-DSC of compound **A<sub>2</sub>** (left) and compound **A<sub>3</sub>** (right).

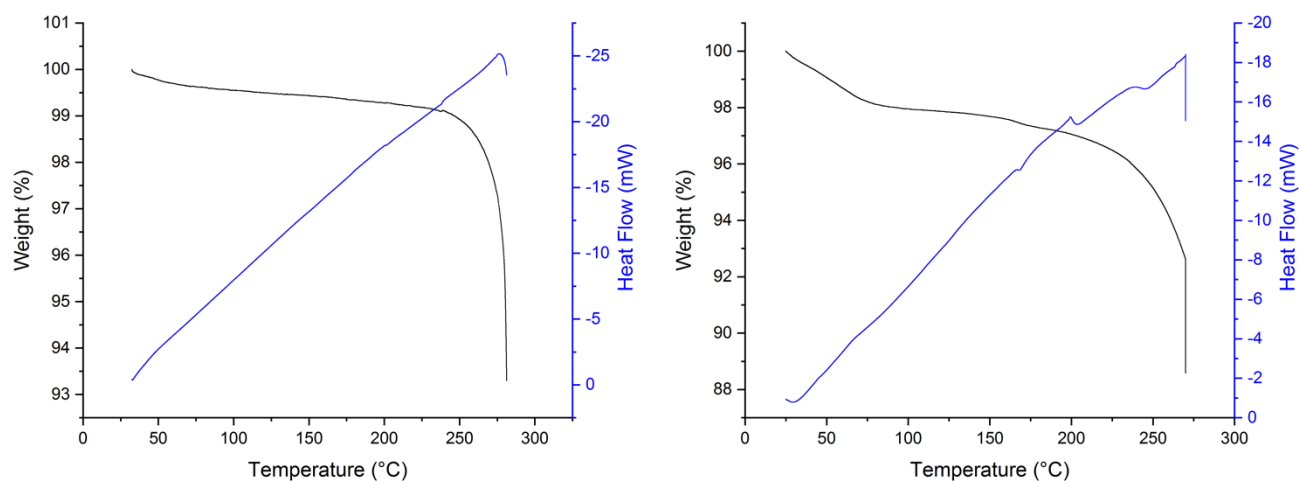


Figure S7.14. TGA-DSC of compound **A<sub>1</sub>B<sub>4</sub>** (left) and compound **A<sub>1</sub>B<sub>7</sub>** (right).

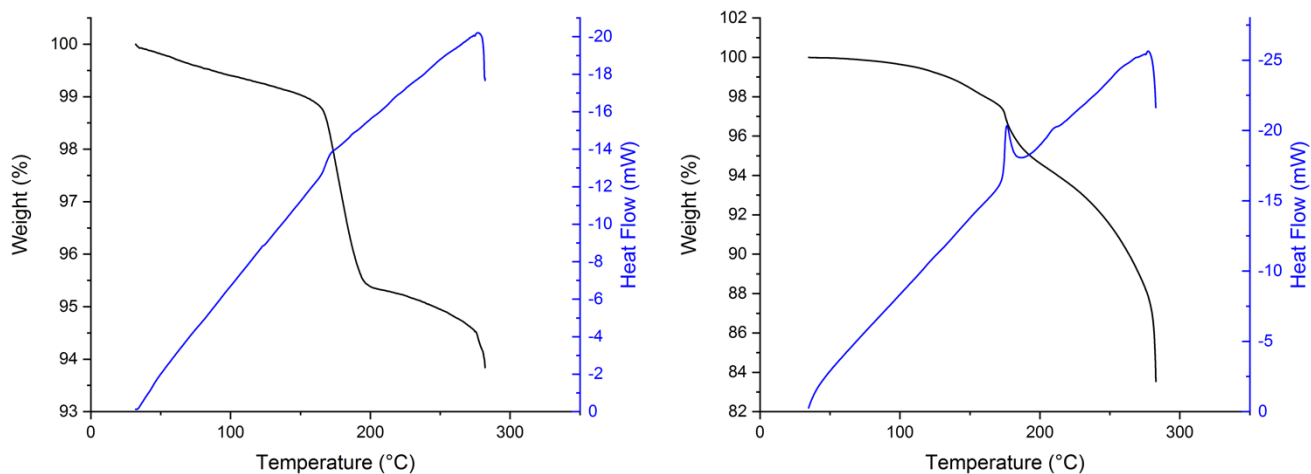


Figure S7.15. TGA-DSC of compound  $A_2B_{1a}$  (left) and compound  $A_2B_{1b}$  (right).

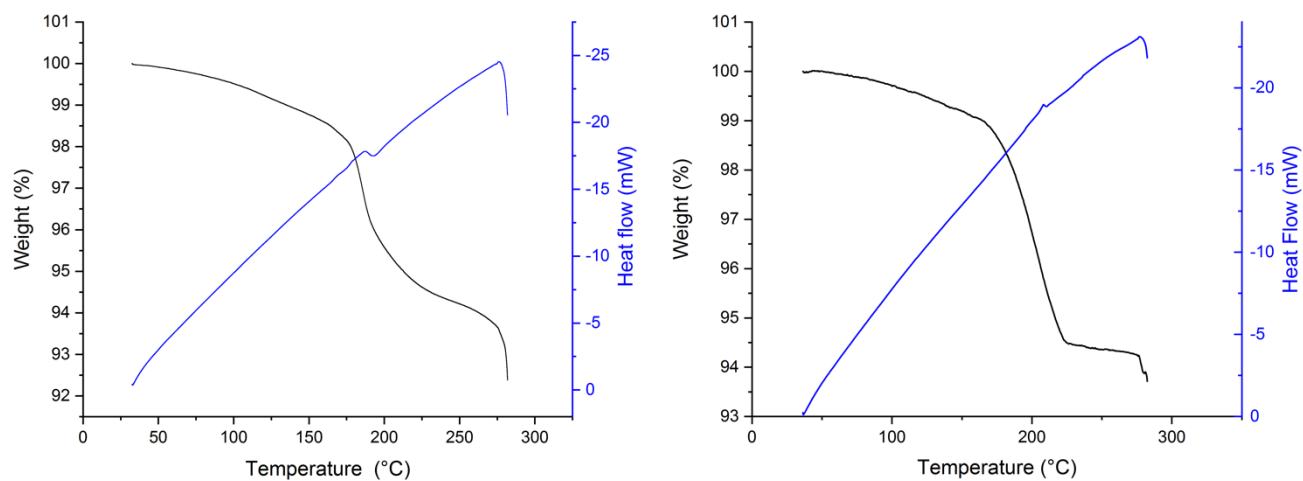


Figure S7.16. TGA-DSC of compound  $A_2B_3$  (left) and compound  $A_2B_4$  (right).

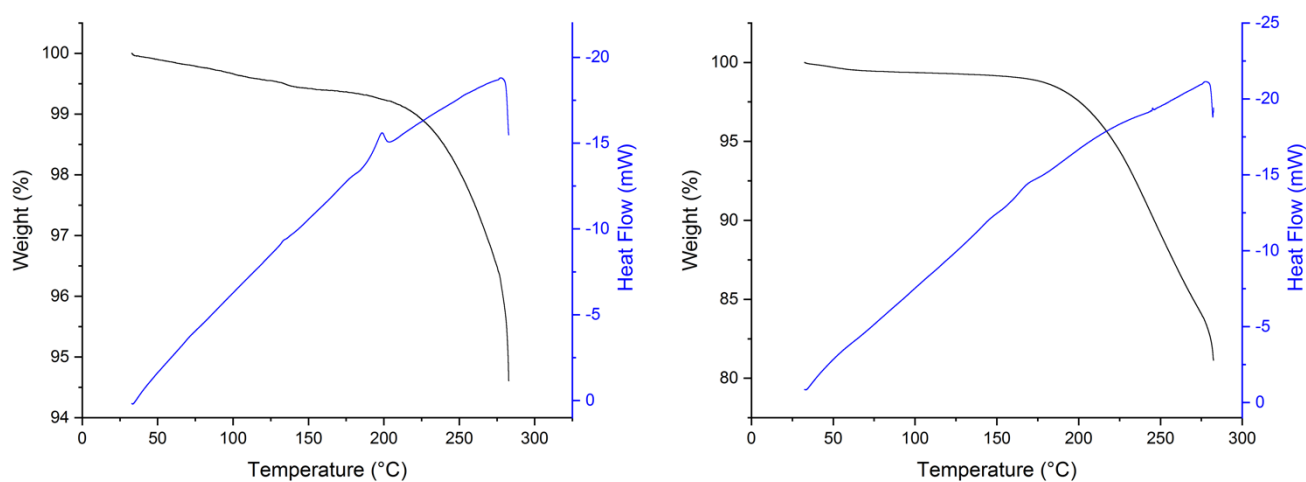


Figure S7.17. TGA-DSC of compound  $A_2B_6$  (left) and compound  $A_2B_7$  (right).

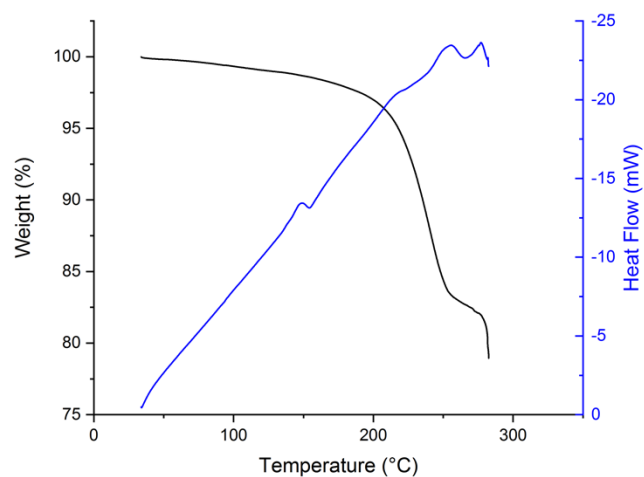


Figure S7.18. TGA-DSC of compound  $A_3B_4$ .

#### 7.4.8 Additional IR spectra

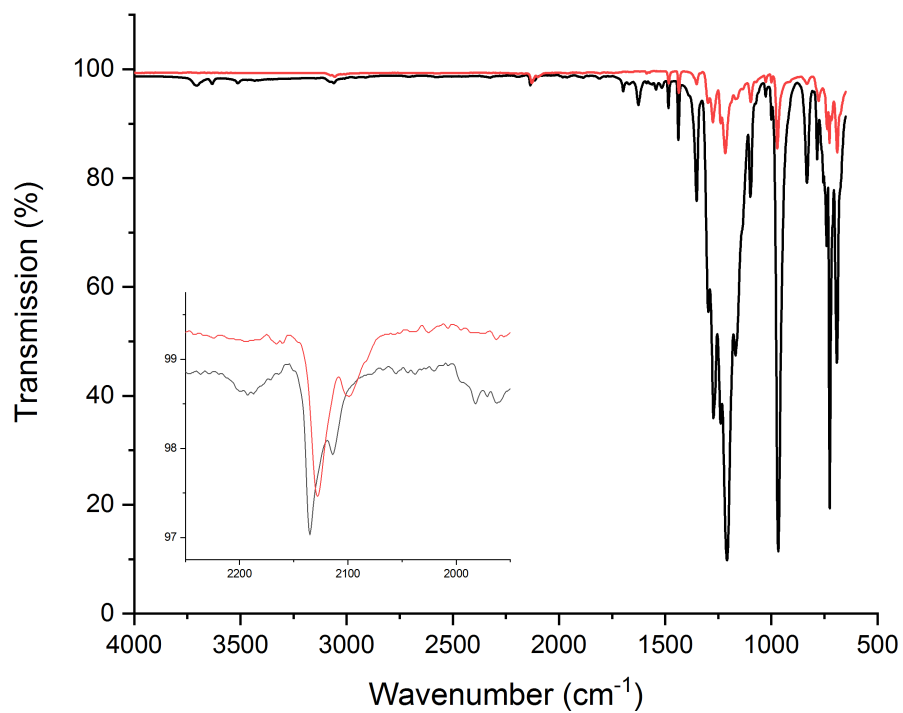
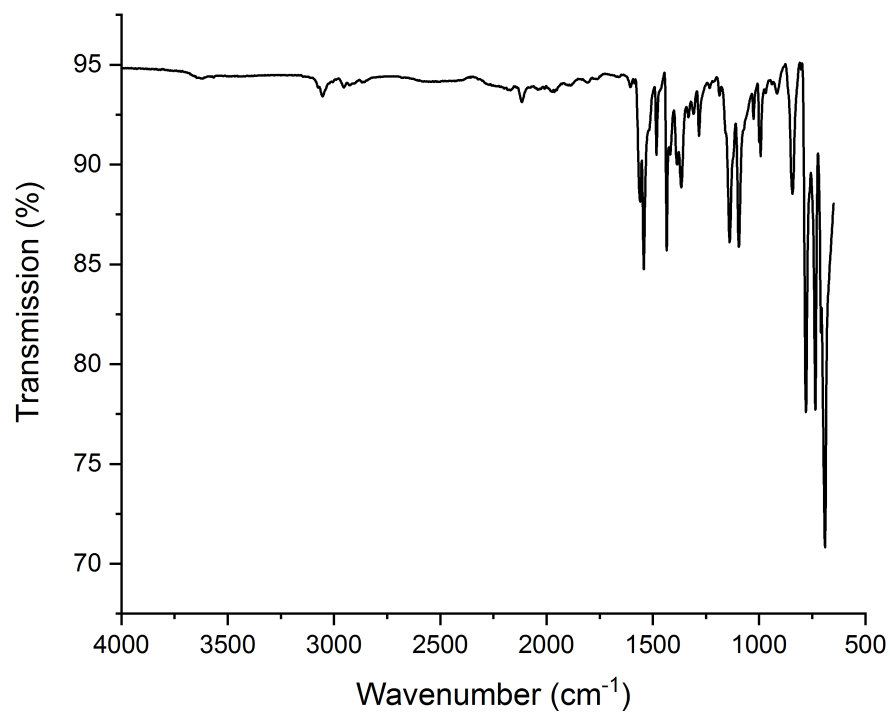
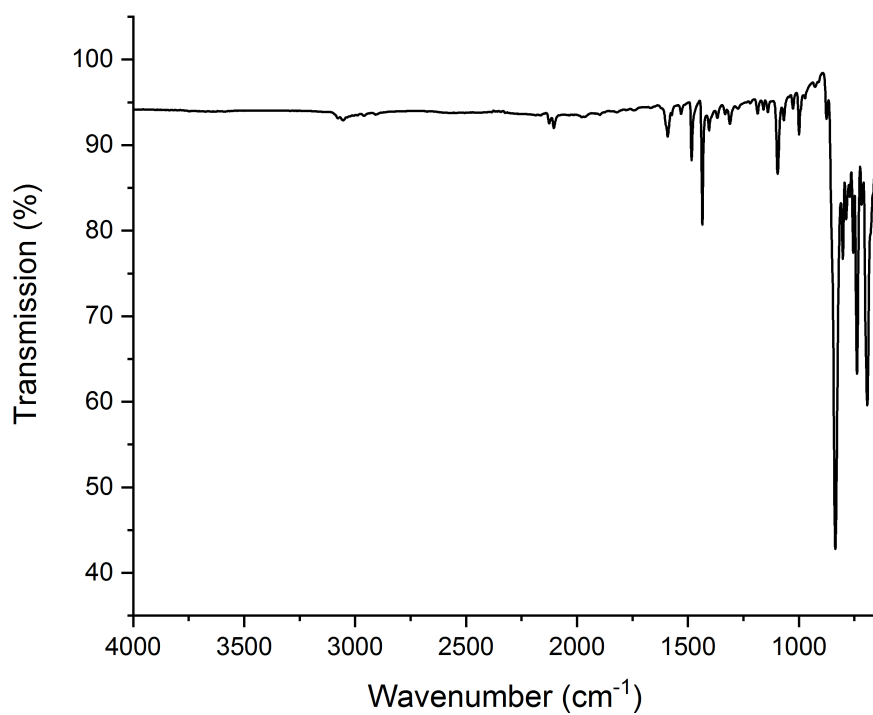


Figure S7.19. IR spectra of compound  $A_2$  before (black) and after the transition (red). Characteristic C≡N vibration bands shown in inset.





**Figure S7.20.** IR spectra of compound **A<sub>3</sub>**.



**Figure S7.21.** IR spectra of compound **A<sub>1</sub>B<sub>1</sub>**.

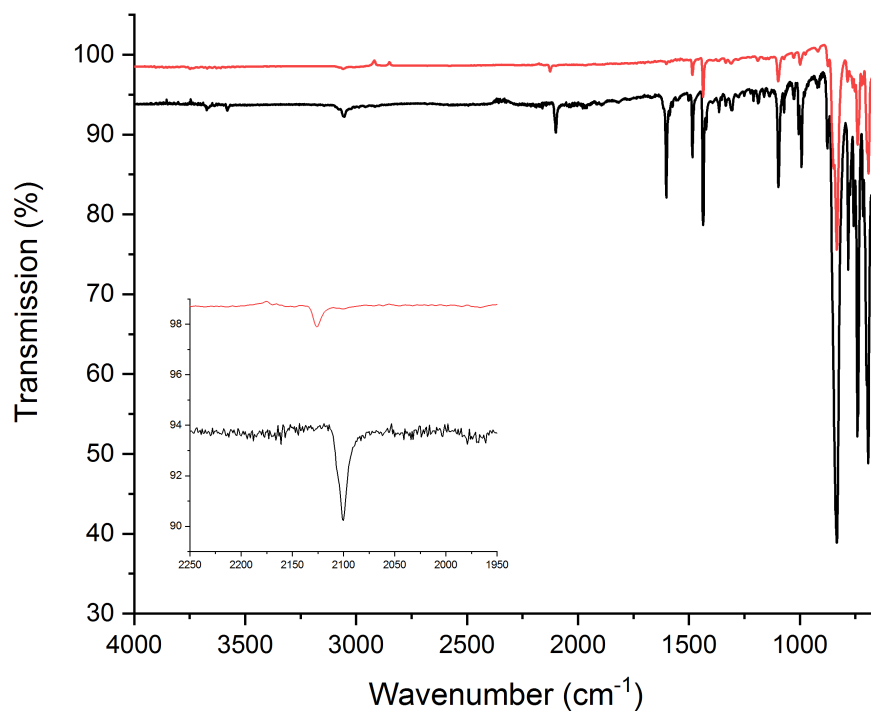


**Figure S7.22.** IR spectra of compound  $A_1B_4$  before (black) and after the transition (red). Characteristic C≡N vibration bands shown in inset.

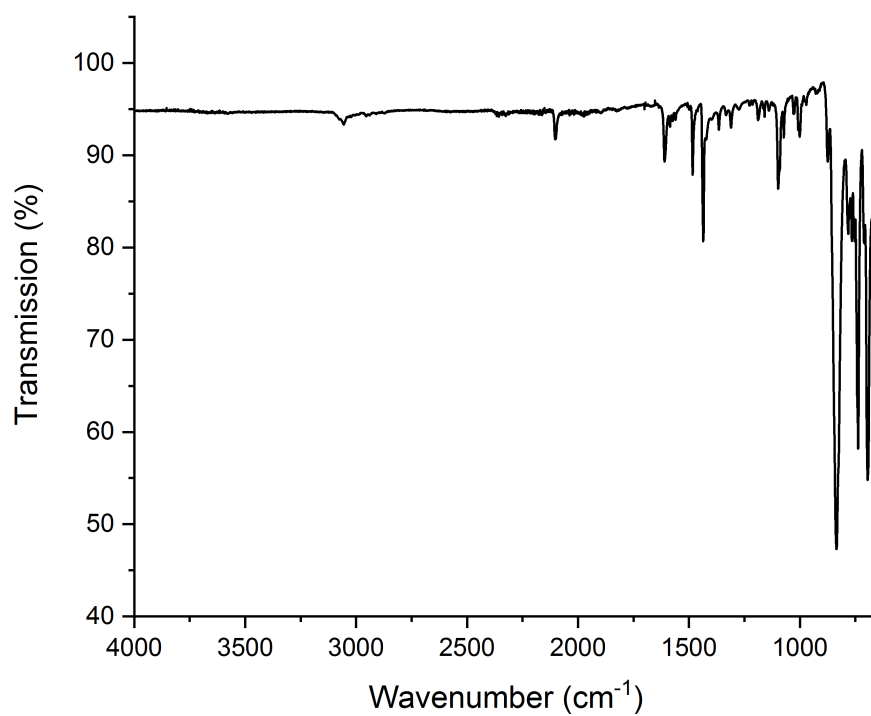


**Figure S7.23.** IR spectra of compound  $A_1B_5$ .

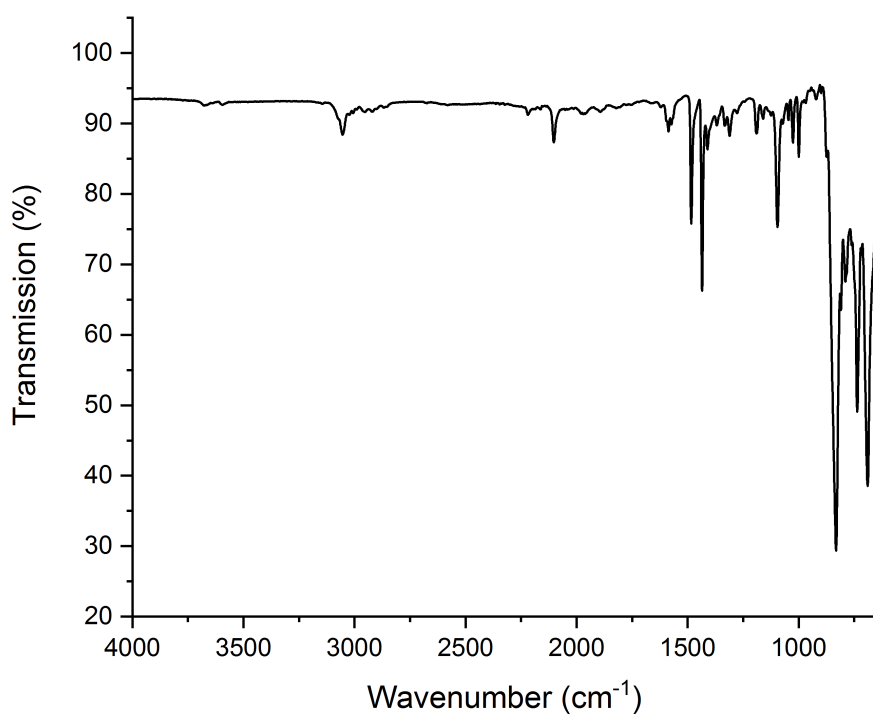


**Figure S7.24.** IR spectra of compound **A<sub>1</sub>B<sub>6</sub>**.

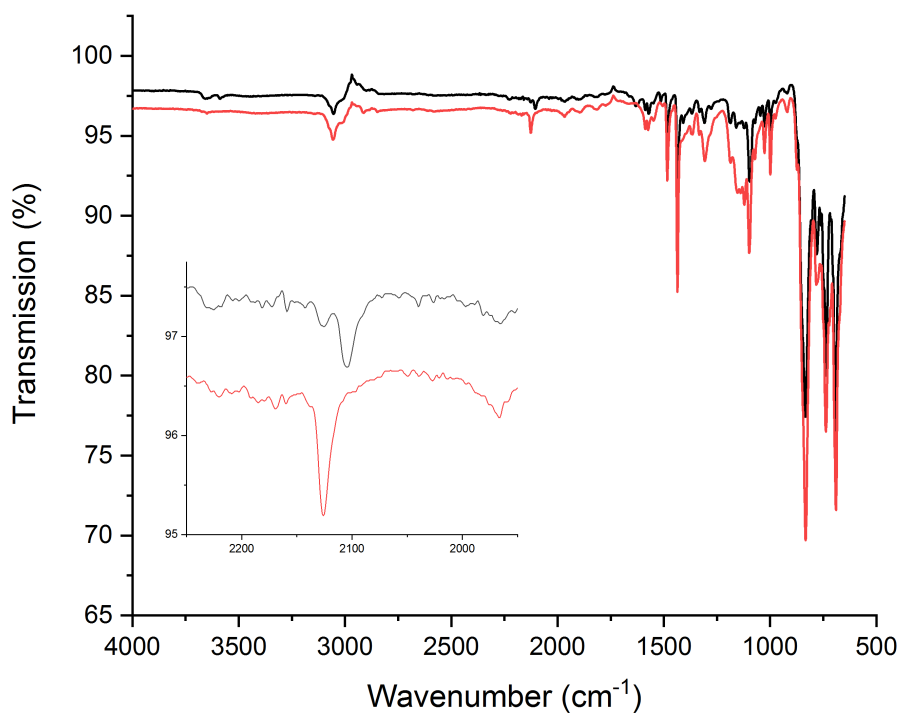


**Figure S7.25.** IR spectra of compound **A<sub>1</sub>B<sub>7</sub>** before (black) and after the transition (red). Characteristic C≡N vibration bands shown in inset.

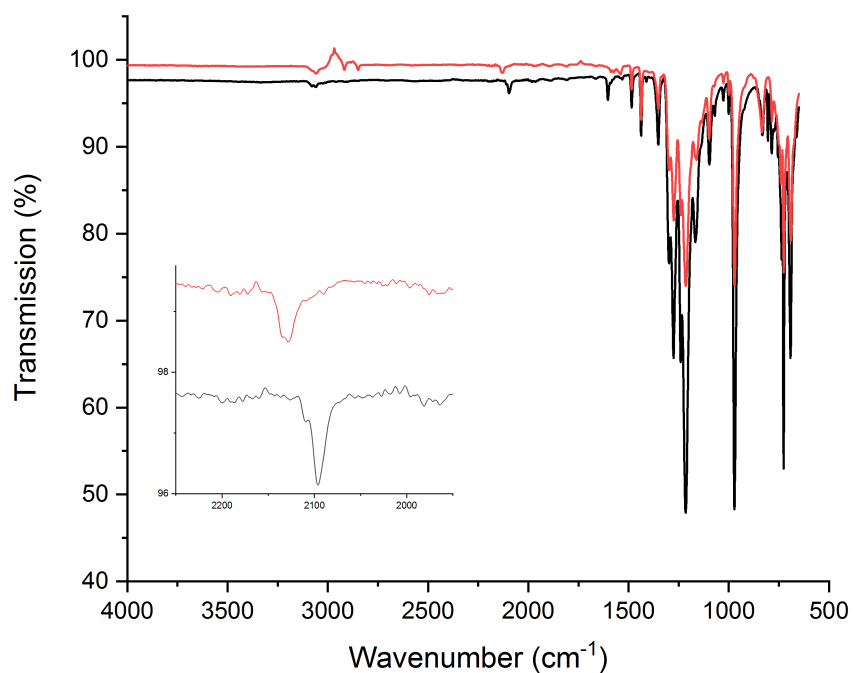


**Figure S7.26.** IR spectra of compound **A<sub>2</sub>B<sub>1</sub>a** before (black) and after the transition (red). Characteristic C≡N vibration bands shown in inset.

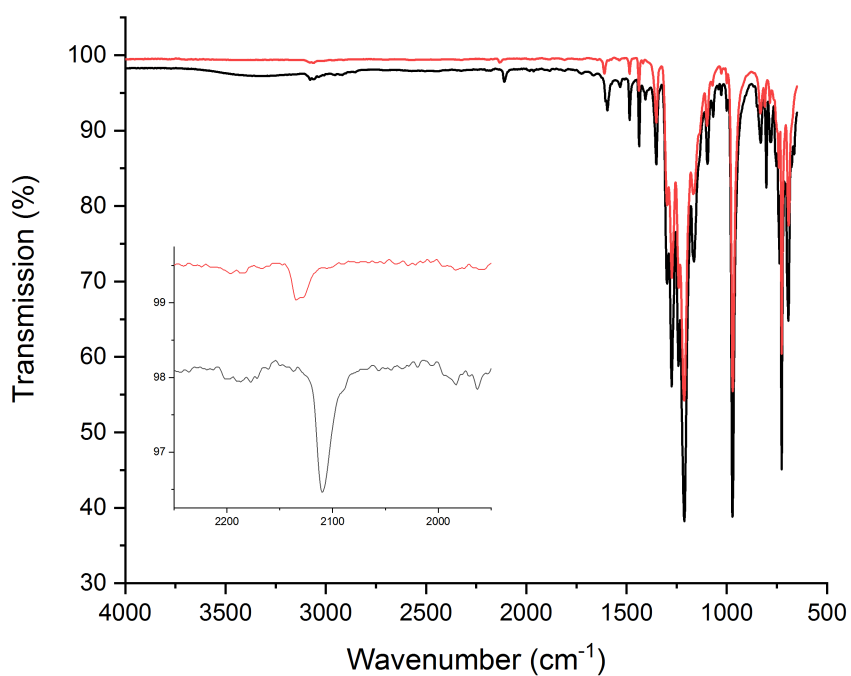


**Figure S7.27.** IR spectra of compound **A<sub>2</sub>B<sub>1</sub>b** before (black) and after the transition (red). Characteristic C≡N vibration bands shown in inset.

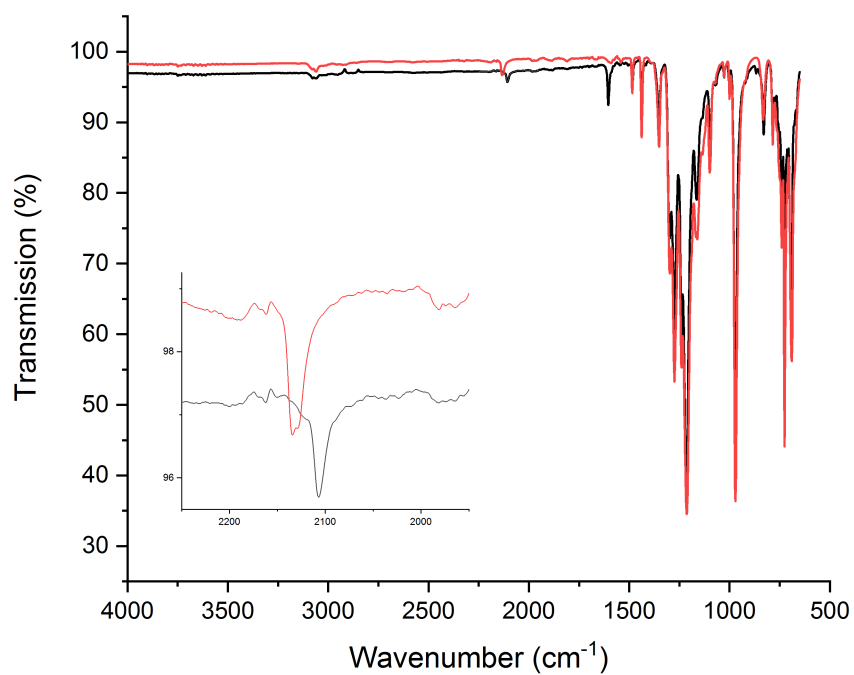


**Figure S7.28.** IR spectra of compound  $A_2B_3$  before (black) and after the transition (red). Characteristic C≡N vibration bands shown in inset.

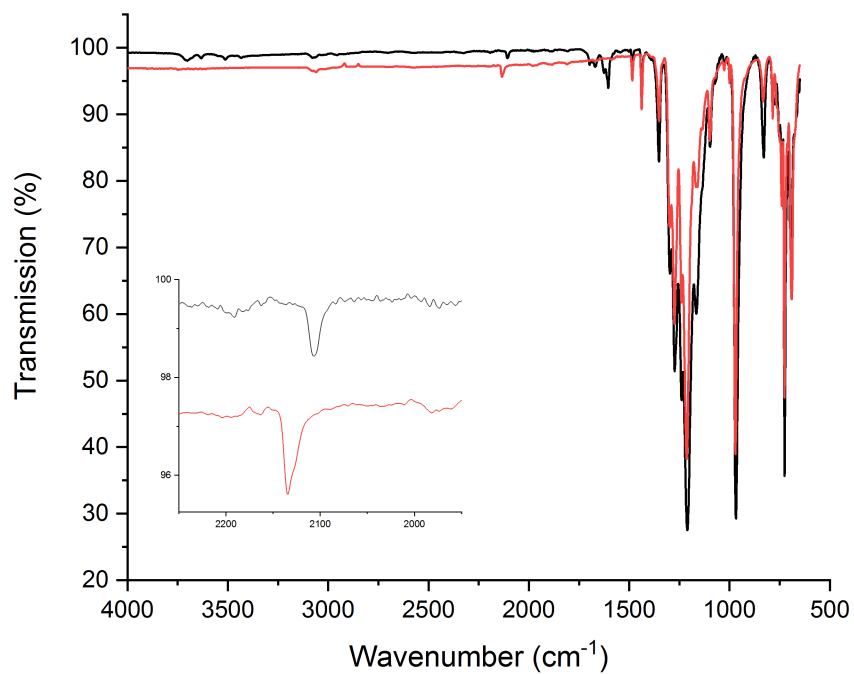


**Figure S7.29.** IR spectra of compound  $A_2B_4$  before (black) and after the transition (red). Characteristic C≡N vibration bands shown in inset.

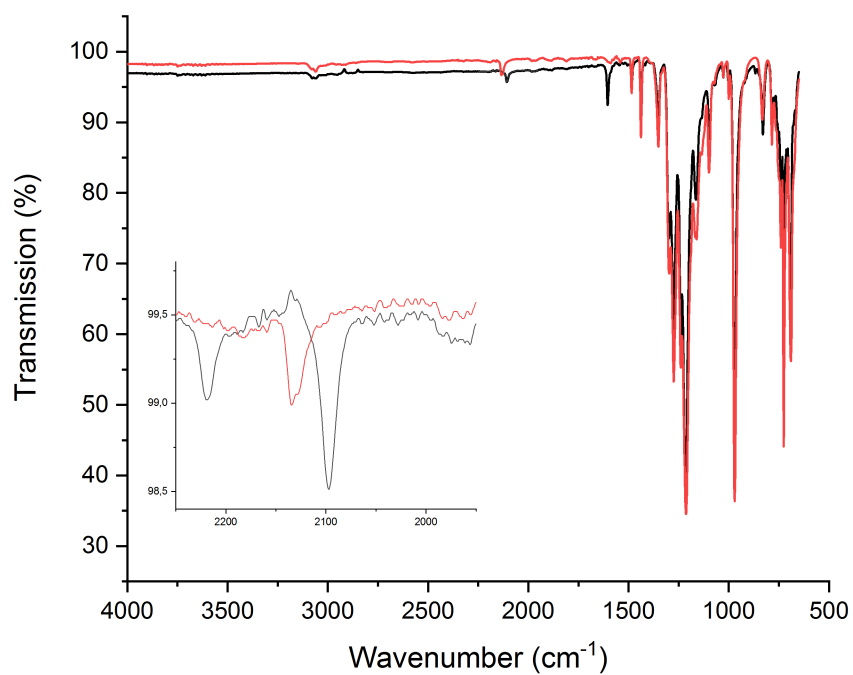


**Figure S7.30.** IR spectra of compound  $A_2B_6$  before (black) and after the transition (red). Characteristic C≡N vibration bands shown in inset.

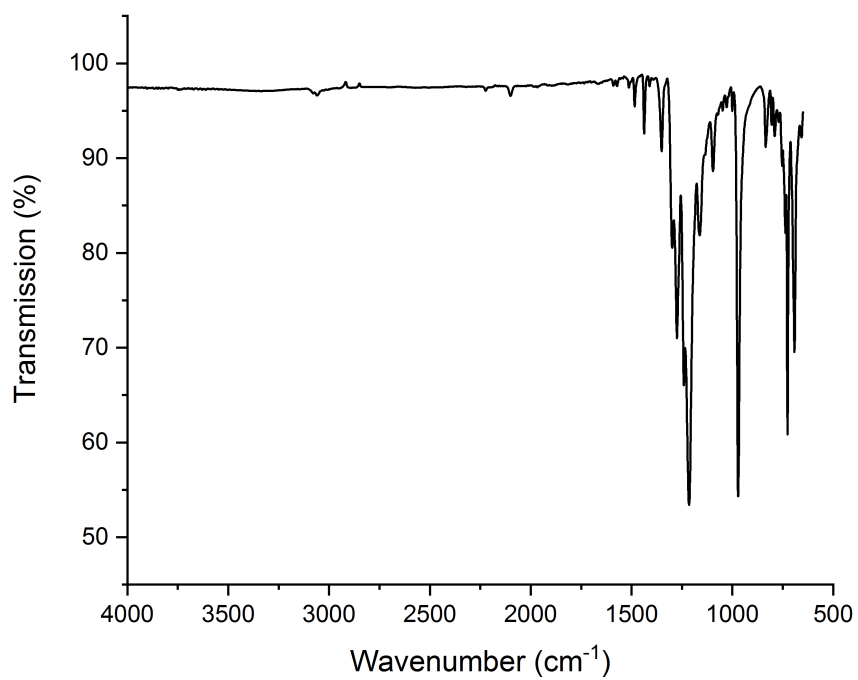


**Figure S7.31.** IR spectra of compound  $A_2B_7$ .

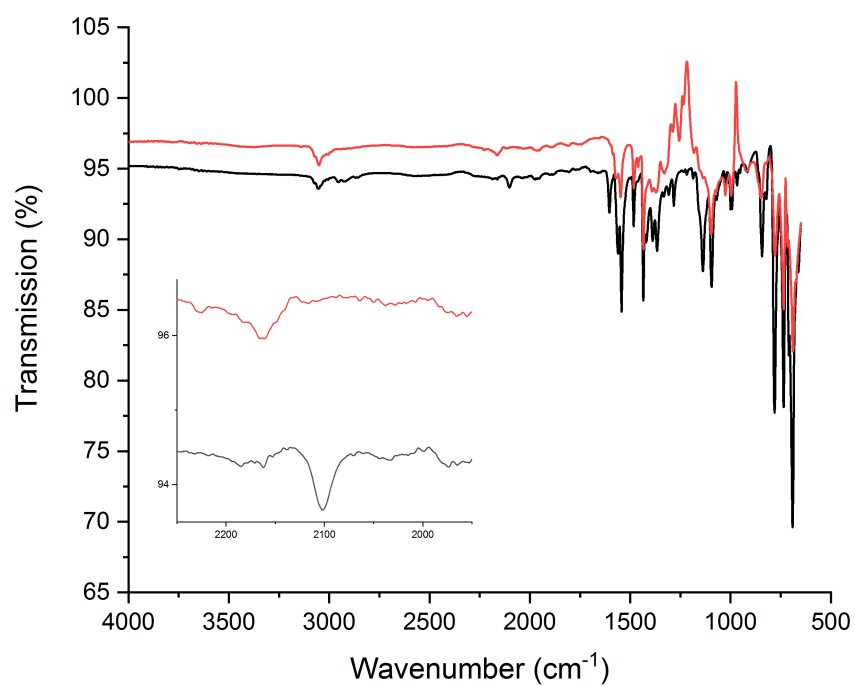


**Figure S7.32.** IR spectra of compound  $A_3B_4$  before (black) and after the transition (red). Characteristic  $C\equiv N$  vibration bands shown in inset.

## 7.5 References

- [1] a) V. W.-W. Yam, V. K.-M. Au, S. Y.-L. Leung, *Chem. Rev.*, **2015**, 115, 7589; b) P. Ai, M. Mauro, L. De Cola, A. A. Danopoulos, P. Braunstein, *Angew. Chem. Int. Ed. Engl.* **2016**, 55, 3338, (c) Czerwieniec, M. J. Leitzl, H. H. H. Homeier, H. Yersin, *Coord. Chem. Rev.* **2016**, 325, 2; d) H. Yersin, Ed., *Highly Efficient OLEDs with Phosphorescent Materials*, Wiley-VCH, Weinheim, **2008**; e) W. Brütting, C. Adachi, Eds., *Physics of Organic Semiconductors*, Wiley-VCH, Weinheim, **2012**.
- [2] M. J. Leitzl, V. A. Krylova, P. I. Djurovich, M. E. Thompson, H. Yersin, *J. Am. Chem. Soc.* **2014**, 136, 16032-16038;
- [3] a) H. Yersin, D. Donges, *Top. Curr. Chem.* **2001**, 214, 81-186; b) W. A. Tarran, G. R. Freeman, L. Murphy, A. M. Katakay, J. A. G. Williams, *Inorg. Chem.* **2014**, 53, 5738-5749.
- [4] a) K.-C. Tang, K. L. Liu, I. C. Chen, *Chem. Phys. Lett.* **2004**, 386, 437-441; b) G. J. Hedley, A. Ruseckas, I. D. W. Samuel, *J. Phys. Chem. A* **2009**, 113, 2-4.
- [5] a) C. Adachi, M. A. Baldo, M. E. Thomson, S. R. Forrest, *J. Appl. Phys.* **2001**, 90, 5048-5051; b) C. Zhao, T. K. Ng, N. Wei, A. Prabaswara, M. S. Alias, B. Janjua, C. Shen, B. S. Ooi, *Nano Lett.* **2016**, 16, 1056-1063; c) R. H. Temperton, N. W. Rosemann, M. Guo, N. Johansson, L. A. Fredin, O. Prakash, K. Wärnmark, K. Handrup, J. Uhlig, J. Schnadt, P. Persson, *J. Phys. Chem. A* **2020**, 124, 1603-0609.
- [6] a) F. Böppler, M. Zimmer, F. Dietrich, M. Gruppe, M. Wallesch, D. Volz, S. Bräse, M. Gerhards, R. Diller, *Phys. Chem. Chem. Phys.* **2017**, 19, 29438-29448; b) T. Hofbeck, U. Monkowius, H. Yersin, *J. Am. Chem. Soc.* **2015**, 137, 399-404; c) M. Osawa, M. Hoshino, M. Hashimoto, I. Kawata, S. Igawa, M. Yashima, *Dalton Trans.* **2015**, 44, 8369-8378; d) L. C. Ravaro, A. C. Mafud, Z. Li, E. Reinheimer, C. A. Carlos, Y. P. Mascarenhas, P. C. Ford, A. S. S. de Camargo, *Dyes and Pigments* **2018**, 158, 464-470.
- [7] a) A. Kobayashi, M. Kato, *Chem. Lett.* **2017**, 46, 154-162; b) L. Bergmann, G. J. Hedley, T. Baumann, S. Bräse, I. D. W. Samuel *Sci. Adv.* **2016**, 2(1), e1500889.
- [8] a) V. W.-W. Yam, V. K.-M. Au, S. Y.-L. Leung, *Chem. Rev.* **2015**, 115, 7589-7728; b) K. M.-C. Wong, M.-Y. Chan, V. W.-W. Yam, *Adv. Mater.* **2014**, 26, 5558-5568; c) K. M.-C. Tang, A. K.-W. Chan, M.-Y. Chan, V. W.-W. Yam, *Top. Curr. Chem.* **2016**, 374, 1-43.
- [9] S. Evarista, A. M. Khalil, M. Elsayed Moussa, A. K.-W. Chan, E. Y.-H. Hong, H.-L. Wong, B. Le Guennic, G. Calvez, K. Costuas, V. W.-W. Yam, C. Lescop, *J. Am. Chem. Soc.* **2018**, 140, 12521-12526.



- [10] M. Elsayed Moussa, S. Evarista, H.-L. Wong, L. Le Bras, C. Roiland, L. Le Polles, B. Le Guennic, K. Costuas, V. W.-W. Yams, C. Lescop, *Chem. Commun.* **2016**, 52, 11370-11373.
- [11] a) B. Nohra, S. Graule, C. Lescop, R. Réau, *J. Am. Chem. Soc.* **2006**, *128*, 3520-3521; b) M. Elsayed Moussa, K. Guillois, W. Shen, R. Réau, J. Crassous, C. Lescop, *Chem. Eur. J.* **2014**, *20*, 14853-14867.
- [12] An additional vibration band is visible at 2114 cm<sup>-1</sup> for **A<sub>2</sub>** which could result from the inversion center crystallographically imposed on the compound.
- [13] a) K. Tsuge, Y. Chishina, H. Hashiguchi, Y. Sasaki, M. Kato, S. Ishizaka, N. Kitamura, *Coord. Chem. Rev.* **2016**, *306*, 636-651; b) M. Elsayed Moussa, S. Welsch, M. Lochner, E. V. Peresykina, A. V. Virovets, M. Scheer, *Eur. J. Inorg. Chem.* **2018**, 2689-2694; c) M. Elsayed Moussa, A. M. Khalil, S. Evarista, H.-L. Wong, V. Delmas, B. Le Guennic, G. Calvez, K. Costuas, V. W.-W. Yam, C. Lescop, *Inorganic Chemistry Frontiers* **2020**, online; d) C. Heintl, E. V. Peresykina, A. V. Virovets, V. Y. Komarov, M. Scheer, *Dalton Trans.* **2015**, *44*, 10245-10252; e) C. Heintl, A. Kuntz, E. V. Peresykina, A. V. Virovets, M. Zabel, D. Lüdeker, G. Brunklaus, M. Scheer, *Dalton Trans.* **2015**, *44*, 6502-6509; f) C. Schenk, F. Henke, G. Santiso-Quinones, I. Krossing, A. Schnepf, *Dalton Trans.* **2008**, 4436-4441.
- [14] Master thesis Florent Moutier **2019**, Université de Rennes 1; PhD thesis Ali Khalil **2019**, Université de Rennes 1.
- [15] An additional vibration band is visible at 2220 cm<sup>-1</sup> for **A<sub>2</sub>B<sub>6</sub>** which could result from the inversion center crystallographically imposed on the compound.
- [16] An additional vibration band is visible at 2223 cm<sup>-1</sup> for **A<sub>2</sub>B<sub>7</sub>** which could result from the inversion center crystallographically imposed on the compound.
- [17] M. Dosen, Y. Kawada, S. Shibata, K. Tsuge, Y. Sasaki, A. Kobayashi, M. Kato, S. Ishizaka, N. Kitamura, *Inorg. Chem.* **2019**, *58*, 8419-8431.
- [18] M. E. Moussa, M. Piesch, M. Fleischmann, A. Schreiner, M. Seidl, M. Scheer, *Dalton Trans.* **2018**, *47*, 16031-16035.
- [19] L. Dütsch, Master thesis **2015**, Universität Regensburg.
- [20] N. Schultheiss, J. M. Ellsworth, E. Bosch, C. L. Barnes, *Eur. J. Inorg. Chem.* **2005**, 45-46.
- [21] Y. Yao, W. Shen, B. Nohra, C. Lescop, R. Reau, *Chem. Eur. J.* **2010**, *16*, 7143-7163.
- [22] H. Yersin, A. F. Rausch, R. Czerwieniec, T. Hofbeck, T. Fischer, *Coord. Chem. Rev.* **2011**, *255*, 2622-2652.

- [23] Z. Otwinowski, W. Minor, In *Methods in Enzymology*, (Ed.: C.W. Carter, Jr. & R.M. Sweet), New York: Academic Press, **1997**, 276, 307.
- [24] A. Altomare, M. C. Burla, M. Camalli, G. Cascarano, C. Giacovazzo, A. Guagliardi, A. G. G. Moliterni, G. Polidori, R. Spagna, *J. Appl. Cryst.* **1999**, 32, 115.
- [25] G.M. Sheldrick, SHELX97, Program for the Refinement of Crystal Structures, University of Göttingen, Germany, **1997**.
- [26] CrysAlisPro Software System, Rigaku Oxford Diffraction, (**2018**).
- [27] Clark, R. C. & Reid, J. S. *Acta Cryst.* **1995**, A51, 887-897.
- [28] O.V. Dolomanov and L.J. Bourhis and R.J. Gildea and J.A.K. Howard and H. Puschmann, Olex2: A complete structure solution, refinement and analysis program, *J. Appl. Cryst.* **2009**, 42, 339-341.
- [29] Sheldrick, G.M., ShelXT-Integrated space-group and crystal-structure determination, *Acta Cryst.* **2015**, A71, 3-8.5.G.
- [30] M. Sheldrick, Crystal structure refinement with ShelXL, *Acta Cryst.* **2015**, C27, 3-8.
- [31] a) A. L. Spek, *J. Appl. Crystallogr.* 2003, 36, 13; b) P. van der Stuis, A. L. Spek, *Acta Cryst.* **1990**, 46, 194.

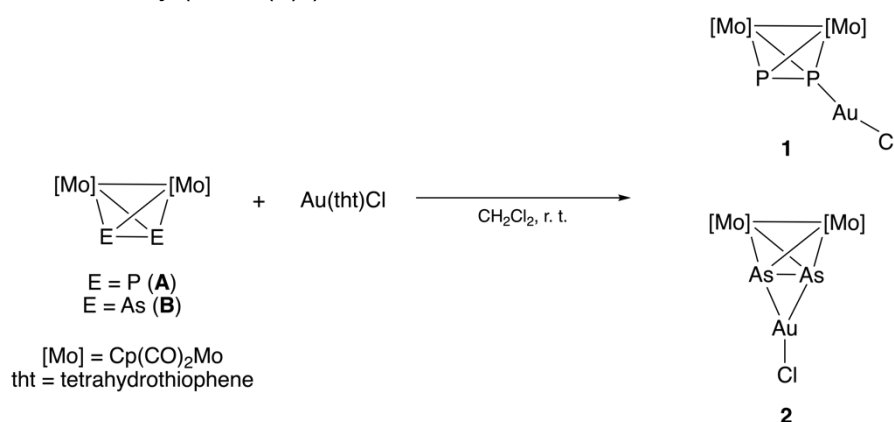


## 8. Thesis Treasury

### 8.1 Coordination Compounds Based on $[(C_5H_5)_2Mo_2(CO)_4(\mu,\eta^2-As_2)]$

#### 8.1.1 Reaction of $[(C_5H_5)_2Mo_2(CO)_4(\mu,\eta^2-As_2)]$ with $Au(tht)Cl$

The already reported reaction of  $[Cp_2Mo_2(CO)_4(\mu,\eta^2-P_2)]$  (**A**) with  $Au(tht)Cl$  (tht = tetrahydrothiophene) yields the molecular compound **1**.<sup>1</sup> The solid-state structure of **1** consists of a Lewis-acidic fragment  $[AuCl]$  coordinated to one phosphorus atom (Scheme 8.1). The coordination mode of the Au(I) cation is not exactly linear, as the P-Au-Cl angle deviates from linearity ( $170.4(2)^\circ$ ).



**Scheme 8.1.** Reaction of  $[Cp_2Mo_2(CO)_4(\mu,\eta^2-P_2)]$  with  $Au(tht)Cl$  yielding compound **1**.<sup>1</sup>

As already reported in chapters 3-5, the tetrahedral arsenic analogue to **A**  $[Cp_2Mo_2(CO)_4(\mu,\eta^2-As_2)]$  (**B**) shows a higher tendency to coordinate towards cations in an  $\eta^2$  fashion. The question arose, what coordination mode the  $As_2$  unit in **B** would take in the reaction outcome with  $Au(tht)Cl$ . The reaction of **B** and this Au(I) salt was conducted under the same reaction conditions, in  $CH_2Cl_2$  at room temperature. Compound **2** was obtained after one week as brownish crystals suitable for X-ray analysis in a moderate yield (37%). As expected, **2** consists of an  $As_2$  moiety coordinating in an  $\eta^2$ -mode towards the Au(I) center (Figure 8.1).

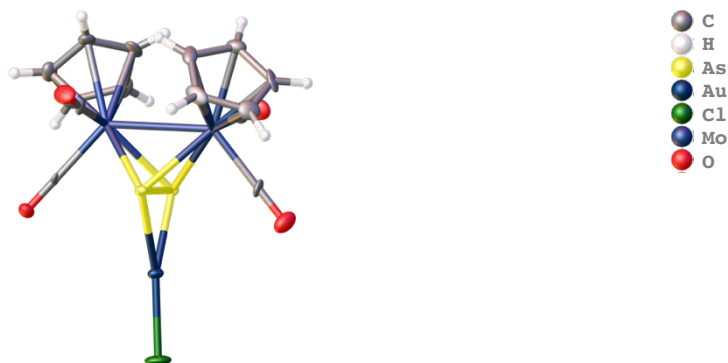
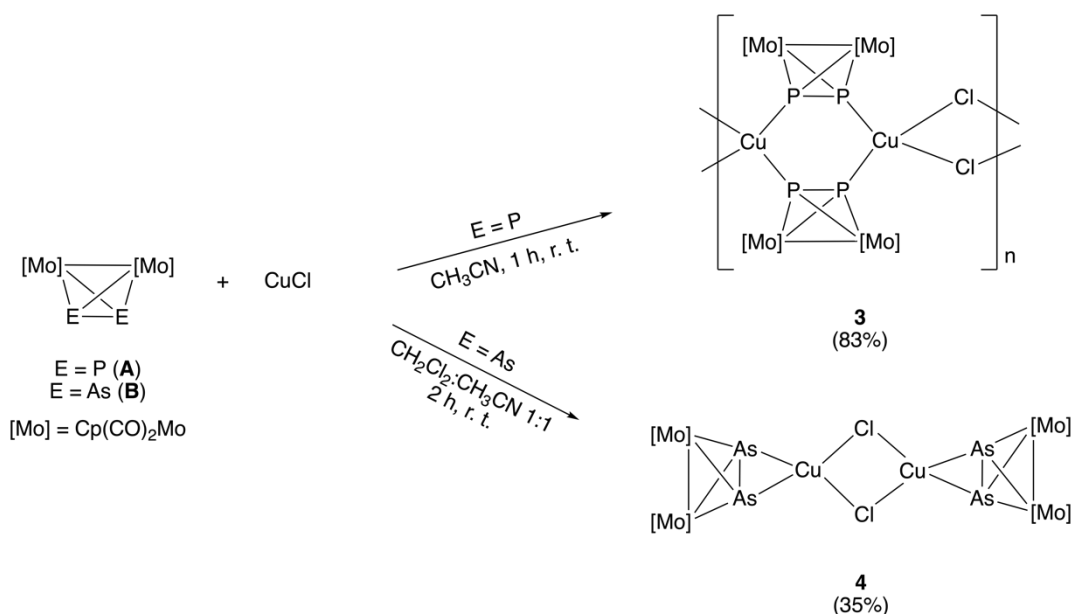


**Figure 8.1.** Solid-state structure of compound **2**. Ellipsoids are shown at 50% probability level.

### 8.1.2 Reaction of $[(C_5H_5)_2Mo_2(CO)_4(\mu,\eta^2-As_2)]$ with CuCl

The already reported reaction of **A** and CuCl leads to the 1D linear polymer  $[CuCl\{Cp_2Mo_2(CO)_4(\mu,\eta^2:\eta^1:\eta^1-P_2)\}]_n$  (**3**) with each phosphorus atom coordinating in a  $\eta^1$ -coordination mode towards the Cu(I) centers.<sup>2</sup> In contrast to **A**, reacting CuCl with  $[Cp_2Mo_2(CO)_4(\mu,\eta^2-As_2)]$  (**B**) leads to the dimer **4** in moderate yields (Scheme 8.2). The  $\eta^2$ -coordination of the  $As_2$  unit towards a CuCl entity results in a dimeric structure.



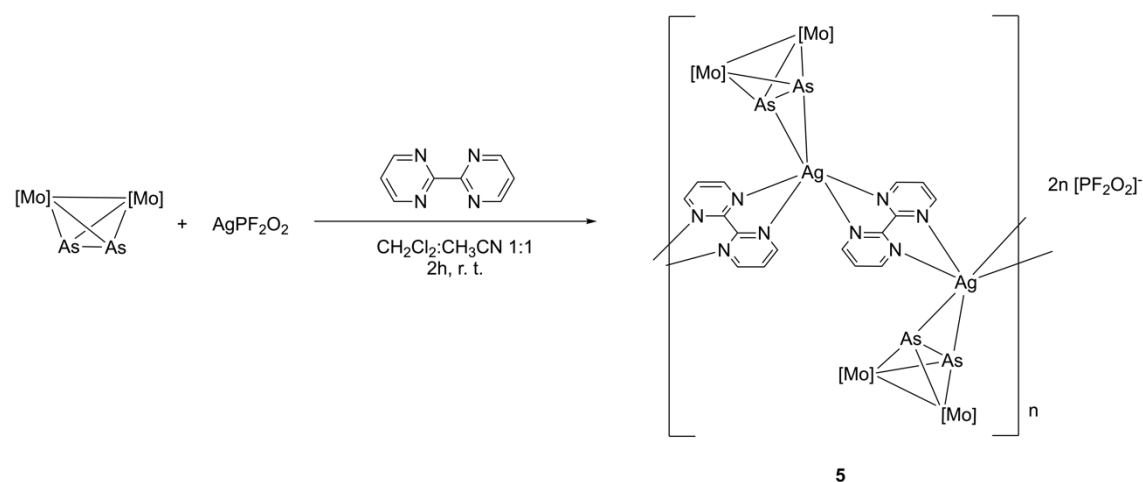
**Scheme 8.2.** Reaction of **A** or **B** and CuCl yielding compounds **3** and **4**, respectively.<sup>2</sup> Yields are given in parentheses.

The orange blocks are soluble in donor solvents, such as  $CH_3CN$ , slightly soluble in  $CH_2Cl_2$  and insoluble in *n*-pentane and toluene. The  $^1H$  and  $^{13}C \{^1H\}$  NMR spectra of **3** show signals for the proton (5.26 ppm) and carbon nuclei (229.54 ppm, 85.85 ppm) of coordinated **B**, respectively. The ESI mass spectra show the cationic fragments  $[B_2Cu]^+$  and  $[BCu(CH_3CN)]^+$ , and the anionic fragment  $[CuCl_2]^-$ .

### 8.1.3 Reaction of $[(C_5H_5)_2Mo_2(CO)_4(\mu,\eta^2-As_2)]$ with hydrolyzed $AgPF_6$ and 2,2'-bipyrimidine

As already reported in chapter 4, the reaction of  $[Cp_2Mo_2(CO)_4(\mu,\eta^2-As_2)]$  (**B**),  $Ag[PF_6]$  and an excess of 2,2'-bipyrimidine (**L**) yields a 1D coordination polymer with the composition 1:1:1. Accidentally using partly hydrolyzed  $Ag[PF_6]$  leads to the similar one-dimensional polymer **5** (Scheme 8.3). The cationic polymeric chain is identical to the one of the already reported polymer, while the anion present is exclusively  $[PF_2O_2]^-$  (Figure

8.2). Since the determination of the anion *via* X-ray structural analysis is rather impossible, NMR spectra were performed. The  $^{31}\text{P}$   $\{^1\text{H}\}$  and the  $^{19}\text{F}$   $\{^1\text{H}\}$  spectra revealed the presence of a  $[\text{PF}_2\text{X}_m]^-$  species.



**Scheme 8.3.** Reaction of **B** and  $\text{AgPF}_6$  with 2,2'-bipyrimidine yielding compound **5**.

This species is most likely an  $[\text{PF}_2\text{O}_2]^-$  anion resulting from partial hydrolysis of the hexafluorophosphate. The  $^{19}\text{F}$   $\{^1\text{H}\}$  spectrum reveals further signals, which indicate a decomposition of  $[\text{PF}_6]^-$  and reaction of formed HF with the glassware.

The ESI mass spectra shows peaks for the cationic fragments  $[\text{BAgL}]^+$ ,  $[\text{AgL}_2]^+$  and  $[\text{AgL}]^+$ . The assignment of negatively charged fragments was not possible.

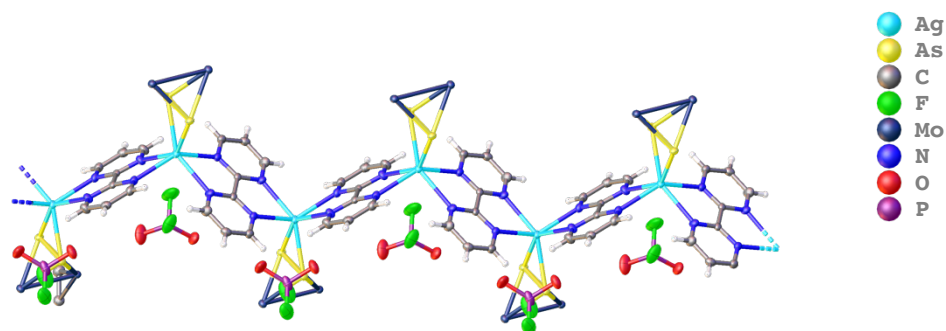


**Figure 8.2.** Solid-state structure of compound **5**. Cp-, CO-fragments and hydrogen atoms are omitted for clarity. Ellipsoids are depicted at 50% probability level.

#### 8.1.4 Reaction of $[(\text{C}_5\text{H}_5)_2\text{Mo}_2(\text{CO})_4(\mu, \eta^2\text{-As}_2)]$ with hydrolyzed $\text{Ag}[\text{PF}_6]$ and 4,4'-bipyridine

As already reported in chapter 4, the reaction of  $[\text{Cp}_2\text{Mo}_2(\text{CO})_4(\mu, \eta^2\text{-As}_2)]$  (**B**),  $\text{Ag}[\text{PF}_6]$  and an excess of 4,4'-bipyridine yields a 1D coordination polymer with linked  $[\text{Ag}_2\text{B}_2]^{2+}$

units. Accidentally using partly hydrolyzed  $\text{Ag}[\text{PF}_6]$  leads to the similar one-dimensional polymer **6** (Figure 8.3.b). This coordination compound consists, as well as the already reported polymer, of  $[\text{Ag}_2\mathbf{B}_2]^{2+}$  moieties linked with each other with 4,4'-bipyridine. However, the partly hydrolyzed anion  $[\text{PF}_2\text{O}_2]^-$  coordinates in an  $\eta^1$ -coordination mode towards the two Ag(I) centers stabilizing a rather short  $\text{Ag}\cdots\text{Ag}$  distance (3.778(4) Å) (Figure 8.3.a). The second anion in the unit cell is disordered,  $[\text{PF}_6]^-$  has an occupancy of 0.8 and another  $[\text{PF}_2\text{O}_2]^-$  anion has an occupancy of 0.2.

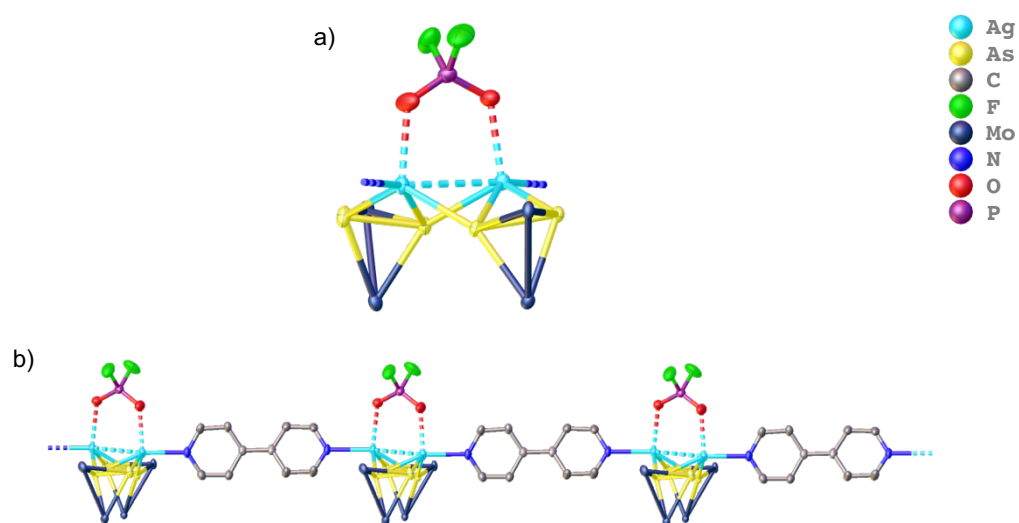


**Figure 8.3.** Solid-state structure of compound **6**. a) Coordination of  $\text{PF}_2\text{O}_2^-$  towards the Ag(I) centers; b) Polymeric structure of **5**. Cp-, CO-fragments and hydrogen atoms, solvent molecules and additional anions are omitted for clarity. Ellipsoids are depicted at 50% probability level.

### 8.1.5 Reaction of $[(\text{C}_5\text{H}_5)_2\text{Mo}_2(\text{CO})_4(\mu, \eta^2\text{-As}_2)]$ with $[\text{Cu}(\text{CH}_3\text{CN})_4][\text{Al}\{\text{OC}(\text{CF}_3)_3\}_4]$ and 1,2-di(4-pyridyl)ethylene

Reaction of the  $\text{As}_2$  complex **B** with  $[\text{Cu}(\text{CH}_3\text{CN})_4][\text{TEF}]$  ( $[\text{TEF}]^- = [\text{Al}\{\text{OC}(\text{CF}_3)_3\}_4]^-$ ) and the ditopic linker 1,2-di(4-pyridyl)ethylene leads to the one-dimensional zig-zag polymer **7**. So far only an incomplete and poor data set could be obtained. The preliminary structure in the solid state shows a Cu(I) ion coordinated in an  $\eta^2$ -fashion by one **B** unit, as well as two linkers (Figure 8.4). An exact determination of bond lengths and angles is not possible due to the incomplete X-ray data set.

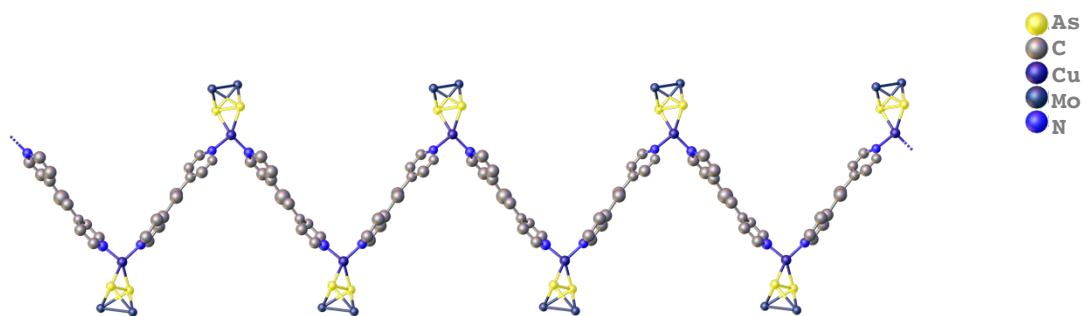


**Figure 8.4.** Preliminary solid-state structure of compound **6**. Hydrogen atoms are omitted for clarity.

## 8.2 Coordination Compounds Based on $[\text{Cp}^*\text{Fe}(\eta^5\text{-P}_5)]$

### 8.2.1 Reaction of $[\text{Cp}^*\text{Fe}(\eta^5\text{-P}_5)]$ with $\text{Ag}[\text{B}(3,5\text{-C}_6\text{H}_3\text{Cl}_2)_4]$

As already reported,<sup>3</sup> the reaction of  $[\text{Cp}^*\text{Fe}(\eta^5\text{-P}_5)]$  (**C**,  $\text{Cp}^* = \text{C}_5(\text{CH}_3)_5$ ) with the weakly coordinating  $\text{Ag}[\text{BAR}^{\text{Cl}}]$  ( $[\text{BAR}^{\text{Cl}}]^- = [\text{B}(3,5\text{-C}_6\text{H}_3\text{Cl}_2)_4]^-$ ) leads to compound **8** consisting of a six-membered  $\text{Ag}_2\text{P}_4$  ring (Figure 8.5). This structural motif was already found in several other compounds containing  $\text{E}_n$  ligand complexes with coinage metal (I) salts. The reaction of **C** and  $\text{Cu}[\text{GaCl}_4]^{4-}$  and  $\text{CuCl}^{5-}$  leads to one dimensional coordination polymers with repeating units of  $\text{Ag}_2\text{P}_4$  ring. Furthermore,  $\text{P}_2$  ligand complexes, such as the tetrahedral  $[\text{Cp}_2(\text{CO})_4\text{Mo}_2\text{P}_2]$  (**A**) form similar six-membered ring motifs with  $\text{Ag}(\text{I})^{1,6}$ ,  $\text{Au}(\text{I})^1$  and  $\text{Cu}(\text{I})^{1,7-9}$  salts. However, these compounds show an additional  $\eta^2$ -coordination of two **A** moieties towards the  $\text{M}(\text{I})$  centers, while compound **8** shows two  $\text{CH}_3\text{CN}$  molecules coordinated to each  $\text{Ag}(\text{I})$  ion.

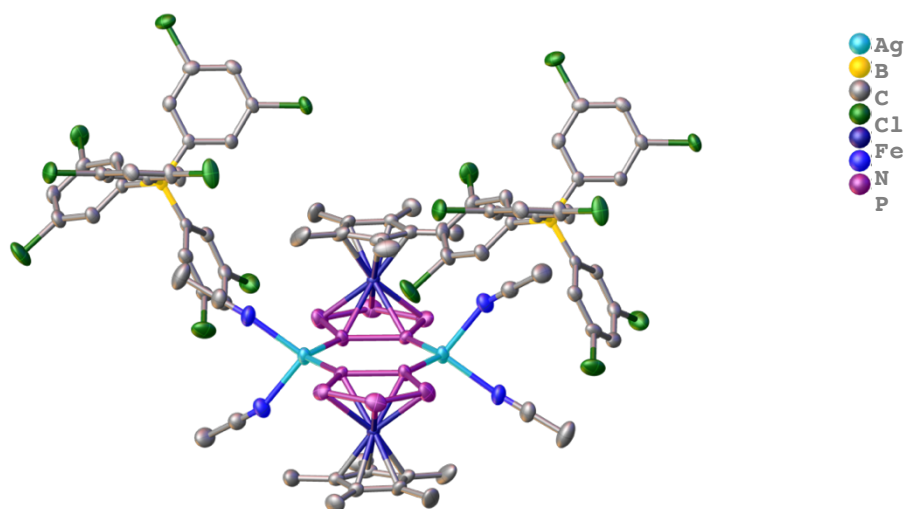


**Figure 8.5.** Molecular structure of **8**.<sup>3</sup> Hydrogen atoms are omitted for clarity. Ellipsoids are depicted at 50% probability level.



Furthermore, two other compounds (**9** and **10**) could be isolated from this reaction (Figure 8.6). At least two of the shown products crystallize simultaneously, sometimes all three. **9** crystallizes as green blocks and **10** as red blocks in the monoclinic space group  $P2_1/n$ . Compound **9** shows, as well as compound **8**, two Ag(I) centers coordinated by two **C** units. However, the cations in **9** are  $\eta^1$  coordinated by one  $P_5$  moiety and  $\eta^2$  coordinated by the other  $P_5$  moiety. Furthermore, two carbon atoms of the anion coordinate towards each silver atom ( $d(\text{Ag}\cdots\text{C}) = 2.593(4)\text{--}2.695(4)\text{ \AA}$ ). The already reported reaction of **C** and  $\text{Ag}[\text{Al}\{\text{OC}(\text{CF}_3)_3\}_4]$  leads to the 1D polymer  $[\text{Ag}\{\text{Cp}^*\text{Fe}(\eta^5\text{:}\eta^2\text{:}\eta^1\text{-P}_5)\}_2]_n [\text{Al}\{\text{OC}(\text{CF}_3)_3\}_4]_n$  with a 1,2,3-coordination mode of **C** towards the Ag(I) ion.<sup>10</sup>

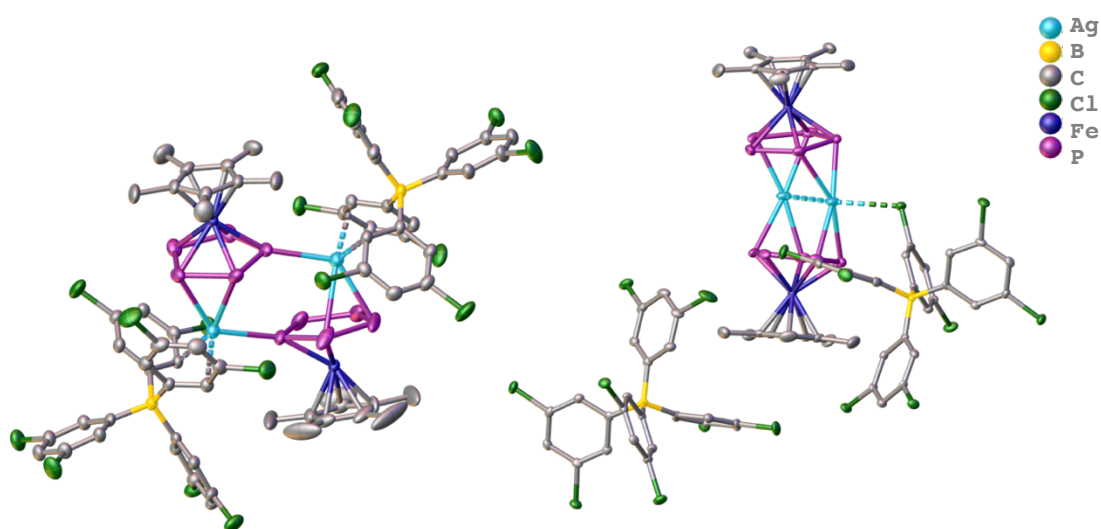


**Figure 8.6.** Molecular structures of **9** (left) and **10** (right). Hydrogen atoms are omitted for clarity. Ellipsoids are depicted at 50% probability level.

However, compound **10** consists of an Ag-Ag dumbbell middle-deck with a short  $\text{Ag}\cdots\text{Ag}$  distance ( $2.9520(8)\text{ \AA}$ ), indicating argentophilic interactions. The two  $P_5$  rings coordinate with two phosphorus atoms each in an  $\eta^2$ -coordination mode towards the  $\text{Ag}_2$  unit from above and below. The solid-state structure of compound **10** is disordered over two positions (90:10) leading to an  $\eta^2$ - $\eta^3$ -coordination towards Ag(I) (cf. Supporting Information). Furthermore, one of the Ag(I) centers is coordinated by a chloride atom of the anion with a rather short  $\text{Ag}\cdots\text{Cl}$  distance of  $2.8506(9)\text{ \AA}$ .

### 8.2.2 Reaction of $[(C_5Me_5)_2Fe(\eta^5-P_5)]$ with $Ag[B(3,5-C_6H_3Cl_2)_4]$ and 4,4'-bipyridine

The reaction of **C** with  $Ag[BAr^{Cl}]$  and ditopic pyridyl-based linkers was studied. The only results obtained contain 4,4'-bipyridine as linking unit. Reacting **C**,  $Ag[BAr^{Cl}]$  and 4,4'-bipyridine in a 2:2:1 ratio yields green rods of compound **11**. Compound **11** consists of  $Ag-P_5$  zig-zag chains cross-linked with each other *via* linker molecules yielding a planar 2D network (Figure 8.7). The two-dimensional network has a composition of  $C:Ag[BAr^{Cl}]:linker$  of 2:2:1, which corresponds to the used stoichiometry.

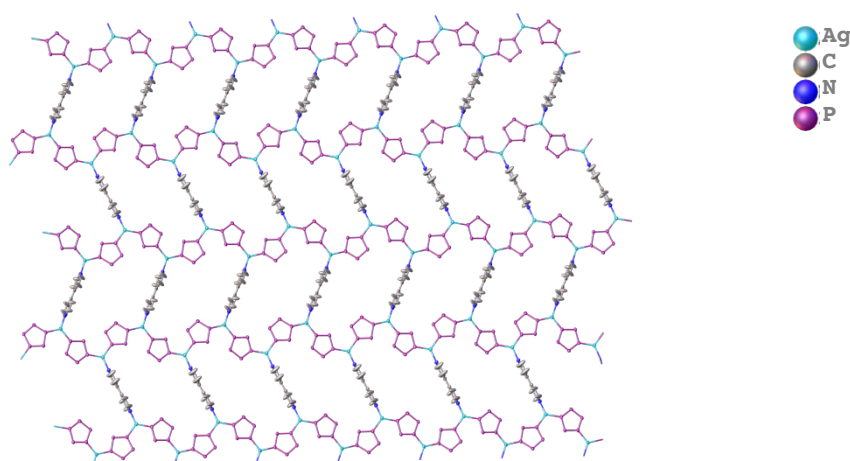


**Figure 8.7.** 2D structure of compound **11**.  $[FeCp^*]$  fragments, hydrogen atoms and anions are omitted for clarity. Ellipsoids are depicted at 50% probability level.

The section shown in figure 8.8 on top shows an entity which is reminiscent of the  $Ag_2P_4$  ring motif. Compared to the already discussed 1,2-coordination, the  $P_5$  rings in **11** reveal a 1,3-coordination towards the  $Ag(I)$  centers. The  $Cp^*$  fragments point alternating up and down the plane.

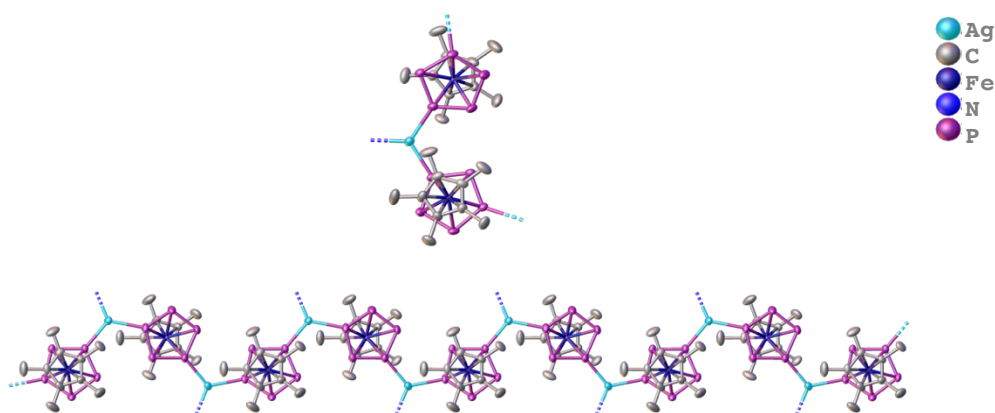


**Figure 8.8.** Sections of compound **11**. Hydrogen atoms and anions are omitted for clarity. Ellipsoids are depicted at 50% probability level.

Using a 1:1:1 ratio of **C**,  $\text{Ag}[\text{BAR}^{\text{Cl}}]$  and 4,4'-bipyridine results in the 3D coordination polymer **12**. The solid-state structure of **12** reveals Ag nodes, which are tetrahedrally coordinated by four linker units and planar  $\text{Ag}_2\text{P}_4$  six membered rings connected to each other *via* the linker units (Figure 8.9). The preliminary solid-state structure reveals a composition of **C**: $\text{Ag}[\text{BAR}^{\text{Cl}}]$ :linker of 1:2:3, which does not corresponds to the used stoichiometry. Colorless crystals containing protonated linker molecules and anions could be isolated, not explaining the excess of linker in the composition. The supernatant was still colored after several months.

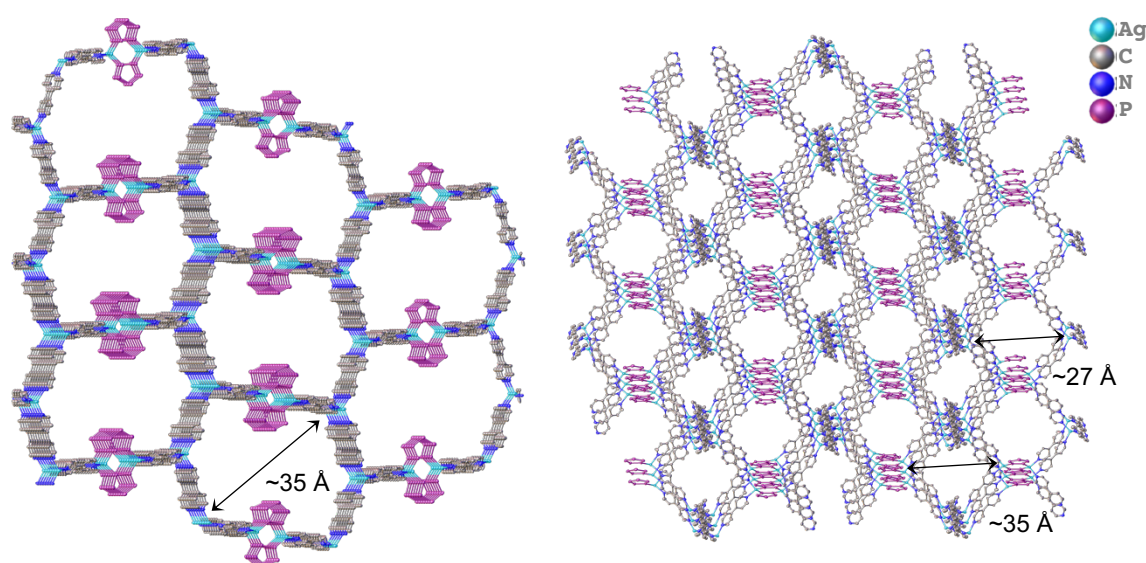


**Figure 8.8.** Solid-state structure of compound **12** along the  $a$ - $c$ -plane (left) and long the  $-a$ - $c$ -plane (right).  $[\text{Cp}^*\text{Fe}]$  fragments, hydrogen atoms and anions are omitted for clarity. Ellipsoids are depicted at 50% probability level.

Along the  $a/c$ -plane the pores of the 3D network reveal a diagonal of  $\sim 35 \text{ \AA}$  (Figure 8.8 left), along the  $-a/c$ -plane two types of pores are present (Figure 8.8 right). The distance of one  $\text{Ag}_2\text{P}_4$  moiety to the opposite one is  $\sim 35 \text{ \AA}$ , while the diagonal of one  $\text{Ag}(\text{I})$  knot to a facing one is  $\sim 27 \text{ \AA}$ . The pores are filled with the bulky weakly coordinating anions.

The  $\text{Ag}(\text{I})$  centers of the planar ring moieties are coordinated by two 4,4'-bipyridine units demonstrating a tetrahedral coordination environment (Figure 8.9.a). The pyridyl rings of the linkers deviate from planarity ( $21^\circ$ ; Figure 8.9.b). The  $\text{Ag}(\text{I})$  knots show a distorted tetrahedral coordination with  $\text{NAgN}$  angles between  $99.8(3)^\circ$  and  $122.4(3)^\circ$  (Figure 8.9.c).

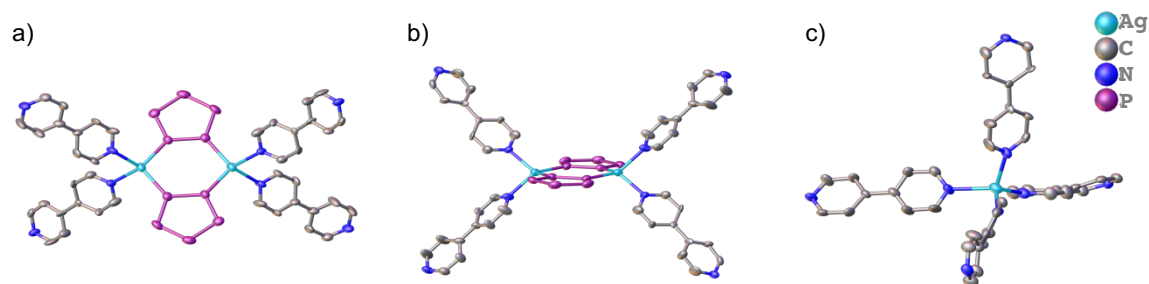


**Figure 8.9.** Extracts of the solid-state structure of compound **12**. a)  $\text{Ag}_2\text{P}_4$  six-membered ring coordinated by linker molecules along the  $c$  axis; b)  $\text{Ag}_2\text{P}_4$  six-membered ring coordinated by linker molecules along the  $-a$ - $c$ -plane; c) distorted tetrahedrally coordinated  $\text{Ag}(\text{I})$  knots.  $[\text{Cp}^*\text{Fe}]$  fragments, hydrogen atoms and anions are omitted for clarity. Ellipsoids are depicted at 50% probability level.

After several months the crystals were measured again as they changed their color from dark green blocks to light green plates in the reaction solution. The obtained solid-state structure of **13** was identical to the one achieved in the reaction with a  $\text{C}:\text{Ag}[\text{BAR}^{\text{Cl}}]:\text{linker}$  ratio of 2:1:2. The 2D polymer **13** consists, similar to compound **11**, of  $\text{AgP}_5$  chains cross-linked with 4,4'-bipyridine units (Figure 8.10.a) with a 1,3-coordination of the  $\text{P}_5$  towards the  $\text{Ag}(\text{I})$ . The difference to the 2D polymer **11** is the coordination mode of the  $\text{Ag}(\text{I})$  ions: in compound **13**, the  $\text{Ag}(\text{I})$  centers are tetrahedrally coordinated by two linkers and two  $\text{P}_5$  entities resulting in a zig-zag polymer (Figure 8.10.b), in contrast to the trigonal planar coordination of the  $\text{Ag}(\text{I})$  ion in **11**.

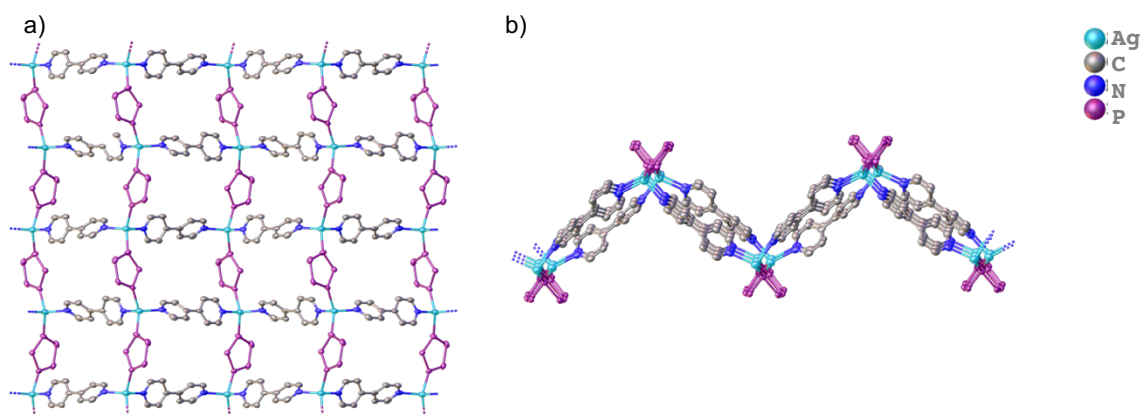


**Figure 8.10.** Solid-state structure of compound **13**. a) Top-view of 2D coordination polymer; b) Section of the zig-zag structural motif.  $[\text{Cp}^*\text{Fe}]$  fragments, hydrogen atoms and anions are omitted for clarity. Ellipsoids are depicted at 50% probability level.

The pyridyl rings in each linker unit are twisted by  $38^\circ$ . Interestingly, the composition of **13** is 1:1:1 and therefore, not matching with the used stoichiometry. However, no other compounds could be determined.

Furthermore, reacting **C**,  $\text{Ag}[\text{BAR}^{\text{Cl}}]$  and 4,4'-bipyridine in a one-pot reaction, in a ratio of 1:1:1 leads to the two-dimensional network **14** (Figure 8.11.a). The 2D polymer contains two layers resulting of the  $\eta^1:\eta^2$ -coordination mode of the  $\text{P}_5$  ring (Figure 8.11.b and c). Every  $\text{Ag}(\text{I})$  center is coordinated by four neighboring atoms, however, there are two types of silver atoms present. One type is  $\eta^1$ -coordinated by one phosphorus atom of **C** and distorted tetrahedrally coordinated by three linker units. The second kind of  $\text{Ag}(\text{I})$  cations has, as well as type I, a tetrahedral coordination environment, however, they are  $\eta^2$ -coordinated by one **C** entity and only two linker units (Figure 8.11.c).

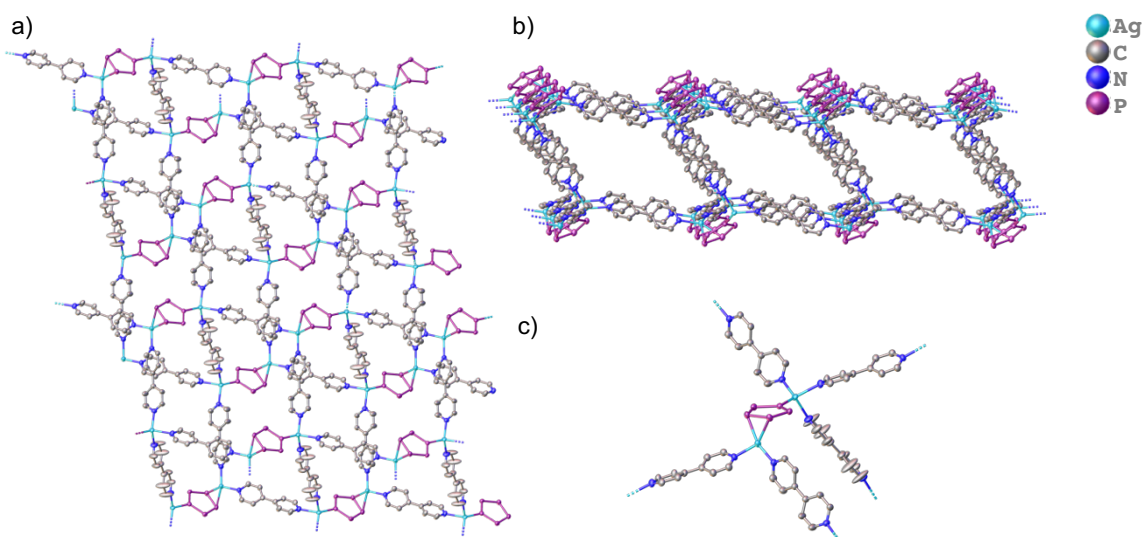


**Figure 8.11.** Solid-state structure of compound **14**. a) Top-view of 2D coordination polymer; b) Layered structure; c)  $\eta^1:\eta^2$ -coordination mode of the  $\text{P}_5$  ring.  $[\text{Cp}^*\text{Fe}]$  fragments, hydrogen atoms and anions are omitted for clarity. Ellipsoids are depicted at 50% probability level.

Compounds **11-14** are hardly reproducible and not selectively formed, therefore, no further analytics was possible.

These different coordination geometries of  $\text{Ag}(\text{I})$  show its flexible coordination sphere and the resulting rich structural diversity of  $\text{Ag}(\text{I})$  coordination compounds. This offers an interesting research area, as well as challenging synthetic tasks.

## 8.3 Supporting Information

### 8.3.1 General

All experiments were performed under an atmosphere of dry argon or nitrogen using standard Schlenk and glovebox techniques. The nitrogen/argon was dried and purified from traces of oxygen with a Cu/MgSO<sub>4</sub> catalyst, concentrated H<sub>2</sub>SO<sub>4</sub> and orange gel. All used solvents were taken from the solvent drying machine MB SPS-800 of the company MBRAUN. The precursors [Cp<sub>2</sub>Mo<sub>2</sub>(CO)<sub>4</sub>(μ,η<sup>2,2</sup>-As<sub>2</sub>)] (**A**)<sup>11</sup>, [Cp\*Fe(η<sup>5</sup>-P<sub>5</sub>)] (**B**)<sup>12</sup>, [Cu(CH<sub>3</sub>CN)<sub>4</sub>][Al{OC(CF<sub>3</sub>)<sub>3</sub>}<sub>4</sub>]<sup>13</sup> and Ag[B(3,5-C<sub>6</sub>H<sub>3</sub>Cl<sub>2</sub>)<sub>4</sub>]<sup>14</sup> were prepared according to literature procedures. Ag[PF<sub>6</sub>] (abcr), 1,2-di(4-pyridyl)ethylene (TCI), 2,2'-bipyrimidine (TCI) and 4,4'-bipyridine (TCI) were used as received without further purification.

Solution NMR spectra were recorded on a Bruker Avance III HD 400 spectrometer (<sup>1</sup>H: 400 MHz, <sup>31</sup>P: 161 MHz, <sup>13</sup>C: 100 MHz, <sup>19</sup>F: 376 MHz) with acetonitrile-d<sub>3</sub> as solvent at room temperature. The chemical shifts  $\delta$  are presented in parts per million ppm and coupling constants  $J$  in Hz. The following samples were used as external reference: TMS (<sup>1</sup>H, <sup>13</sup>C), CFC<sub>3</sub> (<sup>19</sup>F), H<sub>3</sub>PO<sub>4</sub> 85 % (<sup>31</sup>P). The spectra were processed and analyzed using the software Bruker TopSpin 3.0. IR spectra were recorded as solids with an ATR-Ge disc on a Thermo Fisher Nicolet iS5 spectrometer. Elemental analyses were performed on an Elementar Vario MICRO cube apparatus. Mass spectra were recorded on an Agilent Q-TOF 6540 UHD mass spectrometer with acetonitrile as solvent.

The first synthesis of compound **4** was performed by Mehdi Elsayed Moussa.

### 8.3.2 Synthetic Procedure

#### Synthesis and Characterization of **2**

0.05 mmol Au(tht)Cl (16 mg) in 5 mL CH<sub>2</sub>Cl<sub>2</sub> was added to a stirred solution of [Cp<sub>2</sub>Mo<sub>2</sub>(CO)<sub>4</sub>(η<sup>2</sup>-As<sub>2</sub>)] (30 mg, 0.05 mmol) in 5 mL CH<sub>2</sub>Cl<sub>2</sub>, and stirred for 2h at room temperature. The red solution was filtered and carefully layered with threefold amount of *n*-pentane and stored at room temperature in the dark. After one week red brownish crystals were formed. The crystals were washed with *n*-pentane and dried *in vacuo*. Yield 15 mg (37% referred to [Cp<sub>2</sub>Mo<sub>2</sub>(CO)<sub>4</sub>(η<sup>2</sup>-As<sub>2</sub>)])

<sup>1</sup>H NMR (400MHz, CD<sub>3</sub>CN):  $\delta$  = 5.39 (s)

<sup>13</sup>C NMR (100MHz, CD<sub>3</sub>CN):  $\delta$  = 86.99 (C<sub>5</sub>H<sub>5</sub>)

Positive ion ESI-MS (CH<sub>3</sub>CN, r. t.):  $m/z$  (%) = 1364.39 (100) [ $\{\text{Cp}_2(\text{CO})_4\text{Mo}_2\text{As}_2\}_2\text{Au}\}^+$ .

Negative ion ESI-MS (CH<sub>3</sub>CN, r. t.):  $m/z$  (%) = 266.91 (100) [ $\text{AuCl}_2^-$ ], 253.78 (30) [ $\text{CpMo}(\text{CO})_2\text{Cl}^-$ ], the attribution of some additional peaks was not possible, but the fragments do not contain gold or molybdenum.

IR (solid, CO bands):  $\tilde{\nu}/\text{cm}^{-1}$ : 1997 (w), 1982 (w), 1964 (s), 1936 (vs), 1923 (vs);

#### Synthesis and Characterization of 4

0.05 mmol of CuCl in 5 mL CH<sub>2</sub>Cl<sub>2</sub>:CH<sub>3</sub>CN 1:1 was added to a stirred solution of [ $\text{Cp}_2\text{Mo}_2(\text{CO})_4(\eta^2\text{-As}_2)$ ] (29 mg, 0.05 mmol) in 7 mL CH<sub>2</sub>Cl<sub>2</sub>:CH<sub>3</sub>CN 2:1 and stirred for 2h at room temperature. The clear orange solution was carefully layered with threefold amount of *n*-pentane and stored at room temperature in the dark. After three days orange blocks were formed. The crystals were washed with *n*-pentane and dried *in vacuo*. Yield 12 mg (35% referred to [ $\text{Cp}_2\text{Mo}_2(\text{CO})_4(\eta^2\text{-As}_2)$ ])

<sup>1</sup>H NMR (400MHz, CD<sub>3</sub>CN):  $\delta$  = 5.26 (s, 10H)

<sup>13</sup>C NMR (100MHz, CD<sub>3</sub>CN):  $\delta$  = 229.54 (CO), 85.85 (C<sub>5</sub>H<sub>5</sub>)

Positive ion ESI-MS (CH<sub>3</sub>CN, r. t.):  $m/z$  (%) = 1232.36 (100) [ $\{\text{Cp}_2(\text{CO})_4\text{Mo}_2\text{As}_2\}_2\text{Cu}\}^+$ , 687.67 (85) [ $\{\text{Cp}_2(\text{CO})_4\text{Mo}_2\text{As}_2\}\text{Cu}(\text{CH}_3\text{CN})\}^+$ ].

Negative ion ESI-MS (CH<sub>3</sub>CN, r. t.):  $m/z$  (%) = 134.87 (100) [ $\text{CuCl}_2^-$ ].

Elemental analysis, calcd (%) for C<sub>28</sub>H<sub>20</sub>As<sub>4</sub>Cl<sub>2</sub>Cu<sub>2</sub>Mo<sub>4</sub>O<sub>8</sub> (1365.91): C, 24.62; H, 1.48; found: C, 24.85; H, 1.42;

#### Synthesis and Characterization of 5

Hydrolyzed AgPF<sub>6</sub> (1 eq., 4 mg, 0.016 mmol) in 5 mL CH<sub>2</sub>Cl<sub>2</sub>:CH<sub>3</sub>CN 1:1 was added to a stirred solution of [ $\text{Cp}_2\text{Mo}_2(\text{CO})_4(\eta^2\text{-As}_2)$ ] (3 eq., 29 mg, 0.05 mmol) in 5 mL CH<sub>2</sub>Cl<sub>2</sub>:CH<sub>3</sub>CN 1:1 and stirred for 1 h at room temperature. Then 0.1 mmol (6 eq., 16 mg) of the linker 2,2'-bipyrimidine was added and stirred for another 2 h. The red solution was filtered and carefully layered with the threefold amount of *n*-pentane and stored at room temperature in the dark. After several days, compound **5** was obtained as dark red blocks. The supernatant was decanted off, the remaining crystals washed with *n*-pentane and dried *in vacuo*.

<sup>1</sup>H NMR (CD<sub>3</sub>CN):  $\delta$  = 9.05 (broad s, 4H), 7.70 (t,  $J_{H,H}$  = 4.79 Hz, 2H), 5.45 (uncoordinated Cp<sub>2</sub>(CO)<sub>4</sub>Mo<sub>2</sub>As<sub>2</sub>), 5.32 (s, 10H)

<sup>31</sup>P {<sup>1</sup>H} NMR (CD<sub>3</sub>CN):  $\delta/\text{ppm}$  = -12.83 (t,  $^1J_{P,F}$  = 948.19 Hz)

<sup>19</sup>F {<sup>1</sup>H} NMR (CD<sub>3</sub>CN):  $\delta/\text{ppm}$  = -80.22 (d,  $^1J_{F,P}$  = 949.17 Hz), -150.63, -150.69 (decomposition products of HF and glas)

Positive ion ESI-MS (CH<sub>3</sub>CN, r. t.):  $m/z$  (%) = 848.68 (100) [ $\{\text{Cp}_2(\text{CO})_4\text{Mo}_2\text{As}_2\}\text{Ag}(\text{C}_8\text{H}_6\text{N}_4)\}^+$ , 423.02 (19) [ $\text{Ag}(\text{C}_8\text{H}_6\text{N}_4)_2\}^+$ , 264.97 (30) [ $\text{Ag}(\text{C}_8\text{H}_6\text{N}_4)\}^+$ ].



Negative ion ESI-MS (CH<sub>3</sub>CN, r. t.):  $m/z$  (%) = 309.17 (11) [Ag(PF<sub>2</sub>O<sub>2</sub>)<sub>2</sub>]<sup>-</sup>, 144.97 (57) [PF<sub>6</sub>]<sup>-</sup>, 100.96 (31) [PF<sub>2</sub>O<sub>2</sub>]<sup>-</sup>, the attribution of some additional peaks was not possible, however, some peaks could be assigned to linker molecules with anions and H<sub>2</sub>O.

### Synthesis of 6

Hydrolyzed AgPF<sub>6</sub> (1 eq., 4 mg, 0.016 mmol) in 5 mL CH<sub>2</sub>Cl<sub>2</sub>:CH<sub>3</sub>CN 1:1 was added to a stirred solution of [Cp<sub>2</sub>Mo<sub>2</sub>(CO)<sub>4</sub>(η<sup>2</sup>-As<sub>2</sub>)] (3 eq., 29 mg, 0.05 mmol) in 5 mL CH<sub>2</sub>Cl<sub>2</sub>:CH<sub>3</sub>CN 1:1 and stirred for 1 h at room temperature. Then 0.1 mmol (6 eq., 16 mg) of the linker 4,4'-bipyridine was added and stirred for another 2 h. The red solution was filtered and carefully layered with the threefold amount of *n*-pentane and stored at room temperature in the dark. After several days, compound **6** was obtained as orange blocks. The supernatant was decanted off, the remaining crystals washed with *n*-pentane and dried *in vacuo*.

### Synthesis of 7

[Cu(CH<sub>3</sub>CN)<sub>4</sub>][Al{OC(CF<sub>3</sub>)<sub>3</sub>}<sub>4</sub>] (1 eq., 60 mg, 0.05 mmol) in 5 mL CH<sub>2</sub>Cl<sub>2</sub> was added to a stirred solution of [Cp<sub>2</sub>Mo<sub>2</sub>(CO)<sub>4</sub>(η<sup>2</sup>-As<sub>2</sub>)] (1 eq., 29 mg, 0.05 mmol) in 5 mL CH<sub>2</sub>Cl<sub>2</sub> and stirred for 1 h at room temperature. Then 0.05 mmol (1 eq., 9 mg) of the linker 1,2-di(4-pyridyl)ethylene was added and stirred for another 2 h. The red solution was filtered and carefully layered with the threefold amount of *n*-pentane and stored at room temperature in the dark. After several days, compound **7** was obtained as orange blocks. The supernatant was decanted off, the remaining crystals washed with *n*-pentane and dried *in vacuo*.

### Synthesis of 8, 9 and 10

Ag[B(3,5-C<sub>6</sub>H<sub>3</sub>Cl<sub>2</sub>)<sub>4</sub>] (1 eq., 70 mg, 0.1 mmol) in 11 mL CH<sub>2</sub>Cl<sub>2</sub>:CH<sub>3</sub>CN 10:1 was added to a stirred solution of [Cp\*Fe(η<sup>5</sup>-P<sub>5</sub>)] (1 eq., 35 mg, 0.1 mmol) in 10 mL CH<sub>2</sub>Cl<sub>2</sub> and stirred for 1.5 h at room temperature. The green solution was carefully layered with the threefold amount of *n*-hexane and stored at room temperature in the dark. After a few days, compounds **8**, **9** and **10** were obtained as green rods and red blocks. The supernatant was decanted off, the remaining crystals washed with *n*-pentane and dried *in vacuo*.

### Synthesis of 11

Ag[B(3,5-C<sub>6</sub>H<sub>3</sub>Cl<sub>2</sub>)<sub>4</sub>] (1 eq., 70 mg, 0.1 mmol) in 6 mL CH<sub>2</sub>Cl<sub>2</sub>:CH<sub>3</sub>CN 10:1 was added to a stirred solution of [Cp\*Fe(η<sup>5</sup>-P<sub>5</sub>)] (1 eq., 35 mg, 0.1 mmol) in 5 mL CH<sub>2</sub>Cl<sub>2</sub> and stirred for 1 h at room temperature. The green solution was carefully layered with 4,4'-bipyridine (0.5 eq., 8 mg, 0.05 mmol) in 20 mL toluene and stored at room temperature in the dark.



After a few days, compound **11** was obtained as green rods. The supernatant was decanted off, the remaining crystals washed with *n*-pentane and dried *in vacuo*.

### Synthesis of 12

Ag[B(3,5-C<sub>6</sub>H<sub>3</sub>Cl<sub>2</sub>)<sub>4</sub>] (1 eq., 70 mg, 0.1 mmol) in 4 mL CH<sub>2</sub>Cl<sub>2</sub>:CH<sub>3</sub>CN 10:1 was added to a stirred solution of [Cp\*Fe(η<sup>5</sup>-P<sub>5</sub>)] (1 eq., 35 mg, 0.1 mmol) in 2 mL CH<sub>2</sub>Cl<sub>2</sub> and stirred for 1 h at room temperature. The green solution was carefully layered with 4,4'-bipyridine (1 eq., 16 mg, 0.1 mmol) in 20 mL toluene and stored at room temperature in the dark. After 2 weeks, compound **12** was obtained as light green rods. Also colorless plates and dark green blocks were observed, but no structural analysis was possible. The supernatant was decanted off, the remaining crystals washed with *n*-pentane and dried *in vacuo*.

### Synthesis of 13

Ag[B(3,5-C<sub>6</sub>H<sub>3</sub>Cl<sub>2</sub>)<sub>4</sub>] (0.5 eq., 35 mg, 0.05 mmol) in 4 mL CH<sub>2</sub>Cl<sub>2</sub>:CH<sub>3</sub>CN 10:1 was added to a stirred solution of [Cp\*Fe(η<sup>5</sup>-P<sub>5</sub>)] (1 eq., 35 mg, 0.1 mmol) in 2 mL CH<sub>2</sub>Cl<sub>2</sub> and stirred for 1 h at room temperature. The green solution was carefully layered with 4,4'-bipyridine (1 eq., 16 mg, 0.1 mmol) in 20 mL toluene and stored at room temperature in the dark. After 2 weeks, compound **13** was obtained as light green rods. The supernatant was decanted off, the remaining crystals washed with *n*-pentane and dried *in vacuo*.

### Synthesis of 14

Ag[B(3,5-C<sub>6</sub>H<sub>3</sub>Cl<sub>2</sub>)<sub>4</sub>] (1 eq., 35 mg, 0.05 mmol) in 5 mL CH<sub>2</sub>Cl<sub>2</sub>:CH<sub>3</sub>CN 10:1 was added to a stirred solution of [Cp\*Fe(η<sup>5</sup>-P<sub>5</sub>)] (1 eq., 17 mg, 0.05 mmol) in 5 mL CH<sub>2</sub>Cl<sub>2</sub> and stirred for 2.5 h at room temperature. 4,4'-bipyridine (1 eq., 8 mg, 0.05 mmol) was added in 2 mL CH<sub>2</sub>Cl<sub>2</sub>. The green solution was carefully layered with the threefold amount of *n*-hexane and stored at room temperature in the dark. After 2 days, compound **14** was obtained as green rods. The supernatant was decanted off, the remaining crystals washed with *n*-pentane and dried *in vacuo*.

## 8.3.3 Crystallographic Data

Crystals of **2**, **4-14** were taken from a Schlenk flask under a stream of argon and immediately covered with mineral oil to prevent a loss of solvent. The quickly chosen single crystals covered by a thin oil/Fomblin layer were taken to the pre-centered goniometer head with CryoMount® and directly attached to the diffractometer into a stream of cold nitrogen.

The diffraction experiments for **2**, **4-14** were collected on Rigaku Oxford Diffraction diffractometers; on a Xcalibur, Gemini ultra diffractometer equipped with a Atlas2 detector (MoK $\alpha$  radiation,  $\lambda = 0.71073 \text{ \AA}$ ) (**3**); on a SuperNova diffractometer equipped with a Atlas detector (CuK $\alpha$  radiation,  $\lambda = 1.54178 \text{ \AA}$ ) (**11**); on a GV50 diffractometer equipped with a TitanS2 detector (CuK $\alpha$  radiation,  $\lambda = 1.54178 \text{ \AA}$ ) (**2**, **5**, **6**) or on a GV1000 diffractometer equipped with a TitanS2 detector (CuK $\alpha$  radiation,  $\lambda = 1.54178 \text{ \AA}$ ) (**7**, **9**, **10**, **12**, **13**, **14**), respectively. The crystals were kept at  $T = 123(1) \text{ K}$  during data collection. Data collection and reduction were performed with *CrysAlis PRO* [Version V1.171.38.41h, 2015 (**7**), V1.171.38.42b, 2015 (**10**, **11**), V1.171.38.43, 2015 (**9**, **12**, **13**), V1.171.38.46, 2015 (**13**), V1.171.41.54a, 2020 (**2**, **5**, **6**)].<sup>15</sup> For compounds **2**, **5**, **6** and **9** a numerical absorption correction based on gaussian integration over a multifaceted crystal model and an empirical absorption correction using spherical harmonics as implemented in SCALE3 ABSPACK scaling algorithm was applied. For compounds **10**, **11**, **12**, **13** and **14** a multi-scan absorption correction and an empirical absorption correction using spherical harmonics as implemented in SCALE3 ABSPACK scaling algorithm was applied. The crystal structures were solved by dual methods or intrinsic phasing solution method with *SHELXT*<sup>16</sup> or *Olex2*<sup>17</sup> programs and refined by full-matrix least-squares method against  $|F|^2$  in anisotropic approximation using multiprocessor versions of SHELXL.<sup>18</sup> Hydrogen atoms were refined in calculated positions using riding on pivot atom model. In case of the disorder, the site occupancies of the disordered components were refined with their  $U_{\text{iso}}$  fixed at average  $U_{\text{eq}}$  for fully occupied atoms in given structure in order to avoid correlations. After refinement, occupancies were fixed at the resulting values and the refinement of the atomic displacement parameters was performed.

One CH<sub>3</sub>CN molecule in **6** demonstrates disorder. The anion in compound **6** is disordered over two position with an occupancy of 0.2 for [PF<sub>2</sub>O<sub>2</sub>]<sup>-</sup> and 0.8 for [PF<sub>6</sub>]<sup>-</sup>. Furthermore, compound **6** shows a disordered solvent molecule with an occupancy of 0.3 for CH<sub>2</sub>Cl<sub>2</sub> and 0.7 for CH<sub>3</sub>CN. The disorder of compound **10** is discussed in 8.3.2.1. Compound **9** shows a disorder of one Cp ring over two positions. The included toluene molecule of compound **13** was found to be highly disordered and a correct modelling was not possible. We have therefore proceeded to a 'squeeze' treatment<sup>19</sup> in order to remove the scattering contribution of these molecules. Compound **14** shows two disordered CH<sub>2</sub>Cl<sub>2</sub> molecules. The solid-state structures for compound **7**, **9**, **10**, **11**, **11**, **13** and **14** are only preliminary results. The data sets for compound **7**, are not suitable and therefore, they are not depicted. The data sets for compounds **10** and **12** are not complete.

All ORTEP drawings for **2**, **4-14** were made with the Olex2 software.<sup>17</sup>

The solid-state structures of compounds **2**, **5** and **6** were refined by Michael Seidl.

**Table S8.1.** Crystallographic details for **2**, **4**, **5** and **6**.

Compound	<b>2</b>	<b>4</b>	<b>5</b>	<b>6</b> · 0.3 CH <sub>2</sub> Cl <sub>2</sub> / 1.7 CH <sub>3</sub> CN
Data set (internal naming)	JS125	ems_616_aP_abs	JS226	JS225
Formula	C <sub>14</sub> H <sub>10</sub> As <sub>2</sub> AuCl Mo <sub>2</sub> O <sub>4</sub>	C <sub>56</sub> H <sub>40</sub> As <sub>8</sub> Cl <sub>4</sub> Cu <sub>4</sub> Mo <sub>8</sub> O <sub>16</sub>	C <sub>22</sub> H <sub>16</sub> AgAs <sub>2</sub> F <sub>2</sub> Mo <sub>2</sub> N <sub>4</sub> O <sub>6</sub> P	C <sub>41.7</sub> H <sub>33.7</sub> Ag <sub>2</sub> As <sub>4</sub> Cl <sub>0.6</sub> F <sub>7.2</sub> Mo <sub>4</sub> N <sub>3.7</sub> O <sub>10.4</sub> P <sub>2</sub>
<i>D</i> <sub>calc.</sub> / g · cm <sup>-3</sup>	2.982	2.559	2.194	2.1324
μ/mm <sup>-1</sup>	31.547	6.452	16.029	17.542
Formula Weight	816.36	2731.72	950.95	1872.21
Colour	orange	clear orange	orange	orange
Shape	block	block	block	plate
Size/mm <sup>3</sup>	0.13×0.09×0.05	0.21×0.20×0.10	0.14×0.13×0.09	0.11×0.07×0.03
<i>T</i> /K	123.0110)	123(1)	122.91(18)	122.96(13)
Crystal System	trigonal	triclinic	orthorhombic	monoclinic
Flack Parameter	-0.017(17)	-	-	-
Hoof Parameter	0.003(9)	-	-	-
Space Group	<i>P</i> 3 <sub>2</sub>	<i>P</i> $\bar{1}$	<i>Pbcn</i>	<i>P</i> 2 <sub>1</sub> / <i>c</i>
<i>a</i> /Å	8.30060(10)	14.9570(5)	12.5626(3)	19.6075(3)
<i>b</i> /Å	8.30060(10)	14.9928(5)	20.1230(4)	14.3356(2)
<i>c</i> /Å	22.8539(3)	16.9565(6)	11.3876(3)	20.8460(3)
α/°	90	89.238(3)	90	90
β/°	90	88.892(3)	90	114.071(2)
γ/°	120	68.862(3)	90	90
<i>V</i> /Å <sup>3</sup>	1363.67(4)	3545.9(2)	2878.75(12)	5349.96(15)
<i>Z</i>	3	2	4	4
<i>Z'</i>	1	1	0.5	1
Wavelength/Å	1.54184	0.71073	1.54184	1.54184
Radiation type	Cu K <sub>α</sub>	Mo K <sub>α</sub>	Cu K <sub>α</sub>	Cu K <sub>α</sub>
θ <sub>min</sub> /°	5.808	3.392	4.149	3.860
θ <sub>max</sub> /°	73.446	32.429	73.731	74.025
Measured Refl.	5272	34184	6785	30536
Independent Refl.	3045	22087	2826	10532
Reflections with <i>I</i> > 2( <i>I</i> )	2999	18758	2697	9532
<i>R</i> <sub>int</sub>	0.0368	0.0263	0.0235	0.0420
Parameters	217	865	204	776
Restraints	7	0	24	152
Largest Peak	1.766	0.763	2.376	1.178
Deepest Hole	-1.022	-0.761	-1.074	-0.774
GooF	1.057	1.024	1.082	1.086
<i>wR</i> <sub>2</sub> (all data)	0.0967	0.0529	0.0891	0.0714
<i>wR</i> <sub>2</sub>	0.0963	0.0498	0.0877	0.0694
<i>R</i> <sub>1</sub> (all data)	0.0398	0.0405	0.0342	0.0358
<i>R</i> <sub>1</sub>	0.0393	0.0304	0.0326	0.0308

Table S8.2. Crystallographic details for 9, 10, 11 and 12.

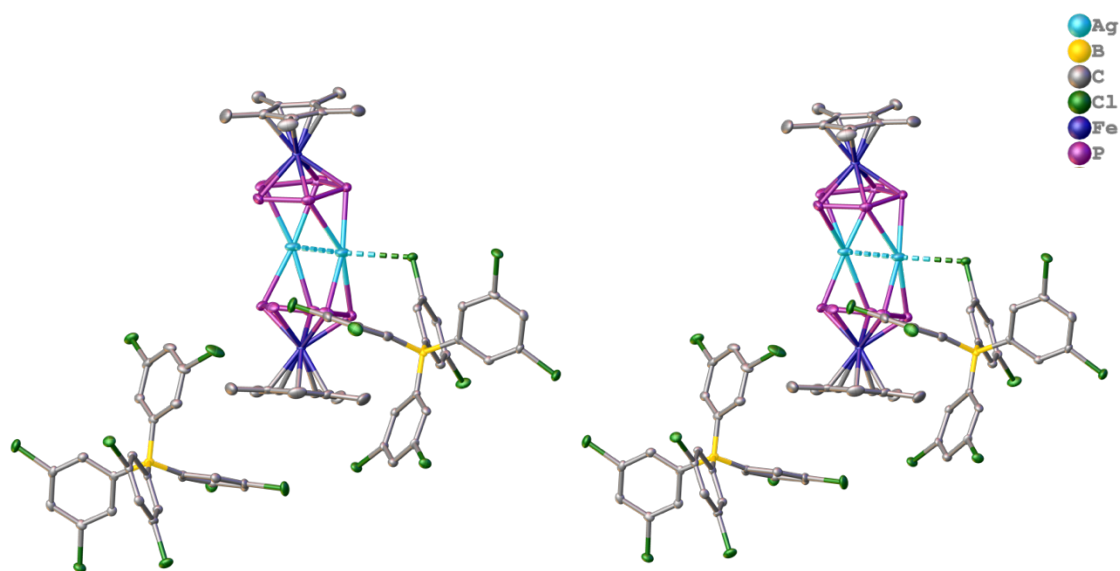
Compound	9	10	11	12 · CH <sub>2</sub> Cl <sub>2</sub>
Data set (internal naming)	JS001_gruen	JS001_rote blöcke_nicht complete	JS007	JS019_hellgruen_wit
Formula	C <sub>276</sub> H <sub>216</sub> B <sub>4</sub> P <sub>40</sub> Cl <sub>64</sub> Fe <sub>8</sub> Ag <sub>8</sub>	C <sub>68</sub> H <sub>54</sub> B <sub>2</sub> P <sub>10</sub> Cl <sub>16</sub> Fe <sub>2</sub> Ag <sub>2</sub>	C <sub>92</sub> H <sub>62</sub> B <sub>2</sub> N <sub>2</sub> P <sub>10</sub> Cl <sub>24</sub> Fe <sub>2</sub> Ag <sub>2</sub>	C <sub>20.94</sub> H <sub>9.18</sub> Ag <sub>0.47</sub> B <sub>0.47</sub> Cl <sub>4.24</sub> Fe <sub>0.24</sub> N <sub>1.41</sub> P <sub>1.18</sub>
<i>D</i> <sub>calc.</sub> / g · cm <sup>-3</sup>	1.734	1.819	2.028	1.611
μ/mm <sup>-1</sup>	10.208	10.712	14.888	10.443
Formula Weight	8393.08	2097.07	2704.99	536.10
Colour	green	red	green	light green
Shape	rods	blocks	rods	rod
Size/mm <sup>3</sup>	0.29×0.12×0.08	?	?	?
<i>T</i> /K	122.98(10)	122.99(10)	123.01(10)	122.96(17)
Crystal System	monoclinic	monoclinic	monoclinic	monoclinic
Space Group	<i>P</i> 2 <sub>1</sub> / <i>n</i>	<i>P</i> 2 <sub>1</sub> / <i>n</i>	<i>P</i> 2 <sub>1</sub> / <i>n</i>	<i>P</i> 2 <sub>1</sub> / <i>n</i>
<i>a</i> /Å	14.4022(2)	16.5700(4)	14.0938(3)	13.4300(4)
<i>b</i> /Å	34.7489(7)	16.8337(2)	12.7788(3)	48.511(4)
<i>c</i> /Å	16.2365(3)	27.4637(3)	24.7703(6)	14.6800(4)
α/°	90	90	90	90
β/°	98.397(2)	91.244(2)	96.883(2)	100.800(3)
γ/°	90	90	90	90
<i>V</i> /Å <sup>3</sup>	8038.6(2)	7658.8(2)	4429.02(18)	9394.6(8)
<i>Z</i>	1	4	2	17
<i>Z'</i>	0.25	1	0.5	4.25
Wavelength/Å	1.39222	1.39222	1.54184	1.54184
Radiation type	Cu K <sub>α</sub>	Cu K <sub>α</sub>	Cu K <sub>α</sub>	Cu K <sub>α</sub>
<i>θ</i> <sub>min</sub> /°	2.737	2.780	3.442	8.359
<i>θ</i> <sub>max</sub> /°	74.644	60.377	74.346	52.773
Measured Refl.	61176	43650	19005	18003
Independent Refl.	21639	12770	8701	8735
Reflections with <i>I</i> > 2( <i>I</i> )	16899	10875	7634	6378
<i>R</i> <sub>int</sub>	0.0617	0.0406	0.0311	0.0533
Parameters	961	915	510	1108
Restraints	0	0	0	0
Largest Peak	1.461	0.819	0.903	0.698
Deepest Hole	-1.604	-0.696	-1.104	-0.740
GooF	1.009	1.036	1.038	1.043
<i>wR</i> <sub>2</sub> (all data)	0.1420	0.0763	0.1023	0.1399
<i>wR</i> <sub>2</sub>	0.1299	0.0715	0.0978	0.1252
<i>R</i> <sub>1</sub> (all data)	0.0756	0.0409	0.0458	0.0873
<i>R</i> <sub>1</sub>	0.0586	0.0317	0.0391	0.0589

Table S8.3. Crystallographic details for **13** and **14**.

Compound	<b>13</b>	<b>14</b> · 3 CH <sub>2</sub> Cl <sub>2</sub>
Data set (internal naming)	JS020_hellgruen	JS029
Formula	C <sub>7.8</sub> H <sub>6.2</sub> N <sub>0.4</sub> Fe <sub>0.2</sub> B <sub>0.2</sub> Ag <sub>0.2</sub> Cl <sub>1.4</sub> P <sub>0.9</sub>	C <sub>86.5</sub> H <sub>59</sub> Ag <sub>2</sub> B <sub>2</sub> Cl <sub>18.1</sub> FeN <sub>5</sub> P <sub>5</sub>
$D_{calc.} / \text{g} \cdot \text{cm}^{-3}$	1.269	1.419
$\mu / \text{mm}^{-1}$	1.364	9.265
Formula Weight	177.55	76.41
Colour	light green	green
Shape	rods	rods
$T / \text{K}$	123.1(4)	123.01(13)
Crystal System	orthorhombic	triclinic
Space Group	<i>Pbca</i>	<i>P</i> $\bar{1}$
$a / \text{\AA}$	18.6535(2)	15.3951(2)
$b / \text{\AA}$	15.69450(10)	16.4937(2)
$c / \text{\AA}$	35.7030(3)	21.9765(4)
$\alpha / ^\circ$	90	82.3150(10)
$\beta / ^\circ$	90	71.7860(10)
$\gamma / ^\circ$	90	70.9900(10)
$V / \text{\AA}^3$	10452.32(16)	5008.47(13)
$Z$	45	56
$Z'$	5.625	28
Wavelength/ $\text{\AA}$	1.54184	1.54184
Radiation type	Cu K $\alpha$	Cu K $\alpha$
$\theta_{min} / ^\circ$	2.475	2.835
$\theta_{max} / ^\circ$	74.148	74.808
Measured Refl.	269383	101951
Independent Refl.	10596	20380
Reflections with $I > 2(I)$	9710	17375
$R_{int}$	0.0886	0.0601
Parameters	564	1032
Restraints	0	0
Largest Peak	2.672	1.166
Deepest Hole	-4.126	-1.297
GooF	1.053	0.985
$wR_2$ (all data)	0.2272	0.1288
$wR_2$	0.2220	0.1175
$R_1$ (all data)	0.0868	0.0543
$R_1$	0.0817	0.0448

### Disorder of compound **10**

The data set for compound **10** is only 85% complete, so these are preliminary results. Compound **10** is disordered over two positions (90:10). The main part, with 90% occupancy, (Figure S8.1 left) shows an Ag-Ag middle-deck between two P<sub>5</sub> rings. Both Ag(I) centers are coordinated in an  $\eta^2$ -fashion by two phosphorus atoms of each P<sub>5</sub> ring, while one Ag(I) is additionally coordinated by one chloride atom of one anion. The minor part (Figure S8.1 right) consists of the same middle deck, furthermore, the Ag(I) not coordinated by the chloride atom is  $\eta^2$ -coordinated by one P<sub>5</sub> ring.



**Figure S8.1.** Disordered solid-state structure of compound **10**. Hydrogen atoms are omitted for clarity. Ellipsoids are shown at 50% probability level.

## 8.4 References

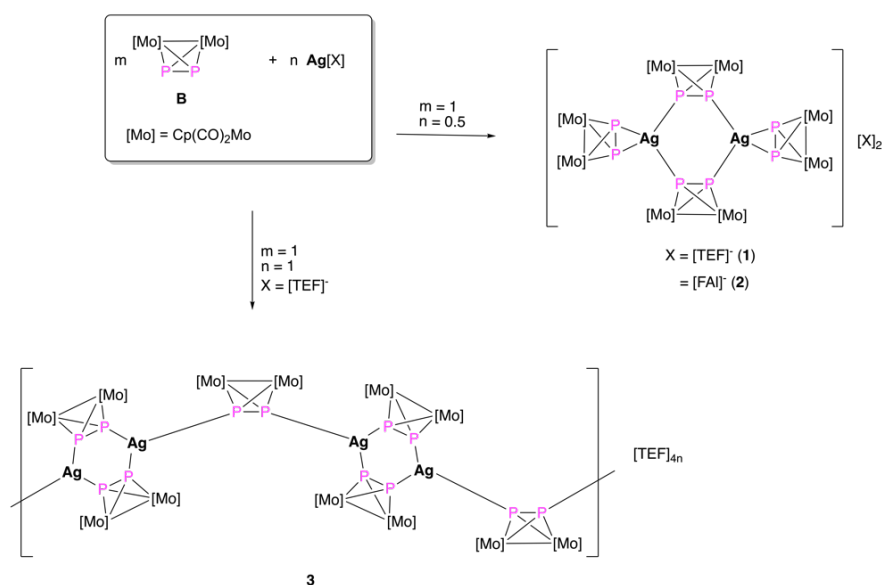
- [1] M. Scheer, L. J. Gregoriades, M. Zabel, J. Bai, I. Krossing, G. Brunklaus, H. Eckert, *Chem. Eur. J.* **2008**, *14*, 282–295.
- [2] M. Scheer, L. J. Gregoriades, J. Bai, M. Sierka, G. Brunklaus, H. Eckert, *Chem. Eur. J.* **2005**, *11*, 2163–2169.
- [3] L. Dütsch, Master thesis, University Regensburg, **2015**.
- [4] C. Heindl, S. Heindl, D. Lüdeker, G. Brunklaus, W. Kremer, M. Scheer, *Inorg. Chim. Acta* **2014**, *422*, 218–223.
- [5] J. Bai, A. V. Virovets, M. Scheer, *Angew. Chem. Int. Ed.* **2002**, *41*, 1737–1740.
- [6] J. Bai, E. Leiner, M. Scheer, *Angew. Chem.* **2002**, *114*, 820–823.
- [7] M. Elsayed Moussa, B. Attenberger, E. V. Peresyphkina, M. Fleischmann, G. Balázs, M. Scheer, *Chem. Commun.* **2016**, *52*, 10004–10007.
- [8] M. Fleischmann, S. Welsch, E. V. Peresyphkina, A. V. Virovets, M. Scheer, *Chem. Eur. J.* **2015**, *21*, 14332–14336.
- [9] M. Elsayed Moussa, M. Piesch, M. Fleischmann, A. Schreiner, M. Seidl, M. Scheer, *Dalton Trans.* **2018**, *47*, 16031–16035.
- [10] M. Scheer, L. J. Gregoriades, A. V. Virovets, W. Kunz, R. Neueder, I. Krossing, *Angew. Chem. Int. Ed.* **2006**, *45*, 5689–5693.
- [11] P. J. Sullivan, A. L. Rheingold, *Organometallics* **1982**, *1*, 1547–1549.
- [12] O. J. Scherer, T. Brück, *Angew. Chem.* **1987**, *1*, 59.
- [13] M. Elsayed Moussa, M. Piesch, M. Fleischmann, A. Schreiner, M. Seidl, M. Scheer, *Dalton Trans.* **2018**, *47*, 16031–16035.
- [14] H. Braunschweig, R. D. Dewhurst, F. Hupp, C. Schneider, *Chem. Commun.* **2014**, *50*, 15685–15688.
- [15] CrysAlisPro Software System, Rigaku Oxford Diffraction, (**2018**).
- [16] Sheldrick, G.M., ShelXT-Integrated space-group and crystal-structure determination, *Acta Cryst.* **2015**, *A71*, 3–8.5.G.
- [17] O.V. Dolomanov, L.J. Bourhis, R.J. Gildea, J.A.K. Howard, H. Puschmann, Olex2: A complete structure solution, refinement and analysis program, *J. Appl. Cryst.* **2009**, *42*, 339–341.
- [18] M. Sheldrick, Crystal structure refinement with ShelXL, *Acta Cryst.* **2015**, *C27*, 3–8.
- [19] a) A. L. Spek, *J. Appl. Crystallogr.* **2003**, *36*, 13; b) P. van der Stuis, A. L. Spek, *Acta Cryst.* **1990**, *46*, 194.

## 9. Conclusion

This work deals with the formation of discrete, polymeric and spherical compounds derived from self-assembly processes of phosphorus and arsenic based ligand complexes and coinage metals salts. Chapter 1 (Introduction) elucidates general aspects of supramolecular chemistry, explains why Weakly Coordinating Anions (WCAs) can be a central tool in coordination chemistry and gives an insight in the use and properties of luminescent Cu(I) complexes. After the research objectives (chapter 2), the results obtained within this thesis are presented in the self-contained chapters 3-8.

### 9.1 Coordination Compounds Based on the Diarsene Complex $[\text{Cp}_2\text{Mo}_2(\text{CO})_4(\mu, \eta^2\text{-As}_2)]$ and $\text{Ag}[\text{WCA}]$

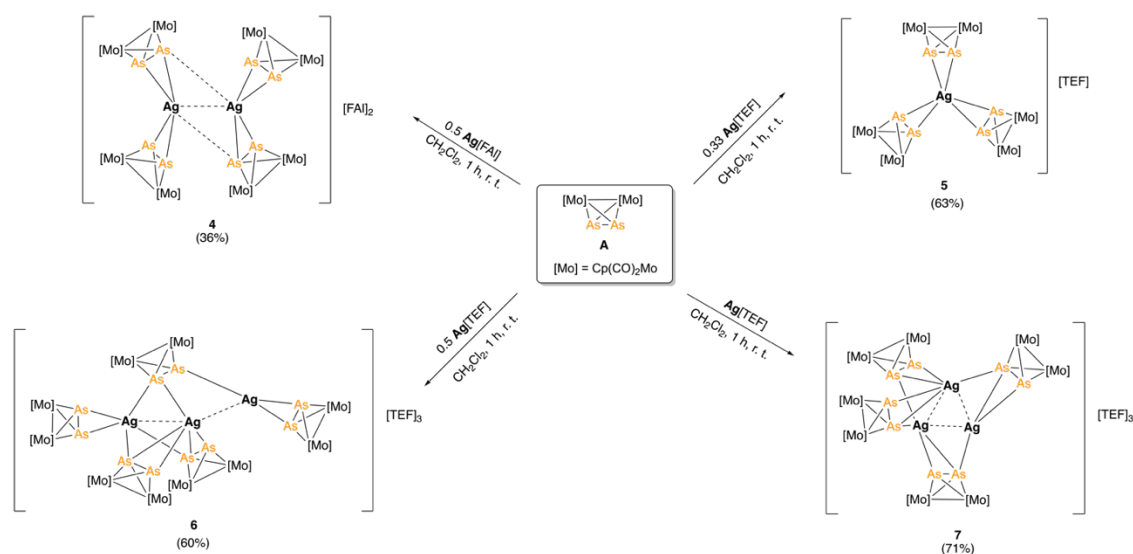
The first part of this thesis describes the synthesis of four unprecedented coordination compounds based on the polypnictogen ligand complex  $[\text{Cp}_2\text{Mo}_2(\text{CO})_4(\mu, \eta^2\text{-As}_2)]$  (**A**) and Ag(I) salts containing the weakly coordinating anions  $[\text{TEF}]^-$  and  $[\text{FAI}]^-$  ( $[\text{TEF}]^- = [\text{Al}\{\text{OC}(\text{CF}_3)_3\}_4]^-$ ,  $[\text{FAI}]^- = [\text{Al}\{\text{OC}(\text{C}_6\text{F}_5)(\text{C}_6\text{F}_{10})\}_3]^-$ ). Specific ratios of reactants were studied in order to compare the obtained products to the ones formed in similar reactions of the P<sub>2</sub> analogue  $[\text{Cp}_2\text{Mo}_2(\text{CO})_4(\mu, \eta^2\text{-P}_2)]$  (**B**). By using an excess of **B** in the reaction with AgWCA ( $[\text{WCA}]^- = [\text{TEF}]^-$  and  $[\text{FAI}]^-$ ) two Ag(I) dimers with the general formula  $[\text{Ag}_2(\eta^2\text{-B})_2(\mu, \eta^1:\eta^1\text{-B})_2][\text{WCA}]$  ( $[\text{WCA}]^- = [\text{TEF}]^-$  (**1**),  $[\text{FAI}]^-$  (**2**), Scheme 9.1) were obtained. However, in the stoichiometric reaction of **B** with Ag[TEF] the one-dimensional polymer  $[\text{Ag}_2(\mu, \eta^1:\eta^1\text{-B})_3]_n[\text{TEF}]_{2n}$  (**3**) is formed (Scheme 9.1).<sup>1</sup>



**Scheme 9.1.** Reaction of **B** with Ag[FAI] and Ag[TEF] yielding the dimer **1** and **2** and the 1D polymer **3**.



In contrast, the reaction of **A** with  $\text{Ag}[\text{FAI}\{\text{OC}(\text{C}_6\text{F}_5)(\text{C}_6\text{F}_{10})\}_3]$  ( $\text{Ag}[\text{FAI}]$ ) in  $\text{CH}_2\text{Cl}_2$  at room temperature yields the supramolecular dimeric assembly  $[(\eta^2\text{-A})_4\text{Ag}_2][\text{FAI}]_2$  (**4**) in a moderate yield (Scheme 9.2). Single crystals of **4** display a disorder which could be resolved as a superposition of three structural isomers **4a-c**. Core **4a** and **4b** possess a 2-fold rotational symmetry, and core **4c** is asymmetric (Figure 9.1). Regardless of the structure **4** adopts in the solid state, it is related to the dimer **2** insofar as both **2** and **4** display a 2:1 ratio of  $\text{E}_2$  to  $\text{Ag}$ . In both compounds one of the two  $\text{E}_2$  units coordinate in an  $\eta^2$ -mode towards one  $\text{Ag}(\text{I})$  center. In compound **2**, the other  $\text{E}_2$  moiety possesses a bridging  $\mu, \eta^1: \eta^1$ -coordination, while the second  $\text{E}_2$  unit in **4** coordinates in a  $\mu, \eta^1: \eta^2$ - or a  $\eta^2$ -fashion.



**Scheme 9.2.** Reaction of **A** with  $\text{Ag}[\text{FAI}\{\text{OC}(\text{C}_6\text{F}_5)(\text{C}_6\text{F}_{10})\}_3]$  ( $\text{Ag}[\text{FAI}]$ ) and  $\text{Ag}[\text{Al}\{\text{OC}(\text{CF}_3)_3\}_4]$  ( $\text{Ag}[\text{TEF}]$ ). Synthesis of the supramolecular compounds **4-7**. Yields are shown in parenthesis.

In order to elucidate whether introducing a higher amount of  $\text{Ag}(\text{I})$  leads to a higher number of  $\text{Ag}(\text{I})$  with possible metal-metal interactions, the stoichiometry in the reaction of **A** with  $\text{Ag}[\text{TEF}]$  in  $\text{CH}_2\text{Cl}_2$  at room temperature was varied, resulting in the compounds **5**, **6** and **7** (Scheme 9.2). Reacting **A** and  $\text{Ag}[\text{TEF}]$  in a 3:1 ratio yields the  $\text{Ag}(\text{I})$  monomer **5** with the general formula  $[\text{Ag}(\mu, \eta^2\text{-A})_3][\text{TEF}]$ . Compound **5** shows an  $\text{Ag}(\text{I})$  center stabilized by six arsenic atoms and demonstrates the second published compound in which a silver center is hexacoordinated by As units.<sup>2</sup> Compound **6** contains three  $\text{Ag}(\text{I})$  atoms, as does compound **7**, however, the central structural motif of **6** displays a bent trinuclear  $\text{Ag}_3$  chain, while it shows an almost perfect equilateral  $\text{Ag}_3$  triangle in **7**. In **6**, five  $\text{Mo}_2\text{As}_2$  ligands (**A**) stabilize these  $\text{Ag}(\text{I})$  ions with two ligands **A** coordinating in an  $\eta^2$ -fashion and the other three in a  $\mu, \eta^2: \eta^1$ -coordination mode. In **7**, all **A** units coordinate

in a  $\mu, \eta^2: \eta^1$ -coordination mode. Interestingly, all Ag(I) centers in compound **6**, as well as in compound **7** show different coordination environments.

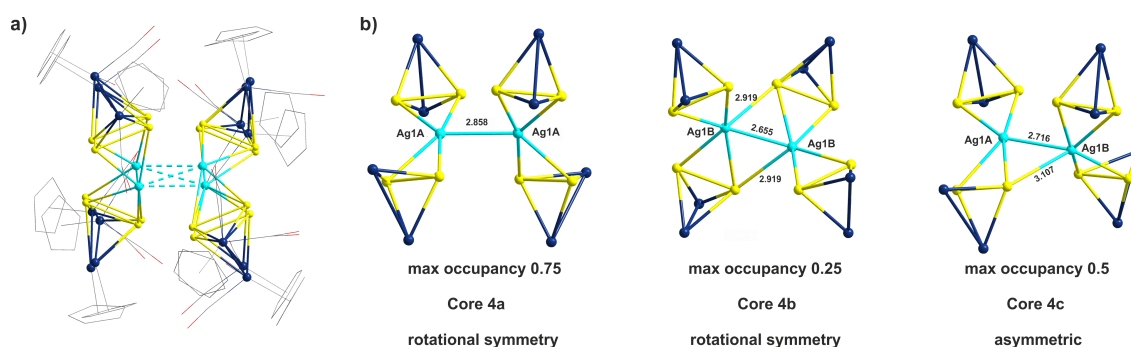


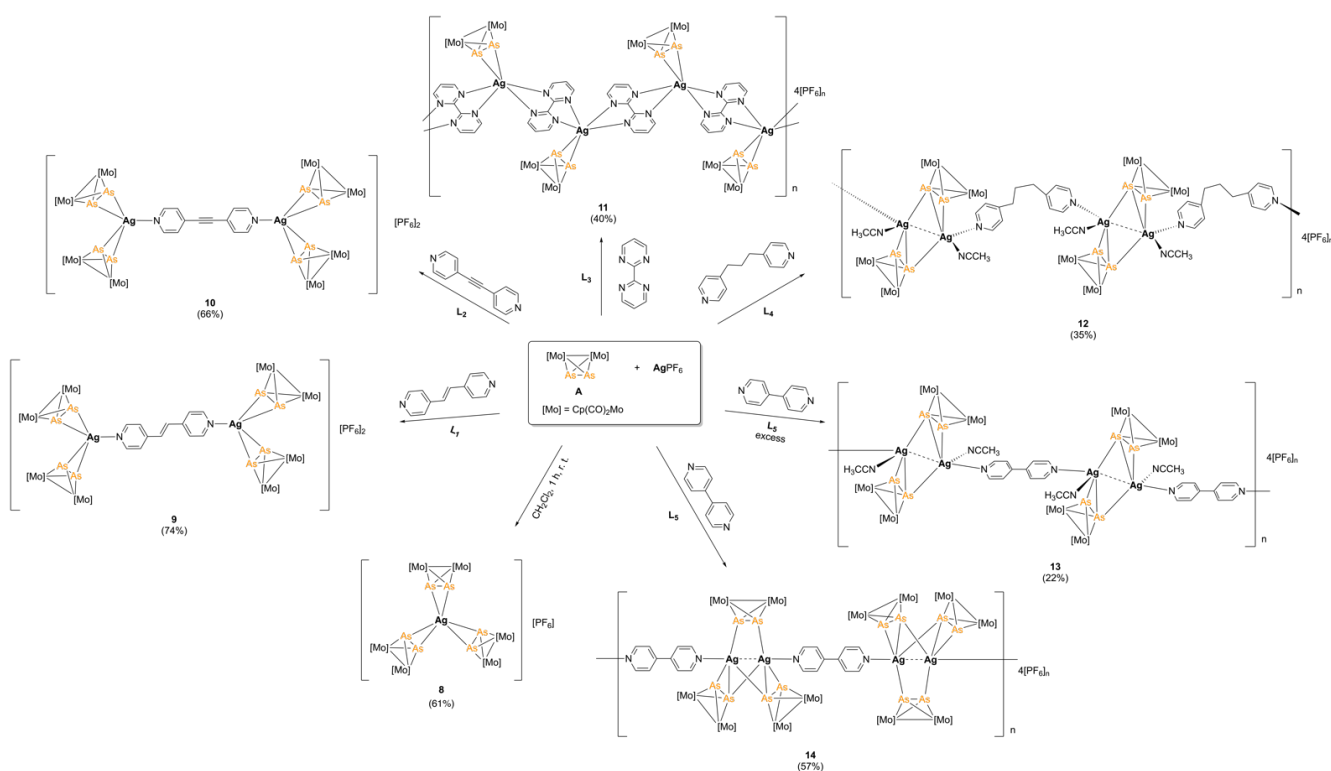
**Figure 9.1.** a) The disordered complex **4** ( $2_z$  axis is directed vertically to the plane of the picture). b) Possible individual cores for compound **4** in the disordered structure.

Compounds **4-7** show a higher tendency of **A** to coordinate in an  $\eta^2$ -fashion compared to the complex **B**. Additionally, compounds **4**, **6** and **7** demonstrate the potential of **A** as a bridging unit stabilizing short Ag...Ag distances. These short distances (2.655(4)-2.9800(8) Å) are much shorter than in compound **2** ( $d(\text{Ag}\cdots\text{Ag}) > 4.85 \text{ \AA}$ )<sup>1</sup> and are indicative of argentophilic interactions ( $\sum_{\text{vdW}}(\text{Ag}-\text{Ag}) = 3.44 \text{ \AA}$ ).<sup>3</sup> These compounds could give rise to more complex coordination polymers by substituting one or more  $\text{Mo}_2\text{As}_2$  ligands.

## 9.2 Discrete and Polymeric coordination Complexes based on the Diarsene Complex $[(\text{Cp}_2\text{Mo}_2(\text{CO})_4(\mu, \eta^2\text{-As}_2))]_n$ , $\text{AgPF}_6$ and Pyridyl-based Linkers

The second part of the thesis deals with the formation of the coordination compound **8** ( $[(\text{Cp}_2(\text{CO})_4\text{Mo}_2\text{As}_2)_3\text{Ag}][\text{PF}_6]$ ) as well as the three-component reactions of  $\text{Cp}_2(\text{CO})_4\text{Mo}_2(\mu, \eta^2\text{-As}_2)$  (**A**) and  $\text{AgPF}_6$  with the pyridyl-based linkers **L**<sub>1</sub>-**L**<sub>5</sub> (**L**<sub>1</sub> = 1,2-di(4-pyridyl)ethylene, **L**<sub>2</sub> = 1,2-di(4-pyridyl)ethyne, **L**<sub>3</sub> = 2,2'-bipyrimidine, **L**<sub>4</sub> = 1,3-di(4-pyridyl)propane and **L**<sub>5</sub> = 4,4'-bipyridine). The reaction of **A** with  $\text{AgPF}_6$  yields the monomeric compound **8** containing one Ag(I) center hexacoordinated by three ligands **A** (Scheme 9.3). This monomeric complex is similar to the compound  $[(\text{Cp}_2(\text{CO})_4\text{Mo}_2\text{As}_2)_3\text{Ag}][\text{TEF}]$  ( $[\text{TEF}]^- = [\text{Al}\{\text{OC}(\text{CF}_3)_3\}_4]^-$ ) obtained in the reaction of **A** and  $\text{Ag}[\text{TEF}]$ . With the aim of substituting the coordinated ligands **A** can be substituted by organic linker molecules. Therefore, **A**,  $\text{AgPF}_6$  and **L**<sub>1</sub>-**L**<sub>5</sub> were reacted in one-pot reactions. Linker **L**<sub>1</sub> and **L**<sub>2</sub> form both a dimeric structure (**9,10**) with two interlinked  $[\text{AgA}_2]^+$  units linked with each other (Scheme 9.3). Reacting **A** and  $\text{AgPF}_6$  with **L**<sub>3</sub> results

in the 1D zig-zag polymer **11**. Its solid-state structure reveals  $[\text{AgA}]^+$  moieties which are linked with  $\text{L}_3$ . Using the flexible linker  $\text{L}_4$  yields the structurally distinct one-dimensional coordination polymer **12** (Scheme 9.3). Compound **12** consists of linked  $[\text{Ag}_2\text{A}_2(\text{CH}_3\text{CN})_2]^{2+}$  entities with short intermetallic  $\text{Ag}\cdots\text{Ag}$  distances of 2.9690(4) Å, indicating argentophilic interactions. Compounds **9-12** are formed regardless of the ratio of  $\text{A}:\text{AgPF}_6:\text{linker}$ .



**Scheme 9.3.** Reaction of **A** and  $\text{AgPF}_6$  in a 3:1 ratio yielding compound **8** and the three component reactions with the linkers  $\text{L}_1$ - $\text{L}_5$  conducted at r. t. in  $\text{CH}_2\text{Cl}_2:\text{CH}_3\text{CN}$  1:1 resulting in compounds **9-14**. Yields are given in parentheses.

In contrast, linker  $\text{L}_5$  forms two structurally distinct compounds **13** and **14**, depending on the stoichiometry (Scheme 9.3). Reacting **A**,  $\text{AgPF}_6$  and  $\text{L}_5$  in a 3:1:2 ratio results in the formation of **14**, while using a threefold excess of  $\text{L}_5$  yields compound **13**. Both solid-state structures consist of  $[\text{Ag}_2]^{2+}$  units. In **13**, two  $\text{As}_2$  moieties coordinate in a  $\mu, \eta^2:\eta^1$ -mode towards the  $\text{Ag}(\text{I})$  centers, while in compound **14** each  $\text{Ag}(\text{I})$  center is bound by three coordinated  $\text{As}_2$  entities. However, **14** displays two  $\mu, \eta^2:\eta^1$ -coordinating ligands and one **A** coordinating in a rare  $\eta^1$ -fashion stabilizing even shorter  $\text{Ag}\cdots\text{Ag}$  distances of 2.7867(6) Å compared to **12**. As reported in the previous chapter, **A** shows a higher tendency to coordinate in an  $\eta^2$ -fashion than **B**. For that reason a pure  $\eta^1$ -coordination mode of **A** towards metal centers had not been observed before.

This chapter has shown anew that **A** can stabilize short Ag···Ag distances, which can be observed both in discrete complexes and in coordination polymers. Furthermore, no influence of the flexibility of the linker to the resulting solid-state structures is apparent, however the stoichiometry can have an effect on the reaction outcome in some of the products.

### 9.3 Mo<sub>2</sub>E<sub>2</sub> (E = P, As) complexes as linking units between Cu(I) ions

The third chapter of this thesis describes the novel linking behavior of tetrahedral Cp<sub>2</sub>(CO)<sub>4</sub>Mo<sub>2</sub>E<sub>2</sub> complexes (E = As (**A**), P (**B**)) towards Cu[WCA] salts ([WCA]<sup>-</sup> = [Al{OC(CF<sub>3</sub>)<sub>3</sub>}<sub>4</sub>]<sup>-</sup>, [BF<sub>4</sub>]<sup>-</sup>, [FAl{OC<sub>6</sub>F<sub>12</sub>(C<sub>6</sub>F<sub>5</sub>)<sub>3</sub>}<sub>3</sub>]<sup>-</sup>). Organometallic compounds containing Cu(I) moieties have attracted a lot of attention in the last decades, due to their versatile coordination chemistry and their wide range of applications.<sup>4</sup> A variety of compounds containing different Cu(I) and organometallic polyphosphorus ligand complexes had previously been reported by us.<sup>5</sup> So far, three coordination modes (**I-III**) have been observed for E<sub>2</sub> ligand complexes (Figure 9.2).<sup>6,7,8</sup> The lone pairs of the E atoms can either coordinate *via* σ-coordination (type **I** and **II**) or the E-E σ-orbital binds in a π-coordination to the metal center (type **III**).

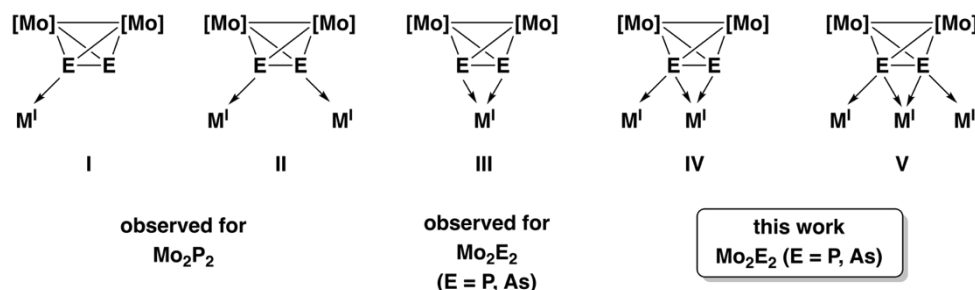
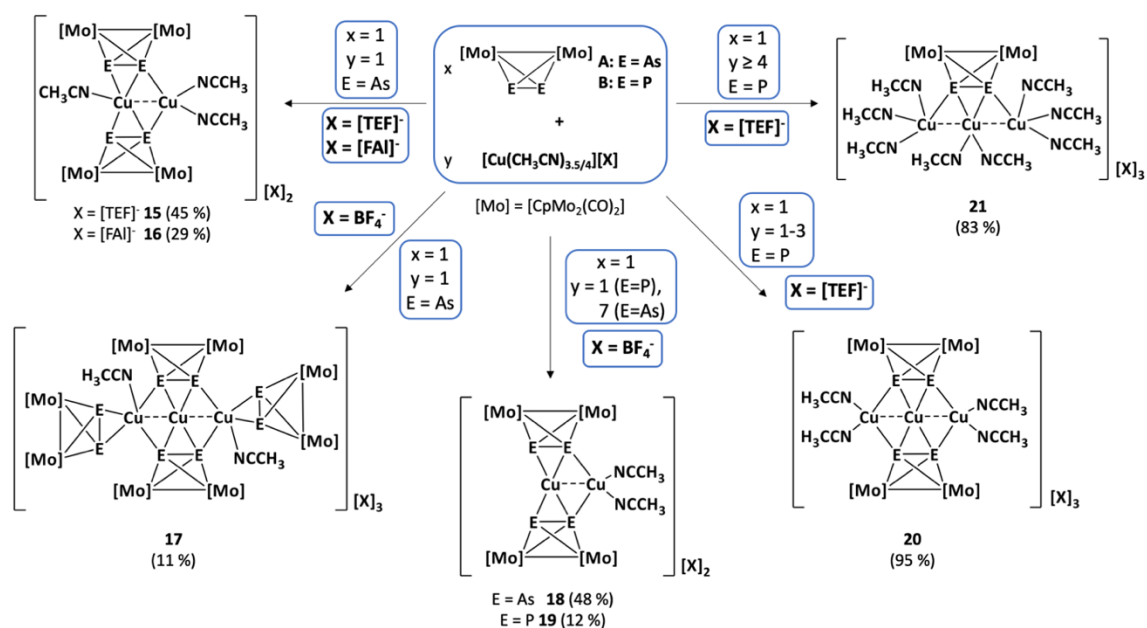


**Figure 9.2.** Reported and new coordination modes of Mo<sub>2</sub>E<sub>2</sub> complexes. M<sup>I</sup> = Ag(I), Cu(I), Au(I). [Mo] = [Cp(CO)<sub>2</sub>Mo<sub>2</sub>].

Reacting the ligand complexes **A** and **B** with suitable Cu(I) precursor salts yields seven unprecedented coordination compounds (**15-21**, Scheme 9.4). Compounds **19-21** show a novel  $\eta^{2:1:1}$  and  $\eta^{2:1}$  coordination behavior (type **IV** and **V**) of the ligand complex **B**. Reacting **B** with [Cu(*o*-DFB)] [Al{OC(CF<sub>3</sub>)<sub>3</sub>}<sub>4</sub>] (*o*-DFB = *ortho*-difluorobenzene) leads to a Cu<sub>2</sub>P<sub>4</sub> six-membered ring motif,<sup>9</sup> while using [Cu(CH<sub>3</sub>CN)<sub>4</sub>][Al{OC(CF<sub>3</sub>)<sub>3</sub>}<sub>4</sub>] leads to two novel trinuclear Cu(I) chains coordinated by one or two **B** units in a coordination mode type **V** depending on the stoichiometry (**20** and **21**). Moreover, compounds **17**, **20** and **21** show Cu···Cu···Cu distances below the sum of the van der Waals radii<sup>10</sup> that are in

the range of Cu(I)-Cu(I) single bonds, suggesting intramolecular metallophilic interactions. DFT calculations for **20** at the B3LYP/def2-TZVP level of theory revealed that the bonding of the peripheral Cu ions to the Mo<sub>2</sub>P<sub>2</sub> ligands takes place via the coordination of the phosphorus lone pairs, while the central Cu ion binds to the P-P σ-orbital of the Mo<sub>2</sub>P<sub>2</sub> unit. Therefore, it can be concluded that there is an interaction present between the central and peripheral Cu ions, as a WBI of 0.11 has been found.



**Scheme 9.4.** Products of the reaction of **A** with the Cu(I) salts [Cu(CH<sub>3</sub>CN)<sub>4</sub>][Al{OC(CF<sub>3</sub>)<sub>3</sub>}<sub>4</sub>] (**15**), [Cu(CH<sub>3</sub>CN)<sub>3.5</sub>][FAI{OC(CF<sub>3</sub>)<sub>3</sub>}<sub>4</sub>] (**16**) and [Cu(CH<sub>3</sub>CN)<sub>4</sub>][BF<sub>4</sub>] (**17/18**, depending on the stoichiometry), and reaction of **B** with [Cu(CH<sub>3</sub>CN)<sub>4</sub>][BF<sub>4</sub>] (**19**) and [Cu(CH<sub>3</sub>CN)<sub>4</sub>][Al{OC(CF<sub>3</sub>)<sub>3</sub>}<sub>4</sub>] (**20/21**, depending on the stoichiometry). Yields are given in parentheses.

The reaction of **A** with [Cu(CH<sub>3</sub>CN)<sub>4</sub>][Al{OC(CF<sub>3</sub>)<sub>3</sub>}<sub>4</sub>] and [Cu(CH<sub>3</sub>CN)<sub>3.5</sub>][FAI{OC(CF<sub>3</sub>)<sub>3</sub>}<sub>4</sub>], respectively, as well as the reaction of **B** with [Cu(CH<sub>3</sub>CN)<sub>4</sub>][BF<sub>4</sub>] yields a coordination compound with a Cu<sub>2</sub> unit coordinated by two Mo<sub>2</sub>E<sub>2</sub> moieties (type **IV**). The previously reported reaction of **B** with [Cu(CH<sub>3</sub>CN)<sub>3.5</sub>][FAI{OC(CF<sub>3</sub>)<sub>3</sub>}<sub>4</sub>] leads to the formation of a compound which is similar to **20** under otherwise identical reaction conditions, however, the compound is missing the central Cu(I) atom, thus forming a Cu<sub>2</sub>P<sub>4</sub> ring.<sup>5a</sup>

The comparison of the obtained compounds **20** and **21** with reported results show the influence of the coordinating solvents in the Cu(I) salts, while all compounds show the decisive influence of the WCA used in the reactions with either Mo<sub>2</sub>As<sub>2</sub> or its phosphorus analogue Mo<sub>2</sub>P<sub>2</sub>.

For the first time, a  $\eta^{2,1,1}$  coordination mode of both  $E_2$  ligand complexes **A** and **B** has been detected, in which both As/P atoms contribute via  $\sigma$ -bonding and  $\pi$ -coordination (type **V**). Moreover, as already discussed in the first two chapters, **B** displays a substantially higher tendency to coordinate in an  $\eta^2$ -fashion in comparison to the  $P_2$  complex **A**.

All the complexes reported here could function as building blocks in supramolecular chemistry to form polymers by substituting the coordinated  $CH_3CN$  molecules with organic N-donor linkers.

#### 9.4 A Superdeficient Sphere based on $[Cp^RFe(\eta^5-P_5)]$

Giant self-assembled supramolecules based on metal cations and rigid bi- or multidentate organic ligands have attracted steadily growing attention during the last decade.<sup>11</sup> Our group already studied various giant spheres reaching 4.6 nm in size *via* coordination of *cyclo*- $P_5$  rings of pentaphosphaferrocenes like  $[Cp^RFe(\eta^5-P_5)]$  ( $Cp^R = C_5(CH_2Ph)_5$  ( $Cp^{Bn}$ , **C**<sub>1</sub>),  $C_5(CH_3)_5$  ( $Cp^*$ , **C**<sub>2</sub>), 1,3- $C_5H_3tBu_2$  ( $Cp^i$ , **C**<sub>3</sub>)) towards Cu(I).<sup>12</sup> In a set of supramolecules with the general formula  $[[Cp^RFe(\eta^5-P_5)]_{12}(CuX)_{20}]$  ( $Cp^R = Cp^*$ ,  $Cp^{Bn}$ ; X = Cl, Br), all phosphorus atoms coordinate towards Cu(I) cations ideally forming an 80-vertex  $\{Cu_{20}P_{60}\}$  core with the fullerene  $I_h-C_{80}$  topology and a pentagonal dodecahedral arrangement of Cu (Figure 9.3a).

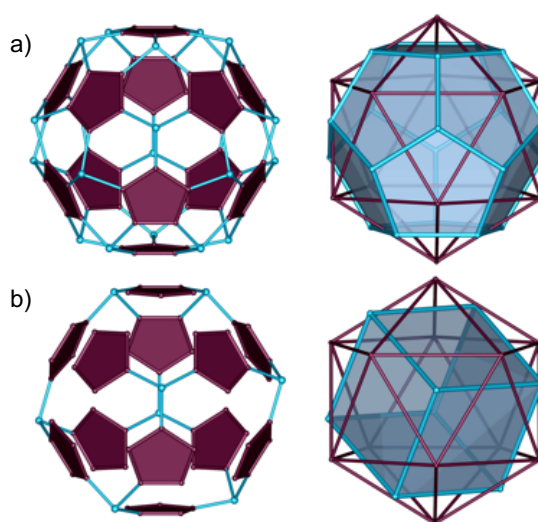


**Figure 9.3.** a) The inorganic core  $\{Cu_{20}P_{60}\}$  of the supramolecule  $[[Cp^RFe(\eta^5-P_5)]_{12}(CuX)_{20}]$  (X = Cl, Br) and corresponding icosahedral representation for centres of *cyclo*- $P_5$  units and dodecahedral for copper; b) Hypothetic 12-fold deficient  $\{Cu_8P_{60}\}$  core and its respective polyhedral representation.

However, previous studies in the solid state as well as in solution have shown that some of the {CuX} sites are statistically vacant.<sup>12f</sup> Molecular modeling of these spherical systems revealed that eight Cu(I) atoms is the minimum number required for a sphere of this overall size to remain stable (Figure 9.3b).<sup>12b</sup> The size of the WCA can control the degree of metal deficiency, due to fact that only a restricted number of large anions can surround multi-charged cations avoiding repulsion.

Using the bulky weakly coordinating anion [Al{OC(CF<sub>3</sub>)<sub>3</sub>}<sub>4</sub>]<sup>-</sup> we were able to selectively synthesize the unprecedented 8+ charged supramolecule [(Cp''Fe(η<sup>5</sup>-P<sub>5</sub>))<sub>12</sub>{CuNCMe}<sub>8</sub>]<sup>8+</sup> (**22**, Cp'' = η<sup>5</sup>-C<sub>5</sub>H<sub>3</sub>tBu<sub>2</sub>) of 2.66 nm in diameter (Figure 9.4a). The sphere possesses the first metal-deficient 68-vertex {Cu<sub>8</sub>P<sub>60</sub>} core with the least possible number of copper atoms (Figure 9.4b).<sup>12b,f</sup>

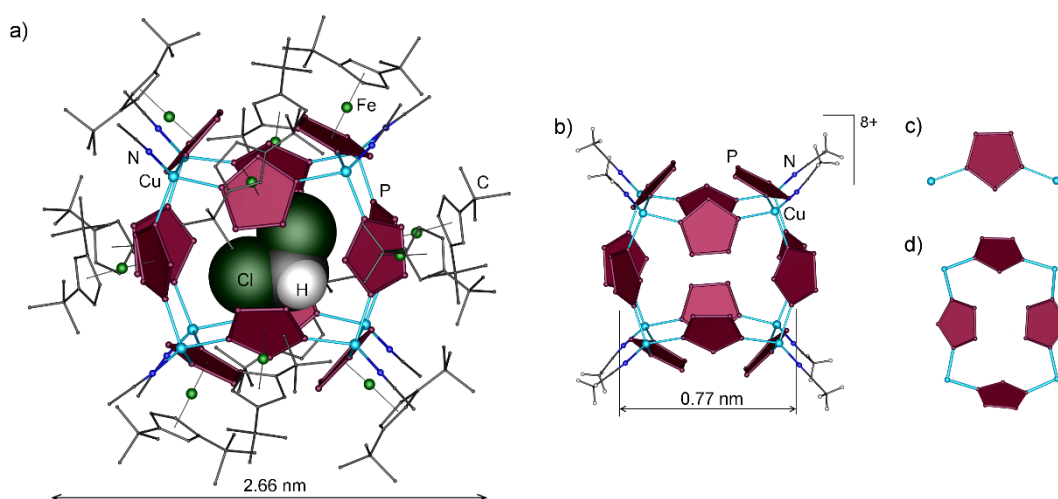


**Figure 9.4.** a) The cationic supramolecular assembly of **22**: b) the 68-vertex cube-like inorganic core, c) 1,3-Coordination mode of the **C**<sub>3</sub> unit and d) 18-membered {Cu<sub>4</sub>P<sub>14</sub>} cycles.

The reaction of two equivalents **C**<sub>3</sub> and three equivalents [Cu(CH<sub>3</sub>CN)<sub>4</sub>][Al{OC(CF<sub>3</sub>)<sub>3</sub>}<sub>4</sub>] in CH<sub>2</sub>Cl<sub>2</sub> at room temperature leads to the formation of **22** and additionally the side-product **23**.

However, the first attempt to fill the free coordination sites with Ni(0) by adding Ni(cod)<sub>2</sub> (cod = 1,5-cyclooctadiene) was unsuccessful because of immediate precipitation of Ni(0). Nevertheless, after filtration and layering with *n*-pentane, compound **23** could be isolated selectively in a moderate yield (36%) with its phase purity confirmed by PXRD.



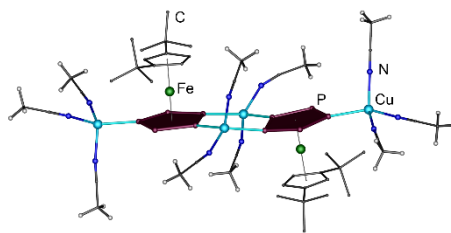


**Figure 9.5.** Molecular structure of the tetracationic dimer **23**.

The solid-state structure of **22** reveals 68-vertex sphere  $[(\text{CH}_2\text{Cl}_2)@[\{\text{Cp}^*\text{Fe}(\eta^5\text{-}\eta^1, \eta^1\text{-P}_5)\}_{12}\text{Cu}_8}]^{8+}$  with 12 units of **C**<sub>3</sub> arranged in an icosahedron, in which Cu(I) ions cap eight of the 20 available trigonal faces (Figure 9.3b). The remaining 12 faces provide six 18-membered rings  $\{\text{Cu}_4\text{P}_{14}\}$  corresponding to a face of an underlying cube of the inorganic core (Figure 9.4d). Moreover, a spherical assembly exclusively composed of two-coordinated units of **C** was predicted, but never observed previously.<sup>12b,f</sup>

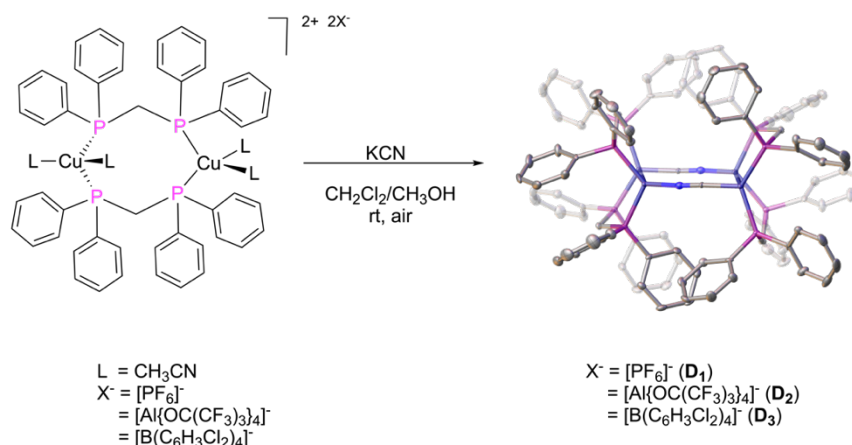
Each copper atom is additionally coordinated by one CH<sub>3</sub>CN molecule. These labile ligands might be substituted by bridging N-donor ligands to build up expanded networks containing the supramolecule. Furthermore, the presence of 12 free metal sites opens a way for further functionalization with heterometals or inner functionalization with small molecules. Future studies could involve the fine tuning with respect to the nature of the Cp ligands and the coinage metal salts.

### 9.5 Tuned emission properties of tetranuclear Cu(I) metallacycles by introducing bulky weakly coordinating anions

In cooperation with Dr. Christophe Lescop (INSA Rennes/France) the impact of changing the nature of the counterion of luminescent Cu(I) complexes was studied. Recently, Cu(I) compounds were discovered to be attractive novel solid-state emitters because of their low costs and accessibility.<sup>13</sup> In the past, emissive Cu(I) precursors acting as pre-organized building blocks to form coordination-driven supramolecular assemblies were only rarely reported. Based on this knowledge, we were interested, how the photophysical properties of Cu(I) complexes can be tuned by introducing different anions and subsequently building up one-dimensional coordination polymers with organic linkers.

The already reported Cu(I) metallacycle  $[\text{Cu}_4(\mu_2\text{-dppm})_4(\text{CN})_2][\text{PF}_6]_2$  (**D**<sub>1</sub>) (dppm = 1,1-bis(diphenylphosphino) methane) is the first Cu(I) coordination-driven supramolecular assembly bearing solid-state Thermally Activated Delayed Fluorescence (TADF) properties (Scheme 9.5).<sup>14</sup>





**Scheme 9.5.** Synthesis of compounds  $\text{D}_1$ - $\text{D}_3$ . Hydrogen atoms, counterions and included solvent molecules were omitted for clarity. Thermal ellipsoids are shown at 50% probability level.

The synthesis of  $\text{D}_2$  and  $\text{D}_3$  was performed under the same reactions conditions as  $\text{D}_1$  in a mixture of  $\text{CH}_2\text{Cl}_2$  and  $\text{CH}_3\text{OH}$  at room temperature. Compound  $\text{D}_2$  ( $\Phi_{298\text{K}} = 86\%$ ), as well as  $\text{D}_3$  ( $\Phi_{298\text{K}} = 91\%$ ) show enhanced absolute luminescent quantum yields at room temperature compared to  $\text{D}_1$  ( $\Phi_{298\text{K}} = 72\%$ ).<sup>14</sup> Upon cooling to 80 K the emission spectra of  $\text{D}_2$  and  $\text{D}_3$  show a bathochromic shift similar to compound  $\text{D}_1$ . Unfortunately, the performed variable-temperature excited state lifetime measurements of  $\text{D}_2$  could not make a statement to elucidate the electronic processes responsible for the luminescence behavior.

As Cu(I) complexes are popular building blocks in supramolecular chemistry,<sup>15</sup> compounds  $\text{D}_1$ - $\text{D}_3$  were reacted with different organic pyridyl-based linkers ( $\text{L}_1$ ,  $\text{L}_2$ ,  $\text{L}_5$ - $\text{L}_{13}$ , Figure 9.5).

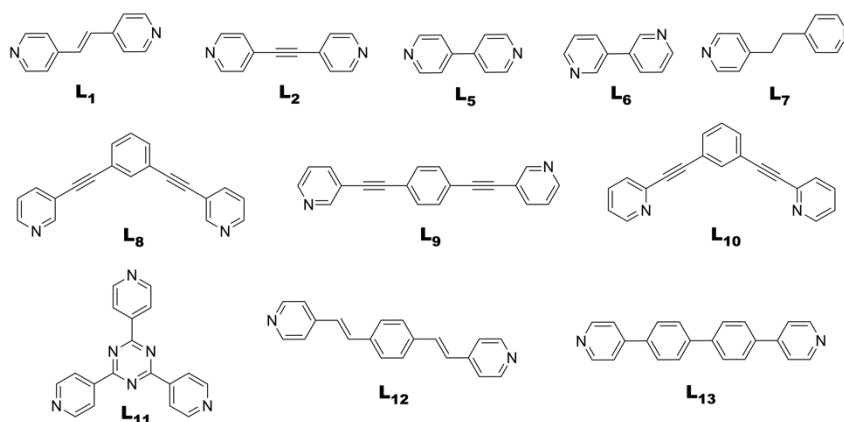


**Figure 9.5.** Organic pyridyl-based linkers  $\text{L}_1$ ,  $\text{L}_2$ ,  $\text{L}_5$ - $\text{L}_{13}$  used in this chapter.

Twelve novel coordination compounds **D<sub>1</sub>L<sub>1</sub>**, **D<sub>1</sub>L<sub>7</sub>-D<sub>1</sub>L<sub>9</sub>**, **D<sub>2</sub>L<sub>1</sub>**, **D<sub>2</sub>L<sub>2</sub>**, **D<sub>2</sub>L<sub>5a</sub>**, **D<sub>2</sub>L<sub>5b</sub>**, **D<sub>1</sub>L<sub>6</sub>**, **D<sub>2</sub>L<sub>8</sub>**, **D<sub>2</sub>L<sub>9</sub>** and **D<sub>3</sub>L<sub>7</sub>** were obtained. All of these compounds, except of **C<sub>2</sub>L<sub>5b</sub>** are 1D polymers in which two opposite Cu(I) are coordinated by the N-donor linkers (Figure 9.6).

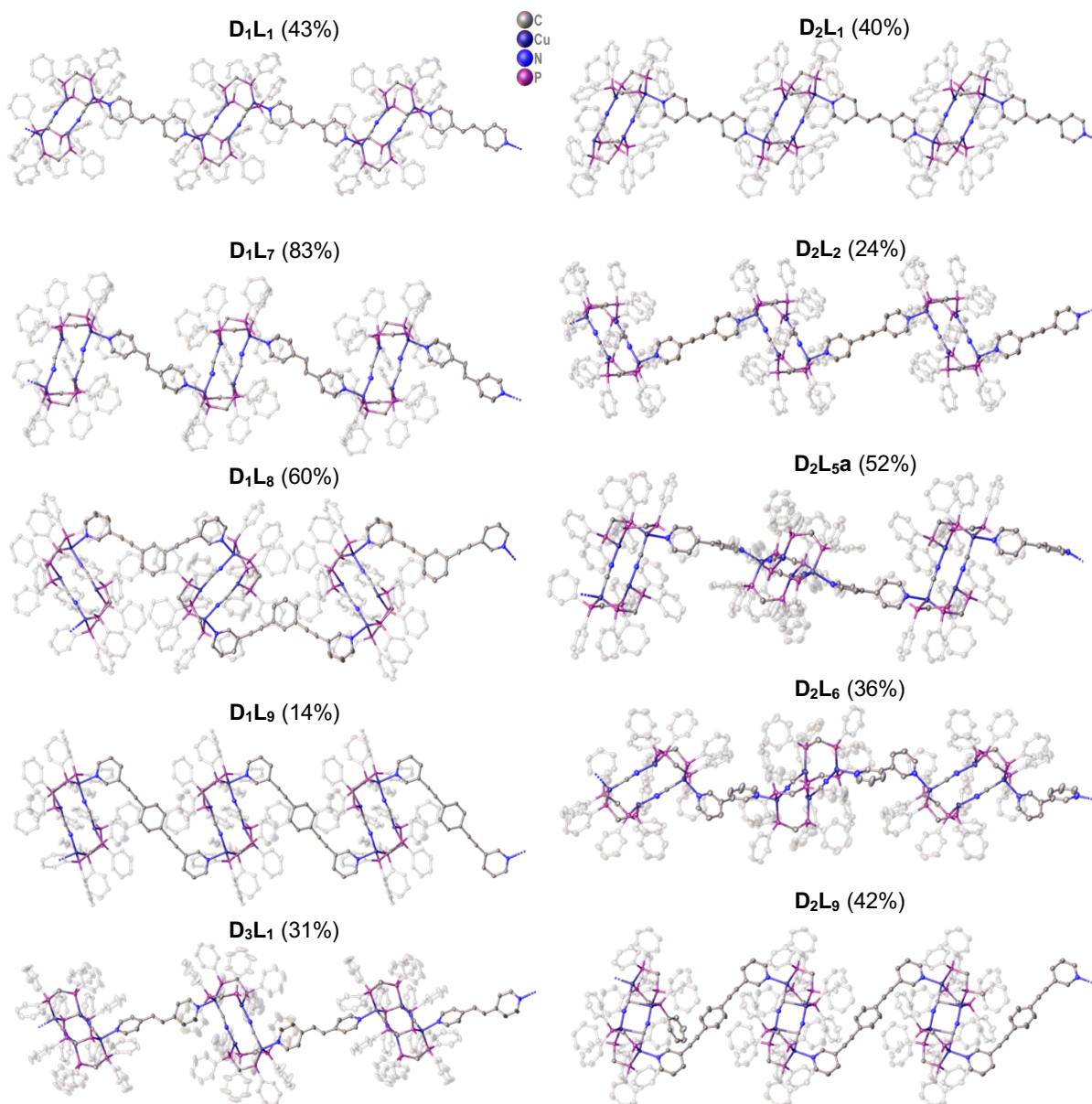


**Figure 9.6.** Obtained coordination polymers in the reactions of **D<sub>1</sub>-D<sub>3</sub>** with linkers **L<sub>1</sub>**, **L<sub>2</sub>** and **L<sub>5</sub>-L<sub>9</sub>**. Anions and hydrogen atoms are omitted for clarity. Phenyl rings are depicted transparent. Thermal ellipsoids are shown at 50% probability level. Yields are given in parentheses.

The comparison of **D<sub>2</sub>L<sub>5</sub>a** with the coordination polymer **D<sub>1</sub>L<sub>5</sub>**<sup>16</sup> shows a major difference in the solid-state structure due to the twisted linker in **D<sub>2</sub>L<sub>5</sub>a**, resulting in distinctive photophysical properties. Although all polymeric structures are similar, each of them demonstrates unique emission behavior. Furthermore, we detected a transformation of the green emissive crystals of **C<sub>2</sub>L<sub>5</sub>a** after one week in the supernatant into the yellow luminescent oligomer **D<sub>2</sub>L<sub>5</sub>b** (Figure 9.7).

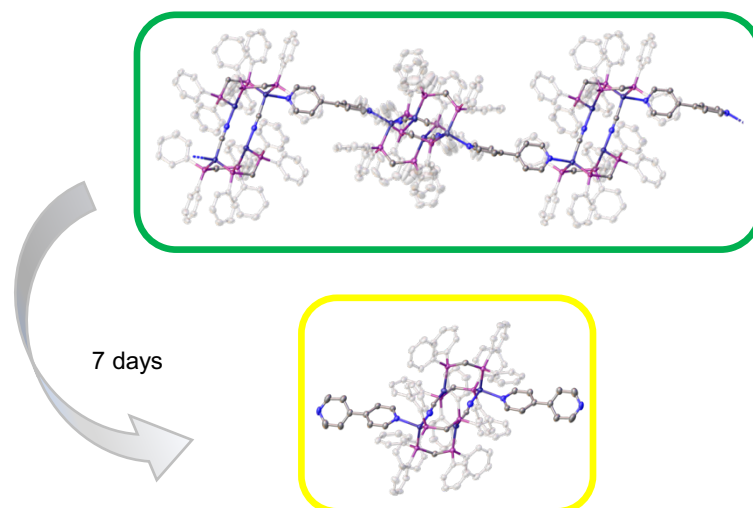


**Figure 9.7.** Transformation of **D<sub>2</sub>L<sub>5</sub>a** into **D<sub>2</sub>L<sub>5</sub>b** within 7 days in the supernatant. Anions and hydrogen atoms are omitted for clarity. Phenyl rings are depicted transparent. Thermal ellipsoids are shown at 50% probability level.

These different structural motifs lead to a wide variety of photophysical properties of the obtained coordination polymers. Future efforts will focus on more detailed studies (*inter alia* quantum yield measurements, variation of the lifetime of the excited state, theoretical calculations, additional VT UV-Vis measurements) in order to rationalize the reported observations.

## 9.6 References

- [1] M. Elsayed Moussa, M. Fleischmann, E. V. Peresykina, L. Dütsch, M. Seidl, G. Balázs, M. Scheer, *Eur. J. Inorg. Chem.* **2017**, 2017, 3222–3226.
- [2] L. J. Gregoriades, H. Krauss, J. Wachter, A. V. Virovets, M. Sierka, M. Scheer, *Angew. Chem. Int. Ed.* **2006**, 45, 4189–4192.
- [3] H. Schmidbauer, A. Schier, *Angew. Chem. Int. Ed.* **2015**, 54, 746–784.
- [4] a) S. T. Li, B. B. Cula, S. Hoof and C. Limberg, *Dalton Trans.* **2018**, 47, 544–560; b) C. Marzano, V. Gandin, M. Pellei, D. Colavito, G. Papini, G. G. Lobbia, E. D. Giudice, M. Porchia, F. Tisato, C. Santini, *J. Med. Chem.* **2008**, 51, 798; c) O. A. Filippov, A. A. Titov, E. A. Guseva, D. A. Loginov, A. F. Smol'yakov, F. M. Dolgushin, N. V. Belkova, L. M. Epstein, E. S. Shubina, *Chem. Eur. J.* **2015**, 21, 13176–13180.
- [5] a) M. E. Moussa, M. Piesch, M. Fleischmann, A. Schreiner, M. Seidl, M. Scheer, *Dalton Trans.* **2018**, 47, 16031–16035; b) M. E. Moussa, M. Seidl, G. Balázs, M. Hautmann, M. Scheer, *Angew. Chem. Int. Ed.* **2019**, 58, 12903–12907; c) M. Scheer, L. J. Gregoriades, M. Zabel, J. Bai, I. Krossing, G. Brunklaus, H. Eckert, *Chem. Eur. J.* **2008**, 14, 282–295; d) M. E. Moussa, B. Attenberger, E. V. Peresykina, M. Fleischmann, G. Balázs, M. Scheer, *Chem. Commun.* **2016**, 52, 10004–10007; e) J. Bai, E. Leiner, M. Scheer, *Angew. Chem.* 2002, 114, 820–823; f) M. Scheer, L. J. Gregoriades, J. Bai, M. Sierka, G. Brunklaus, H. Eckert, *Chem. Eur. J.* **2005**, 11, 2163–2169; g) M. E. Moussa, P. A. Shelyganov, B. Wegley, M. Seidl, M. Scheer, *Eur. J. Inorg. Chem.* **2019**, 4241–4248.
- [6] J. Bai, E. Leiner, M. Scheer *Angew. Chem. Int. Ed.* 2002, 41, 783–786.
- [7] M. Scheer, L. J. Gregoriades, M. Zabel, J. Bai, I. Krossing, G. Brunklaus, H. Eckert, *Chem. Eur. J.* **2008**, 14, 282–295.
- [8] a) J. Schiller, M. Elsayed Moussa, M. Seidl, E. V. Peresykina, G. Balázs, M. Scheer, *manuscript in preparation*; b) M. Elsayed Moussa, M. Seidl, G. Balázs, M. Hautmann, M. Scheer, *Angew. Chem. Int. Ed.* **2019**, 58, 12903–12907.
- [9] M. Fleischmann, S. Welsch, E. V. Peresykina, A. V. Virovets, M. Scheer, *Chem. Eur. J.* **2015**, 21, 14332–14336.
- [10] A. Bondi, *J. Phys. Chem.* **1964**, 68, 441–451.
- [11] a) F. J. Rizzuto, L. K. S. von Krbek, J. R. Nitschke, *Nat. Rev. Chem.* **2019**, 3, 204–222; b) M. Han, D. M. Engelhard, G. Clever, *Chem. Soc. Rev.* **2014**, 43, 1848–1860; c) P. S. Bols, H. L. Anderson, *Acc. Chem. Res.* **2018**, 51, 2083–2092;

- d) M. D. Ward, C. A. Hunter, N. H. Williams, *Acc. Chem. Res.* **2018**, *51*, 2073–2082; e) C. M. Hong, R. G. Bergman, K. N. Raymond, F. D. Toste, *Acc. Chem. Res.* **2018**, *51*, 2447–2455.
- [12] a) J. Bai, A. V. Virovets, M. Scheer, *Science* **2003**, *300*, 781-783; b) E. Peresyphkina, C. Heindl, A. Virovets, M. Scheer in *Structure and Bonding, Vol. 174* (Eds.: S. Dehnen), Springer International Publishing, Switzerland, **2016**, pp. 321–373; c) C. Schwarzmaier, A. Schindler, C. Heindl, S. Scheuermayer, E. Peresyphkina, A. Virovets, M. Neumeier, R. Gschwind, M. Scheer. *Angew. Chem. Int. Ed.* **2013**, *52*, 10896-10899; d) C. Heindl, E. Peresyphkina, A. V. Virovets, I. S. Bushmarinov, M. G. Medvedev, B. Krämer, B. Dittrich M. Scheer, *Angew. Chem. Int. Ed.*, **2017**, *56*, 13237-13243; e) H. Brake, E. Peresyphkina, C. Heindl, A. V. Virovets, W. Kremer, M. Scheer, *Chem. Sci.* **2019**, *10*, 2940-2944; f) F. Dielmann, M. Fleischmann, C. Heindl, E.V. Peresyphkina, A.V. Virovets, R. Gschwind, M. Scheer, *Chem. Eur. J.* **2015**, *21*, 6208–6214.
- [13] a) F. Böppler, M. Zimmer, F. Dietrich, M. Gruppe, M. Wallesch, D. Volz, S. Bräse, M. Gerhards, R. Diller, *Phys. Chem. Chem. Phys.* **2017**, *19*, 29438-29448; b) T. Hofbeck, U. Monkowius, H. Yersin, *J. Am. Chem. Soc.* **2015**, *137*, 399-404; c) M. Osawa, M. Hoshino, M. Hashimoto, I. Kawata, S. Igawa, M. Yashima, *Dalton Trans.* **2015**, *44*, 8369-8378; d) L. C. Ravaro, A. C. Mafud, Z. Li, E. Reinheimer, C. A. Carlos, Y. P. Mascarenhas, P. C. Ford, A. S. S. de Camargo, *Dyes and Pigments* **2018**, *158*, 464-470.
- [14] M. Elsayed Moussa, S. Evarista, H.-L. Wong, L. Le Bras, C. Roiland, L. Le Polles, B. Le Guennic, K. Costuas, V. W.-W. Yams, C. Lescop, *Chem. Commun.* **2016**, *52*, 11370-11373.
- [15] a) K. Tsuge, Y. Chishina, H. Hashiguchi, Y. Sasaki, M. Kato, S. Ishizaka, N. Kitamura, *Coord. Chem. Rev.* **2016**, *306*, 636-651; b) M. Elsayed Moussa, S. Welsch, M. Lochner, E. V. Peresyphkina, A. V. Virovets, M. Scheer, *Eur. J. Inorg. Chem.* **2018**, 2689-2694; c) M. Elsayed Moussa, A. M. Khalil, S. Evarista, H.-L. Wong, V. Delmas, B. Le Guennic, G. Calvez, K. Costuas, V. W.-W. Yam, C. Lescop, *Inorganic Chemistry Frontiers* **2020**, online; d) C. Heindl, E. V. Peresyphkina, A. V. Virovets, V. Y. Komarov, M. Scheer, *Dalton Trans.* **2015**, *44*, 10245-10252; e) C. Heindl, A. Kuntz, E. V. Peresyphkina, A. V. Virovets, M. Zabel, D. Lüdeker, G. Bruncklaus, M. Scheer, *Dalton Trans.* **2015**, *44*, 6502-6509; f) C. Schenk, F. Henke, G. Santiso-Quinones, I. Krossing, A. Schnepf, *Dalton Trans.* **2008**, 4436-4441.
- [16] Master thesis Florent Moutier **2019**, Université de Rennes 1; PhD thesis Ali Khalil **2019**, Université de Rennes 1.

## A. Appendices

### Alphabetic List of Abbreviations

Å	Angstroem, $1 \text{ \AA} = 1 \cdot 10^{-10} \text{ m}$
°C	degree Celsius
[BAr <sup>Cl</sup> ] <sup>-</sup>	[B(3,5-C <sub>6</sub> H <sub>3</sub> Cl <sub>2</sub> ) <sub>4</sub> ]
<sup>t</sup> Bu	<i>tert</i> -butyl, C <sub>4</sub> H <sub>9</sub>
CP	coordination polymer
Cp	cyclopentadienyl, $\eta^5\text{-C}_5\text{H}_5$
Cp*	pentamethylcyclopentadienyl, $\eta^5\text{-C}_5\text{Me}_5$
Cp''	1,3-di- <i>tert</i> -butylcyclopentadienyl, $\eta^5\text{-C}_5\text{H}_3\text{tBu}_2$
Cp'''	1,2,4-tris- <i>tert</i> -butylcyclopentadienyl, $\eta^5\text{-C}_5\text{H}_2\text{tBu}_3$
d(NMR)	doublet
dbp	2,9-di- <i>n</i> -butyl-1,10-phenanthroline
dmp	2,9-di- <i>tert</i> -butyl-1,10-phenanthroline
dppb	1,2-bis(diphenylphosphino)benzene
dppm	1,1-bis(diphenylphosphino)methane
DSC	differential scanning calorimetry
dtp	2,9-di- <i>n</i> -butyl-1,10-phenanthroline
δ	chemical shift
DFT	density functional theory
DNA	deoxyribonucleic acid
E	element of the group 15, E = P, As, Sb, Bi
e <sup>-</sup>	electron, elemental charge
EMIM <sup>+</sup>	1-ethyl-3-methyl imidazolium
ESI MS	electron spray ionization mass spectrometry
EQY	emission quantum yield
[FAI] <sup>-</sup>	[FAI{OC <sub>6</sub> F <sub>10</sub> (C <sub>6</sub> F <sub>5</sub> ) <sub>3</sub> }] <sup>-</sup>
h	hour
HOMO	highest occupied molecular orbital
IR	infrared spectroscopy
J(NMR)	coupling constant
K	Kelvin
L	ligand (specified in text)
L	liter
LUMO	lowest unoccupied molecular orbital
M	metal (specified in text)
m(NMR)	multiplet
<i>m/z</i>	mass to charge ratio
Me	methyl, CH <sub>3</sub>
MHz	Megahertz, 10 <sup>6</sup> Hz
min	minutes
mL	milliliter, 10 <sup>-3</sup> L
MLCT	metal-to-ligand charge transfer
MOF	metal organic framework
NMR	nuclear magnetic resonance

<i>o</i> -DFB	<i>ortho</i> -difluorobenzene
OLED	organic light emitting diode
[OTf] <sup>-</sup>	triflate, [CF <sub>3</sub> SO <sub>3</sub> ] <sup>-</sup>
$\tilde{\nu}$	frequency/wavenumber
PAG	photoacid generator
Ph	phenyl, C <sub>6</sub> H <sub>5</sub>
P-N	[2-(diisopropylphosphino)diphenyl]amide
PNP	bis[2-(diisobutylphosphino)phenyl]amide
POM	polyoxometallate
POP	bis[2-(diphenylphosphino)phenyl]ether
ppm	parts per million
q(NMR)	quartett
R	organic substituent
r	radius
RISC	reversed intersystem crossing
r.t.	room temperature
S <sub>0</sub>	singlet ground state
S <sub>1</sub>	lowest excited singlet state
s(IR)	strong
s(NMR)	singlet
SOC	spin-orbit coupling
T <sub>1</sub>	lowest excited triplet state
[TEF] <sup>-</sup>	[Al{OC(CF <sub>3</sub> ) <sub>3</sub> } <sub>4</sub> ] <sup>-</sup>
<sup>t</sup> Bu	<i>tert</i> -butyl, C <sub>4</sub> H <sub>9</sub>
t(NMR)	triplet
TADF	Thermally Activated Delayed Fluorescence
TGA	thermogravimetical analysis
THF/thf	tetrahydrofurane, C <sub>4</sub> H <sub>8</sub> O
UV	ultra violet
vdW	van der Waals
VE	valence electrons
vs(IR)	very strong
VT	variable temperature
WBI	Wiberg bond index
WCA	weakly coordinating anion
w(IR)	weak
1D	one-dimensional
2D	two-dimensional

## Danksagung

Mein besonderer Dank gilt Prof. Dr. Manfred Scheer, dass er mich als Doktorand aufgenommen hat und mir eine ideale Umgebung geschaffen hat, mich weiter zu entwickeln und zu entfalten. Bei Prof. Dr. Henri Brunner bedanke ich mich für die Übernahme des Zweitgutachtens. PD Dr. David Díaz-Díaz und Prof. Dr. Hubert Motschmann danke ich für die Übernahme der Drittprüferschaft und des Vorsitzes des Promotionsausschusses.

Weiter möchte ich mich bei den Leitern und Mitarbeitern der zentralen Analytik und den Werkstätten bedanken, insbesondere Dr. Michael Bodensteiner und Birgit Hischa (Röntgenstrukturanalyse), Barbara Baumann und Helmut Schüller (Elementaranalyse) und Josef Kirmaier und Wolfgang Söllner (Massenspektrometrie).

Mein weiterer Dank gilt Gabór Balázs und Barbara Bauer. Vielen Dank Gabór für die unzähligen Ratschläge und Hilfestellungen, egal ob Analytikauswertungen, Kirschen einkochen oder Marathontraining. Und ohne Barbara wäre die Zeit nur halb so lustig und doppelt so schwer gewesen. Vielen Dank für Alles! Ganz besonders möchte ich mich bei unserem Kooperationspartner Dr. Christophe Lescop (INSA Rennes) bedanken, für die neuen Herausforderungen im Labor, für die tolle Zeit in Rennes, und dass er immer ein offenes Ohr für mich hat, egal um was es geht.

Außerdem möchte ich mich bei meinen Kooperationspartner (Andrea Schreiner, Dr. Michael Seidl, Dr. Eugenia Peresykina, Dr. Alexander Virovets, Dr. Mehdi Elsayed Moussa) und allen aktuellen und ehemaligen Kollegen aus dem AK Scheer bedanken, besonders bei Michael Weinhart, Corinna Gruber (AK Buschauer), Anna Garbagnati, Nicolás Fontana (AK Bauer), Luis Dütsch und Christoph Riesinger. Vielen Dank für die aufrichtigen und unterstützenden Gespräche, die schönen Abende und Mittagspausen. Ganz besonderen Dank gebührt Rebecca. Ohne sie (und Siggi und Frieda) wäre ich nicht wo ich jetzt bin. Tausend Dank für Alles!

Bei den Kollegen der Nachbar-Arbeitskreise Bauer, Díaz-Díaz, Garcia, Fleischer und Gschwind bedanke ich mich für die schöne gemeinsame Zeit und die gegenseitige Unterstützung. Außerdem bedanke ich mich bei allen Freunden und Kommilitonen, die mich während des Studiums und der Promotion begleitet haben.

Besonders möchte ich mich bei meiner Familie für ihre andauernde Unterstützung in allen Lebenslagen bedanken. Vielen Dank, dass ihr immer für mich da seid. Mein größter Dank gilt meinem Mann Dirk für seine unermüdliche Unterstützung, Forderung und Förderung.



## Lebenslauf

### Persönliche Daten

---

Vorname                   Jana Eva-Maria  
Nachname                 Schiller  
Geburtsdatum            08.01.1991  
Geburtsort                Regensburg

### Werdegang

---

- 08/2016 – 05/2020    **Promotion Anorganische Chemie (Prof. Scheer)**  
                          **Universität Regensburg**  
                          Phosphorus and Arsenic Based Ligands in Supramolecular  
                          Chemistry
- 01/2016 - 04/2016    **Wissenschaftlicher Mitarbeiter Organische Chemie (Prof. Díaz**  
                          **Díaz)**  
                          **Universität Regensburg**
- 10/2013 - 01/2016    **Studium Master Chemie**  
                          **Universität Regensburg, Abschlussnote 1,7**  
                          Fächerbelegung: Organische Chemie, Anorganische Chemie,  
                          Analytische Chemie  
                          Masterarbeit: Hydrogen bonding organocatalysts meet material  
                          synthesis: functional supramolecular organogels, Note 1,0
- 10/2010 - 09/2013    **Studium Bachelor Chemie**  
                          **Universität Regensburg, Abschlussnote 2,7**  
                          Bachelorarbeit: Genauere Untersuchungen zur  
                          Spannungsabhängigkeit einer voltostatischen, NHC-katalysierten  
                          Michael-Addition an  $\alpha,\beta$ -ungesättigten Aldehyden durch Redox-  
                          Aktivierung, Note 1,7
- 09/2001 - 06/2010    **Gymnasium Parsberg, Abiturnote 1,8**  
                          Leistungskurse: Chemie, Kunst

### Publikationen

---

- J. Schiller, J. V. Alegre-Requena, E. Marqués-López, R. P. Herrera, J. Casanovas, C. Alemán, D. Díaz Díaz, *Soft Matter* **2016**, *12*, 4361-4374.
- J. Schiller, R. Pérez-Ruiz, D. Sampedro, E. Marqués-López, R. P. Herrera, D. Díaz Díaz, *Sensors* **2016**, *16*, 658.
- M. Häring, J. Schiller, J. Mayr, S. Grijalvo, R. Eritja, D. Díaz Díaz, D.; *Gels* **2015**, *1*, 135-161.
- J. Mayr, M. Häring, J. Schiller, D. Díaz Díaz, *Nachr. Chem.* **2015**, *63*, 899-903.
- J. Schiller, E. V. Peresykina, A. V. Virovets, M. Scheer, *Angew. Chem. Int. Ed.* **2020**, *accepted*.

**Teilnahme an Konferenzen**

---

- 09/2019            **Deutsch-Französisches Symposium**  
**Universität Regensburg**  
Organisation und aktive Teilnahme
- 05/2019            **Gecom Conoord, Group d'étude de chimie organométallique & Concertation en chimie de coordination**  
**Erquy, Frankreich**  
Aktive Teilnahme
- 09/2018            **19. Vortragstagung für Anorganische Chemie der FG Wöhler-Vereinigung und Festkörperchemie und Materialforschung**  
**Universität Regensburg**  
Organisation
- 07/2018            **ICCC, 43rd International Conference on Coordination Chemistry**  
**Sendai, Japan**  
Aktive Teilnahme
- 08/2017            **Wissenschaftliches Kolloquium für Anorganische Chemie**  
**Hirschegg, Kleinwalsertal**  
Aktive Teilnahme

**Auslandsaufenthalte**

---

- 02/2020            **Forschungsaufenthalt (Gruppe Dr. C. Lescop)**  
**INSA Rennes, Frankreich**  
Charakterisierung von photodynamischen supramolekularen Cu(I) Komplexen
- 05/2019 - 07/2019   **Forschungsaufenthalt (Gruppe Dr. C. Lescop)**  
**INSA Rennes, Frankreich**  
Modifikation, Synthese und Charakterisierung von neuartigen photodynamischen supramolekularen Verbindungen
- 05/2018- 06/2018   **Forschungsaufenthalt (Gruppe Dr. C. Lescop)**  
**INSA Rennes, Frankreich**  
Synthese und Charakterisierung von kupferhaltigen photodynamischen Materialien

**Berufserfahrung**

---

- 05/2016-07/2016   **Wissenschaftliche Mitarbeiterin**  
**TriOptoTec GmbH**
- 08/2012-09/2014   **Studentische/Wissenschaftliche Hilfskraft**  
**Sensorik-Bayern/Universitätsklinikum Regensburg**  
Darstellung, Reinigung und Charakterisierung von photodynamisch aktiven Wirkstoffen

## **Praktika**

---

- 07/2010-09/2010      **Assistenz der Geschäftsleitung**  
**Institut für Überdruckmedizin, Regensburg**  
 - Terminorganisation  
 - Praxis-/Qualitätsmanagement
- 08/2009-09/2009      **Praktikum im Bereich Management und Patientenbetreuung**  
**Institut für Überdruckmedizin, Regensburg**  
 - Ordnungsmanagement  
 - Hilfestellung bei ärztlichen Maßnahmen

## **Ehrenamtliches Engagement**

---

- 12/2017 - dato      Stellvertretende Vorsitzende im Alumniverein Chemie der  
 Universität Regensburg e.V.
- 12/2016 - 12/2017      Beisitzerin im Alumniverein Chemie der Uni Regensburg e.V.
- 04/2007-05/2009      Jugendsprecherin bei den "Jungen Wilden aus'm Labertal"
- 09/2007-01/2009      Jugendsprecherin bei der TSG Laaber (Würdigung für  
 ehrenamtliche Tätigkeit)
- 03/2008      Ausbildung zur Clubassistentin (Bayerische Sportjugend)
- 09/2008-07/2010      Kollegstufensprecherin am Gymnasium Parsberg (Würdigung für  
 ehrenamtliche Tätigkeit)

## **Sprachkenntnisse**

---

- |             |                                      |
|-------------|--------------------------------------|
| Englisch    | verhandlungssicher                   |
| Französisch | erweiterte Grundkenntnisse (DELF B1) |
| Spanisch    | Grundkenntnisse                      |
| Arabisch    | Grundkenntnisse                      |

## **EDV-Kenntnisse & Qualifikationen**

---

- MS-Office  
 OriginLab  
 ChemDraw  
 TopSpin/MestReNova  
 Qualitätsmanagement in der analytischen Chemie-  
 Nachweis der umfassenden Sachkunde nach §5 i. V. m. §2 ChemVerbotsV

## **Eidesstattliche Erklärung**

Ich erkläre hiermit an Eides statt, dass ich die vorliegende Arbeit ohne unzulässige Hilfe Dritter und ohne Benutzung anderer als der angegebenen Hilfsmittel angefertigt habe; die aus anderen Quellen direkt oder indirekt übernommenen Daten und Konzepte sind unter Angabe des Literaturzitats gekennzeichnet.

---

Jana Schiller